



Fachgebiet für Peptidbiochemie

**Synthesen und biochemische und biophysikalische
Untersuchungen von Amyloidpeptidabkömmlingen**

Michael Beißwenger

Vollständiger Abdruck der von der Fakultät Wissenschaftszentrum Weihenstephan für Ernährung, Landnutzung und Umwelt der Technischen Universität München zur Erlangung des akademischen Grades eines
Doktors der Naturwissenschaften
genehmigten Dissertation.

Vorsitzende:

Univ.-Prof. Dr. I. Antes

Prüfer der Dissertation:

1. Univ.-Prof. Dr. A. Kapurniotu
2. Univ.-Prof. Dr. B. Reif

Die Dissertation wurde am 28.04.2015 bei der Technischen Universität München eingereicht und durch die Fakultät Wissenschaftszentrum Weihenstephan für Ernährung, Landnutzung und Umwelt am 21.09.2015 angenommen.

Abstract

Protein misfolding and aggregation are linked to many severe diseases like Alzheimer's disease (AD) and type 2 diabetes (T2D). AD is associated with the formation of amyloid plaques consisting mainly of the β -amyloid peptide ($A\beta$), whereas T2D is associated with the aggregation of islet amyloid polypeptide (IAPP). Emerging pathophysiological, epidemiological and biochemical evidence suggests that the pathogeneses of these two diseases are linked to each other. At the molecular level, $A\beta$ and IAPP share a 25% sequence similarity and a 50% homology and the two polypeptides have been shown to bind to each other with high affinity and to form non-fibrillar and non-toxic hetero-oligomers. The $A\beta$ -IAPP cross-interaction results in suppression of amyloidogenic self-association and has been thus suggested to be a potential molecular link between AD and T2D. Recent studies have identified the two IAPP segments IAPP(8-18) and IAPP(22-28) as hot segments of both the IAPP self- and the IAPP- $A\beta$ hetero-association interface.

The first aim of this work was to investigate the role of the IAPP loop region IAPP(19-21) which connects hot segments IAPP(8-18) and IAPP(22-28) with each other in amyloid self-association of the IAPP partial sequence IAPP(8-28). Toward this aim, biophysical and biochemical studies on a number of analogues of IAPP(8-28) containing various different tripeptide segments consisting of amino acids with varying charge, hydrophobicity, aromaticity, steric hindrance, flexibility, or secondary structure-stabilizing propensity instead of the native segment IAPP(19-21) were performed. The results showed that the amino acid composition of IAPP(19-21) plays a crucial role in conformation and amyloidogenic and cytotoxic potential of IAPP(8-28). For instance, results of CD studies on analogues of IAPP(8-28)-OH with hydrophobic amino acids in the IAPP(19-21) region were consistent with large amounts of β -sheet/ β -turn structural contents. These analogues also exhibited high amounts of exposed hydrophobic surface, high aggregation potentials and medium to high cytotoxicity. By contrast, analogues containing charged amino acids in the IAPP(19-21) region were unable to form amyloid fibrils and most of them were non-cytotoxic. Intriguingly, analogues with a charged loop region adopted in their non-aggregated state a similar overall conformation -mainly random coil- to the highly amyloidogenic IAPP(8-28)-OH based on CD spectroscopy. Their weak amyloidogenic and cytotoxic potentials might be explained by electrostatic repulsion of the charged residues in the IAPP(19-21) region that prevent the formation of a hydrophobic core likely required for fibril formation. Importantly, IAPP(8-28) and the strongly amyloidogenic analog S20G-IAPP(8-28) contain small or polar amino acid residues in the IAPP(19-21) region which are usually found in β -turns and the CD spectra of the non-aggregated states suggested mostly unordered states or polyproline II helices (PPII). Taken together, the results suggested that tripeptide segments consisting of polar β -turn stabilizing residues had similar strong effects on amyloidogenicity and cytotoxicity as segments consisting of hydrophobic β -sheet-stabilizing ones.

The aim of the second part of this work was to investigate the conformation, amyloidogenic and cytotoxic potential of designed model peptides consisting of two covalently linked hot segments of the $A\beta$ -IAPP interaction interface. To achieve this aim, the segments $A\beta$ (27-32) and IAPP(22-28) were chosen. These two segments, which are amyloidogenic and able to cross-interact with each other, were connected by various different tripeptide segments or flexible linkers containing non-native amino acids. The tripeptide linkers varied with respect to charge, hydrophobicity, steric hindrance, polarity, or flexibility of the involved amino acids. The effect of these different connecting elements on β -sheet formation, cytotoxicity, and fibril formation was studied. Peptides with hydrophobic connecting elements displayed in general high fibril forming potentials. Among the studied peptides only the ones with a hydrophobic connecting element like Aoc (8-aminooctanoic acid), Adc (10-aminodecanoic acid) and the tripeptide LLL were found to form β -sheets, cytotoxic assemblies and amyloid fibrils. Peptides with hydrophilic or charged connecting elements were unable to form amyloid fibrils and only expressed weak cytotoxicity. Positive and negative charges were found to block

fibril formation most likely due to electrostatic repulsion. CD spectra of peptides with charged connecting motifs displayed mainly random coil structure. This was an additional hint that charges disrupted the formation of ordered structures. A flexible connecting element seemed to be rather disadvantageous for fibril formation and toxicity. Hydrophobic connecting elements were found to be a key factor for the formation of amyloid structures whereas charged elements turned out to be less important.

In an attempt to force the two amyloidogenic sequences A β (27-32) and IAPP(22-28) into an intramolecular interaction, cyclic peptides containing these two sequences were synthesized and studied with regard to their conformation, fibril forming and cytotoxic properties. Three different connecting elements (LLL, KKK, and Aoc) were chosen for these cyclic peptides based on the results of the studies performed with linear peptides. Again, the hydrophobic connecting elements LLL and Aoc were found to induce the formation of β -sheet structures. Cyclic peptides containing these connecting elements were found to exhibit a high fibril forming potential and cytotoxicity. However, only the cyclic peptides containing Aoc as a connecting element showed similar fibril forming potentials and toxicity as the respective linear peptides. Cyclic peptides containing the charged and hydrophilic element KKK on the other hand displayed a low fibril forming potential and cytotoxicity. In general, cyclization did not lead to large changes in the biophysical properties of the peptides when compared with their linear equivalents. This might be because the open and the cyclized equivalents possessed similar structural features indicating a U-shaped structure for the linear peptides. The results of this work should contribute to a better understanding of the molecular mechanisms underlying protein aggregation and related cell toxicity in AD and T2D.

Zusammenfassung

Die Fehlfaltung und Aggregation von Proteinen steht im Zusammenhang mit vielen schwerwiegenden Erkrankungen, wie z.B. die Alzheimer Erkrankung (AD) und Typ 2 Diabetes (T2D). AD steht im Zusammenhang mit der Bildung von Ablagerungen, die hauptsächlich aus dem β -Amyloid Peptid ($A\beta$) bestehen, wohingegen bei T2D das Insel-Amyloid-Polypeptid (IAPP) Ablagerungen bildet. Neu auftauchende pathophysiologische, epidemiologische und biochemische Erkenntnisse legen nahe, dass die Pathogenesen dieser beiden Erkrankungen miteinander verknüpft sind. Auf molekularer Ebene sind die Sequenzen von $A\beta$ und IAPP zu 25% identisch und zu 50% homolog. Zudem wurde kürzlich gezeigt, dass die beiden Peptide mit hoher Affinität zu einander binden und nicht-fibrilläre, nicht-toxische Hetero-Oligomere bilden können. Die $A\beta$ -IAPP Kreuzwechselwirkung führt zu einer Unterdrückung der amyloidogenen Selbstassoziation und wurde deshalb als potentieller molekularer Zusammenhang zwischen AD und T2D vorgeschlagen. Aktuelle Untersuchungen haben die beiden IAPP Segmente IAPP(8-18) und IAPP(22-28) als „Hot-Segmente“ der IAPP Selbst- und der IAPP- $A\beta$ Heteroassoziation identifiziert.

Das erste Ziel dieser Arbeit war es, die Funktion der IAPP Schleifenregion IAPP(19-21), die die beiden Hot-Segmente IAPP(8-18) und IAPP(22-28) miteinander verbindet, bei der Amyloid-Selbstassoziation der IAPP Teilsequenz IAPP(8-28) zu untersuchen. Um dies zu erreichen wurden biophysikalische und biochemische Untersuchungen mit einer Reihe von IAPP(8-28) Analoga durchgeführt, die anstelle des nativen Segments IAPP(19-21) vielfältige, verschiedene Tripeptidsegmente enthalten, die aus Aminosäuren mit unterschiedlicher Ladung, Hydrophobizität, Aromatizität, sterischer Hinderung, Flexibilität oder Sekundärstruktur stabilisierenden Eigenschaften bestehen, durchgeführt. Die Ergebnisse deuten darauf hin, dass die Aminosäurezusammensetzung der Region IAPP(19-21) eine wichtige Rolle für die Konformation, das amyloidogene Potential und die Zytotoxizität von IAPP(8-28) spielt. Die Ergebnisse von CD Studien mit Analoga von IAPP(8-28) mit hydrophoben Aminosäuren in der Region IAPP(19-21) weisen auf einen großen Anteil an β -Faltblatt/ β -Schleifen Strukturelementen hin. Diese Analoga besitzen auch einen hohen Anteil an exponierten hydrophoben Oberflächen, ein hohes Aggregationspotential und eine mittlere bis hohe Zytotoxizität. Im Gegensatz dazu waren Analoga mit geladenen Aminosäuren in der Region IAPP(19-21) nicht fähig, Amyloidfibrillen zu bilden und die meisten dieser Analoga waren nicht zytotoxisch. Interessanterweise nahmen Analoga mit einer geladenen Schleifenregion im nicht-aggregierten Zustand, basierend auf CD spektroskopischen Studien, eine ähnliche Gesamtkonformation ein - hauptsächlich Random Coil - wie das hochgradig amyloidogene IAPP(8-28)-OH. Ihre schwachen amyloidogenen und zytotoxischen Potentiale lassen sich möglicherweise durch elektrostatische Abstoßung der geladenen Reste in der Region IAPP(19-21) erklären, die die Ausbildung eines hydrophoben Kerns, der wahrscheinlich für die Fibrilbildung notwendig ist, verhindern. Bedeutenderweise besitzen IAPP(8-28) und das hochgradig amyloidogene Analogon S20G-IAPP(8-28) kleine oder polare Aminosäurereste in der Region IAPP(19-21), die man üblicherweise in β -Schleifen findet und die CD Spektren der nicht-aggregierten Zustände deuten auf großteils ungeordnete oder Polyprolin-II-Helix Strukturen hin. Zusammengenommen deuten die Ergebnisse darauf hin, dass Tripeptidsegmente die aus polaren, β -Schleifen stabilisierenden Resten bestehen, ähnlich starke Effekte auf Amyloidogenität und Zytotoxizität haben, wie Segmente, die aus hydrophoben, β -Faltblätter stabilisierenden Resten bestehen.

Ziel des zweiten Teils dieser Arbeit war es, die Konformation und die amyloidogenen und zytotoxischen Potentiale von speziell entworfenen Modellpeptiden, die aus zwei kovalent verknüpften Segmenten der IAPP- $A\beta$ Wechselwirkungsdomäne bestehen. Um dies zu ermöglichen, wurden die Segmente $A\beta$ (27-32) und IAPP(22-28) ausgewählt. Diese beiden Segmente, die amyloidogen und in der Lage sind, miteinander zu interagieren, wurden mit verschiedenen unterschiedlichen Tripeptidsegmenten oder mit flexiblen Verknüpfungselementen, die nicht-native Aminosäuren enthalten, verbunden. Die

Tripeptidverknüpfungselemente unterschieden sich hinsichtlich der Ladung, Hydrophobizität, sterischen Hinderung, Polarität oder Flexibilität der verwendeten Aminosäuren. Der Einfluss dieser verschiedenen Verknüpfungselemente auf β -Faltblattbildung, Zytotoxizität und Fibrilbildung wurde untersucht. Peptide mit hydrophoben Verknüpfungselementen zeigten allgemein hohe Fibrilbildungspotentiale. Von den untersuchten Peptiden bildeten nur jene mit hydrophoben Verknüpfungselementen β -Faltblattstrukturen, zytotoxische Aggregate und Amyloidfibrillen. Peptide mit hydrophilen oder geladenen Verknüpfungselementen waren nicht dazu in der Lage, Amyloidfibrillen auszubilden und zeigten nur schwache Zytotoxizität. Positive und negative Ladungen verhinderten eine Fibrilbildung höchstwahrscheinlich wegen elektrostatischer Abstoßung. CD Spektren von Peptiden mit geladenen Verknüpfungselementen wiesen hauptsächlich auf Random Coil Elemente hin. Dies war ein weiterer Hinweis dafür, dass Ladungen die Bildung von geordneten Strukturen verhindern können. Ein flexibles Rückgrat schien für Fibrilbildung und Zytotoxizität eher hinderlich zu sein. Peptide mit einem flexiblen Verknüpfungselement besaßen niedrige Fibrilbildungspotentiale und Zytotoxizität. Hydrophobe Verknüpfungselemente schienen der zentrale Faktor für die Ausbildung von Amyloidstrukturen zu sein, wohingegen sich geladene Elemente als weniger bedeutsam herausstellten.

In einem Versuch, die beiden amyloidogenen Sequenzen A β (27-32) und IAPP(22-28) zu intramolekularen Wechselwirkungen zu zwingen, wurden zyklische Peptide, die diese beiden Sequenzen enthalten, synthetisiert und hinsichtlich ihrer strukturellen, Fibril-bildenden und zytotoxischen Eigenschaften untersucht. Basierend auf den Ergebnissen vorangehender Untersuchungen wurden drei unterschiedliche Verknüpfungselemente (LLL, KKK, und Aoc) ausgewählt. Erneut wurde festgestellt, dass hydrophobe Verknüpfungselemente die Bildung von β -Faltblattstrukturen herbeiführen können. Zyklische Peptide, die solche Verknüpfungselemente enthalten, zeigten hohe Fibrilbildungspotentiale und Zytotoxizität. Dennoch besaßen nur die zyklischen Peptide mit Aoc als Verknüpfungselement ähnliche Fibrilbildungspotentiale und Toxizitäten wie ihre linearen Äquivalente. Zyklische Peptide, die das hydrophile Verknüpfungselement KKK enthalten, besaßen hingegen schwache Fibrilbildungspotentiale und Zytotoxizität. Dies könnte daran liegen, dass die offenen und die zyklischen Äquivalente ähnliche strukturelle Eigenschaften besitzen, was auf eine U-förmige Struktur hinweist.

Die Ergebnisse dieser Arbeit sollen zu einem besseren Verständnis der molekularen Mechanismen führen, die der Aggregation und der damit verbundenen Zelltoxizität der AD und T2D zugrunde liegen.

Table of Content

1 Introduction	1
1.1 Amyloid	1
1.1.1 Toxic amyloid species	1
1.1.2 Formation of amyloid fibrils	1
1.1.3 Structure of amyloid	2
1.1.4 Functional amyloid	3
1.2 Alzheimer's disease and A β	4
1.3 IAPP	5
1.3.1 Structure of IAPP	7
1.4 Link between IAPP and A β	9
1.5 Aim	10
2 Materials and Methods	11
2.1 Chemicals	11
2.2 Instruments	12
2.3 Laboratory utensils	13
2.4 Cell culture media	13
2.5 Methods	13
2.5.1 Solid phase peptide synthesis	13
2.5.1.1 Loading of the resin	13
2.5.1.2 Determination of the substitution level	14
2.5.1.3 Chain elongation	14
2.5.1.4 Kaiser test	14
2.5.1.5 Cleavage of Mtt and PiP protecting groups	15
2.5.1.6 Cleavage of the ivDde protecting group	15
2.5.1.7 Cyclization strategies	15
2.5.1.8 Cleavage from the resin	16
2.5.2 MALDI mass spectrometry	16
2.5.3 HPLC	18
2.5.4 Circular dichroism spectroscopy	18
2.5.5 Thioflavin T fluorescence assay	19
2.5.6 Congo Red staining	19
2.5.7 Transmission electron microscopy	19
2.5.8 ANS binding assay	19
2.5.9 Concentration determination of carboxyfluorescein-labeled peptides	20
2.5.9.1 Self-association studies using Fluorescence Spectroscopy	20
2.5.10 Size-exclusion chromatography	20
2.5.11 SDS PAGE	20
2.5.11.1 Coomassie staining	21
2.5.11.2 Silver staining	21
2.5.12 Cell viability studies	21
3 Results and Discussion	23
3.1 Analogues of IAPP(8-28)	23
3.1.1 Design of the analogues	23
3.1.1.1 IAPP(8-18)-OH	25
3.1.1.2 IAPP(22-28)-OH	26
3.1.1.3 IAPP(8-28)-OH	28
3.1.1.4 IAPP(8-18)-SGN-(22-28)-OH	30
3.1.1.5 IAPP(8-18)-Aoc-(22-28)-OH	31
3.1.1.6 IAPP(8-18)-Peg-(22-28)-OH	33
3.1.1.7 IAPP(8-18)-KKK-(22-28)-OH	35
3.1.1.8 IAPP(8-18)-Dap ₃ -(22-28)-OH	37
3.1.1.9 IAPP(8-18)-RRR-(22-28)-OH	39
3.1.1.10 IAPP(8-18)-DDD-(22-28)-OH	40
3.1.1.11 IAPP(8-18)-GGG-(22-28)-OH	42
3.1.1.12 IAPP(8-18)-AAA-(22-28)-OH	44
3.1.1.13 IAPP(8-18)-VVV-(22-28)-OH	45

3.1.1.14 IAPP(8-18)-LLL-(22-28)-OH	47
3.1.1.15 IAPP(8-18)-III-(22-28)-OH	49
3.1.1.16 IAPP(8-18)-Nle ₃ -(22-28)-OH	51
3.1.1.17 IAPP(8-18)-2Aoc ₃ -(22-28)-OH	53
3.1.1.18 IAPP(8-18)-TTT-(22-28)-OH	54
3.1.1.19 IAPP(8-18)-FFF-(22-28)-OH	56
3.1.1.20 IAPP(8-18)-Cha ₃ -(22-28)-OH	58
3.1.1.21 IAPP(8-18)-SpG-(22-28)-OH	60
3.1.1.22 IAPP(8-18)-pGN-(22-28)-OH	61
3.1.1.23 IAPP(8-18)-PPP-(22-28)-OH	63
3.1.1.24 IAPP(8-18)-(K(Ac)) ₃ -(22-28)-OH	65
3.1.1.25 IAPP(8-18)-KK(Ac)K(Ac)-(22-28)-OH	67
3.1.1.26 IAPP(8-18)-K(Ac)KK(Ac)-(22-28)-OH	69
3.1.1.27 IAPP(8-18)-K(Ac)K(Ac)K-(22-28)-OH	71
3.1.1.28 IAPP(8-18)-KKK(Ac)-(22-28)-OH	72
3.1.1.29 IAPP(8-18)-KK(Ac)K-(22-28)-OH	74
3.1.1.30 IAPP(8-18)-K(Ac)KK-(22-28)-OH	76
3.1.2 Comparison of the analogues	79
3.1.2.1 IAPP(8-28), partial segments IAPP(8-18) and IAPP(22-28), S20G-IAPP(8-28), and IAPP(8-28) analogues with nonpeptidic substituents for the region IAPP(19-21)	79
3.1.2.2 Analogues with charged side chains in the region IAPP(19-21)	81
3.1.2.3 Analogues with side chains with differences in steric hindrance and hydrophobicity in the IAPP(19-21) region	82
3.1.2.4 Analogues with a branch in the gamma position of the side chain in the IAPP(19-21) region	85
3.1.2.5 Analogues with secondary structure inducing elements in the IAPP(19-21) region	87
3.1.2.6 Comparison of the analogues concerning their toxicity	89
3.1.2.6.1 High toxicity	89
3.1.2.6.2 Medium toxicity	91
3.1.2.6.3 Low toxicity	93
3.1.2.7 Scanning of the IAPP(19-21) region with Lys and Lys(Ac)	94
3.1.3 Thermal denaturation studies on selected analogues	99
3.1.4 ANS binding	109
3.1.5 Size exclusion chromatography (SEC) studies with selected analogues	114
3.1.6 NuPAGE	119
3.1.7 Fluos self-association	120
3.1.8 Conclusions	122
3.2 Hybrids of A β (27-32) and IAPP(22-28)	124
3.2.1 Introduction	124
3.2.1.1 Aim and Design	125
3.2.2 Peptides containing the segments A β (27-32) and IAPP(22-28)	126
3.2.2.1 IAPP(22-28) or H-NFGAILS-OH	126
3.2.2.2 A β (27-32) or H-NKGAIL-OH	127
3.2.2.3 H-NKGAIL-Peg-NFGAILS-OH (H5)	128
3.2.2.4 H-NKGAIL-Aoc-NFGAILS-OH (H5a)	130
3.2.2.5 H-NKGAIL-Aoc-NFGAILS- β A-KKK-OH (H5aK3)	132
3.2.2.6 H-KKK- β A-NKGAIL-Aoc-NFGAILS- β A-KKK-OH (H5aK6)	133
3.2.2.7 H-NKGAIL-Adc-NFGAILS-OH (H5b)	134
3.2.2.8 H-NKGAIL-GGG-NFGAILS-OH (H16)	136
3.2.2.9 H-NKGAIL-AAA-NFGAILS-OH (H18)	137
3.2.2.10 H-NKGAIL-LLL-NFGAILS-OH (H12)	139
3.2.2.11 H-KKK- β A-NKGAIL-LLL-NFGAILS- β A-KKK-OH (H12K6)	140
3.2.2.12 H-NKGAIL-KKK-NFGAILS-OH (H13)	142
3.2.2.13 H-NKGAIL-K(Ac)K(Ac)K(Ac)-NFGAILS-OH (H20)	143
3.2.2.14 H-NKGAIL-EEE-NFGAILS-OH (H22)	145
3.2.3 Peptides containing the segments A β (32-27) and IAPP(22-28)	147
3.2.3.1 A β (32-27) or H-IIAGKN-OH	147
3.2.3.2 H-IIAGKN-Peg-NFGAILS-OH (H6)	149

3.2.3.3 H-IIAGKN-Aoc-NFGAILS-OH (H6a)	150
3.2.3.4 H-IIAGKN-Adc-NFGAILS-OH (H6b)	151
3.2.3.5 H-IIAGKN-GGG-NFGAILS-OH (H24)	153
3.2.3.6 H-IIAGKN-AAA-NFGAILS-OH (H23)	154
3.2.3.7 H-IIAGKN-LLL-NFGAILS-OH (H14)	156
3.2.3.8 H-IIAGKN-KKK-NFGAILS-OH (H15)	157
3.2.3.9 H-IIAGKN-K(Ac)K(Ac)K(Ac)-NFGAILS-OH (H19)	159
3.2.3.10 H-IIAGKN-EEE-NFGAILS-OH (H17)	160
3.2.4 Other combinations of the segments A β (27-32) and IAPP(22-28)	162
3.2.4.1 H-NFGAILS-LLL-NFGAILS-OH (CB1)	162
3.2.4.2 H-NKGAIL-LLL-NKGAIL-OH (CB3)	164
3.2.4.3 H-NFGAILS-Aoc-NFGAILS-OH (CB5)	165
3.2.4.4 H-NKGAIL-Aoc-NKGAIL-OH (CB6)	167
3.2.4.5 H-NFGAILS-Aoc-NKGAIL-OH (CB7)	168
3.2.4.6 H-NFGAILS-KKK-NFGAILS-OH (CB2)	170
3.2.4.7 H-NKGAIL-KKK-NKGAIL-OH (CB4)	171
3.2.5 Comparisons	173
3.2.5.1 Influence of the different connecting elements	173
3.2.5.2 Peptides with the connecting element LLL	177
3.2.5.3 Peptides with the connecting element Aoc	179
3.2.5.4 Peptides with the connecting element KKK	181
3.2.5.5 Influence of the sequence	182
3.2.5.6 Conclusions	184
3.3 Cyclic peptides containing the segments A β (27-32) and IAPP(22-28)	186
3.3.1 Design of the peptides	186
3.3.2 Synthesis and studies of cyclic peptides and their linear equivalents	188
3.3.2.1 H-C-NKGAIL-LLL-NFGAILS-C-OH (H12CC)	188
3.3.2.2 H-S-NKGAIL-LLL-NFGAILS-S-OH (H12Ser)	190
3.3.2.3 Linear H-Lys-NKGAIL-LLL-NFGAILS-Asp-OH (Lys-LLL-lin)	191
3.3.2.4 Cyclic H-Lys-NKGAIL-LLL-NFGAILS-Asp-OH (Lys-LLL-cyclo)	193
3.3.2.5 Linear H-Dap-NKGAIL-LLL-NFGAILS-Asp-OH (Dap-LLL-lin)	194
3.3.2.6 Linear H-C-NKGAIL-KKK-NFGAILS-C-OH (H13CC-red)	196
3.3.2.7 Cyclic H-C-NKGAIL-KKK-NFGAILS-C-OH (H13CC-ox)	197
3.3.2.8 H-S-NKGAIL-KKK-NFGAILS-S-OH (H13Ser)	199
3.3.2.9 Linear H-Lys-NKGAIL-KKK-NFGAILS-Asp-OH (Lys-KKK-lin)	200
3.3.2.10 Linear H-Dap-NKGAIL-KKK-NFGAILS-Asp-OH (Dap-KKK-lin)	202
3.3.2.11 Cyclic H-Dap-NKGAIL-KKK-NFGAILS-Asp-OH (Dap-KKK-cyclo)	203
3.3.2.12 Linear H-C-NKGAIL-Aoc-NFGAILS-C-OH (H5aCC-red)	205
3.3.2.13 Cyclic H-C-NKGAIL-Aoc-NFGAILS-C-OH (H5aCC-ox)	207
3.3.2.14 Dimer 3 red	208
3.3.2.15 Dimer 3 ox	210
3.3.3 Comparisons	212
3.3.3.1 Peptides with the connecting element LLL	213
3.3.3.2 Peptides with the connecting element KKK	214
3.3.3.3 Peptides with the connecting element Aoc	216
3.3.3.4 Conclusions	217
4 References	220
5 List of Abbreviations	226
6 Amino Acid Codes	227
7 Curriculum Vitae	228
8 Acknowledgments	229
9 Declaration	229

1 Introduction

1.1 Amyloid

The term “amyloid” is used to describe insoluble aggregates of a particular protein or peptide consisting of fibrils having mainly „cross- β “-structures.

The transition of soluble protein into insoluble aggregates often correlates with the loss of its physiological function and the formation of cytotoxic assemblies. Misfolded and aggregated proteins play a crucial role in many chronic degenerative diseases. For example A β in Alzheimer’s disease (AD) and Down’s syndrome [1], islet amyloid polypeptide (IAPP) in type 2 diabetes (T2D) [2], prion protein in BSE, Creutzfeldt–Jakob disease and kuru [3], serum amyloid A in secondary amyloidosis [4], α -synuclein in Parkinson’s disease [5], medin in aortic medial amyloidosis [6], superoxide dismutase in amyotrophic lateral sclerosis [7], tau in tauopathies or AD [8, 9], and huntingtin in Huntington’s disease [10].

1.1.1 Toxic amyloid species

The nature of the specific toxic amyloid species is still unknown. Early models related the presence of amyloid depots to cell degeneration and toxicity. These models stated that disease and fibril formation have the same cause [11-14].

Studies could even show the toxicity of amyloid fibrils for example from A β [15, 16].

There is however no linear relation between the amount of amyloid plaques and the severeness of the disease [17-19].

Increasing evidence suggests that soluble oligomers are the main cytotoxic species [20-27]. The term oligomers is thereby used for different species ranging from dimers up to prefibrillar aggregates consisting of hundreds of peptides.

A number of studies revealed the structure of amyloid fibrils (see chapter 1.1.3), whereas little is known about the structure of oligomers and their formation. Details of their molecular structure and their function in amyloid diseases now begin to emerge [28-30].

Oligomers of different amyloidogenic peptides however seem to have a common structural motif as they all bind to a specifically designed antibody despite having no sequence similarity [31].

Since these different oligomers seem to have similar structural properties, their mechanism of toxicity might also be similar. They most likely mediate membrane disruption and toxicity by forming channels and pores through the cell membrane [32-35] or simply by inducing membrane defects upon assembling on the membrane surface [36-38].

1.1.2 Formation of amyloid fibrils

The formation of amyloid fibrils follows a nucleation dependent polymerisation mechanism. Above a critical concentration, proteins or peptides start to self-associate into several metastable intermediates, including dimers, trimers, and tetramers. This cooperative process is called the lag phase, in which nucleation takes place, initiating amyloid formation. The exposure of hydrophobic patches resulting in a hydrophobic collapse is a key step in the process leading towards the formation of insoluble aggregates and fibrils [39].

During the fibril elongation phase, monomers add to the protofibrils and resulting in amyloid fibrils. Fibrils are thermodynamically favoured compared to monomers or oligomers. The end-point of fibril formation is the so called plateau in which the association and the dissociation of monomers are in equilibrium with each other [40-42] (Fig. 1).

The exact molecular steps of amyloid formation are not yet completely understood.

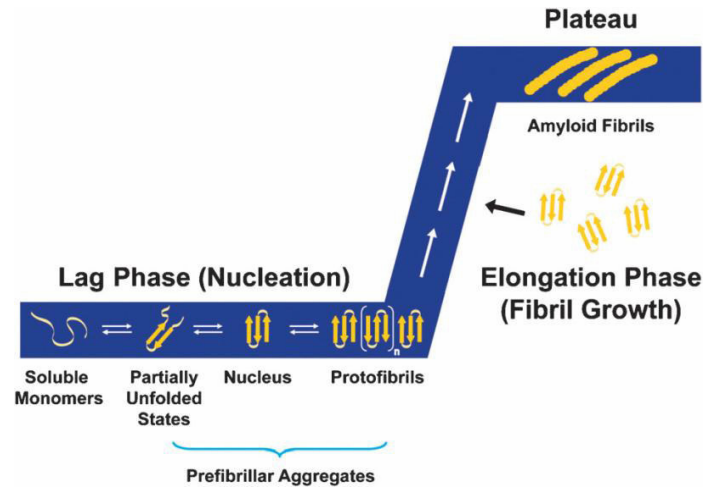


Fig. 1: A schematic representation of the nucleation polymerization model of amyloid aggregation. Soluble monomeric forms self-associate during the lag phase. Thereby a nucleus is formed that can be exponentially extended during the elongation phase. Mature amyloid fibrils are the final product of this process and the plateau phase represents the steady state when maximum fibril growth has been reached. The aggregation processes follows a sigmoidal kinetic trace that is depicted in the figure (blue). Picture from [43].

1.1.3 Structure of amyloid

A large variety of proteins are able to form amyloid. These proteins share no apparent sequence similarities except of glutamine and asparagine rich domains that seem to promote aggregation and the formation of antiparallel β -sheet structures by establishing polar side-chain interactions with main-chain amides [44-49].

However, one thing they all have in common is their ability to form β -sheet rich aggregates. Atomic resolution X-ray diffraction studies of amyloid fibrils showed that they contain a repetitive spine, commonly built from a pair of β -sheets. These two β -sheets run perpendicular to the fibril direction and are tightly packed together by interdigitated side chains of these β -strands creating a compact dehydrated interface. This structural motif is termed a 'steric zipper' [50, 51].

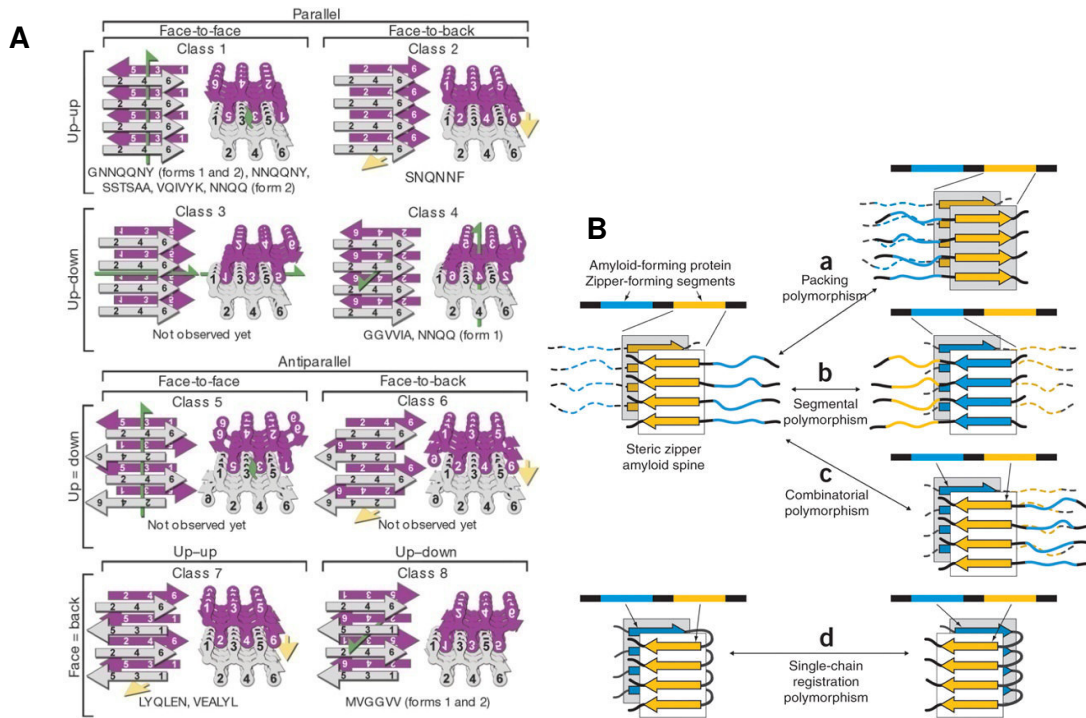


Fig. 2: Classification of steric zipper interfaces. (A) Classification depending on the arrangement of the segments within the β -sheets and on the packing and relative orientation of the β -sheets towards each other (from [51]). (B) Classification depending on the steric zipper forming segments and their arrangement to each other (from [52]).

There are eight classes of steric-zipper interfaces. They differ in orientation of the β -sheets towards each other and symmetry between two adjacent β -sheets. The strands of adjacent β -sheets can be aligned either parallel or anti-parallel to each other. These β -sheets can either align with the same surface (face-to-face) or with different surfaces (face-to-back) adjacent to each other. The β -sheets themselves can be oriented either parallel (up-up) or anti-parallel (up-down) relative to each other (Fig. 2A [51]).

Another way to classify steric zippers is according to the segments they are formed of. Steric zippers can form from one type of segment according to the eight different classes mentioned before. They can also be formed from two different types of segments. These two segments can either be located on two different peptides forming an intermolecular zipper motif or even be located on the same peptide strand and form an intramolecular steric zipper motif. Steric zippers consisting of two different amyloidogenic segments have not yet been described in atomic resolution (Fig. 2B [52]).

Despite their common β -spine structure, amyloid fibrils formed even from the same protein can occur in different structural morphologies.

1.1.4 Functional amyloid

In recent years, the so called “functional amyloid” hypothesis was developed. It states, that amyloidogenic aggregates can have an important biological function for the organism despite being toxic. The reason is that they possess properties like high stability and resistance to proteolytic digestion as well as degradation. These unique features of amyloids are also more and more used for bionanotechnological applications.

Functional amyloids have been found in many organisms. For example biofilms forming proteins like chaplins and curli in bacteria [53, 54].

Functional amyloids were even found in humans.

Pmel 17 is a type I transmembrane glycoprotein that is expressed by melanocytes and retinal pigment epithelial cells. Pmel17 is intralumenally cleaved by proprotein convertase leading to

a 28-kDa transmembrane fragment called M β and an 80-kDa luminal fragment called M α . M α is able to self-associate into fibrils that form the core of mature melanosomes. These fibrils are essential for the storage of melanin [55, 56].

1.2 Alzheimer's disease and A β

"I now begin the journey that will lead me into the sunset of my life."

Ronald Reagan's letter to Americans after learning he had Alzheimer's disease

Alzheimer's disease is the most common form of dementia. In Germany, approximately 1.4 million people are affected by dementia, two third of those suffer from Alzheimer's disease. It is estimated that this number will rise up to 3 million in 2050 [57].

AD can be separated into two groups depending on the patient's age when AD is diagnosed. Early-onset Alzheimer's disease (EOAD) is used for cases where Alzheimer's disease is diagnosed before the patient is 65 years old. Approximately 5-10% of the patients suffer from EOAD. Among these are also the cases of Familial Alzheimer's disease, a rather unusual form of Alzheimer's disease [58].

Late-onset Alzheimer's disease (LOAD) is the most common form of Alzheimer's disease and usually occurs after the age of 65 [59].

Alzheimer's disease was first described by the Bavarian psychiatrist and neuropathologist Alois Alzheimer in 1906. He discovered unusual protein deposits in the brain of a patient suffering from severe dementia and related them to the progressive cognitive decline [60].

It took almost 80 years until these deposits were characterized as an aggregated form of a polypeptide named A β . It was also possible to solubilize a monomeric form of A β with an estimated mass of 4.2-4.3 kDa and partially determine its sequence [1, 61-63].

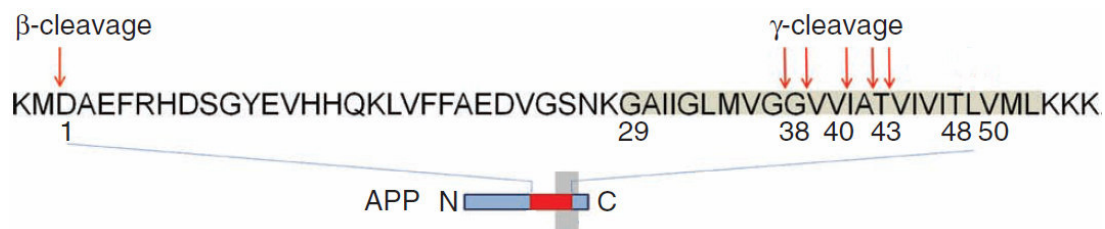


Fig. 3: Processing pathway of A β from amyloid precursor protein. The cleavage sites of β - and γ -secretase are marked with red arrows. Cleavage by γ -secretase produces a pool of A β fragments with varying length and hydrophobicity. The transmembrane domain of APP is highlighted in gray. Picture from [64].

A β is a polypeptide derived from APP, the Amyloid Precursor Protein, by proteolytic cleavage. Various different variants of A β with a length of 37 to 43 residues are known, depending on where APP is cut by the γ -secretase ([65], Fig. 3).

Due to these A β length variants and posttranslational modifications like phosphorylation [66-68], oxidation [69, 70], or pyroglutamylation [71-73], more than 20 different variants of A β are involved in its aggregation and pathological function.

Among those variants A β ₁₋₄₀ is the most abundant one, whereas the less abundant variant A β ₁₋₄₂ is much more fibrillogenic. Until now, research was mainly focused on these two variants.

As mentioned above, A β is processed from APP. APP is a transmembrane protein consisting of a small intracellular C-terminal region and a much larger extracellular region. The gene for APP is located on chromosome 21 [65].

During biosynthesis APP undergoes extensive post-translational modifications, such as N-glycosylation, O-glycosylation and tyrosine sulfation [74].

Mature APP can be processed by at least two proteolytic pathways. The non-amyloidogenic pathway involves cleavage by the α -secretase and the amyloidogenic pathway leading to A β formation. In the amyloidogenic pathway APP is cleaved by β - and γ -secretase [75].

A model of A β 40 fibrils using combined ssNMR and TEM data was developed by the Tycko group. In this model, A β 40 fibrils consist of in-register parallel β -sheets. The two β -strands of this model span from residues 10-22 and residues 30-40 [76].

The side chains of the hydrophobic residues L17, F19, I34, L34, and V36 create an internal hydrophobic core by forming internal quaternary contacts thereby stabilizing the fold of a single molecular layer. Another stabilizing feature shown by this model is the intramolecular salt bridge between D23 and K28. The side chain of M35 is forming external quaternary contacts to the backbone of G33, thereby forming an intermolecular interface. Oxidation of the side chain of M35 is known to prevent fibril formation [77-79] (Fig. 4).

H/D exchange data of A β 40 fibrils also indicate that residues 15-23 and 27-35 are involved in the formation of extremely stable structures, like the spine of a steric zipper [80].

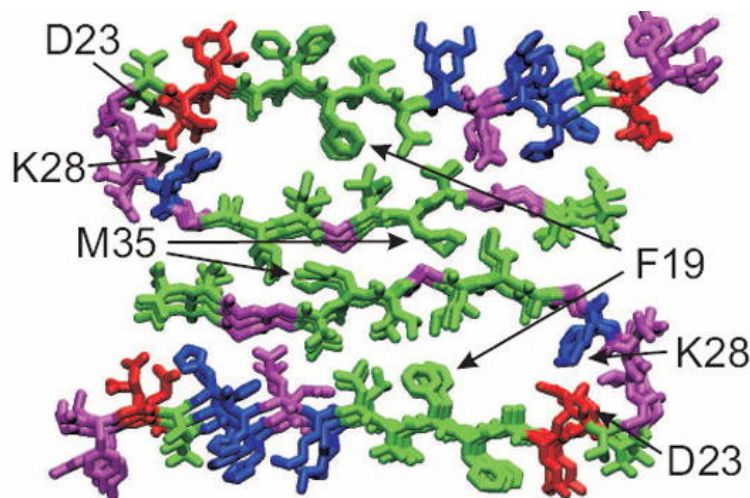


Fig. 4: Molecular structural models for A β 40 fibrils developed primarily from solid state NMR data with additional constraints from electron microscopy. The model shows residues 9-40. Residues 1-8 are conformationally disordered and therefore omitted. Hydrophobic residues are colored green, negatively charged red, positively charged (including His) blue, and polar (including Gly) magenta. Picture from [81].

Recent studies from the same group done with fibrils from Alzheimer's disease brain tissues also show in-register parallel β -sheet conformation for A β 40 fibrils. A β 40 fibrils were taken from brain tissues of patients suffering from Alzheimer's disease and used as seeds for further fibril growth in vitro [82].

1.3 IAPP

Deposits in the pancreatic islets of Langerhans of patients having type 2 diabetes were first described in 1901 [83].

In 1986, the peptide forming these deposits was identified as IAPP, a 37 residue long polypeptide with a similarity to the known neuropeptide calcitonin gene related peptide (CGRP) [2, 84-86].

This peptide is sometimes also called "amylin" [87].

Islet Amyloid Polypeptide is synthesized as an 89 residue pre-pro peptide and then processed in the Golgi apparatus and in the insulin secretory granule [88].

It consists of a 22 amino acid signal peptide which is cleaved shortly after translation and two regions flanking the actual IAPP part which are cleaved by prohormone convertases PC1/3 and PC2 at two consecutive basic amino acid residues in a similar way as proinsulin [88-90].

Final steps in the processing of mature IAPP include amidation of the C-terminus and the formation of a disulfide-bridge between Cys2 and Cys7 (Fig. 5).

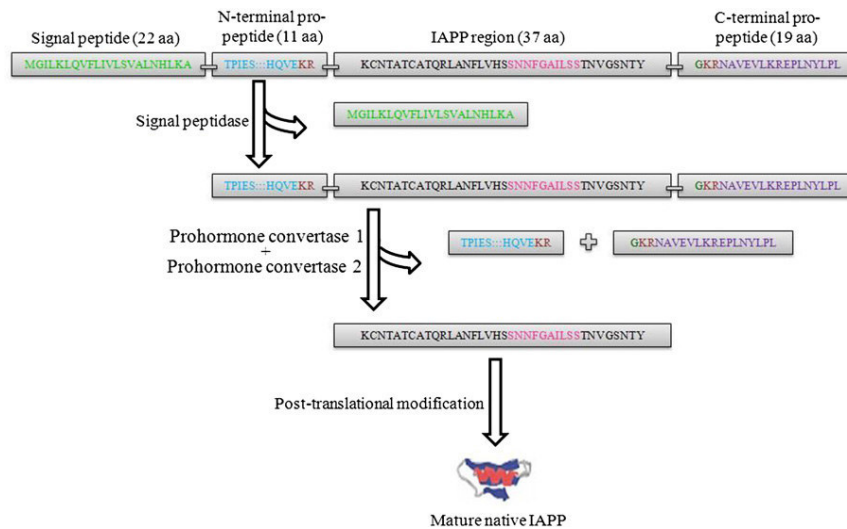


Fig. 5: Processing pathway of pre-pro IAPP leading towards native IAPP. Picture from [91].

The sequence of IAPP is highly conserved among the various species [92]. In contrast, IAPP from rats (rIAPP) does not form fibrils. rIAPP differs from hIAPP in six residues. Five out of those six difference occur in the region of IAPP(20-29) [93, 94]. Furthermore, rIAPP contains three proline residues, whereas hIAPP contains none. These three prolines are at position 25, 28 and 29. Proline is a known β -sheet breaker and it was therefore postulated that this was the reason why rIAPP is not fibrillogenic [94, 95].

Results of studies ([94, 96, 97]) also suggested the important role of IAPP(20-29) for fibril formation.

The replacement of residues 25, 28 and 29 of hIAPP by prolines leads to a non-fibrillogenic IAPP analog called Pramlintide. This analog is used for the treatment of diabetes type 1 and 2 [98, 99] (Fig. 6).

The shortest sequences of hIAPP that is able to self-assemble into amyloid fibrils are hIAPP(23-27) and hIAPP(15-18) [100, 101]. The identification of such short amyloid forming sequences can assist in the design of novel inhibitors of hIAPP aggregation [100].

hIAPP:	KCNTATCATQRLANFLVHSSNFGAILSSTNVGSNTY
rIAPP:	KCNTATCATQRLANFLV R SSNN LGPVLP P TNVGSNTY
Pramlintide:	KCNTATCATQRLANFLVHSSNFG P IL PP TNVGSNTY

Fig. 6: Comparison of the sequence of hIAPP with rIAPP and Pramlintide. Differences from the sequence of hIAPP are marked in red.

One known natively occurring hIAPP mutation is the S20G mutant. This mutation is known to increase the fibril forming potential of IAPP and is associated with an increased risk to develop early-onset type 2 diabetes [102-104].

Human IAPP contains three aromatic residues, F15, F23, and Y37. Systematic mutations of these residues with leucine to investigate the role of aromatic interactions in fibril formation revealed that the Y37L mutation dramatically slowed down the rate of fibril formation compared to wild-type IAPP. The F23L mutation also lowered the fibril forming potential, but not as much as Y37L. Contrary to that, the F15L mutation even increased the fibril forming potential [105]. In the core region of IAPP, hydrophobic interactions seem to be more important for fibril formation than aromatic interactions [105, 106].

The fibril forming potential of IAPP is also strongly pH-dependent [107]. Studies showed that the fibril formation is faster at pH 8.8 than at pH 4.0 [108]. At this pH-range, only the α -amino group and His18 of IAPP are able to get ionized. Studies showed that the ionization state of His-18 significantly affects the fibril formation of IAPP. A charged His-18 side chain increases solubility and reduces the fibril forming potential of IAPP [106, 109].

1.3.1 Structure of IAPP

Native, soluble IAPP adopts a mixture consisting of mainly random-coil and some β -sheet or β -turn structure [110-114]. Upon incubation in solution, the amount of β -sheet or β -turn elements increases, indicating a structural conversion from the native, soluble state to an aggregation prone structure [115].

A model for IAPP aggregation established by the group of David Eisenberg from the x-ray structure of hIAPP fused to maltose binding protein also predicts equilibrium between disordered and helical conformation for IAPP monomers. The helical structure is adopted by residues 8–18 and 22–27. It also showed that IAPP dimerizes and that the dimer leads towards fibril formation. In this model, the fibrillogenic IAPP consists of two β -strands ranging from residues 8-18 and 23-37 and a loop region in between them (Fig. 7).

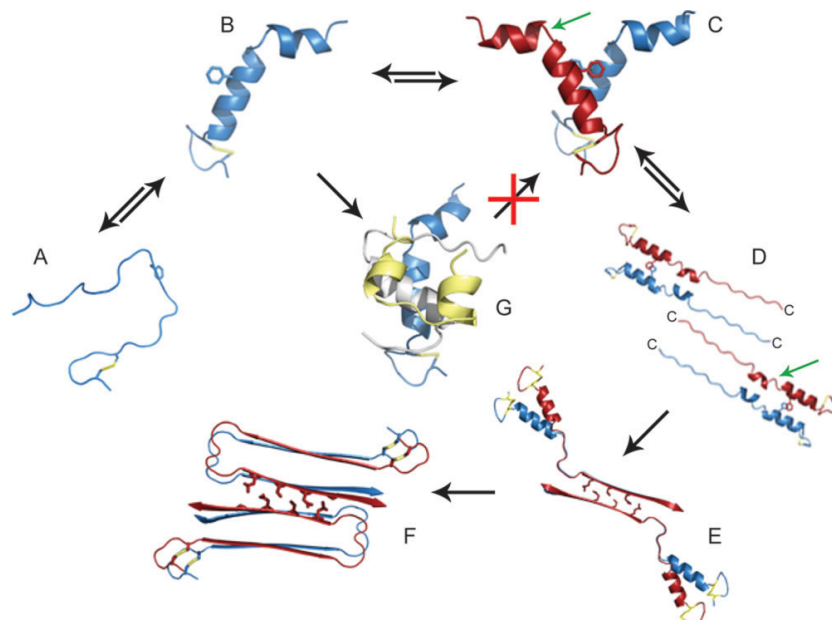


Fig. 7: Model of the IAPP fibril formation and the inhibition of fibrillation by insulin. Soluble monomers of IAPP are assumed to be in equilibrium between disordered (A) and helical (B) state. IAPP is then aligning into dimers (C). Two IAPP dimers align their C-terminal amyloid domains in an antiparallel orientation. The position of residue S20 is indicated by the green arrow. When this residue is mutated to Glycine, fibrils form more rapidly (D). Residues 23–37 are involved in the formation of a steric zipper spine. This is done by interdigitating sidechains of a second IAPP dimer (E). The formation of the N-terminal strand occurs subsequent to spine formation (F). Insulin can prevent the homoaggregation of IAPP by binding to monomeric IAPP. The insulin A-chain is shown in gold and the B chain is shown in gray (G). Picture from [52].

The model also suggests a mechanism for the prevention of IAPP fibril formation by insulin. Insulin binds to monomeric helical IAPP and thereby blocks the dimerization of IAPP [52].

A similar model for the molecular structure of IAPP fibrils was created by the group of Robert Tycko based on NMR data. This model also proposes a β -strand-loop- β -strand motif. The two β -strand forming regions consist of residues 8-17 and 28-37. The loop is formed by residues 18-27. The model actually contains two different structures differing in the side chain orientations. In one structure, the side chains of residues 9, 11, 13, and 15 are solvent

exposed, in the other structure they are buried in the hydrophobic core of the molecule (Fig. 8) [116].

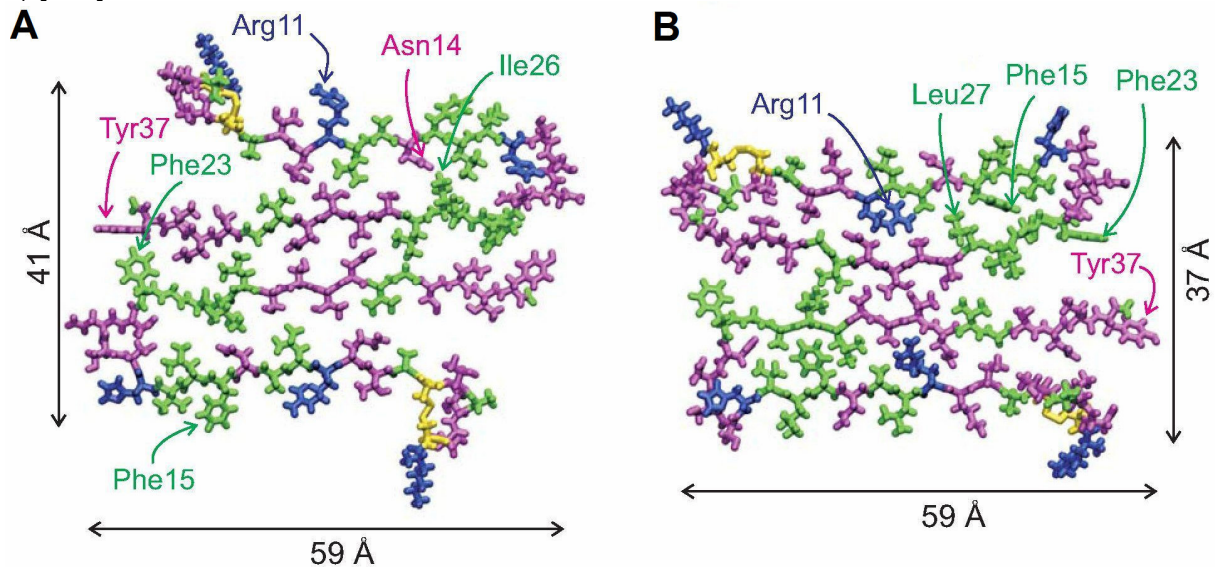


Fig. 8: Two different structural models of IAPP fibrils. In one structure residues 9, 11, 13, and 15 are exposed to the solvent (A) whereas they are buried inside the molecule in the second structure (B). Picture from [116].

A third model proposes a β -serpentine structure with three β -strands and two turns. The β -strands are formed by residues 12-17, 22-27 and 31-37, while the turns are formed by residues 18-21 and 28-30 (Fig. 9) [117].

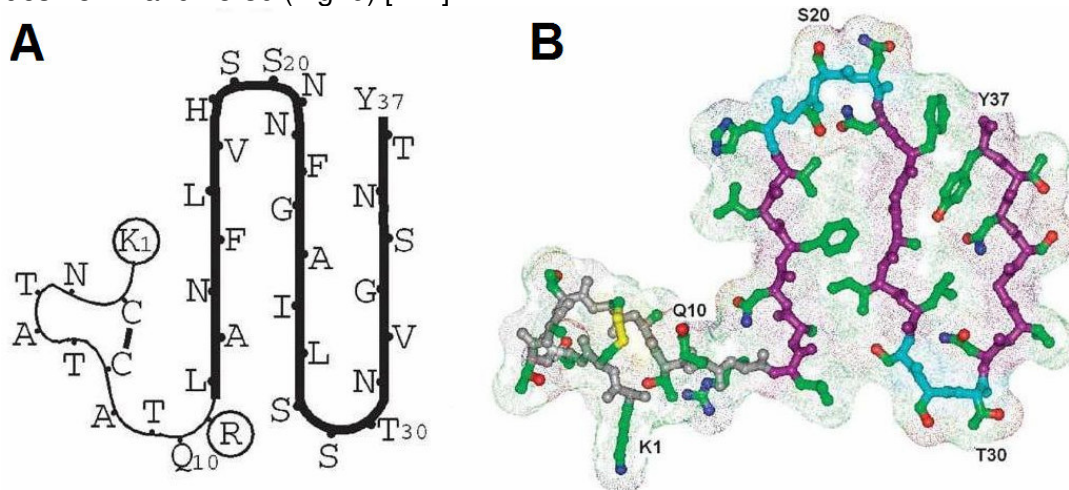


Fig. 9: The β -serpentine model for IAPP. In A, the β -serpentine motif is shown as a thick black line. In the ball-and-stick representation (B), the backbones of the β -strands are colored in purple and the backbones of the loops in cyan. Carbon atoms are in green, oxygen atoms in red, nitrogen atoms in blue and sulfur atoms in yellow. The first 11 N-terminal residues are not considered to be part of the serpentine motif. Picture from [117].

All these models have some things in common. First of all, the N-terminal part of IAPP has a rigid structure and is not involved in β -sheet formation. This is most likely due to the disulfide bridge between residues 2 and 7. The residues from at least 12 to 17 form a β -sheet in all these models. From residue 18 onward, there is a loop or turn structure. This structure ranges until residue 21 to 29, depending on the model. The C-terminus from residue 31 onwards is again a β -sheet in all models.

This means the mayor differences might be in the sequence between residues 18-30. In the different models, this part is either involved in the formation of a turn- β -sheet-turn structure, or a β -sheet-turn- β -sheet structure.

These differences might be due to different sample preparations required for the different experimental setups, the different methods of modeling used, which a priori assumptions were made, or they can be the result of the structural polymorphism of IAPP fibrils.

Circular dichroism studies showed that the IAPP monomer adopts random coil conformation in solution that is converted to a β -sheet rich structure upon time. These studies also predicted the existence of two different IAPP conformations in equilibrium with each other, an amyloidogenic one and a non-amyloidogenic one [115]. This was verified by combined results of mobility mass spectrometry and molecular dynamics which have shown that two different types of conformers of IAPP monomers are present. One conformer containing an extended β -hairpin motif one and one with a helix-coil structure [118]. The extended β -hairpin motif was not detected in experiments performed with rIAPP suggesting that this conformer might be an intermediate in the aggregation pathway of human IAPP.

1.4 Link between IAPP and A β

When comparing A β and IAPP, one realizes that they share 25% sequence identity and 50% sequence similarity. Both peptides are intrinsically disordered, highly amyloidogenic, and undergo structural changes followed by self association and deposition.

Studies showed that IAPP and A β are able to interact with each other in vitro and can form hetero-complexes.

For A β , the sequences A β (27-32) (NKGAI), A β (35-40) (MLVGGV), and A β (19-22) (FFAED) have been identified as hot regions, which are able to bind itself at nanomolar concentrations. Self association of IAPP is mediated by the two regions IAPP(8-18) and IAPP(22-28) that are able to bind each other with nano- to low micromolar affinity [119].

These hot spot regions of the A β and IAPP homo-interaction also modulate the hetero-interaction between A β and IAPP (Fig. 10) [120].

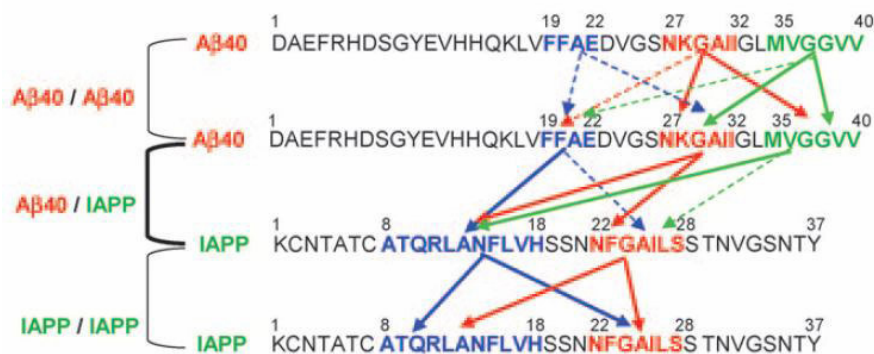


Fig. 10: Cross- and self-association domains of A β 40 and IAPP. The hot regions are colored in blue, red, and green. The same regions are promoting both homo- and hetero-association of A β 40 and IAPP. Picture from [120].

Epidemiological studies indicate an increased risk for developing Alzheimer's disease in people with type 2 diabetes and vice versa [121].

Recent studies even indicated that these two peptides interact in vivo [122, 123]. These studies could show that IAPP accumulates in the brain of AD patients and were even able to identify deposits containing both IAPP and A β . This indicates an association between brain derived IAPP and AD. Whether IAPP is able to cross-seed A β in the brain remains unclear and needs further investigation.

1.5 Aims

The focus of my work was to identify molecular features underlying IAPP self-association and its hetero-association with A β .

The first aim was to investigate the role of the IAPP loop region IAPP(19-21) in self-association of the IAPP partial sequence IAPP(8-28). Toward this aim, the properties of a number of different synthetic analogues of IAPP(8-28), which contains the hot regions of IAPP self- and its hetero-association with A β , IAPP(8-18) and IAPP(22-28), were to be studied. These analogues contained different tripeptide segments instead the IAPP loop region IAPP(19-21). The tripeptide segments consisted of hydrophobic, charged, flexible, sterically hindered, or polar amino acids as well as combinations of them. These analogues were to be studied with respect to their conformations, cytotoxicities, and their abilities to form amyloid structures using various different biophysical and biochemical methods.

The second aim was to synthesize and characterize the biophysical properties of a number of short peptides consisting of the hot regions of the A β /IAPP interaction interface. These studies should contribute in learning more about the structural features involved in A β -IAPP hetero-association. The two short sequences of A β and IAPP NKGAIL (A β (27-32)) and NFGAILS (IAPP(22-28)), which have been previously shown to both self- and cross-interact with each other, were selected. The plan was to covalently link these two sequences to each other with various connecting elements. The selected connecting elements should exhibit different features with regard to hydrophobicity, positive or negative charges, flexibility, and polarity. The effects of these different features on structure, fibril forming potential and cytotoxicity of the synthetic A β -IAPP hybrid peptides should then be investigated.

The third aim of this work was to constrain the conformation of some of the above A β /IAPP hybrids via intramolecular cyclization in order to induce formation of β -sheet structure likely based on a specific amyloid "steric zipper" motif. Several conformationally constrained cyclic peptides were to be synthesized and studied with regard to their conformation, amyloidogenicity and cytotoxicity.

2 Materials and Methods

2.1 Chemicals

Chemical

Amino acids (Fmoc and side chain protected)
Acetic acid (100% ACS)
Acetic anhydride
Acetone
Acetonitrile (HPLC-R)
Ammonium acetate
2-(7-Aza-1H-benzotriazole-1-yl)-1,1,3,3-tetramethyluronium hexafluorophosphate (HATU)
8-Anilinoanthracene-1-sulfonic acid (ANS)
4-Benzyloxybenzyl Alcohol Resin (Wang-resin)
Biotin
5(6)-Carboxyfluorescein
Chloranil
Congo Red
Dichloromethane (DCM)
Dimethylsulfoxid (DMSO)
N,N'-Diisopropylcarbodiimide
N,N-Diisopropylethylamine (DIEA)
3-[4,5-dimethylthiazol-2-yl]-2,5-diphenyltetrazolium bromide (MTT)
Dimethylformamid (DMF)
Diethylether
Dithiothreitol (DTT)
1,2-ethanedithiol (>98% GC) (EDT)
Ethanol (>96%)
Fmoc-2-aminooctanoic acid
Fmoc-8-aminooctanoic acid
Fmoc-10-aminodecanoic acid
Fmoc-Peg-OH
Formic acid
Glycin
Guanidinium-HCl
HCl
Hellmanex
1,1,1,3,3,3-hexafluoro-2-propanol (grade 99%) (HFiP)
H₂SO₄
1-Hydroxybenzotriazole (HOBT)
Isopropanol
Methanol (p.a.)
NaCl
NaOH
NaH₂PO₄
Na₂B₄O₇
Na₂HPO₄

Company

IRIS Biotech GmbH (Germany)
RAPP Polymere GmbH (Tübingen)
Merck (Darmstadt)
Biosolve (Netherland)
Sigma-Aldrich (Steinheim)
Biosolve (Netherland)
Fluka (Steinheim)
Merck (Darmstadt)
Aldrich (Steinheim)
IRIS Biotech GmbH (Germany)
Sigma-Aldrich (Steinheim)
Sigma-Aldrich (Steinheim)
Fluka (Steinheim)
Sigma-Aldrich (Steinheim)
Roth (Karlsruhe)
Roth (Karlsruhe)
Sigma-Aldrich (Steinheim)
Biosolve (Netherland)
Aldrich (Steinheim)
Biosolve (Netherland)
Roth (Karlsruhe)
Sigma-Aldrich (Steinheim)
Fluka (Steinheim)
Roth (Karlsruhe)
IRIS Biotech GmbH (Germany)
IRIS Biotech GmbH (Germany)
IRIS Biotech GmbH (Germany)
PolyPeptide Group
Sigma-Aldrich (Steinheim)
Fluka (Steinheim)
Roth (Karlsruhe)
Sigma-Aldrich (Steinheim)
Hellma
Sigma-Aldrich (Steinheim)
Merck (Darmstadt)
Fluka (Steinheim)
Roth (Karlsruhe)
Roth (Karlsruhe)
KMF (Lohmar)
Merck (Darmstadt)
Merck (Darmstadt)
Merck (Darmstadt)
Merck (Darmstadt)

NH ₄ HCO ₃	Fluka (Steinheim)
Ninhydrin	Fluka (Steinheim)
Phenol (99% A.C.S reagent)	Sigma-Aldrich (Steinheim)
Piperidin	Biosolve (Netherland)
Pyridin	Sigma-Aldrich (Steinheim)
Polylysine	Sigma-Aldrich (Steinheim)
2-propanol (p.a grade)	Merck (Darmstadt)
Proteinmarker-Muti Mark TM	Invitrogen (Karlsruhe)
Sodium acetate	Merck (Darmstadt)
Sodium dodecyl sulfate (SDS)	Merck (Darmstadt)
N,N,N',N'-Tetramethyl-O-(benzotriazol-1-yl)uronium tetrafluoroborate (TBTU)	IRIS Biotech GmbH (Germany)
Thioanisole (>99% GC)	Fluka (Steinheim)
Thioflavin T (ThT)	Sigma (Steinheim)
Trifluoroacetic acid (>99.5%) (TFA for synthesis)	Biosolve (Netherland)
Trifluoroacetic acid (>99.9%) (TFA for HPLC)	Biosolve (Netherland)
Triisopropylsilan (TIS)	Sigma-Aldrich (Steinheim)
2-Amino-2-(hydroxymethyl)-1,3-propanediol, hydrochloride (Tris-HCl)	Roth (Darmstadt)
Triton X-100	
Uranyl acetate	Sigma (München)

2.2 Instruments

Instrument

Analytical balance
 BLOWZARD Silver Line Microbiological Safety Cabinet
 Electrophoresis system XCell SureLock™ Mini-Cell
 Freeze-dryer Alpha 1-2 LD Plus
 Heating bloc neoBlock-1
 HPLC-system
 - PU-2080 Plus Intelligent HPLC pump
 - DG-2080-53 3 Line Degasser
 - LG-2080-02 Ternary Gradient Unit
 - UV-2077 Plus 4 λ Intelligent UV/VIS Detector
 Jasco 715-Spectropolarimeter
 Mass spectrometer Ultraflexxtreme
 Optical microscope Olympus CKX41

pH meter
 Shaker CAT S20
 Tabletop centrifuge 5417 C
 Ultracentrifuge Z400K

V-630 Spectrophotometer (UV/VIS)
 Viktor X3 multiplate reader 2030

Vortex Genie 2

Company

Denver Instruments, Bohemia NY, USA
 Kojair Tech Oy, Vilppula, Finland

Invitrogen Europa Holding GmbH, Darmstadt, Germany
 Christ, Osterode am Harz, Germany
 neoLab, Heidelberg, Germany
 Jasco, Gross-Umstadt, Germany
 Grace, Worms, Germany

Jasco, Gross-Umstadt, Germany
 Bruker Daltonik GmbH, Bremen, Germany
 Olympus Deutschland GmbH, Hamburg, Germany
 Mettler TOLEDO
 CAT, Staufen, Germany
 Eppendorf, Hamburg, Germany
 Hermle Labortechnik GmbH, Wehingen, Germany
 Jasco, Gross-Umstadt, Germany
 PerkinElmer Life and Analytical Sciences Inc., Rodgau, Germany
 Scientific Industries, Bohemia, USA

2.3 Laboratory utensils

Utensil

Cell culture plate (polystyrol) (96-well)
Cell culture plate (polystyrol) (F-bottom) (96-well)
HPLC-columns
- C18 Nucleosil-100 column
(L: 250 mm, ID: 8 mm, 7µm pore size)
- C18 Nucleosil-100 pre-column
(L: 33 mm, ID: 8 mm, 7µm pore size)
Quartz cuvettes (1 cm; 0,5 cm; 0,2 cm)
Reaction vessel 1,5 ml
Rotilabo reaction glasses
Syringes (10 ml, 2 ml)
Tissue culture flasks (75 cm², 250 mL, PS, filter cap, sterile)
16% Tricine gel 1.00 mm x 10 well

Company

Brand GmbH + Co KG, Wertheim, Germany
Greiner Bio-One, Frickenhausen, Germany
Grace Davidson Discovery Sciences - Alltech Grom GmbH, Worms, Deutschland
Hellma GmbH & Co. KG, Müllheim, Germany
Sarstedt, Nümbrecht, Germany
Roth, Karlsruhe, Germany
BD Discardit, Fraga, Spain
Greiner Bio-One, Frickenhausen, Germany
Invitrogen Europa Holding GmbH, Darmstadt, Germany

2.4 Cell culture media

Cell culture medium

Bovine serum albumin (BSA)
Glucose
Horse serum
L-Glutamine
NEAA (Non-essential amino acids)
Nutrient mixture F-12 (Ham)
Penicillin/Streptomycin
RPMI-1640 Medium
Sodium Pyruvate
Trypsin/EDTA

Company

Sigma-Aldrich, Steinheim, Germany
Sigma-Aldrich, Steinheim, Germany
Gibco Life Technologies, Carlsbad, USA
Gibco Life Technologies, Carlsbad, USA
Gibco Life Technologies, Carlsbad, USA
Gibco Life Technologies, Carlsbad, USA
Gibco Life Technologies, Carlsbad, USA
Gibco Life Technologies, Carlsbad, USA
Gibco Life Technologies, Carlsbad, USA
Invitrogen (Karlsruhe)

2.5 Methods

2.5.1 Solid phase peptide synthesis

Peptides were synthesized using Fmoc/tBu chemistry [124, 125]. The following side-chain protecting groups were applied for standard couplings: tBu (Asp, Glu, Ser, Thr), Boc (Lys), Trt (Cys, His, Asn, Gln) and Pbf (Arg). For the purpose of side-chain modification, different protecting groups were selected according to the targeted task.

2.5.1.1 Loading of the resin

For the peptide synthesis, Wang-resin [126, 127] (substitution level 1.1 mmol/g) was used. The first amino acid was coupled using two fold molar excess of the wanted amino acid (N-

terminally Fmoc protected and acid lable protecting group on the side chain), two fold molar excess of TBTU, two equivalent of HOBt, and four fold molar excess of DIEA for 2 h.

The success of the loading of the resin was controlled by UV/VIS spectroscopy. If the desired substitution level was not achieved, this procedure was repeated.

If the achieved substitution level was sufficient, the remaining free hydroxyl groups of the Wang-resin were acetylated using 10 eq. acetic anhydride and 10 eq. DIEA for 40 min.

2.5.1.2 Determination of the substitution level

The success of the coupling of the first amino acid to the resin was controlled via UV/VIS spectroscopy. Therefore, 3 mg of dried resin was dissolved in 10 ml 25% piperidine in DMF, mixed and incubated for 10 minutes at room temperature. Afterwards, 1.5 ml of this solution was filled into a cuvette and the absorbance was measured at a wavelength of 290 nm. At this wavelength, the Fmoc group absorbs light with a specific extinction coefficient and its concentration can be determined using the Lambert-Beer law:

$$C = \frac{A}{\epsilon \cdot l}$$

$\epsilon = 5800 \text{ [l}\cdot\text{mol}^{-1}\cdot\text{cm}^{-1}\text{]}$; l – length of the cuvette [cm]; A – absorbance at 290 nm

Using this equation, the substitution level can be determined:

$$\text{Substitution level [mmol/g]} = \frac{A \cdot V[\text{ml}]}{\epsilon \cdot m[\text{g}]}$$

The substitution level is important to calculate the needed amount of amino acids, activator and base used for the following couplings.

2.5.1.3 Chain elongation

To remove the N-terminal Fmoc group, 25% piperidine in DMF was added to the resin until it is completely covered. The reaction was incubated for 5 minutes under agitation and was repeated for additional 20 minutes. Afterwards, the resin was washed 4 times with DMF for 1 minute.

For each coupling step 3 eq. of Fmoc protected amino acid and TBTU referred to the substitution level of the resin were dissolved in DMF and added to the resin. Then, 4.5 eq. DIEA were added and the resin was incubated for 40 minutes under agitation. Excessive reagents were removed and the step is repeated one time. Afterwards the resin was washed with DMF for three times 1 minute.

Afterwards, a Kaiser test was performed to check for remaining free amines. If this test was negative, the next coupling step was started.

2.5.1.4 Kaiser test

The Kaiser test is based on the reaction of ninhydrine with primary amines. It is a very sensitive test, visualized by an intense blue color in the presence of primary amines [128].

The Kaiser test was performed using a solution of 500 mg ninhydrine in 10 ml ethanol, a solution of 80 g phenol in 20 ml ethanol and a third solution of 2 ml 0.001 M aqueous KCN solution in 98 ml pyridine. A few resin beads were placed in a small glass tube and 2-3 drops of each solution were added. The tube was placed in an oven and the reaction was left to develop for 3-5 min at 110°C.

2.5.1.5 Cleavage of Mtt and PiP protecting groups

The methyltrityl (Mtt) protecting group was utilized to protect the side chain amine groups of lysine and 2,3-diaminopropionic acid. It can be selectively removed under mild acidic conditions, allowing further modification of peptides on resin at the side chains of these amino acids. The Mtt group can already be removed with 1-2% trifluoroacetic acid (TFA) in dichloromethane (DCM) [129, 130].

Similar to Mtt, the phenylisopropyl (PiP) protecting group was used to protect the side chain carboxyl group of aspartic acid. It can also be selectively removed under mild acidic conditions using 1-2% trifluoroacetic acid (TFA) in dichloromethane (DCM) [131].

For the cleavage of these protecting groups, the resin was suspended in TFA/TIS/DCM (1:5:94 v:v:v) for 2x2 min and 6x10 min. Afterwards, the resin was washed three times with DCM for 1 min and then three times with DMF for 1 min. Remaining amounts of TFA on the resin were neutralized using 1% DIEA in DMF for 2x2 min. The resin is then washed three times with DMF for 1 min. The successful deprotection of the Mtt-group was verified by a Kaiser-test.

2.5.1.6 Cleavage of the ivDde protecting group

The 1-(4,4-dimethyl-2,6-dioxocyclohex-1-ylidene)-3-methylbutyl (ivDde) protecting group is utilized to protect the side chain amine group of lysine. It is not removed under standard Fmoc or Boc deprotection protocols and can be selectively removed to allow site-specific modification of peptides on resin. The standard method of removing the ivDde group utilizes 2% hydrazine in DMF [132].

These conditions also remove Fmoc protecting groups. Therefore the N-terminal residue should be protected with a Boc group or should be acetylated.

Cleavage of ivDde deprotection was done using hydrazine. A solution of 2% hydrazine in DMF was added to the resin (completely cover the resin with solution). The resin was shaken at room temperature for 3 minutes, and then the solution was removed. The hydrazine solution was collected from the syringe and the absorbance at 290 nm is measured. The treatment with hydrazine solution was repeated until the absorbance at 290 nm decreased to zero. Finally, the resin was washed three times with DMF.

2.5.1.7 Cyclization strategies

Cyclization of Lys-LLL-lin

A side-chain-to-side-chain-cyclization [133, 134] on the resin was applied to achieve cyclic peptide. Therefore, a peptide bond was formed between a carboxylic side chain group (C-terminal, from aspartic acid) and a primary amine side chain (N-terminal, from lysine or 2,3-diaminopropionic acid).

At first, the acid labile side chain protective groups Mtt (from the side chain of Lys) and OPiP (from the side chain of Asp) were removed using 1 % TFA, 5% TIS (v/v) in DCM for 2 times 2 minutes and 6 times 10 minutes. The resin was then washed with DCM and DMF for three times each, neutralized with 1 % DIEA in DMF for twice two minutes, and washed again with DMF for three times.

Afterwards, the cyclisation was done using 4 equivalents of each 2-(7-Aza-1H-benzotriazol-1-yl)-1,1,3,3-tetramethyluronium hexafluorophosphat (HATU) and DIEA in DMF for 4 h and then for additional 16 h with new coupling reagents. The success of the cyclisation was then controlled with a Kaiser test.

Then, the resin was treated with 10 eq. Ac₂O and 10 eq. DIEA in DMF for 45 minutes in order to acetylate potentially remaining reactive groups.

Cyclization of H13CC-red

To force the peptide into a cyclic conformation an oxidation of the cysteine residues was performed. 1 mg of the crude product was dissolved in 20% DMSO in 0.1 M NH_4HCO_3 . The solution was incubated at room temperature for 3h under agitation.

Afterwards, the oxidation was controlled and the oxidized product was purified by HPLC.

Cyclization of H5aCC-red

Oxidation of H5aCC was achieved using 0.15 mg purified H5aCC-red in 1.5 ml H_2O containing 10% DMSO and 3% H_2O_2 (0.1 mg/ml). The peptide completely oxidised after a few minutes forming cyclic monomeric H5aCC-ox which was then purified by HPLC.

Cyclization of Dimer 3 red

0.1 mg/ml of purified Dimer 3 red was incubated in 10% DMSO in 0.1M NH_4HCO_3 for 6h at room temperature under agitation. The product was then purified by HPLC.

2.5.1.8 Cleavage from the resin

In the end of the synthesis the peptide was cleaved from the Wang-resin and all protective groups were removed.

Cleavage of simple unproblematic peptide sequences was achieved using TFA/dd H_2O 95/5 % v/v for 2.5 h.

Peptides containing Pbf side chain protecting groups were cleaved using TFA/dd H_2O /TIS 95/2.5/2.5 % v/v for 3 h.

Peptides containing cysteine or methionine residues were cleaved using Reagent K to avoid oxidation of the sulfur atoms. Reagent K contained 75 mg phenol, 25 μl EDT, 50 μl thioanisol and 50 μl dd H_2O in 1 ml TFA. For 20 mg resin, 600 μl Reagent K were used [135].

After 3 h of agitation, approximately 5 ml dd H_2O of ice cold were put into a falcon tube and the cleavage solution is added. The falcon tube was then filled up with ice cold diethylether. The solution was mixed and centrifuged for 1 minute at 2500 rpm at 1°C. Afterwards, the diethylether was removed. These steps were repeated two more times. The water peptide solution was then frozen and lyophilized over night.

2.5.2 MALDI mass spectrometry

For the mass spectrometry measurements a small sample of the peptide was dissolved either in 0.1% TFA and 30% ACN in dd H_2O or in 0.1% TFA and 97% acetone in dd H_2O .

The sample was mixed with a saturated solution of α -cyano-4-hydroxycinnamic acid in the same solvent mixture, spotted onto a target played and allowed to dry. Afterwards, the dry spot was washed with 10 mM $\text{NH}_4\text{H}_2\text{PO}_4$ in dd H_2O .

The mass spectra were then recorded on a Bruker MALDI-TOF mass spectrometer.

Table 1: Results of MALDI-MS measurements of all studied peptides.

ID-Nr.	Peptide	Monoisotopic MW calculated $[\text{M}+\text{H}]^+$	MW found $[\text{M}+\text{H}]^+$ (if not stated otherwise)
1	H-NKGAIL-OH	615.36	653.38 $[\text{M}+\text{K}]^+$
2	H-NKGAIL-Peg(2)-NFGAILS-OH	1462.81	1462.83
3	H-NKGAIL-Aoc-NFGAILS-OH	1458.96	1458.83
4	H-NKGAIL-Aoc-NFGAILS- β A-KKK-OH	1914.29	1914.19
5	H-KKK- β A-NKGAIL-Aoc-NFGAILS- β A-KKK-OH	2369.61	2370.46
6	H-NKGAIL-Adc-NFGAILS-OH	1487.02	1486.86
7	H-NKGAIL-GGG-NFGAILS-OH	1488.80	1488.80
8	H-NKGAIL-AAA-NFGAILS-OH	1530.85	1530.92

9	H-NKGAI-LLL-NFGAILS-OH	1656.99	1657.019
10	H-KKK-βA-NKGAI-LLL-NFGAILS-βA-KKK-OH	2567.63	2567.69
11	H-NKGAI-KKK-NFGAILS-OH	1702.02	1702.14
12	H-NKGAI-K(Ac)K(Ac)K(Ac)-NFGAILS-OH	1828.05	1828.17
13	H-NKGAI-EEE-NFGAILS-OH	1704.86	1705.00
14	H-IIAGKN-OH	615.36	615.35
15	H-IIAGKN-Peg-NFGAILS-OH	1462.81	1463.04
16	H-IIAGKN-Aoc-NFGAILS-OH	1458.96	1458.82
17	H-IIAGKN-Adc-NFGAILS-OH	1487.02	1486.90
18	H-IIAGKN-GGG-NFGAILS-OH	1488.80	1488.78
19	H-IIAGKN-AAA-NFGAILS-OH	1530.85	1552.83 [M+Na] ⁺
20	H-IIAGKN-LLL-NFGAILS-OH	1656.99	1656.97
21	H-IIAGKN-KKK-NFGAILS-OH	1702.02	1702.06
22	H-IIAGKN-K(Ac)K(Ac)K(Ac)-NFGAILS-OH	1828.05	1829.08
23	H-IIAGKN-EEE-NFGAILS-OH	1704.86	1704.94
24	H-NFGAILS-LLL-NFGAILS-OH	1762.99	1785.06 [M+Na] ⁺
25	H-NKGAI-LLL-NKGAI-OH	1550.98	1551.08
26	H-NFGAILS-Aoc-NFGAILS-OH	1564.97	1587.51 [M+Na] ⁺
27	H-NKGAI-Aoc-NKGAI-OH	1352.96	1353.11
28	H-NFGAILS-Aoc-NKGAI-OH	1458.96	1458.98
29	H-NFGAILS-KKK-NFGAILS-OH	1808.03	1808.24
30	H-NKGAI-KKK-NKGAI-OH	1596.01	1596.11
31	H12CC	1863.01	1862.20
32	H12Ser	1831.05	1870.01 [M+K] ⁺
33	Lys-LLL-lin	1900.11	1900.15
34	Lys-LLL-cyclo	1882.11	1882.18
35	Dap-LLL-lin	1858.12	1860.07
36	H13CC-red	1908.04	1909.15
37	H13CC-ox	1906.04	1906.31
38	H13Ser	1876.08	1876.20
39	Lys-KKK-lin	1945.14	1945.26
40	Dap-KKK-lin	1903.16	1903.30
41	Dap-KKK-cyclo	1885.25	3770.67 [2M+H] ⁺
42	H5aCC-red	1664.98	1664.90
43	H5aCC-ox	1662.98	1663.15
44	Dimer3-red	4185.70	4186.58
45	Dimer3-ox	4183.70	4184.03
46	IAPP(8-18)-OH	1269.69	1269.77
47	IAPP(22-28)-OH	721.37	759.30 [M+K] ⁺
48	IAPP(8-28)-OH	2260.17	2260.66
49	IAPP(8-18)-SGN-(22-28)-OH	2230.15	2230.46
50	IAPP(8-18)-Aoc-(22-28)-OH	2113.29	2113.19
51	IAPP(8-18)-Peg-(22-28)-OH	2118.09	2118.20
52	IAPP(8-18)-KKK-(22-28)-OH	2356.34	2356.39
53	Fluos-IAPP(8-18)-KKK-(22-28)-OH	2714.66	2714.41
54	IAPP(8-18)-Dap ₃ -(22-28)-OH	2230.75	2230.27
55	IAPP(8-18)-RRR-(22-28)-OH	2440.36	2440.64
56	Fluos-IAPP(8-18)-RRR-(22-28)-OH	2798.68	2799.74
57	IAPP(8-18)-DDD-(22-28)-OH	2317.14	2318.39
58	IAPP(8-18)-GGG-(22-28)-OH	2143.12	2143.24
59	IAPP(8-18)-AAA-(22-28)-OH	2185.17	2185.26
60	IAPP(8-18)-VVV-(22-28)-OH	2269.26	2270.42
61	IAPP(8-18)-LLL-(22-28)-OH	2311.31	2311.39
62	Fluos-IAPP(8-18)-LLL-(22-28)-OH	2669.63	2669.96
63	IAPP(8-18)-III-(22-28)-OH	2311.31	2311.29
64	IAPP(8-18)-Nle ₃ -(22-28)-OH	2311.31	2310.25
65	IAPP(8-18)-2Aoc ₃ -(22-28)-OH	2395.75	2395.56

66	IAPP(8-18)-TTT-(22-28)-OH	2275.20	2275.31
67	IAPP(8-18)-FFF-(22-28)-OH	2413.26	2413.61
68	IAPP(8-18)-Cha ₃ -(22-28)-OH	2431.78	2431.58
69	IAPP(8-18)-SpG-(22-28)-OH	2213.16	2213.44
70	IAPP(8-18)-pGN-(22-28)-OH	2240.18	2240.33
71	IAPP(8-18)-PPP-(22-28)-OH	2263.23	2265.03
72	IAPP(8-18)-(K(Ac)) ₃ -(22-28)-OH	2482.38	2482.47
73	Fluos-IAPP(8-18)-(K(Ac)) ₃ -(22-28)-OH	2840.70	2840.91
74	IAPP(8-18)-KK(Ac)K(Ac)-(22-28)-OH	2440.37	2440.39
75	IAPP(8-18)-K(Ac)KK(Ac)-(22-28)-OH	2440.37	2440.42
76	IAPP(8-18)-K(Ac)K(Ac)K-(22-28)-OH	2440.37	2440.34
77	IAPP(8-18)-KKK(Ac)-(22-28)-OH	2398.35	2398.53
78	IAPP(8-18)-KK(Ac)K-(22-28)-OH	2398.35	2398.39
79	IAPP(8-18)-K(Ac)KK-(22-28)-OH	2398.35	2398.40

2.5.3 HPLC

All peptides were analyzed and purified using HPLC systems with a C18 Nucleosil column (7 μ m, 8 mm \times 250 mm) and a C18 Nucleosil pre-column (7 μ m, 8 mm \times 33 mm).

The absorbance at 214 nm and 280 nm were detected during the runs. At a wavelength of 214 nm, the peptide bond is absorbing light, whereas at a wavelength of 280 nm aromatic structures absorb. The buffer system used was 0.058% TFA in ddH₂O (buffer A) and 0.05% TFA in 90% acetonitrile 10% ddH₂O (buffer B). Peptides were dissolved in 10% TFA, 80% buffer B in buffer A prior to injection.

Typical gradients are listed below:

Schnell A β

Time / min	Buffer A / %	Buffer B / %
0	90	10
1	90	10
31	10	90

Peptides with following ID-Numbers were purified using the gradient Schnell A β :

1, 4, 5, 6, 7, 10, 12-23, 25-32, 36-38, 43, 46-49, 53, 56, 57, 69-71, and 73-79.

10-100% stay

Time / min	Buffer A / %	Buffer B / %
0	90	10
1	90	10
21	0	100
31	0	100
31	10	90

Peptides with following ID-Numbers were purified using the gradient 10-100% stay:

24, 44, 45, 62, and 65.

2.5.4 Circular dichroism spectroscopy

Far-UV CD spectra were recorded at room temperature on a Jasco J-715 spectropolarimeter. Quartz cuvettes were used for all CD spectra. Data were recorded from 195 to 250 nm using the following parameters: 0.1 nm data pitch, 1 nm band width, 1 s response time, and 100 nm min⁻¹ scan speed. Accumulation was set on 3.

The measurements were performed in 1x 1% HFIP at different peptide concentrations. The samples used in CD experiments were freshly prepared.

The CD spectrum of the solvent was subtracted from that of the peptide solutions to eliminate interferences from the cell, solvent and optical equipment.

For measurements done without HFiP, the peptides were taken from a stock in HFiP. The HFiP was evaporated and the dried peptide was redissolved in 1 mM HCl, added to the 1xb in the cuvette and directly measured.

For temperature dependant studies, following parameters were used: A temperature slope of 1°C/min for both heating up and cooling down and a delay time of 60 s. Spectra were measured every 10°C.

All CD data were analysed and smoothed using Microcal Origin software.

2.5.5 Thioflavin T fluorescence assay

The incubations at a specific peptide concentration were prepared in 1xb (10mM phosphate buffer, pH 7.4) containing 1% v/v HFiP. The peptide was taken from a stock in HFiP, peptide concentration 1 mM. The HFiP was removed by air.

An excess of 6.8 fold ThT compared to the peptide concentration was used.

The time dependence of fluorescence intensity was monitored immediately after the peptide incubation was prepared, after 30 minutes incubation at room temperature with shaking, and in intervals of 24 h from the starting point of the incubation for 5 d.

Thioflavin T fluorescence was measured using a Victor X3 multiplate reader at an emission wavelength of 482 nm and an excitation wavelength of 440 nm. All experiments were repeated at least three times by individually prepared incubations to ensure the results were reproducible.

2.5.6 Congo Red staining

The peptide was dissolved at a concentration of 1 mM in 1xb, 1% HFiP, pH 7.4. The sample was incubated for half an hour at room temperature under agitation and then for 3 days at room temperature without agitation.

Then, one drop of the incubation was put on a glass slide and dried over night. The next day one drop of 200 µM Congo Red in ddH₂O was put on top of the dried spot of the peptide incubation and also dried over night [136].

Afterwards, the spot was examined under the microscope and pictures of representative areas were taken under both normal field and cross-polarized light.

2.5.7 Transmission electron microscopy

TEM grids were usually prepared from aged peptide solutions in 1xb, 1% HFiP, pH 7.4. A drop of the peptide solution was put on the grid and incubated for 3 min. Then, the solution was carefully removed using a filter paper. Negative staining was done by incubating the grid with one drop of 2% uranyl acetate in ddH₂O g/v for 1 min. Afterwards this solution was again carefully removed with a filter paper. The grid was examined after complete drying (examination in the JEOL JEM 100CX TEM was done by Michael Kracklauer).

2.5.8 ANS binding assay

ANS (8-Anilinonaphthalene-1-sulfonic acid) is a hydrophobic fluorescent dye that specifically binds to solvent-exposed hydrophobic surfaces of other molecules. This binding is characterized by a blue shift of the maximum and an enhancement of the fluorescence emission spectrum [137].

The spectra were measured in 1xb containing 1% HFIP at different peptide concentrations. A twofold excess of ANS compared to the peptide concentration was used. The measurements were done immediately after preparation.

For the measurements, following parameters were used: Excitation wavelength of 355 nm, emission wavelength from 355 to 650 nm, a bandwidth (emission) of 5 nm, a response time of 1 s, a Data Pitch of 1 nm and a scanning speed of 100 nm/min.

2.5.9 Concentration determination of carboxyfluorescein-labeled peptides

HPLC purified peptides were first dissolved in HFIP and then filtered (0,2 µm PTFE filter). UV absorbance of the peptide solution was measured between 200 and 600 nm and the absorbance at 432 nm was used to determine the exact peptide concentration. At this wavelength, the extinction coefficient of carboxyfluorescein was determined to be

$$\epsilon_{432} = 22770 \text{ M}^{-1} \text{ cm}^{-1} \text{ [138].}$$

Peptide concentrations were calculated according to the Lambert-Beer law.

2.5.9.1 Self-association studies using Fluorescence Spectroscopy

Fluorescence measurements were performed with a Jasco FP-6500 spectrofluorometer. All titrations were carried out using 5 nM N-terminally fluorescein labeled peptides and increasing concentrations of un-labeled peptides in 1xb, pH 7.4, 1% HFIP. For the measurements, an excitation wavelength of 492 nm was applied and fluorescence emission spectra were recorded between 500 and 600 nm.

The changes of the fluorescence emission at a wavelength of 522 nm were used to generate the binding curve.

Apparent affinities (app. K_d) were estimated using 1/1 binding models. Sigmoidal curve fittings and estimation of affinities of interaction (K_d) were performed with Origin software.

2.5.10 Size-exclusion chromatography

For SEC studies, a Superdex 75 10/300 GL column was used. As buffer, 10 mM phosphate buffer containing 150 mM NaCl were taken. The buffer was filtered and degassed prior to use. The flow rate was 0.5 ml/min.

Peptides were incubated at various concentrations in 1xb.

2.5.11 SDS PAGE

Polyacrylamide gel electrophoresis is a technique that allows separating proteins and peptides according to their electrophoretic mobility. Mobility is a function of the length, conformation and charge of the molecule. By adding an anionic detergent like sodium dodecyl sulfate (SDS) peptides and proteins are denatured and charged according to their size, resulting in a fractionation by mass during electrophoresis.

It was used to determine if the peptides formed oligomers, what kind of oligomeric order was formed and to which amount they were formed.

10 µg of the peptides were dissolved in 1xb, pH 7.4, 1% HFIP at a concentration of 200 µM and then either incubated for 24h at room temperature or directly mixed with NuPAGE LDS sample buffer without reducing agents (1/4). Afterwards, the solutions were transferred into the pockets of a 4-12% Bis-Tris gel 10 without boiling and also 3 µl Novex® Sharp pre-stained protein standard were used as marker. Equal amounts of peptides were loaded throughout all pockets. The gel was running for 35 minutes at 200 V. Then the gel was

stained using either silver or Coomassie Brilliant Blue R-250 and pictures of the gel were made using a LAS-4000 plate reader.

2.5.11.1 Coomassie staining

For the staining solution, 1 mg/ml Coomassie Brilliant Blue R-250 was dissolved in 50% methanol and 5% acetic acid in ddH₂O. The gel was incubated at room temperature under shaking for around 50 minutes until the bands were intensely coloured. Excessive colour was removed with 50% methanol and 5% acetic acid in ddH₂O two times for 20 minutes and then with ddH₂O over night.

2.5.11.2 Silver staining

For the silver staining method, the gel was first incubated in 20% trichloroacetic acid g/v for 30 min. After that, it was washed with 50% MeOH in ddH₂O v/v for 2x10 min and then in ddH₂O for 3x5 min. The gel was stained in freshly prepared staining solution. Afterwards, the gel was again washed with ddH₂O for 3x5 min. Then, the gel was kept in developing solution until the bands were clearly visible while the background became unstained. Finally, this process was stopped with 50% MeOH in ddH₂O v/v for 2 x 10 min.

Staining solution:

For the staining solution 700 µl 25% NH₃ were added to 11ml 0.36% NaOH under agitation on ice. Then, 0.3 g AgNO₃ dissolved in 1 ml ddH₂O were put drop by drop into this solution. Finally, 50 ml ddH₂O were added and the solution was used.

Developing solution:

For the developing solution 250 µl 1% citric acid in ddH₂O and 25 µl 37% formaldehyde were mixed and 50 ml ddH₂O were added.

2.5.12 Cell viability studies

For cell viability studies both the rat insulinoma cell line RIN5fm and the rat pheochromocytoma cell line PC-12 were used.

PC-12 cells were cultured in RPMI 1640 medium containing 10% heat-inactivated horse serum, 5% fetal calf serum, 25 units/ml penicillin, and 25 µg/ml streptomycin. 24h prior to cell viability assays, PC-12 cells were then plated at a density of 1x10⁵ cells/ml in 96-well plates. Peptides were incubated at a concentration of 5 mM in 1xb, 1% HFiP, pH 7.4 for 4d. Prior to addition to the cells, the peptide incubations were diluted using cell medium and then added to the cells at final concentrations between 50 µM and 1 µM.

PC-12 cells were then incubated for 24h with these aged peptide solutions. Afterwards, 3-[4,5-dimethylthiazol-2-yl]-2,5-diphenyltetrazolium bromide (MTT) (final concentration of 1 mg/ml) was added and the cells were kept for 90 minutes at 37°C in the CO₂ incubator (5% CO₂) and then incubated with cell lysis buffer containing 10% SDS in 20 mM HCl, pH 4.5 over night at room temperature.

Cellular MTT reduction was measured at 570 nm using a 2030 Multilabel Reader VictorX3 (PerkinElmer).

RIN cells were cultured in RPMI 1640 containing 10% heat-inactivated fetal bovine serum, 2 mM L-glutamine, 0.1 mM non-essential amino acids, 1 mM sodium pyruvate, 1 mg/ml glucose, and 0.1 mg/ml penicillin/streptomycin.

RIN cells were plated at a density of 5×10^5 cells/ml in 96-well plates 24h prior to use. Aged peptide incubations (5 mM peptide concentration) were diluted with cell culture medium, added to the cells at the indicated final concentrations, and were left at 37°C in the CO₂ incubator (5% CO₂) for 24h. RIN cells were then incubated with 3-[4,5-dimethylthiazol-2-yl]-2,5-diphenyltetrazolium bromide (MTT) (1 mg/ml) for 90-120 minutes at 37°C in the CO₂ incubator (5% CO₂).

Then, the cell medium was sucked off, 100 µl 0.04 N HCl in isopropanol were added to each well and the 96-well plate was shaken for 10 min. Afterwards, 100 µl H₂O were added to each well and the MTT reduction was directly measured as above.

Complete loss of cell viability was defined as the absorbance value obtained in wells containing 0.1% Triton X-100 for 90-120 minutes at 37°C in the CO₂ incubator (5% CO₂). No loss of cell viability was defined as the absorbance value obtained in wells containing cells without the addition of peptide solution. Cell viability of cells treated with peptide solution was calculated using following formula:

$$\text{cell viability [\%]} = \frac{A(\text{incubation}) - A(\text{dead cells})}{A(\text{untreated cells}) - A(\text{dead cells})} \cdot 100$$

3 Results and Discussion

3.1 Analogues of IAPP(8-28)

3.1.1 Design of the analogues

The two regions IAPP(8-18) and IAPP(22-28) are known for their ability to both homo- and hetero-associate [120]. These regions were connected by a linking region with a length of three amino acids instead of the native tripeptide sequence SSN. This region was exchanged by different motifs with varying charge, hydrophobicity, steric hindrance as well as motifs forming specific secondary structures.

The studies presented here were done to get a better understanding of the role of the IAPP(19-21) region for amyloidogenesis and fibril formation.



Fig. 11: Homo-association domains of IAPP; gray: domains responsible for association; blue: hot regions of the homo-association [120].

Different connecting elements were chosen according to their individual features. The following substitutions in the IAPP(19-21) region were made:

The natively occurring IAPP mutation S20G is known to increase the fibril forming potential of IAPP and is associated with an increased risk to develop early-onset type 2 diabetes [102-104]. This is one of the substitutions chosen.

Amyloid fibrils typically display a rigid conformation. To evaluate the influence of flexible elements in the IAPP(19-21) region on structure and fibril formation Aoc (8-amino-octanoic acid) and Peg (8-amino-3,6-dioxo-octanoic acid) were chosen as connecting elements to replace the native IAPP(19-21) sequence. Both amino acids display a length similar to that of the backbone of a tripeptide. Aoc is a strongly hydrophobic whereas Peg is rather hydrophilic. A third flexible substituent was the GGG tripeptide for the IAPP(19-21) region. Glycine is the proteinogenic amino acid with the smallest side chain consisting of only one hydrogen atom. It can therefore display a bigger range of torsion angle values compared to other amino acids.

Net charges have a rather negative effect on fibril formation whereas alternating charges can promote association and fibril formation [139-142]. Hydrophilic and charged motifs were thought to reduce fibril formation due to electrostatic repulsion and by preventing the formation of a hydrophobic core that is considered a crucial step leading towards fibril formation. Both positive and negatively charged amino acids were incorporated in the IAPP(19-21) region and tested for their biophysical properties.

Hydrophobic elements are known to favor fibril formation by generating a hydrophobic core leading towards fibril formation [143-146]. A set of different hydrophobic elements were used starting with alanine which has the smallest hydrophobic side chain among all proteinogenic amino acids. Apart from that, amino acids with varying side chain length and position of the branch within the side chain creating different steric hindrance and strength of hydrophobicity were incorporated in the IAPP(19-21)-OH region. Additionally, hydrophobic elements in combination with other features like flexibility or aromaticity were used.

The TTT motif was chosen because its side chain structure is similar to of the VVV motif, whereas the hydrophobicity is disrupted by hydrophilic hydroxyl groups that also makes it similar to the Ser side chains in position 19 and 20.

The dipeptide sequence D-Pro-Gly (abbreviated pG) is known for its ability to stabilize a type II' β -turn conformation [147].

Since it is thought that the IAPP(19-21) region is involved in the formation of a turn motif, the sequence pG was put into the IAPP(19-21) region to investigate the role of turn motifs on amyloid fibril formation. There are two possibilities to incorporate the pG element into the IAPP(19-21) region: at positions 19 and 20 and at positions 20 and 21. Both analogues were synthesized and tested.

The PPP motif was used for the IAPP(19-21) region to initiate and stabilize polyproline II helical structure. The polyproline II helix possesses an extended, flexible structure and is not forming intrachain backbone hydrogen bonds.

Some amyloid forming peptides seem to have a high content of PPII structure in their unaggregated form. There is however no direct relationship between the amount of PPII structure for a specific protein and its ability to form fibrils. It has been suggested that PPII might be a transient structure along the fibril forming pathway [148-151].

On the other hand, proline residues prevent the formation of intra- and intermolecular H-bonds which are required for the formation of β -sheet structures and amyloid fibrils. The introduction of prolines into amyloidogenic peptide sequences can thereby reduce or even prevent the formation of amyloid fibrils [152-155].

K(Ac) was chosen because of the polar character of its side chain that makes its features comparable to glutamine and because it is similar to lysine, but without a charge in the side chain. Polyglutamine repeats are associated with several neurodegenerative diseases like e.g. Huntington's disease [156, 157].

Table 2: List of the analogues of IAPP(8-28) presented in this chapter.

IAPP(8-18)-OH
IAPP(22-28)-OH
IAPP(8-28)-OH
IAPP(8-18)-SGN-(22-28)-OH
IAPP(8-18)-Aoc-(22-28)-OH
IAPP(8-18)-Peg-(22-28)-OH
IAPP(8-18)-KKK-(22-28)-OH
IAPP(8-18)-Dap ₃ -(22-28)-OH
IAPP(8-18)-RRR-(22-28)-OH
IAPP(8-18)-DDD-(22-28)-OH
IAPP(8-18)-GGG-(22-28)-OH
IAPP(8-18)-AAA-(22-28)-OH
IAPP(8-18)-VVV-(22-28)-OH
IAPP(8-18)-LLL-(22-28)-OH
IAPP(8-18)-III-(22-28)-OH
IAPP(8-18)-NIe ₃ -(22-28)-OH
IAPP(8-18)-2Aoc ₃ -(22-28)-OH
IAPP(8-18)-TTT-(22-28)-OH
IAPP(8-18)-FFF-(22-28)-OH
IAPP(8-18)-Cha ₃ -(22-28)-OH
IAPP(8-18)-SpG-(22-28)-OH
IAPP(8-18)-pGN-(22-28)-OH
IAPP(8-18)-PPP-(22-28)-OH
IAPP(8-18)-(K(Ac)) ₃ -(22-28)-OH
IAPP(8-18)-KK(Ac)K(Ac)-(22-28)-OH
IAPP(8-18)-K(Ac)KK(Ac)-(22-28)-OH
IAPP(8-18)-K(Ac)K(Ac)K-(22-28)-OH
IAPP(8-18)-KKK(Ac)-(22-28)-OH
IAPP(8-18)-KK(Ac)K-(22-28)-OH
IAPP(8-18)-K(Ac)KK-(22-28)-OH

3.1.1.1 IAPP(8-18)-OH

Far-UV CD spectra of IAPP(8-18)-OH (Fig. 12) displayed a random coil structure for the peptide as indicated by an intense minimum at 195 nm. There was almost no signal intensity for IAPP(8-18)-OH at around 220 nm. This indicated a lack of other structural motifs apart from random coil elements. The signal intensity of that minimum was reduced for concentrations larger than 2.5 μM indicating the formation of soluble oligomers.

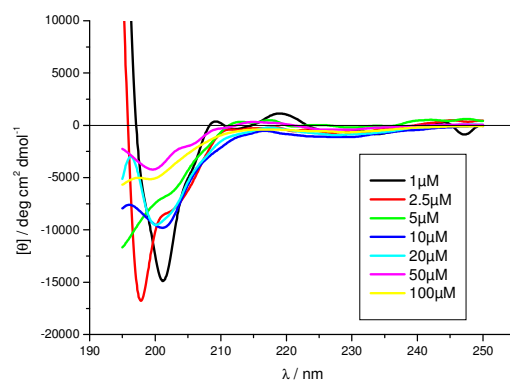


Fig. 12: Far-UV CD spectra of H-IAPP(8-18)-OH at different concentrations in 1xb 1% HFiP, pH 7.4 (from [158]).

ThT assays of IAPP(8-18)-OH revealed that IAPP(8-18)-OH did not form fibrils at concentrations of 100 and 200 μM within the examined time range of 5 days. However, at a concentration of 500 μM IAPP(8-18)-OH was forming fibrils which was confirmed by TEM imaging (Fig. 13A and B).

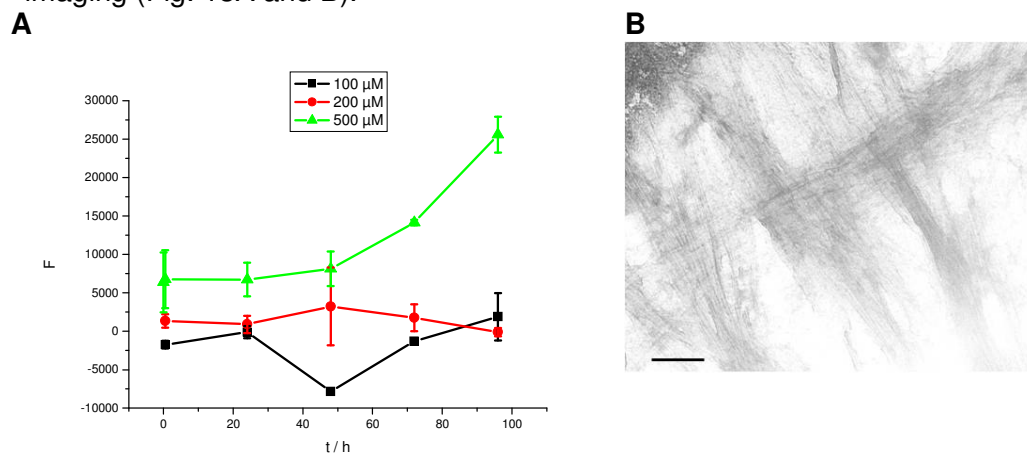


Fig. 13: (A) ThT assays of IAPP(8-18)-OH at different concentrations in 1xb 1% HFiP, pH 7.4. Data are means of 3 assays after subtraction of buffer values \pm standard error of the mean (SEM) with each experiment performed in multiple replicates ($n = 3$).

(B) TEM picture of IAPP(8-28)-OH. The peptide was incubated at 500 μM for 7 d in 1xb 1% HFiP. Scale bar: 100 nm.

Fibrillar aggregates of IAPP(8-28)-OH stained with Congo Red displayed intense red color under normal light (Fig. 14A) and revealed green birefringence under cross polarized light (Fig. 14B). This birefringence was an indication for the formation of amyloid structures.

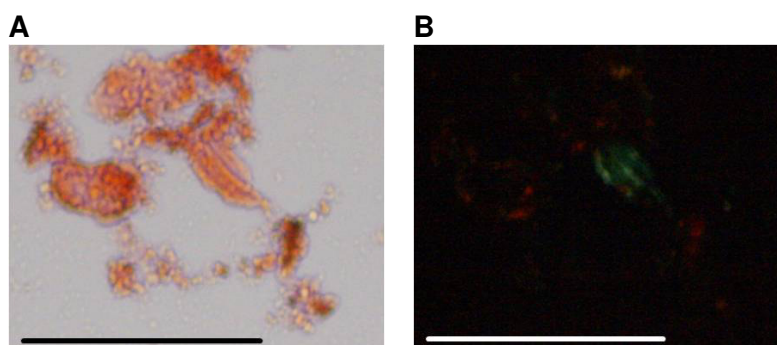


Fig. 14: Microscopic examination of an aged incubation of IAPP(8-18)-OH stained with Congo Red. The peptide was incubated at a concentration of 1 mM in 1xb 1% HFIP for 3 days. Pictures were taken under A normal and B cross polarized light. Scale bar: 100 µm.

However, aggregates formed by IAPP(8-18)-OH were not toxic to RIN cells (Fig. 15).

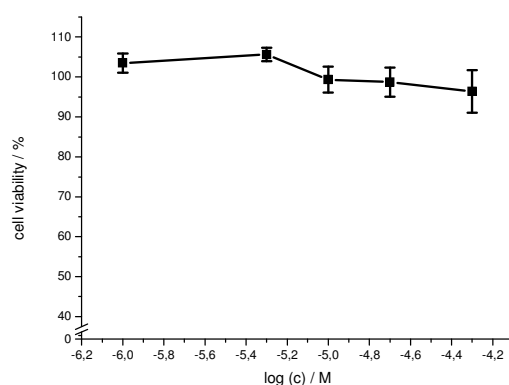


Fig. 15: Cell viability assay of an aged solution of IAPP(8-18)-OH (5 mM in 1xb 1% HFIP for 4 days, pH 7.4) using RIN cells. Data are percentages of control and are the mean (+/-SEM) of three independent experiments with each experiment performed in multiple replicates (n = 3).

3.1.1.2 IAPP(22-28)-OH

The far-UV CD spectra of H-NFGAILS-OH (Fig. 16) displayed a random coil structure for the peptide as indicated by an intense minimum at 195 nm. The signal intensity of that minimum was reduced for concentrations larger than 10 µM intending the formation of soluble oligomers.

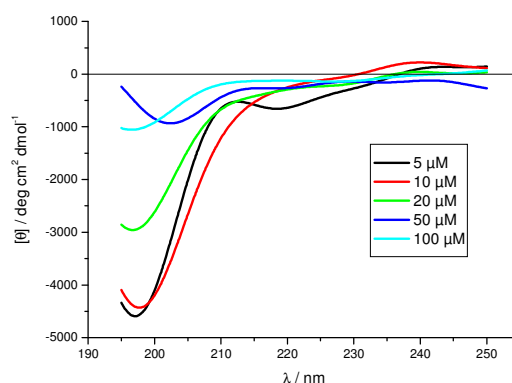


Fig. 16: Far-UV CD spectra of H-NFGAILS-OH at different concentrations in 1xb 1% HFIP, pH 7.4 (from [159]).

As shown in Fig. 17A IAPP(22-28)-OH did not form fibrils up to 10 mM under the conditions used. Also the TEM picture of 10 mM IAPP(22-28)-OH only displayed amorphous aggregates (Fig. 17B).

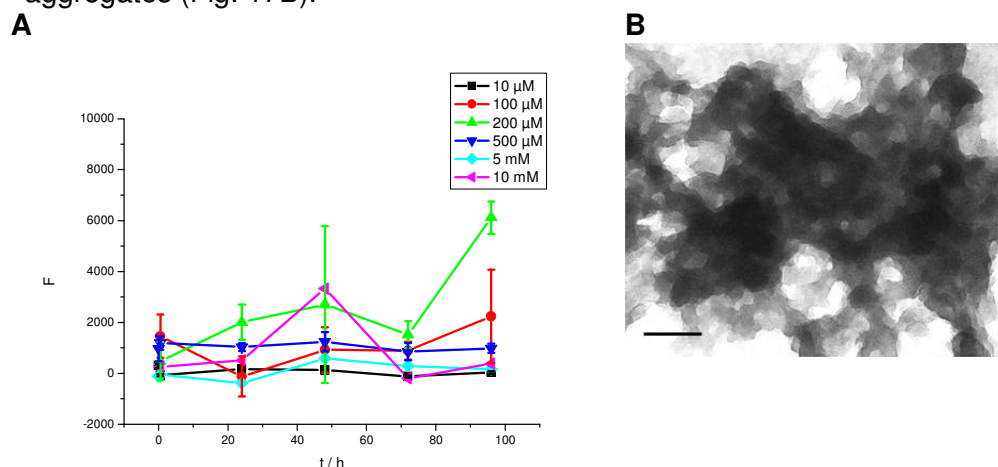


Fig. 17: (A) ThT assays of H-NFGAILS-OH at different concentrations in 1xb 1% HFiP, pH 7.4 (partially from [160], [161], and [162]). Data are means of 3 assays after subtraction of buffer values +/- standard error of the mean (SEM) with each experiment performed in multiple replicates (n = 3). (B) TEM picture of H-FGAILS-OH. The peptide was incubated at 10 mM for 7 d in 1xb 1% HFiP. Scale bar: 100 nm.

Congo Red stained aggregates of IAPP(22-28)-OH revealed binding to the dye Congo Red as shown by red color under normal light (Fig. 18 A). They however did not display birefringence under cross polarized light (Fig. 18 B). This was yet another indication for the presence of amorphous aggregates rather than amyloid fibrils.

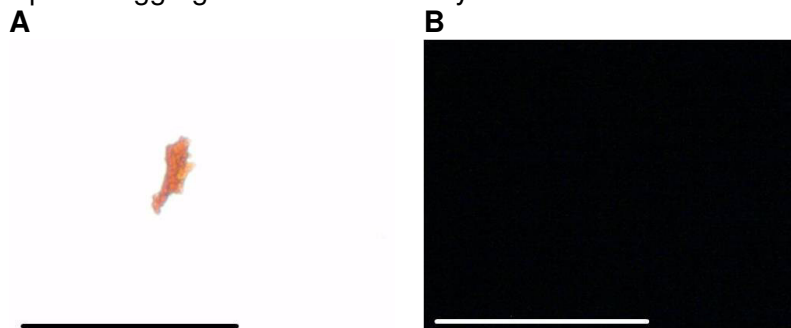


Fig. 18: Microscopic examination of an aged incubation of IAPP(22-28)-OH stained with Congo Red. The peptide was incubated at a concentration of 1 mM in 1xb 1% HFiP for 3 days. Pictures were taken under A normal and B cross polarized light. Scale bar: 100 μm.

Aggregates of IAPP(22-28)-OH were also only weakly toxic to RIN cells (Fig. 19).

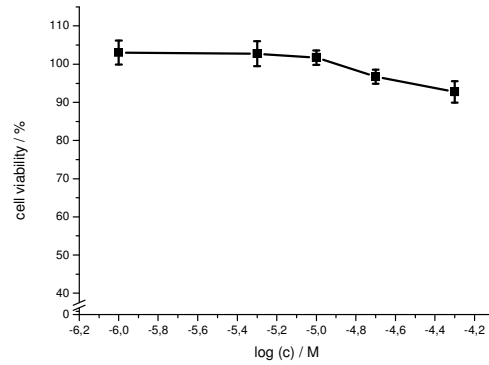


Fig. 19: Cell viability assay of an aged solution of IAPP(22-28)-OH (5 mM in 1xb 1% HFiP for 4 days, pH 7.4) using RIN cells. Data are percentages of control and are the mean (+/-SEM) of three independent experiments with each experiment performed in multiple replicates (n = 3).

3.1.1.3 IAPP(8-28)-OH

The concentration dependent CD spectra showed a strong minimum at 195 - 200 nm that could be related to random coil structures but might also be polyproline II helices [163]. The weaker negative signal between 210 nm and 230 nm indicated the presence of additional structural elements like β -sheets and β -turns (Fig. 20A). Already at a peptide concentration of 10 μ M, the signal intensity was reduced. For the spectrum at 10 μ M, this reduction mainly occurred in the random coil signal. At higher concentrations, also the signal between 210 nm and 230 nm was losing its intensity. At a concentration of 100 μ M, there was almost no signal left. This indicated an aggregation of IAPP(8-28)-OH in solution and the formation of soluble oligo- or multimers at higher concentrations.

CD spectra measured in aqueous solution without HFiP (Fig. 20B) displayed similar shape, intensity, and aggregation potential as the spectra measured in solutions containing 1% HFiP.

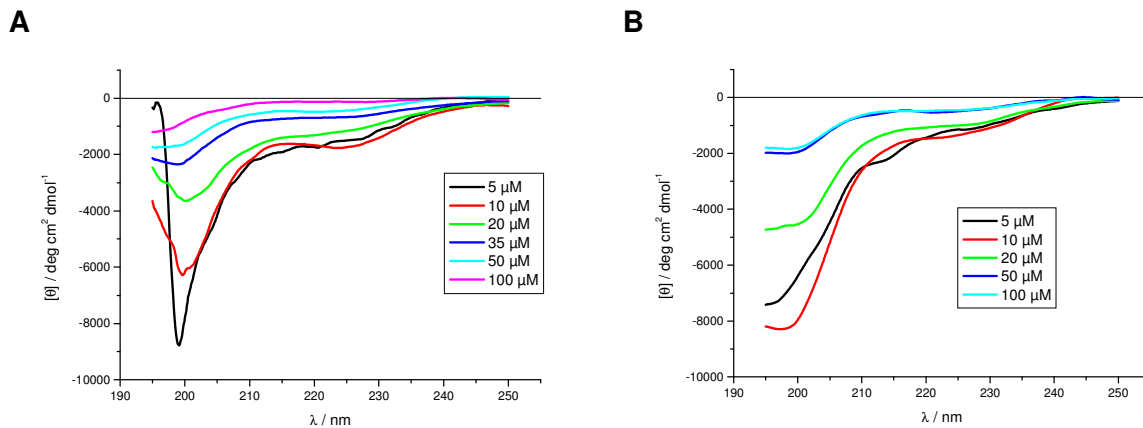


Fig. 20: Concentration dependent CD spectra of IAPP(8-28)-OH.

(A) Peptide was taken from a stock solution of 1 mM in HFiP measured in 1xb 1% HFiP, pH 7.4 (from [162]).
 (B) Incubations were made with peptide from stock solutions in 1 mM HCl measured in 1xb 1 μ M HCl, pH 7.

ThT studies at different concentrations revealed that IAPP(8-28)-OH started forming fibrils at a concentration of 35 μ M, as shown in Fig. 21A. At a concentration of 20 μ M, no fibrils were formed. The concentration dependent CD spectrum at 20 μ M already showed a signal loss related to oligomerization. These oligomers were obviously unable to transform into amyloid fibrils within 96h. At a concentration of 100 μ M, IAPP(8-28)-OH was forming fibrils without a lag time and the ThT fluorescence signal reached a plateau after 48 h. This meant that most

of IAPP(8-28)-OH has already formed fibrils and an equilibrium between fibril growth and dissolution was reached. This fibril formation could be verified by TEM (Fig. 21B).

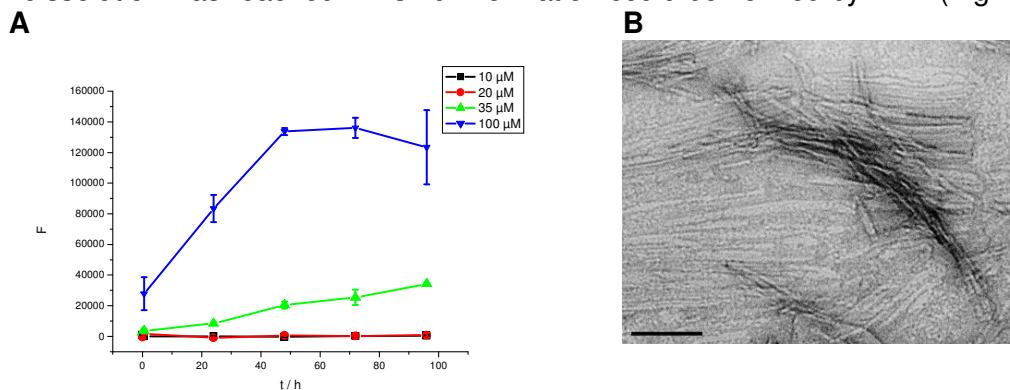


Fig. 21: (A) ThT assays of IAPP(8-28)-OH at different concentrations in 1xb 1% HFIP, pH 7.4 (from [162]). Data are means of 3 assays after subtraction of buffer values \pm standard error of the mean (SEM) with each experiment performed in multiple replicates ($n = 3$).

(B) TEM picture of IAPP(8-28)-OH. The peptide was incubated at 100 μ M for 7 d in 10 mM sodium phosphate buffer at pH 7.4 containing 1% HFIP. Scale bar: 100 nm.

Staining of aggregates of IAPP(8-28)-OH with Congo Red also revealed the formation of amyloid fibrils. Stained aggregates showed intense red color under normal light (Fig. 22A) and displayed green but also bright red color under cross polarized light (Fig. 22B).

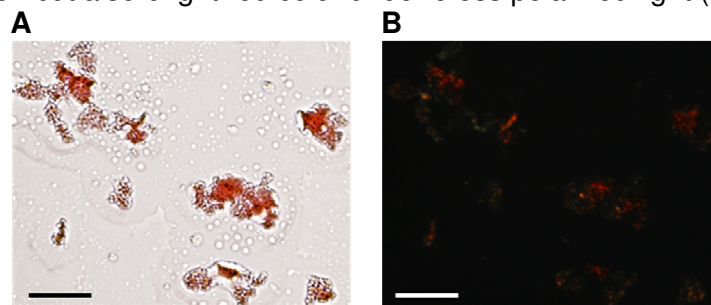


Fig. 22: Microscopic examination of fibrillar aggregates of IAPP(8-28)-OH stained with Congo Red. 1 mM peptide was incubated in 10 mM sodium phosphate buffer at pH 7.4 containing 1% HFIP for 3d and then spotted on a slide. The dried droplet was stained with 200 μ M Congo Red in H₂O. Pictures were taken under A normal and B cross polarized light. Scale bar: 100 μ m.

Aggregates of IAPP(8-28)-OH were highly toxic to RIN cells as indicated by MTT assays (Fig. 23). This correlated with a fast and intense fibril formation as indicated by ThT assays (Fig. 21A).

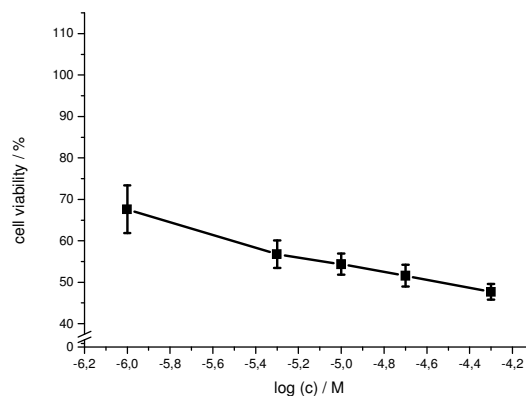


Fig. 23: Cell viability assay of an aged solution of IAPP(8-28)-OH (5 mM in 1xb 1% HFIP for 4 days, pH 7.4) using RIN cells. Data are percentages of control and are the mean (\pm SEM) of three independent experiments with each experiment performed in multiple replicates ($n = 3$).

3.1.1.4 IAPP(8-18)-SGN-(22-28)-OH

Similar to IAPP(8-28)-OH, the CD spectra of IAPP(8-18)-SGN-(22-28)-OH displayed mainly signals related to random coil structures (Fig. 24A). The signal intensity was slightly weaker and the concentration dependent decay of signal was also slower. The major difference was that at a concentration of 50 μM IAPP(8-18)-SGN-(22-28)-OH was already forming insoluble aggregates. Therefore no CD spectrum was measured at 50 μM .

CD studies were also performed in aqueous solution without HFiP (Fig. 24B). These spectra displayed properties similar to the spectra measured in solutions containing 1% HFiP.

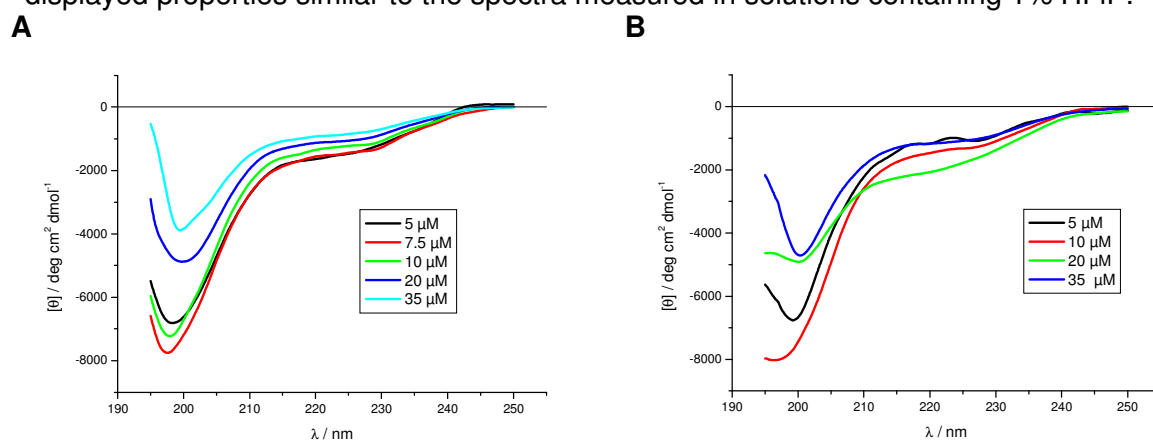


Fig. 24: Concentration dependent CD spectra of IAPP(8-18)-SGN-(22-28)-OH.

(A) Peptide was taken from a stock solution of 1 mM in HFiP measured in 1x 1% HFiP, pH 7.4.

(B) Incubations were made with peptide from stock solutions in 1 mM HCl measured in 1x 1 μM HCl, pH 7.

The results of the ThT binding assays showed that IAPP(8-18)-SGN-(22-28)-OH already started to form fibrils at 10 μM (Fig. 25A), corresponding to a lower concentration than the concentration required for IAPP(8-28)-OH for fibril formation (Fig. 21A). Also the signal intensity at 100 μM IAPP(8-18)-SGN-(22-28)-OH is much higher than that of native IAPP(8-28)-OH. The plateau at 100 μM was reached after 96h which was similar to IAPP(8-28)-OH. This might be an indication for a similar fibril forming mechanism between IAPP(8-28)-OH and IAPP(8-18)-SGN-(22-28)-OH.

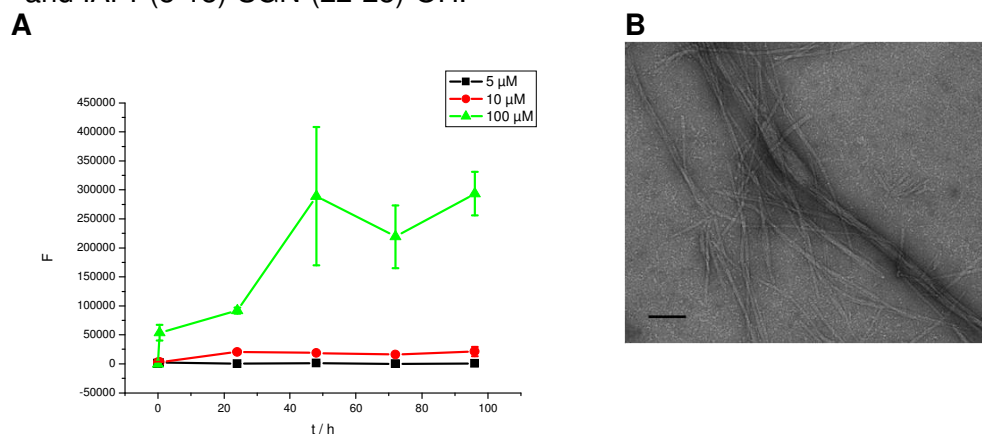


Fig. 25: (A) ThT assays of IAPP(8-18)-SGN-(22-28)-OH at different concentrations in 1x 1% HFiP, pH 7.4. Data are means of 3 assays after subtraction of buffer values \pm standard error of the mean (SEM) with each experiment performed in multiple replicates ($n = 3$).

(B) TEM picture of IAPP(8-18)-SGN-(22-28)-OH. The peptide was incubated at 100 μM for 7 d in 10 mM sodium phosphate buffer at pH 7.4 containing 1% HFiP. Scale bar: 100 nm.

Congo Red stained fibrillar aggregates of IAPP(8-18)-SGN-(22-28)-OH exhibited an intense gold/green birefringence under cross polarized light which was consistent with the formation of amyloid fibrils (Fig. 26B).

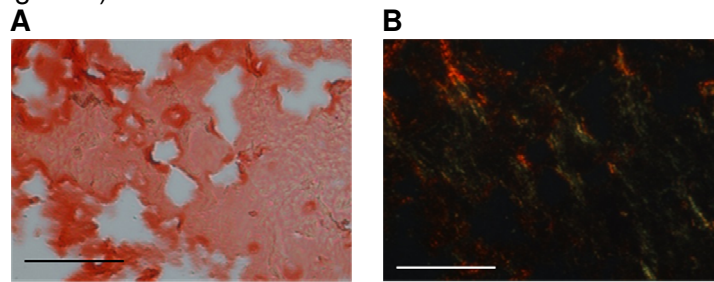


Fig. 26: Microscopic examination of fibrillar aggregates of IAPP(8-18)-SGN-(22-28)-OH stained with Congo Red. 1 mM peptide was incubated in 10 mM sodium phosphate buffer at pH 7.4 containing 1% HFIP for 3d and then spotted on a slide. The dried droplet was stained with 200 μ M Congo Red in H₂O. Pictures were taken under A normal and B cross polarized light. Scale bar: 100 μ m.

Fibrillar aggregates of IAPP(8-18)-SGN-(22-28)-OH (Fig. 27) were even more toxic than those of IAPP(8-28)-OH. This was expected since the natively occurring IAPP mutant S20G is also more toxic and has a higher fibril forming potential than hIAPP [102].

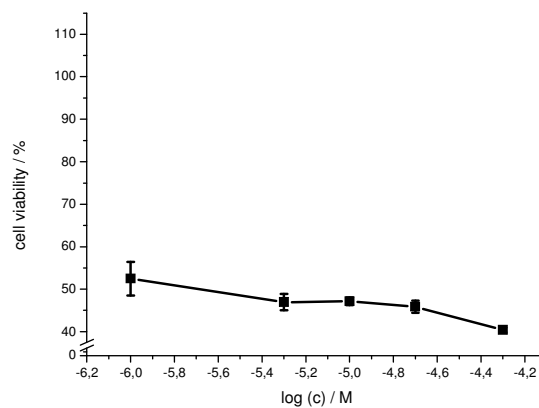


Fig. 27: Cell viability assay of an aged solution of IAPP(8-18)-SGN-(22-28)-OH (5 mM in 1x 1% HFIP for 4 days, pH 7.4) using RIN cells. Data are percentages of control and are the mean (+/-SEM) of three independent experiments with each experiment performed in multiple replicates (n = 3).

3.1.1.5 IAPP(8-18)-Aoc-(22-28)-OH

CD spectra of IAPP(8-18)-Aoc-(22-28)-OH revealed a broad and intense minimum at 215 nm (Fig. 28). This was a strong indication for a β -sheet structure of the peptide. The signal intensity decreased already at a peptide concentration of 5 μ M. At a concentration of 15 μ M peptide, there was only a small signal detectable. At concentrations > 15 μ M the peptide started to form insoluble oligomers and the solutions were getting turbid. Therefore, no CD spectra were measured.

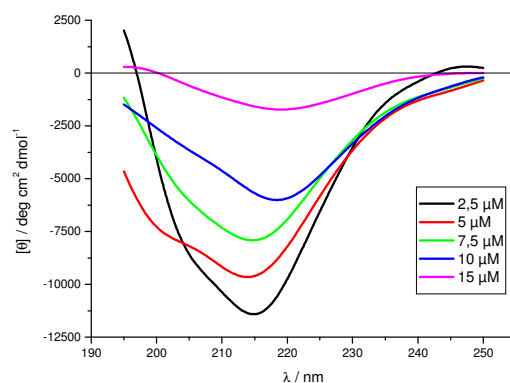


Fig. 28: Concentration dependent CD spectra of IAPP(8-18)-Aoc-(22-28)-OH in 1xb 1% HFIP, pH 7.4 (from [162]).

ThT assays showed that IAPP(8-18)-Aoc-(22-28)-OH was forming fibrils extremely fast (Fig. 29A). The plateau of fibril formation at both 35 and 100 μM was reached already after 30 min of shaking. However, the lowest peptide concentration at which the formation of amyloid fibrils occurred was similar to that of IAPP(8-28)-OH. This means that the faster formation of both soluble and insoluble aggregates observed for IAPP(8-18)-Aoc-(22-28)-OH did not result in a faster formation of amyloid fibrils. This indicated a conformational switch of IAPP(8-18)-Aoc-(22-28)-OH during the transition from oligomers to fibrils. This switch might have been hindered by a hydrophobic IAPP(19-21) sequence even though it increased the aggregation potential of IAPP(8-18)-Aoc-(22-28)-OH.

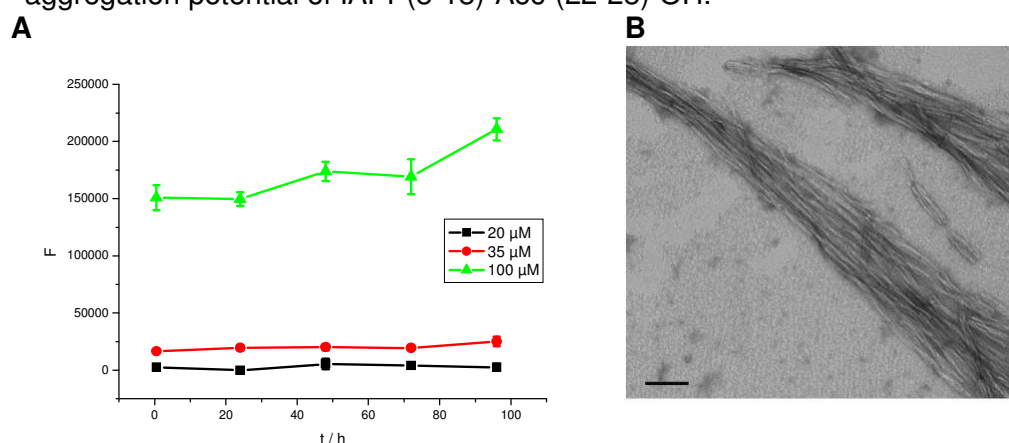


Fig. 29: (A) ThT assays of IAPP(8-18)-Aoc-(22-28)-OH at different concentrations in 1xb 1% HFIP, pH 7.4 (from [162]). Data are means of 3 assays after subtraction of buffer values \pm standard error of the mean (SEM) with each experiment performed in multiple replicates ($n = 3$).

(B) TEM picture of IAPP(8-18)-Aoc-(22-28)-OH. The peptide was incubated at 500 μM for 7 d in 10 mM sodium phosphate buffer at pH 7.4 containing 1% HFIP. Scale bar: 100 nm.

The formation of amyloid fibrils could be confirmed by Congo red staining (Fig. 30A and B) and TEM (Fig. 29B).

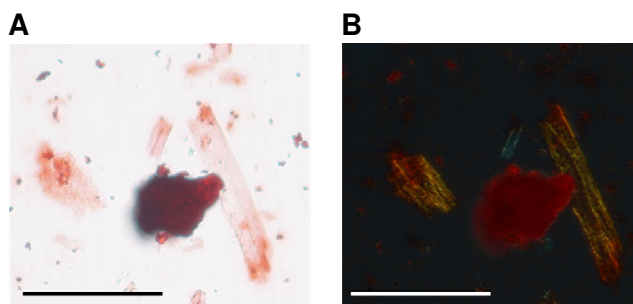


Fig. 30: Microscopic examination of fibrillar aggregates of IAPP(8-18)-Aoc-(22-28)-OH stained with Congo Red. 1 mM peptide was incubated in 10 mM sodium phosphate buffer at pH 7.4 containing 1% HFIP for 3d and then spotted on a slide. The dried droplet was stained with 2 mM Congo Red in H₂O. Pictures were taken under A normal and B cross polarized light. Scale bar: 100 µm.

The results of the MTT assays revealed that IAPP(8-18)-Aoc-(22-28)-OH was about as toxic as IAPP(8-28)-OH. This correlated with the fibril forming potential of the two peptides but not with their aggregation potential.

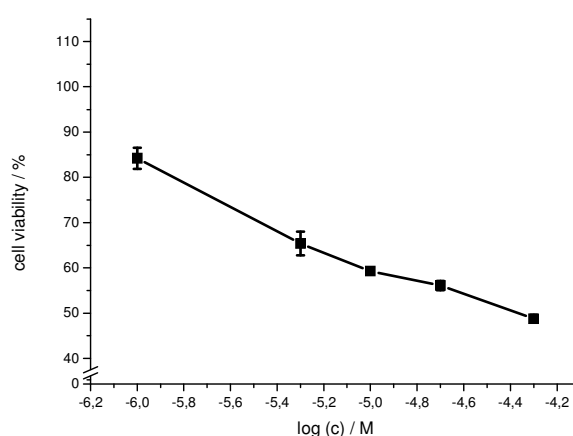


Fig. 31: Cell viability assay of an aged solution of IAPP(8-18)-Aoc-(22-28)-OH (5 mM in 1xb 1% HFIP for 4 days, pH 7.4) using RIN cells. Data are percentages of control replicates and are the mean (+/-SEM) of three independent experiments with each experiment performed in multiple replicates (n = 3).

3.1.1.6 IAPP(8-18)-Peg-(22-28)-OH

As seen on Fig. 32, IAPP(8-18)-Peg-(22-28)-OH displayed mainly random coil structures in CD, indicated by a minimum at around 200 nm. A weak minimum at 210-230 nm indicated the presence of β -sheet and β -turn elements. The signal intensity of spectra at a concentration between 5 and 20 μ M were nearly identical. A reduction of signal intensity first occurred at a peptide concentration of 35 μ M. This indicated a much lower aggregation potential of IAPP(8-18)-Peg-(22-28)-OH compared to IAPP(8-28)-OH (Fig. 21A) or IAPP(8-18)-Aoc-(22-28)-OH (Fig. 28). In general, the intensity of the CD spectra of IAPP(8-18)-Peg-(22-28)-OH was low, whereas the overall shape of the spectra was similar to IAPP(8-28)-OH. The weaker signal intensity, especially in the random coil area was an indication for the presence of less structural elements. The Peg liker seemed to have a strong influence on the aggregation potential and structure of the analogue.

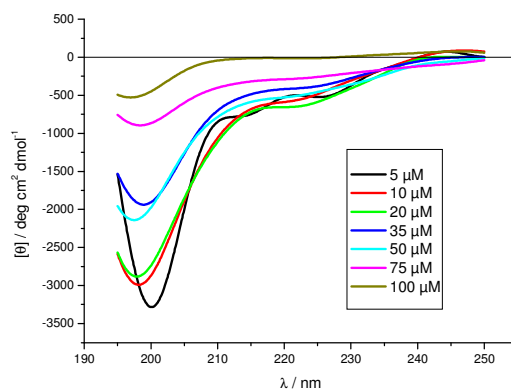


Fig. 32: Concentration dependent CD spectra of IAPP(8-18)-Peg-(22-28)-OH in 1xb 1% HFIP, pH 7.4 (from [162]).

IAPP(8-18)-Peg-(22-28)-OH started forming fibrils at a concentration of 100 μM (Fig. 33A), at a concentration where a loss of intensity was detected by CD.

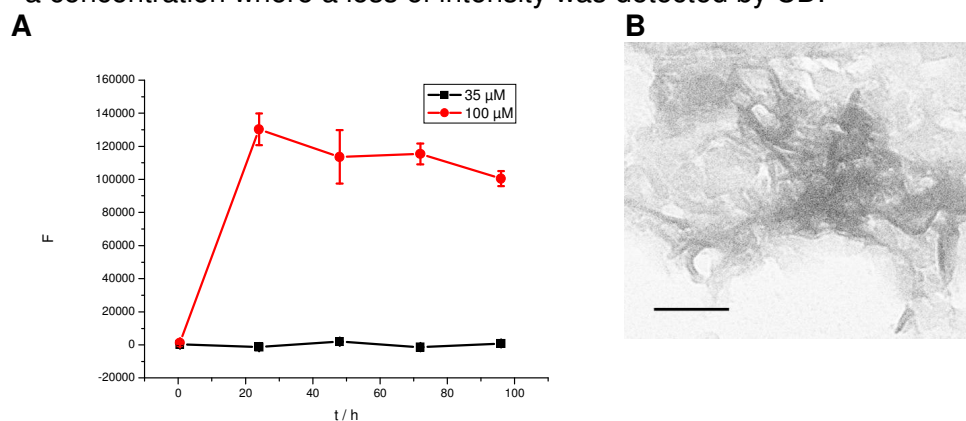


Fig. 33: (A) ThT assays of IAPP(8-18)-Peg-(22-28)-OH at different concentrations in 1xb 1% HFIP, pH 7.4 (from [162]). Data are means of 3 assays after subtraction of buffer values \pm standard error of the mean (SEM) with each experiment performed in multiple replicates ($n = 3$).

(B) TEM picture of IAPP(8-18)-Peg-(22-28)-OH. The peptide was incubated at 100 μM for 7 d in 10 mM sodium phosphate buffer at pH 7.4 containing 1% HFIP. Scale bar: 100 nm.

Fibril formation was confirmed by Congo Red staining (Fig. 34) and TEM (Fig. 33B). The TEM picture revealed the formation of small fibril bundles. Pictures of fibrils stained with Congo Red displayed weak green birefringence under cross polarized light.

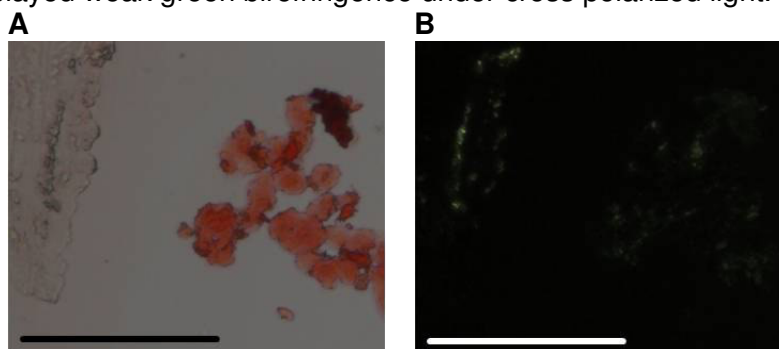


Fig. 34: Microscopic examination of fibrillar aggregates of IAPP(8-18)-Peg-(22-28)-OH stained with Congo Red. 1 mM peptide was incubated in 10 mM sodium phosphate buffer at pH 7.4 containing 1% HFIP for 3d and then spotted on a slide. The dried droplet was stained with 200 μM Congo Red in H_2O . Pictures were taken under A normal and B cross polarized light. Scale bar: 100 μm .

Cell viability assays of aged incubations of IAPP(8-18)-Peg-(22-28)-OH (Fig. 35) were less toxic than incubations of IAPP(8-28)-OH (Fig. 23). This was in good agreement to the fibril forming and aggregation potentials of IAPP(8-18)-Peg-(22-28)-OH.

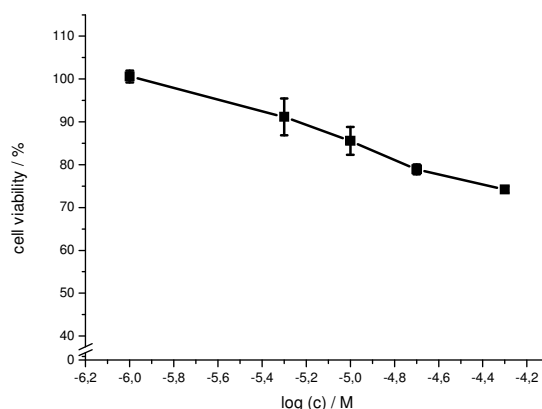


Fig. 35: Cell viability assay of an aged solution of IAPP(8-18)-Peg-(22-28)-OH (5 mM in 1xb 1% HFiP for 4 days, pH 7.4) using RIN cells. Data are percentages of control and are the mean (+/-SEM) of three independent experiments with each experiment performed in multiple replicates (n = 3).

3.1.1.7 IAPP(8-18)-KKK-(22-28)-OH

The CD spectra of IAPP(8-18)-KKK-(22-28)-OH (Fig. 36A) were similar to those of IAPP(8-28)-OH (Fig. 20). They showed a strong minimum at 195 - 200 nm which could have been due to random coil structures and weaker negative signal between 210 nm and 230 nm which could have been due to β -sheets and β -turns. All features of the concentration dependent CD spectra such as the overall shape, the signal intensity and the concentration dependent signal loss were comparable to IAPP(8-28)-OH (Fig. 20A). The connecting element KKK had obviously no strong influence on the structure and the aggregation potential of the peptide.

CD spectra measured in aqueous solution without HFiP (Fig. 36B) showed a similar shape and intensity compared to measurements in solutions containing 1% HFiP, whereas the aggregation potential of IAPP(8-18)-KKK-(22-28)-OH was much lower in aqueous solution. Under these conditions, the peptide seemed to remain monomeric up to a concentration of 100 μ M.

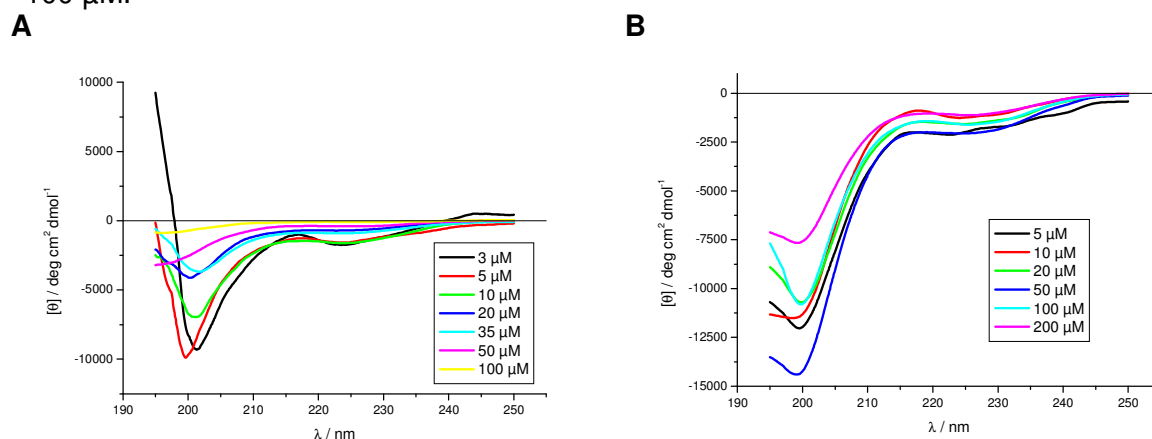


Fig. 36: Concentration dependent CD spectra of IAPP(8-18)-KKK-(22-28)-OH. (A) Peptide was taken from a stock solution of 1 mM in HFiP measured in 1xb 1% HFiP, pH 7.4 (from [162]). (B) Incubations were made with peptide from stock solutions in 1 mM HCl measured in 1xb 1 μ M HCl, pH 7.

ThT studies of IAPP(8-18)-KKK-(22-28)-OH showed no fibril formation at concentrations up to 500 μM (Fig. 37A). This could be verified by TEM which indicated the presence of amorphous aggregates but no fibrils (Fig. 37B).

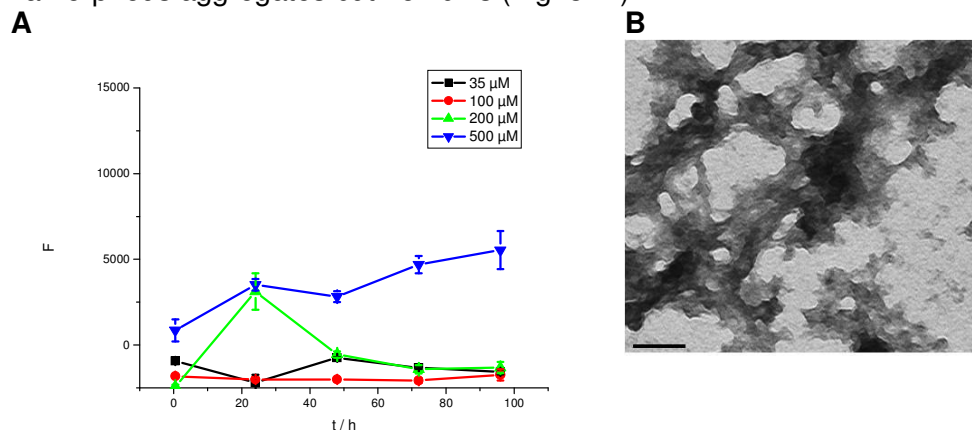


Fig. 37: (A) ThT assays of IAPP(8-18)-KKK-(22-28)-OH at different concentrations in 1x 1% HFIP, pH 7.4 (partially from [162]). Data are means of 3 assays after subtraction of buffer values \pm standard error of the mean (SEM) with each experiment performed in multiple replicates ($n = 3$). (B) TEM picture of IAPP(8-18)-KKK-(22-28)-OH. The peptide was incubated at 5 mM for 7 d in 10 mM sodium phosphate buffer at pH 7.4 containing 1% HFIP. Scale bar: 100 nm.

Congo Red stained aggregates of IAPP(8-18)-KKK-(22-28)-OH showed red color under normal light but no birefringence under cross polarized light at all (Fig. 38A and B). Aggregates of IAPP(8-18)-KKK-(22-28)-OH were able to bind to Congo Red but they did not possess the typical cross- structure that is responsible for the appearance of birefringence under cross polarized light.

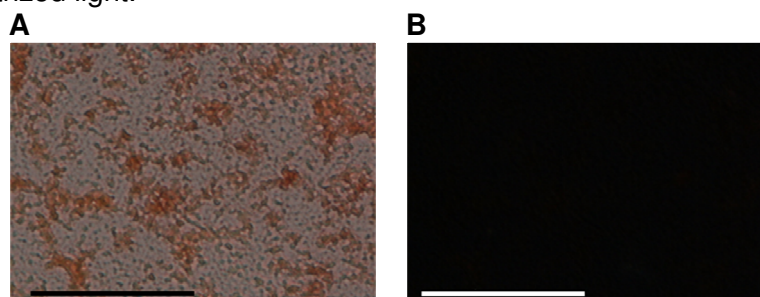


Fig. 38: Microscopic examination of aggregates of IAPP(8-18)-KKK-(22-28)-OH stained with Congo Red. 1 mM peptide was incubated in 10 mM sodium phosphate buffer at pH 7.4 containing 1% HFIP for 3d and then spotted on a slide. The dried droplet was stained with 200 μM Congo Red in H_2O . Pictures were taken under A normal and B cross polarized light. Scale bar: 100 μm .

Aggregates of IAPP(8-18)-KKK-(22-28)-OH were toxic to RIN cells (Fig. 39) but not as toxic as IAPP(8-28)-OH. Since IAPP(8-18)-KKK-(22-28)-OH was not able to form amyloid fibrils, the oligomers formed by IAPP(8-18)-KKK-(22-28)-OH seem to be toxic themselves.

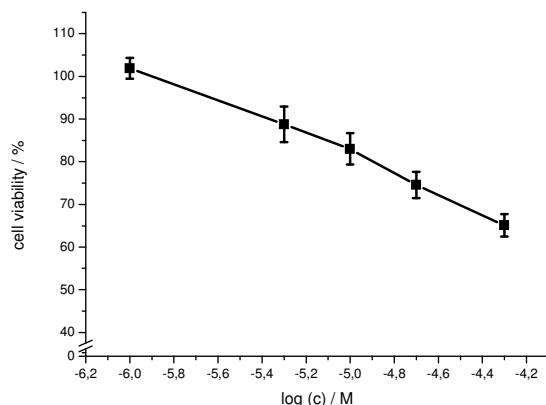


Fig. 39: Cell viability assay of an aged solution of IAPP(8-18)-KKK-(22-28)-OH (5 mM in 1xb 1% HFiP for 4 days, pH 7.4) using RIN cells. Data are percentages of control and are the mean (+/-SEM) of three independent experiments with each experiment performed in multiple replicates (n = 3).

3.1.1.8 IAPP(8-18)-Dap₃-(22-28)-OH

The CD spectra of IAPP(8-18)-Dap₃-(22-28)-OH showed a strong minimum at around 200 nm that were related to random coil structures and weaker negative signal at 210 - 230 nm that were related to β -sheets and β -turns (Fig. 40). The shape of the concentration dependent CD spectra of IAPP(8-18)-Dap₃-(22-28)-OH were comparable to those of IAPP(8-18)-KKK-(22-28)-OH. The signal intensity was lower and the signal reduction occurred at higher concentrations as in the case of IAPP(8-18)-KKK-(22-28)-OH (Fig. 36A). The aggregation potential of IAPP(8-18)-Dap₃-(22-28)-OH was apparently weaker than that of IAPP(8-18)-KKK-(22-28)-OH.

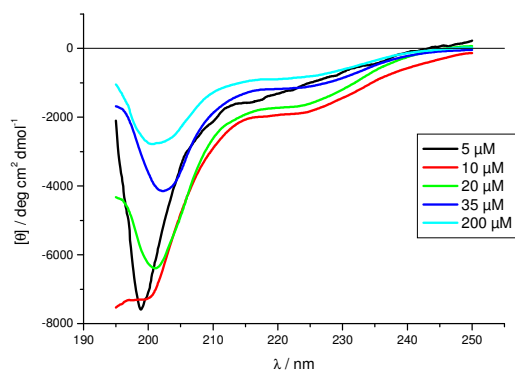


Fig. 40: Concentration dependent CD spectra of IAPP(8-18)-Dap₃-(22-28)-OH in 1xb 1% HFiP, pH 7.4 (from [164]).

ThT binding assays showed that IAPP(8-18)-Dap₃-(22-28)-OH did not form fibrils at concentrations up to 500 μ M (Fig. 41A) as observed in the case for IAPP(8-18)-KKK-(22-28)-OH (Fig. 37A).

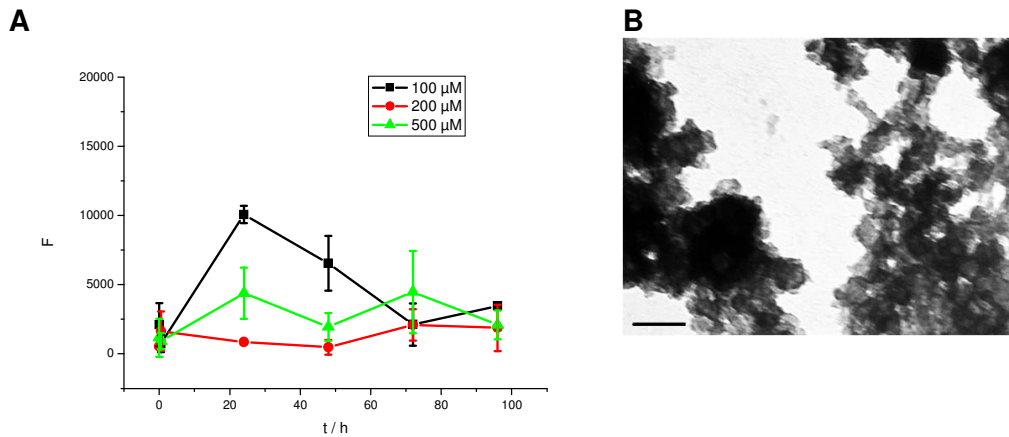


Fig. 41: (A) ThT assays of IAPP(8-18)-Dap₃-(22-28)-OH at different concentrations in 1x 1% HFiP, pH 7.4 (partially from [Altmann, 2012]). Data are means of 3 assays after subtraction of buffer values +/- standard error of the mean (SEM) with each experiment performed in multiple replicates (n = 3). (B) TEM picture of IAPP(8-18)-Dap₃-(22-28)-OH. The peptide was incubated at 500 μM for 7 d in 10 mM sodium phosphate buffer at pH 7.4 containing 1% HFiP. Scale bar: 100 nm.

The TEM picture of the incubation at a concentration of 500 μM (Fig. 41B) and the Congo Red staining at a concentration of 1 mM IAPP(8-18)-Dap₃-(22-28)-OH (Fig. 42) revealed no fibril formation. The TEM picture of IAPP(8-18)-Dap₃-(22-28)-OH showed amorphous aggregates but no fibrils.

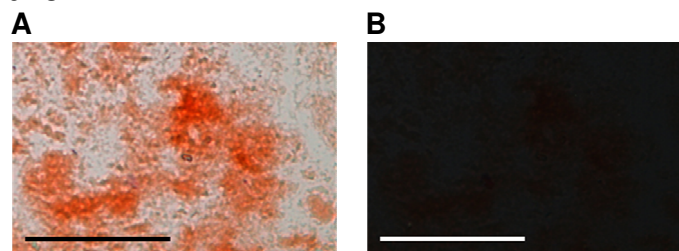


Fig. 42: Microscopic examination of aggregates of IAPP(8-18)-Dap₃-(22-28)-OH stained with Congo Red. 1 mM peptide was incubated in 10 mM sodium phosphate buffer at pH 7.4 containing 1% HFiP for 3d and then spotted on a slide. The dried droplet was stained with 200 μM Congo Red in H₂O. Pictures were taken under A normal and B cross polarized light. Scale bar: 100 μm.

The results of the MTT assays showed that IAPP(8-18)-Dap₃-(22-28)-OH was almost not toxic to RIN cells (Fig. 43).

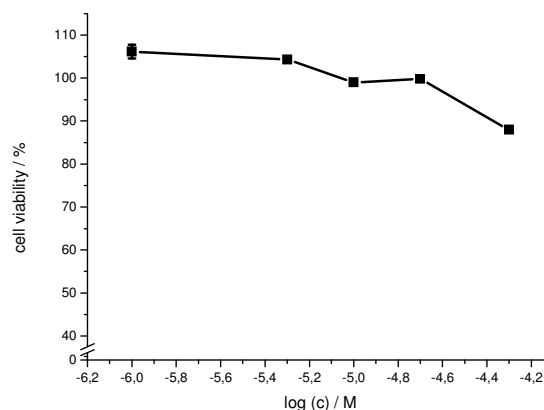


Fig. 43: Cell viability assay of an aged solution of IAPP(8-18)-Dap₃-(22-28)-OH (5 mM in 1x 1% HFiP for 4 days, pH 7.4) using RIN cells. Data are percentages of control and are the mean (+/-SEM) of three independent experiments with each experiment performed in multiple replicates (n = 3).

3.1.1.9 IAPP(8-18)-RRR-(22-28)-OH

Concentration dependent CD spectra of IAPP(8-18)-RRR-(22-28)-OH displayed a strong minimum at around 200 nm that was related to random coil structures (Fig. 44A). There were additional negative signals at 210 - 230 nm related to β -sheets and β -turns. A significant reduction of signal intensity, an indication for the formation of soluble oligomers, was observed already at a concentration of 20 μ M. The shape and the concentration dependent signal reduction were similar to those of IAPP(8-18)-KKK-(22-28)-OH (Fig. 36A).

Additionally, CD spectra were measured in aqueous solution without HFIP (Fig. 44B). These studies showed a lower aggregation potential of IAPP(8-18)-KKK-(22-28)-OH in aqueous solution.

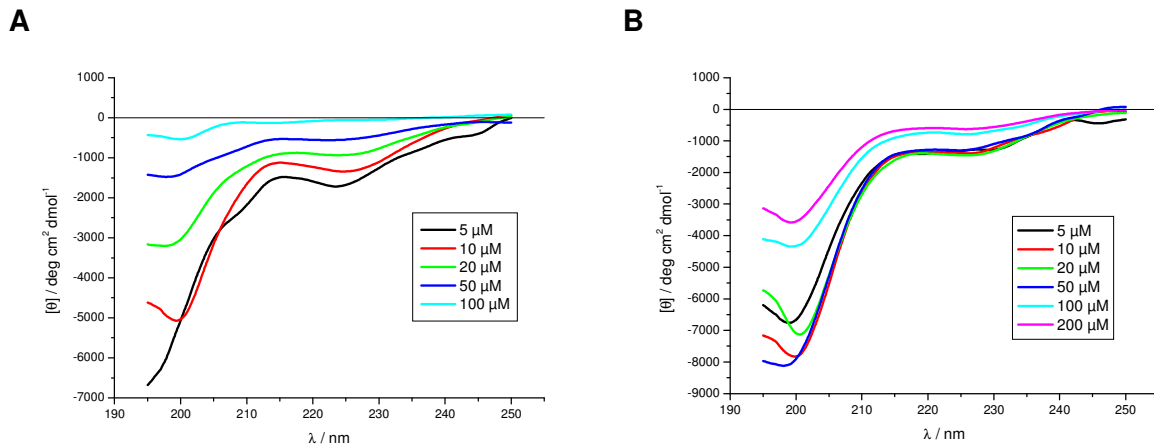


Fig. 44: Concentration dependent CD spectra of IAPP(8-18)-RRR-(22-28)-OH.

(A) Peptide was taken from a stock solution of 1 mM in HFIP measured in 1x 1% HFIP, pH 7.4 (from [161]).

(B) Incubations were made with peptide from stock solutions in 1 mM HCl measured in 1x 1 μ M HCl, pH 7.

ThT studies of IAPP(8-18)-RRR-(22-28)-OH showed no fibril formation at concentrations up to 500 μ M (Fig. 45A). The TEM picture at a concentration of 5 mM peptide also just showed amorphous aggregates but no fibrils (Fig. 45B). This incubation was done under the same conditions used to study toxicity.

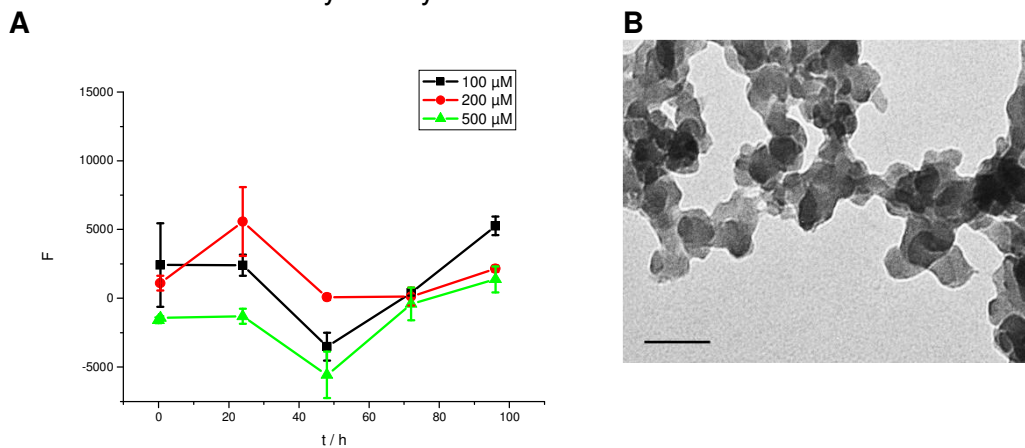


Fig. 45: (A) ThT assays of IAPP(8-18)-RRR-(22-28)-OH at different concentrations in 1x 1% HFIP, pH 7.4 (partially from [161]). Data are means of 3 assays after subtraction of buffer values \pm standard error of the mean (SEM) with each experiment performed in multiple replicates ($n = 3$).

(B) TEM picture of IAPP(8-18)-RRR-(22-28)-OH. The peptide was incubated at 5 mM for 4 d in 10 mM sodium phosphate buffer at pH 7.4 containing 1% HFIP. Scale bar: 100 nm.

Congo Red stained aggregates of IAPP(8-18)-RRR-(22-28)-OH showed red color under normal light (Fig. 46A) but no birefringence under cross polarized light at all (Fig. 46B) just like aggregates of IAPP(8-18)-KKK-(22-28)-OH.

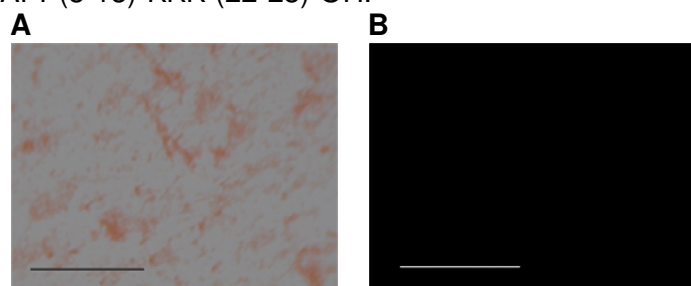


Fig. 46: Microscopic examination of aggregates of IAPP(8-18)-RRR-(22-28)-OH stained with Congo Red. 1 mM peptide was incubated in 10 mM sodium phosphate buffer at pH 7.4 containing 1% HFIP for 3d and then spotted on a slide. The dried droplet was stained with 200 μ M Congo Red in H₂O. Pictures were taken under A normal and B cross polarized light. Scale bar: 100 μ m.

IAPP(8-18)-RRR-(22-28)-OH displayed slight toxicity (Fig. 47), similar to that of IAPP(8-18)-Dap₃-(22-28)-OH.

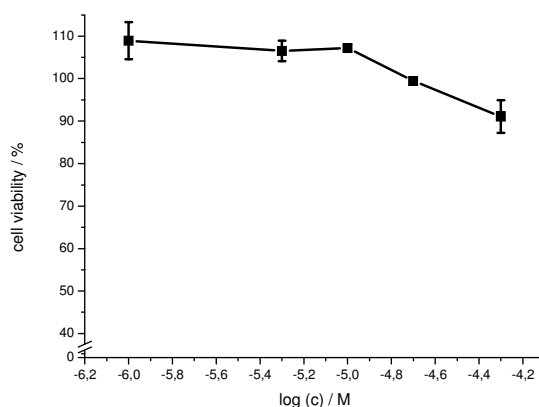


Fig. 47: Cell viability assay of an aged solution of IAPP(8-18)-RRR-(22-28)-OH (5 mM in 1x 1% HFIP for 4 days, pH 7.4) using RIN cells. Data are percentages of control and are the mean (+/-SEM) of three independent experiments with each experiment performed in multiple replicates (n = 3).

3.1.1.10 IAPP(8-18)-DDD-(22-28)-OH

The concentration dependent CD spectra of IAPP(8-18)-DDD-(22-28)-OH showed a strong minimum at 195 - 200 nm that can be related to random coil structures (Fig. 48). A weaker negative signal between 210 nm and 230 nm intended the presence of additional structural elements like β -sheets and β -turns. The lowest peptide concentration where a reduction of the intensity of the CD signal was observed was 20 μ M indicating the formation of oligomers.

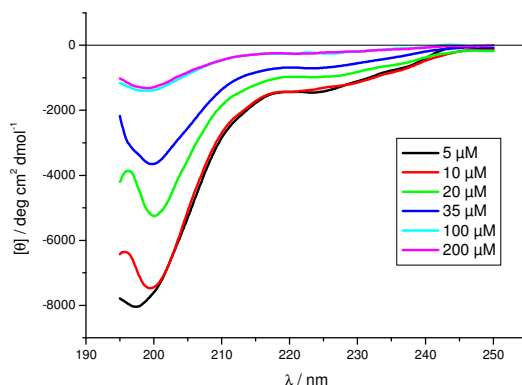


Fig. 48: Concentration dependent CD spectra of IAPP(8-18)-DDD-(22-28)-OH in 1x 1% HFIP, pH 7.4.

Like other analogues with charged elements in the IAPP(19-21) region, IAPP(8-18)-DDD-(22-28)-OH did not display fibril formation according to the results of ThT (Fig. 49A), TEM (Fig. 39B) and Congo Red studies (Fig. 50). Only non amyloid aggregates were visible.

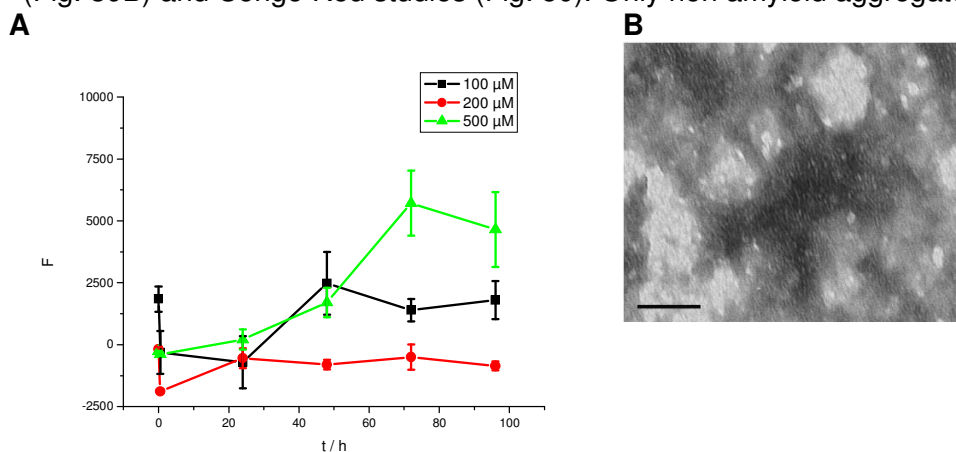


Fig. 49: (A) ThT assays of IAPP(8-18)-DDD-(22-28)-OH at different concentrations in 1x 1% HFIP, pH 7.4. Data are means of 3 assays after subtraction of buffer values \pm standard error of the mean (SEM) with each experiment performed in multiple replicates ($n = 3$).

(B) TEM picture of IAPP(8-18)-DDD-(22-28)-OH. The peptide was incubated at 500 μ M for 7 d in 10 mM sodium phosphate buffer at pH 7.4 containing 1% HFIP. Scale bar: 100 nm.

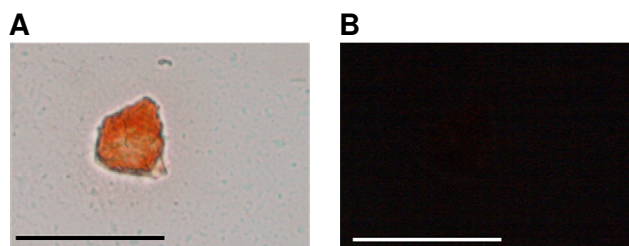


Fig. 50: Microscopic examination of aggregates of IAPP(8-18)-DDD-(22-28)-OH stained with Congo Red. 1 mM peptide was incubated in 10 mM sodium phosphate buffer at pH 7.4 containing 1% HFIP for 3d and then spotted on a slide. The dried droplet was stained with 200 μ M Congo Red in H₂O. Pictures were taken under A normal and B cross polarized light. Scale bar: 100 μ m.

Results of MTT reduction assays showed that IAPP(8-18)-DDD-(22-28)-OH was nontoxic to RIN cells at all (Fig. 51).

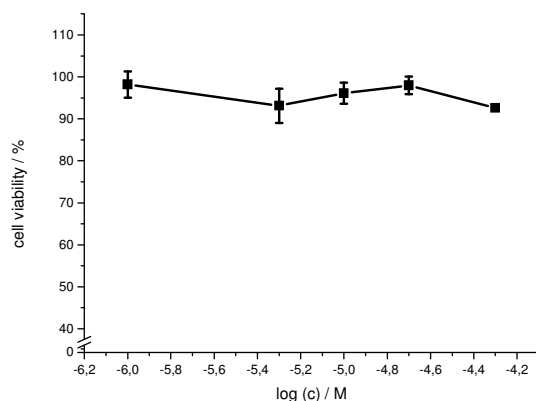


Fig. 51: Cell viability assay of an aged solution of IAPP(8-18)-DDD-(22-28)-OH (5 mM in 1xb 1% HFIP for 4 days, pH 7.4) using RIN cells. Data are percentages of control and are the mean (+/-SEM) of three independent experiments with each experiment performed in multiple replicates (n = 3).

3.1.1.11 IAPP(8-18)-GGG-(22-28)-OH

Similar to IAPP(8-28)-OH, the CD spectra of IAPP(8-18)-GGG-(22-28)-OH displayed mainly signals related to random coil structures (Fig. 52A). The signal intensity was slightly weaker than for IAPP(8-28)-OH. The lowest peptide concentration where a reduction of the intensity of the CD signal was observed was 20 μ M. At a concentration of 50 μ M, IAPP(8-18)-GG-(22-28)-OH already displayed no signal at all. The solution was still clear.

CD spectra of IAPP(8-18)-GGG-(22-28)-OH measured in aqueous solution without HFIP (Fig. 52B) showed a similar shape and intensity, but a slightly lower aggregation potential compared to the spectra measured in solutions containing 1% HFIP.

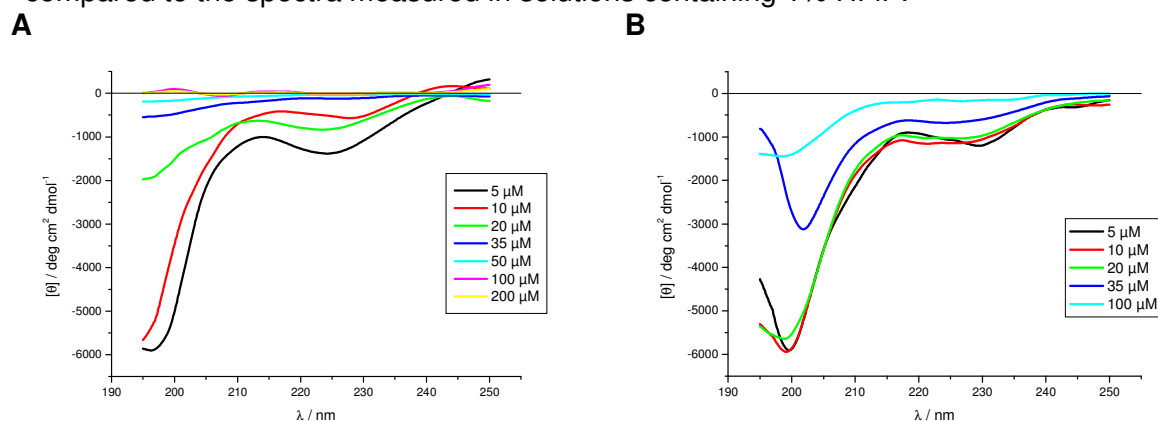


Fig. 52: Concentration dependent CD spectra of IAPP(8-18)-GGG-(22-28)-OH.

(A) Peptide was taken from a stock solution of 1 mM in HFIP measured in 1xb 1% HFIP, pH 7.4 (from [161]).

(B) Incubations were made with peptide from stock solutions in 1 mM HCl measured in 1xb 1 μ M HCl, pH 7.

The results of ThT assays revealed that IAPP(8-18)-GGG-(22-28)-OH started forming fibrils at a concentration of 100 μ M. At a concentration of 35 μ M, IAPP(8-18)-GGG-(22-28)-OH was not forming fibrils within 96h (Fig. 53A).

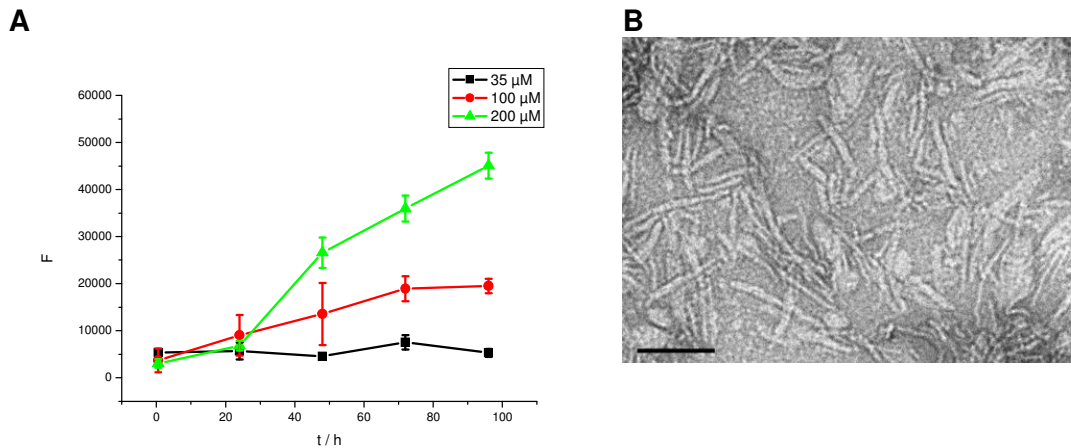


Fig. 53: (A) ThT assays of IAPP(8-18)-GGG-(22-28)-OH at different concentrations in 1xb 1% HFIP, pH 7.4 (from [161]). Data are means of 3 assays after subtraction of buffer values +/- standard error of the mean (SEM) with each experiment performed in multiple replicates (n = 3). (B) TEM picture of IAPP(8-18)-GGG-(22-28)-OH. The peptide was incubated at 200 μ M for 7 d in 10 mM sodium phosphate buffer at pH 7.4 containing 1% HFIP. Scale bar: 100 nm.

The formation of amyloid fibrils could be confirmed by Congo Red staining (Fig. 54) and TEM imaging (Fig. 53B).

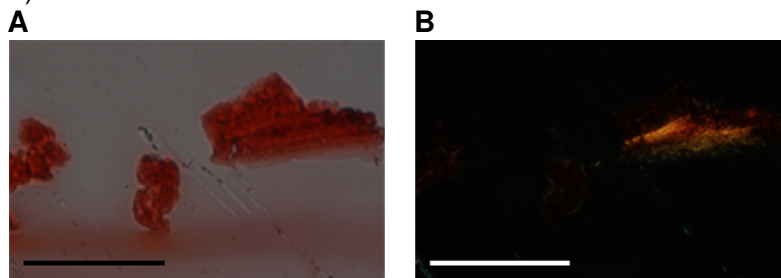


Fig. 54: Microscopic examination of fibrillar aggregates of IAPP(8-18)-GGG-(22-28)-OH stained with Congo Red. 1 mM peptide was incubated in 10 mM sodium phosphate buffer at pH 7.4 containing 1% HFIP for 3d and then spotted on a slide. The dried droplet was stained with 200 μ M Congo Red in H₂O. Pictures were taken under A normal and B cross polarized light. Scale bar: 100 μ m.

The toxicity of IAPP(8-18)-GGG-(22-28)-OH as shown by MTT reduction assays (Fig. 55) was similar to that of IAPP(8-18)-Peg-(22-28)-OH. The fibril forming potential of both peptides was also similar.

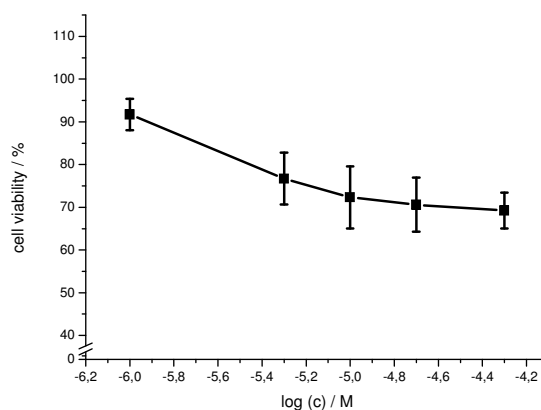


Fig. 55: Cell viability assay of an aged solution of IAPP(8-18)-GGG-(22-28)-OH (5 mM in 1xb 1% HFIP for 4 days, pH 7.4) using RIN cells. Data are percentages of control and are the mean (+/-SEM) of three independent experiments with each experiment performed in multiple replicates (n = 3).

3.1.1.12 IAPP(8-18)-AAA-(22-28)-OH

CD spectra of IAPP(8-18)-AAA-(22-28)-OH also revealed a minimum at 195 - 200 nm referred to as random coil structures and weak negative signals between 220 nm and 230 nm indicating the presence of additional structural elements like β -sheets and β -turns (Fig. 56). The intensity of the signal at 220 - 230 nm was more dominant and the intensity of the minimum at 195 - 200 nm much weaker compared to IAPP(8-28)-OH (Fig. 20A). The lowest peptide concentration where a reduction of the intensity of the CD signal was observed was 10 μ M.

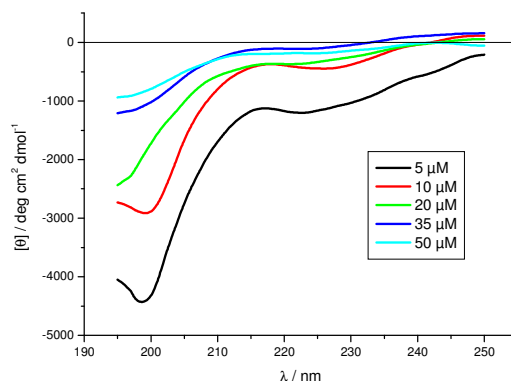


Fig. 56: Concentration dependent CD spectra of IAPP(8-18)-AAA-(22-28)-OH in 1xb 1% HFIP, pH 7.4 (from [161]).

For IAPP(8-18)-AAA-(22-28)-OH, clear fibril formation occurred at a concentration of 200 μ M, as intended by ThT studies (Fig. 57A). At a concentration of 100 μ M IAPP(8-18)-AAA-(22-28)-OH, only a weak increase of ThT fluorescence was visible. The fibril formation at 200 μ M could be conferred by TEM studies which also indicated the presence of amorphous aggregates (Fig. 57B).

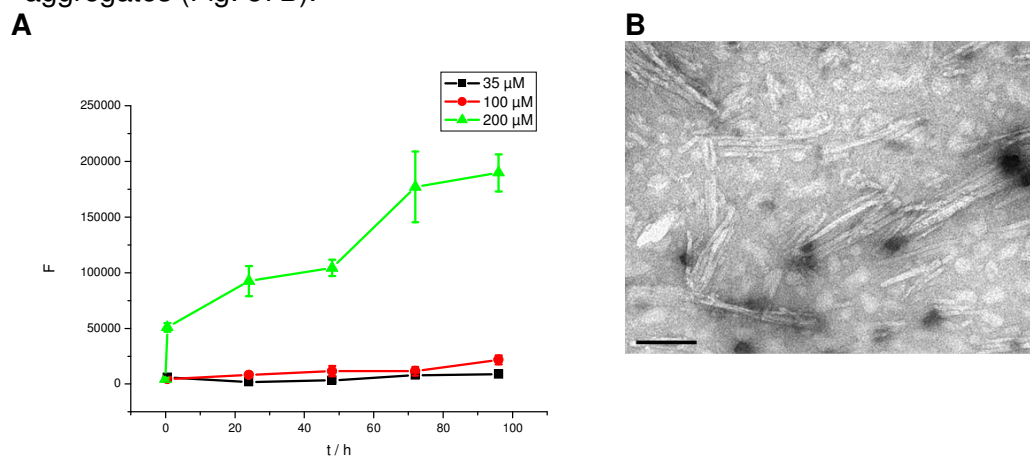


Fig. 57: (A) ThT assays of IAPP(8-18)-AAA-(22-28)-OH at different concentrations in 1xb 1% HFIP, pH 7.4 (from [161]). Data are means of 3 assays after subtraction of buffer values \pm standard error of the mean (SEM) with each experiment performed in multiple replicates ($n = 3$).

(B) TEM picture of IAPP(8-18)-AAA-(22-28)-OH. The peptide was incubated at 200 μ M for 7 d in 10 mM sodium phosphate buffer at pH 7.4 containing 1% HFIP. Scale bar: 100 nm.

Congo Red staining of IAPP(8-18)-AAA-(22-28)-OH showed gold/yellow birefringence under cross polarized light related to amyloid structures (Fig. 58B).

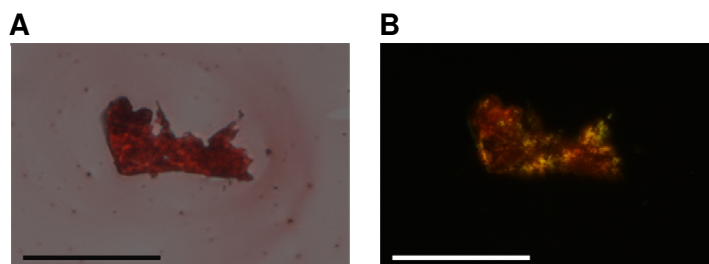


Fig. 58: Microscopic examination of fibrillar aggregates of IAPP(8-18)-AAA-(22-28)-OH stained with Congo Red. 1 mM peptide was incubated in 10 mM sodium phosphate buffer at pH 7.4 containing 1% HFiP for 3d and then spotted on a slide. The dried droplet was stained with 200 μ M Congo Red in H₂O. Pictures were taken under A normal and B cross polarized light. Scale bar: 100 μ m.

Fibrillar aggregates of IAPP(8-18)-AAA-(22-28)-OH (Fig. 59) were more toxic than aggregates of IAPP(8-18)-GGG-(22-28)-OH or IAPP(8-18)-Peg-(22-28)-OH, though significantly less than IAPP(8-28)-OH. Based on the results obtained from CD and ThT studies IAPP(8-18)-AAA-(22-28)-OH had a strong aggregation potential but only a weak fibril forming potential.

The analogue IAPP(8-18)-AAA-(22-28)-OH partially displayed features typical for peptides with hydrophobic residues in the sequence IAPP(19-21) such as strong aggregation potential and intense β -sheet and β -turn elements in CD. The hydrophobicity of the alanine side chain was however not strong enough to display all features of hydrophobic analogues.

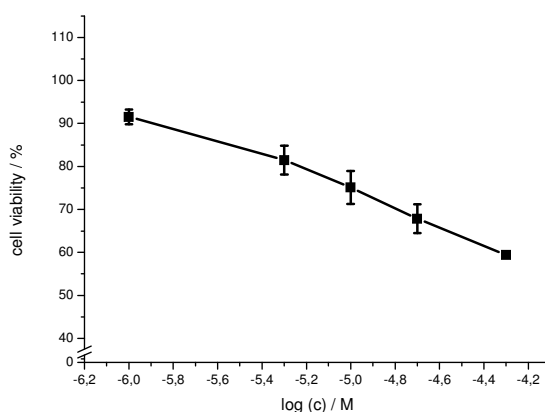


Fig. 59: Cell viability assay of an aged solution of IAPP(8-18)-AAA-(22-28)-OH (5 mM in 1x 1% HFiP for 4 days, pH 7.4) using RIN cells. Data are percentages of control and are the mean (+/-SEM) of three independent experiments with each experiment performed in multiple replicates (n = 3).

3.1.1.13 IAPP(8-18)-VVV-(22-28)-OH

CD spectra of IAPP(8-18)-VVV-(22-28)-OH (Fig. 60A) showed a broad and intense minimum at 215 nm, an indication for a β -sheet structure of the peptide. This signal was shifted towards higher wavelengths upon aggregation. At a concentration of 35 μ M, the minimum was around 230 nm which might have been related to a structural change from mainly β -sheet elements to more β -turn elements upon aggregation. The lowest peptide concentration where a reduction of the intensity of the CD signal was observed was 5 μ M, indicating a strong aggregation potential.

CD spectra performed in the absence of HFiP (Fig. 60B) displayed similar results. The minimum at 215 nm was sharper. There was no intense red shift of the minimum upon aggregation. This indicated a β -sheet structure for IAPP(8-18)-VVV-(22-28)-OH in aqueous solution with a much lower amount of β -turn elements.

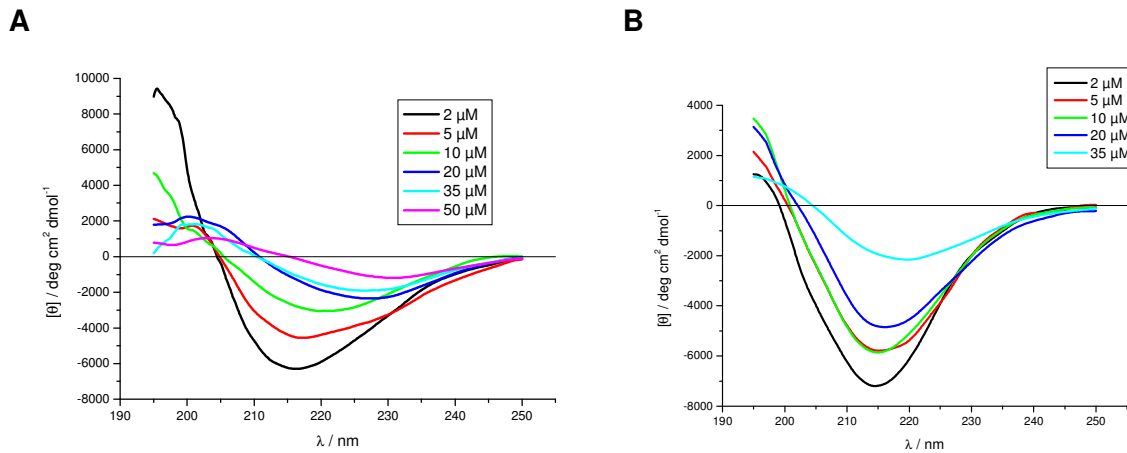


Fig. 60: Concentration dependent CD spectra of IAPP(8-18)-VTV-(22-28)-OH
 (A) Peptide was taken from a stock solution of 1 mM in HFIP measured in 1x 1% HFIP, pH 7.4 (from [164]).
 (B) Incubations were made with peptide from stock solutions in 1 mM HCl measured in 1x 1 μM HCl, pH 7.

ThT studies of IAPP(8-18)-VTV-(22-28)-OH showed that fibril formation already occurred at a concentration of 20 μM (Fig. 61A) which was consistent with a strong aggregation potential. The TEM picture (Fig. 61B) and pictures of Congo Red stained IAPP(8-18)-VTV-(22-28)-OH (Fig. 62) were also consistent with the formation of amyloid fibrils.

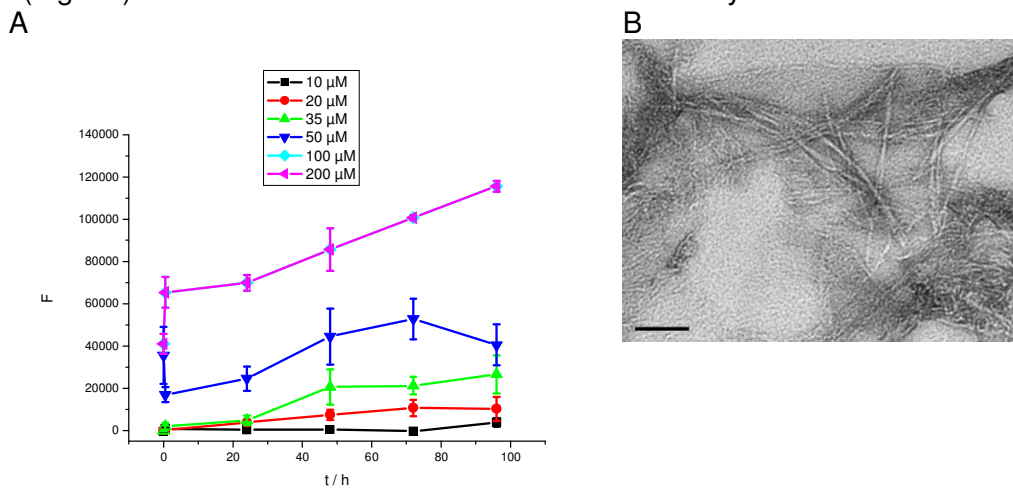


Fig. 61: (A) ThT assays of IAPP(8-18)-VTV-(22-28)-OH at different concentrations in 1x 1% HFIP, pH 7.4 (partially from [164]). Data are means of 3 assays after subtraction of buffer values +/- standard error of the mean (SEM) with each experiment performed in multiple replicates (n = 3).
 (B) TEM picture of IAPP(8-18)-VTV-(22-28)-OH. The peptide was incubated at 35 μM for 7 d in 10 mM sodium phosphate buffer at pH 7.4 containing 1% HFIP. Scale bar: 100 nm.

However as for IAPP(8-18)-Aoc-(22-28)-OH, the faster formation of both soluble and insoluble aggregates at lower peptide concentrations did not correlate with a fibril formation at lower peptide concentrations.

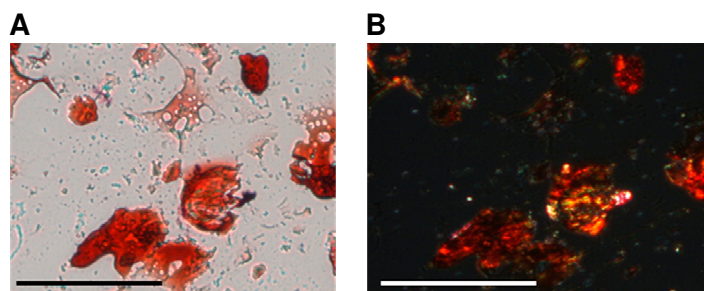


Fig. 62: Microscopic examination of fibrillar aggregates of IAPP(8-18)-VTV-(22-28)-OH stained with Congo Red. 1 mM peptide was incubated in 10 mM sodium phosphate buffer at pH 7.4 containing 1% HFiP for 3d and then spotted on a slide. The dried droplet was stained with 200 µM Congo Red in H₂O. Pictures were taken under A normal and B cross polarized light. Scale bar: 100 µm.

As shown on Fig. 63 IAPP(8-18)-VTV-(22-28)-OH was thus found to be about as toxic to RIN cells as IAPP(8-28)-OH (Fig. 23). The aggregation potential of IAPP(8-18)-VTV-(22-28)-OH was higher than that of IAPP(8-28)-OH, while fibril forming and toxic potential were similar.

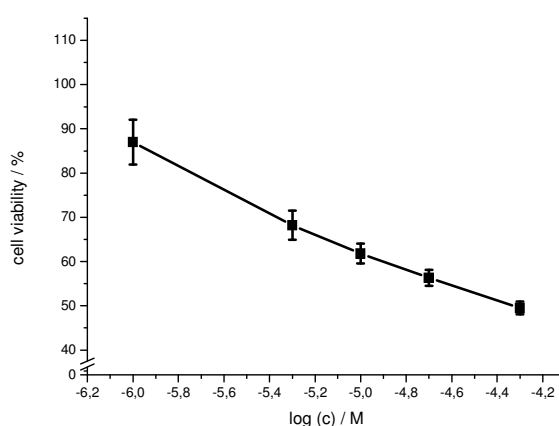


Fig. 63: Cell viability assay of an aged solution of IAPP(8-18)-VTV-(22-28)-OH (5 mM in 1xb 1% HFiP for 4 days, pH 7.4) using RIN cells. Data are percentages of control and are the mean (+/-SEM) of three independent experiments with each experiment performed in multiple replicates (n = 3).

3.1.1.14 IAPP(8-18)-LLL-(22-28)-OH

CD spectra of IAPP(8-18)-LLL-(22-28)-OH at different concentrations displayed a strong minimum at around 225 - 230 nm indicating the presence of β -sheet and β -turn elements (Fig. 64A). The signal intensity of spectra at a concentration between 2.5 and 7.5 µM was almost similar indicating the presence of monomeric IAPP(8-18)-LLL-(22-28)-OH at these concentrations. A reduction of the intensity of the CD signal occurred first at a peptide concentration of 10 µM.

CD studies done with a peptide stock in HCl instead of HFiP showed a distinct shift of the minimum towards 216 nm (Fig. 64B). This minimum is typical for proteins having β -sheet structure [165]. The signal reduction which indicated peptide aggregation was similar to that in 1xb containing 1% HFiP but without a redshift of the minimum upon aggregation.

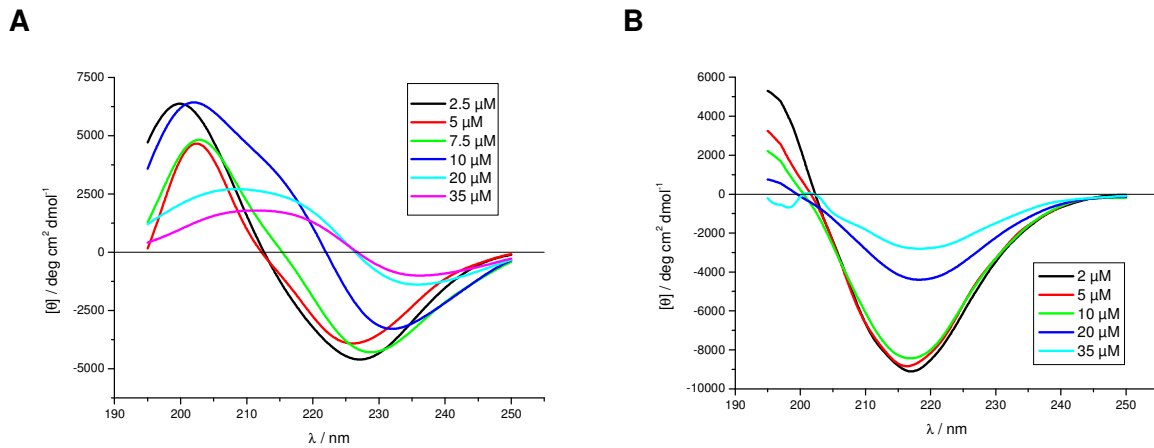


Fig. 64: Concentration dependent CD spectra of IAPP(8-18)-LLL-(22-28)-OH. (A) Peptide was taken from a stock solution of 1 mM in HFIP measured in 1x 1% HFIP, pH 7.4 (from [162]). (B) Incubations were made with peptide from stock solutions in 1 mM HCl measured in 1x 1 μM HCl, pH 7.

The fibril forming potential of IAPP(8-18)-LLL-(22-28)-OH was low (Fig. 65A). At a concentration of 100 and 200 μM only a weak increase in the ThT fluorescence was visible. Strong and intense fibril formation was only seen at a peptide concentration of 500 μM (Fig. 65A). Also only at a concentration of 500 μM, fibrils were visible on the TEM picture (Fig. 65B).

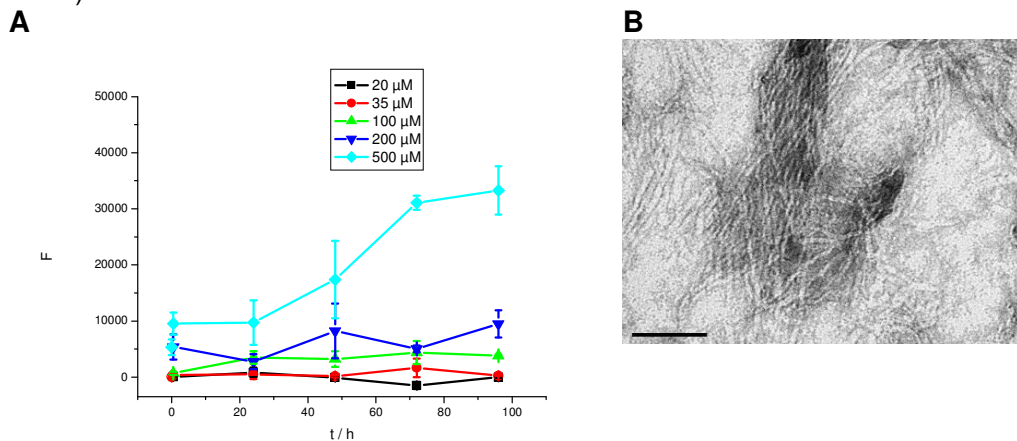


Fig. 65: (A) ThT assays of IAPP(8-18)-LLL-(22-28)-OH at different concentrations in 1x 1% HFIP, pH 7.4 (partially from [162]). Data are means of 3 assays after subtraction of buffer values \pm standard error of the mean (SEM) with each experiment performed in multiple replicates ($n = 3$). (B) TEM picture of IAPP(8-18)-LLL-(22-28)-OH. The peptide was incubated at 500 μM for 7 d in 10 mM sodium phosphate buffer at pH 7.4 containing 1% HFIP. Scale bar: 100 nm.

IAPP(8-18)-LLL-(22-28)-OH bound to Congo Red (Fig. 66), however only weak birefringence was found under cross polarized light. This also correlated with the low fibril forming potential expressed by ThT and TEM studies.

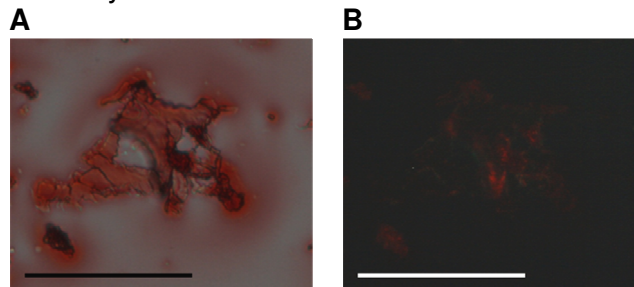


Fig. 66: Microscopic examination of fibrillar aggregates of IAPP(8-18)-LLL-(22-28)-OH stained with Congo Red. 1 mM peptide was incubated in 10 mM sodium phosphate buffer at pH 7.4 containing 1% HFiP for 3d and then spotted on a slide. The dried droplet was stained with 200 μ M Congo Red in H₂O. Pictures were taken under A normal and B cross polarized light. Scale bar: 100 μ m.

The toxicity of IAPP(8-18)-LLL-(22-28)-OH was lower than that of IAPP(8-18)-AAA-(22-28)-OH or IAPP(8-18)-GGG-(22-28)-OH (Fig. 67). This was consistent with the weaker fibril forming potential of IAPP(8-18)-LLL-(22-28)-OH.

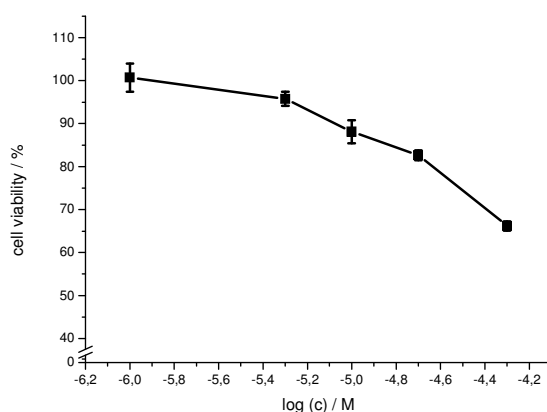


Fig. 67: Cell viability assay of an aged solution of IAPP(8-18)-LLL-(22-28)-OH (5 mM in 1xb 1% HFiP for 4 days, pH 7.4) using RIN cells. Data are percentages of control and are the mean (+/-SEM) of three independent experiments with each experiment performed in multiple replicates (n = 3).

3.1.1.15 IAPP(8-18)-III-(22-28)-OH

The CD spectra of IAPP(8-18)-III-(22-28)-OH (Fig. 68A) were similar to those of IAPP(8-18)-LLL-(22-28)-OH (Fig. 64A). They showed a strong minimum at around 220 - 230 nm indicating the presence of β -sheet and β -turn elements and a red shift of this minimum upon aggregation. The intensity of the minimum was higher for IAPP(8-18)-III-(22-28)-OH than for IAPP(8-18)-LLL-(22-28)-OH. The signal intensity of spectra at a concentration between 2 and 10 μ M was almost similar indicating the presence of monomeric IAPP(8-18)-III-(22-28)-OH at these concentrations. A reduction of signal intensity occurred first at a peptide concentration of 15 μ M. This indicated a lower aggregation potential compared to other analogues with hydrophobic elements in the sequence at position IAPP(19-21).

CD spectra of IAPP(8-18)-III-(22-28)-OH in 1xb without HFiP (Fig. 68B) displayed a minimum at 216 nm, similar to IAPP(8-18)-LLL-(22-28)-OH (Fig. 64B). This minimum did also not shift towards higher wavelengths upon aggregation.

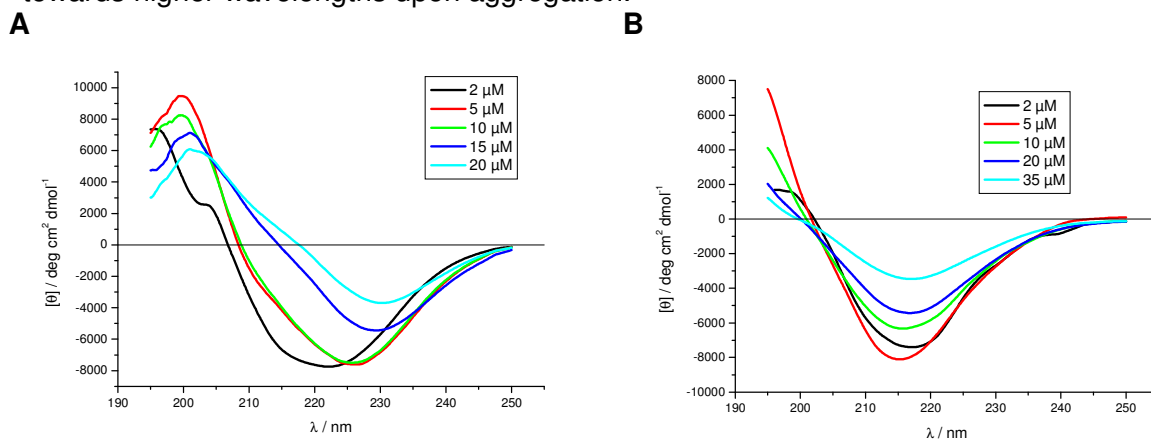


Fig. 68: Concentration dependent CD spectra of IAPP(8-18)-III-(22-28)-OH.
 (A) Peptide was taken from a stock solution of 1 mM in HFIP measured in 1xb 1% HFIP, pH 7.4 (from [164]).
 (B) Incubations were made with peptide from stock solutions in 1 mM HCl measured in 1xb 1 μ M HCl, pH 7.

As seen on Fig. 69A, IAPP(8-18)-III-(22-28)-OH started forming fibrils at a concentration of 35 μ M. This fibril formation could be verified by TEM (Fig. 69B).

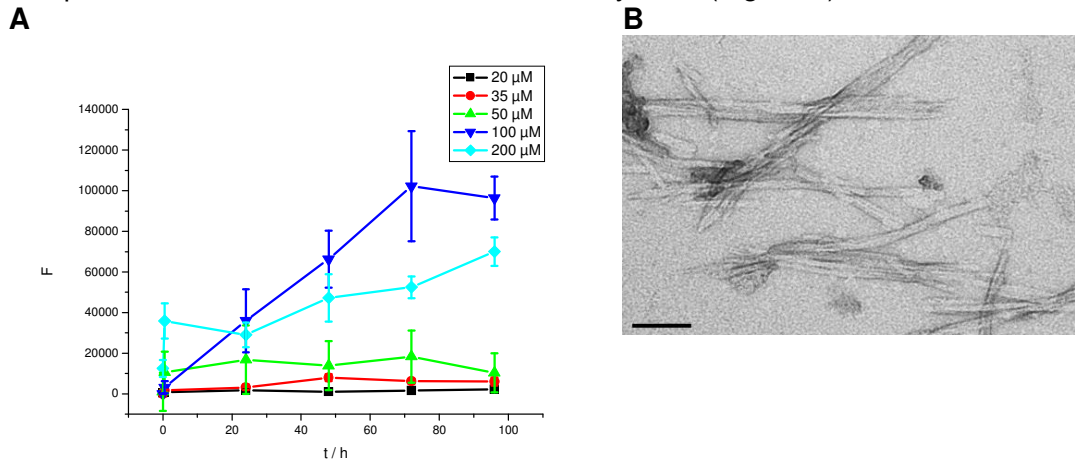


Fig. 69: (A) ThT assays of IAPP(8-18)-III-(22-28)-OH at different concentrations in 1xb 1% HFIP, pH 7.4 (partially from [164]). Data are means of 3 assays after subtraction of buffer values \pm standard error of the mean (SEM) with each experiment performed in multiple replicates (n = 3).
 (B) TEM picture of IAPP(8-18)-III-(22-28)-OH. The peptide was incubated at 35 μ M for 7 d in 10 mM sodium phosphate buffer at pH 7.4 containing 1% HFIP. Scale bar: 100 nm.

Congo Red staining of IAPP(8-18)-III-(22-28)-OH showed weak green/yellow birefringence under cross polarized light related to amyloid structures (Fig. 70B).

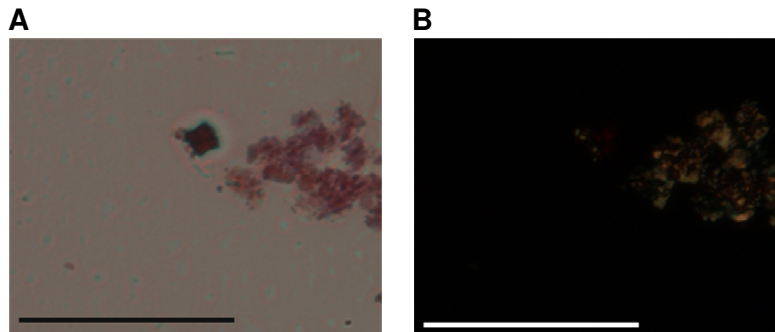


Fig. 70: Microscopic examination of fibrillar aggregates of IAPP(8-18)-III-(22-28)-OH stained with Congo Red. 1 mM peptide was incubated in 10 mM sodium phosphate buffer at pH 7.4 containing 1% HFIP for 3d and then spotted on a slide. The dried droplet was stained with 200 μ M Congo Red in H₂O. Pictures were taken under A normal and B cross polarized light. Scale bar: 100 μ m.

The toxicity of IAPP(8-18)-III-(22-28)-OH (Fig. 71) was slightly weaker than that of native IAPP(8-28)-OH, similar to that of IAPP(8-18)-Aoc-(22-28)-OH and IAPP(8-18)-VVV-(22-28)-OH. The fibril forming potential of all these peptides was similar, correlating with their toxicity. Compared to IAPP(8-18)-LLL-(22-28)-OH IAPP(8-18)-III-(22-28)-OH was much more toxic and fibrillogenic. This indicated the role of steric hindrance in the IAPP(19-21) region on toxicity and fibril formation.

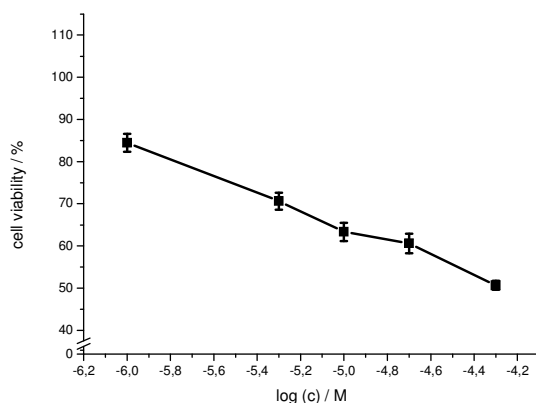


Fig. 71: Cell viability assay of an aged solution of IAPP(8-18)-III-(22-28)-OH (5 mM in 1x 1% HFiP for 4 days, pH 7.4) using RIN cells. Data are percentages of control and are the mean (+/-SEM) of three independent experiments with each experiment performed in multiple replicates (n = 3).

3.1.1.16 IAPP(8-18)-Nle₃-(22-28)-OH

CD spectra of IAPP(8-18)-Nle₃-(22-28)-OH displayed a minimum between 225 nm and 230 nm (Fig. 72A). This indicated a β -sheet conformation of the peptide. The lowest peptide concentration where a reduction of the intensity of the CD signal was observed was 20 μ M. At concentrations > 35 μ M the peptide started to form insoluble oligomers and the solutions were getting turbid. Therefore no CD spectra were measured. The concentration dependent CD spectra of IAPP(8-18)-Nle₃-(22-28)-OH displayed an overall shape typical for analogues with hydrophobic elements at the positions IAPP(19-21).

Similar to other analogues with hydrophobic elements in the IAPP(19-21) region CD spectra of IAPP(8-18)-Nle₃-(22-28)-OH performed in the absence of HFiP (Fig. 72B) displayed a sharp minimum at 215 nm. There was no intense red shift of the minimum upon aggregation. This indicated a β -sheet structure for IAPP(8-18)-Nle₃-(22-28)-OH in aqueous solution.

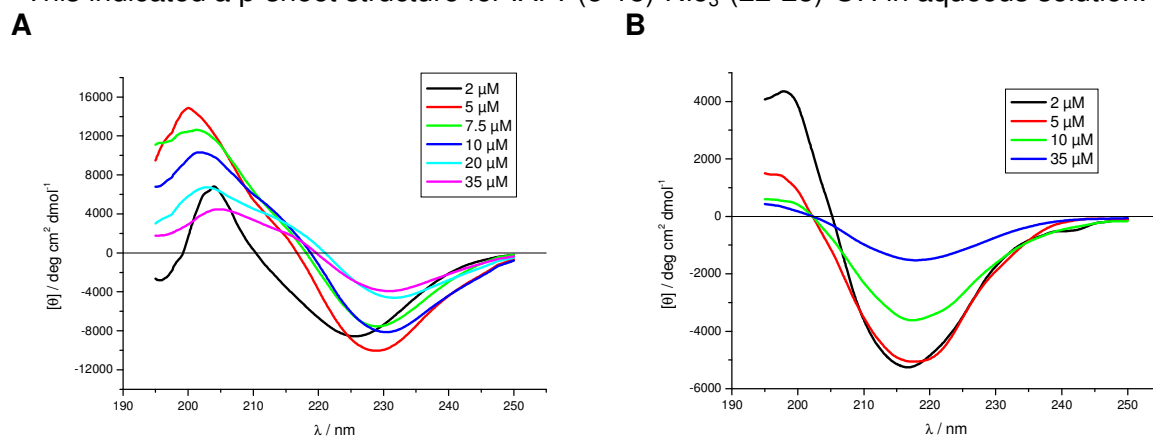


Fig. 72: Concentration dependent CD spectra of IAPP(8-18)-Nle₃-(22-28)-OH.

(A) Peptide was taken from a stock solution of 1 mM in HFiP measured in 1x 1% HFiP, pH 7.4 (from [164]).
 (B) Incubations were made with peptide from stock solutions in 1 mM HCl measured in 1x 1 μ M HCl, pH 7.

ThT studies of IAPP(8-18)-Nle₃-(22-28)-OH at different concentrations revealed the start of fibril formation at 35 μ M (Fig. 73A).

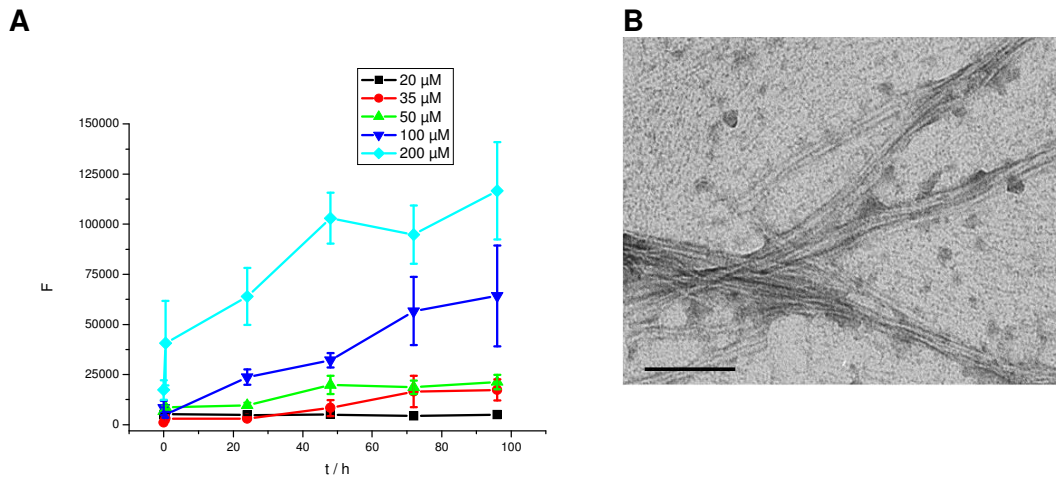


Fig. 73: (A) ThT assays of IAPP(8-18)-Nle₃-(22-28)-OH at different concentrations in 1x 1% HFIP, pH 7.4 (partially from [164]). Data are means of 3 assays after subtraction of buffer values +/- standard error of the mean (SEM) with each experiment performed in multiple replicates (n = 3). (B) TEM picture of IAPP(8-18)-Nle₃-(22-28)-OH. The peptide was incubated at 100 μM for 7 d in 10 mM sodium phosphate buffer at pH 7.4 containing 1% HFIP. Scale bar: 100 nm.

Staining of fibrillar aggregates of IAPP(8-18)-Nle₃-(22-28)-OH with Congo Red also indicated the presence of cross-β structures. Stained aggregates showed intense red color under normal light (Fig. 74A) and displayed yellow birefringence under cross polarized light (Fig. 74B).

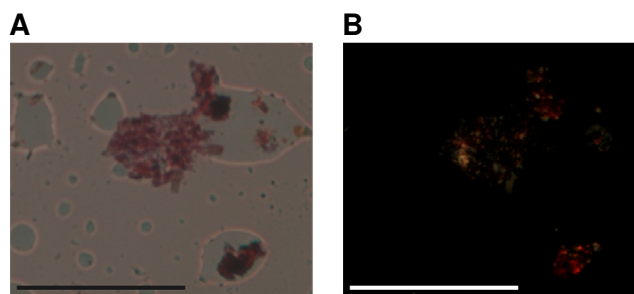


Fig. 74: Microscopic examination of fibrillar aggregates of IAPP(8-18)-Nle₃-(22-28)-OH stained with Congo Red. 1 mM peptide was incubated in 10 mM sodium phosphate buffer at pH 7.4 containing 1% HFIP for 3d and then spotted on a slide. The dried droplet was stained with 200 μM Congo Red in H₂O. Pictures were taken under A normal and B cross polarized light. Scale bar: 100 μm.

As seen on Fig. 75, IAPP(8-18)-Nle₃-(22-28)-OH was less toxic than IAPP(8-18)-III-(22-28)-OH but more toxic than for example IAPP(8-18)-LLL-(22-28)-OH. The fibril forming potential of IAPP(8-18)-Nle₃-(22-28)-OH and IAPP(8-18)-III-(22-28)-OH were similar.

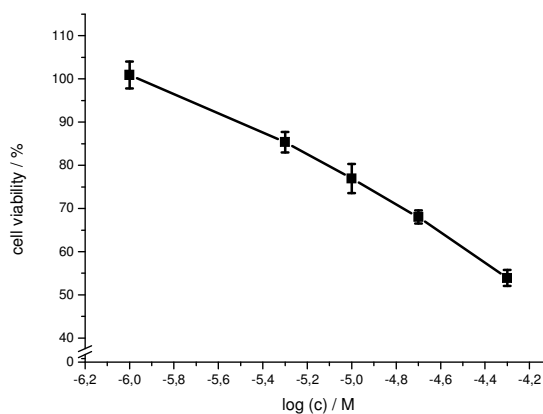


Fig. 75: Cell viability assay of an aged solution of IAPP(8-18)-Nle₃-(22-28)-OH (5 mM in 1xb 1% HFiP for 4 days, pH 7.4) using RIN cells. Data are percentages of control and are the mean (+/-SEM) of three independent experiments with each experiment performed in multiple replicates (n = 3).

3.1.1.17 IAPP(8-18)-2Aoc₃-(22-28)-OH

IAPP(8-18)-2Aoc₃-(22-28)-OH displayed both β -sheet and β -turn structures in CD, indicated by a broad minimum at around 225 nm (Fig. 76A). The signal intensity of spectra at a concentration between 5 and 10 μ M was almost similar. IAPP(8-18)-2Aoc₃-(22-28)-OH displayed the highest signal intensity for monomeric peptide among the analogues with hydrophobic elements in the sequence IAPP(19-21). A reduction of signal intensity was observed first at a peptide concentration of 20 μ M. At a concentration of 35 μ M peptide, only a weak CD signal was observed. At concentrations > 35 μ M the peptide formed insoluble oligomers and the solutions were getting turbid.

CD studies of IAPP(8-18)-2Aoc₃-(22-28)-OH done with a peptide stock in HCl instead of HFiP showed a distinct shift of the minimum towards 216 nm (Fig. 76B). There was however still a strong signal intensity between 220 and 225 nm. Compared to other analogues with hydrophobic elements in the IAPP(19-21) region, IAPP(8-18)-2Aoc₃-(22-28)-OH seemed to possess a big content of β -turn structures even without the presence of HFiP.

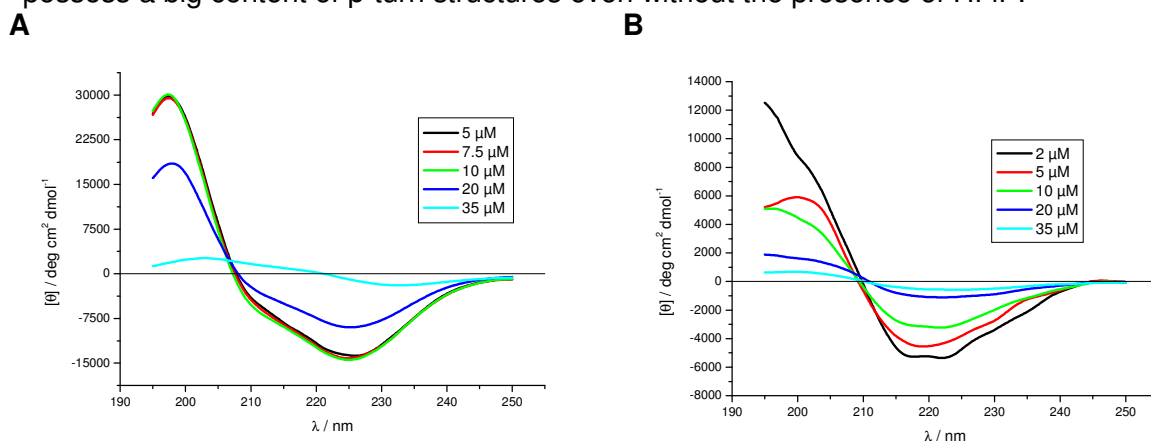


Fig. 76: Concentration dependent CD spectra of IAPP(8-18)-2Aoc₃-(22-28)-OH. (A) Peptide was taken from a stock solution of 1 mM in HFiP measured in 1xb 1% HFiP, pH 7.4. (B) Incubations were made with peptide from stock solutions in 1 mM HCl measured in 1xb 1 μ M HCl, pH 7.

ThT assays of IAPP(8-18)-2Aoc₃-(22-28)-OH showed that the peptide started to form amyloid fibrils at a concentration of 35 μ M (Fig. 77A). Fibril formation was verified by TEM (Fig. 77B).

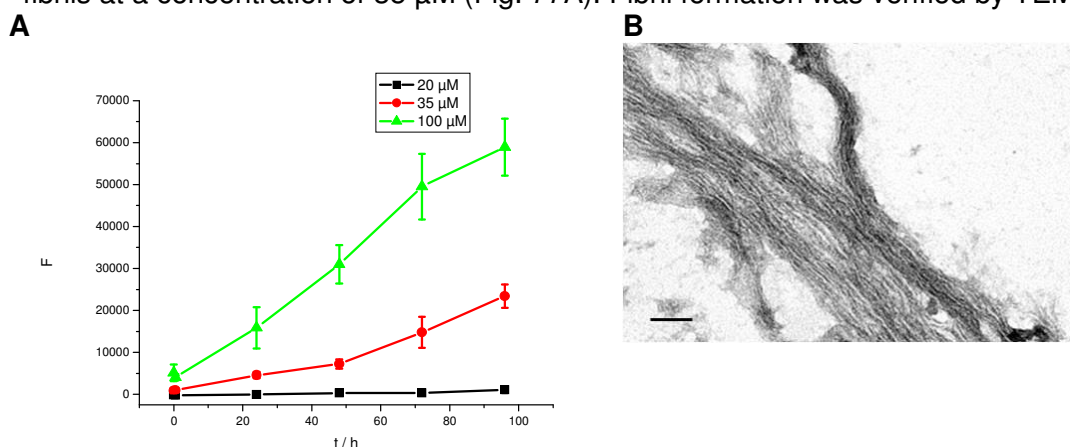


Fig. 77: (A) ThT assays of IAPP(8-18)-2Aoc₃-(22-28)-OH at different concentrations in 1x 1% HFiP, pH 7.4. Data are means of 3 assays after subtraction of buffer values +/- standard error of the mean (SEM) with each experiment performed in multiple replicates (n = 3). (B) TEM picture of IAPP(8-18)-2Aoc₃-(22-28)-OH. The peptide was incubated at 100 μM for 7 d in 10 mM sodium phosphate buffer at pH 7.4 containing 1% HFiP. Scale bar: 100 nm.

Staining of fibrillar aggregates of IAPP(8-18)-2Aoc₃-(22-28)-OH with Congo Red also revealed the formation of amyloid fibrils (Fig. 78). Stained aggregates showed intense red color under normal light and also mainly red color under cross polarized light. The red birefringence under cross polarized light was due to Congo Red bound to fibrils that was shining through unbound and therefore red Congo Red.

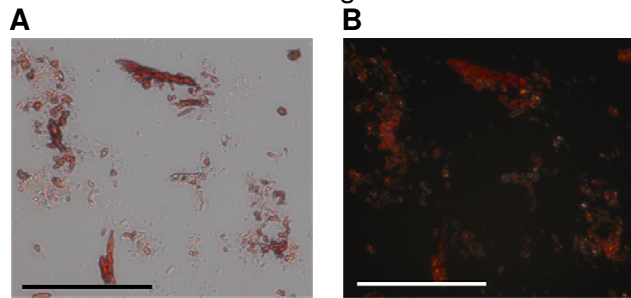


Fig. 78: Microscopic examination of fibrillar aggregates of IAPP(8-18)-2Aoc₃-(22-28)-OH stained with Congo Red. 1 mM peptide was incubated in 10 mM sodium phosphate buffer at pH 7.4 containing 1% HFiP for 3d and then spotted on a slide. The dried droplet was stained with 200 μM Congo Red in H₂O. Pictures were taken under A normal and B cross polarized light. Scale bar: 100 μm.

MTT reduction assays of IAPP(8-18)-2Aoc₃-(22-28)-OH (Fig. 79) revealed that the peptide was about as toxic as IAPP(8-18)-Nle₃-(22-28)-OH (Fig. 75).

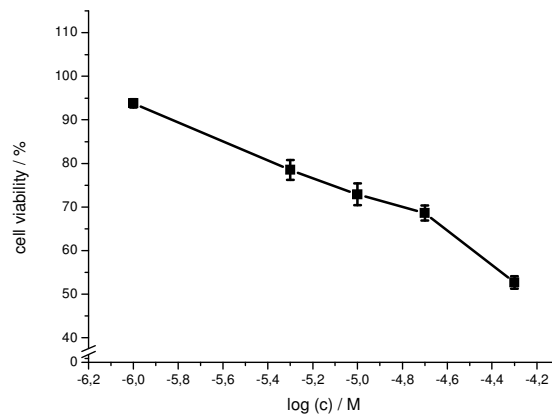


Fig. 79: Cell viability assay of an aged solution of IAPP(8-18)-2Aoc₃-(22-28)-OH (5 mM in 1x 1% HFiP for 4 days, pH 7.4) using RIN cells. Data are percentages of control and are the mean (+/-SEM) of three independent experiments with each experiment performed in multiple replicates (n = 3).

3.1.1.18 IAPP(8-18)-TTT-(22-28)-OH

The CD spectra of IAPP(8-18)-TTT-(22-28)-OH displayed a strong minimum at 195 - 200 nm that can be related to random coil structures and also a negative signal between 210 nm and 230 nm related to β-sheet or β-turn elements (Fig. 80). Already at a peptide concentration of 7.5 μM, the signal intensity was slightly reduced. Just like for IAPP(8-28)-OH, the signal loss upon aggregation occurred first in the area at 195 – 200 nm and then in the area between 210 nm and 230 nm. The shape of the spectra was similar to the shape of the spectra of IAPP(8-18)-AAA-(22-28)-OH (Fig. 56).

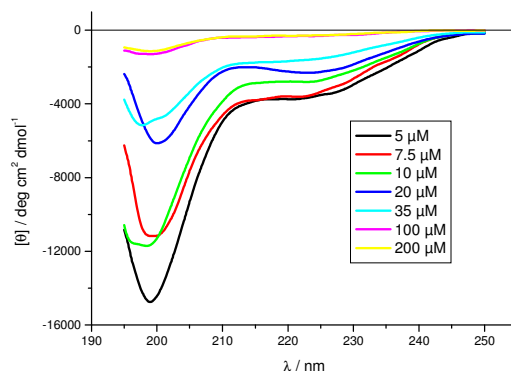


Fig. 80: Concentration dependent CD spectra of IAPP(8-18)-TTT-(22-28)-OH in 1xb 1% HFIP, pH 7.4.

As shown by ThT fluorescence assays IAPP(8-18)-TTT-(22-28)-OH started forming fibrils at a concentration of 35 μM (Fig. 81A). There was no lag time in the ThT assays. Fibril formation obviously occurred already during the 30 min of shaking at the beginning of the assays.

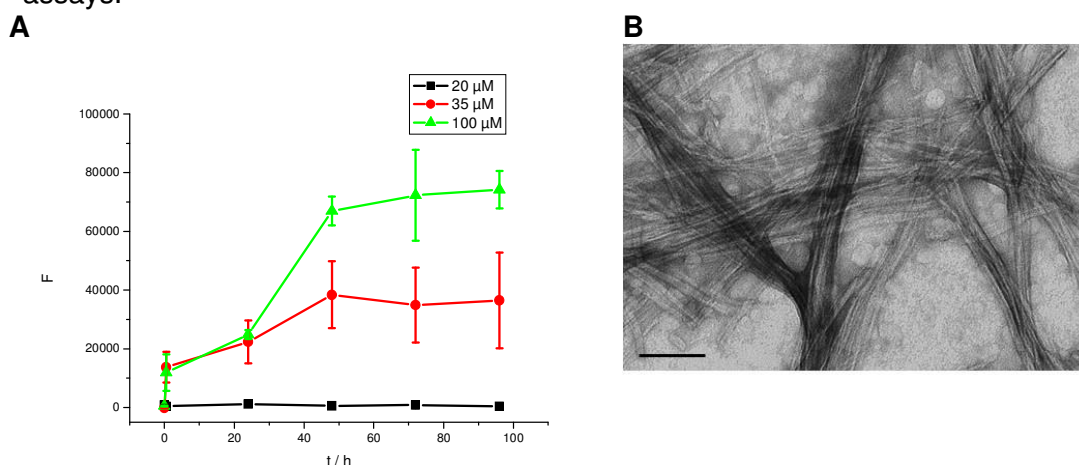


Fig. 81: (A) ThT assays of IAPP(8-18)-TTT-(22-28)-OH at different concentrations in 1xb 1% HFIP, pH 7.4. Experiments were done in 10 mM sodium phosphate buffer at pH 7.4 containing 1% HFIP. Data are means of 3 assays after subtraction of buffer values \pm standard error of the mean (SEM) with each experiment performed in multiple replicates ($n = 3$).

(B) TEM picture of IAPP(8-18)-TTT-(22-28)-OH. The peptide was incubated at 100 μM for 7 d in 10 mM sodium phosphate buffer at pH 7.4 containing 1% HFIP. Scale bar: 100 nm.

Staining of fibrillar aggregates of IAPP(8-18)-TTT-(22-28)-OH with Congo Red also revealed the formation of amyloid fibrils (Fig. 82). Stained aggregates showed intense red color under normal light and apple green but also red birefringence under cross polarized light. The red birefringence under polarized light was due to Congo Red bound to fibrils that was shining through unbound Congo Red. The areas that were red under polarized light also seemed to be thicker than areas showing green birefringence.

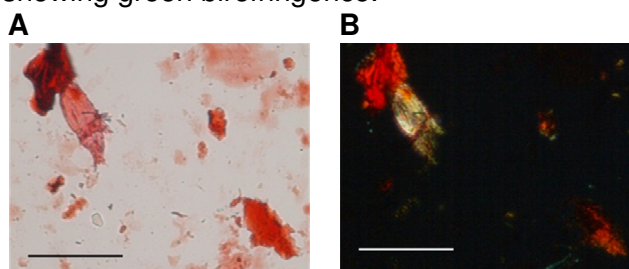


Fig. 82: Microscopic examination of fibrillar aggregates of IAPP(8-18)-TTT-(22-28)-OH stained with Congo Red. 1 mM peptide was incubated in 10 mM sodium phosphate buffer at pH 7.4 containing 1% HFiP for 3d and then spotted on a slide. The dried droplet was stained with 200 μ M Congo Red in H₂O. Pictures were taken under A normal and B cross polarized light. Scale bar: 100 μ m.

IAPP(8-18)-TTT-(22-28)-OH is highly toxic to RIN cells (Fig. 83), but not as toxic as IAPP(8-28)-OH (Fig. 23).

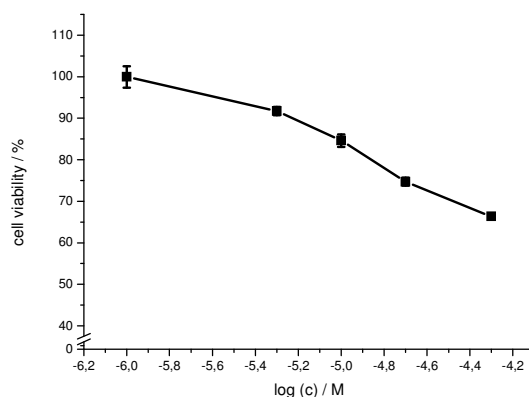


Fig. 83: Cell viability assay of an aged solution of IAPP(8-18)-TTT-(22-28)-OH (5 mM in 1xb 1% HFiP for 4 days, pH 7.4) using RIN cells. Data are percentages of control and are the mean (+/-SEM) of three independent experiments with each experiment performed in multiple replicates (n = 3).

3.1.1.19 IAPP(8-18)-FFF-(22-28)-OH

CD spectra of IAPP(8-18)-FFF-(22-28)-OH measured in 1xb 1% HFiP showed a minimum at 225 nm. This indicated β -sheet and β -turn structures for the peptide. Spectra could only be obtained at concentrations from 3 μ M to 7.5 μ M (Fig. 84A). These spectra revealed only small concentration dependent differences assuming a monomeric structure for IAPP(8-18)-FFF-(22-28)-OH under these conditions. At concentrations > 7.5 μ M the peptide started to precipitate and no CD spectra could be obtained under these conditions. Therefore IAPP(8-18)-FFF-(22-28)-OH was kept in a stock solution containing HCl. Spectra measured under these conditions showed slight differences to those measured in solutions containing 1% HFiP. With HCl, CD spectra of IAPP(8-18)-FFF-(22-28)-OH displayed a minimum at 216 nm which is typical for β -sheets (Fig. 84B). The signal intensity for 5 μ M was also slightly higher than for the same peptide in HFiP. It was also possible to measure spectra up to a concentration of 50 μ M showing a concentration related signal loss.

Spectra measured under both conditions displayed β -sheet structures and a high aggregation potential for IAPP(8-18)-FFF-(22-28)-OH.

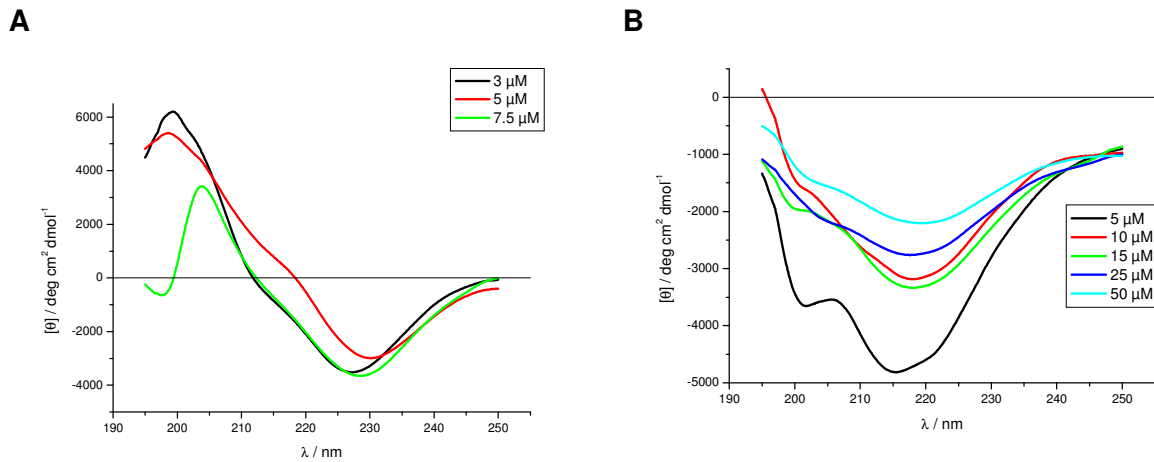


Fig. 84: Concentration dependent CD spectra of IAPP(8-18)-FFF-(22-28)-OH.

(A) Peptide was taken from a stock solution of 1 mM in HFIP measured in 1x 1% HFIP, pH 7.4 (from [161]).

(B) Incubations were made with peptide from stock solutions in 1 mM HCl measured in 1x 1 μM HCl, pH 7 (from [161]).

IAPP(8-18)-FFF-(22-28)-OH started forming fibrils in ThT assays at a concentration of 50 μM (Fig. 85A). The TEM picture of an incubation at a peptide concentration of 100 μM showed mainly fibrils but also some amorphous aggregates (Fig. 85B).

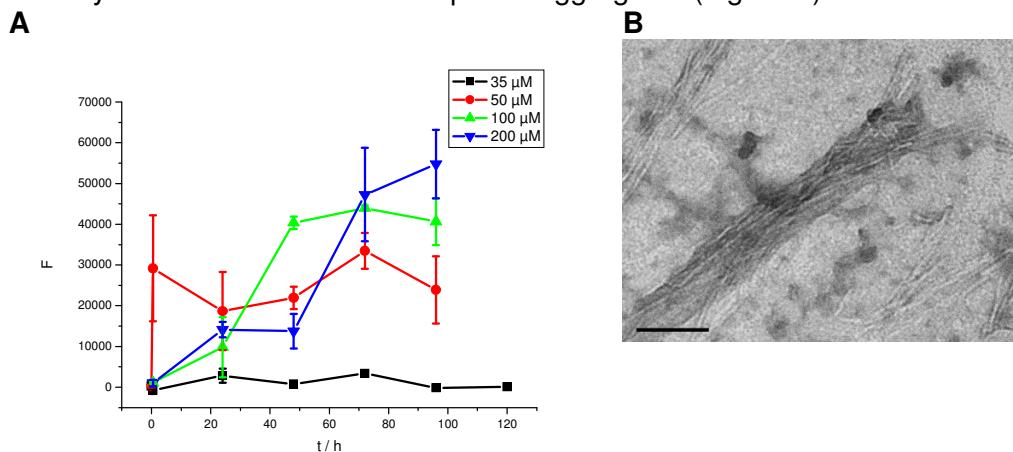


Fig. 85: (A) ThT assays of IAPP(8-18)-FFF-(22-28)-OH at different concentrations in 1x 1% HFIP, pH 7.4 (partially from [161]). Data are means of 3 assays after subtraction of buffer values +/- standard error of the mean (SEM) with each experiment performed in multiple replicates (n = 3).

(B) TEM picture of IAPP(8-18)-FFF-(22-28)-OH. The peptide was incubated at 100 μM for 7 d in 10 mM sodium phosphate buffer at pH 7.4 containing 1% HFIP. Scale bar: 100 nm.

Staining of fibrillar aggregates of IAPP(8-18)-FFF-(22-28)-OH with Congo Red also indicated the presence of cross-β structures. Stained aggregates showed red color under normal light (Fig. 86A) and displayed orange/yellow birefringence under cross polarized light (Fig. 86B).

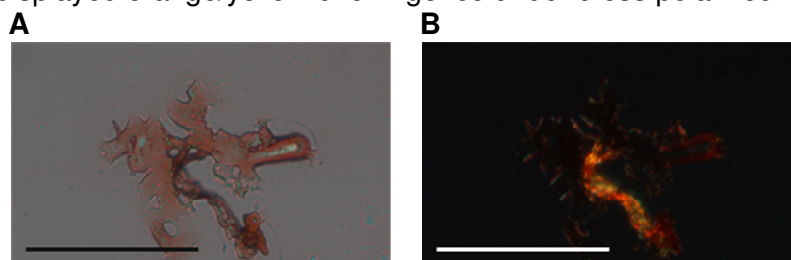


Fig. 86: Microscopic examination of fibrillar aggregates of IAPP(8-18)-FFF-(22-28)-OH stained with Congo Red. 1 mM peptide was incubated in 10 mM sodium phosphate buffer at pH 7.4 containing 1% HFIP for 3d and then

spotted on a slide. The dried droplet was stained with 200 μM Congo Red in H_2O . Pictures were taken under A normal and B cross polarized light. Scale bar: 100 μm .

Results of cell viability assays showed that IAPP(8-18)-FFF-(22-28)-OH was toxic to RIN cells (Fig. 87). The toxicity of IAPP(8-18)-FFF-(22-28)-OH was in relation to its fibril forming potential when compared with other analogues of IAPP(8-28)-OH.

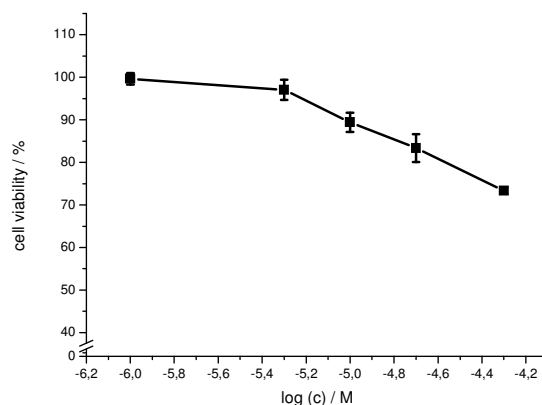


Fig. 87: Cell viability assay of an aged solution of IAPP(8-18)-FFF-(22-28)-OH (5 mM in 1xb 1% HFiP for 4 days, pH 7.4) using RIN cells. Data are percentages of control and are the mean (+/-SEM) of three independent experiments with each experiment performed in multiple replicates (n = 3).

3.1.1.20 IAPP(8-18)-Cha₃-(22-28)-OH

CD spectra of IAPP(8-18)-Cha₃-(22-28)-OH revealed a broad and intense minimum related to β -sheets and β -turns (Fig. 88A). At a concentration of 3 μM the minimum was around 225 nm. At 5 μM , the minimum was shifted towards 230 nm. The signal intensity of these two spectra was comparable. IAPP(8-18)-Cha₃-(22-28)-OH also displayed a strong signal loss upon aggregation. At a concentration of 20 μM , there was almost no CD signal detectable. In case of IAPP(8-18)-Cha₃-(22-28)-OH, CD measurements done with a peptide stock in HCl instead of HFiP showed a minimum around 225 nm (Fig. 88B). The minimum was only slightly shifted towards lower wavelengths but with a higher signal intensity at around 216 nm when compared to that in 1xb containing 1% HFiP. Even in aqueous solution without HFiP CD spectra of IAPP(8-18)-Cha₃-(22-28)-OH seemed to contain more β -turn than β -sheet content.

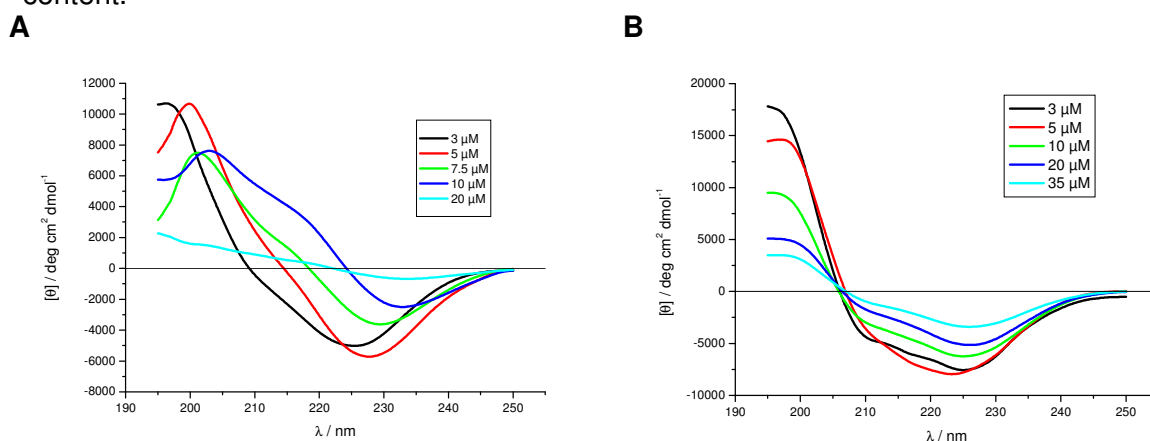


Fig. 88: Concentration dependent CD spectra of IAPP(8-18)-Cha₃-(22-28)-OH. (A) Peptide was taken from a stock solution of 1 mM in HFiP measured in 1xb 1% HFiP, pH 7.4 (from [161]). (B) Incubations were made with peptide from stock solutions in 1 mM HCl measured in 1xb 1 μM HCl, pH 7.

IAPP(8-18)-Cha₃-(22-28)-OH did not form fibrils as suggested by the results of ThT assays (Fig. 89A), Congo Red staining (Fig. 90) and TEM imaging (Fig. 89B).

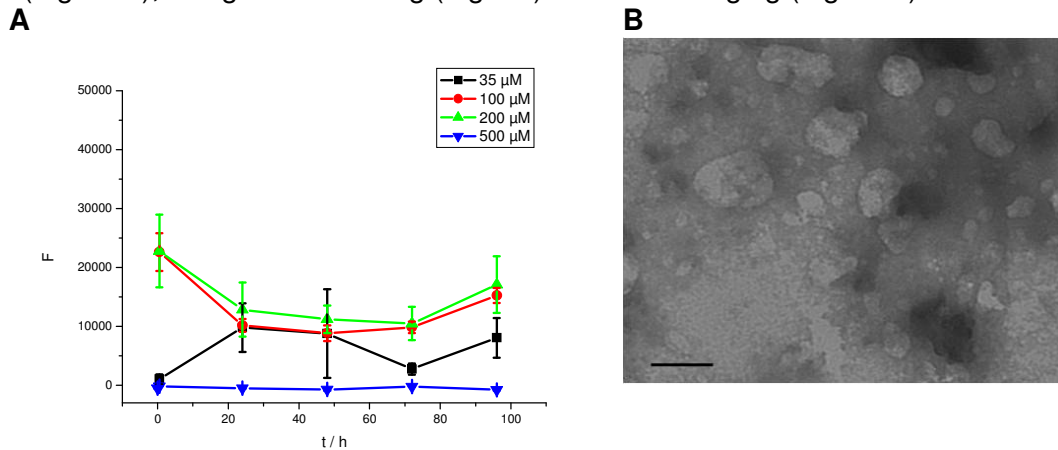


Fig. 89: (A) ThT assays of IAPP(8-18)-Cha₃-(22-28)-OH at different concentrations in 1x 1% HFiP, pH 7.4 (partially from [161]). Data are means of 3 assays after subtraction of buffer values +/- standard error of the mean (SEM) with each experiment performed in multiple replicates (n = 3). (B) TEM picture of IAPP(8-18)-Cha₃-(22-28)-OH. The peptide was incubated at 500 μM for 7 d in 10 mM sodium phosphate buffer at pH 7.4 containing 1% HFiP. Scale bar: 100 nm.

Even though the ThT assays displayed unspecific binding of IAPP(8-18)-Cha₃-(22-28)-OH to ThT, the TEM picture only showed amorphous aggregates. Congo Red staining also revealed no birefringence under cross polarized light.

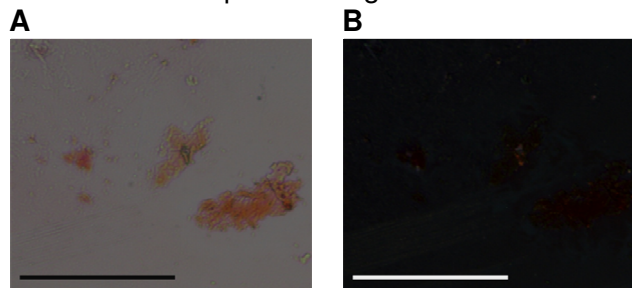


Fig. 90: Microscopic examination of fibrillar aggregates of IAPP(8-18)-Cha₃-(22-28)-OH stained with Congo Red. 1 mM peptide was incubated in 10 mM sodium phosphate buffer at pH 7.4 containing 1% HFiP for 3d and then spotted on a slide. The dried droplet was stained with 200 μM Congo Red in H₂O. Pictures were taken under A normal and B cross polarized light. Scale bar: 100 μm.

IAPP(8-18)-Cha₃-(22-28)-OH was weakly toxic to RIN cells (Fig. 91), comparable to IAPP(8-18)-RRR-(22-28)-OH for example.

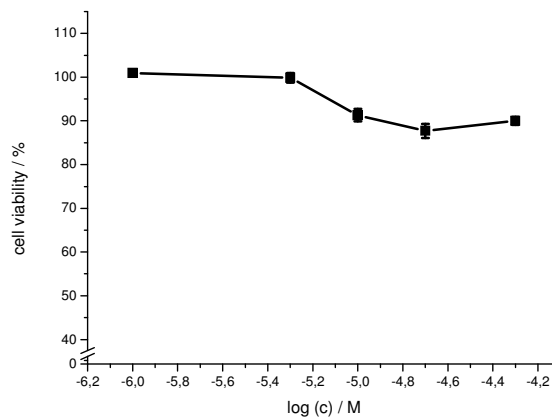


Fig. 91: Cell viability assay of an aged solution of IAPP(8-18)-Cha₃-(22-28)-OH (5 mM in 1xb 1% HFiP for 4 days, pH 7.4) using RIN cells. Data are percentages of control and are the mean (+/-SEM) of three independent experiments with each experiment performed in multiple replicates (n = 3).

3.1.1.21 IAPP(8-18)-SpG-(22-28)-OH

Concentration dependent CD spectra of IAPP(8-18)-SpG-(22-28)-OH displayed a strong minimum at 195 - 200 nm that can be related to random coil structures. The weaker negative signal between 210 nm and 230 nm intended the presence of additional structural elements like β -sheets or β -turns (Fig. 92A). This was somehow a typical spectrum for analogues without hydrophobic elements in the IAPP(19-21) region. At concentrations > 10 μ M the signal intensity started to decrease indicating an aggregation of the peptide.

Additional CD spectra measured in aqueous solution without HFiP (Fig. 92B) showed similar shape and intensity, but a lower aggregation potential compared to the spectra measured in solutions containing 1% HFiP. This behavior was similar to that of IAPP(8-18)-GGG-(22-28)-OH (Fig. 52B).

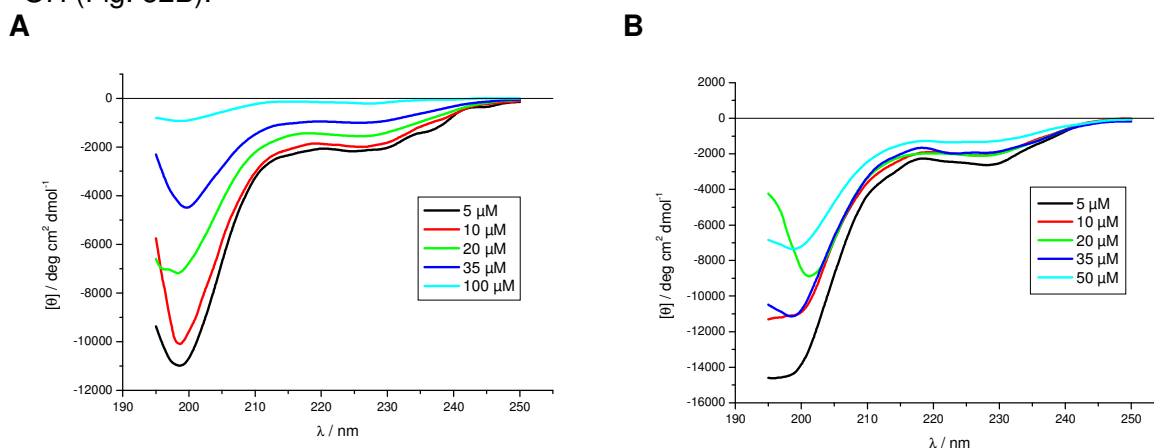


Fig. 92: Concentration dependent CD spectra of IAPP(8-18)-SpG-(22-28)-OH. (A) Peptide was taken from a stock solution of 1 mM in HFiP measured in 1xb 1% HFiP, pH 7.4. (B) Incubations were made with peptide from stock solutions in 1 mM HCl measured in 1xb 1 μ M HCl, pH 7.

The fibril forming potential of IAPP(8-18)-SpG-(22-28)-OH was difficult to interpret. At a concentration of 50 μ M, fibrils were formed but they seemed to get dissolved over time (Fig. 93A). The TEM picture of IAPP(8-18)-SpG-(22-28)-OH at a concentration of 100 μ M showed mixtures of amorphous aggregates and black bundle-like fibrils (Fig. 93B).

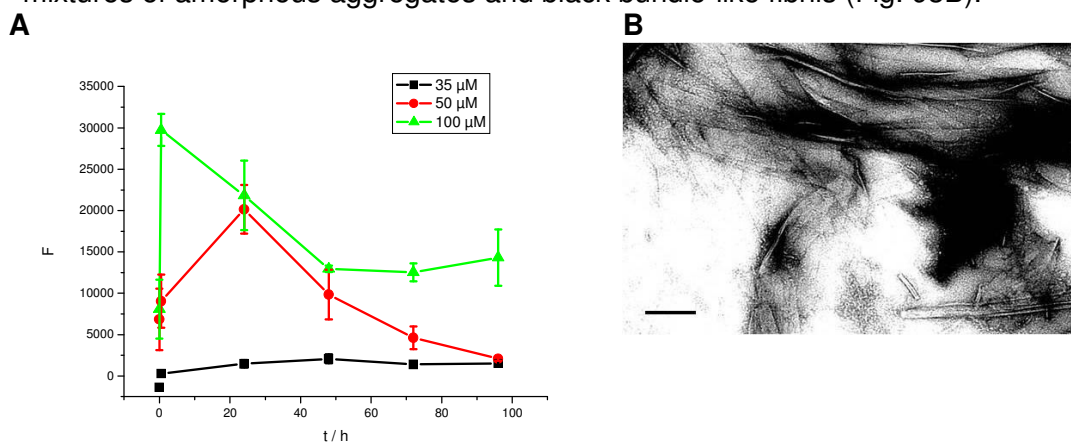


Fig. 93: (A) ThT assays of IAPP(8-18)-SpG-(22-28)-OH at different concentrations in 1xb 1% HFiP, pH 7.4. Data are means of 3 assays after subtraction of buffer values +/- standard error of the mean (SEM) with each experiment performed in multiple replicates (n = 3).

(B) TEM picture of IAPP(8-18)-SpG-(22-28)-OH. The peptide was incubated at 100 μ M for 7 d in 10 mM sodium phosphate buffer at pH 7.4 containing 1% HFIP. Scale bar: 100 nm.

Congo Red staining of aggregates formed by IAPP(8-18)-SpG-(22-28)-OH also displayed large aggregates that were stained with Congo Red and displayed only weak birefringence under cross polarized light (Fig. 94A and B). The pictures obviously displayed mainly amorphous aggregates.

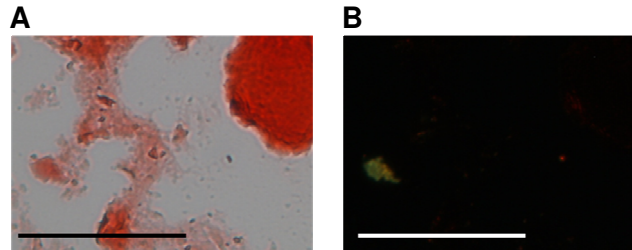


Fig. 94: Microscopic examination of fibrillar aggregates of IAPP(8-18)-SpG-(22-28)-OH stained with Congo Red. 1 mM peptide was incubated in 10 mM sodium phosphate buffer at pH 7.4 containing 1% HFIP for 3d and then spotted on a slide. The dried droplet was stained with 200 μ M Congo Red in H₂O. Pictures were taken under A normal and B cross polarized light. Scale bar: 100 μ m.

Earlier and more recent studies of oligomers formed by IAPP [100, 166] revealed a structure in which FGAIL (IAPP(23-27)) is forming a β -sheet. The sequence NFGAILS alone was shown to form an out-of-register steric zipper [167].

pG is a motif known to induce hairpin formation. In the case of IAPP(8-18)-SpG-(22-28)-OH this might lead to a delayed formation of oligomers with a rigid β -sheet-hairpin- β -sheet structure that cannot be converted into amyloid fibrils. A partial reduction of already formed fibrils might appear due to a newly established equilibrium between fibrils, flexible oligomers that can transform into fibrils and rigid oligomers that cannot be converted into amyloid fibrils.

As seen on Fig. 95 IAPP(8-18)-SpG-(22-28)-OH was toxic to RIN cells, though less toxic than native IAPP(8-28)-OH (Fig. 23).

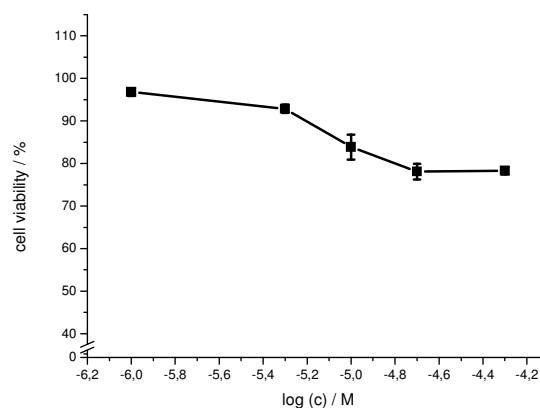


Fig. 95: Cell viability assay of an aged solution of IAPP(8-18)-SpG-(22-28)-OH (5 mM in 1x 1% HFIP for 4 days, pH 7.4) using RIN cells. Data are percentages of control and are the mean (+/-SEM) of three independent experiments with each experiment performed in multiple replicates (n = 3).

3.1.1.22 IAPP(8-18)-pGN-(22-28)-OH

The concentration dependent CD spectra of IAPP(8-18)-pGN-(22-28)-OH (Fig. 96) were similar to those of IAPP(8-18)-SpG-(22-28)-OH. They also displayed a strong minimum at 195 - 200 nm and a weaker negative signal between 210 nm and 230 nm. The signal loss was also occurring at concentrations > 10 μ M, but was not as intense as for IAPP(8-18)-

SpG-(22-28)-OH. This indicated a slightly lower aggregation potential for IAPP(8-18)-pGN-(22-28)-OH compared to IAPP(8-18)-SpG-(22-28)-OH.

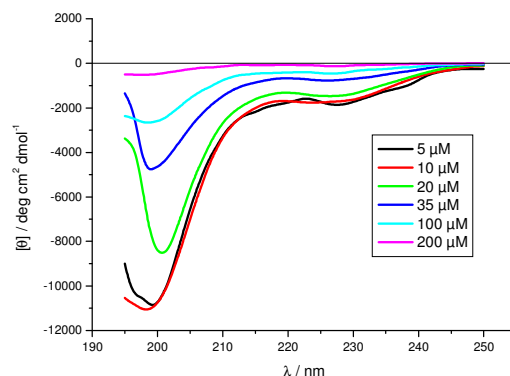


Fig. 96: Concentration dependent CD spectra of IAPP(8-18)-pGN-(22-28)-OH in 1x 1% HFIP, pH 7.4.

ThT fluorescence assays revealed that IAPP(8-18)-pGN-(22-28)-OH started forming fibrils at a concentration of 100 μM (Fig. 97A), at a slightly higher concentration than for IAPP(8-18)-SpG-(22-28)-OH. This correlated with the aggregation potential of both peptides. The TEM image of IAPP(8-18)-pGN-(22-28)-OH at a peptide concentration of 100 μM only displayed fibrils (Fig. 97B).

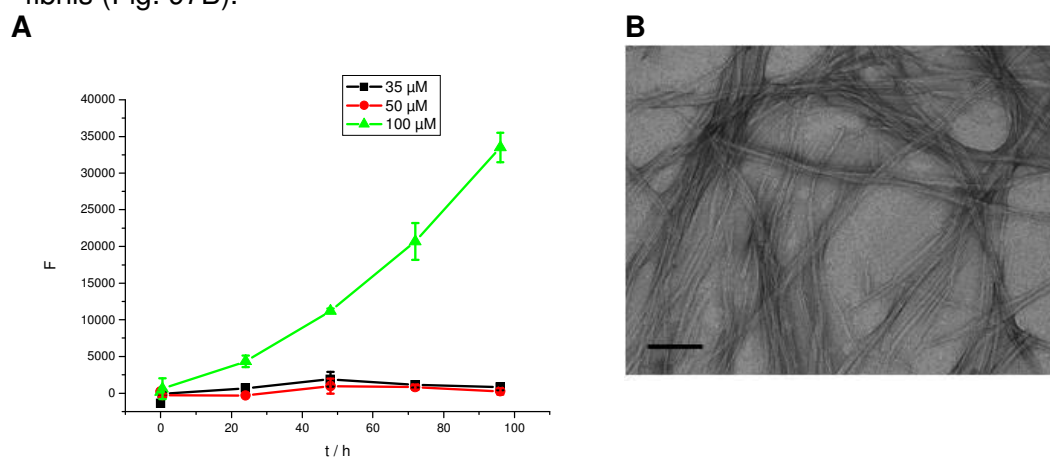


Fig. 97: (A) ThT assays of IAPP(8-18)-pGN-(22-28)-OH at different concentrations in 1x 1% HFIP, pH 7.4. Data are means of 3 assays after subtraction of buffer values \pm standard error of the mean (SEM) with each experiment performed in multiple replicates ($n = 3$).

(B) TEM picture of IAPP(8-18)-pGN-(22-28)-OH. The peptide was incubated at 100 μM for 7 d in 10 mM sodium phosphate buffer at pH 7.4 containing 1% HFIP. Scale bar: 100 nm.

Congo Red stained aggregates of IAPP(8-18)-pGN-(22-28)-OH displayed orange birefringence under cross polarized light (Fig. 98B).

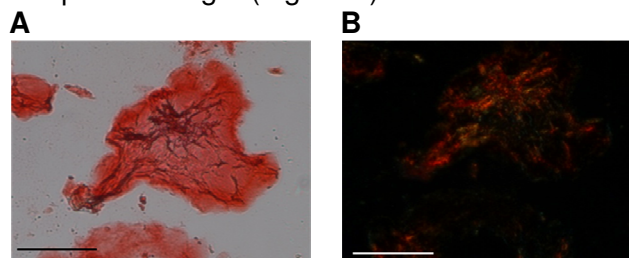


Fig. 98: Microscopic examination of fibrillar aggregates of IAPP(8-18)-pGN-(22-28)-OH stained with Congo Red. 1 mM peptide was incubated in 10 mM sodium phosphate buffer at pH 7.4 containing 1% HFIP for 3d and then spotted on a slide. The dried droplet was stained with 200 μM Congo Red in H_2O . Pictures were taken under A normal and B cross polarized light. Scale bar: 100 μm .

A pathway leading towards the formation of oligomers that cannot be transformed into fibrils like for IAPP(8-18)-SpG-(22-28)-OH did not seem to occur for IAPP(8-18)-pGN-(22-28)-OH. One might conclude, that a hairpin inducing motif like pG at position 20,21 results in oligomers with a structure more similar to native IAPP oligomers since IAPP(8-18)-SpG-(22-28)-OH has a higher aggregation and fibril forming potential than IAPP(8-18)-pGN-(22-28)-OH.

Compared to IAPP(8-18)-SpG-(22-28)-OH IAPP(8-18)-pGN-(22-28)-OH was more toxic to RIN cells (Fig. 99) though also less toxic than IAPP(8-28)-OH (Fig. 23).

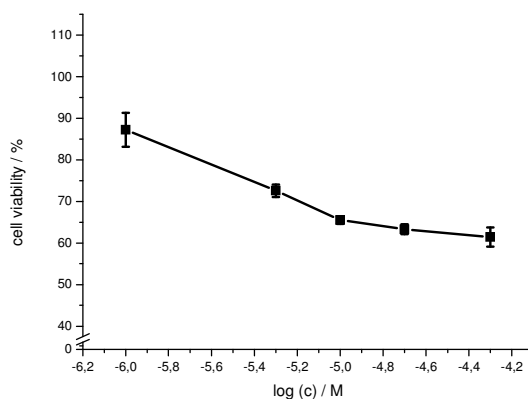


Fig. 99: Cell viability assay of an aged solution of IAPP(8-18)-pGN-(22-28)-OH (5 mM in 1xb 1% HFiP for 4 days, pH 7.4) using RIN cells. Data are percentages of control and are the mean (+/-SEM) of three independent experiments with each experiment performed in multiple replicates (n = 3).

3.1.1.23 IAPP(8-18)-PPP-(22-28)-OH

As shown on Fig. 100, IAPP(8-18)-PPP-(22-28)-OH displayed mainly random coil structures in CD, indicated by a minimum at around 200 nm. A weak minimum at 230 nm indicated the presence of β -sheet and β -turn elements. The signal intensity of spectra at a concentration between 2 and 5 μ M was almost similar. The lowest peptide concentration where a reduction of the intensity of the CD signal was observed was 10 μ M. In general, the intensity of the signal of the CD spectra of IAPP(8-18)-PPP-(22-28)-OH was high. The PPP motif was expected to adopt a PPII helical structure. At room temperature, this structure shows CD spectra typically referred to as random coil with a strong minimum around 200 nm. The high intensity of the signal at around 200 nm might have been due to the formation of a PPII helix.

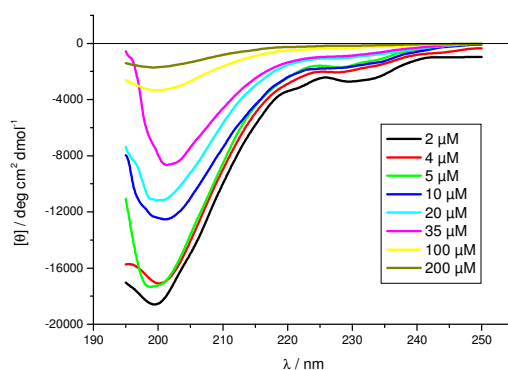


Fig. 100: Concentration dependent CD spectra of IAPP(8-18)-PPP-(22-28)-OH in 1xb 1% HFiP, pH 7.4.

Under the conditions used for ThT assays, IAPP(8-18)-PPP-(22-28)-OH was not forming fibrils (Fig. 101A). The TEM picture of IAPP(8-18)-PPP-(22-28)-OH only showed amorphous

aggregates (Fig. 101B) and the Congo Red staining assay revealed only weak Congo Red binding and no birefringence under cross polarized light (Fig. 102A and B).

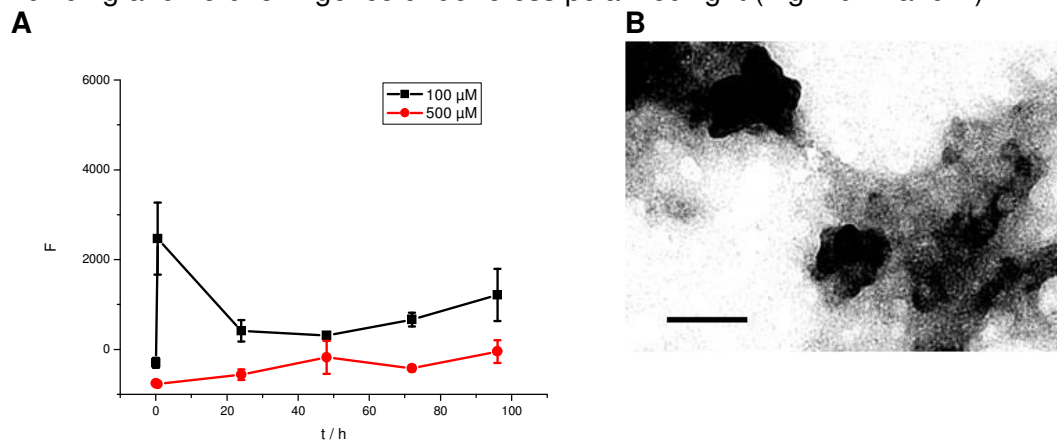


Fig. 101: (A) ThT assays of IAPP(8-18)-PPP-(22-28)-OH at different concentrations in 1x 1% HFIP, pH 7.4. Data are means of 3 assays after subtraction of buffer values \pm standard error of the mean (SEM) with each experiment performed in multiple replicates ($n = 3$). (B) TEM picture of IAPP(8-18)-PPP-(22-28)-OH. The peptide was incubated at 500 μ M for 7 d in 10 mM sodium phosphate buffer at pH 7.4 containing 1% HFIP. Scale bar: 100 nm.

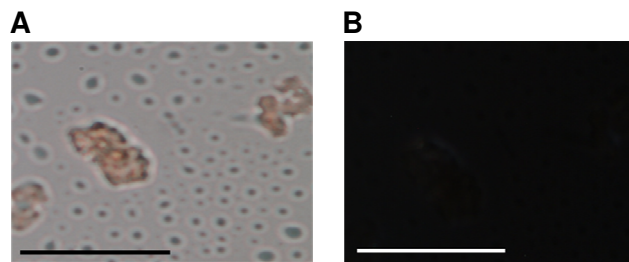


Fig. 102: Microscopic examination of aggregates of IAPP(8-18)-PPP-(22-28)-OH stained with Congo Red. 1 mM peptide was incubated in 10 mM sodium phosphate buffer at pH 7.4 containing 1% HFIP for 3d and then spotted on a slide. The dried droplet was stained with 200 μ M Congo Red in H₂O. Pictures were taken under A normal and B cross polarized light. Scale bar: 100 μ m.

As indicated by MTT reduction assays using RIN cells, IAPP(8-18)-PPP-(22-28)-OH was not toxic (Fig. 103). Due to the introduction of Prolines into the sequence of IAPP(8-28)-OH, the formation of several intra- and intermolecular hydrogen bonds. This could have been the reason for the lack of amyloidogenicity and toxicity of IAPP(8-18)-PPP-(22-28)-OH.

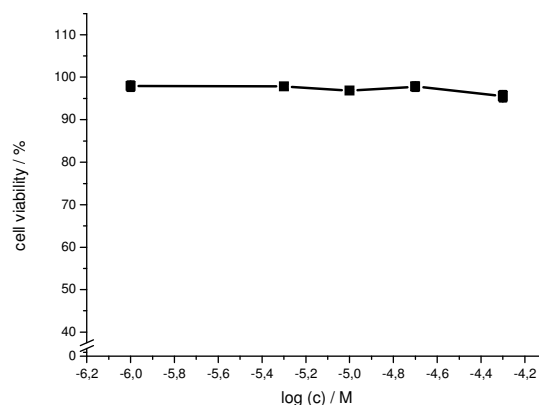


Fig. 103: Cell viability assay of an aged solution of IAPP(8-18)-PPP-(22-28)-OH (5 mM in 1x 1% HFIP for 4 days, pH 7.4) using RIN cells. Data are percentages of control and are the mean (\pm SEM) of three independent experiments with each experiment performed in multiple replicates ($n = 3$).

3.1.1.24 IAPP(8-18)-(K(Ac))₃-(22-28)-OH

The CD spectra of IAPP(8-18)-(K(Ac))₃-(22-28)-OH showed a strong minimum at 195 - 200 nm related to random coil structures and weaker negative signal between 210 nm and 230 nm related to β -sheets and β -turns (Fig. 104A). The signal intensity decreased already at a peptide concentration of 2 μ M, indicating the presence of soluble oligomers at 5 μ M. All aspects of the concentration dependent CD spectra of IAPP(8-18)-(K(Ac))₃-(22-28)-OH like the overall shape, the signal intensity and the concentration dependent signal loss were similar to those of IAPP(8-28)-OH (Fig. 23A).

In aqueous solution without HFiP, IAPP(8-18)-(K(Ac))₃-(22-28)-OH also displayed mainly random coil structures in CD measurements (Fig. 104B). At a peptide concentration of 100 μ M, the CD spectrum showed a negative signal between 210 nm and 230 nm related to β -sheets and β -turns that was even more intense than the negative signal at around 200 nm. Oligomers of IAPP(8-18)-(K(Ac))₃-(22-28)-OH formed in aqueous solution obviously possessed more β -sheet and β -turn structure than oligomers formed in solutions containing 1% HFiP.

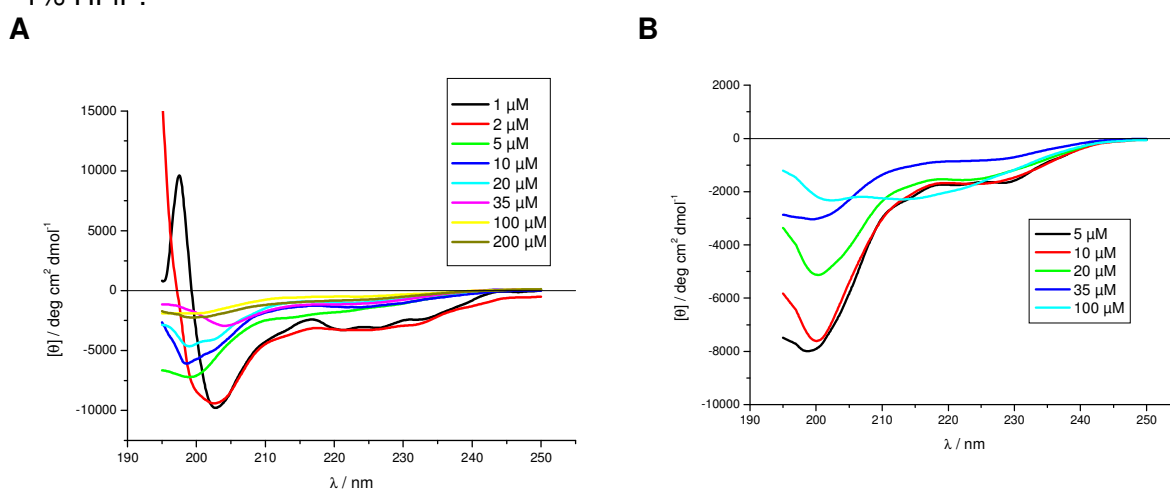


Fig. 104: Concentration dependent CD spectra of IAPP(8-18)-(K(Ac))₃-(22-28)-OH.

(A) Peptide was taken from a stock solution of 1 mM in HFiP measured in 1xb 1% HFiP, pH 7.4 (partially from [164]).

(B) Incubations were made with peptide from stock solutions in 1 mM HCl measured in 1xb 1 μ M HCl, pH 7.

ThT fluorescence assays revealed that IAPP(8-18)-(K(Ac))₃-(22-28)-OH started forming fibrils already at 10 μ M (Fig. 105A) meaning it had a similar fibril forming potential as IAPP(8-18)-SGN-(22-28)-OH (Fig. 25A). The TEM picture of IAPP(8-18)-(K(Ac))₃-(22-28)-OH also clearly showed fibrillar structures (Fig. 105B).

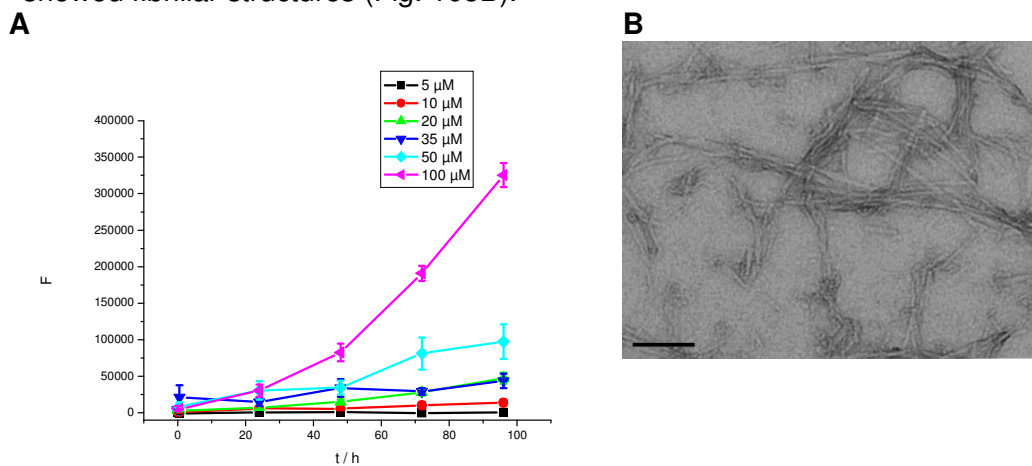


Fig. 105: (A) ThT assays of IAPP(8-18)-(K(Ac))₃-(22-28)-OH at different concentrations in 1xb 1% HFIP, pH 7.4 (partially from [164]). Data are means of 3 assays after subtraction of buffer values +/- standard error of the mean (SEM) with each experiment performed in multiple replicates (n = 3). (B) TEM picture of IAPP(8-18)-(K(Ac))₃-(22-28)-OH. The peptide was incubated at 100 μM for 7 d in 10 mM sodium phosphate buffer at pH 7.4 containing 1% HFIP. Scale bar: 100 nm.

Congo Red staining of fibrillar aggregates of IAPP(8-18)-(K(Ac))₃-(22-28)-OH displayed a clear yellow/green birefringence under cross polarized light (Fig. 106B). This was a strong indication for fibril formation.

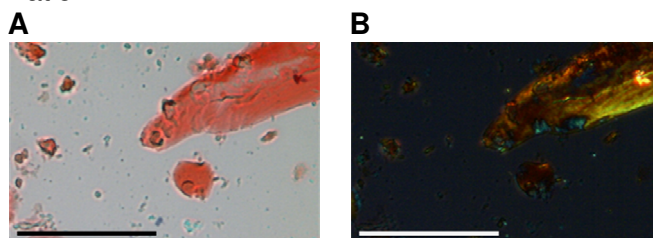


Fig. 106: Microscopic examination of fibrillar aggregates of IAPP(8-18)-(K(Ac))₃-(22-28)-OH stained with Congo Red. 1 mM peptide was incubated in 10 mM sodium phosphate buffer at pH 7.4 containing 1% HFIP for 3d and then spotted on a slide. The dried droplet was stained with 200 μM Congo Red in H₂O. Pictures were taken under A normal and B cross polarized light. Scale bar: 100 μm.

Cell viability assays showed that IAPP(8-18)-(K(Ac))₃-(22-28)-OH was the most toxic peptide among the designed analogues (Fig. 107) and the only one that was more toxic than the native IAPP(8-28)-OH (Fig. 23). It also had a higher fibril forming potential than IAPP(8-28)-OH (Fig. 21A).

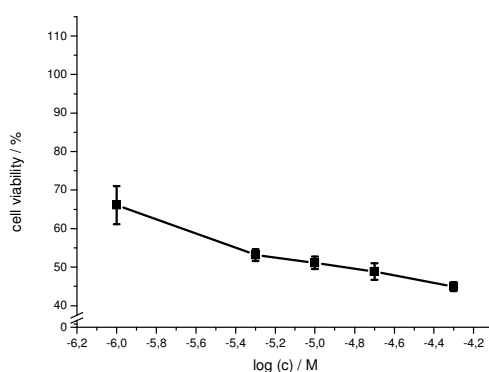


Fig. 107: Cell viability assay of an aged solution of IAPP(8-18)-(K(Ac))₃-(22-28)-OH (5 mM in 1xb 1% HFIP for 4 days, pH 7.4) using RIN cells. Data are percentages of control and are the mean (+/-SEM) of three independent experiments with each experiment performed in multiple replicates (n = 3).

Table 3: Overview of ThT and cell viability assays performed of the analogues of IAPP(8-28). Results of “+” indicate fibril formation, whereas “-” indicate no fibril formation within the 5 days of incubation of the solution at the given peptide concentration. For the cell viability assays, results of “+++” mean high toxicity towards RIN cells, “++” means medium toxicity, “+/-” means low toxicity and “-” mean no toxicity.

Sequence	ThT										Tox
	5 μM	10 μM	20 μM	35 μM	50 μM	100 μM	200 μM	500 μM	5 mM	10 mM	
IAPP(8-18)-OH						-	-	+			-
IAPP(22-28)-OH						-	-	-	-	-	-
IAPP(8-28)-OH			-	+	+	+					+++
IAPP(8-18)-SGN-(22-28)-OH	-	+				+					+++
IAPP(8-18)-Aoc-(22-28)-OH			-	+		+					+++
IAPP(8-18)-Peg-(22-28)-OH				-		+					++
IAPP(8-18)-KKK-(22-28)-OH				-		-	-	-			++
IAPP(8-18)-Dap ₃ -(22-28)-OH						-	-	-			-
IAPP(8-18)-RRR-(22-28)-OH						-	-	-			-
IAPP(8-18)-DDD-(22-28)-OH						-		-			-
IAPP(8-18)-GGG-(22-28)-OH				-		+	+				++
IAPP(8-18)-AAA-(22-28)-OH				-		+	+				++
IAPP(8-18)-VVV-(22-28)-OH		-	+	+	+	+	+				+++
IAPP(8-18)-LLL-(22-28)-OH			-	-		-	+	+			++
IAPP(8-18)-III-(22-28)-OH			-	+	+	+	+				+++
IAPP(8-18)-Nle ₃ -(22-28)-OH			-	+	+	+	+				+++
IAPP(8-18)-2(Aoc) ₃ -(22-28)-OH			-	+		+					+++
IAPP(8-18)-TTT-(22-28)-OH			-	+		+					++
IAPP(8-18)-FFF-(22-28)-OH				-	+	+	+				++
IAPP(8-18)-Cha ₃ -(22-28)-OH				-		-	-	-			+/-
IAPP(8-18)-SpG-(22-28)-OH				-	+	+					+/-
IAPP(8-18)-pGN-(22-28)-OH				-	-	+					++
IAPP(8-18)-PPP-(22-28)-OH						-		-			-
IAPP(8-18)-K(Ac) ₃ -(22-28)-OH	-	+	+	+	+	+	+				+++

3.1.1.25 IAPP(8-18)-KK(Ac)K(Ac)-(22-28)-OH

The concentration dependent CD spectra of IAPP(8-18)-KK(Ac)K(Ac)-(22-28)-OH showed a strong minimum at 195 - 200 nm that can be related to random coil structures. A weaker negative signal between 210 nm and 230 nm indicated the presence of additional structural elements like β -sheets and β -turns (Fig. 108). The signal intensity of spectra at a concentration between 5 and 10 μ M was almost similar. The lowest peptide concentration where a reduction of the intensity of the CD signal was observed was 20 μ M. This indicated a lower aggregation potential of IAPP(8-18)-KK(Ac)K(Ac)-(22-28)-OH as compared to IAPP(8-18)-(K(Ac))₃-(22-28)-OH. The magnitude of the CD spectra was much higher for IAPP(8-18)-KK(Ac)K(Ac)-(22-28)-OH compared to the spectra of IAPP(8-18)-(K(Ac))₃-(22-28)-OH (Fig. 104A). This can be interpreted as a sign that IAPP(8-18)-(K(Ac))₃-(22-28)-OH was not monomeric at a concentration of 5 μ M.

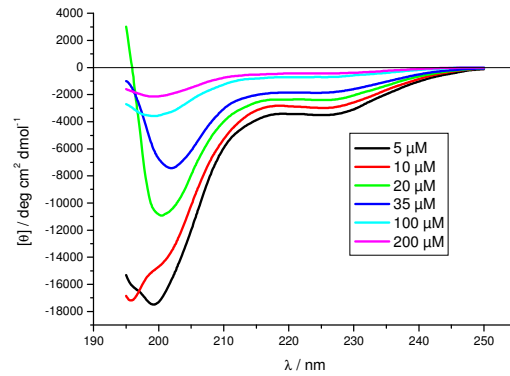


Fig. 108: Concentration dependent CD spectra of IAPP(8-18)-KK(Ac)K(Ac)-(22-28)-OH in 1x 1% HFIP, pH 7.4.

ThT studies of IAPP(8-18)-KK(Ac)K(Ac)-(22-28)-OH indicated a lower fibril formation potency as compared to IAPP(8-18)-(K(Ac))₃-(22-28)-OH. IAPP(8-18)-KK(Ac)K(Ac)-(22-28)-OH started forming fibrils at a concentration of 35 μM (Fig. 109A) which was verified by TEM (Fig. 109B).

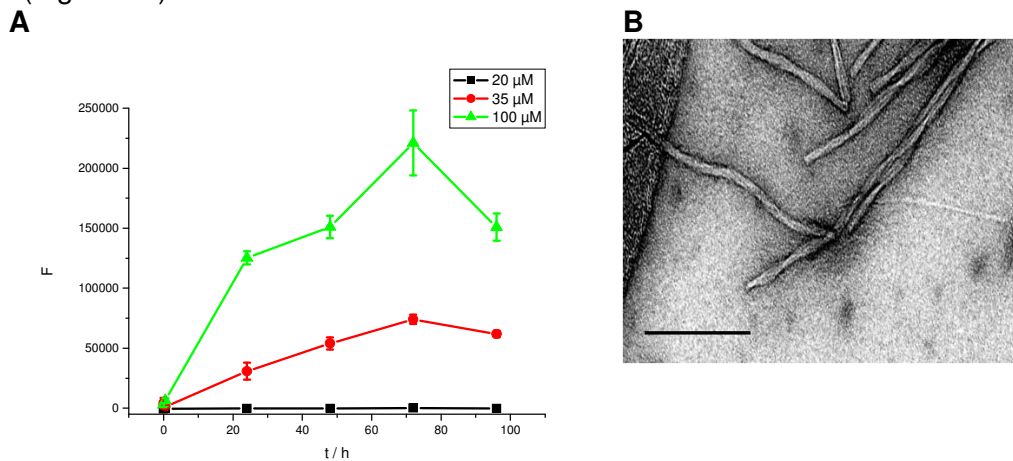


Fig. 109: (A) ThT assays of IAPP(8-18)-KK(Ac)K(Ac)-(22-28)-OH at different concentrations in 1x 1% HFIP, pH 7.4. Data are means of 3 assays after subtraction of buffer values +/- standard error of the mean (SEM) with each experiment performed in multiple replicates (n = 3). (B) TEM picture of IAPP(8-18)-KK(Ac)K(Ac)-(22-28)-OH. The peptide was incubated at 35 μM for 7 d in 10 mM sodium phosphate buffer at pH 7.4 containing 1% HFIP. Scale bar: 100 nm.

Congo Red staining and microscopic examination of aggregates formed by IAPP(8-18)-KK(Ac)K(Ac)-(22-28)-OH displayed orange/yellow birefringence under cross polarized light (Fig. 110B). This was another proof for the fibril forming ability of IAPP(8-18)-KK(Ac)K(Ac)-(22-28)-OH.

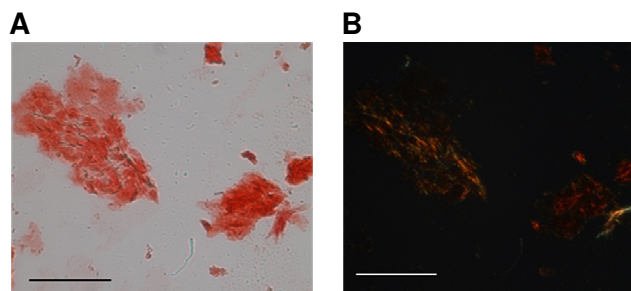


Fig. 110: Microscopic examination of fibrillar aggregates of IAPP(8-18)-KK(Ac)K(Ac)-(22-28)-OH stained with Congo Red. 1 mM peptide was incubated in 10 mM sodium phosphate buffer at pH 7.4 containing 1% HFIP for 3d and then spotted on a slide. The dried droplet was stained with 200 μM Congo Red in H₂O. Pictures were taken under A normal and B cross polarized light. Scale bar: 100 μm.

As shown on Fig. 111 aggregates of IAPP(8-18)-KK(Ac)K(Ac)-(22-28)-OH were highly toxic to RIN cells. Their toxicity was about as high as for aggregates of IAPP(8-28)-OH (Fig. 23) but lower than for aggregates of IAPP(8-18)-(K(Ac))₃-(22-28)-OH (Fig. 107). This also correlated with the fibril forming potential of these peptides.

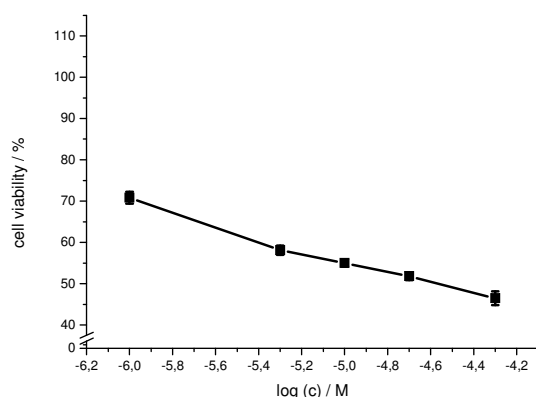


Fig. 111: Cell viability assay of an aged solution of IAPP(8-18)-KK(Ac)K(Ac)-(22-28)-OH (5 mM in 1xb 1% HFIP for 4 days, pH 7.4) using RIN cells. Data are percentages of control and are the mean (+/-SEM) of three independent experiments with each experiment performed in multiple replicates (n = 3).

3.1.1.26 IAPP(8-18)-K(Ac)KK(Ac)-(22-28)-OH

The concentration dependent CD spectra of IAPP(8-18)-K(Ac)KK(Ac)-(22-28)-OH (Fig. 112) exhibited a strong minimum at 195 - 200 nm related to random coil structures. The weaker negative signal between 210 nm and 230 nm indicated the presence of β -sheets and β -turns. Between 5 and 10 μ M the signal intensity was only slightly reduced. The lowest peptide concentration where a reduction of the intensity of the CD signal was observed was 20 μ M.

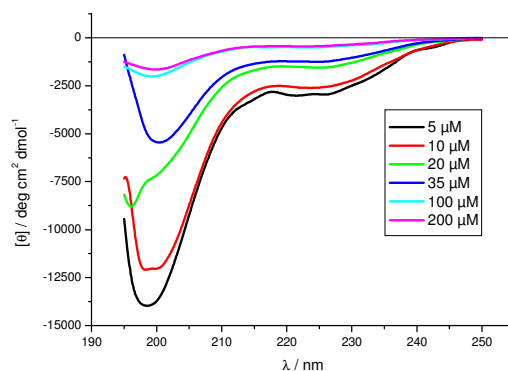


Fig. 112: Concentration dependent CD spectra of IAPP(8-18)-K(Ac)KK(Ac)-(22-28)-OH in 1xb 1% HFIP, pH 7.4.

ThT fluorescence assays revealed that IAPP(8-18)-K(Ac)KK(Ac)-(22-28)-OH started to form fibrils at a peptide concentration of 35 μ M (Fig. 113A). IAPP(8-18)-KK(Ac)K(Ac)-(22-28)-OH also started forming fibrils at 35 μ M (Fig. 109A) but displayed a more intense fluorescence signal. The TEM image of an aged solution of IAPP(8-18)-K(Ac)KK(Ac)-(22-28)-OH at a concentration of 35 μ M showed mainly fibrils but also a small amount of amorphous aggregates (Fig. 113B). This indicated a slightly weaker fibril forming potential for IAPP(8-18)-K(Ac)KK(Ac)-(22-28)-OH than for IAPP(8-18)-KK(Ac)K(Ac)-(22-28)-OH.

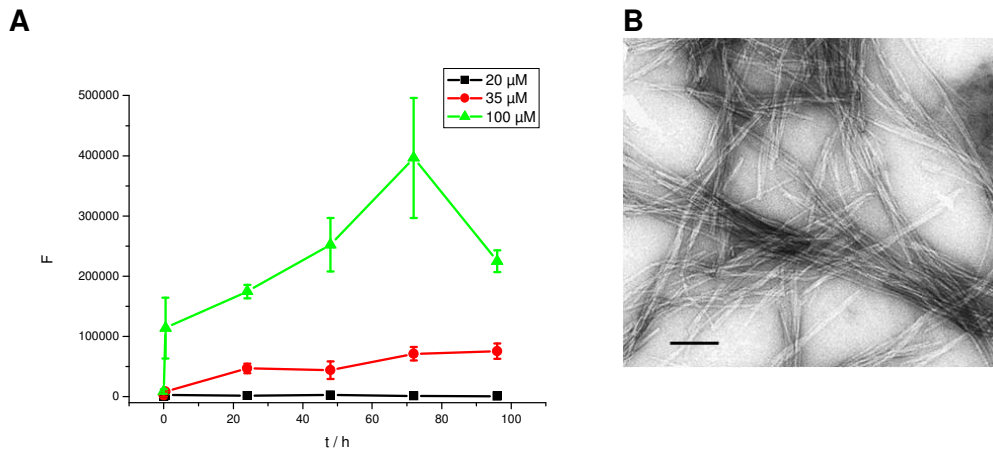


Fig. 113: (A) ThT assays of IAPP(8-18)-K(Ac)KK(Ac)-(22-28)-OH at different concentrations in 1xb 1% HFIP, pH 7.4. Data are means of 3 assays after subtraction of buffer values +/- standard error of the mean (SEM) with each experiment performed in multiple replicates (n = 3).

(B) TEM picture of IAPP(8-18)-K(Ac)KK(Ac)-(22-28)-OH. The peptide was incubated at 35 μM for 7 d in 10 mM sodium phosphate buffer at pH 7.4 containing 1% HFIP. Scale bar: 100 nm.

Staining of aggregates of IAPP(8-18)-K(Ac)KK(Ac)-(22-28)-OH with Congo Red also revealed the formation of amyloid fibrils. Stained aggregates showed intense red color under normal light (Fig. 114A) and displayed green, yellow and orange birefringence under cross polarized light (Fig. 114B).

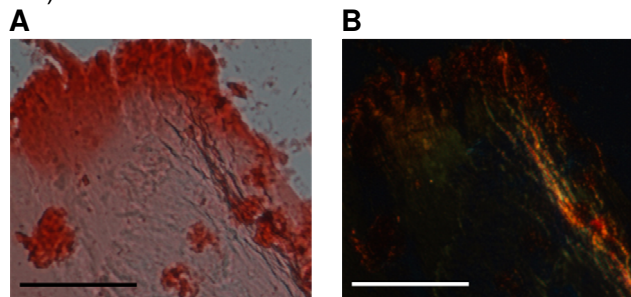


Fig. 114: Microscopic examination of fibrillar aggregates of IAPP(8-18)-K(Ac)KK(Ac)-(22-28)-OH stained with Congo Red. 1 mM peptide was incubated in 10 mM sodium phosphate buffer at pH 7.4 containing 1% HFIP for 3d and then spotted on a slide. The dried droplet was stained with 200 μM Congo Red in H₂O. Pictures were taken under A normal and B cross polarized light. Scale bar: 100 μm.

Aged solutions of IAPP(8-18)-K(Ac)KK(Ac)-(22-28)-OH were toxic to RIN cells (Fig. 115), but less toxic than aged solutions of IAPP(8-18)-KK(Ac)K(Ac)-(22-28)-OH (Fig. 111). This correlated with the fibril forming potentials of these two peptides.

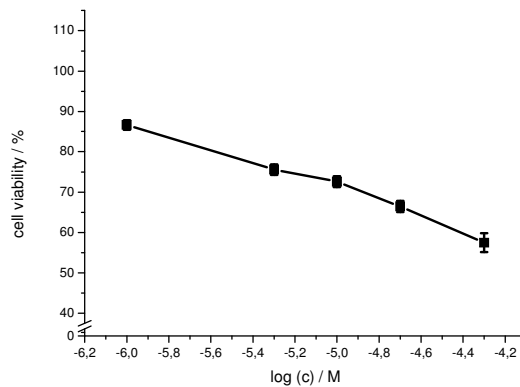


Fig. 115: Cell viability assay of an aged solution of IAPP(8-18)-K(Ac)K(Ac)-(22-28)-OH (5 mM in 1xb 1% HFIP for 4 days, pH 7.4) using RIN cells. Data are percentages of control and are the mean (+/-SEM) of three independent experiments with each experiment performed in multiple replicates (n = 3).

3.1.1.27 IAPP(8-18)-K(Ac)K(Ac)K-(22-28)-OH

The concentration dependent CD spectra of IAPP(8-18)-K(Ac)K(Ac)K-(22-28)-OH showed a strong minimum at 195 - 200 nm (Fig. 116). This was related to random coil structures. The weaker negative signal between 210 nm and 230 nm indicated the presence of structural elements like β -sheets and β -turns. The signal intensities of the CD spectra at 5 μ M and at 10 μ M was almost identical. The lowest peptide concentration where a reduction of the intensity of the CD signal was observed was 20 μ M. Overall shape, signal intensity and the concentration dependent signal loss of the CD spectra are comparable to the CD data of IAPP(8-18)-K(Ac)K(Ac)K-(22-28)-OH (Fig. 128).

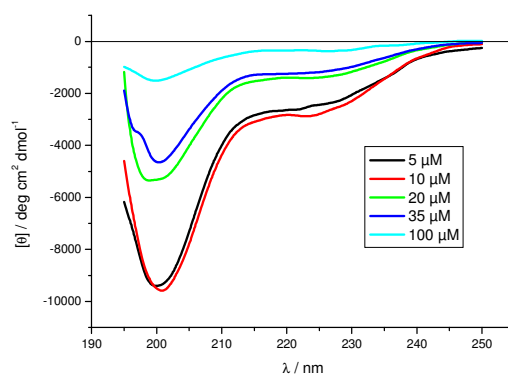


Fig. 116: Concentration dependent CD spectra of IAPP(8-18)-K(Ac)K(Ac)K-(22-28)-OH in 1xb 1% HFIP, pH 7.4.

IAPP(8-18)-K(Ac)K(Ac)K-(22-28)-OH started forming fibrils at a concentration of 200 μ M. Clear fibril formation was observed in the ThT assay at 500 μ M peptide concentration (Fig. 117A). The TEM picture of IAPP(8-18)-K(Ac)K(Ac)K-(22-28)-OH at a concentration of 200 μ M showed the presence of both fibrils and amorphous aggregates (Fig. 117B).

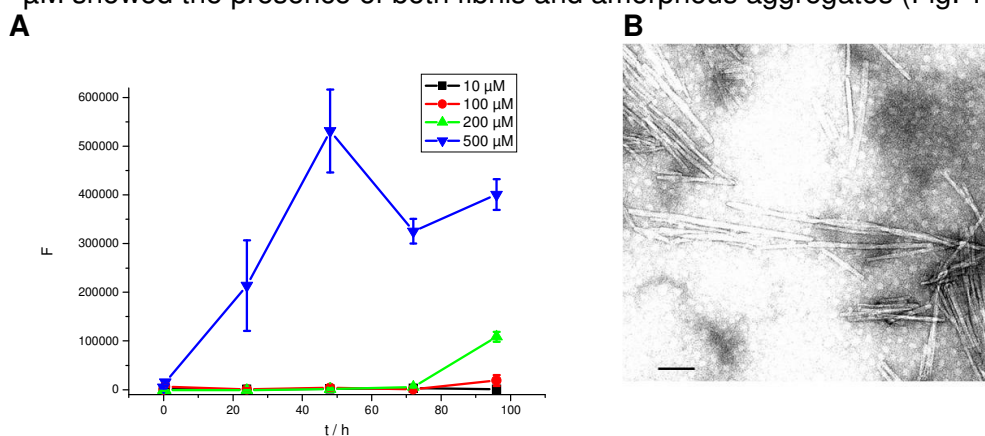


Fig. 117: (A) ThT assays of IAPP(8-18)-K(Ac)K(Ac)K-(22-28)-OH at different concentrations in 1xb 1% HFIP, pH 7.4. Data are means of 3 assays after subtraction of buffer values +/- standard error of the mean (SEM) with each experiment performed in multiple replicates (n = 3).

(B) TEM picture of IAPP(8-18)-K(Ac)K(Ac)K-(22-28)-OH. The peptide was incubated at 200 μ M for 7 d in 10 mM sodium phosphate buffer at pH 7.4 containing 1% HFIP. Scale bar: 100 nm.

Congo Red staining of IAPP(8-18)-K(Ac)K(Ac)K-(22-28)-OH revealed clear orange and weak green birefringence under cross polarized light (Fig. 118B). This indicated the formation of amyloid fibrils.

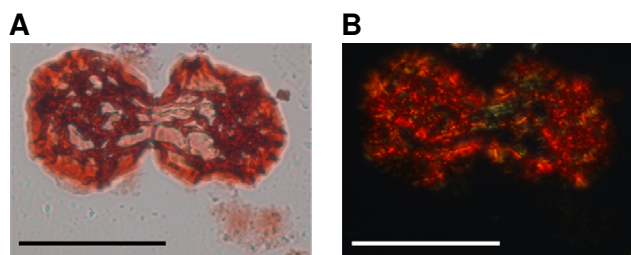


Fig. 118: Microscopic examination of fibrillar aggregates of IAPP(8-18)-K(Ac)K(Ac)K-(22-28)-OH stained with Congo Red. 1 mM peptide was incubated in 10 mM sodium phosphate buffer at pH 7.4 containing 1% HFIP for 3d and then spotted on a slide. The dried droplet was stained with 200 µM Congo Red in H₂O. Pictures were taken under A normal and B cross polarized light. Scale bar: 100 µm.

Cell viability assays showed that aged aggregates of IAPP(8-18)-K(Ac)K(Ac)K-(22-28)-OH were toxic to RIN cells (Fig. 119).

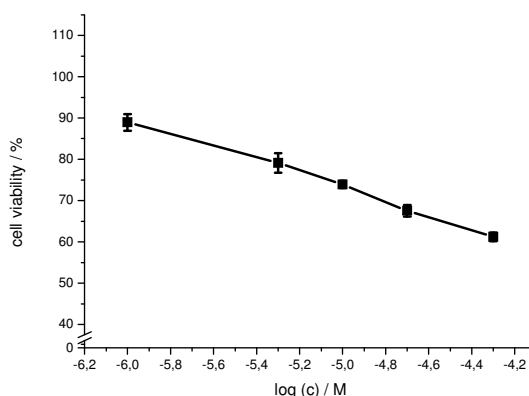


Fig. 119: Cell viability assay of an aged solution of IAPP(8-18)-K(Ac)K(Ac)K-(22-28)-OH (5 mM in 1x1% HFIP for 4 days, pH 7.4) using RIN cells. Data are percentages of control and are the mean (+/-SEM) of three independent experiments with each experiment performed in multiple replicates (n = 3).

3.1.1.28 IAPP(8-18)-KKK(Ac)-(22-28)-OH

CD spectra of IAPP(8-18)-KKK(Ac)-(22-28)-OH displayed a strong minimum at 195 - 200 nm related to random coil structures. The weaker negative signal between 210 nm and 230 nm can be related to the presence of additional structural elements like β -sheets and β -turns (Fig. 120). The signal intensity of spectra at a concentration between 5 and 10 µM was almost similar. The lowest peptide concentration where a reduction of the intensity of the CD signal was observed was 20 µM. This indicated a much lower aggregation potential of IAPP(8-18)-KKK(Ac)-(22-28)-OH as compared to IAPP(8-18)-(K(Ac))₃-(22-28)-OH (Fig. 104).

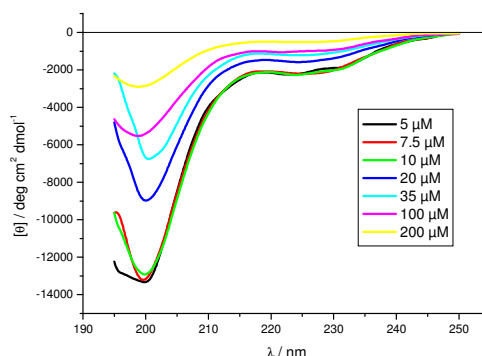


Fig. 120: Concentration dependent CD spectra of IAPP(8-18)-KKK(Ac)-(22-28)-OH in 1x1% HFIP, pH 7.4.

IAPP(8-18)-KKK(Ac)-(22-28)-OH did not form fibrils until a concentration of 500 μM . The fibrils formed at 500 μM exhibited strong ThT binding as evidenced ThT binding studies (Fig. 121A) and a TEM picture that was full of fibrils (Fig. 121B).

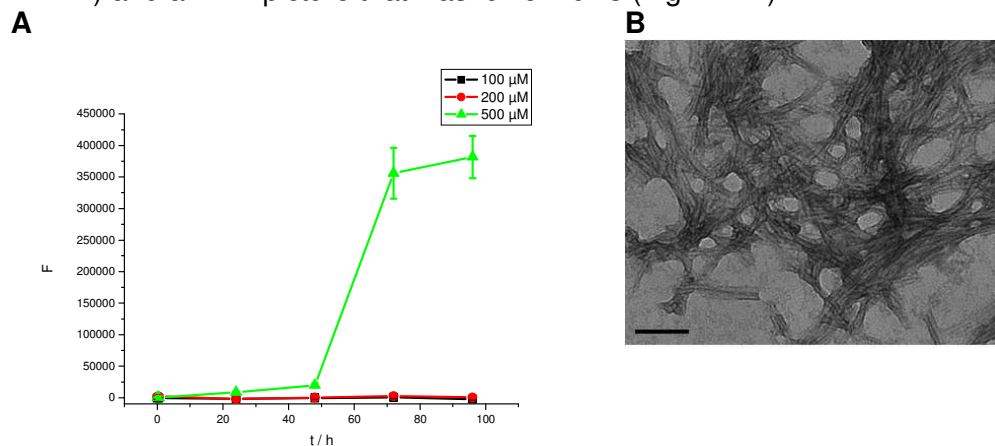


Fig. 121: (A) ThT assays of IAPP(8-18)-KKK(Ac)-(22-28)-OH at different concentrations in 1xb 1% HFIP, pH 7.4. Data are means of 3 assays after subtraction of buffer values \pm standard error of the mean (SEM) with each experiment performed in multiple replicates ($n = 3$).

(B) TEM picture of IAPP(8-18)-KKK(Ac)-(22-28)-OH. The peptide was incubated at 500 μM for 7 d in 10 mM sodium phosphate buffer at pH 7.4 containing 1% HFIP. Scale bar: 100 nm.

Results of the Congo Red staining assay of aggregates of IAPP(8-18)-KKK(Ac)-(22-28)-OH also supported the presence of cross- β -structures indicated by a yellow/green birefringence under cross polarized light (Fig. 122B).

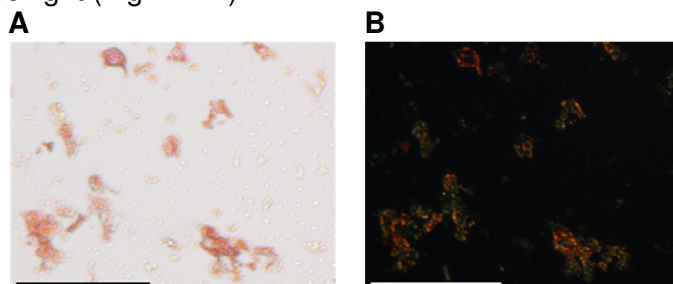


Fig. 122: Microscopic examination of fibrillar aggregates of IAPP(8-18)-KKK(Ac)-(22-28)-OH stained with Congo Red. 1 mM peptide was incubated in 10 mM sodium phosphate buffer at pH 7.4 containing 1% HFIP for 3d and then spotted on a slide. The dried droplet was stained with 200 μM Congo Red in H_2O . Pictures were taken under A normal and B cross polarized light. Scale bar: 100 μm .

The toxicity of aggregates of IAPP(8-18)-KKK(Ac)-(22-28)-OH (Fig. 123) was much lower than that of aggregates of IAPP(8-18)-(K(Ac))₃-(22-28)-OH (Fig. 107) and almost similar to that of aggregates of IAPP(8-18)-KKK-(22-28)-OH (Fig. 39). It appeared thus that the presence of two non-acetylated lysines at position 19 and 20 played a role for the toxicity of the aggregates of the peptide.

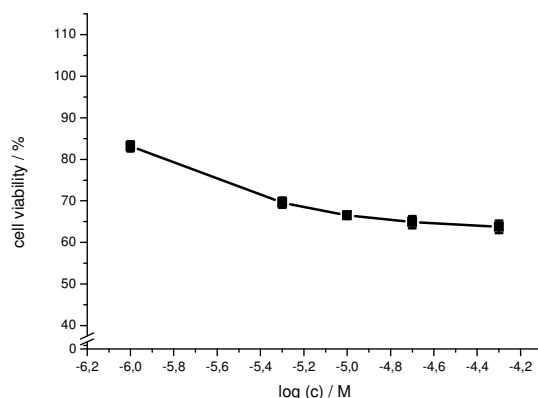


Fig. 123: Cell viability assay of an aged solution of IAPP(8-18)-KKK(Ac)-(22-28)-OH (5 mM in 1xb 1% HFIP for 4 days, pH 7.4) using RIN cells. Data are percentages of control and are the mean (+/-SEM) of three independent experiments with each experiment performed in multiple replicates (n = 3).

3.1.1.29 IAPP(8-18)-KK(Ac)K-(22-28)-OH

CD spectra of IAPP(8-18)-KK(Ac)K-(22-28)-OH displayed a strong minimum at 195 - 200 nm that indicated predominantly random coil structures (Fig. 124). A weaker negative signal between 210 nm and 230 nm intended the presence of additional structural elements like β -sheets and β -turns. The signal intensity of spectra at a concentration between 5 and 10 μ M was almost similar. The lowest peptide concentration where a reduction of the intensity of the CD signal was observed was 20 μ M. The signal intensity for spectra of monomeric IAPP(8-18)-KK(Ac)K-(22-28)-OH was the lowest compared to the spectra of other analogues with intermixing K and K(Ac) in the IAPP(19-21) region.

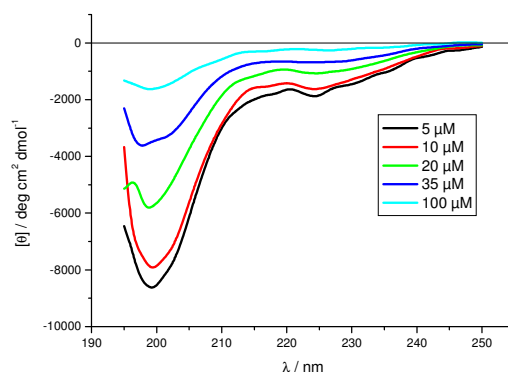


Fig. 124: Concentration dependent CD spectra of IAPP(8-18)-KK(Ac)K-(22-28)-OH in 1xb 1% HFIP, pH 7.4.

ThT fluorescence assays showed that IAPP(8-18)-KK(Ac)K-(22-28)-OH was forming fibrils at a concentration of 500 μ M (Fig. 125A). The TEM picture of IAPP(8-18)-KK(Ac)K-(22-28)-OH at 500 μ M displayed thick bundles of fibrils but also to a small amount amorphous aggregates (Fig. 125B).

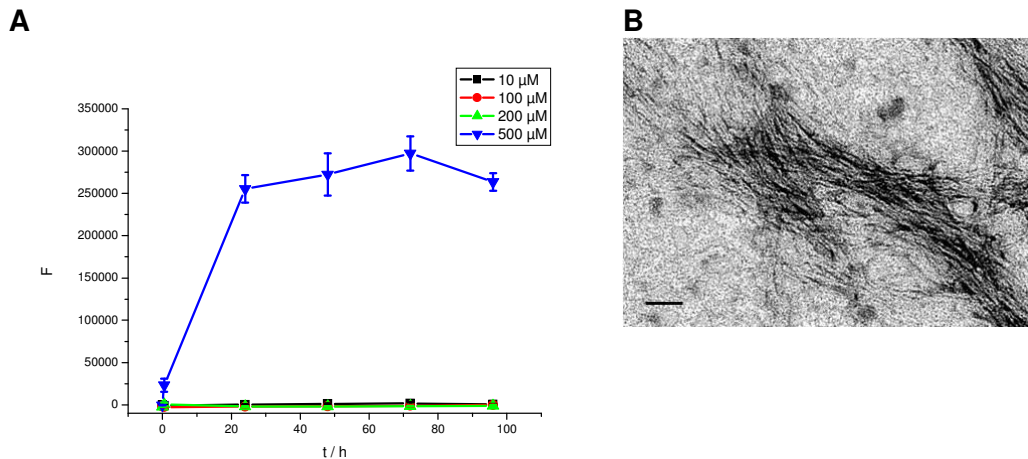


Fig. 125: (A) ThT assays of IAPP(8-18)-KK(Ac)K-(22-28)-OH at different concentrations in 1x 1% HFIP, pH 7.4. Data are means of 3 assays after subtraction of buffer values \pm standard error of the mean (SEM) with each experiment performed in multiple replicates ($n = 3$). (B) TEM picture of IAPP(8-18)-KK(Ac)K-(22-28)-OH. The peptide was incubated at 500 μ M for 7 d in 10 mM sodium phosphate buffer at pH 7.4 containing 1% HFIP. Scale bar: 100 nm.

Staining of aggregates of IAPP(8-18)-KK(Ac)K-(22-28)-OH with Congo Red revealed the formation of amyloid fibrils. Stained aggregates showed intense red color under normal light (Fig. 126A) and displayed green but also bright red birefringence under cross polarized light (Fig. 126B). The red light under cross polarized light was due to Congo Red bound to fibrils that was shining through unbound and therefore red Congo Red. Some aggregates were colored red under normal light but displayed no birefringence under cross polarized light. These seemed to be amorphous aggregates.

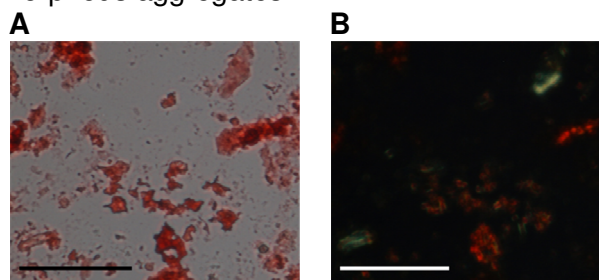


Fig. 126: Microscopic examination of fibrillar aggregates of IAPP(8-18)-KK(Ac)K-(22-28)-OH stained with Congo Red. 1 mM peptide was incubated in 10 mM sodium phosphate buffer at pH 7.4 containing 1% HFIP for 3d and then spotted on a slide. The dried droplet was stained with 200 μ M Congo Red in H₂O. Pictures were taken under A normal and B cross polarized light. Scale bar: 100 μ m.

According to MTT reduction assays aged incubations of IAPP(8-18)-KK(Ac)K-(22-28)-OH were slightly toxic to RIN cells (Fig. 127).

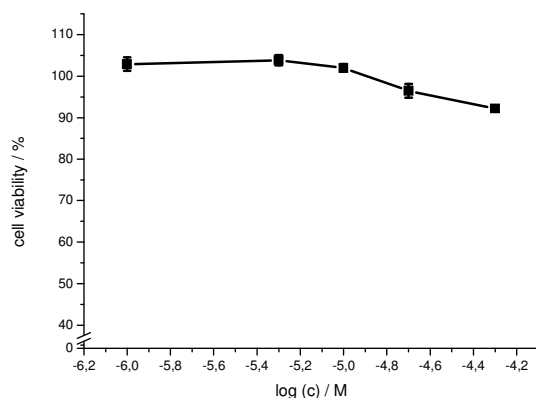


Fig. 127: Cell viability assay of an aged solution of IAPP(8-18)-KK(Ac)K-(22-28)-OH (5 mM in 1xb 1% HFIP for 4 days, pH 7.4) using RIN cells. Data are percentages of control and are the mean (+/-SEM) of three independent experiments with each experiment performed in multiple replicates (n = 3).

3.1.1.30 IAPP(8-18)-K(Ac)KK-(22-28)-OH

As seen on Fig. 128, IAPP(8-18)-K(Ac)KK-(22-28)-OH showed a strong minimum at 195 - 200 nm in the measured CD spectra that can be related to random coil structures. The weaker negative signal between 210 nm and 230 nm was related to β -sheet and β -turn elements. The signal intensity of spectra at a concentration between 5 and 10 μ M was almost similar. The lowest peptide concentration where a reduction of the intensity of the CD signal occurred was 20 μ M. This can be interpreted as a sign that IAPP(8-18)-K(Ac)KK-(22-28)-OH was a monomer at a concentration of up to 10 μ M. The signal intensity was in general lower for IAPP(8-18)-K(Ac)KK-(22-28)-OH compared to the spectra of IAPP(8-18)-KKK(Ac)-(22-28)-OH (Fig. 120).

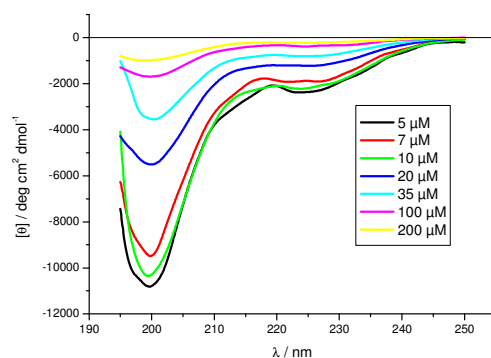


Fig. 128: Concentration dependent CD spectra of IAPP(8-18)-K(Ac)KK-(22-28)-OH in 1xb 1% HFIP, pH 7.4.

Under the conditions tested with ThT fluorescence assays IAPP(8-18)-K(Ac)KK-(22-28)-OH did not display fibril formation (Fig. 129A). The TEM picture of IAPP(8-18)-K(Ac)KK-(22-28)-OH also only showed amorphous aggregates (Fig. 129B).

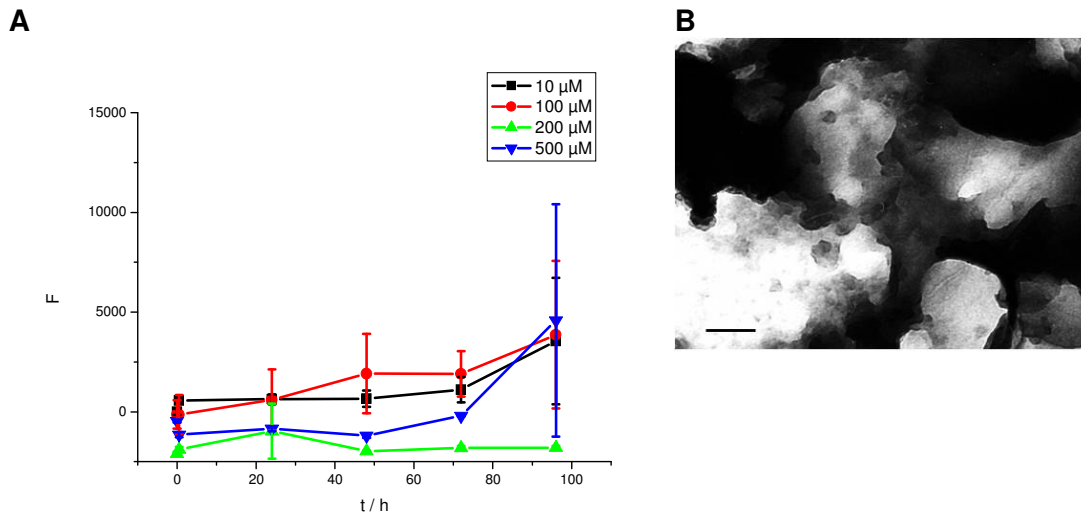


Fig. 129: (A) ThT assays of IAPP(8-18)-K(Ac)KK-(22-28)-OH at different concentrations in 1x 1% HFiP, pH 7.4. Data are means of 3 assays after subtraction of buffer values +/- standard error of the mean (SEM) with each experiment performed in multiple replicates (n = 3). (B) TEM picture of IAPP(8-18)-K(Ac)KK-(22-28)-OH. The peptide was incubated at 500 μM for 7 d in 10 mM sodium phosphate buffer at pH 7.4 containing 1% HFiP. Scale bar: 100 nm.

Congo Red staining of aged aggregates of IAPP(8-18)-K(Ac)KK-(22-28)-OH also revealed no birefringence under cross polarized light (Fig. 130B), a sign for the lack of amyloid structures.

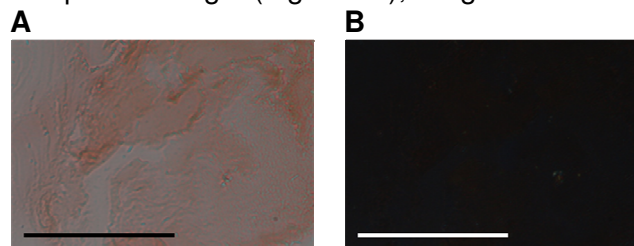


Fig. 120: Microscopic examination of aggregates of IAPP(8-18)-K(Ac)KK-(22-28)-OH stained with Congo Red. 1 mM peptide was incubated in 10 mM sodium phosphate buffer at pH 7.4 containing 1% HFiP for 3d and then spotted on a slide. The dried droplet was stained with 200 μM Congo Red in H₂O. Pictures were taken under A normal and B cross polarized light. Scale bar: 100 μm.

Aged aggregates of IAPP(8-18)-K(Ac)KK-(22-28)-OH were also non toxic to RIN cells (Fig. 131).

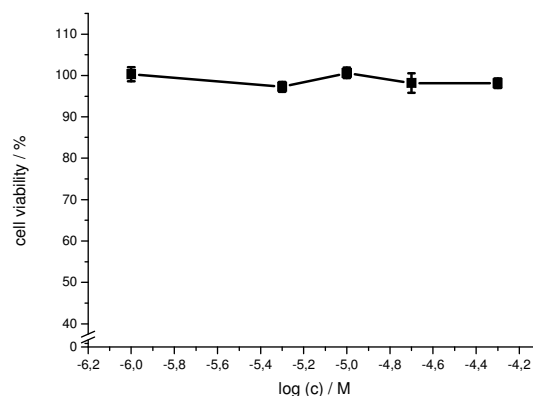


Fig. 131: Cell viability assay of an aged solution of IAPP(8-18)-K(Ac)KK-(22-28)-OH (5 mM in 1x 1% HFiP for 4 days, pH 7.4) using RIN cells. Data are percentages of control and are the mean (+/-SEM) of three independent experiments with each experiment performed in multiple replicates (n = 3).

Table 4: Overview of ThT and cell viability assays performed of the analogues of IAPP(8-28). Results of “+” indicate fibril formation, whereas “-” indicate no fibril formation within the 5 days of incubation of the solution at the given peptide concentration. For the cell viability assays, results of “+++” mean high toxicity towards RIN cells, “++” mean medium toxicity, “+/-” means low toxicity and “-“ mean no toxicity.

Sequence	ThT										Tox.
	5 μM	10 μM	20 μM	35 μM	50 μM	100 μM	200 μM	500 μM	5 mM	10 mM	
IAPP(8-18)-OH						-	-	+			-
IAPP(22-28)-OH						-	-	-	-	-	-
IAPP(8-28)-OH			-	+	+	+					+++
IAPP(8-18)-SGN-(22-28)-OH	-	+				+					+++
IAPP(8-18)-Aoc-(22-28)-OH			-	+		+					+++
IAPP(8-18)-Peg-(22-28)-OH				-		+					++
IAPP(8-18)-KKK-(22-28)-OH				-		-	-	-			++
IAPP(8-18)-Dap ₃ -(22-28)-OH						-	-	-			-
IAPP(8-18)-RRR-(22-28)-OH						-	-	-			-
IAPP(8-18)-DDD-(22-28)-OH						-		-			-
IAPP(8-18)-GGG-(22-28)-OH				-		+	+				++
IAPP(8-18)-AAA-(22-28)-OH				-		+	+				++
IAPP(8-18)-VVV-(22-28)-OH		-	+	+	+	+	+				+++
IAPP(8-18)-LLL-(22-28)-OH			-	-		-	+	+			++
IAPP(8-18)-III-(22-28)-OH			-	+	+	+	+				+++
IAPP(8-18)-Nle ₃ -(22-28)-OH			-	+	+	+	+				+++
IAPP(8-18)-2(Aoc) ₃ -(22-28)-OH			-	+		+					+++
IAPP(8-18)-TTT-(22-28)-OH			-	+		+					++
IAPP(8-18)-FFF-(22-28)-OH				-	+	+	+				++
IAPP(8-18)-Cha ₃ -(22-28)-OH				-		-	-	-			+/-
IAPP(8-18)-SpG-(22-28)-OH				-	+	+					+/-
IAPP(8-18)-pGN-(22-28)-OH				-	-	+					++
IAPP(8-18)-PPP-(22-28)-OH						-		-			-
IAPP(8-18)-K(Ac) ₃ -(22-28)-OH	-	+	+	+	+	+					+++
IAPP(8-18)-KK(Ac)K(Ac)-(22-28)-OH			-	+		+					+++
IAPP(8-18)-K(Ac)KK(Ac)-(22-28)-OH			-	+		+					++
IAPP(8-18)-K(Ac)K(Ac)K-(22-28)-OH		-				-	+	+			++
IAPP(8-18)-KKK(Ac)-(22-28)-OH						-	-	+			++
IAPP(8-18)-KK(Ac)K-(22-28)-OH		-				-	-	+			-
IAPP(8-18)-K(Ac)KK-(22-28)-OH		-				-	-	-			-

3.1.2 Comparison of the analogues

3.1.2.1 IAPP(8-28), partial segments IAPP(8-18) and IAPP(22-28), S20G-IAPP(8-28), and IAPP(8-28) analogues with nonpeptidic substituents for the region IAPP(19-21)

Under the here applied conditions, the segments IAPP(8-18)-OH and IAPP(22-28)-OH alone exhibited weak to no fibril forming potential and no toxicity. In fact, IAPP(22-28)-OH did not form fibrils at concentrations up to 10 mM under the conditions used.

The peptide IAPP(8-18)-SGN-(22-28)-OH with the natively occurring mutation S20G in the IAPP(19-21) region was more toxic and fibrillogenic than the native IAPP(8-28)-OH. However they showed almost identical CD spectra at 5 μ M peptide with a dominant minimum slightly below 200 nm indicating random coil structure and a smaller negative bulge at around 220-230 nm displaying β -sheet and β -turn elements (Fig. 132A).

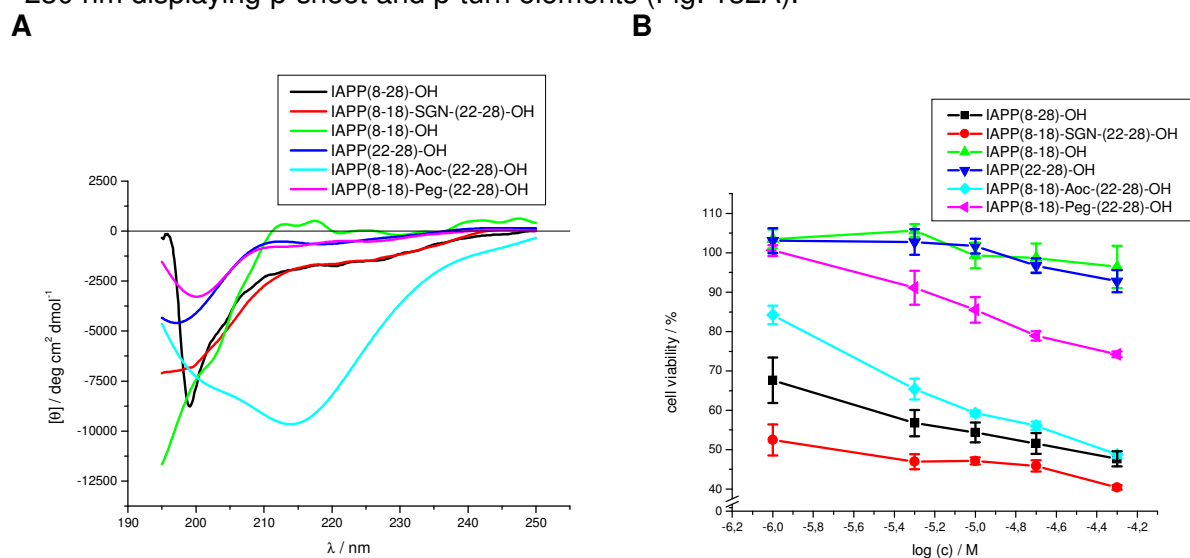


Fig. 132: (A) Comparison of the CD spectra of IAPP(8-28)-OH, IAPP(8-18)-SGN-(22-28)-OH, IAPP(8-18)-Aoc-(22-28)-OH and IAPP(8-18)-Peg-(22-28)-OH at a peptide concentration of 5 μ M in 1x 1% HFIP, pH 7.4.

(B) Comparison of the cytotoxicity of fibrillar aggregates of peptides IAPP(8-28)-OH, IAPP(8-18)-SGN-(22-28)-OH, IAPP(8-18)-Aoc-(22-28)-OH, IAPP(8-18)-Peg-(22-28)-OH, IAPP(8-18)-OH and IAPP(22-28)-OH to RIN5fm cells. Data are percentages of control and are the mean (+/-SEM) of three independent experiments with each experiment performed in multiple replicates ($n = 3$).

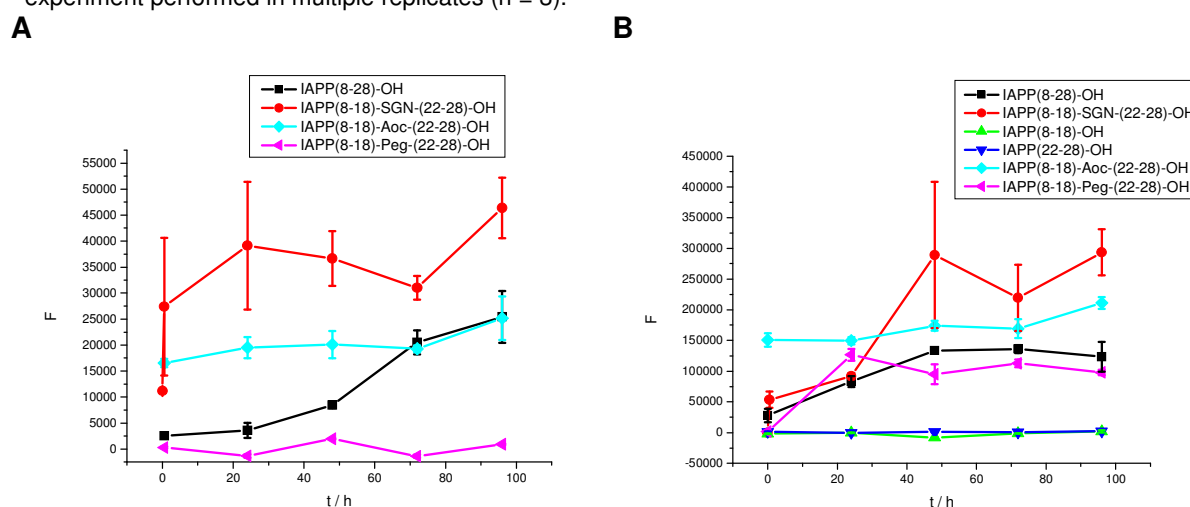


Fig. 133: (A) Comparison of ThT assays of peptides IAPP(8-28)-OH, IAPP(8-18)-SGN-(22-28)-OH, IAPP(8-18)-Aoc-(22-28)-OH and IAPP(8-18)-Peg-(22-28)-OH at a concentration of 35 μ M for each peptide in 1x 1% HFIP,

pH 7.4. Data are means of 3 assays after subtraction of buffer values +/- standard error of the mean (SEM) with each experiment performed in multiple replicates (n = 3).

(B) Comparison of ThT assays of peptides IAPP(8-28)-OH, IAPP(8-18)-SGN-(22-28)-OH, IAPP(8-18)-Aoc-(22-28)-OH, IAPP(8-18)-Peg-(22-28)-OH, IAPP(8-18)-OH and IAPP(22-28)-OH at a concentration of 100 μ M for each peptide in 1x 1% HFIP, pH 7.4. Data are means of 3 assays after subtraction of buffer values +/- standard error of the mean (SEM) with each experiment performed in multiple replicates (n = 3).

The two peptides with nonpeptidic backbones in the region IAPP(19-21) differed both from each other and the native IAPP(8-28)-OH. IAPP(8-18)-Peg-(22-28)-OH was less toxic and fibrillogenic than IAPP(8-28)-OH (Fig. 132B and Fig. 133). Its CD spectrum at a concentration of 5 μ M peptide displayed a much weaker signal and there was also no bulge at 220-230 nm (Fig. 132A). On the other hand, IAPP(8-18)-Aoc-(22-28)-OH was as fibrillogenic and almost as toxic as IAPP(8-28)-OH (Fig. 133 and Fig. 132A). The CD spectrum of IAPP(8-18)-Aoc-(22-28)-OH at 5 μ M showed an intense, broad minimum at 215 nm. This minimum was a strong indication that the peptide formed a β -sheet structure. The Aoc-linker is more flexible but also more hydrophobic than the Peg-linker. These features seemed to promote fibril formation and toxicity maybe because they benefited the formation of a hydrophobic core upon oligomerization and fibril formation. To address this issue, ANS binding studies were performed with these analogues (see chapter 3.1.4).

Table 5: Overview of ThT and cell viability assays performed of the analogues compared in chapter 3.1.2.1. Results of "+" indicate fibril formation, whereas "-" indicate no fibril formation within the 5 days of incubation of the solution at the given peptide concentration. For the cell viability assays, results of "+++" mean high toxicity towards RIN cells, "++" mean medium toxicity, and "-" mean no toxicity.

Sequence	ThT										Tox.
	5 μ M	10 μ M	20 μ M	35 μ M	50 μ M	100 μ M	200 μ M	500 μ M	5 mM	10 mM	
IAPP(8-18)-OH						-	-	+			-
IAPP(22-28)-OH						-	-	-	-	-	-
IAPP(8-28)-OH			-	+	+	+					+++
IAPP(8-18)-SGN-(22-28)-OH	-	+				+					+++
IAPP(8-18)-Aoc-(22-28)-OH			-	+		+					+++
IAPP(8-18)-Peg-(22-28)-OH				-		+					++

3.1.2.2 Analogues with charged side chains in the region IAPP(19-21)

Different analogues with charged side chains in the region IAPP(19-21) were designed to examine the influence of net charge upon fibril formation. It was expected that net charges would reduce the fibril forming potential of amyloidogenic peptides [139, 141, 168].

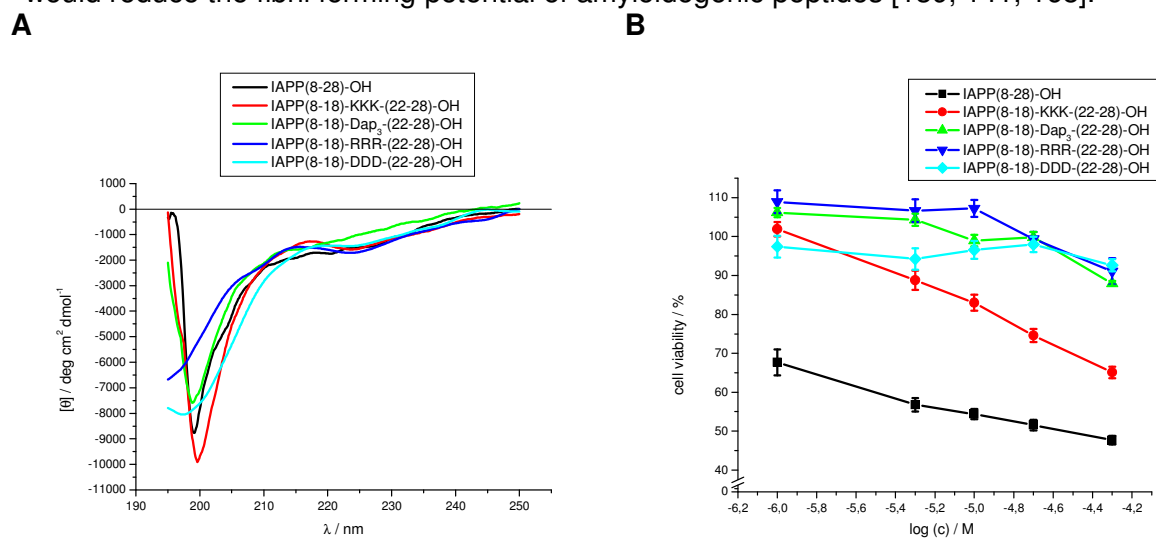


Fig. 134: (A) Comparison of the CD spectra of IAPP(8-28)-OH, IAPP(8-18)-KKK-(22-28)-OH, IAPP(8-18)-Dap₃-(22-28)-OH, IAPP(8-18)-RRR-(22-28)-OH and IAPP(8-18)-DDD-(22-28)-OH at a peptide concentration of 5 μM in 1x1% HFIP, pH 7.4.

(B) Comparison of the cytotoxicity of fibrillar aggregates of peptides IAPP(8-28)-OH, IAPP(8-18)-KKK-(22-28)-OH, IAPP(8-18)-Dap₃-(22-28)-OH, IAPP(8-18)-RRR-(22-28)-OH and IAPP(8-18)-DDD-(22-28)-OH to RIN5fm cells. Data are percentages of control and are the mean (+/-SEM) of three independent experiments with each experiment performed in multiple replicates ($n = 3$).

Both under physiological conditions positively and negatively charged amino acids were incorporated into the IAPP(19-21) region. Their presence prevented fibril formation most likely due to electrostatic repulsion between the positively or negatively charged side chains of the peptide monomers at pH 7.4. Except for IAPP(8-18)-KKK-(22-28)-OH, all peptides with charged side chains in the region IAPP(19-21) were non-toxic to RIN5fm cells (Fig. 134B). The specific toxicity of IAPP(8-18)-KKK-(22-28)-OH might be due to interactions between the lysine side chains and the negatively charged cell membrane since other positively charged motifs in the region IAPP(19-21) showed no cytotoxicity. The reason for this specific interaction and its underlying molecular mechanism still need to be further investigated. But it might be possible that IAPP(8-18)-KKK-(22-28)-OH aligned on the cell surface and formed pores in the membrane leading to cellular degeneration [169-171].

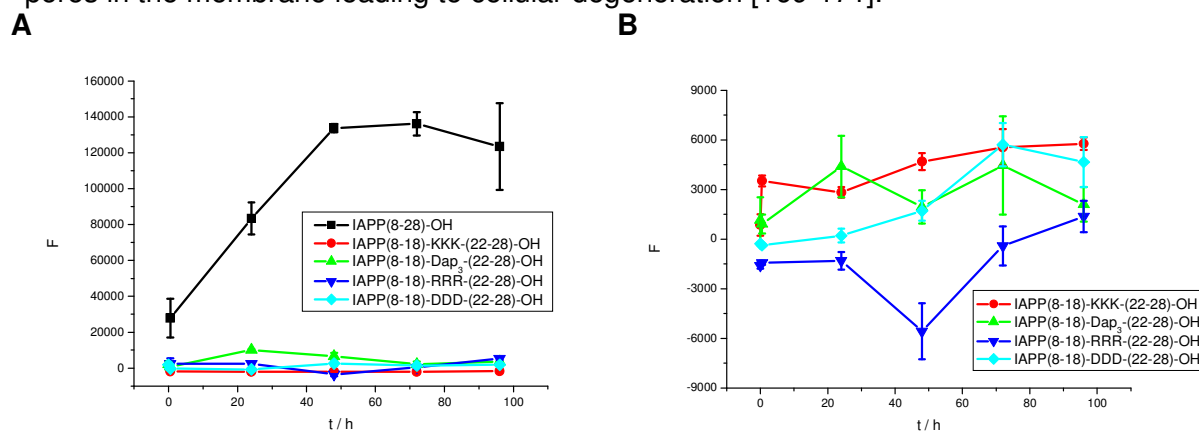


Fig. 135: (A) Comparison of ThT assays of peptides IAPP(8-28)-OH, IAPP(8-18)-KKK-(22-28)-OH, IAPP(8-18)-Dap₃-(22-28)-OH, IAPP(8-18)-RRR-(22-28)-OH and IAPP(8-18)-DDD-(22-28)-OH at a concentration of 100 μ M for each peptide. Data are means of 3 assays after subtraction of buffer values \pm standard error of the mean (SEM) with each experiment performed in multiple replicates (n = 3). (B) Comparison of ThT assays of peptides IAPP(8-18)-KKK-(22-28)-OH, IAPP(8-18)-Dap₃-(22-28)-OH, IAPP(8-18)-RRR-(22-28)-OH and IAPP(8-18)-DDD-(22-28)-OH at a concentration of 500 μ M for each peptide in 1x 1% HFIP, pH 7.4. Data are means of 3 assays after subtraction of buffer values \pm standard error of the mean (SEM) with each experiment performed in multiple replicates (n = 3).

CD spectra of these peptides at a concentration of 5 μ M all showed a minimum below 200 nm indicating random coil structure and a smaller negative bulge at around 220-230 nm displaying β -sheet and β -turn elements (Fig. 134A). These spectra were similar to the spectrum of native IAPP(8-28)-OH (Fig. 20A). The most intense minimum at 200 nm was present in the spectrum of IAPP(8-18)-KKK-(22-28)-OH.

This indicated that these peptides exhibited similar overall conformation in their monomeric state in solution, whereas the huge difference between their weak fibril forming ability and the strong fibril forming potential of IAPP(8-28)-OH can be explained by the electric repulsion due to the charges in the region IAPP(19-21). This repulsion may have prevented a close alignment of the monomers which might be necessary for the formation of fibrils. This suggestion was further supported by the results of studies performed with the IAPP(8-18)-(K(Ac))₃-(22-28)-OH analogue which was found to be highly amyloidogenic and cytotoxic (see Fig. 105A and Fig. 107).

Table 6: Overview of ThT and cell viability assays performed of the analogues of IAPP(8-28) with charged side chains in the IAPP(19-21) region.

Results of "+" indicate fibril formation, whereas "-" indicate no fibril formation within the 5 days of incubation of the solution at the given peptide concentration.

For the cell viability assays, results of "++" mean medium toxicity towards RIN cells and "-" mean no toxicity.

Sequence	ThT								Tox.
	5 μ M	10 μ M	20 μ M	35 μ M	50 μ M	100 μ M	200 μ M	500 μ M	
IAPP(8-18)- KKK -(22-28)-OH				-		-	-	-	++
IAPP(8-18)- Dap₃ -(22-28)-OH						-	-	-	-
IAPP(8-18)- RRR -(22-28)-OH						-	-	-	-
IAPP(8-18)- DDD -(22-28)-OH						-		-	-

3.1.2.3 Analogues with side chains with differences in steric hindrance and hydrophobicity in the IAPP(19-21) region

Steric hindrance can have a negative effect on fibril formation since the hydrophobic core of fibrils is normally tightly packed [52, 143, 172].

To systematically investigate this phenomenon, a set of peptides with increasing steric hindrance in the side chain of amino acids forming the IAPP(19-21) region and a peptidic backbone was designed. A second feature displayed by analogues of this group was an increased hydrophobicity of the residues in the IAPP(19-21) region. Hydrophobic residues also play an important role in promoting the aggregation of amyloid peptides [173].

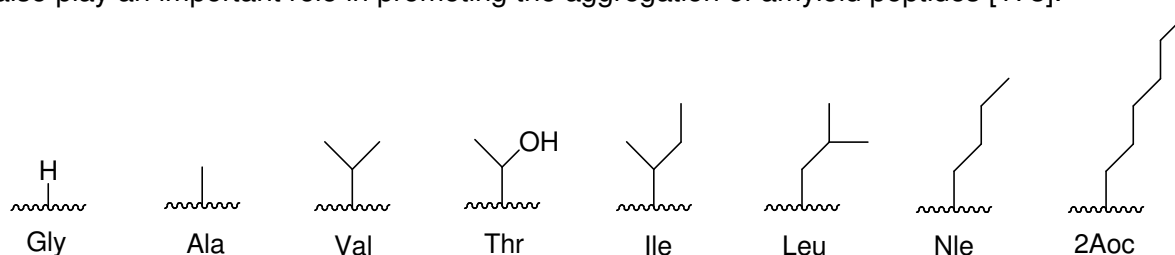


Fig. 136: Side chain structure of amino acids used to determine the effect of steric hindrance and hydrophobicity on fibril formation.

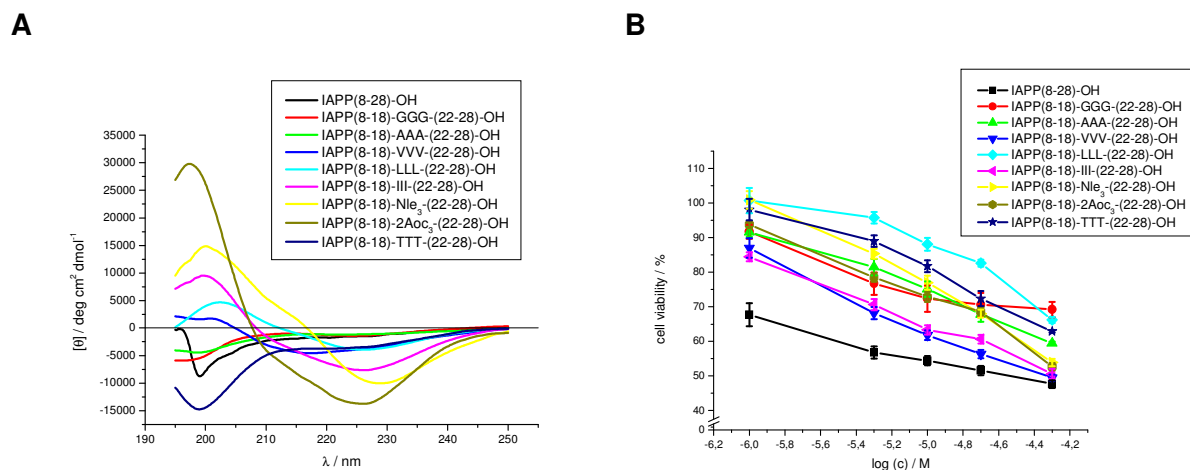
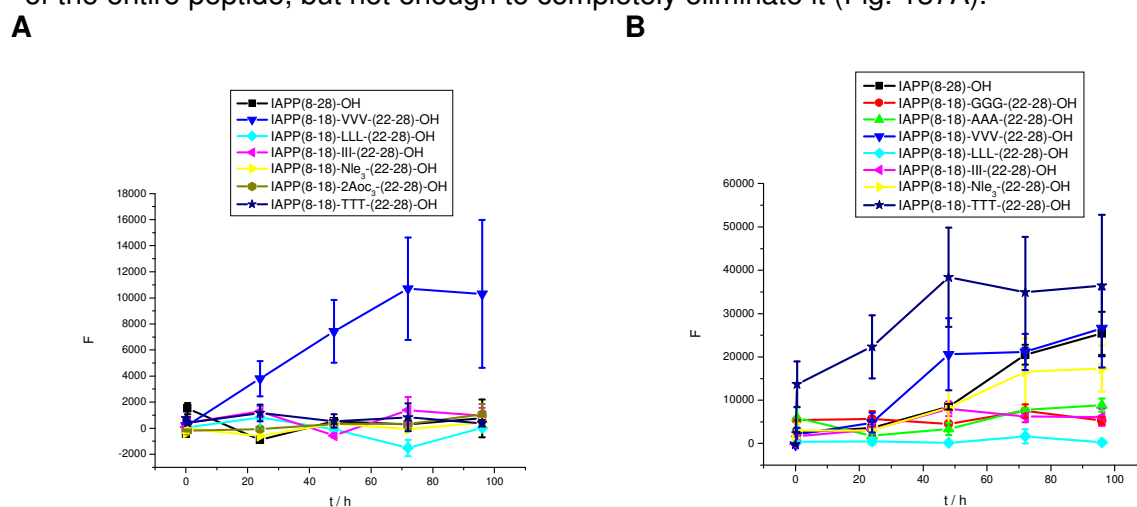


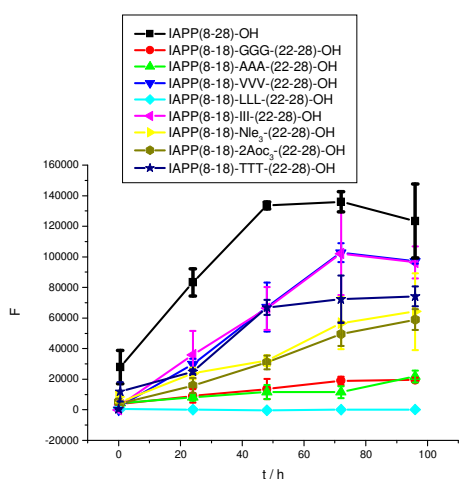
Fig. 137: (A) Comparison of the CD spectra of IAPP(8-28)-OH, IAPP(8-18)-GGG-(22-28)-OH, IAPP(8-18)-AAA-(22-28)-OH, IAPP(8-18)-VVV-(22-28)-OH, IAPP(8-18)-LLL-(22-28)-OH, IAPP(8-18)-III-(22-28)-OH, IAPP(8-18)-Nle₃-(22-28)-OH, IAPP(8-18)-2Aoc₃-(22-28)-OH and IAPP(8-18)-TTT-(22-28)-OH at a peptide concentration of 5 μM in 1x1 1% HFIP, pH 7.4.

(B) Comparison of the cytotoxicity of fibrillar aggregates of peptides IAPP(8-28)-OH, IAPP(8-18)-GGG-(22-28)-OH, IAPP(8-18)-AAA-(22-28)-OH, IAPP(8-18)-VVV-(22-28)-OH, IAPP(8-18)-LLL-(22-28)-OH, IAPP(8-18)-III-(22-28)-OH, IAPP(8-18)-Nle₃-(22-28)-OH, IAPP(8-18)-2Aoc₃-(22-28)-OH and IAPP(8-18)-TTT-(22-28)-OH to RIN5fm cells. Data are percentages of control and are the mean (\pm SEM) of three independent experiments with each experiment performed in multiple replicates ($n = 3$).

Most of the peptides with hydrophobic side chains in the IAPP(19-21) region showed significant β -sheet and β -turn elements in their CD spectra. IAPP(8-18)-AAA-(22-28)-OH and IAPP(8-18)-GGG-(22-28)-OH displayed mainly random coil structures in their CD spectra with a weak minimum at around 220-230 nm relating to β -sheet and β -turn elements. The CD of IAPP(8-18)-TTT-(22-28)-OH at a concentration of 5 μM showed both a bulge at around 220-230 nm and an intense minimum at 195-200 nm intending the presence of β -sheet, β -turn, and random coil structures. The hydroxyl group in the side chains of the three threonine residues instead of a methyl group in the case of the three valine side chains in the IAPP(19-21) region already seemed to be enough to disrupt the β -sheet and β -turn forming potential of the entire peptide, but not enough to completely eliminate it (Fig. 137A).



C



D

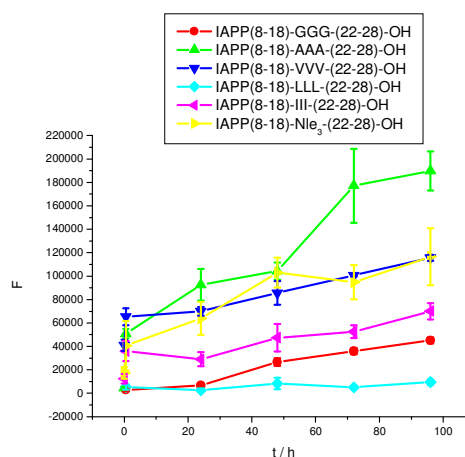


Fig. 138: (A) Comparison of ThT assays of peptides IAPP(8-28)-OH, IAPP(8-18)-VVV-(22-28)-OH, IAPP(8-18)-LLL-(22-28)-OH, IAPP(8-18)-III-(22-28)-OH, IAPP(8-18)-Nle₃-(22-28)-OH, IAPP(8-18)-2Aoc₃-(22-28)-OH and IAPP(8-18)-TTT-(22-28)-OH at a concentration of 20 μM for each peptide in 1xb 1% HFIP, pH 7.4. Data are means of 3 assays after subtraction of buffer values +/- standard error of the mean (SEM) with each experiment performed in multiple replicates (n = 3).

(B) Comparison of ThT assays of peptides IAPP(8-28)-OH, IAPP(8-18)-GGG-(22-28)-OH, IAPP(8-18)-AAA-(22-28)-OH, IAPP(8-18)-VVV-(22-28)-OH, IAPP(8-18)-LLL-(22-28)-OH, IAPP(8-18)-III-(22-28)-OH, IAPP(8-18)-Nle₃-(22-28)-OH and IAPP(8-18)-TTT-(22-28)-OH at a concentration of 35 μM for each peptide in 1xb 1% HFIP, pH 7.4. Data are means of 3 assays after subtraction of buffer values +/- standard error of the mean (SEM) with each experiment performed in multiple replicates (n = 3).

(C) Comparison of ThT assays of peptides IAPP(8-28)-OH, IAPP(8-18)-GGG-(22-28)-OH, IAPP(8-18)-AAA-(22-28)-OH, IAPP(8-18)-VVV-(22-28)-OH, IAPP(8-18)-LLL-(22-28)-OH, IAPP(8-18)-III-(22-28)-OH, IAPP(8-18)-Nle₃-(22-28)-OH, IAPP(8-18)-2Aoc₃-(22-28)-OH and IAPP(8-18)-TTT-(22-28)-OH at a concentration of 100 μM for each peptide in 1xb 1% HFIP, pH 7.4. Data are means of 3 assays after subtraction of buffer values +/- standard error of the mean (SEM) with each experiment performed in multiple replicates (n = 3).

(D) Comparison of ThT assays of peptides IAPP(8-18)-GGG-(22-28)-OH, IAPP(8-18)-AAA-(22-28)-OH, IAPP(8-18)-VVV-(22-28)-OH, IAPP(8-18)-LLL-(22-28)-OH, IAPP(8-18)-III-(22-28)-OH and IAPP(8-18)-Nle₃-(22-28)-OH at a concentration of 200 μM for each peptide in 1xb 1% HFIP, pH 7.4. Data are means of 3 assays after subtraction of buffer values +/- standard error of the mean (SEM) with each experiment performed in multiple replicates (n = 3).

Concerning fibril forming potential and cytotoxicity, the peptides IAPP(8-18)-VVV-(22-28)-OH and IAPP(8-18)-III-(22-28)-OH were the most toxic and fibrillogenic ones from this group, IAPP(8-18)-VVV-(22-28)-OH even a little more than IAPP(8-18)-III-(22-28)-OH (Fig. 138A and table 7). Valines and isoleucines in the IAPP(19-21) region were hydrophobic enough to enhance fibril formation and β-sheet and β-turn structure of the peptide, but not that sterically hindered. The side chains of valine and isoleucine are branched in the β position, whereas the leucine side chain is branched in the γ position and norleucine and 2Aoc have longer side chains.

IAPP(8-18)-LLL-(22-28)-OH was by far the least toxic and fibrillogenic peptide from this group. The reason could be the position of the branch in the side chains of the three leucine residues in the IAPP(19-21) region.

Both norleucine and 2Aoc have long unbranched hydrophobic side chains. An increase of the length of the side chains did not lead to faster fibril formation or higher toxicity. However IAPP(8-18)-Nle₃-(22-28)-OH and IAPP(8-18)-2Aoc₃-(22-28)-OH displayed a fibril forming potential similar to that of IAPP(8-18)-III-(22-28)-OH and were even slightly less toxic than IAPP(8-18)-III-(22-28)-OH (Fig. 137A and Fig. 138). Negative effects on fibril formation and toxicity like the bigger steric hindrance of these side chains in the IAPP(19-21) region might have counteracted the positive effect of higher hydrophobicity.

IAPP(8-18)-AAA-(22-28)-OH and IAPP(8-18)-GGG-(22-28)-OH had only a very weakly hydrophobic IAPP(19-21) region displaying almost no steric hindrance which resulted in

weaker toxicity and fibril forming potential. Hydrophobicity was obviously a key feature for the formation of β -sheet and β -turn structures, fibrillar structures, and cytotoxic behaviour.

Taken together, the results from this group suggested that sterically unhindered hydrophobic side chains in the IAPP(19-21) region were the best choice for increasing the fibril forming potential of IAPP(8-28)-OH. Larger, more hydrophobic but more sterically hindered side chains in the IAPP(19-21) region were rather counterproductive since they seemed to slow down the formation of a hydrophobic core, which was an essential step towards the formation of amyloidogenic structures.

Table 7: Overview of ThT and cell viability assays performed of the analogues of IAPP(8-28) with varying hydrophobicity and steric hindrance of the side chains in the IAPP(19-21) region.

Results of “+” indicate fibril formation, whereas “-” indicate no fibril formation within the 5 days of incubation of the solution at the given peptide concentration.

For the cell viability assays, results of “+++” mean high toxicity towards RIN cells and “++” mean medium toxicity.

Sequence	ThT								Tox
	5 μ M	10 μ M	20 μ M	35 μ M	50 μ M	100 μ M	200 μ M	500 μ M	
IAPP(8-18)-GGG-(22-28)-OH				-		+	+		++
IAPP(8-18)-AAA-(22-28)-OH				-		+	+		++
IAPP(8-18)-VVV-(22-28)-OH		-	+	+	+	+	+		+++
IAPP(8-18)-LLL-(22-28)-OH			-	-		-	+	+	++
IAPP(8-18)-III-(22-28)-OH			-	+	+	+	+		+++
IAPP(8-18)-Nle ₃ -(22-28)-OH			-	+	+	+	+		+++
IAPP(8-18)-2(Aoc) ₃ -(22-28)-OH			-	+		+			+++
IAPP(8-18)-TTT-(22-28)-OH			-	+		+			++

3.1.2.4 Analogues with a branch in the gamma position of the side chain in the IAPP(19-21) region

To further investigate the effect of steric hindrance on fibril formation, analogues with a branch in the γ position of the side chain were used for the IAPP(19-21) region. The amino acids used for the IAPP(19-21) region were leucine, phenylalanine, and cyclohexylalanine. Leucine has a simple branch in the γ position of the side chain, phenylalanine has a planar phenyl group in that position, and cyclohexylalanine has a large hydrophobic and sterically hindered cyclohexyl group in the γ position.

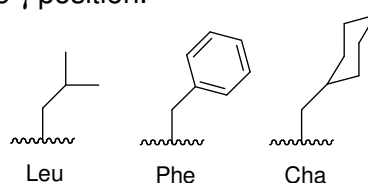


Fig. 139: Side chain structure of γ -branched amino acids used to determine the effects of hydrophobicity and aromaticity.

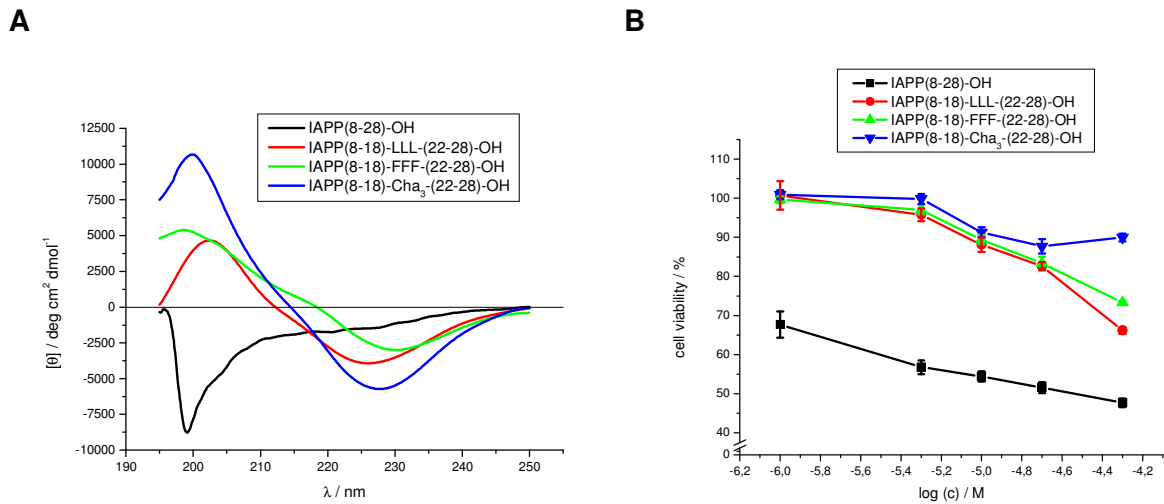


Fig. 140: (A) Comparison of the CD spectra of IAPP(8-28)-OH, IAPP(8-18)-LLL-(22-28)-OH, IAPP(8-18)-FFF-(22-28)-OH and IAPP(8-18)-Cha₃-(22-28)-OH at a peptide concentration of 5 μM in 1xb 1% HFIP, pH 7.4. (B) Comparison of the cytotoxicity of fibrillar aggregates of peptides IAPP(8-28)-OH, IAPP(8-18)-LLL-(22-28)-OH, IAPP(8-18)-FFF-(22-28)-OH and IAPP(8-18)-Cha₃-(22-28)-OH to RIN5fm cells. Data are percentages of control and are the mean (+/-SEM) of three independent experiments with each experiment performed in multiple replicates (n = 3).

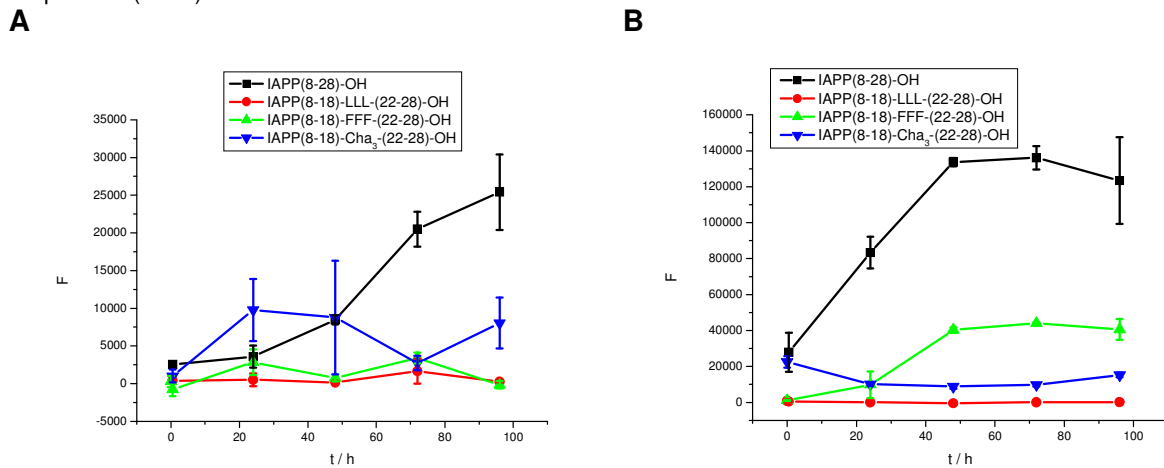


Fig. 141: (A) Comparison of ThT assays of peptides IAPP(8-28)-OH, IAPP(8-18)-LLL-(22-28)-OH, IAPP(8-18)-FFF-(22-28)-OH and IAPP(8-18)-Cha₃-(22-28)-OH at a concentration of 35 μM for each peptide in 1xb 1% HFIP, pH 7.4. Data are means of 3 assays after subtraction of buffer values +/- standard error of the mean (SEM) with each experiment performed in multiple replicates (n = 3). (B) Comparison of ThT assays of peptides IAPP(8-28)-OH, IAPP(8-18)-LLL-(22-28)-OH, IAPP(8-18)-FFF-(22-28)-OH and IAPP(8-18)-Cha₃-(22-28)-OH at a concentration of 100 μM for each peptide in 1xb 1% HFIP, pH 7.4. Data are means of 3 assays after subtraction of buffer values +/- standard error of the mean (SEM) with each experiment performed in multiple replicates (n = 3).

As shown in table 8 and Fig. 141, the fibril forming potential followed the order IAPP(8-28)-OH > IAPP(8-18)-FFF-(22-28)-OH > IAPP(8-18)-LLL-(22-28)-OH > IAPP(8-18)-Cha₃-(22-28)-OH.

Even though IAPP(8-18)-Cha₃-(22-28)-OH had the most hydrophobic sequence at positions IAPP(19-21), it had the lowest toxicity and fibril forming potential.

In this group, IAPP(8-18)-LLL-(22-28)-OH and IAPP(8-18)-FFF-(22-28)-OH displayed similar toxicities while IAPP(8-18)-FFF-(22-28)-OH was the most fibrillogenic peptide.

These results further support the thesis that an increased steric hindrance of the side chains in the IAPP(19-21) region prevented an amyloidogenic alignment of the peptide.

The clear difference between the fibril forming potential of IAPP(8-18)-FFF-(22-28)-OH and IAPP(8-18)-Cha₃-(22-28)-OH suggested an important role also for aromatic interactions for the fibril forming capacity of IAPP(8-28).

Table 8: Overview of ThT and cell viability assays performed of the analogues of IAPP(8-28) with a branch in the gamma position of the side chains in the IAPP(19-21) region.

Results of “+” indicate fibril formation, whereas “-” indicate no fibril formation within the 5 days of incubation of the solution at the given peptide concentration.

For the cell viability assays, results of “++” mean medium toxicity towards RIN cells and “+/-” mean low toxicity .

Sequence	ThT								Tox
	5 μM	10 μM	20 μM	35 μM	50 μM	100 μM	200 μM	500 μM	
IAPP(8-18)-LLL-(22-28)-OH			-	-		-	+	+	++
IAPP(8-18)-FFF-(22-28)-OH				-	+	+	+		++
IAPP(8-18)-Cha ₃ -(22-28)-OH				-		-	-	-	+/-

3.1.2.5 Analogues with secondary structure inducing elements in the IAPP(19-21) region

In order to specifically modulate the structure of the analogues, several known secondary structure inducing elements were incorporated into the IAPP(19-21) region. pG is a known β -turn inducing motif [147]. There are two possibilities for introducing this motif into the IAPP(19-21) region: at position 19, 20 (IAPP(8-18)-pGN-(22-28)-OH) and at position 20, 21 (IAPP(8-18)-SpG-(22-28)-OH). The second structure inducing motif was PPP which was introduced here to stabilize polyproline-II helical structure.

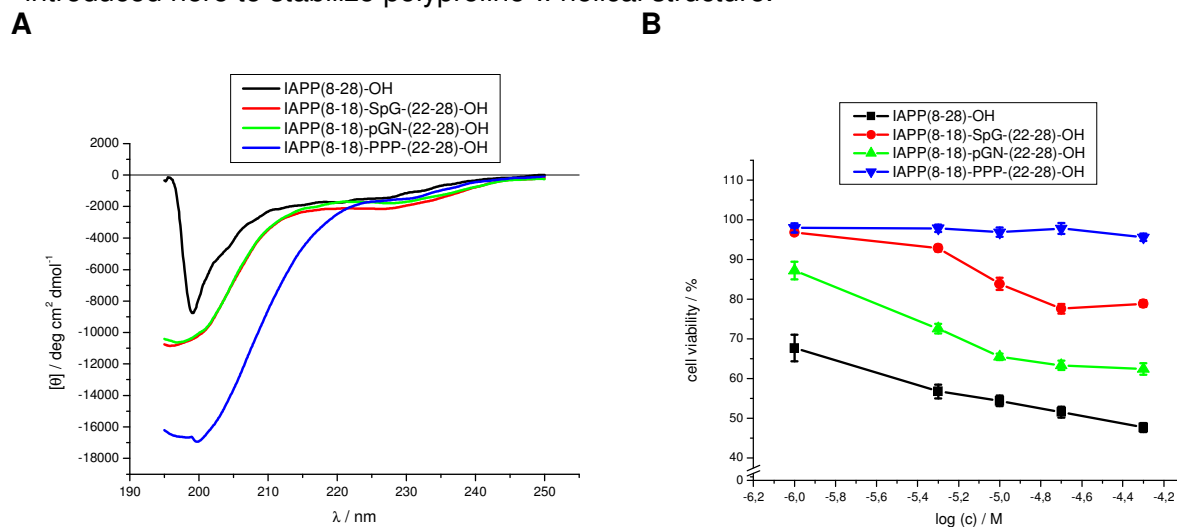


Fig. 142: (A) Comparison of the CD spectra of IAPP(8-28)-OH, IAPP(8-18)-SpG-(22-28)-OH, IAPP(8-18)- pGN-(22-28)-OH and IAPP(8-18)-PPP-(22-28)-OH at a peptide concentration of 5 μM in 1xβ 1% HFIP, pH 7.4.

(B) Comparison of the cytotoxicity of fibrillar aggregates of peptides IAPP(8-28)-OH, IAPP(8-18)-SpG-(22-28)-OH, IAPP(8-18)- pGN-(22-28)-OH and IAPP(8-18)-PPP-(22-28)-OH to RIN5fm cells. Data are percentages of control and are the mean (+/-SEM) of three independent experiments with each experiment performed in multiple replicates (n = 3).

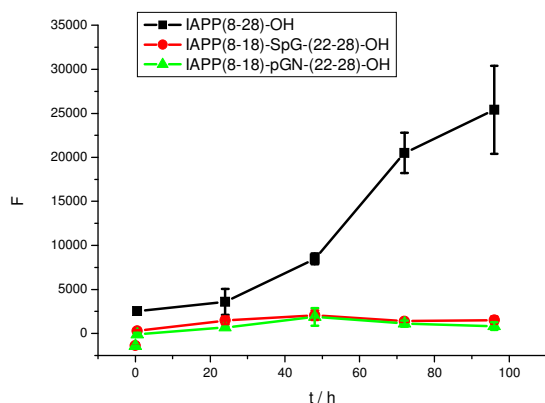
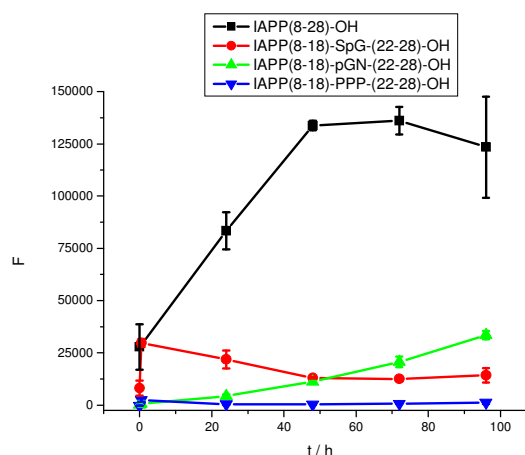
A**B**

Fig. 143: (A) Comparison of ThT assays of peptides IAPP(8-28)-OH, IAPP(8-18)-SpG-(22-28)-OH and IAPP(8-18)-pGN-(22-28)-OH at a concentration of 35 μ M for each peptide in 1xb 1% HFIP, pH 7.4. Data are means of 3 assays after subtraction of buffer values \pm standard error of the mean (SEM) with each experiment performed in multiple replicates ($n = 3$).

(B) Comparison of ThT assays of peptides IAPP(8-28)-OH, IAPP(8-18)-SpG-(22-28)-OH, IAPP(8-18)-pGN-(22-28)-OH and IAPP(8-18)-PPP-(22-28)-OH at a concentration of 100 μ M for each peptide in 1xb 1% HFIP, pH 7.4. Data are means of 3 assays after subtraction of buffer values \pm standard error of the mean (SEM) with each experiment performed in multiple replicates ($n = 3$).

The two analogues IAPP(8-18)-pGN-(22-28)-OH and IAPP(8-18)-SpG-(22-28)-OH displayed almost identical CD spectra at a concentration of 5 μ M with a strong minimum at 195-200 nm indicating random coil structure and a weak minimum at around 220-230 nm indicating the presence of β -sheet and β -turn elements. This minimum was a little stronger in the case of IAPP(8-18)-SpG-(22-28)-OH (Fig. 142A).

The incorporation of this β -turn inducing motif did not lead to a faster fibril formation or a higher toxicity as compared to IAPP(8-28)-OH. Among those two peptides, IAPP(8-18)-SpG-(22-28)-OH was slightly more fibrillogenic while IAPP(8-18)-pGN-(22-28)-OH was more toxic. A number of studies indicate that FGAIL (IAPP(23-27)) is involved in the formation of β -sheets, at least for oligomers of IAPP [100]. For IAPP(8-18)-SpG-(22-28)-OH there might be a pathway leading towards the formation of oligomers that cannot be transformed into amyloid fibrils. These oligomers seem to possess a rigid β -sheet-hairpin- β -sheet structure. Such a pathway does not occur for IAPP(8-18)-pGN-(22-28)-OH. This might also be the reason why IAPP(8-18)-pGN-(22-28)-OH was less fibrillogenic but more toxic than IAPP(8-18)-SpG-(22-28)-OH. Fibrils formed by IAPP(8-18)-SpG-(22-28)-OH could partially get transformed into rigid oligomers that could not be transformed back into amyloid structures and were also not toxic.

On the other hand, these findings might also be explained by the assumption that these peptides despite having the pG motif in the IAPP(19-21) region did not form a β -turn. Another explanation might be that they did not form the appropriate turn structure needed as an intermediate in fibril formation. This question could only be solved by determining the structure of these peptides on the molecular level for example by NMR or X-ray crystallography.

One issue was also to further investigate the random coil structure occurring in the CD spectra of many of the analogues. The term random coil is used for several extended structural motifs that can't be distinguished by CD spectroscopy. One of these structures is the polyproline II helix. In order to create an analogue having this structural motif, three prolines were put into the IAPP(19-21) region. The CD spectrum of 5 μ M IAPP(8-18)-PPP-(22-28)-OH had an intense, broad minimum at 200 nm and no bulge at 220-230 nm. Such a spectrum was expected for a polyproline II helix at room temperature (Fig. 142A). However

the typical behavior of the polyproline II helix in CD can only be investigated by thermal denaturation experiments. These were performed and are described in chapter 3.1.3. As expected, IAPP(8-18)-PPP-(22-28)-OH is non toxic and non fibrillogenic since Proline residues prevent the formation of intra- and intermolecular H-bonds which are required for the β -sheet structure and the formation of fibrils (table 9).

Table 9: Overview of ThT and cell viability assays performed with analogues of IAPP(8-28) with secondary structure inducing elements in the IAPP(19-21) region. Results of “+” indicate fibril formation, whereas “-” indicate no fibril formation within the 5 days of incubation of the solution at the given peptide concentration. For the cell viability assays, results of “++” mean medium toxicity towards RIN cells, “+/-” means low toxicity and “-” mean no toxicity.

Sequence	ThT								Tox
	5 μ M	10 μ M	20 μ M	35 μ M	50 μ M	100 μ M	200 μ M	500 μ M	
IAPP(8-18)-SpG-(22-28)-OH				-	+	+			+
IAPP(8-18)-pGN-(22-28)-OH				-	-	+			++
IAPP(8-18)-PPP-(22-28)-OH						-		-	-

3.1.2.6 Comparison of the analogues concerning their toxicity

The here studied analogues were additionally sorted into three different groups concerning their toxicity. This was done to point out which features in the IAPP(19-21) region were positive and which were negative for the toxicity of the tested analogues. The three groups created were called high (cell viability < 60%), medium (cell viability of 60-80%), and low toxicity (cell viability > 80%).

3.1.2.6.1 High toxicity

As expected, the natively occurring mutant S20G was the most toxic analogue. The analogue with the 3 K(Ac) in the IAPP(19-21) region was more toxic and fibrillogenic than the native IAPP(8-28)-OH. In fact, it was as fibrillogenic as the S20G mutant.

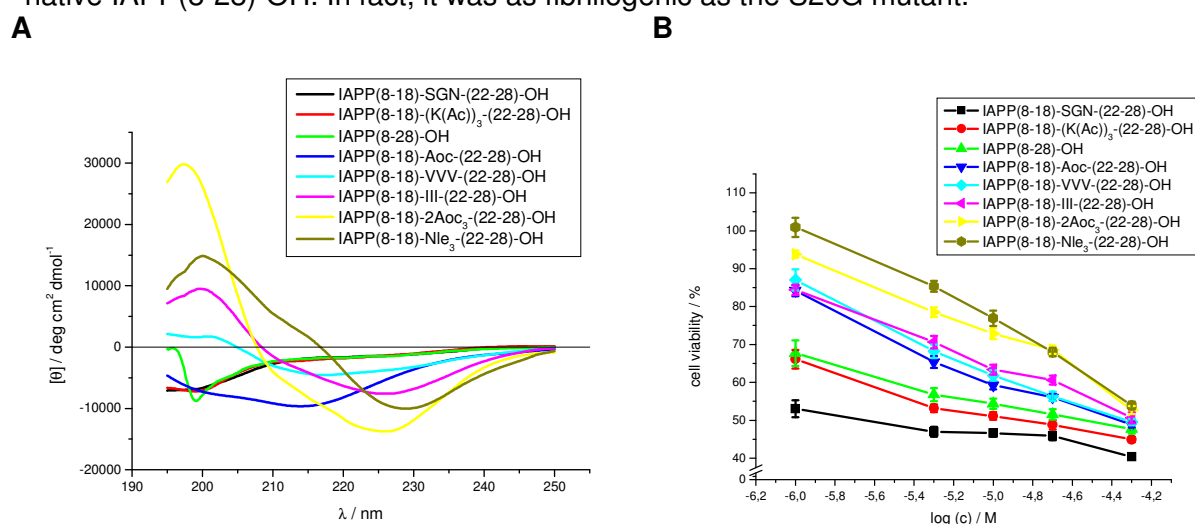


Fig. 144: (A) Comparison of the CD spectra of IAPP(8-18)-SGN-(22-28)-OH, IAPP(8-18)-(K(Ac))₃-(22-28)-OH, IAPP(8-28)-OH, IAPP(8-18)-Aoc-(22-28)-OH, IAPP(8-18)-VTV-(22-28)-OH, IAPP(8-18)-III-(22-28)-OH, IAPP(8-18)-2Aoc₃-(22-28)-OH and IAPP(8-18)-Nle₃-(22-28)-OH at a peptide concentration of 5 μ M in 1x1% HFIP, pH 7.4.

(B) Comparison of the cytotoxicity of fibrillar aggregates of peptides IAPP(8-18)-SGN-(22-28)-OH, IAPP(8-18)-(K(Ac))₃-(22-28)-OH, IAPP(8-28)-OH, IAPP(8-18)-Aoc-(22-28)-OH, IAPP(8-18)-VVV-(22-28)-OH, IAPP(8-18)-III-(22-28)-OH, IAPP(8-18)-2Aoc₃-(22-28)-OH and IAPP(8-18)-Nle₃-(22-28)-OH to RIN5fm cells. Data are percentages of control and are the mean (+/-SEM) of three independent experiments with each experiment performed in multiple replicates (n = 3).

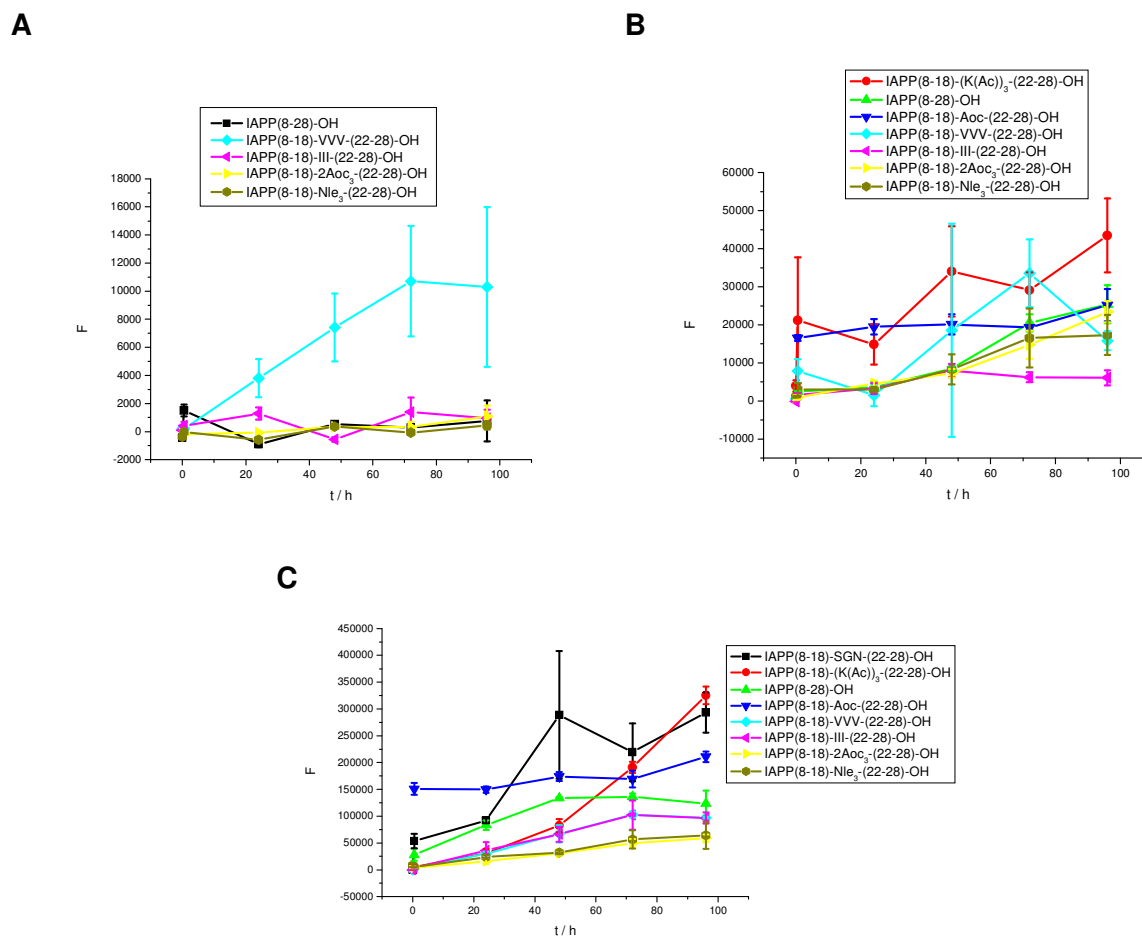


Fig. 145: (A) Comparison of ThT assays at 20 μ M of peptides IAPP(8-28)-OH, IAPP(8-18)-VVV-(22-28)-OH, IAPP(8-18)-III-(22-28)-OH, IAPP(8-18)-2Aoc₃-(22-28)-OH and IAPP(8-18)-Nle₃-(22-28)-OH in 1xb 1% HFiP, pH 7.4. Data are means of 3 assays after subtraction of buffer values +/- standard error of the mean (SEM) with each experiment performed in multiple replicates (n = 3).

(B) Comparison of ThT assays at 35 μ M of peptides IAPP(8-18)-(K(Ac))₃-(22-28)-OH, IAPP(8-28)-OH, IAPP(8-18)-Aoc-(22-28)-OH, IAPP(8-18)-VVV-(22-28)-OH, IAPP(8-18)-III-(22-28)-OH, IAPP(8-18)-2Aoc₃-(22-28)-OH and IAPP(8-18)-Nle₃-(22-28)-OH in 1xb 1% HFiP, pH 7.4. Data are means of 3 assays after subtraction of buffer values +/- standard error of the mean (SEM) with each experiment performed in multiple replicates (n = 3).

(C) Comparison of ThT assays of 100 μ M of peptides IAPP(8-18)-SGN-(22-28)-OH, IAPP(8-18)-(K(Ac))₃-(22-28)-OH, IAPP(8-28)-OH, IAPP(8-18)-Aoc-(22-28)-OH, IAPP(8-18)-VVV-(22-28)-OH, IAPP(8-18)-III-(22-28)-OH, IAPP(8-18)-2Aoc₃-(22-28)-OH and IAPP(8-18)-Nle₃-(22-28)-OH in 1xb 1% HFiP, pH 7.4. Data are means of 3 assays after subtraction of buffer values +/- standard error of the mean (SEM) with each experiment performed in multiple replicates (n = 3).

Among the most toxic analogues were several of the ones with hydrophobic elements in the IAPP(19-21) region which were almost as toxic and fibrillogenic as the native sequence (Fig. 144B and Fig. 145). As mentioned above (chapter 3.1.2.4), not only the hydrophobicity but also the steric hindrance of the side chain of the amino acids forming the IAPP(19-21) region was responsible for expressing these features.

A common feature of all those peptides was that they seem to have β -sheet and β -turn elements in their structure as shown by a negative signal in the CD spectra from around 210-240 nm (Fig. 144A).

Table 10: Overview of ThT and cell viability assays performed of the analogues of IAPP(8-28) that displayed high toxicity to RIN cells.

Results of “+” indicate fibril formation, whereas “-” indicate no fibril formation within the 5 days of incubation of the solution at the given peptide concentration.

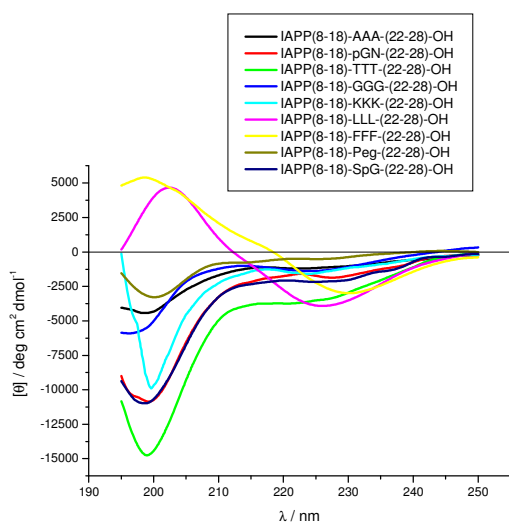
For the cell viability assays, results of “+++” mean high toxicity towards RIN cells.

Sequence	ThT								Tox
	5 μ M	10 μ M	20 μ M	35 μ M	50 μ M	100 μ M	200 μ M	500 μ M	
IAPP(8-18)-SGN-(22-28)-OH	-	+		+		+			+++
IAPP(8-18)-K(Ac) ₃ -(22-28)-OH	-	+	+	+	+	+			+++
IAPP(8-28)-OH			-	+	+	+			+++
IAPP(8-18)-Aoc-(22-28)-OH			-	+		+			+++
IAPP(8-18)-VVV-(22-28)-OH		-	+	+	+	+	+		+++
IAPP(8-18)-III-(22-28)-OH			-	+	+	+	+		+++
IAPP(8-18)-2(Aoc) ₃ -(22-28)-OH			-	+		+			+++
IAPP(8-18)-Nle ₃ -(22-28)-OH			-	+	+	+	+		+++

3.1.2.6.2 Medium toxicity

This group contained analogues with a wide variety of different attributes in the IAPP(19-21) region. Amino acids with aromatic, hydrophobic and charged side chains as well as secondary structure inducing elements belonged to this group. It was quite likely that many different aspects like steric hindrance and hydrophobicity of the side chains, rigidity of the IAPP(19-21) region and also interactions of the flanking regions IAPP(8-18) and IAPP(22-28) both with each other and with the IAPP(19-21) region were responsible for this rather complex picture.

A



B

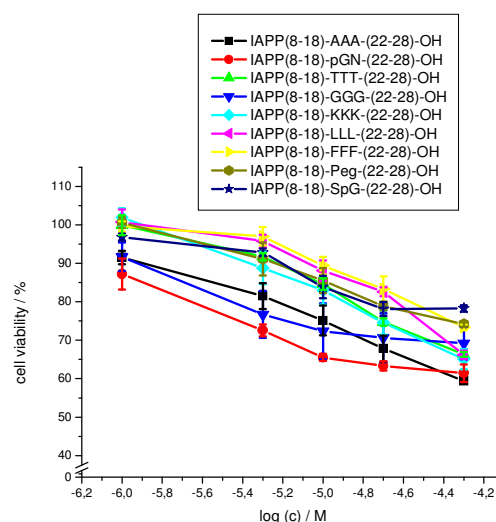
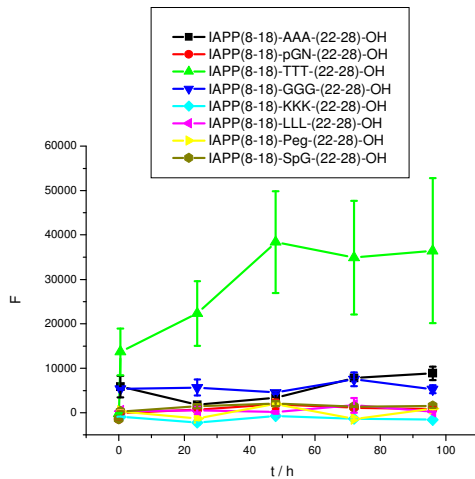


Fig. 146: (A) Comparison of the CD spectra of IAPP(8-18)-AAA-(22-28)-OH, IAPP(8-18)-pGN-(22-28)-OH, IAPP(8-18)-TTT-(22-28)-OH, IAPP(8-18)-GGG-(22-28)-OH, IAPP(8-18)-KKK-(22-28)-OH, IAPP(8-18)-LLL-(22-28)-OH, IAPP(8-18)-FFF-(22-28)-OH, IAPP(8-18)-Peg-(22-28)-OH and IAPP(8-18)-SpG-(22-28)-OH at a peptide concentration of 5 μ M in 1xb 1% HFIP, pH 7.4.

(B) Comparison of the cytotoxicity of fibrillar aggregates of peptides IAPP(8-18)-AAA-(22-28)-OH, IAPP(8-18)-pGN-(22-28)-OH, IAPP(8-18)-TTT-(22-28)-OH, IAPP(8-18)-GGG-(22-28)-OH, IAPP(8-18)-KKK-(22-28)-OH, IAPP(8-18)-LLL-(22-28)-OH, IAPP(8-18)-FFF-(22-28)-OH, IAPP(8-18)-Peg-(22-28)-OH, and IAPP(8-18)-SpG-(22-28)-OH to RIN5fm cells. Data are percentages of control and are the mean (+/-SEM) of three independent experiments with each experiment performed in multiple replicates (n = 3).

A



B

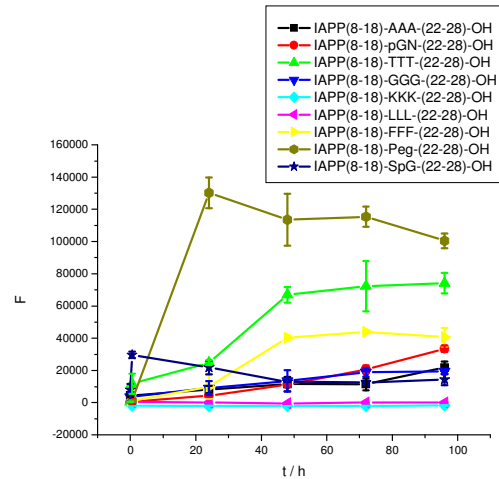


Fig. 147: (A) Comparison of ThT assays of peptides IAPP(8-18)-AAA-(22-28)-OH, IAPP(8-18)-pGN-(22-28)-OH, IAPP(8-18)-TTT-(22-28)-OH, IAPP(8-18)-GGG-(22-28)-OH, IAPP(8-18)-KKK-(22-28)-OH, IAPP(8-18)-LLL-(22-28)-OH, IAPP(8-18)-Peg-(22-28)-OH and IAPP(8-18)-SpG-(22-28)-OH at a concentration of 35 μ M for each peptide in 1xb 1% HFIP, pH 7.4. Data are means of 3 assays after subtraction of buffer values \pm standard error of the mean (SEM) with each experiment performed in multiple replicates ($n = 3$).

(B) Comparison of ThT assays of peptides IAPP(8-18)-AAA-(22-28)-OH, IAPP(8-18)-pGN-(22-28)-OH, IAPP(8-18)-TTT-(22-28)-OH, IAPP(8-18)-GGG-(22-28)-OH, IAPP(8-18)-KKK-(22-28)-OH, IAPP(8-18)-LLL-(22-28)-OH, IAPP(8-18)-FFF-(22-28)-OH, IAPP(8-18)-Peg-(22-28)-OH and IAPP(8-18)-SpG-(22-28)-OH at a concentration of 100 μ M for each peptide in 1xb 1% HFIP, pH 7.4. Data are means of 3 assays after subtraction of buffer values \pm standard error of the mean (SEM) with each experiment performed in multiple replicates ($n = 3$).

In most of the here studied analogues, lower toxicity seemed to be linked to lower fibril forming potential, even though this was not always the case (Fig. 146B and Fig. 147).

Table 11: Overview of ThT and cell viability assays performed of the analogues of IAPP(8-28) that displayed medium toxicity to RIN cells.

Results of “+” indicate fibril formation, whereas “-” indicate no fibril formation within the 5 days of incubation of the solution at the given peptide concentration.

For the cell viability assays, results of “++” mean medium toxicity towards RIN cells and “+/-” mean low toxicity.

Sequence	ThT								Tox
	5 μ M	10 μ M	20 μ M	35 μ M	50 μ M	100 μ M	200 μ M	500 μ M	
IAPP(8-18)- AAA -(22-28)-OH				-		+	+		++
IAPP(8-18)- pGN -(22-28)-OH				-	-	+			++
IAPP(8-18)- TTT -(22-28)-OH			-	+		+			++
IAPP(8-18)- GGG -(22-28)-OH				-		+	+		++
IAPP(8-18)- KKK -(22-28)-OH				-		-	-	-	++
IAPP(8-18)- LLL -(22-28)-OH			-	-		-	+	+	++
IAPP(8-18)- FFF -(22-28)-OH						+	+		++
IAPP(8-18)- Peg -(22-28)-OH				-		+			++
IAPP(8-18)- SpG -(22-28)-OH				-	+	+			+/-

3.1.2.6.3 Low toxicity

Peptides in this group showed very low or no fibril forming potential and toxicity (Fig. 148B). They displayed mainly a random coil structure in CD and showed no minimum at around 220 nm (Fig. 148A).

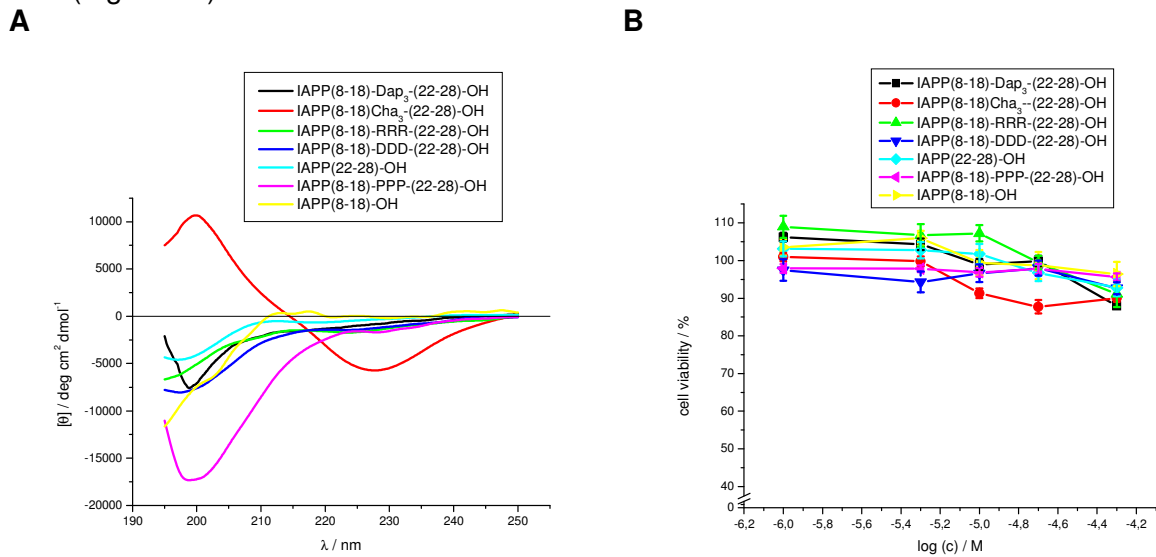


Fig. 148: (A) Comparison of the CD spectra of IAPP(8-18)-Dap₃-(22-28)-OH, IAPP(8-18)-Cha₃-(22-28)-OH, IAPP(8-18)-RRR-(22-28)-OH, IAPP(8-18)-DDD-(22-28)-OH and IAPP(8-18)-PPP-(22-28)-OH at a peptide concentration of 5 μ M in 1xb 1% HFIP, pH 7.4.

(B) Comparison of the cytotoxicity of aggregates of peptides IAPP(8-18)-Dap₃-(22-28)-OH, IAPP(8-18)-Cha₃-(22-28)-OH, IAPP(8-18)-RRR-(22-28)-OH, IAPP(8-18)-DDD-(22-28)-OH, IAPP(22-28)-OH, IAPP(8-18)-PPP-(22-28)-OH and IAPP(8-18)-OH to RIN5fm cells. Data are percentages of control and are the mean (+/-SEM) of three independent experiments with each experiment performed in multiple replicates (n = 3).

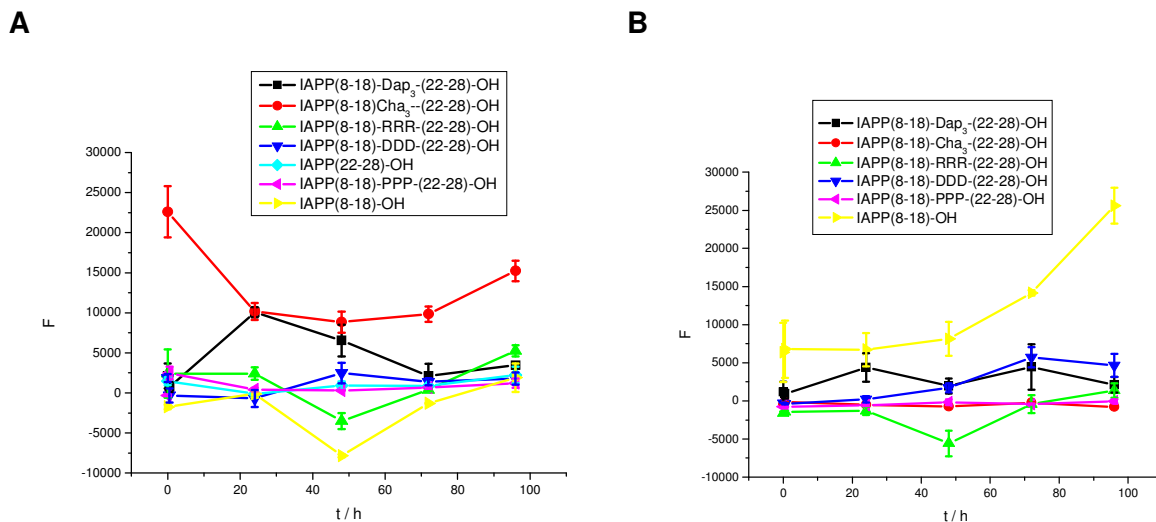


Fig. 149: (A) Comparison of ThT assays of peptides IAPP(8-18)-Dap₃-(22-28)-OH, IAPP(8-18)-Cha₃-(22-28)-OH, IAPP(8-18)-RRR-(22-28)-OH, IAPP(8-18)-DDD-(22-28)-OH, IAPP(22-28)-OH, IAPP(8-18)-PPP-(22-28)-OH and IAPP(8-18)-OH at a concentration of 100 μ M for each peptide in 1xb 1% HFIP, pH 7.4. Data are means of 3 assays after subtraction of buffer values +/- standard error of the mean (SEM) with each experiment performed in multiple replicates (n = 3).

(B) Comparison of ThT assays of peptides IAPP(8-18)-Dap₃-(22-28)-OH, IAPP(8-18)-Cha₃-(22-28)-OH, IAPP(8-18)-RRR-(22-28)-OH, IAPP(8-18)-DDD-(22-28)-OH, IAPP(8-18)-PPP-(22-28)-OH and IAPP(8-18)-OH at a concentration of 500 μ M for each peptide in 1xb 1% HFIP, pH 7.4. Data are means of 3 assays after subtraction of buffer values +/- standard error of the mean (SEM) with each experiment performed in multiple replicates (n = 3).

The assays performed, revealed no simple linear relationship between the toxicity and other features typical for the different analogues – except for their fibril forming potential (Fig. 148B, Fig. 149 and table 12). The reason therefore was that the analogues presented different features with contrary effects on toxicity at the same time. For example Cha is an extremely hydrophobic but also sterically hindered building block. Therefore IAPP(8-18)-Cha₃-(22-28)-OH displayed features typical for hydrophobic analogues like intense β -turn and β -sheet structures in CD but the peptide was not toxic and did not form fibrils. Therefore more detailed studies were performed with selected analogues to address this issue (chapter 3.1.3 and 3.1.4).

Table 12: Overview of ThT and cell viability assays performed of the analogues of IAPP(8-28) that displayed low toxicity to RIN cells.

Results of “+” indicate fibril formation, whereas “-” indicate no fibril formation within the 5 days of incubation of the solution at the given peptide concentration.

For the cell viability assays, results of “+/-” mean low toxicity towards RIN cells and “-“ mean no toxicity.

Sequence	ThT										Tox
	5 μ M	10 μ M	20 μ M	35 μ M	50 μ M	100 μ M	200 μ M	500 μ M	5 mM	10 mM	
IAPP(8-18)-Dap ₃ -(22-28)-OH						-	-	-			-
IAPP(8-18)-Cha ₃ -(22-28)-OH				-		-	-	-			+/-
IAPP(8-18)-RRR-(22-28)-OH						-	-	-			-
IAPP(8-18)-DDD-(22-28)-OH						-		-			-
IAPP(22-28)-OH						-	-	-	-	-	-
IAPP(8-18)-PPP-(22-28)-OH						-		-			-
IAPP(8-18)-OH						-	-	+			-

3.1.2.7 Scanning of the IAPP(19-21) region with Lys and Lys(Ac)

IAPP(8-18)-(K(Ac))₃-(22-28)-OH was the most toxic and fibrillogenic among the designed analogues. On the other hand, IAPP(8-18)-KKK-(22-28)-OH did not form fibrils. The big difference between Lys and Lys(Ac) lies in the side chain. While the side chain of Lys is charged, this charge is eliminated in the side chain of Lys(Ac) by acetylation of the amino group of the side chain, creating a polar noncharged side chain.

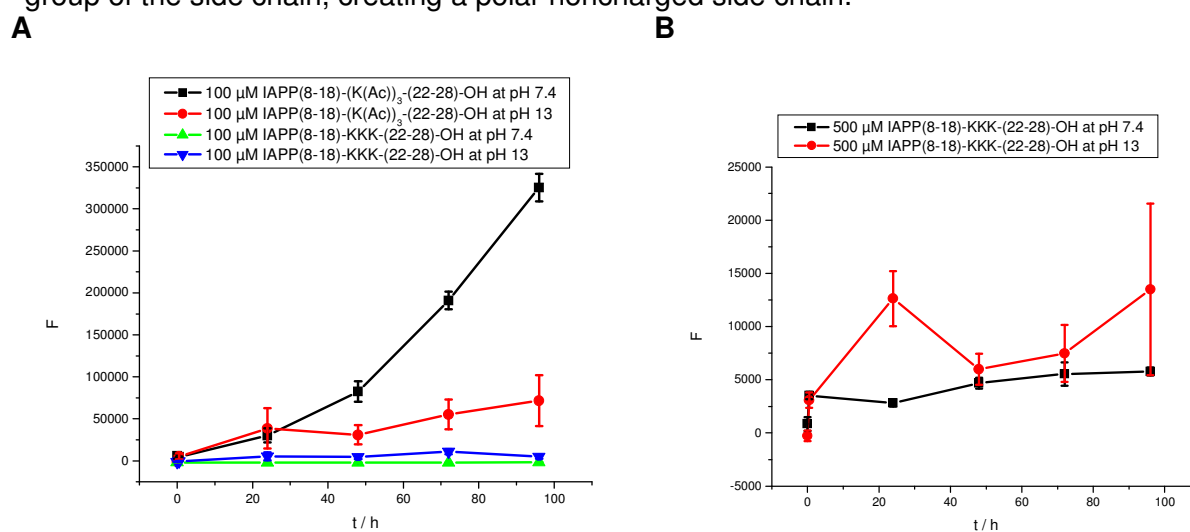


Fig. 150: (A) Comparison of ThT assays of IAPP(8-18)-(K(Ac))₃-(22-28)-OH and IAPP(8-18)-KKK-(22-28)-OH at a concentration of 100 μ M for each peptide in 10 mM sodium phosphate buffer at pH 7.4 and pH 13 containing 1%

HFiP. Data are means of 3 assays after subtraction of buffer values \pm standard error of the mean (SEM) with each experiment performed in multiple replicates ($n = 3$).

(B) Comparison of ThT assays of IAPP(8-18)-KKK-(22-28)-OH at a concentration of 500 μ M in 10 mM sodium phosphate buffer at pH 7.4 and pH 13 containing 1% HFiP. Data are means of 3 assays after subtraction of buffer values \pm standard error of the mean (SEM) with each experiment performed in multiple replicates ($n = 3$).

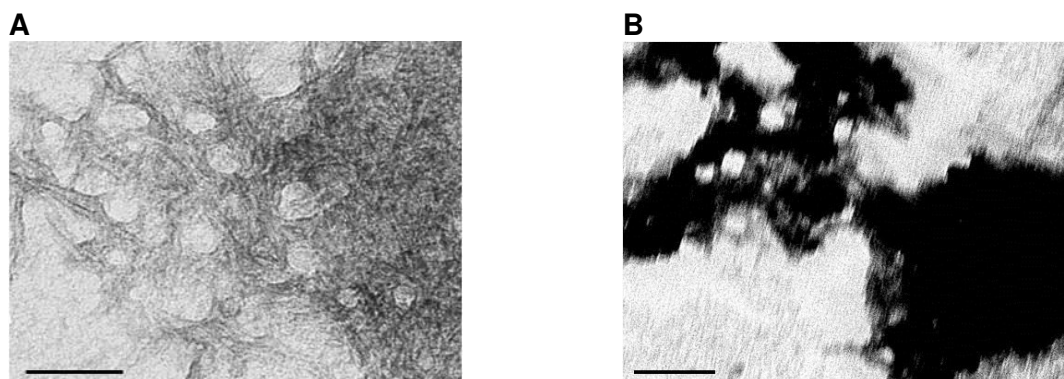


Fig. 151: (A) TEM picture of IAPP(8-18)-(K(Ac))₃-(22-28)-OH. The peptide was incubated at 100 μ M for 7 d in 1x 1% HFiP at pH 13. Scale bar: 100 nm.

(B) TEM picture of IAPP(8-18)-KKK-(22-28)-OH. The peptide was incubated at 500 μ M for 7 d in 1x 1% HFiP at pH 13. Scale bar: 100 nm.

ThT studies at different pH values revealed, that the presence or absence of charge was not the only factor determining the fibril forming potential. IAPP(8-18)-KKK-(22-28)-OH was also not forming fibrils when incubated at pH 13 where the side chain of Lys was uncharged (Fig. 150). By contrast IAPP(8-18)-(K(Ac))₃-(22-28)-OH was able to form fibrils at pH 13. This could be verified by TEM (Fig. 151A and B).

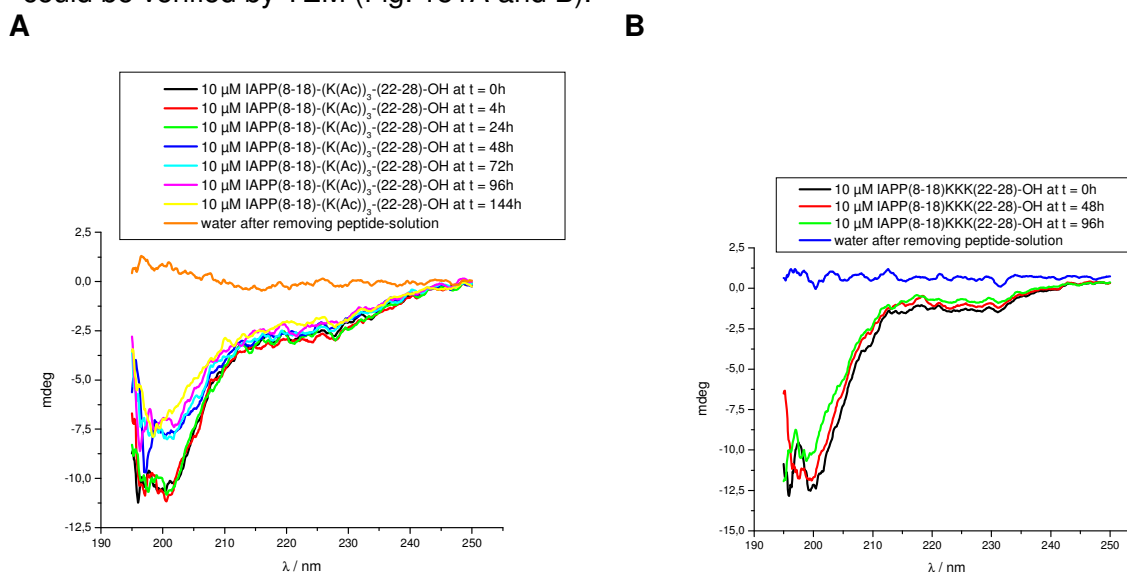
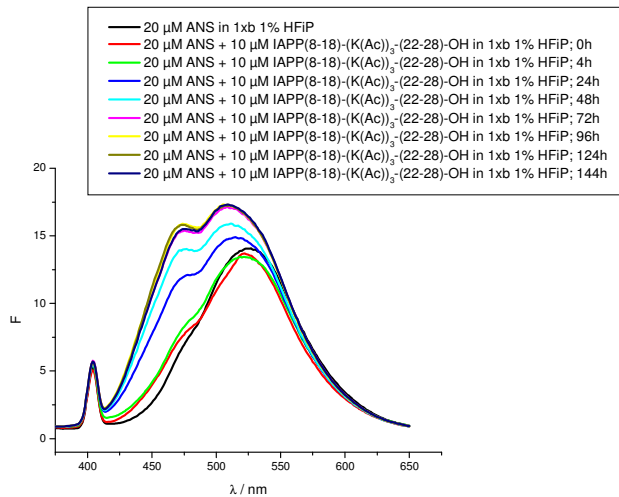


Fig. 152: Time dependent CD spectra of IAPP(8-18)-(K(Ac))₃-(22-28)-OH (A) and IAPP(8-18)-KKK(22-28)-OH (B) at a concentration of 10 μ M. Experiments were done in 10 mM sodium phosphate buffer at pH 7.4 containing 1% HFiP.

Time dependent CD studies showed that the signal of IAPP(8-18)-(K(Ac))₃-(22-28)-OH was undergoing weak changes in the process of fibril formation. The random coil signal was getting reduced after more than 24 h incubation, whereas the β -sheet and β -turn structural content at around 220 nm remained unchanged (Fig. 152). These changes were further confirmed by ThT and ANS analysis (Fig. 153). All these studies were done at a peptide concentration of 10 μ M in 10 mM sodium phosphate buffer at pH 7.4 containing 1% HFiP.

A



B

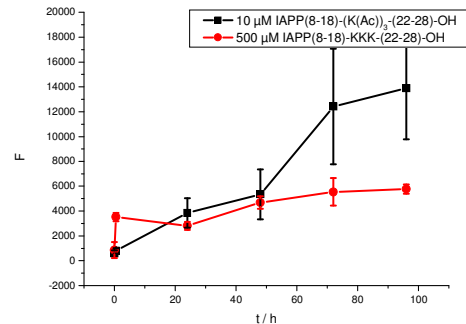


Fig. 153: (A) Time dependent ANS assays of IAPP(8-18)-(K(Ac))₃-(22-28)-OH at a peptide concentration of 10 μM in 1xb 1% HFiP, pH 7.4.

(B) ThT assays of IAPP(8-18)-(K(Ac))₃-(22-28)-OH at a peptide concentration of 10 μM and of IAPP(8-18)-KKK-(22-28)-OH at a peptide concentration of 500 μM in 1xb 1% HFiP, pH 7.4. Data are means of 3 assays after subtraction of buffer values +/- standard error of the mean (SEM) with each experiment performed in multiple replicates (n = 3).

The changes in the ANS binding ability of IAPP(8-18)-(K(Ac))₃-(22-28)-OH (Fig. 153A) occurred before changes in the CD structure and a significant increase in the ThT binding ability, indicating that an exposure of hydrophobic surfaces appeared before structural changes were made and fibrils were formed which is also consistent with existing literature [174]. In all cases, the plateau of these changes was reached between 48-72 h.

The small increase in the ThT signal of IAPP(8-18)-(K(Ac))₃-(22-28)-OH already after 24 h (Fig. 153B) might be related to the formation of protofibrils. During the process of fibril formation, increased binding affinity to ANS occurred in general faster than an increased binding to ThT, suggesting that an increased hydrophobic exposure was a feature of early aggregation and assembly into protofibrils before the actual formation of mature amyloidogenic fibrils.

To further investigate the role of Lys(Ac) and Lys in the IAPP(19-21) region and their effects on cytotoxicity and fibril formation, a set of peptides displaying every possible combination of Lys and Lys(Ac) in the IAPP(19-21) region was synthesized and tested.

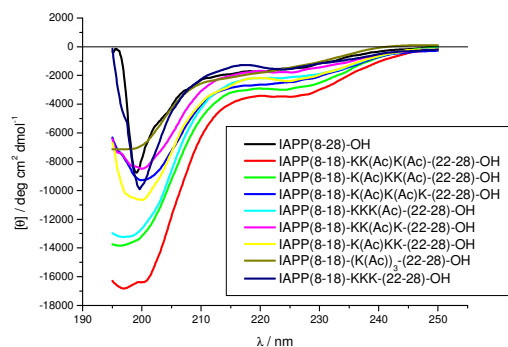


Fig. 154: Comparison of the CD spectra of IAPP(8-18)-KK(Ac)K(Ac)-(22-28)-OH, IAPP(8-18)-K(Ac)KK(Ac)-(22-28)-OH, IAPP(8-18)-K(Ac)K(Ac)K-(22-28)-OH, IAPP(8-18)-KKK(Ac)-(22-28)-OH, IAPP(8-18)-KK(Ac)K-(22-28)-OH, IAPP(8-18)-K(Ac)KK-(22-28)-OH, IAPP(8-18)-(K(Ac))₃-(22-28)-OH and IAPP(8-18)-KKK-(22-28)-OH at a peptide concentration of 5 μM in 1xb 1% HFiP, pH 7.4.

The CD spectra of all peptides showed mainly random coil signals and a weak minimum at around 210-230 nm. This minimum was a little more intense for peptides with two Lys(Ac) in the IAPP(19-21) region than for peptides with only one Lys(Ac) in the IAPP(19-21) region (Fig. 155). IAPP(8-18)-KK(Ac)K(Ac)-(22-28)-OH was the most toxic one among the peptides with a mixed IAPP(19-21) sequence and had also the highest magnitude in the CD signal at a peptide concentration of 5 μ M. The two peptides with homogeneous IAPP(19-21) sequences, IAPP(8-18)-(K(Ac))₃-(22-28)-OH and IAPP(8-18)-KKK-(22-28)-OH, had weaker signals in CD than the peptides with a mixed IAPP(19-21) sequence (Fig. 154 and Fig. 155).

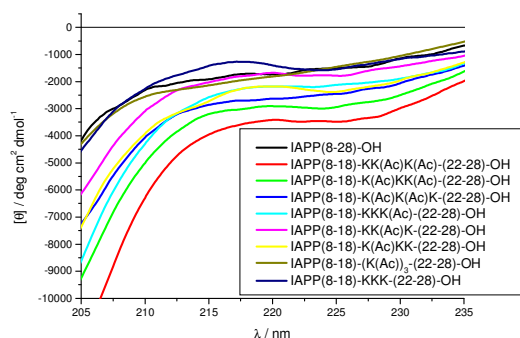


Fig. 155: Comparison of the CD spectra of IAPP(8-18)-KK(Ac)K(Ac)-(22-28)-OH, IAPP(8-18)-K(Ac)KK(Ac)-(22-28)-OH, IAPP(8-18)-K(Ac)K(Ac)K-(22-28)-OH, IAPP(8-18)-KKK(Ac)-(22-28)-OH, IAPP(8-18)-KK(Ac)K-(22-28)-OH, IAPP(8-18)-K(Ac)KK-(22-28)-OH, IAPP(8-18)-(K(Ac))₃-(22-28)-OH and IAPP(8-18)-KKK-(22-28)-OH at a peptide concentration of 5 μ M in 1x 1% HFIP, pH 7.4.

When taking a closer look at the CD signal between 210 nm and 230 nm (Fig. 155) it was obvious that peptides with two Lys(Ac) in the IAPP(19-21) region displayed a more intense signal than peptides with only one Lys(Ac). The spectrum of IAPP(8-18)-KK(Ac)K(Ac)-(22-28)-OH showed the most intense signal between 210 nm and 230 nm. IAPP(8-18)-KK(Ac)K(Ac)-(22-28)-OH was also the most toxic and fibrillogenic among the analogues with intermixing Lys(Ac) and Lys in the IAPP(19-21) sequence. The weak signal of IAPP(8-18)-(K(Ac))₃-(22-28)-OH might have been due to an aggregation of the peptide already occurring at a concentration of 5 μ M.

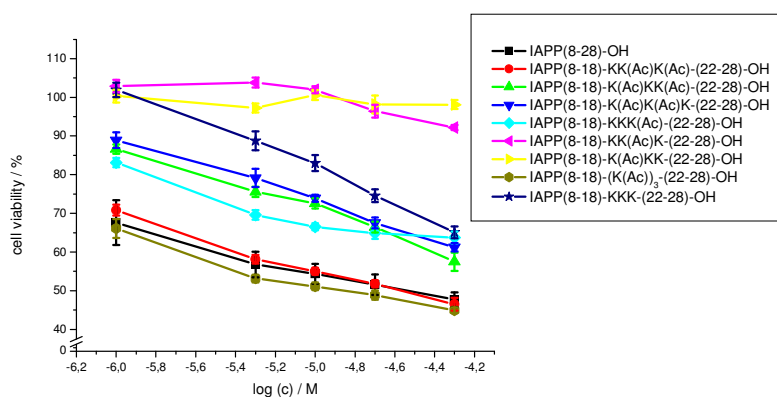


Fig. 156: Comparison of the cytotoxicity of fibrillar aggregates of IAPP(8-18)-KK(Ac)K(Ac)-(22-28)-OH, IAPP(8-18)-K(Ac)KK(Ac)-(22-28)-OH, IAPP(8-18)-K(Ac)K(Ac)K-(22-28)-OH, IAPP(8-18)-KKK(Ac)-(22-28)-OH, IAPP(8-18)-KK(Ac)K-(22-28)-OH, IAPP(8-18)-K(Ac)KK-(22-28)-OH, IAPP(8-18)-(K(Ac))₃-(22-28)-OH and IAPP(8-18)-KKK-(22-28)-OH to RIN5fm cells. Data are percentages of control and are the mean (+/-SEM) of three independent experiments with each experiment performed in multiple replicates (n = 3).

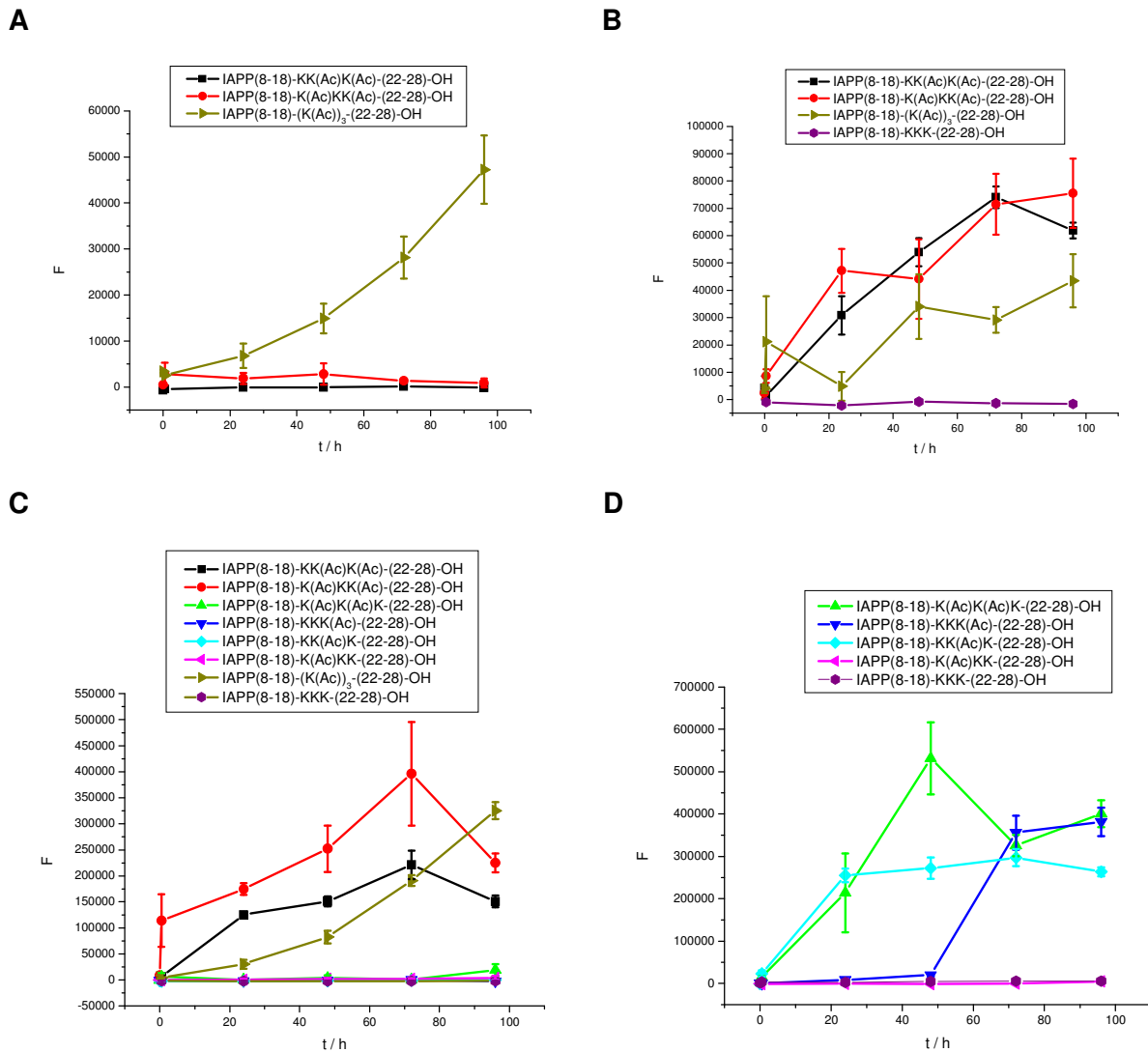


Fig. 157: (A) Comparison of ThT assays of IAPP(8-18)-KK(Ac)K(Ac)-(22-28)-OH, IAPP(8-18)-K(Ac)KK(Ac)-(22-28)-OH and IAPP(8-18)-(K(Ac))₃-(22-28)-OH at a concentration of 20 μM for each peptide in 1xb 1% HFIP, pH 7.4. Data are means of 3 assays after subtraction of buffer values +/- standard error of the mean (SEM) with each experiment performed in multiple replicates (n = 3).

(B) Comparison of ThT assays of IAPP(8-18)-KK(Ac)K(Ac)-(22-28)-OH, IAPP(8-18)-K(Ac)KK(Ac)-(22-28)-OH, IAPP(8-18)-(K(Ac))₃-(22-28)-OH and IAPP(8-18)-KKK-(22-28)-OH at a concentration of 35 μM for each peptide in 1xb 1% HFIP, pH 7.4. Data are means of 3 assays after subtraction of buffer values +/- standard error of the mean (SEM) with each experiment performed in multiple replicates (n = 3).

(C) Comparison of ThT assays of IAPP(8-18)-KK(Ac)K(Ac)-(22-28)-OH, IAPP(8-18)-K(Ac)KK(Ac)-(22-28)-OH, IAPP(8-18)-K(Ac)K(Ac)K(Ac)-(22-28)-OH, IAPP(8-18)-KKK(Ac)-(22-28)-OH, IAPP(8-18)-KK(Ac)K(Ac)-(22-28)-OH, IAPP(8-18)-K(Ac)KK(Ac)-(22-28)-OH, IAPP(8-18)-(K(Ac))₃-(22-28)-OH and IAPP(8-18)-KKK-(22-28)-OH at a concentration of 100 μM for each peptide in 1xb 1% HFIP, pH 7.4. Data are means of 3 assays after subtraction of buffer values +/- standard error of the mean (SEM) with each experiment performed in multiple replicates (n = 3).

(D) Comparison of ThT assays of IAPP(8-18)-K(Ac)K(Ac)K(Ac)-(22-28)-OH, IAPP(8-18)-KKK(Ac)-(22-28)-OH, IAPP(8-18)-KK(Ac)K(Ac)-(22-28)-OH, IAPP(8-18)-K(Ac)KK(Ac)-(22-28)-OH and IAPP(8-18)-KKK-(22-28)-OH at a concentration of 500 μM for each peptide in 1xb 1% HFIP, pH 7.4. Data are means of 3 assays after subtraction of buffer values +/- standard error of the mean (SEM) with each experiment performed in multiple replicates (n = 3).

In general, peptides with two Lys(Ac) in the IAPP(19-21) region were more toxic and displayed a higher fibril forming potential than peptides with only one Lys(Ac) in the IAPP(19-21) region. IAPP(8-18)-KK(Ac)K(Ac)-(22-28)-OH with two consecutive Lys(Ac) in position 20 and 21 was the most toxic and fibrillogenic peptide among these analogues, whereas

IAPP(8-18)-K(Ac)KK-(22-28)-OH with one Lys(Ac) in position 19 was the least toxic and fibrillogenic one. The analogue IAPP(8-18)-KKK(Ac)-(22-28)-OH with one Lys(ac) at position 12 was mediate toxic (Fig. 156 and table 13). These data suggested that a Lys(Ac) at position 21 was the most important for toxicity and fibril formation while a Lys(Ac) at position 19 was the least important. IAPP(8-18)-KKK(Ac)-(22-28)-OH was similar toxic but less fibrillogenic than IAPP(8-18)-K(Ac)K(Ac)K-(22-28)-OH and IAPP(8-18)-K(Ac)KK(Ac)-(22-28)-OH. The toxicity of IAPP(8-18)-KKK(Ac)-(22-28)-OH seemed to be linked to the presence of both a Lys(Ac) at position 21 and two Lys at position 19 and 20. IAPP(8-18)-K(Ac)KK-(22-28)-OH and IAPP(8-18)-KK(Ac)K-(22-28)-OH were both non toxic and had no consecutive Lys at position 19 and 20 both also only one Lys(Ac) in the IAPP(19-21) region (Fig. 156 and table 13).

Table 13: Overview of ThT and cell viability assays performed of the analogues of IAPP(8-28) with different combinations of Lys and Lys(Ac) residues in the IAPP(19-21) region.

Results of “+” indicate fibril formation, whereas “-” indicate no fibril formation within the 5 days of incubation of the solution at the given peptide concentration.

For the cell viability assays, results of “+++” mean high toxicity towards RIN cells, “++” mean medium toxicity, and “-” mean no toxicity.

Sequence	ThT								Tox.
	5 μ M	10 μ M	20 μ M	35 μ M	50 μ M	100 μ M	200 μ M	500 μ M	
IAPP(8-18)- KKK (Ac)-(22-28)-OH				-		-	-	-	++
IAPP(8-18)- K(Ac)KK (Ac)-(22-28)-OH		-				-	-	-	-
IAPP(8-18)- KK(Ac)K (Ac)-(22-28)-OH		-				-	-	+	-
IAPP(8-18)- KKK(Ac) (Ac)-(22-28)-OH						-	-	+	++
IAPP(8-18)- K(Ac)K(Ac)K (Ac)-(22-28)-OH		-				-	+	+	++
IAPP(8-18)- K(Ac)KK(Ac) (Ac)-(22-28)-OH			-	+		+			++
IAPP(8-18)- KK(Ac)K(Ac) (Ac)-(22-28)-OH			-	+		+			+++
IAPP(8-18)- K(Ac)₃ (Ac)-(22-28)-OH	-	+	+	+	+	+			+++

3.1.3 Thermal denaturation studies on selected analogues

Thermal denaturation studies were done to get additional information about structure and thermodynamic stability of selected analogues. A second goal was to determine whether PPII helices were formed. The CD spectra of PPII helices are quite characteristic. Typical spectra measured at low temperature display a minimum around 200 nm and a weak positive band at about 217 nm [163, 175].

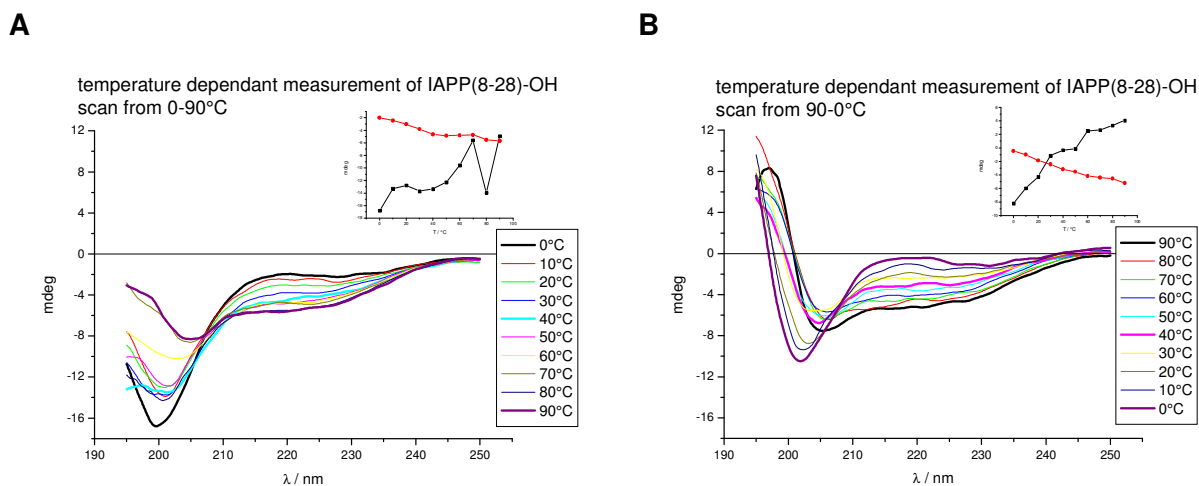


Fig. 158: Temperature dependent CD spectra of IAPP(8-28)-OH at a concentration of 5 μ M in 1xb 1% HFIP, pH 7.4. Inset: Temperature dependent changes of the CD signal intensity of the local minima at 199.6 nm (black) and 218.8 nm (red).

The CD spectrum of IAPP(8-28)-OH at 0°C showed an intense negative signal at around 200 nm indicating an extended structure. The reduction of this signal upon increased temperature correlated with an increased signal intensity between 210-230 nm which can be related to β -sheet, β -turn or even α -helical structures. A higher temperature also meant a higher energy of the system. This additional energy might have induced a reversible folding [176, 177] or aggregation of the extended structure of IAPP(8-28)-OH. Upon cooling down from 90-0°C, the increase of the signal intensity between 210-230 nm was completely inverted, whereas the intensity of their signal at around 200 nm was not completely restored (Fig. 158).

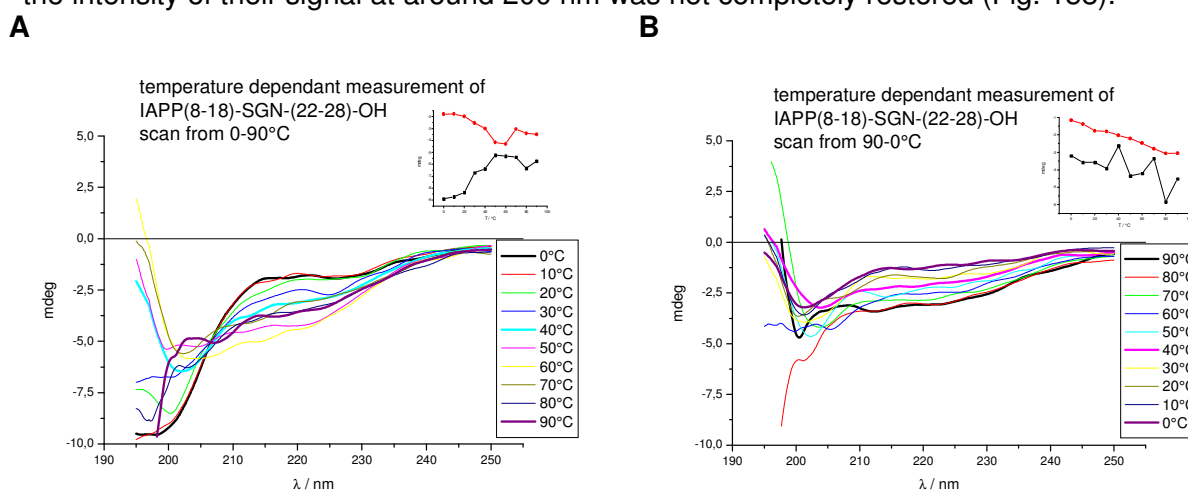


Fig. 159: Temperature dependent CD spectra of IAPP(8-18)-SGN-(22-28)-OH at a concentration of 5 μ M in 1xb 1% HFIP, pH 7.4. Inset: Temperature dependent changes of the CD signal intensity of the local minima at 201 nm (black) and 222 nm (red).

Thermal denaturation studies of IAPP(8-18)-SGN-(22-28)-OH revealed a similarity in the signal changes to those of IAPP(8-28)-OH. The signal intensities, especially the intensity of the negative signal at around 200 nm, and also the intensity of signal changes were lower than in the case of IAPP(8-28)-OH. The CD spectrum of IAPP(8-18)-SGN-(22-28)-OH at 0°C displayed a weak positive signal at 215-220 nm and a small negative band directly adjacent to that at 220-225 nm. The positive signal was typical for polyproline II helices, the negative signal at 220-225 nm an indication for β -turn elements (Fig. 159).

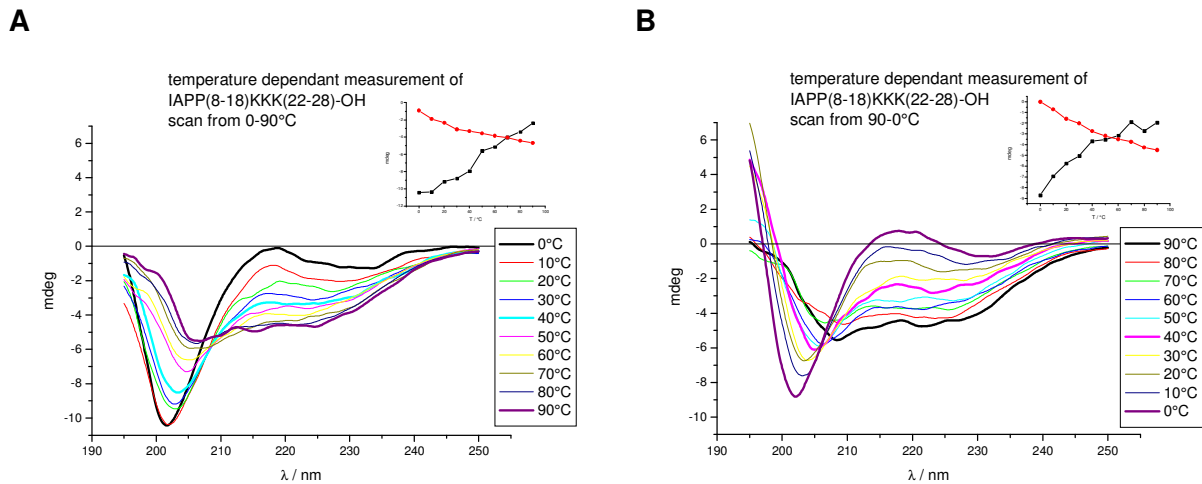


Fig. 160: Temperature dependent CD spectra of IAPP(8-18)-KKK(22-28)-OH at a concentration of 10 μ M in 1x 1% HFIP, pH 7.4. Inset: Temperature dependent changes of the CD signal intensity of the local minima at 201.6 nm (black) and 224.5 nm (red).

At 0°C, IAPP(8-18)-KKK-(22-28)-OH displayed a spectrum similar to that of IAPP(8-18)-PPP-(22-28)-OH with an intense minimum at around 200 nm and a weak positive signal at around 220 nm that is characteristic for the PII helix structure. There was also a small negative signal intensity between 220 and 230 nm in the spectra at 0°C and 10°C similar to those of IAPP(8-18)-SpG-(22-28)-OH. The temperature dependent changes of IAPP(8-18)-KKK-(22-28)-OH however were more similar to those of IAPP(8-28)-OH, especially when comparing the shape of the negative signal from 210-240 nm at higher temperatures. IAPP(8-18)-KKK-(22-28)-OH was definitely more flexible than IAPP(8-18)-RRR-(22-28)-OH, but also not able to form fibrils. These studies also indicated, that there was not much structural difference between IAPP(8-18)-KKK-(22-28)-OH and native IAPP(8-28)-OH indicating that the differences in toxicity and the fibril forming potential were related to the charges and electrostatic repulsion of the KKK motif (Fig. 160).

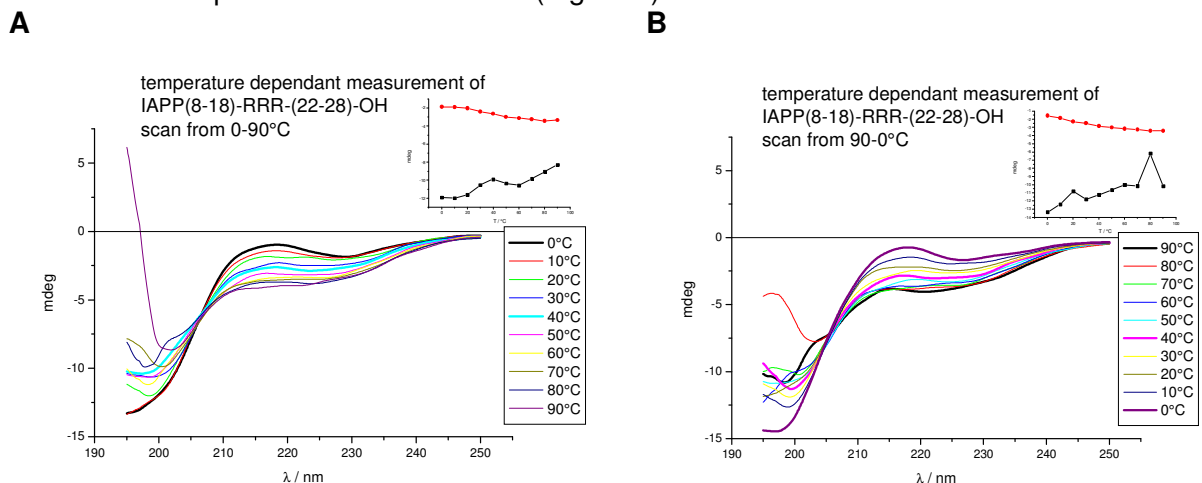


Fig. 161: Temperature dependent CD spectra of IAPP(8-18)-RRR-(22-28)-OH at a concentration of 10 μ M in 1x 1% HFIP, pH 7.4. Inset: Temperature dependent changes of the CD signal intensity of the local minima at 200 nm (black) and 229 nm (red).

Temperature dependent CD spectra of IAPP(8-18)-RRR-(22-28)-OH displayed weak changes upon increasing temperature at a peptide concentration of 10 μ M (Fig. 161). The reduction of the intensity of the negative signal at 200 nm upon increased temperature correlated with an increased signal intensity between 210-230 nm which can be related to β -

sheet, β -turn or even α -helical structures. These changes were however much weaker when compared to for example IAPP(8-28)-OH. Monomers of IAPP(8-18)-RRR-(22-28)-OH had a rigid, extended structure that could not easily be folded differently or more compactly therefore preventing fibril formation.

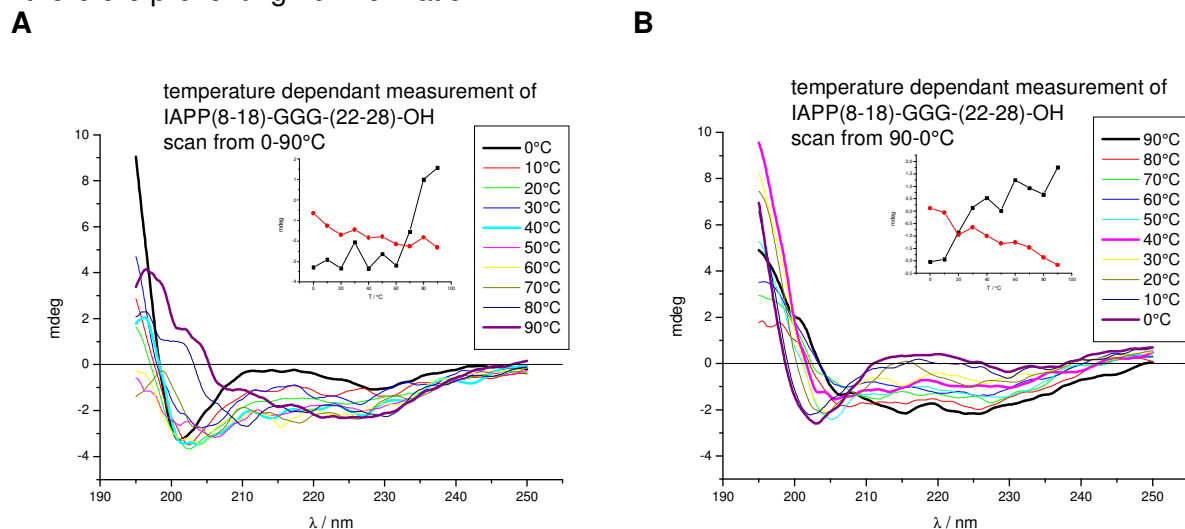


Fig. 162: Temperature dependent CD spectra of IAPP(8-18)-GGG-(22-28)-OH at a concentration of 5 μ M in 1xb 1% HFIP, pH 7.4. Inset: Temperature dependent changes of the CD signal intensity of the local minima at 201.1 nm (black) and 223.9 nm (red).

The temperature dependent CD spectra of IAPP(8-18)-GGG-(22-28)-OH were similar to those of IAPP(8-18)-SGN-(22-28)-OH and IAPP(8-18)-(K(Ac))₃-(22-28)-OH. The intensity of the CD signal was in general lower than those of IAPP(8-18)-SGN-(22-28)-OH and IAPP(8-18)-(K(Ac))₃-(22-28)-OH (Fig. 162). IAPP(8-18)-GGG-(22-28)-OH was also less toxic and had a weaker fibril forming potential than IAPP(8-18)-SGN-(22-28)-OH and IAPP(8-18)-(K(Ac))₃-(22-28)-OH.

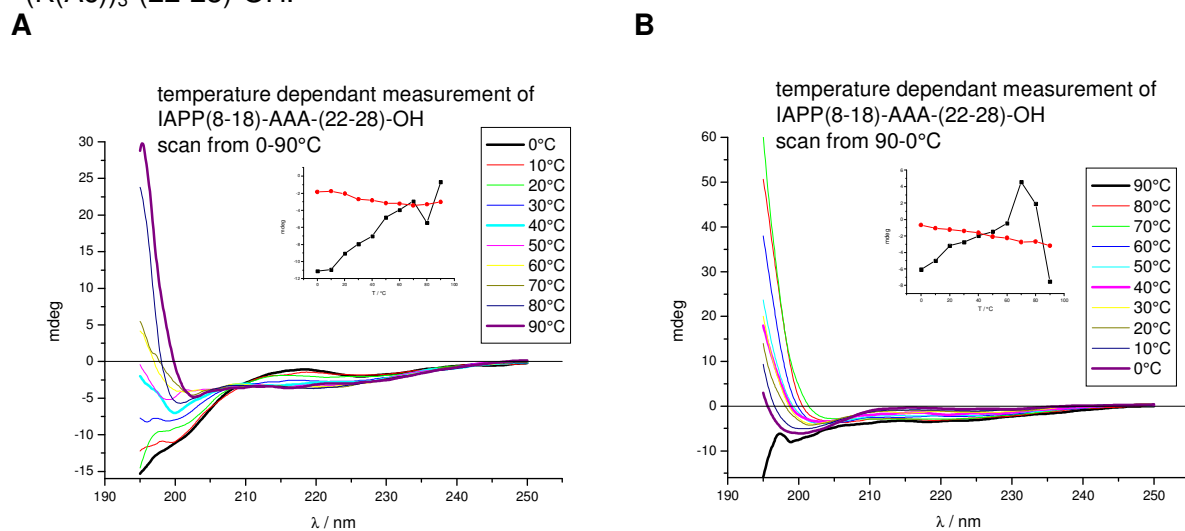


Fig. 163: Temperature dependent CD spectra of IAPP(8-18)-AAA-(22-28)-OH at a concentration of 5 μ M in 1xb 1% HFIP, pH 7.4. Inset: Temperature dependent changes of the CD signal intensity of the local minima at 200 nm (black) and 224.1 nm (red).

IAPP(8-18)-AAA-(22-28)-OH showed an intense negative signal at around 200 nm indicating a random coil or polyproline II structure. The decrease of this signal upon heating correlated with an increased signal intensity between 210-230 nm which can be related to β -sheet and β -turn structures. Upon cooling down from 90-0°C, the increase of the signal intensity

between 210-230 nm was completely inverted, whereas the intensity at around 200 nm was not completely restored. These features were similar to the changes occurring for IAPP(8-28)-OH. The CD spectra of IAPP(8-18)-AAA-(22-28)-OH at 0°C and 10°C showed a weak minimum at around 220-230 nm similar to those in the spectra of IAPP(8-18)-SpG-(22-28)-OH. This signal might be related to β -turn elements. At room temperature, these signals were not directly visible since they overlap with signals of other structural elements (Fig. 163).

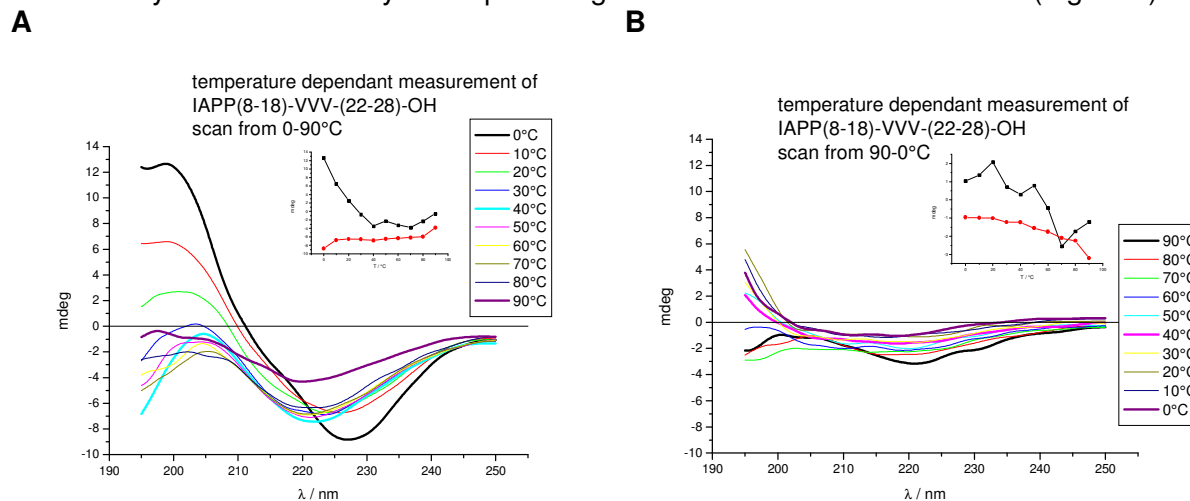


Fig. 164: Temperature dependent CD spectra of IAPP(8-18)-VVV-(22-28)-OH at a concentration of 5 μ M in 1xb 1% HFIP, pH 7.4. Inset: Temperature dependent changes of the CD signal intensity of the local maximum at 198.8 nm (black) and of the local minimum at 221.1 nm (red).

IAPP(8-18)-VVV-(22-28)-OH seemed to be the most stable among the hydrophobic peptides. The complete loss of the signal occurred only after some time at 90°C. There was even no complete loss of signal during the scan from 0-90°C (Fig. 164). The minimum of the signal between 210 and 240 nm was shifting towards lower wavelengths upon heating. This shift of the signal was intense between 0 and 10°C, but only weak during further heating indicating an initial cold denaturation process for the peptide [178]. The higher stability might be one of the reasons, why IAPP(8-18)-VVV-(22-28)-OH was also more toxic and fibrillogenic than other peptides with hydrophobic IAPP(19-21) region.

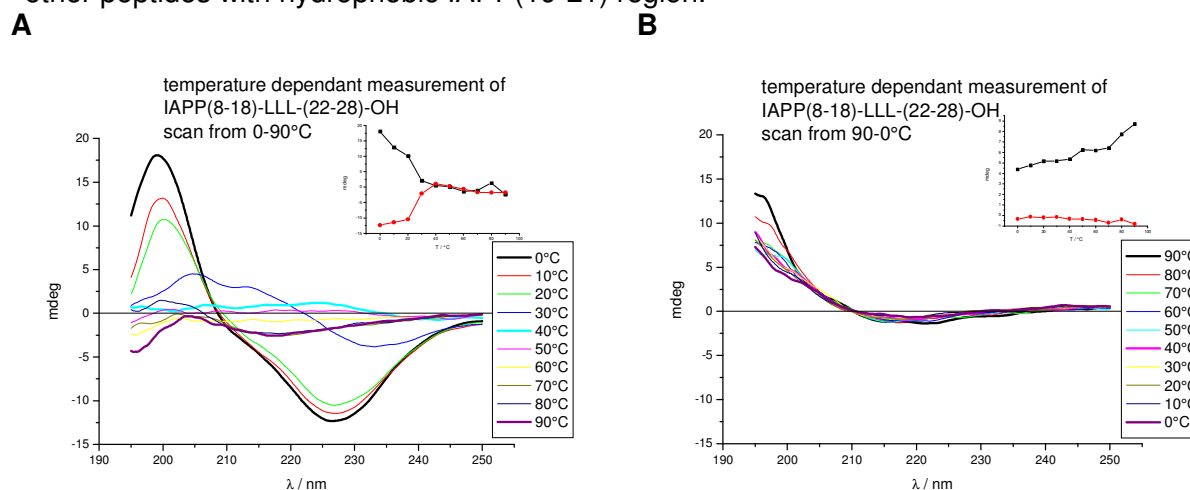


Fig. 165: Temperature dependent CD spectra of IAPP(8-18)-LLL-(22-28)-OH at a concentration of 5 μ M in 1xb 1% HFIP, pH 7.4. Inset: Temperature dependent changes of the CD signal intensity of the local maximum at 199 nm (black) and of the local minimum at 226.4 nm (red).

In the case of IAPP(8-18)-LLL-(22-28)-OH, the signal loss occurred between 20 and 30°C (Fig. 165). This indicated that IAPP(8-18)-LLL-(22-28)-OH was at least partially denatured or

refolded at room temperature. These changes appeared quiet fast, since most of the signal loss occurred between 20 and 40°C.

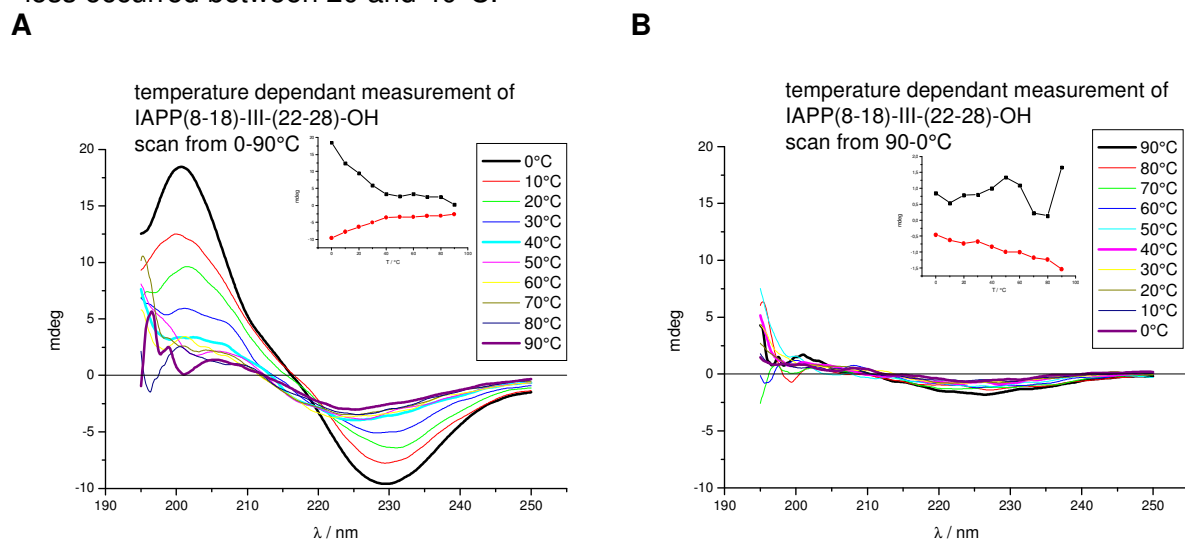


Fig. 166: Temperature dependent CD spectra of IAPP(8-18)-III-(22-28)-OH at a concentration of 5 μM in 1xb 1% HFIP, pH 7.4. Inset: Temperature dependent changes of the CD signal intensity of the local maximum at 200.7 nm (black) and of the local minimum at 229.4 nm (red).

IAPP(8-18)-III-(22-28)-OH was the least stable among the tested peptides. The reduction of the signal occurred already between 0 and 10°C. The peptide was already completely denatured at 40°C indicated by a complete loss of the signal between 220 and 230 nm. This loss of signal was irreversible (Fig. 166). The minimum of this signal was slightly shifted towards higher wavelengths upon heating.

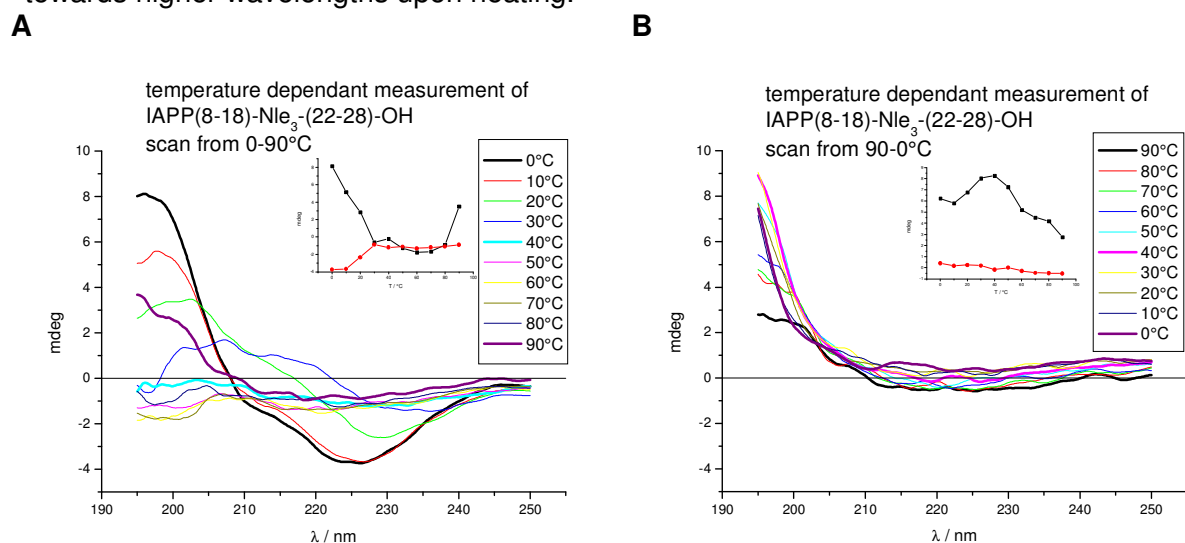


Fig. 167: Temperature dependent CD spectra of IAPP(8-18)-Nle₃-(22-28)-OH at a concentration of 5 μM in 1xb 1% HFIP, pH 7.4. Inset: Temperature dependent changes of the CD signal intensity of the local maximum at 196 nm (black) and of the local minimum at 226.3 nm (red).

For IAPP(8-18)-Nle₃-(22-28)-OH, the reduction of the signal occurred between 10 and 20°C (Fig. 167). The peptide was completely denatured at 40°C indicated by a complete loss of the signal between 210 and 240 nm. The minimum of this signal was slightly shifted towards higher wavelengths upon heating. The signal loss occurred between 10 and 40°C. Like IAPP(8-18)-LLL-(22-28)-OH, IAPP(8-18)-Nle₃-(22-28)-OH was at least partially denatured or refolded at room temperature.

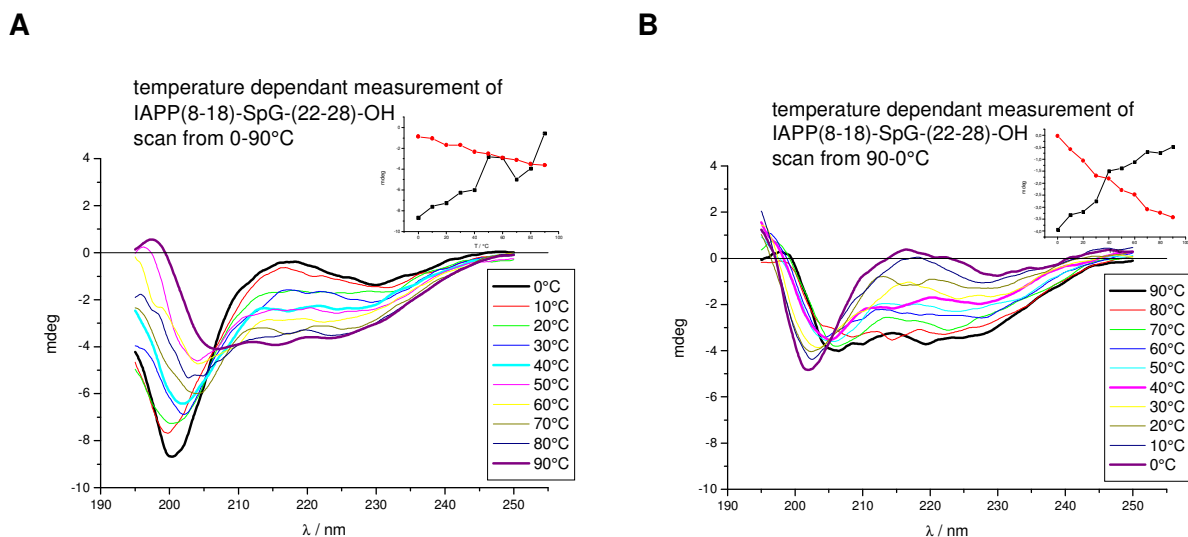


Fig. 168: Temperature dependent CD spectra of IAPP(8-18)-SpG-(22-28)-OH at a concentration of 5 μ M in 1xb 1% HFIP, pH 7.4. Inset: Temperature dependent changes of the CD signal intensity of the local minima at 200.2 nm (black) and 223.2 nm (red).

The temperature dependent CD spectra of IAPP(8-18)-SpG-(22-28)-OH were similar to those of IAPP(8-28)-OH. The intensity of the signal was in general lower than in the case of IAPP(8-28)-OH. One interesting difference was a small negative shoulder in the CD spectra of IAPP(8-18)-SpG-(22-28)-OH at 0°C and 10°C at around 220-230 nm. This signal was similar to the negative signals displayed by analogues with hydrophobic elements in the IAPP(19-21) region and might be related to β -turn elements. pG is a structural motif known for its ability to induce the formation of type II β -turns (Fig. 168). These CD spectra indicated the presence of β -turn elements in the structure of IAPP(8-18)-SpG-(22-28)-OH. At room temperature, these signals were not directly visible since they overlapped with signals of other structural elements.

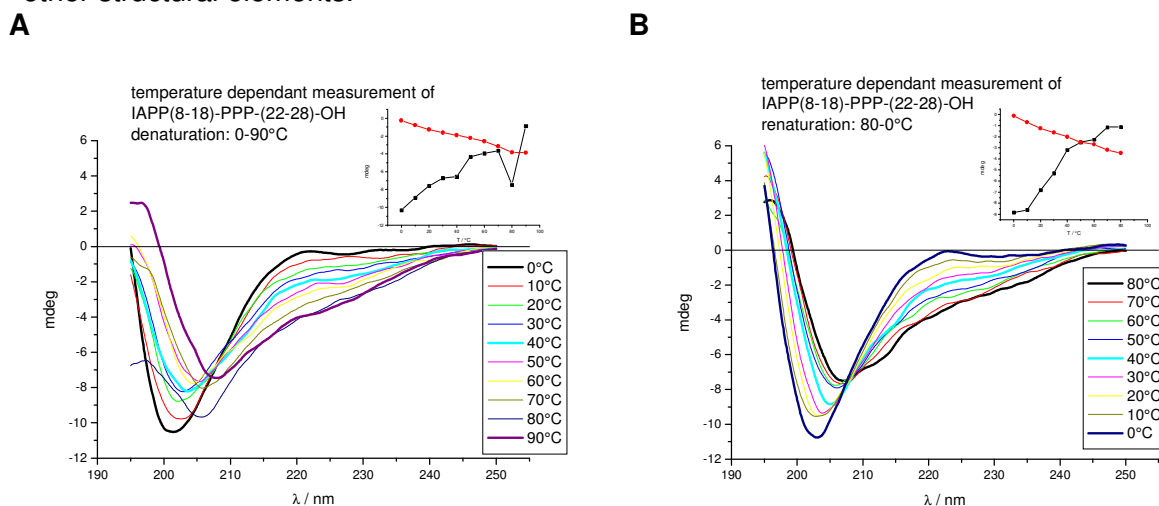
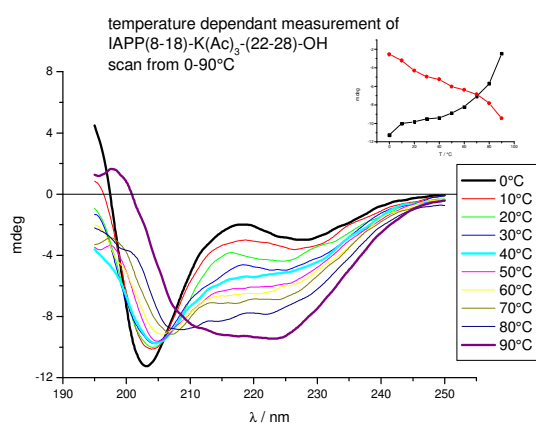


Fig. 169: Temperature dependent CD spectra of IAPP(8-18)-PPP-(22-28)-OH at a concentration of 5 μ M in 1xb 1% HFIP, pH 7.4. Inset: Temperature dependent changes of the CD signal intensity of the local minima at 200 nm (black) and 222.1 nm (red).

IAPP(8-18)-PPP-(22-28)-OH displayed temperature dependent CD spectra characteristic for the poly-L-proline type II (PPII) helix structure (Fig. 169). At 0°C, the spectrum showed an intense minimum at around 200 nm and a weak positive signal at around 220 nm. Upon increasing temperature, the minimum at 200 nm was losing its intensity whereas the positive

signal disappeared as the signal in that area decreased and finally produced a negative signal, but without a real local minimum. At room temperature, the PII helix displays a typical random coil spectrum in CD studies and can therefore not be distinguished from other extended structures normally summed up under the phrase *random coil*. Only temperature dependent CD studies can specifically identify PII helices [163, 175]. The PII helix is a structural motif commonly occurring in proline-rich sequences but is also found in fibrillar proteins. The introduction of prolines in the IAPP(19-21) region successfully lead to a PII like structure. IAPP(8-18)-PPP-(22-28)-OH was nontoxic and was also not forming fibrils under the conditions tested. Prolines do not have a hydrogen atom at the backbone amide and are therefore disrupting the formation of both intra- and intermolecular hydrogen bonds which are essential for the formation of fibrillar aggregates. The similarity of the temperature dependent CD spectra of IAPP(8-18)-PPP-(22-28)-OH with temperature dependent CD spectra of other analogues of IAPP(8-28)-OH, especially the ones displaying intense random coil structures in CD, indicated that the PII structure could be a common, but not the only structural feature of IAPP(8-28)-OH analogues.

A



B

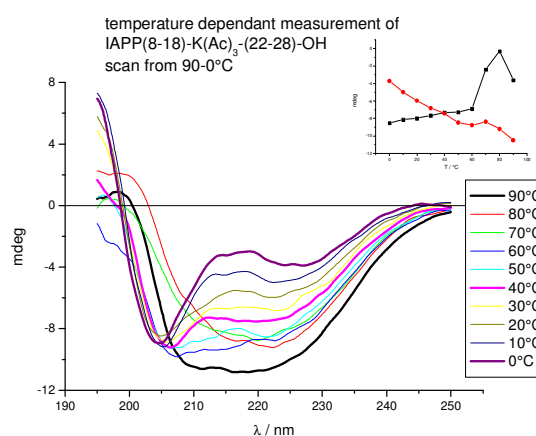


Fig. 170: Temperature dependent CD spectra of IAPP(8-18)-(K(Ac))₃-(22-28)-OH at a concentration of 10 μM in 1xb 1% HFIP, pH 7.4. Inset: Temperature dependent changes of the CD signal intensity of the local minima at 203.2 nm (black) and 222.6 nm (red).

IAPP(8-18)-(K(Ac))₃-(22-28)-OH displayed the strongest changes in the CD signal upon temperature changes (Fig. 170). This might also be due to the fact, than the thermal denaturation of IAPP(8-18)-(K(Ac))₃-(22-28)-OH was performed at a peptide concentration of 10 μM. Time dependent CD studies of IAPP(8-18)-(K(Ac))₃-(22-28)-OH performed at the same concentration revealed also a reduction of the intensity of the random coil structure upon aggregation, but no changes in the signal intensity between 210-230 nm. The spectrum of IAPP(8-18)-(K(Ac))₃-(22-28)-OH at 0°C also contained a small negative signal at 220-230 nm similar to that of IAPP(8-18)-SpG-(22-28)-OH.

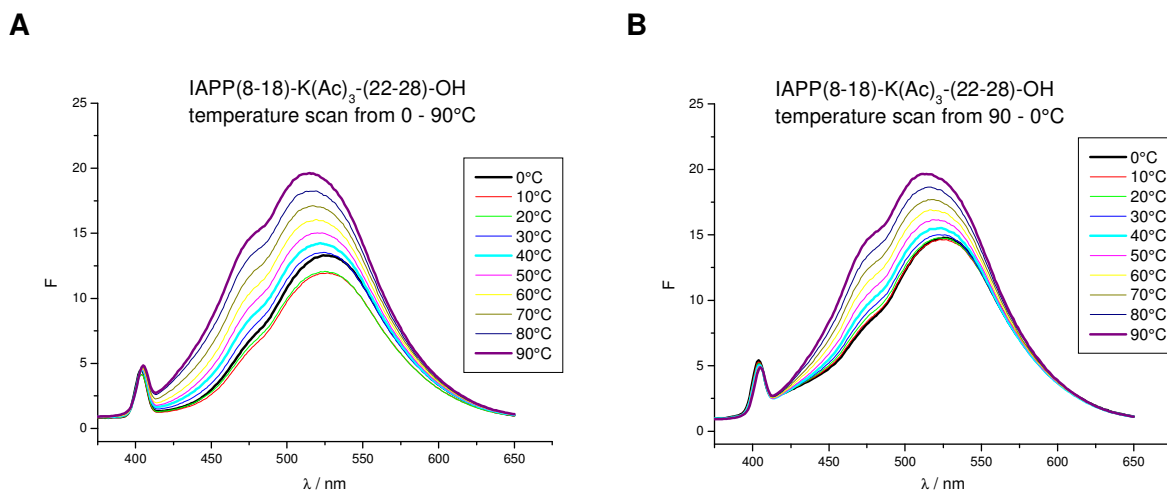


Fig. 171: Temperature dependent ANS binding of IAPP(8-18)-(K(Ac)₃)-(22-28)-OH at a concentration of 10 μM in 1x 1% HFIP, pH 7.4.

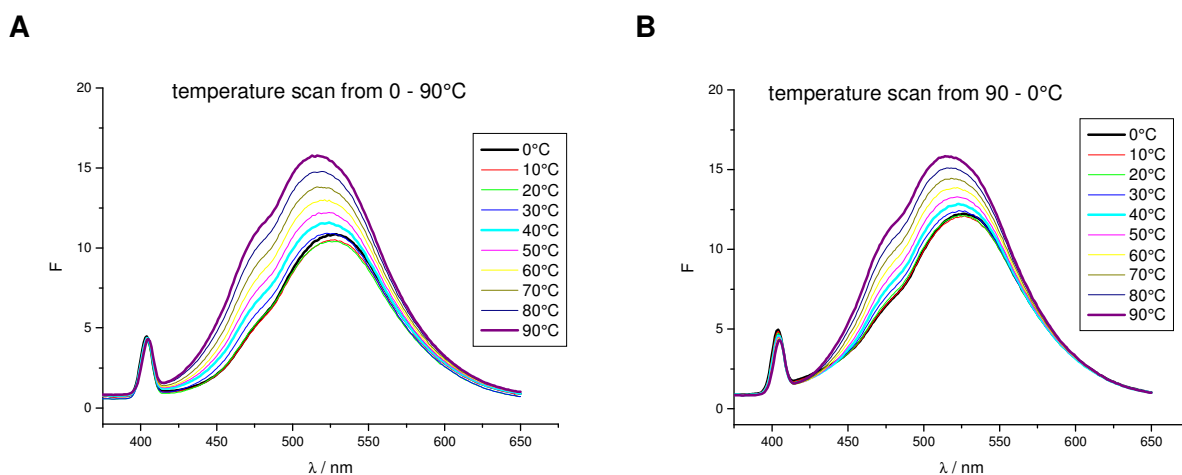


Fig. 172: Temperature dependent changes of the ANS emission spectrum, 20 μM in 1x 1% HFIP, pH 7.4.

Temperature dependent ANS studies of IAPP(8-18)-(K(Ac)₃)-(22-28)-OH at a peptide concentration of 10 μM could not provide additional information since the signal change upon heating was similar to the changes in the signal of ANS alone (Fig. 171 and Fig. 172). Additionally, thermal denaturation studies of IAPP(8-18)-LLL-(22-28)-OH and IAPP(8-18)-VVV-(22-28)-OH were done in aqueous solution without HFIP.

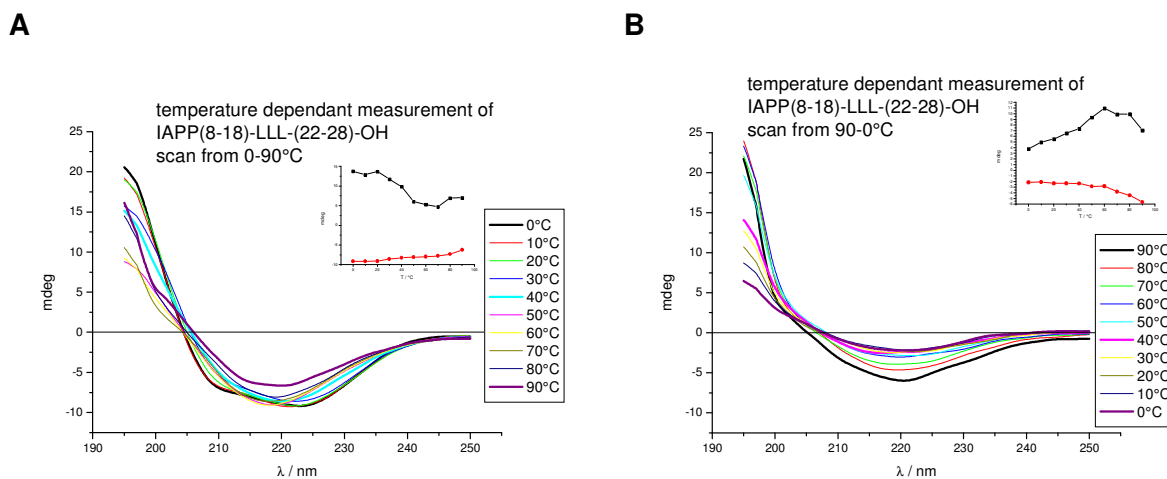


Fig. 173: Temperature dependent CD spectra of IAPP(8-18)-LLL-(22-28)-OH at a concentration of 5 μM in aqueous solution without HFIP. Inset: Temperature dependent changes of the CD signal intensity of the local maximum at 199 nm (black) and of the local minimum at 222.9 nm (red).

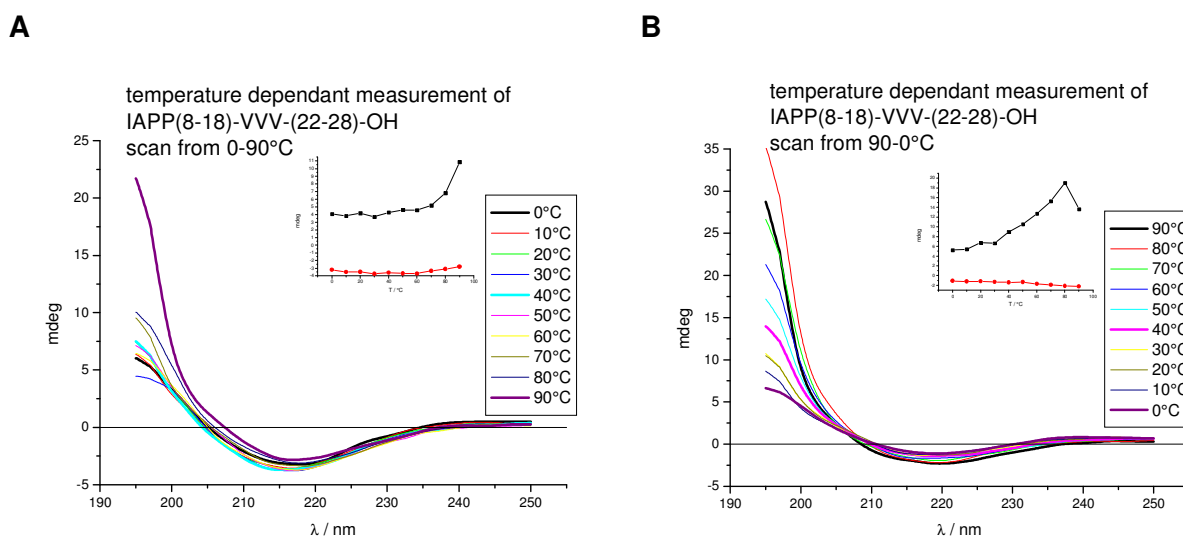


Fig. 174: Temperature dependent CD spectra of IAPP(8-18)-VVV-(22-28)-OH at a concentration of 5 μM in aqueous solution without HFIP. Inset: Temperature dependent changes of the CD signal intensity of the local maximum at 198.8 nm (black) and of the local minimum at 218.1 nm (red).

Both analogues displayed a higher stability in completely aqueous solution when compared with studies done in solutions containing 1% HFIP since complete denaturation occurred only at high temperatures, at 90°C. For IAPP(8-18)-LLL-(22-28)-OH, the signal measured between 0 and 20°C (Fig. 173) displayed almost α -helical structure. The structure was converted to β -sheet at 40°C indicated by a minimum at around 217 nm.

The CD signal of IAPP(8-18)-VVV-(22-28)-OH remained almost identical until a temperature of 90°C. Signal loss occurred only upon cooling down, probably after soluble oligomers were formed that then continued to further aggregate as indicated by a loss of signal intensity (Fig. 174B).

With temperature dependent CD studies it was possible to gain deeper insights into the structure and stability of IAPP(8-28)-OH analogues. The CD spectra of analogues with hydrophobic elements in the IAPP(19-21) region did not only differ from those of the other analogues indicating a completely different structure for soluble monomers of different peptides, these analogues also behaved totally different during thermal denaturation. The

hydrophobic peptides displayed a complete, irreversible signal loss during temperature dependent CD studies which could be due to irreversible aggregation. They seemed to have in general a less stable conformation, as also indicated by a loss of signal at low concentrations compared to the other analogues in concentration dependent CD studies.

The random coil elements detected in CD spectra at room temperature seemed to be PPII helices as indicated by the CD spectra of IAPP(8-18)-SGN-(22-28)-OH, IAPP(8-18)-PPP-(22-28)-OH, IAPP(8-18)-(K(Ac))₃-(22-28)-OH and IAPP(8-18)-KKK-(22-28)-OH at 0°C. In the spectra of IAPP(8-18)-SGN-(22-28)-OH, IAPP(8-18)-SpG-(22-28)-OH, IAPP(8-18)-(K(Ac))₃-(22-28)-OH and IAPP(8-18)-KKK-(22-28)-OH at low temperature there was also a small minimum at 220-230 nm. This signal was an indication for β -turn and β -hairpin elements. The signal was also very weak at room temperature and overlapping with signals of other structural elements. Therefore it was not clearly visible during concentration dependent CD studies. In general, the information gained by temperature dependent CD studies suggest a PPII helix-turn like structure for analogues of IAPP(8-28)-OH that mainly showed random coil signals at room temperature.

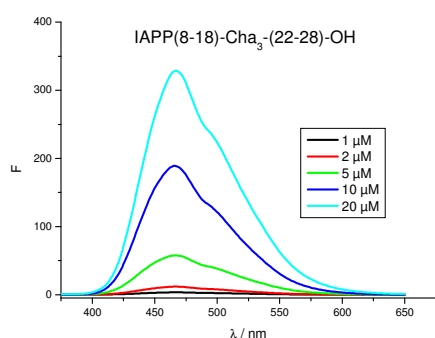
Peptides with hydrophobic elements in the IAPP(19-21) region proved to be extremely instable towards thermal studies. They displayed a loss of signal already at around 10°C. They were also completely and irreversibly denatured during the experiments although they remained in a soluble state.

3.1.4 ANS binding

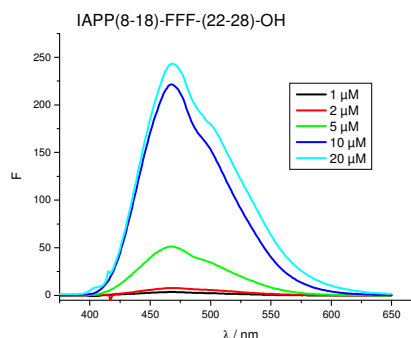
ANS (8-Anilinonaphthalene-1-sulfonic acid) is a hydrophobic fluorescent dye that specifically binds to solvent-exposed hydrophobic surfaces of other molecules. This binding is characterized by a blue shift of the maximum and an enhancement of the fluorescence emission spectrum [137].

Several analogues were selected and tested for their ANS binding affinity. Among these analogues were many with a hydrophobic IAPP(19-21) region, also in combination with other features like aromaticity, steric hindrance, and flexibility. The native IAPP(8-28)-OH, IAPP(8-18)-SGN-(22-28)-OH, and IAPP(8-18)-(K(Ac))₃-(22-28)-OH, that all had a high fibril forming potential as well as analogues with flexible or charged or secondary structure inducing elements in the IAPP(19-21) region were also tested.

A



B



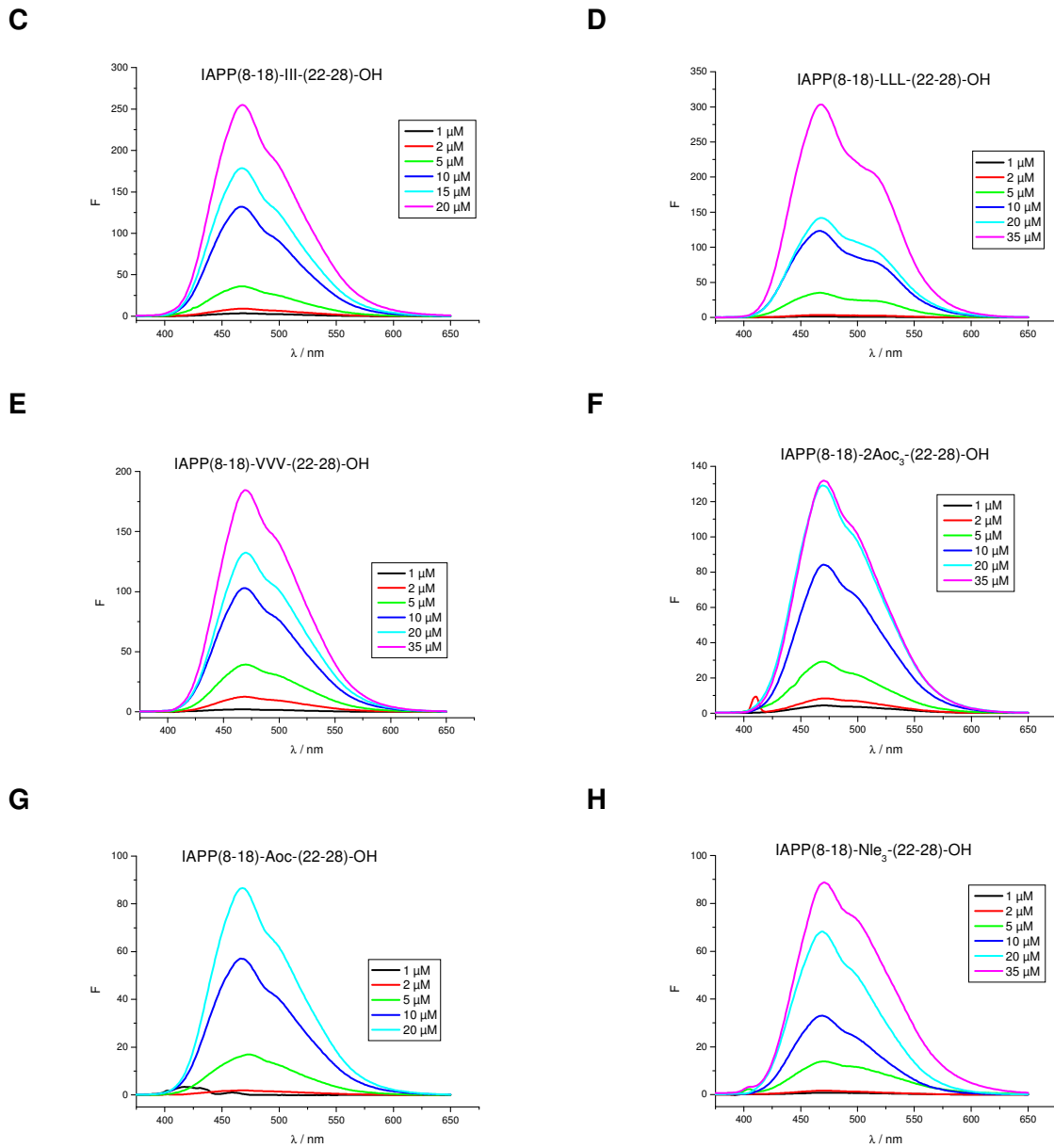


Fig. 175: (A) ANS binding affinity of IAPP(8-18)-Cha₃-(22-28)-OH at different concentrations in 1xb 1% HFiP, pH 7.4.

(B) ANS binding affinity of IAPP(8-18)-FFF-(22-28)-OH at different concentrations in 1xb 1% HFiP, pH 7.4.

(C) ANS binding affinity of IAPP(8-18)-III-(22-28)-OH at different concentrations in 1xb 1% HFiP, pH 7.4.

(D) ANS binding affinity of IAPP(8-18)-LLL-(22-28)-OH at different concentrations in 1xb 1% HFiP, pH 7.4.

(E) ANS binding affinity of IAPP(8-18)-VVV-(22-28)-OH at different concentrations in 1xb 1% HFiP, pH 7.4.

(F) ANS binding affinity of IAPP(8-18)-2Aoc₃-(22-28)-OH at different concentrations in 1xb 1% HFiP, pH 7.4.

(G) ANS binding affinity of IAPP(8-18)-Aoc-(22-28)-OH at different concentrations in 1xb 1% HFiP, pH 7.4.

(H) ANS binding affinity of IAPP(8-18)-Nle₃-(22-28)-OH at different concentrations in 1xb 1% HFiP, pH 7.4.

Fluorescence emission spectra were measured at various peptide concentrations. Spectra of ANS alone were subtracted from the spectra of peptide with ANS.

As expected, the peptides with hydrophobic amino acids in the IAPP(19-21) region were binding strongly to ANS, already at low concentrations (Fig. 175). IAPP(8-18)-Cha₃-(22-28)-OH, IAPP(8-18)-FFF-(22-28)-OH, IAPP(8-18)-III-(22-28)-OH, IAPP(8-18)-LLL-(22-28)-OH, and IAPP(8-18)-VVV-(22-28)-OH, the peptides with a branch in the hydrophobic region, bound even stronger to ANS than the ones without a branch in their hydrophobic region like IAPP(8-18)-2Aoc₃-(22-28)-OH, IAPP(8-18)-Aoc-(22-28)-OH and IAPP(8-18)-Nle₃-(22-28)-OH.

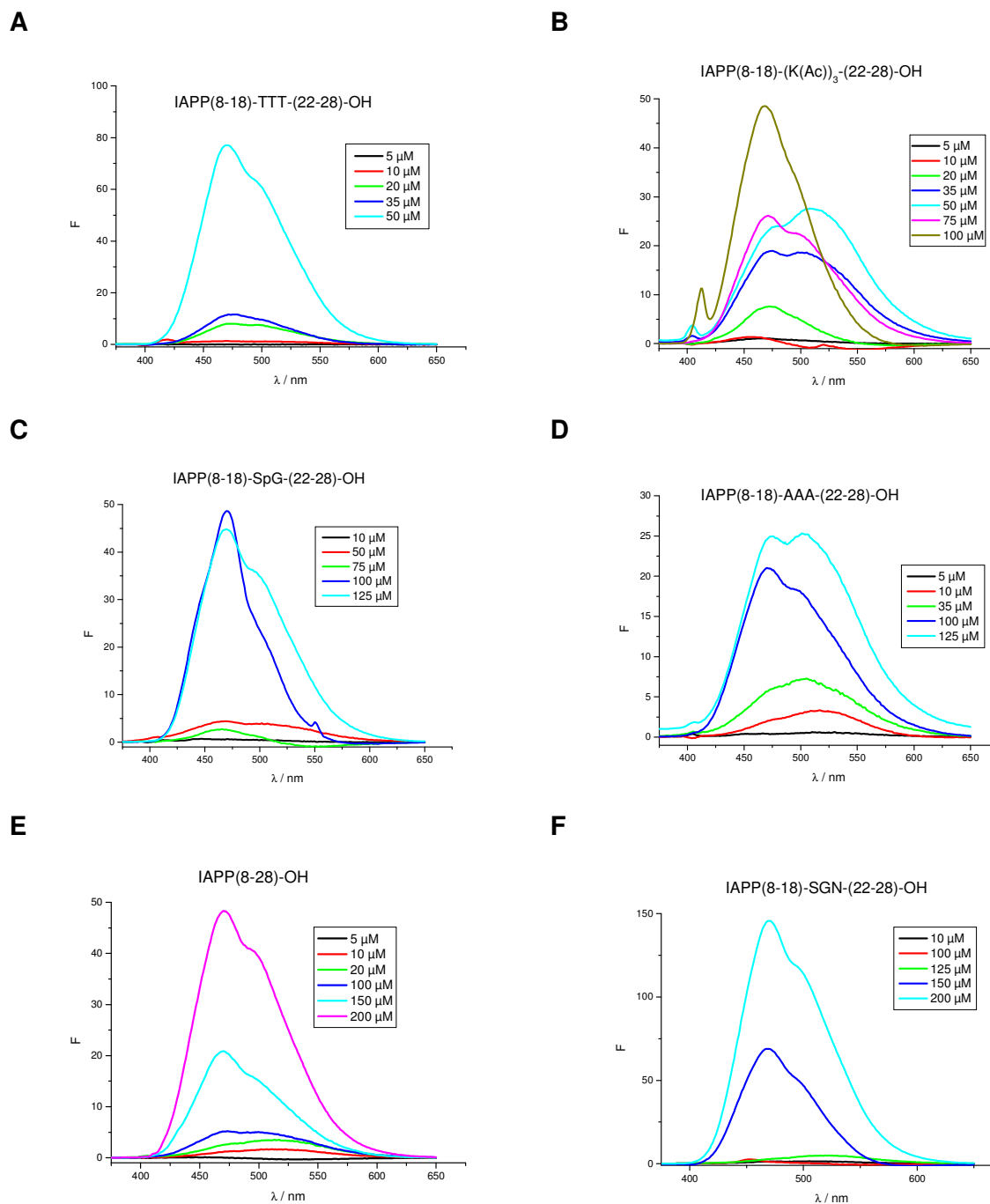


Fig. 176: (A) ANS binding affinity of IAPP(8-18)-TTT-(22-28)-OH at different concentrations in 1xb 1% HFIP, pH 7.4.

(B) ANS binding affinity of IAPP(8-18)-(K(Ac))₃-(22-28)-OH at different concentrations in 1xb 1% HFIP, pH 7.4.

(C) ANS binding affinity of IAPP(8-18)-SpG-(22-28)-OH at different concentrations in 1xb 1% HFIP, pH 7.4.

(D) ANS binding affinity of IAPP(8-18)-AAA-(22-28)-OH at different concentrations in 1xb 1% HFIP, pH 7.4.

(E) ANS binding affinity of IAPP(8-28)-OH at different concentrations in 1xb 1% HFIP, pH 7.4.

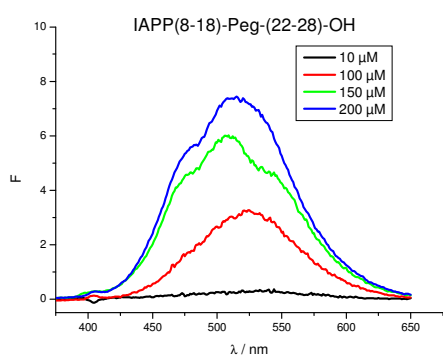
(F) ANS binding affinity of IAPP(8-18)-SGN-(22-28)-OH at different concentrations in 1xb 1% HFIP, pH 7.4.

Fluorescence emission spectra were measured at various peptide concentrations. Spectra of ANS alone were subtracted from the spectra of peptide with ANS.

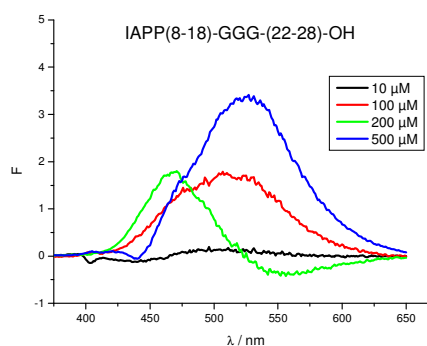
The analogue IAPP(8-18)-TTT-(22-28)-OH contains weakly hydrophobic elements in the IAPP(19-21) region. Therefore it displayed a binding to ANS with a weaker signal compared to the peptides with more hydrophobic IAPP(19-21) region, but still stronger than analogues lacking hydrophobic elements in the IAPP(19-21) region.

In case of IAPP(8-18)-(K(Ac))₃-(22-28)-OH, the exposure of hydrophobic surfaces occurred at a much lower concentration compared to the native IAPP(8-28)-OH, but with a weaker signal compared to the peptides with hydrophobic elements in the IAPP(19-21) region. IAPP(8-18)-SGN-(22-28)-OH displayed a strong binding to ANS but only at concentrations from 150 μM peptide and higher. But in that case the binding was even stronger than that of the native IAPP(8-28)-OH. Both IAPP(8-18)-SGN-(22-28)-OH and IAPP(8-18)-(K(Ac))₃-(22-28)-OH were not only binding stronger to ANS than IAPP(8-28)-OH, they were also more toxic and fibrillogenic than the native sequence. This suggested, that the exposure of hydrophobic surfaces was related to a structural change along the amyloidogenic pathway that seemed to occur before the formation of fibrils. IAPP(8-18)-SpG-(22-28)-OH was also binding to ANS at higher concentrations. This binding was even stronger than the binding of native IAPP(8-28)-OH. IAPP(8-18)-SpG-(22-28)-OH was also forming fibrils and was toxic to RIN cells, but not as much as the native IAPP(8-28)-OH. The analogue IAPP(8-18)-AAA-(22-28)-OH was binding to ANS at higher concentrations as well and was also able to form fibrils at higher concentration (Fig. 176).

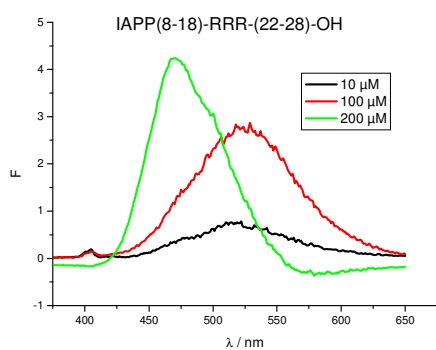
A



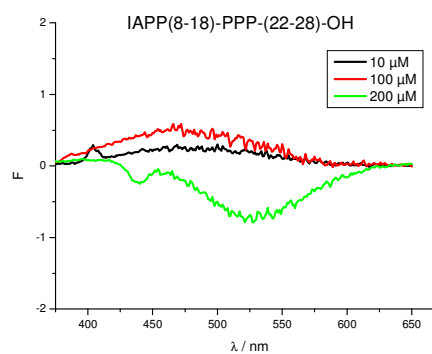
B



C



D



E

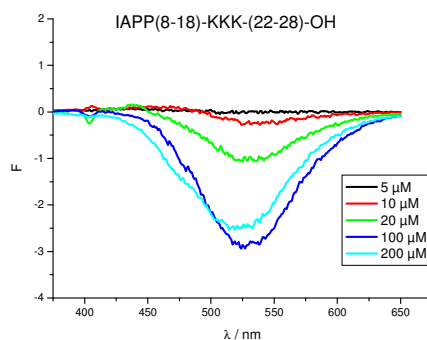


Fig. 177: (A) ANS binding affinity of IAPP(8-18)-Peg-(22-28)-OH at different concentrations in 1xb 1% HFIP, pH 7.4.

(B) ANS binding affinity of IAPP(8-18)-GGG-(22-28)-OH at different concentrations in 1xb 1% HFIP, pH 7.4.

(C) ANS binding affinity of IAPP(8-18)-RRR-(22-28)-OH at different concentrations in 1xb 1% HFIP, pH 7.4.

(D) ANS binding affinity of IAPP(8-18)-PPP-(22-28)-OH at different concentrations in 1xb 1% HFIP, pH 7.4.

(E) ANS binding affinity of IAPP(8-18)-KKK-(22-28)-OH at different concentrations in 1xb 1% HFIP, pH 7.4.

Fluorescence emission spectra were measured at various peptide concentrations. Spectra of ANS alone were subtracted from the spectra of peptide with ANS.

As shown in Fig. 177, IAPP(8-18)-RRR-(22-28)-OH, IAPP(8-18)-PPP-(22-28)-OH, and IAPP(8-18)-KKK-(22-28)-OH, peptides with no fibril forming potential also did not bind to ANS. The exposure of hydrophobic surfaces seemed to be a specific feature of the amyloidogenic pathway that leads towards fibril formation.

IAPP(8-18)-GGG-(22-28)-OH and IAPP(8-18)-Peg-(22-28)-OH have a weak fibril forming potential, but they did not bind ANS. The exposure of hydrophobic areas obviously occurred not immediately but may needed some incubation time, just like the formation of fibrils.

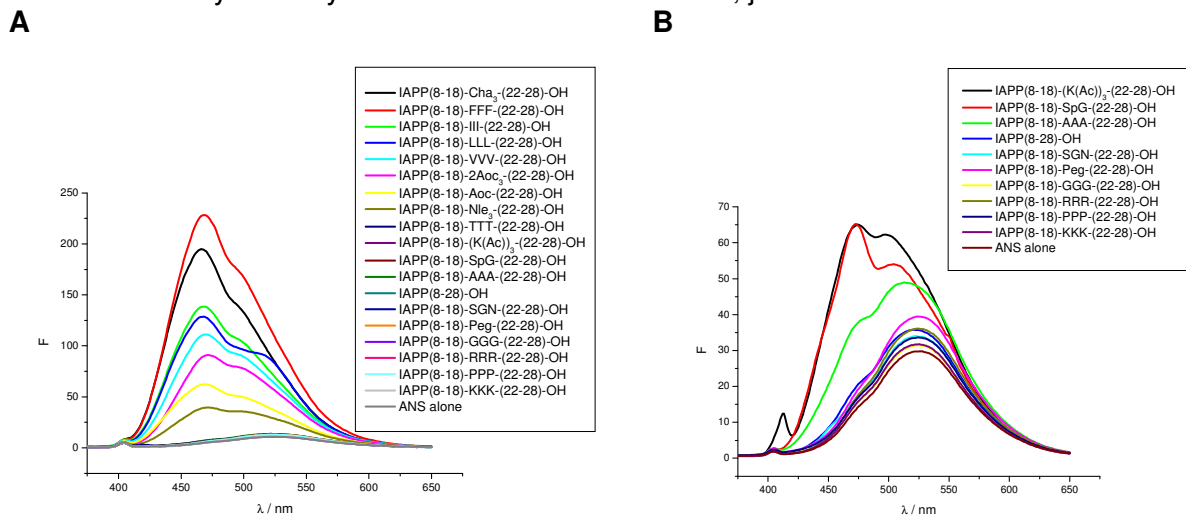


Fig. 178: Comparison of the ANS binding affinity of different peptides at A 10 μM peptide concentration and B 100 μM peptide concentration.

To verify the results obtained by the ANS binding studies, additional studies were done with IAPP(8-18)-Aoc-(22-28)-OH and IAPP(8-18)-LLL-(22-28)-OH (Fig. 179). These experiments were done under the same conditions as the ANS binding studies, just with ThT instead of ANS. ThT binds specifically to cross- β -structures that form during amyloid formation. At the chosen concentrations, these two peptides were found to display strong binding to ANS, showed clear solutions during CD studies and did not yet form fibrils, as indicated by ThT studies (table 3).

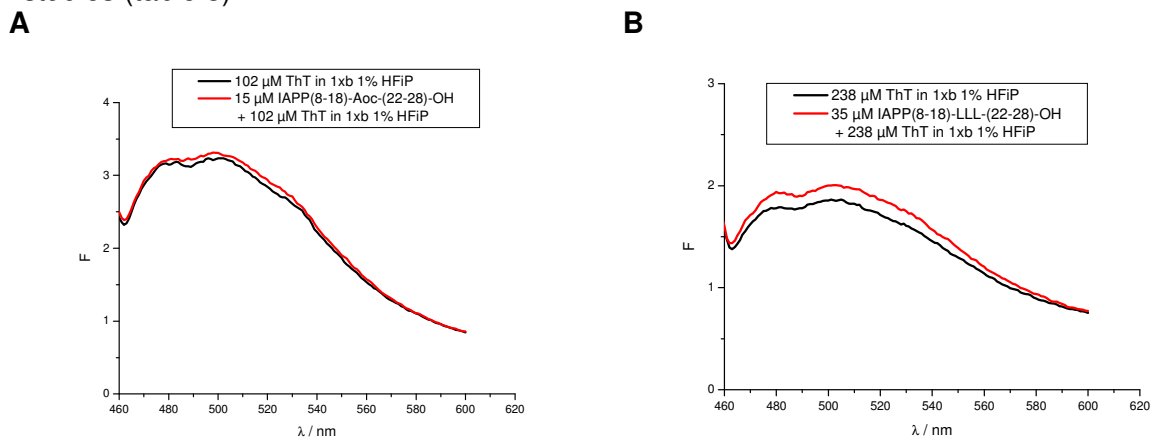


Fig. 179: ThT binding studies of A 15 μM IAPP(8-18)-Aoc-(22-28)-OH and B 35 μM IAPP(8-18)-LLL-(22-28)-OH in 10 mM sodium phosphate buffer at pH 7.4 containing 1% HFIP.

These experiments suggested that there was no binding to ThT under the ANS-binding assay conditions. This was another indication that hydrophobic exposure occurred before fibril formation and that the increase in the fluorescence emission of ANS in the mixtures with peptides at low concentrations was not due to fibril formation but rather due to oligomer formation. To study the self-assembly state, oligomerization assays and fluorescence self-binding studies were performed.

Table 14: Overview of ANS binding assays performed with analogues of IAPP(8-28). Results of “+” indicate an increase of ANS fluorescence, whereas “-” indicate no increase of ANS fluorescence of the solution at the given peptide concentration.

Sequence	Concentration													
	1 μM	2 μM	5 μM	10 μM	15 μM	20 μM	35 μM	50 μM	75 μM	100 μM	125 μM	150 μM	200 μM	500 μM
IAPP(8-18)- Cha ₃ -(22-28)-OH	+	+	+	+		+								
IAPP(8-18)- FFF -(22-28)-OH	+	+	+	+		+								
IAPP(8-18)- III -(22-28)-OH	+	+	+	+	+	+								
IAPP(8-18)- LLL -(22-28)-OH	+	+	+	+		+	+							
IAPP(8-18)- VVV -(22-28)-OH	+	+	+	+		+	+							
IAPP(8-18)- 2Aoc ₃ -(22-28)-OH	+	+	+	+		+	+							
IAPP(8-18)- Aoc -(22-28)-OH	-	+	+	+	+	+								
IAPP(8-18)- Nle ₃ -(22-28)-OH	-	+	+	+		+	+							
IAPP(8-18)- TTT -(22-28)-OH			-	-		+	+	+						
IAPP(8-18)- K(Ac) ₃ -(22-28)-OH			-	-		+	+	+	+	+				
IAPP(8-18)- SpG -(22-28)-OH				-				-	-	+		+		
IAPP(8-18)- AAA -(22-28)-OH			-	-			-			+	+			
IAPP(8-28)-OH			-	-		-				-		+	+	
IAPP(8-18)- SGN -(22-28)-OH				-						-	-	+	+	
IAPP(8-18)- Peg -(22-28)-OH				-						-		-	-	
IAPP(8-18)- GGG -(22-28)-OH				-						-			-	-
IAPP(8-18)- RRR -(22-28)-OH				-						-			-	
IAPP(8-18)- PPP -(22-28)-OH				-						-			-	
IAPP(8-18)- KKK -(22-28)-OH			-	-		-				-			-	

3.1.5 Size exclusion chromatography (SEC) studies with selected analogues

To get an insight into the fibril forming pathway and to specifically determine what kind of multimers, how fast and to which amount they may form, size exclusion chromatography (SEC) studies were performed.

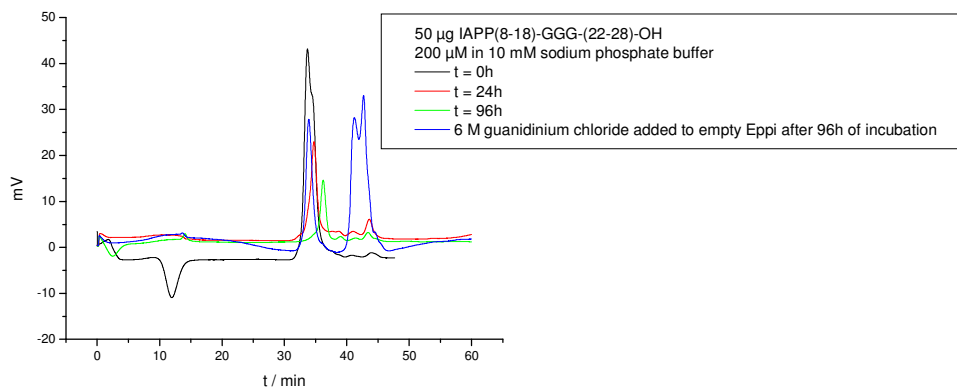


Fig. 180: SEC data of IAPP(8-18)-GGG-(22-28)-OH. For each run, 50 μg of the peptide was incubated at a concentration of 200 μM .

The signal of 50 μg IAPP(8-18)-GGG-(22-28)-OH incubated at a concentration of 200 μM in 10 mM sodium phosphate buffer was decreasing upon time. This decrease was comparable with the increase of the fluorescence signal in the ThT assay at a concentration of 200 μM in 10 mM sodium phosphate buffer. To the Eppendorf tube, in which the incubation for 96h was done, a solution of 6 M guanidinium chloride in 10 mM sodium phosphate buffer was added. After a short incubation time, this solution was injected onto the SEC column. The solution displayed a signal similar to that of 50 μg IAPP(8-18)-GGG-(22-28)-OH at $t = 0\text{h}$ but a little weaker. The small shift in the retention time after 96h of incubation might be due to conformational changes of IAPP(8-18)-GGG-(22-28)-OH monomers leading to a more compact configuration (Fig. 180).

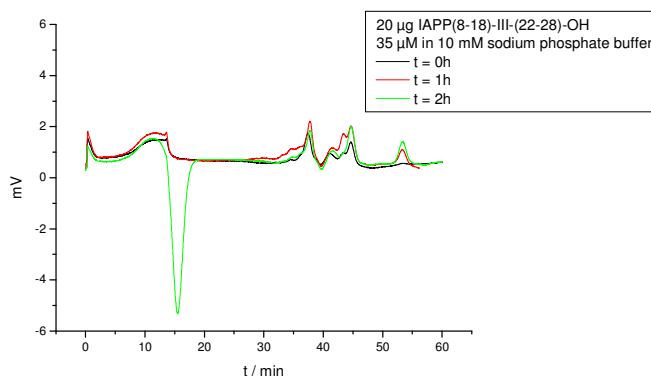


Fig. 181: SEC data of IAPP(8-18)-III-(22-28)-OH. For each run, 20 μg of the peptide was incubated at a concentration of 35 μM .

For IAPP(8-18)-III-(22-28)-OH, there could be no clear peptide peak detected. The peptide was most likely adsorbed by the column material (Fig. 181).

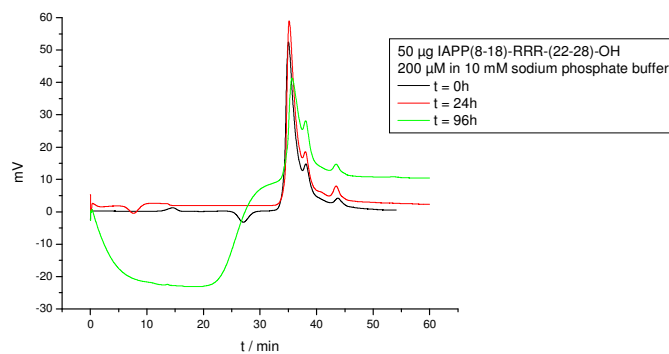


Fig. 182: SEC data of IAPP(8-18)-RRR-(22-28)-OH. For each run, 50 μg of the peptide was incubated at a concentration of 200 μM .

In case of IAPP(8-18)-RRR-(22-28)-OH, there were no changes during the first 24h of incubation at 200 μM in 10 mM sodium phosphate buffer. After 96h, the peak was slightly smaller but broader. This might also have been the result of a more compact structure of the monomers like in the case of IAPP(8-18)-GGG-(22-28)-OH. The negative peak between 0 and 20 minutes might be due to oligomers or multimers (Fig. 182).

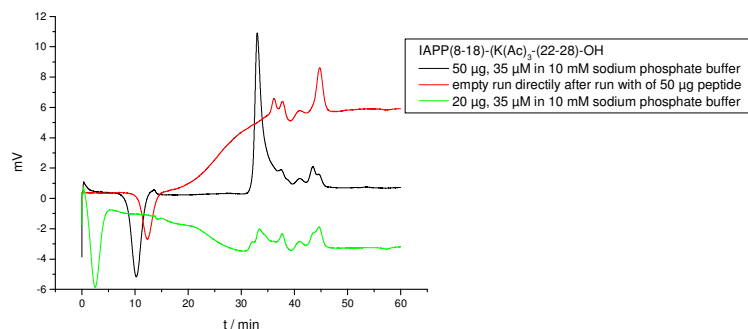
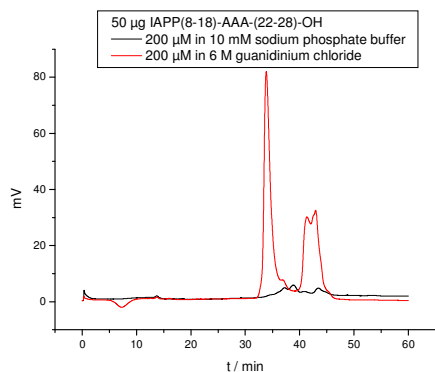


Fig. 183: SEC data of IAPP(8-18)-(K(Ac)₃)-(22-28)-OH. For each run, 50 μg of the peptide was incubated at a concentration of 200 μM .

The spectrum of 50 μg IAPP(8-18)-(K(Ac)₃)-(22-28)-OH at 35 μM in 10 mM sodium phosphate buffer was showing a clear peak. The signal intensity of this peak was quiet low for 50 μg peptide. An empty run performed directly after the run of IAPP(8-18)-(K(Ac)₃)-(22-28)-OH revealed the fate of the remaining peptide: It got adsorbed by the column material and was washed off during that empty run. A reduction of the amount of peptide used for one run to 20 μg did not improve the outcome. In order to protect the column, no further studies were performed using IAPP(8-18)-(K(Ac)₃)-(22-28)-OH (Fig. 183).

A



B

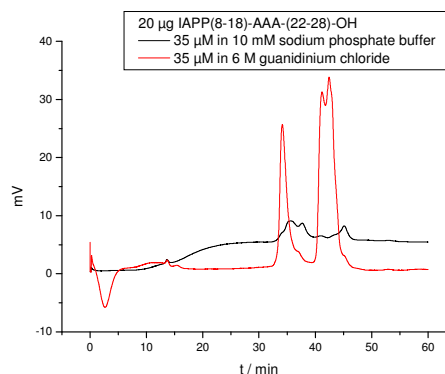


Fig. 184: SEC data of IAPP(8-18)-AAA-(22-28)-OH. For each run, 50 μg of the peptide was incubated at a concentration of 200 μM (A) or 20 μg of the peptide was incubated at a concentration of 35 μM (B).

IAPP(8-18)-AAA-(22-28)-OH displayed a clear peak only when dissolved in 6 M guanidinium chloride, so under conditions where no aggregation is possible (Fig. 184).

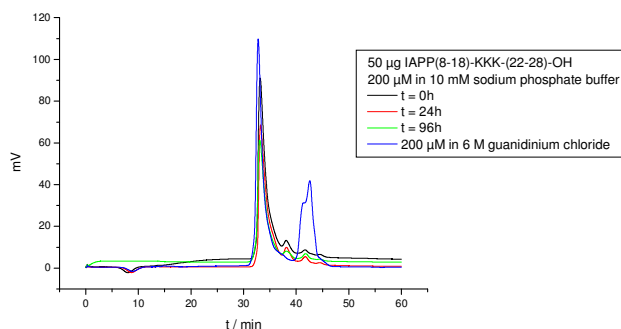
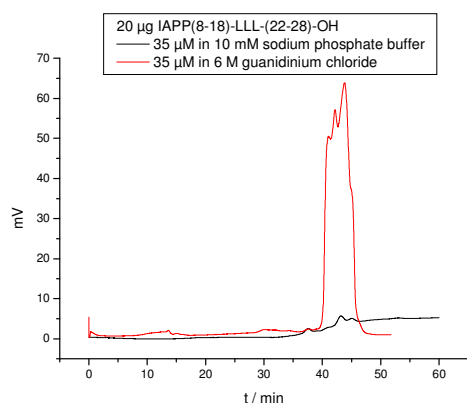


Fig. 185: SEC data of IAPP(8-18)-KKK-(22-28)-OH. For each run, 50 μg of the peptide was incubated at a concentration of 200 μM .

50 μg IAPP(8-18)-KKK-(22-28)-OH incubated at 200 μM in 10 mM sodium phosphate buffer displayed a weak signal loss over time indicating nonspecific binding of oligomers by the column matrix. The peptide was not forming fibrils and there were no oligomers visible in the SEC spectra (Fig. 185).

A



B

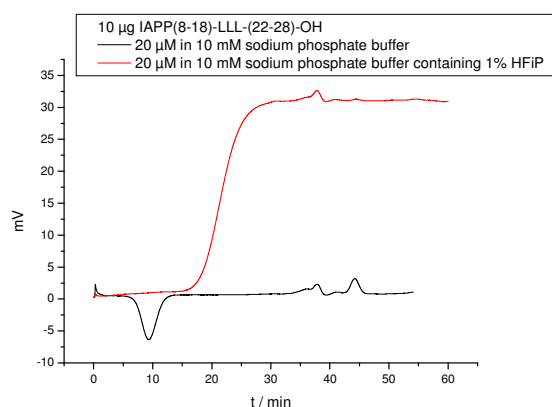


Fig. 186: SEC data of IAPP(8-18)-LLL-(22-28)-OH. For each run, 20 μg of the peptide was incubated at a concentration of 35 μM (A) or 10 μg of the peptide was incubated at a concentration of 20 μM (B).

Like for IAPP(8-18)-III-(22-28)-OH, there was no clear peak in the spectra of IAPP(8-18)-LLL-(22-28)-OH. The peptide also seemed to get adsorbed by the column matrix (Fig. 186).

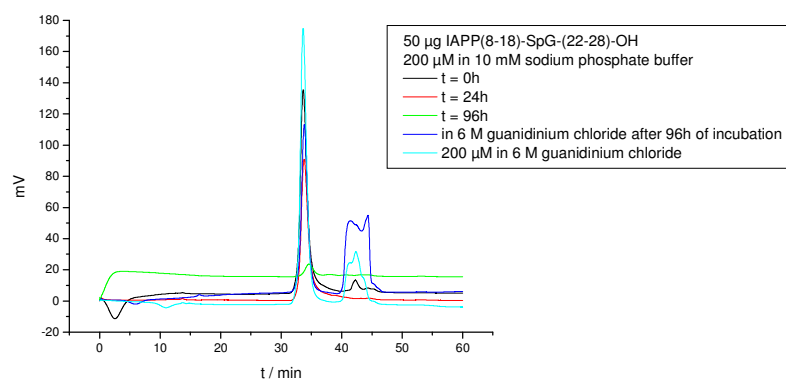


Fig. 187: SEC data of IAPP(8-18)-SpG-(22-28)-OH. For each run, 50 μg of the peptide was incubated at a concentration of 200 μM .

50 μg IAPP(8-18)-SpG-(22-28)-OH was incubated at a concentration of 200 μM in 1xb. Spectra were measured after 0h, 24h and 96h. A strong decrease of the signal of the peak related to IAPP(8-18)-SpG-(22-28)-OH monomers was detected. This decrease was related to fibril formation. After 96h of incubation, there was almost no monomer left. To the Eppendorf tube, in which the incubation for 96h was done, a solution of 6 M guanidinium chloride in 10 mM sodium phosphate buffer was added. After a short incubation time, this solution was injected onto the SEC column. The solution displayed a signal similar to that of 50 μg IAPP(8-18)-SpG-(22-28)-OH at $t = 0\text{h}$. The fibrils formed during the incubation in 10 mM sodium phosphate buffer obviously precipitated in the Eppendorf tube and were then redissolved in 6 M guanidinium chloride. The fibril forming pathway of IAPP(8-18)-SpG-(22-28)-OH might lead to insoluble oligomers or fibrils immediately after the initial aggregation step. This might also explain, why no oligomers were detected using SEC (Fig. 187).

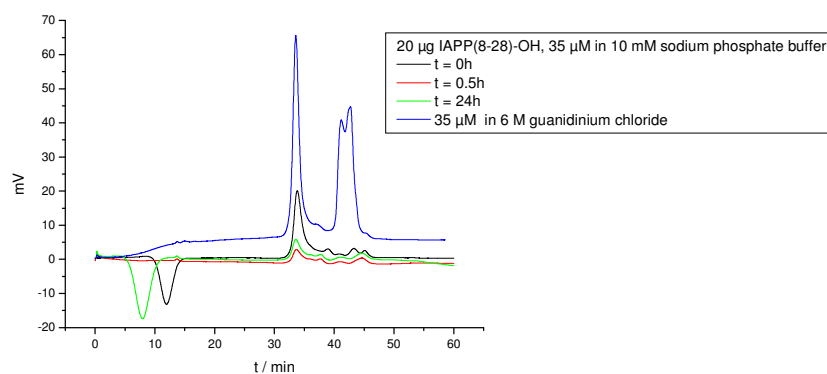


Fig. 188: SEC data of IAPP(8-28)-OH. For each run, 20 μg of the peptide was incubated at a concentration of 35 μM .

The signal of 20 μg IAPP(8-28)-OH incubated in 1xb at a concentration of 35 μM was decreasing extremely fast. Compared to the same amount of peptide dissolved in 6 M guanidinium chloride, even the spectrum at $t = 0\text{h}$ already displayed a strong loss of signal. This also indicated, that after an initial aggregation step either fibrils were formed extremely fast or the multimers formed in this step were insoluble in 10 mM sodium phosphate buffer and precipitated (Fig. 188).

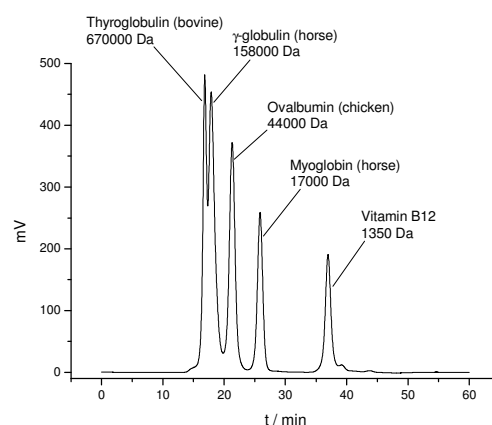


Fig. 189: SEC data of the BIO-RAD gel filtration standard.

The molecular weights correlating to the peaks detected were calculated using the data determined with the BIO-RAD gel filtration standard (Fig. 189). According to this calculation, all analogues that did elute, eluted as monomers.

In total, only the changes in the amount of monomers could be detected using SEC. In some cases, not even the monomers were seen, since they were sticking on the filter of the column or even adsorbed on the column material itself and therefore did not elute as a distinct peak.

3.1.6 NuPAGE

An oligomerization assay was performed with several chosen analogues. Among these analogues was one with a high fibril forming potential, IAPP(8-18)-(K(Ac))₃-(22-28)-OH, one with a medium fibril forming potential, IAPP(8-18)-AAA-(22-28)-OH, one with a low fibril forming potential, IAPP(8-18)-LLL-(22-28)-OH, and one analogue that did not form fibrils under the conditions tested, IAPP(8-18)-RRR-(22-28)-OH.

Aim was to detect the oligomers which were nondetectable by SEC.

The fibril forming potential of IAPP(8-18)-LLL-(22-28)-OH was low (Fig. 65A). At a concentration of 100 and 200 μ M only a weak increase in the ThT fluorescence was visible. Strong and intense fibril formation was only seen at a peptide concentration of 500 μ M (Fig. 65A). Also only at a concentration of 500 μ M, fibrils were visible on the TEM picture (Fig. 65B).

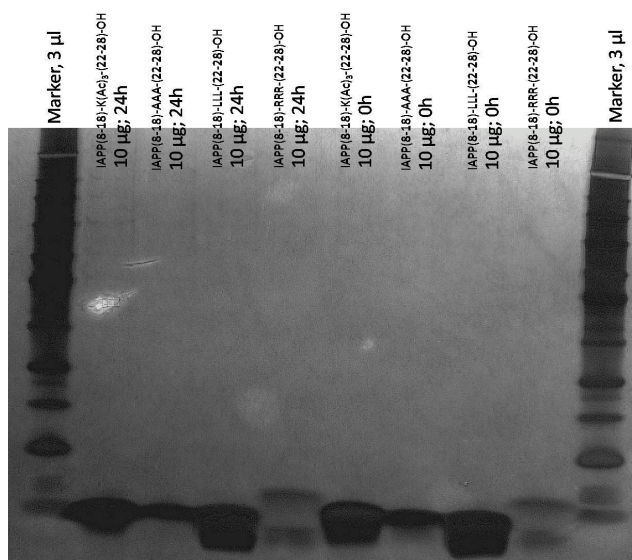


Fig. 190: NuPAGE oligomerization assay of IAPP(8-18)-(K(Ac))₃-(22-28)-OH, IAPP(8-18)-AAA-(22-28)-OH, IAPP(8-18)-LLL-(22-28)-OH and IAPP(8-18)-RRR-(22-28)-OH. 10 μ g of the peptides were dissolved in 1x, pH 7.4, 1% HFiP at a concentration of 200 μ M and then either incubated for 24h at room temperature or directly mixed with NuPAGE LDS sample buffer and loaded onto the gel.

The peptides were incubated at a concentration of 200 μ M for this assay.

For IAPP(8-18)-(K(Ac))₃-(22-28)-OH and IAPP(8-18)-AAA-(22-28)-OH a higher population of dimers was visible after 24h. In contrast, for IAPP(8-18)-LLL-(22-28)-OH and IAPP(8-18)-KKK-(22-28)-OH the observed population of monomers and dimers remained unchanged when compared to the state at 0h (Fig. 190).

Only monomers and dimers of the tested analogues were visible on the gel. Higher order oligomers were obviously not stable under the conditions used for NuPAGE.

Similar to the SEC studies, also the NuPAGE oligomerization assay could not reveal information about the aggregation pathway leading towards amyloid fibril formation because higher order multimers could not be detected.

3.1.7 Fluos self-association

Self-association studies by titrating N-terminally fluorescein labeled analogues were done with some four analogues.

The analogues selected for these studies were IAPP(8-18)-(K(Ac))₃-(22-28)-OH that displayed high fibril forming potential and toxicity, IAPP(8-18)-LLL-(22-28)-OH with a low fibril forming potential and toxicity but a hydrophobic IAPP(19-21) region, and two analogue that did not form fibrils under the conditions tested, IAPP(8-18)-KKK-(22-28)-OH and IAPP(8-18)-RRR-(22-28)-OH. However IAPP(8-18)-KKK-(22-28)-OH was toxic to RIN cells, whereas IAPP(8-18)-RRR-(22-28)-OH did not display any cytotoxicity.

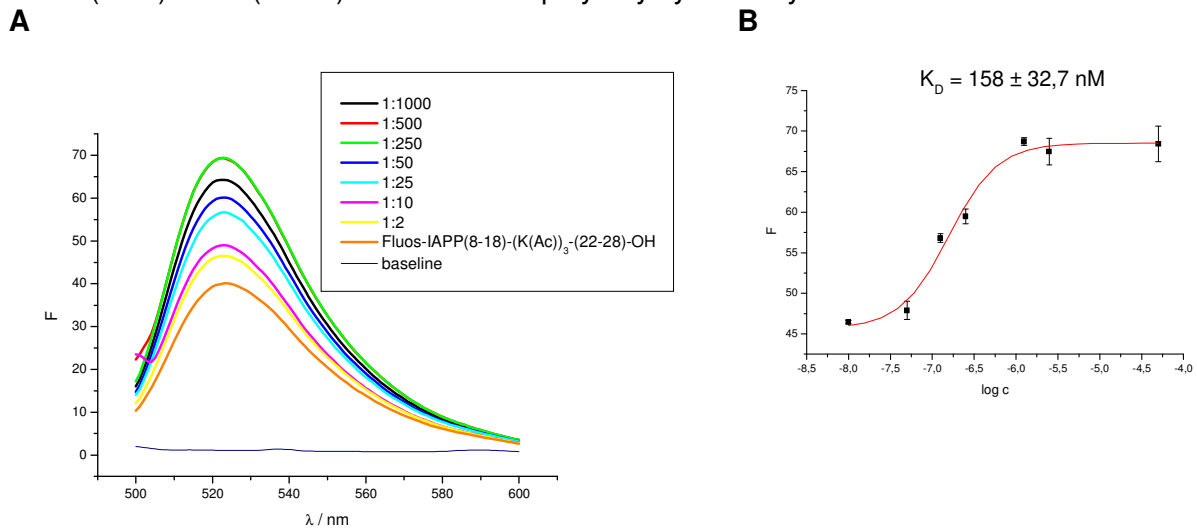


Fig. 191: (A) Fluorescence emission spectra of Fluos-IAPP(8-18)-(K(Ac))₃-(22-28)-OH alone and following titration with IAPP(8-18)-(K(Ac))₃-(22-28)-OH (at the indicated Fluos-IAPP(8-18)-(K(Ac))₃-(22-28)-OH / IAPP(8-18)-(K(Ac))₃-(22-28)-OH molar ratios). Measurements were done in 1xb 1% HFiP, pH 7.4.

(B) Binding curve of the fluorescence titration and app. K_D of the interaction. Data are means (\pm SEM) from three titration curves.

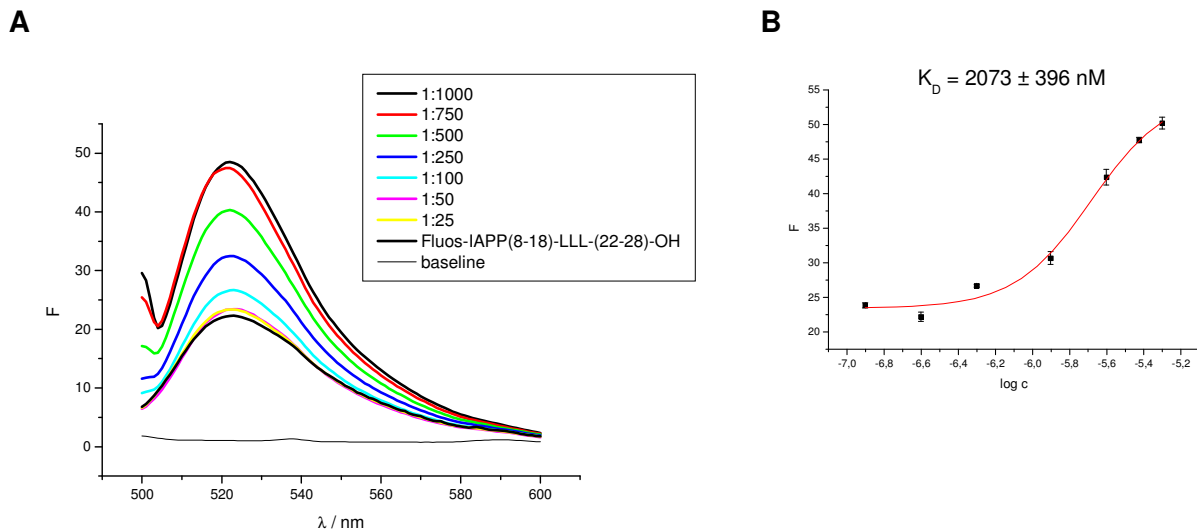


Fig. 192: (A) Fluorescence emission spectra of Fluos-IAPP(8-18)-LLL-(22-28)-OH alone and following titration with IAPP(8-18)-(K(Ac))₃-(22-28)-OH (at the indicated Fluos-IAPP(8-18)-LLL-(22-28)-OH / IAPP(8-18)-LLL-(22-28)-OH molar ratios). Measurements were done in 1xb 1% HFiP, pH 7.4.

(B) Binding curve of the fluorescence titration and app. K_D of the interaction. Data are means (\pm SEM) from three titration curves.

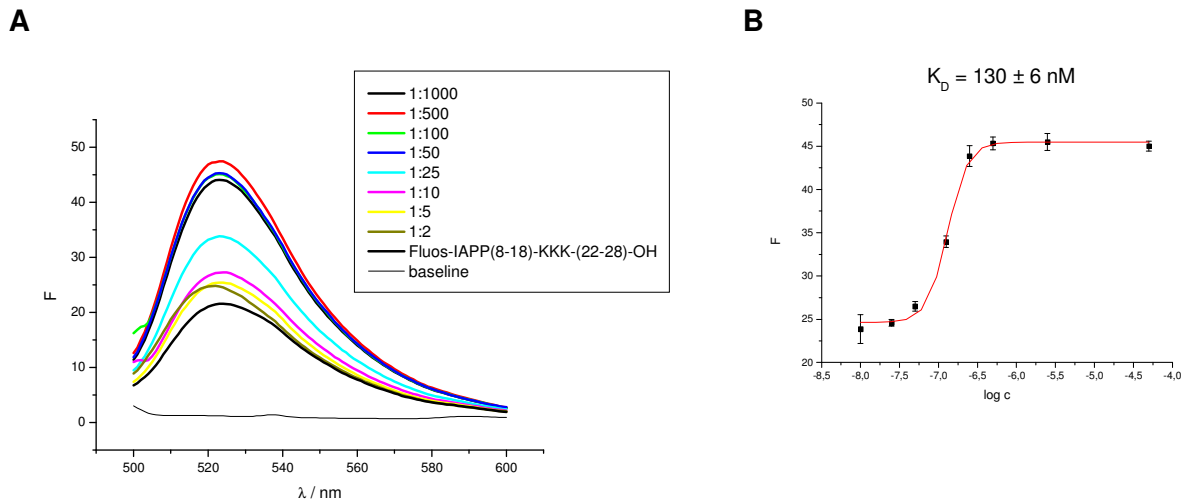


Fig. 193: (A) Fluorescence emission spectra of Fluos-IAPP(8-18)-KKK-(22-28)-OH alone and following titration with IAPP(8-18)-(K(Ac))₃-(22-28)-OH (at the indicated Fluos-IAPP(8-18)-KKK-(22-28)-OH / IAPP(8-18)-KKK-(22-28)-OH molar ratios). Measurements were done in 1xb 1% HFIP, pH 7.4. (B) Binding curve of the fluorescence titration and app. K_D of the interaction. Data are means (\pm SEM) from three titration curves.

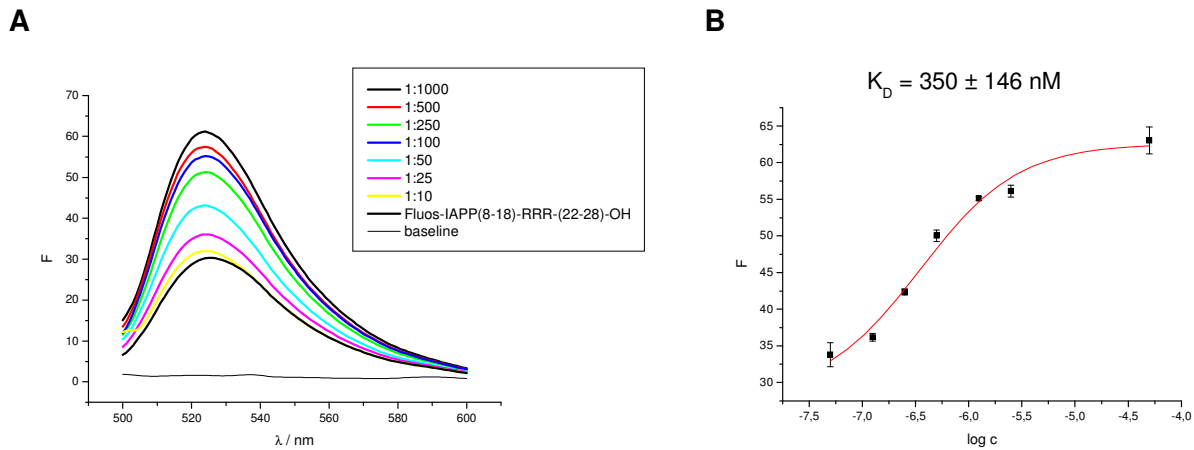


Fig. 194: (A) Fluorescence emission spectra of Fluos-IAPP(8-18)-RRR-(22-28)-OH alone and following titration with IAPP(8-18)-(K(Ac))₃-(22-28)-OH (at the indicated Fluos-IAPP(8-18)-RRR-(22-28)-OH / IAPP(8-18)-RRR-(22-28)-OH molar ratios). Measurements were done in 1xb 1% HFIP, pH 7.4. (B) Binding curve of the fluorescence titration and app. K_D of the interaction. Data are means (\pm SEM) from three titration curves.

Among the analogues tested, IAPP(8-18)-LLL-(22-28)-OH showed the weakest self-association potential. The self association constants of IAPP(8-18)-KKK-(22-28)-OH and IAPP(8-18)-(K(Ac))₃-(22-28)-OH were almost identical indicating no direct influence of the charge upon self-association. The negative effects of repelling charges seem to prevent the formation of amyloid fibers rather than the aggregation of peptides.

No direct correlations between apparent affinities of self-association and fibril forming potential or celltoxicity could be determined.

Table 15: Overview of the binding constants determined for analogues of IAPP(8-28).

Peptide	App. K_D
IAPP(8-18)-(K(Ac)) ₃ -(22-28)-OH	158 \pm 32,7 nM
IAPP(8-18)-LLL-(22-28)-OH	2073 \pm 396 nM
IAPP(8-18)-KKK-(22-28)-OH	130 \pm 6 nM
IAPP(8-18)-RRR-(22-28)-OH	350 \pm 146 nM

3.1.8 Conclusion

The performed studies revealed a unique behavior for analogues of IAPP(8-28)-OH with a hydrophobic IAPP(19-21) region. These peptides display a clear and intense signal in the region of 220-230 nm in CD spectra that suggest the presence of large amounts of β -sheet and β -turn structure. Peptides with hydrophobic elements in the IAPP(19-21) region generally had a high aggregation potential, a high binding affinity to ANS and became denatured or aggregated upon heating. Even though they had many common features, these peptides varied widely among each other concerning their toxicity and fibril forming potentials. This indicates that other aspects also played a role for effects like fibril formation and toxicity. Steric hindrance for example seemed to have a big influence on fibril formation. Big sterically hindered elements in the IAPP(19-21) region, like Cha for example, could disrupt and even prevent fibril formation. This is a strong indication for a conformational and structural switch from oligomers to fibrils. Large, sterically hindered elements might not be able to form a tight, closely packed structure typically found for amyloid fibrils.

The CD spectra of analogues of IAPP(8-28)-OH containing non-hydrophobic elements in the IAPP(19-21) region indicated a PPII-turn-PPII structure for monomeric and oligomeric peptides. The random coil structure displayed by CD spectra at room temperature was most likely a PPII helix as proved by temperature dependent CD spectra. This could also be verified by data obtained from IAPP(8-18)-PPP-(22-28)-OH, an analogue intended to induce the formation of PPII helix. Data from analogues with the pG motif in the IAPP(19-21) region indicated the importance of a turn structure in the IAPP(19-21) region, especially in the case of IAPP(8-18)-SpG-(22-28)-OH.

Some aspects like flexibility or aromaticity in the IAPP(19-21) region seem to have no big influence on structure and fibril forming potential especially compared with the influence of hydrophobic elements.

Charged elements in the IAPP(19-21) region have a huge influence on fibril formation and toxicity. Their weak fibril forming potential compared to native IAPP(8-28)-OH might be explained by the electric repulsion of similar charged elements. This repulsion may have prevented a close alignment of monomers and oligomers which might be necessary for the formation of fibrils even though CD data revealed similar structural motifs for native IAPP(8-28)-OH and analogues with charged elements in the IAPP(19-21) region. This suggestion was further supported by the results of studies performed with the IAPP(8-18)-(K(Ac))₃-(22-28)-OH analogue which was highly toxic and had a strong fibril forming potential.

Future investigations on the structure of oligomers and fibrils formed by these analogues using ssNMR and x-ray diffraction might lead to a deeper understanding of the role of the the IAPP(19-21) region in IAPP aggregation and fibril formation. Some of these peptides might assist in obtaining insight on the molecular basis of the here identified strong effects of the IAPP(19-21) region on IAPP self-assembly.

Table 17: Overview of ThT, cell viability, and ANS binding assays as well as results from CD studies performed with analogues of IAPP(8-28).

Results of “+” indicate fibril formation, whereas “-” indicate no fibril formation within the 5 days of incubation of the solution at the given peptide concentration.

For the cell viability assays, results of “+++” mean high toxicity towards RIN cells, “++” mean medium toxicity, “+/-” mean low toxicity and “-” mean no toxicity.

In the case of ANS binding, results of “+++” mean strong increase in ANS fluorescence, “++” mean medium increase in ANS fluorescence, “+/-” mean weak increase in ANS fluorescence and “-” mean no increase in ANS fluorescence.

The abbreviation r.c. means random coil structure, β means β -sheet and β -turn structure in CD studies.

Sequence	ThT										Tox	ANS	CD
	5 μ M	10 μ M	20 μ M	35 μ M	50 μ M	100 μ M	200 μ M	500 μ M	5 mM	10 mM			
IAPP(8-18)-OH						-	-	+			-		r.c.
IAPP(22-28)-OH						-	-	-	-	-	-		r.c.
IAPP(8-28)-OH			-	+	+	+					+++	+/-	r.c.
IAPP(8-18)-SGN-(22-28)-OH	-	+		+		+					+++	+/-	r.c.
IAPP(8-18)-Aoc-(22-28)-OH			-	+		+					+++	++	β
IAPP(8-18)-Peg-(22-28)-OH				-		+					++	-	r.c.
IAPP(8-18)-KKK-(22-28)-OH				-		-	-	-			++	-	r.c.
IAPP(8-18)-Dap ₃ -(22-28)-OH						-	-	-			-		r.c.
IAPP(8-18)-RRR-(22-28)-OH						-	-	-			-	-	r.c.
IAPP(8-18)-DDD-(22-28)-OH						-		-			-		r.c.
IAPP(8-18)-GGG-(22-28)-OH				-		+	+				++	-	r.c.
IAPP(8-18)-AAA-(22-28)-OH				-		+	+				++	+/-	r.c.
IAPP(8-18)-VVV-(22-28)-OH		-	+	+	+	+	+				+++	+++	β
IAPP(8-18)-LLL-(22-28)-OH			-	-		-	+	+			++	+++	β
IAPP(8-18)-III-(22-28)-OH			-	+	+	+	+				+++	+++	β
IAPP(8-18)-Nle ₃ -(22-28)-OH			-	+	+	+	+				+++	++	β
IAPP(8-18)-2Aoc ₃ -(22-28)-OH			-	+		+	+				+++	+++	β
IAPP(8-18)-TTT-(22-28)-OH			-	+		+	+				++		r.c.
IAPP(8-18)-FFF-(22-28)-OH				-	+	+	+				++	+++	β
IAPP(8-18)-Cha ₃ -(22-28)-OH				-		-	-	-			+/-	+++	β
IAPP(8-18)-SpG-(22-28)-OH				-	+	+					+/-	+/-	r.c.
IAPP(8-18)-pGN-(22-28)-OH				-	-	+					++	+	r.c.
IAPP(8-18)-PPP-(22-28)-OH						-		-			-	-	r.c.
IAPP(8-18)-(K(Ac)) ₃ -(22-28)-OH	-	+	+	+	+	+					+++	+	r.c.
IAPP(8-18)-KK(Ac)K(Ac)-(22-28)-OH			-	+		+					+++		r.c.
IAPP(8-18)-K(Ac)KK(Ac)-(22-28)-OH			-	+		+					++		r.c.
IAPP(8-18)-K(Ac)K(Ac)K-(22-28)-OH		-				-	+	+			++		r.c.
IAPP(8-18)-KKK(Ac)-(22-28)-OH						-	-	+			++		r.c.
IAPP(8-18)-KK(Ac)K-(22-28)-OH		-				-	-	+			-		r.c.
IAPP(8-18)-K(Ac)KK-(22-28)-OH		-				-	-	-			-		r.c.

3.2 Hybrids of A β (27-32) and IAPP(22-28)

3.2.1 Introduction

Both, NKGAI (A β (27-32)) and NFGAILS (IAPP(22-28)) alone are known to be able to form amyloid fibrils. They share a high sequence similarity and more than 50% of the sequence is identical.

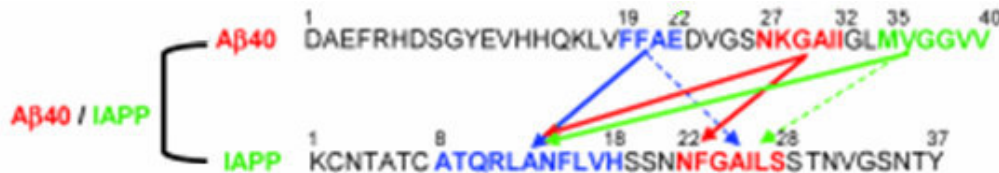


Fig. 195: Cross-interactions between the hot regions (solid arrows) of the A β 40-IAPP interaction interface. The hot regions are colored in blue, red, and green (from [120]).

The two regions are involved in both the homo- and heteroassociation of IAPP and A β (Fig. 195 [120]). Crystallographic structure analysis reveals that both sequences are involved in the formation of interdigitated β -sheets called steric zippers.

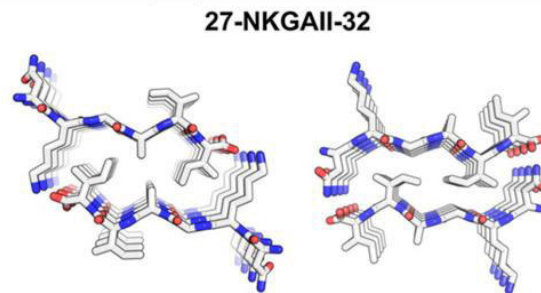


Fig. 196: Steric zipper motifs formed by NKGAI (from[179]).

NKGAI is a segment of A β that is able to form steric zippers (Fig 196, [179]). The segment forms a parallel β -sheet stacking with two different interfaces. One interface displays a face-to-face orientation and the other a back-to-back orientation. Both interfaces show β -sheets packed together via interdigitating hydrophobic side chains.

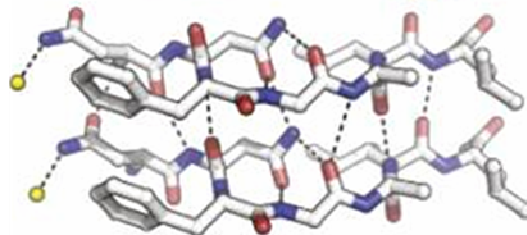


Fig. 197: Structure of NNFGAIL. The segment is not forming a typical steric zipper and might rather form a turn element [from [52]].

There is no crystal structure available from NFGAILS; nevertheless there is one from NNFGAIL. NNFGAIL is not forming a typical steric zipper motif. Its structure does not display interdigitated β -sheets that are characteristic for steric zippers (Fig 197). The segment contains a tight main-chain to main-chain interface formed by the Phe, Gly, and Ala residues from opposing sheets. It also contains a bend in the backbone facilitated by the Gly residue. The NNFGAIL segment may rather be involved in the formation of a turn leading to a steric zipper than a steric zipper itself [52]. It has however been shown, that NFGAIL (IAPP(22-27)) and FGAIL (IAPP(23-27)) alone are able to form β -sheet containing amyloidogenic fibrils [100].

3.2.1.1 Aim and Design

In my work, I attempted to create peptides with a specific steric zipper motif, consisting of two amyloidogenic sequences from two different peptides. Therefore, the two sequences NKGAI (A β (27-32)) and NFGAILS (IAPP(22-28)) were chosen. These two sequences were connected by different linker elements with a common length of 3 amino acids. The linkers vary in aspects like charge, hydrophobicity or steric hindrance.

Different linking elements were chosen to investigate their influence on the formation of an intramolecular steric zipper motif by these hot regions. The influence of both the sequences and the different linking elements on β -sheet formation and fibril formation was studied.

For example, hydrophobic elements like Aoc, Adc and LLL were chosen because they might support the formation of a hydrophobic core promoting fibril formation.

Other linkers contained charged elements like KKK and EEE that should rather prevent fibril formation due to repelling charges and the formation of a hydration shell [180].

Another issue was to test the influence of flexible connecting elements on the formation of fibrils and a steric zipper motif. Therefore variable flexible elements were chosen with additional hydrophobic (Aoc and Adc) or hydrophilic (Peg) features and a more flexible but peptidic backbone structure (GGG) were tested.

Table 18: List of the designed and tested peptide hybrids.

Abbreviation	Sequence
H5	H-NKGAI-Peg-NFGAILS-OH
H5a	H-NKGAI-Aoc-NFGAILS-OH
H5aK3	H-NKGAI-Aoc-NFGAILS- β A-KKK-OH
H5aK6	H-KKK- β A-NKGAI-Aoc-NFGAILS- β A-KKK-OH
H5b	H-NKGAI-Adc-NFGAILS-OH
H16	H-NKGAI-GGG-NFGAILS-OH
H18	H-NKGAI-AAA-NFGAILS-OH
H12	H-NKGAI-LLL-NFGAILS-OH
H12K6	H-KKK- β A-NKGAI-LLL-NFGAILS- β A-KKK-OH
H13	H-NKGAI-KKK-NFGAILS-OH
H20	H-NKGAI-K(Ac)K(Ac)K(Ac)-NFGAILS-OH
H22	H-NKGAI-EEE-NFGAILS-OH
H6	H-IIAGKN-Peg-NFGAILS-OH
H6a	H-IIAGKN-Aoc-NFGAILS-OH
H6b	H-IIAGKN-Adc-NFGAILS-OH
H24	H-IIAGKN-GGG-NFGAILS-OH
H23	H-IIAGKN-AAA-NFGAILS-OH
H14	H-IIAGKN-LLL-NFGAILS-OH
H15	H-IIAGKN-KKK-NFGAILS-OH
H19	H-IIAGKN-K(Ac)K(Ac)K(Ac)-NFGAILS-OH
H17	H-IIAGKN-EEE-NFGAILS-OH
CB1	H-NFGAILS-LLL-NFGAILS-OH
CB3	H-NKGAI-LLL-NKGAI-OH
CB5	H-NFGAILS-Aoc-NFGAILS-OH
CB6	H-NKGAI-Aoc-NKGAI-OH
CB7	H-NFGAILS-Aoc-NKGAI-OH
CB2	H-NFGAILS-KKK-NFGAILS-OH
CB4	H-NKGAI-KKK-NKGAI-OH

3.2.2 Peptides containing the segments A β (27-32) and IAPP(22-28)

3.2.2.1 IAPP(22-28) or H-NFGAILS-OH

At first, the sequence NFGAILS (IAPP(22-28)) alone was tested for its amyloidogenic potential under the conditions used for the different assays.

The far-UV CD spectra of H-NFGAILS-OH (Fig. 198A) displayed a random coil structure for the peptide as indicated by an intense minimum at 195 nm. The signal intensity of that minimum was reduced for concentrations larger than 10 μ M intending the formation of soluble oligomers.

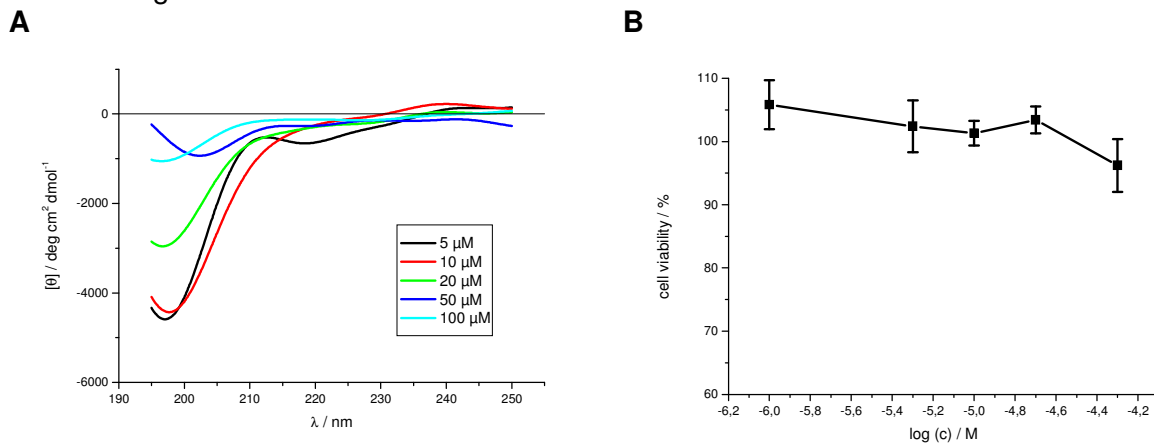


Fig. 198: (A) Far-UV CD spectra of H-NFGAILS-OH at different concentrations in 1xb 1% HFIP, pH 7.4 (from [159]).

(B) Cell viability assay of an aged solution of H-NFGAILS-OH (5 mM in 1xb 1% HFIP for 4 days, pH 7.4) using PC-12 cells. Data are percentages of control and are the mean (+/-SEM) of three independent experiments with each experiment performed in multiple replicates (n = 3).

H-NFGAILS-OH was not toxic to PC-12 cells under the conditions tested (Fig. 198B).

As shown in Fig. 199A, H-NFGAILS-OH did not form fibrils up to a concentration of 10 mM under the conditions used within 96h.

The TEM picture of an aged solution of 10 mM H-NFGAILS-OH (Fig. 199B) confirmed this finding by only displaying amorphous aggregates.

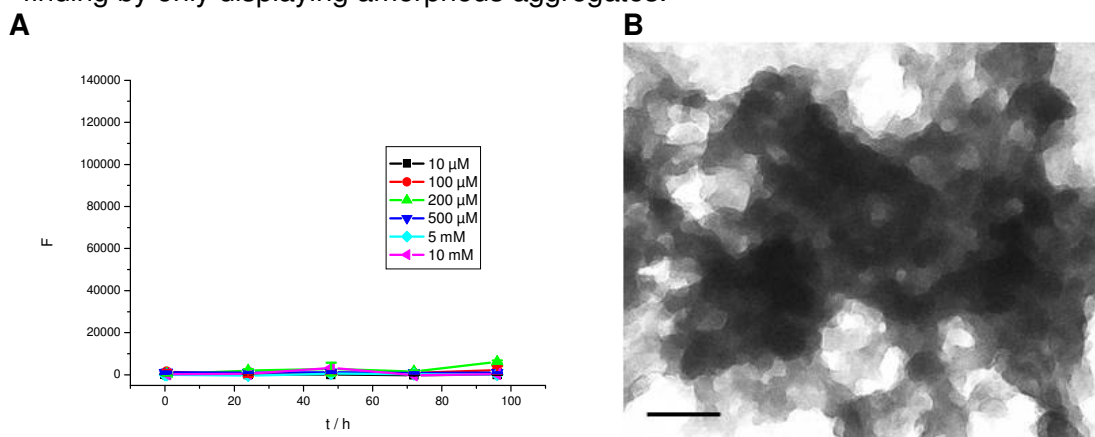


Fig. 199: (A) ThT binding assays of H-NFGAILS-OH at different concentrations in 1xb 1% HFIP, pH 7.4 (partially from [160-162]). Data are means of 3 assays after subtraction of buffer values +/- standard error of the mean (SEM) with each experiment performed in multiple replicates (n = 3).

(B) TEM picture of H-NFGAILS-OH. The peptide was incubated at 10 mM for 7 d in 1xb 1% HFIP, pH 7.4. Scale bar: 100 nm.

Staining of aged incubations of H-NFGAILS-OH with Congo Red (Fig. 200A and B) also revealed no birefringence under cross-polarized light. Stained aggregates showed intense red color under normal light which indicates a nonspecific binding to H-NFGAILS-OH. The lack of green/yellow birefringence under cross-polarized light albeit indicates that these aggregates are rather amorphous and did not display a typical amyloidogenic structure. It has however been shown that NFGAILS is able to form amyloid fibrils under conditions differing from the ones used here [100].

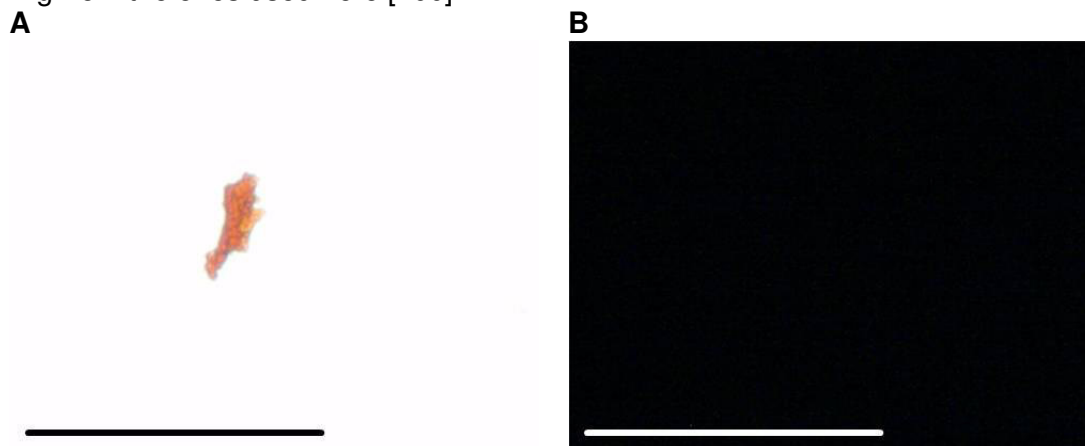


Fig. 200: Microscopic examination of an aged incubation of H-NFGAILS-OH stained with Congo Red. The peptide was incubated at a concentration of 1 mM in 1xb 1% HFIP, pH 7.4 for 3 days. Pictures were taken under A normal and B cross-polarized light. Scale bar: 100 μm .

3.2.2.2 A β (27-32) or H-NKGAIL-OH

The other sequence used, NKGAIL (A β (27-32)), was also studied with regard to its biophysical properties.

The CD spectra of H-NKGAIL-OH showed both a minimum at 200 nm related to random coil structure but also a strong negative signal at 215-220 nm that could be related to β -sheet structure (Fig. 201A) similar to H-NFGAILS-OH, H-NKGAIL-OH also started to form soluble oligomers at concentrations higher than 10 μM .

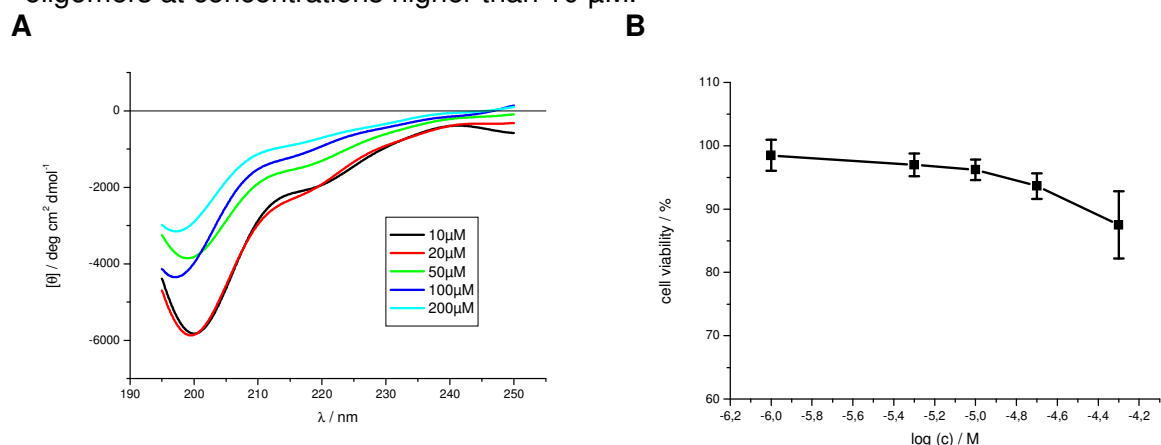


Fig. 201: (A) Far-UV CD spectra of H-NKGAIL-OH at different concentrations in 1xb 1% HFIP, pH 7.4 (from [159]).

(B) Cell viability assay of an aged solution of H-NKGAIL-OH (5 mM in 1xb 1% HFIP, pH 7.4 for 4 days) using PC-12 cells. Data are percentages of control and are the mean (+/-SEM) of three independent experiments with each experiment performed in multiple replicates (n = 3).

H-NKGAIL-OH was slightly toxic to PC-12 cells (Fig. 201B).

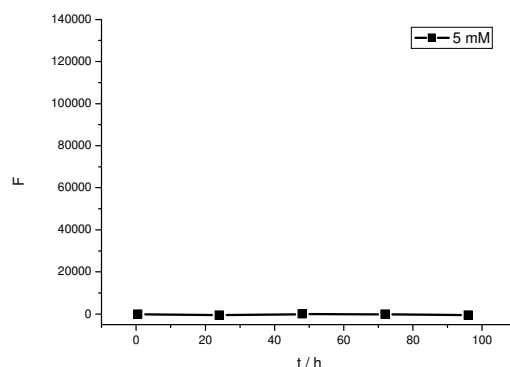


Fig. 202: ThT binding assay of H-NKGAI-OH at a peptide concentration of 5 mM in 1xb, 1% HFIP, pH 7.4.

The ThT assay of H-NKGAI-OH at a peptide concentration of 5 mM did not show fibril formation within 96h as shown in Fig. 202.

Staining of aged incubations of H-NKGAI-OH with Congo Red (Fig. 203A and B) also revealed no birefringence under cross-polarized light. Under normal light there were only small Congo Red stained aggregates of H-NKGAI-OH visible.

Similar to NFGAILS, NKGAI did not form fibrils under the conditions tested in this work. It is however able to form amyloid fibrils under conditions differing from the ones used here [179].

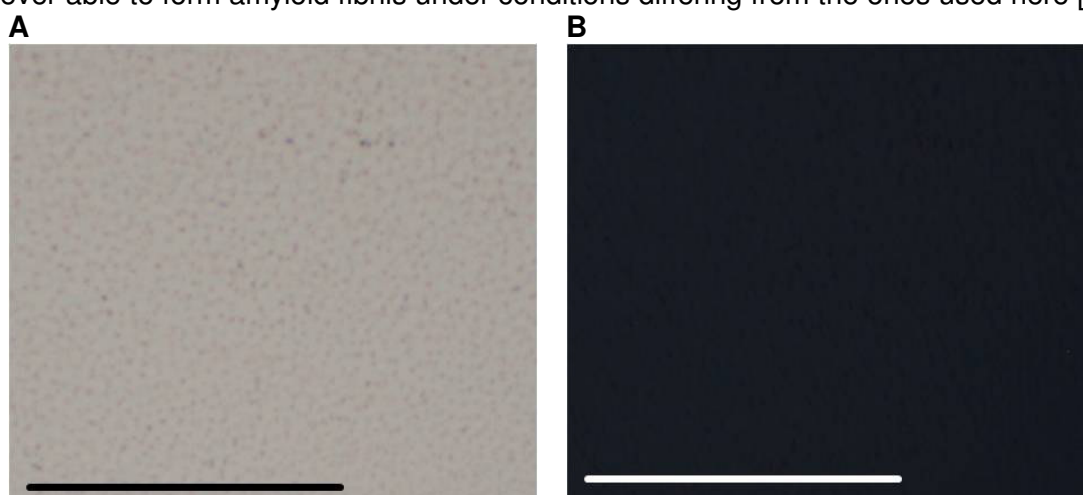


Fig. 203: Microscopic examination of an aged incubation of H-NKGAI-OH stained with Congo Red. The peptide was incubated at a concentration of 1 mM in 1xb 1% HFIP for 3 days. Pictures were taken under A normal and B cross-polarized light. Scale bar: 100 μ m.

3.2.2.3 H-NKGAI-Peg-NFGAILS-OH (H5)

The concentration dependent CD spectra of H-NKGAI-Peg-NFGAILS-OH (Fig. 204A) showed a strong minimum at 195 - 200 nm that can be related to random coil structure. The weaker negative signal between 210 nm and 220 nm intend the presence of additional structural elements like β -sheets and β -turns. H-NKGAI-Peg-NFGAILS-OH expressed only a weak aggregation potential as indicated by a small signal reduction upon increasing concentrations.

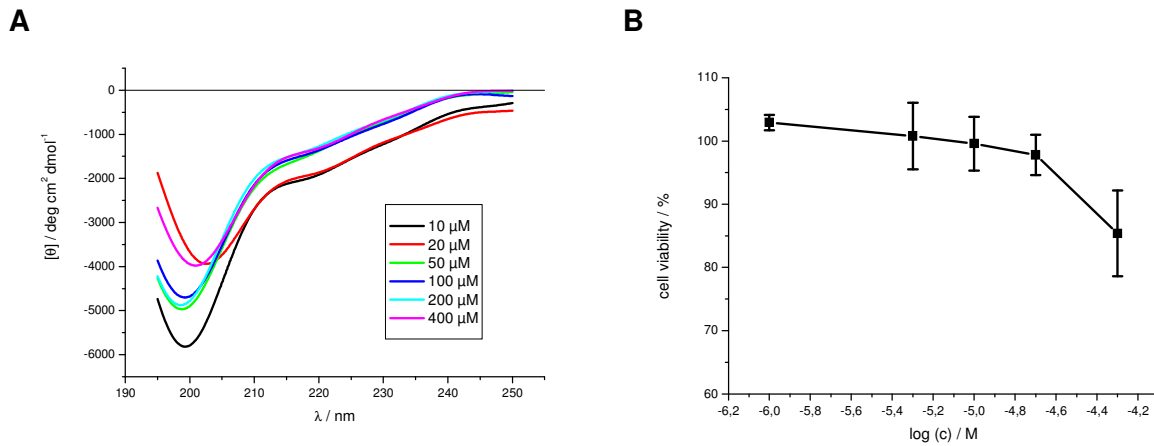


Fig. 204: (A) Far-UV CD spectra of H-NKGAI-Peg-NFGAILS-OH at different concentrations in 1x 1% HFIP, pH 7.4 (from [159]). (B) Cell viability assay of an aged solution of H-NKGAI-Peg-NFGAILS-OH (5 mM in 1x 1% HFIP for 4 days) using PC-12 cells. Data are percentages of control and are the mean (+/-SEM) of three independent experiments with each experiment performed in multiple replicates (n = 3).

As shown in Fig. 204B H-NKGAI-Peg-NFGAILS-OH was toxic to PC-12 cells.

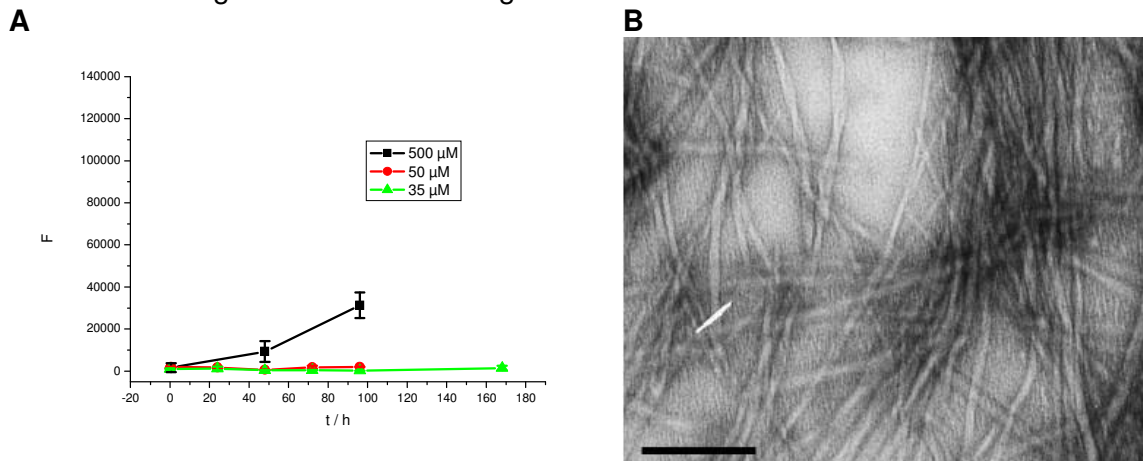


Fig. 205: (A) ThT binding assays of H-NKGAI-Peg-NFGAILS-OH at different concentrations in 1x 1% HFIP, pH 7.4 (partially from [159]). Data are means of 3 assays after subtraction of buffer values +/- standard error of the mean (SEM) with each experiment performed in multiple replicates (n = 3). (B) TEM picture of H-NKGAI-Peg-NFGAILS-OH. The peptide was incubated at 500 μM for 7 d in 1x 1% HFIP, pH 7.4. Scale bar: 100 nm.

The fibril forming potential of H-NKGAI-Peg-NFGAILS-OH was low. At concentrations of 35 and 50 μM it was not forming fibrils within 96h. Fibril formation was only seen at a peptide concentration of 500 μM (Fig. 205A).

Fibril formation could be confirmed by Congo Red staining. Pictures of fibrils stained with Congo Red displayed clear green birefringence under cross-polarized light (Fig. 206B).

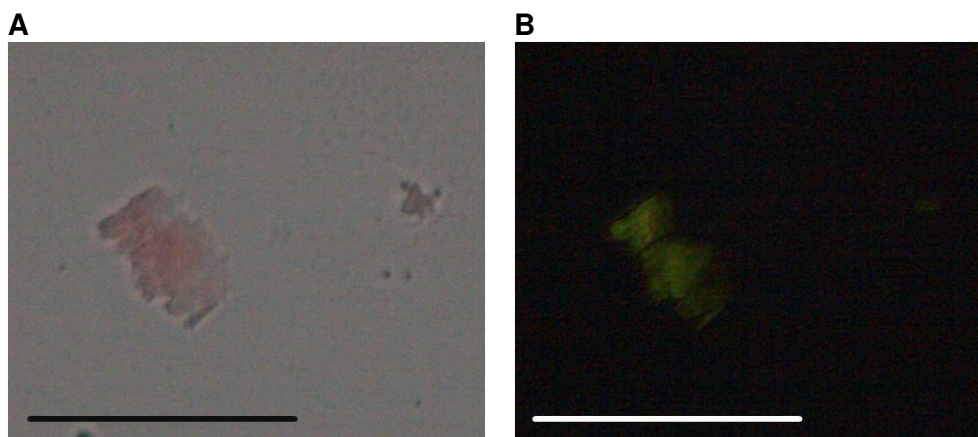


Fig. 206: Microscopic examination of an aged incubation of H-NKGAI-Peg-NFGAILS-OH stained with Congo Red. The peptide was incubated at a concentration of 1 mM in 1xb 1% HFIP for 3 days. Pictures were taken under A normal and B cross-polarized light. Scale bar: 100 µm.

3.2.2.4 H-NKGAI-Aoc-NFGAILS-OH (H5a)

CD spectra of H-NKGAI-Aoc-NFGAILS-OH (Fig. 207A) revealed a broad and intense minimum. At a peptide concentration of 1 µM, the minimum of this signal was at around 200 nm indicating the presence of random coil structure. The minimum of this signal was shifted to 210 nm at higher peptide concentrations. At a concentration of 5 µM the signal displayed no random coil structure anymore but a clear shape related to the presence of β -sheet structure. The signal intensity decreased at peptide concentrations higher than 10 µM. This signal decrease might be related to the formation of soluble oligomers. These data suggest that H-NKGAI-Aoc-NFGAILS-OH undergoes structural changes from random coil to a more ordered β -sheet conformation prior to aggregation.

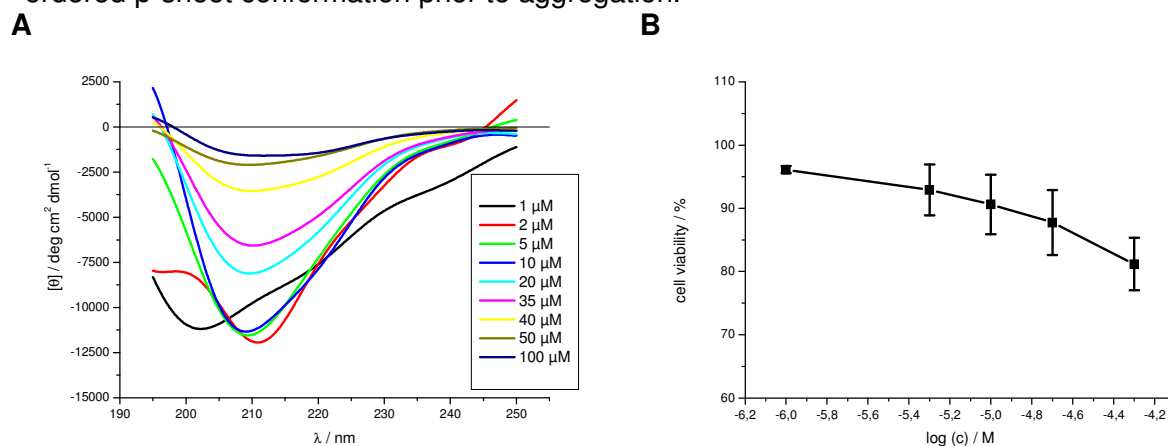


Fig. 207: (A) Far-UV CD spectra of H-NKGAI-Aoc-NFGAILS-OH at different concentrations in 1xb 1% HFIP, pH 7.4 (from [159]).

(B) Cell viability assay of an aged solution of H-NKGAI-Aoc-NFGAILS-OH (5 mM in 1xb 1% HFIP, pH 7.4 for 4 days) using PC-12 cells. Data are percentages of control and are the mean (+/-SEM) of three independent experiments with each experiment performed in multiple replicates (n = 3).

Compared to H-NKGAI-Peg-NFGAILS-OH (Fig. 204B), H-NKGAI-Aoc-NFGAILS-OH displayed a significantly higher toxicity towards PC-12 cells (Fig. 207B).

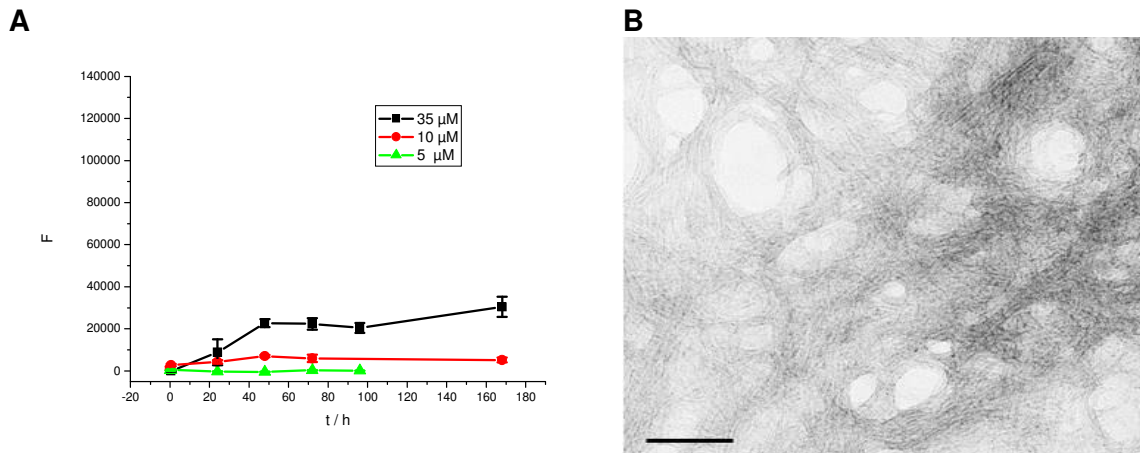


Fig. 208: (A) ThT binding assays of H-NKGAI-Aoc-NFGAILS-OH at different concentrations in 1xb 1% HFIP, pH 7.4 (partially from [159]). Data are means of 3 assays after subtraction of buffer values \pm standard error of the mean (SEM) with each experiment performed in multiple replicates ($n = 3$). (B) TEM picture of an aged incubation of H-NKGAI-Aoc-NFGAILS-OH. The peptide was incubated at 50 μ M for 7 d in 1xb 1% HFIP, pH 7.4. Scale bar: 100 nm.

ThT studies at different concentrations revealed, that H-NKGAI-Aoc-NFGAILS-OH started forming fibrils at a concentration of 10 μ M (Fig. 208A). Fibril formation occurred quite fast, already after 30 minutes of incubation. The concentration dependent CD spectrum at 20 μ M already showed a signal loss related to oligomerization (Fig. 207A). This correlates with a fast fibril formation observed by ThT assays. At a concentration of 35 μ M, the ThT fluorescence signal reaches a plateau after 48 h. This means that either the total amount of H-NKGAI-Aoc-NFGAILS-OH has already formed fibrils or that an equilibrium between fibril growth and depletion was reached.

The results of staining of aged incubations of H-NKGAI-Aoc-NFGAILS-OH with Congo Red were consistent with the amyloid nature of the aggregates which showed intense red color under normal light (Fig. 209A) and displayed green color under cross-polarized light (Fig. 209B).

This fibril formation was verified by TEM. The TEM image of an aged incubation of H-NKGAI-Aoc-NFGAILS-OH at a concentration of 50 μ M aggregates of H-NKGAI-Aoc-NFGAILS-OH consisted of amyloid fibrils (Fig. 208B).

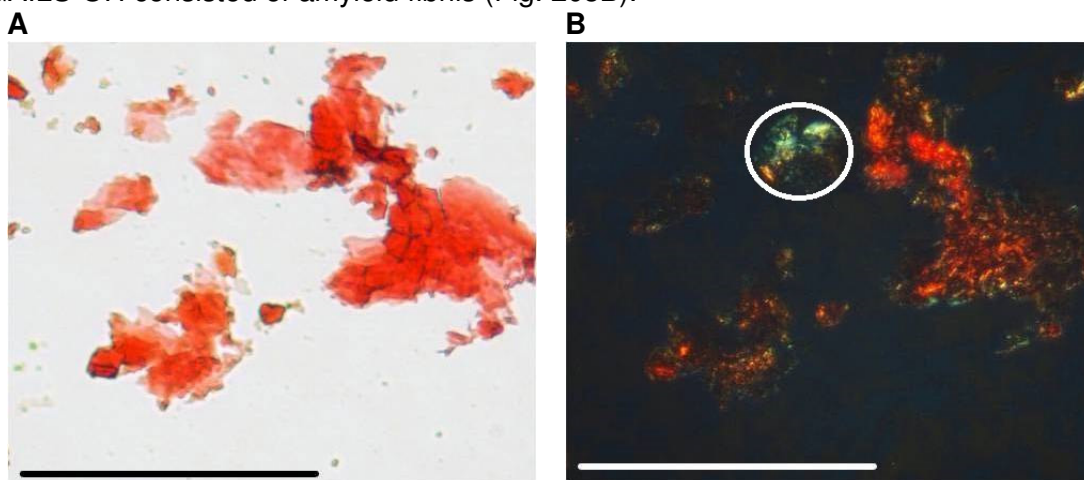


Fig. 209: Microscopic examination of an aged incubation of H-NKGAI-Aoc-NFGAILS-OH stained with Congo Red. The peptide was incubated at a concentration of 1 mM in 1xb 1% HFIP, pH 7.4 for 3 days. Pictures were taken under A normal and B cross-polarized light (from [159]). Scale bar: 100 μ m.

3.2.2.5 H-NKGAI-Aoc-NFGAILS-βA-KKK-OH (H5aK3)

To improve the solubility of H-NKGAI-Aoc-NFGAILS-OH three lysines and β-alanine as a spacer were added on the C-terminus of the peptide.

CD spectra of H-NKGAI-Aoc-NFGAILS-βA-KKK-OH (Fig. 210) displayed a strong negative signal at 195 nm indicating random coil structure and a broad negative bulge at 210-230 nm indicating the presence of significant amounts of β-sheet or β-turn elements. For comparison, the CD spectra of H-NKGAI-Aoc-NFGAILS-OH (Fig. 207A) indicated mainly β-sheet structure and only at a very low peptide concentration, where H-NKGAI-Aoc-NFGAILS-OH was potentially monomeric, random coil elements were present.

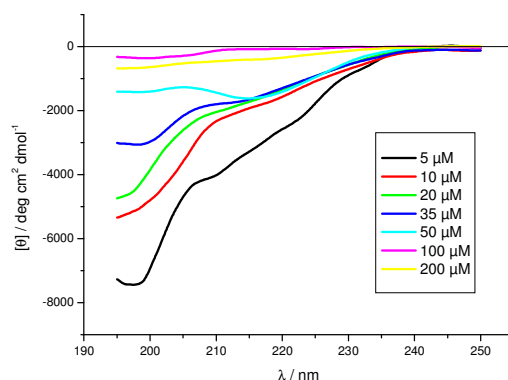


Fig. 210: Far-UV CD spectra of H-NKGAI-Aoc-NFGAILS-βA-KKK-OH at different concentrations in 1xb 1% HFIP, pH 7.4.

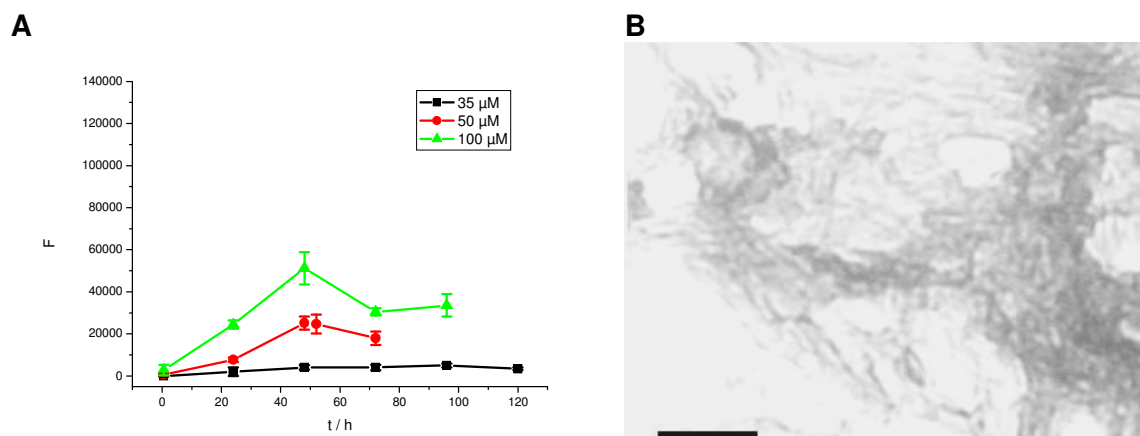


Fig. 211: (A) ThT binding assays of H-NKGAI-Aoc-NFGAILS-βA-KKK-OH at different concentrations in 1xb 1% HFIP, pH 7.4. Data are means of 3 assays after subtraction of buffer values +/- standard error of the mean (SEM) with each experiment performed in multiple replicates (n = 3).

(B) TEM picture of an aged incubation of H-NKGAI-Aoc-NFGAILS-βA-KKK-OH. The peptide was incubated at 100 μM for 7 d in 1xb 1% HFIP, pH 7.4. Scale bar: 100 nm.

H-NKGAI-Aoc-NFGAILS-βA-KKK-OH started forming fibrils at a peptide concentration of 50 μM as indicated by an increase of ThT fluorescence intensity (Fig. 211A). This indicated that the fibril forming potential of H-NKGAI-Aoc-NFGAILS-βA-KKK-OH was lower than that of H-NKGAI-Aoc-NFGAILS-OH (Fig. 208A).

The TEM picture of an aged incubation at 100 μM showed mainly fibrils but also some amorphous aggregates (Fig. 211B).

Congo Red staining of an aged incubation of H-NKGAI-Aoc-NFGAILS-βA-KKK-OH (Fig. 212B) showed weak green/yellow birefringence under cross-polarized light related to amyloid structures.

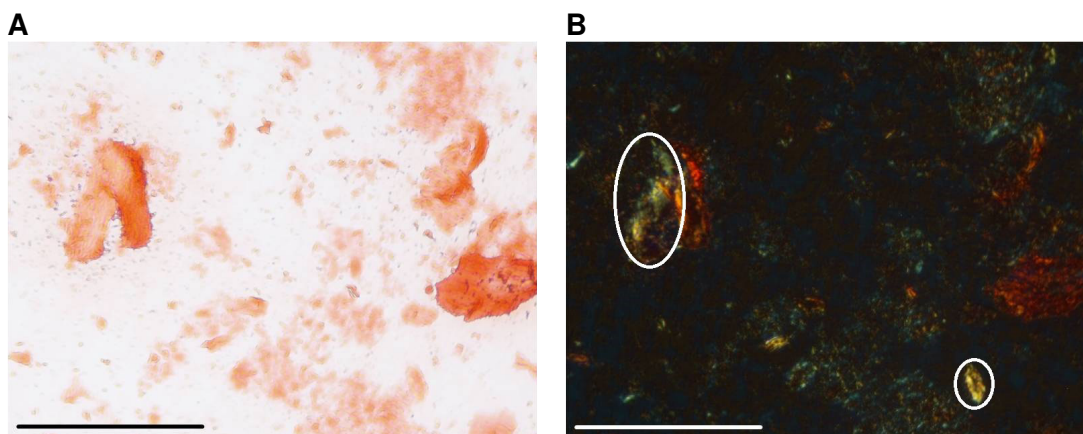


Fig. 212: Microscopic examination of an aged incubation of H-NKGAI-Aoc-NFGAILS-βA-KKK-OH stained with Congo Red. The peptide was incubated at a concentration of 1 mM in 1xb 1% HFIP, pH 7.4 for 3 days. Pictures were taken under A normal and B cross-polarized light. Scale bar: 100 μm.

3.2.2.6 H-KKK-βA-NKGAI-Aoc-NFGAILS-βA-KKK-OH (H5aK6)

Concentration dependent CD spectra of H-KKK-βA-NKGAI-Aoc-NFGAILS-βA-KKK-OH (Fig. 213A) revealed an almost complete loss of β-sheet structure compared to H-NKGAI-Aoc-NFGAILS-OH (Fig. 14A) and H-NKGAI-Aoc-NFGAILS-βA-KKK-OH (Fig. 210). Instead the peptide exhibited mainly random coil structure as indicated by the pronounced minimum at 198 nm. At a concentration of 5 μM the intensity of this minimum is similar to that of H-NKGAI-Aoc-NFGAILS-βA-KKK-OH.

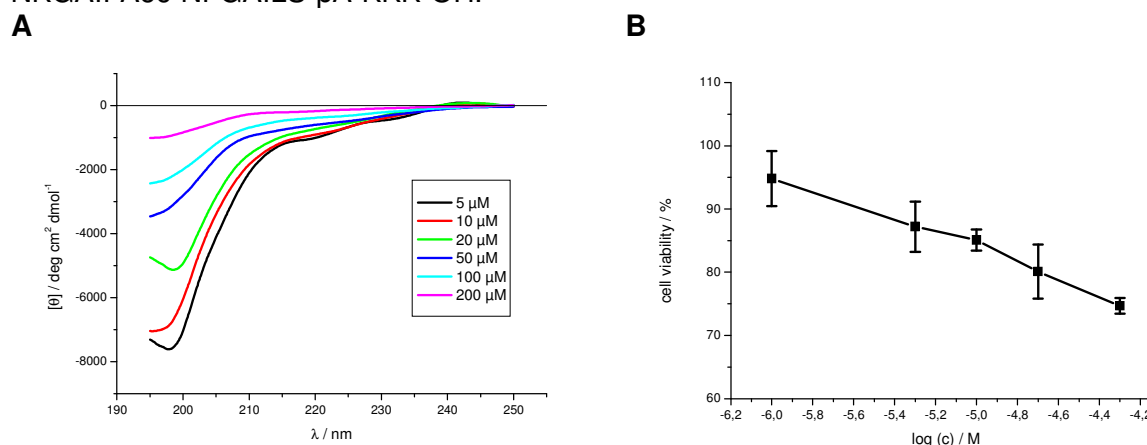


Fig. 213: (A) Far-UV CD spectra of H-KKK-βA-NKGAI-Aoc-NFGAILS-βA-KKK-OH at different concentrations in 1xb 1% HFIP, pH 7.4. (B) Cell viability assay of an aged solution of H-KKK-βA-NKGAI-Aoc-NFGAILS-βA-KKK-OH (5 mM in 1xb 1% HFIP, pH 7.4 for 4 days) using PC-12 cells. Data are percentages of control and are the mean (+/-SEM) of three independent experiments with each experiment performed in multiple replicates (n = 3).

H-KKK-βA-NKGAI-Aoc-NFGAILS-βA-KKK-OH displayed some toxicity to PC-12 cells (Fig. 213B) similar to H-NKGAI-Aoc-NFGAILS-OH (Fig. 207B).

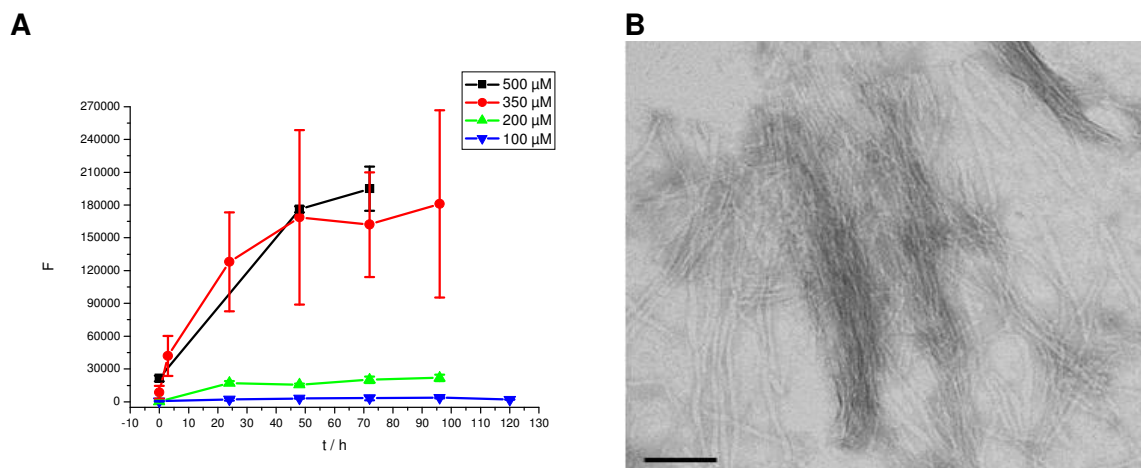


Fig. 214: (A) ThT binding assays of H-KKK- β A-NKGAI-Aoc-NFGAILS- β A-KKK-OH at different concentrations in 1xb 1% HFIP, pH 7.4. Data are means of 3 assays after subtraction of buffer values \pm standard error of the mean (SEM) with each experiment performed in multiple replicates ($n = 3$). (B) TEM picture of an aged incubation of H-KKK- β A-NKGAI-Aoc-NFGAILS- β A-KKK-OH. The peptide was incubated at 500 μ M for 7 d in 1xb 1% HFIP, pH 7.4. Scale bar: 100 nm.

ThT assays of H-KKK- β A-NKGAI-Aoc-NFGAILS- β A-KKK-OH at different concentrations indicated that the peptide started forming amyloid fibrils at a concentration of 200 μ M (Fig. 214A). The fibril forming potential of H-KKK- β A-NKGAI-Aoc-NFGAILS- β A-KKK-OH was thus lower than that of H-NKGAI-Aoc-NFGAILS- β A-KKK-OH (Fig. 211A). This can be due to the presence of C- and N-terminal lysines in H-KKK- β A-NKGAI-Aoc-NFGAILS- β A-KKK-OH.

Congo Red staining of an aged solution of H-KKK- β A-NKGAI-Aoc-NFGAILS- β A-KKK-OH (Fig. 215A and B) showed red staining under normal light and green/yellow birefringence under cross-polarized light indicating the presence of amyloid structures.

TEM imaging of an aged solution of 500 μ M H-KKK- β A-NKGAI-Aoc-NFGAILS- β A-KKK-OH confirmed the presence of fibrillar aggregates (Fig. 214B).

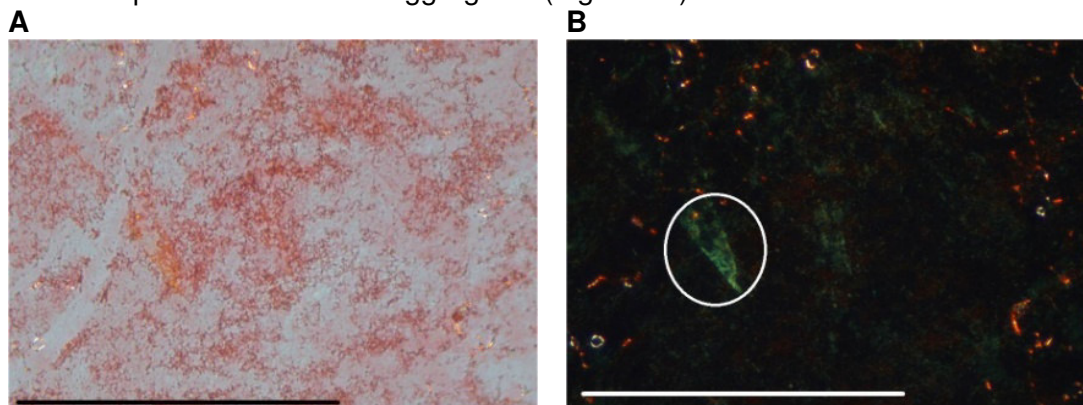


Fig. 215: Microscopic examination of an aged incubation of H-KKK- β A-NKGAI-Aoc-NFGAILS- β A-KKK-OH stained with Congo Red. The peptide was incubated at a concentration of 1 mM in 1xb 1% HFIP, pH 7.4 for 3 days. Pictures were taken under A normal and B cross-polarized light. Scale bar: 100 μ m.

3.2.2.7 H-NKGAI-Adc-NFGAILS-OH (H5b)

Similar to H-NKGAI-Aoc-NFGAILS-OH (Fig. 207A), the CD spectra of IAPP(8-18)-Adc-(22-28)-OH (Fig. 216A) displayed a broad and intense minimum at 215 nm. Compared to H-NKGAI-Aoc-NFGAILS-OH, this signal was broader but less intense. The signal intensity decreased already at a peptide concentration of 5 μ M. This indicates a higher aggregation potential compared to e.g. H-NKGAI-Peg-NFGAILS-OH (Fig. 204A) or H-NKGAI-Aoc-NFGAILS-OH (Fig. 207A).

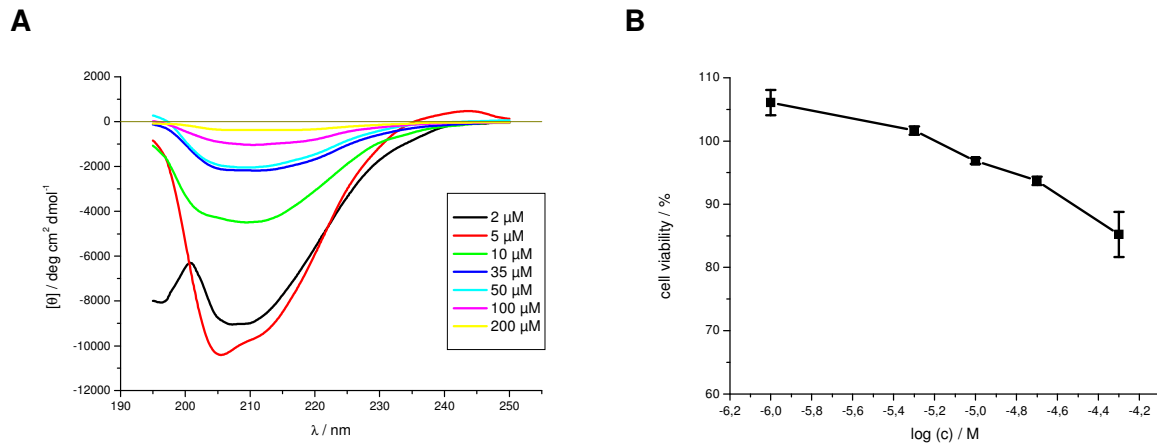


Fig. 216: (A) Far-UV CD spectra of H-NKGAI-Adc-NFGAILS-OH at different concentrations in 1xb 1% HFiP, pH 7.4. (B) Cell viability assay of an aged solution of H-NKGAI-Adc-NFGAILS-OH (5 mM in 1xb 1% HFiP, pH 7.4 for 4 days) using PC-12 cells. Data are percentages of control and are the mean (+/-SEM) of three independent experiments with each experiment performed in multiple replicates (n = 3).

However, H-NKGAI-Adc-NFGAILS-OH was found to be slightly less toxic to PC-12 cells (Fig. 216B) than H-NKGAI-Aoc-NFGAILS-OH (Fig. 207B).

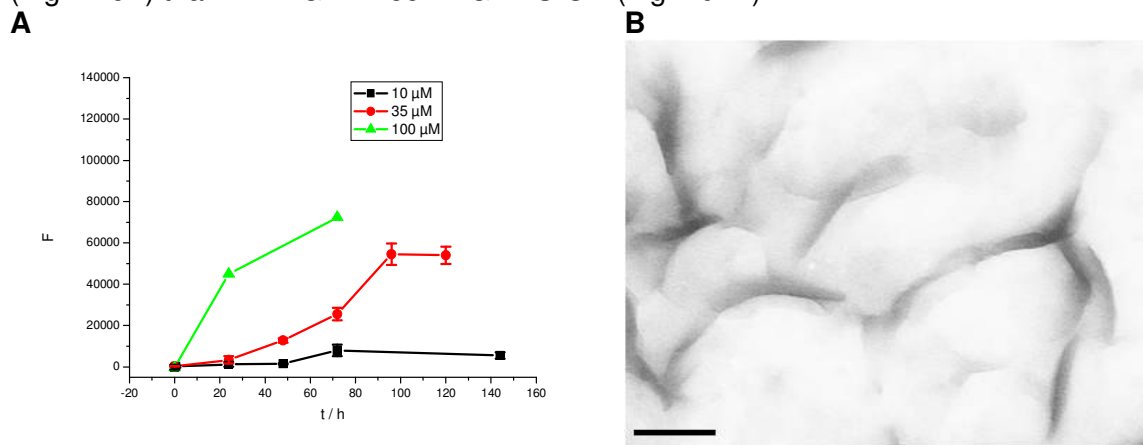


Fig. 217: (A) ThT binding assays of H-NKGAI-Adc-NFGAILS-OH at different concentrations in 1xb 1% HFiP, pH 7.4. Data are means of 3 assays after subtraction of buffer values +/- standard error of the mean (SEM) with each experiment performed in multiple replicates (n = 3). (B) TEM picture of an aged incubation of H-NKGAI-Adc-NFGAILS-OH. The peptide was incubated at 100 μM for 7 d in 1xb 1% HFiP, pH 7.4. Scale bar: 100 nm.

ThT binding studies on H-NKGAI-Adc-NFGAILS-OH revealed fibril formation at a concentration of 35 μM (Fig. 217A). Congo Red staining of an aged incubation of H-NKGAI-Adc-NFGAILS-OH (Fig. 218A and B) showed aggregates colored red under normal light and in part green/yellow birefringence under cross-polarized light. This was a clear indication for the formation of amyloid structures. Fibril formation was confirmed by TEM (Fig. 217B).

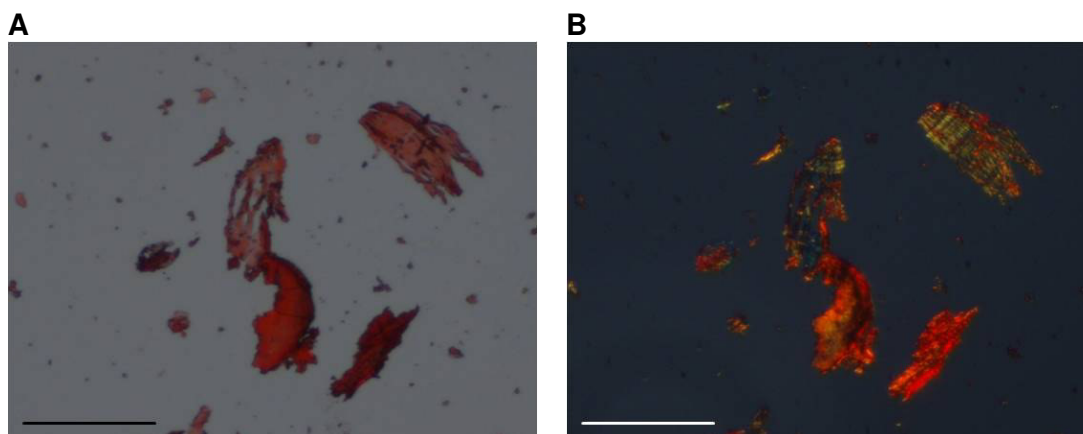


Fig. 218: Microscopic examination of an aged incubation of H-NKGAI-Adc-NFGAILS-OH stained with Congo Red. The peptide was incubated at a concentration of 1 mM in 1xb 1% HFiP, pH 7.4 for 3 days. Pictures were taken under A normal and B cross-polarized light. Scale bar: 100 μm .

3.2.2.8 H-NKGAI-GGG-NFGAILS-OH (H16)

The CD spectra of H-NKGAI-GGG-NFGAILS-OH (Fig. 219A) showed a strong minimum at 195 - 200 nm that was due to random coil structure. The weaker negative signal between 210 nm and 230 nm indicated the presence of additional structural elements like β -sheet and β -turn. Already at a peptide concentration of 10 μM , the signal intensity was slightly reduced. For the spectrum at 10 μM this reduction mainly occurred in the random coil signal. At higher concentrations, also the signal between 210 nm and 230 nm was losing its intensity. At a concentration of 100 μM , there was almost no signal left the solution was however clear. This indicated the formation of soluble oligomers of H-NKGAI-GGG-NFGAILS-OH.

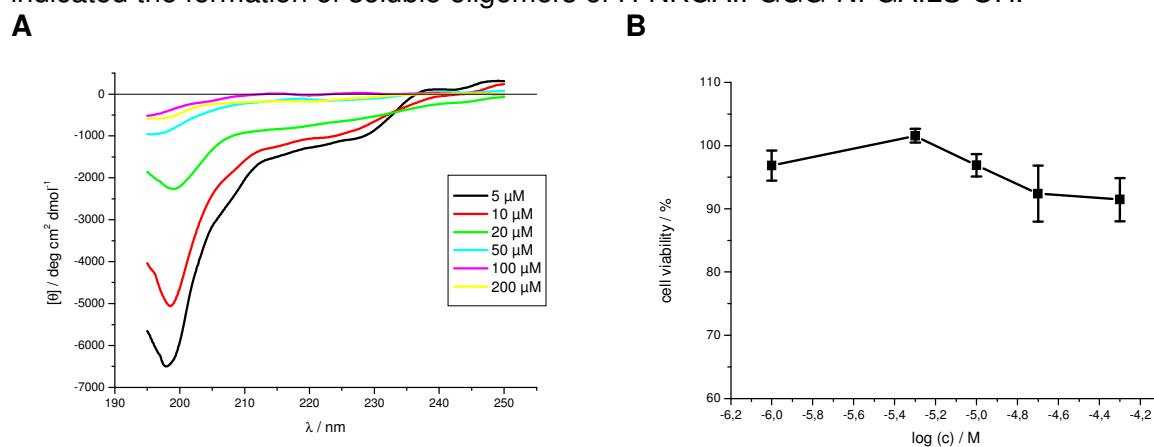


Fig. 219: (A) Far-UV CD spectra of H-NKGAI-GGG-NFGAILS-OH at different concentrations in 1xb 1% HFiP, pH 7.4.

(B) Cell viability assay of an aged solution of H-NKGAI-GGG-NFGAILS-OH (5 mM in 1xb 1% HFiP, pH 7.4 for 4 days) using PC-12 cells. Data are percentages of control and are the mean (+/-SEM) of three independent experiments with each experiment performed in multiple replicates ($n = 3$).

H-NKGAI-GGG-NFGAILS-OH was only weakly toxic to PC-12 cells (Fig. 219B).

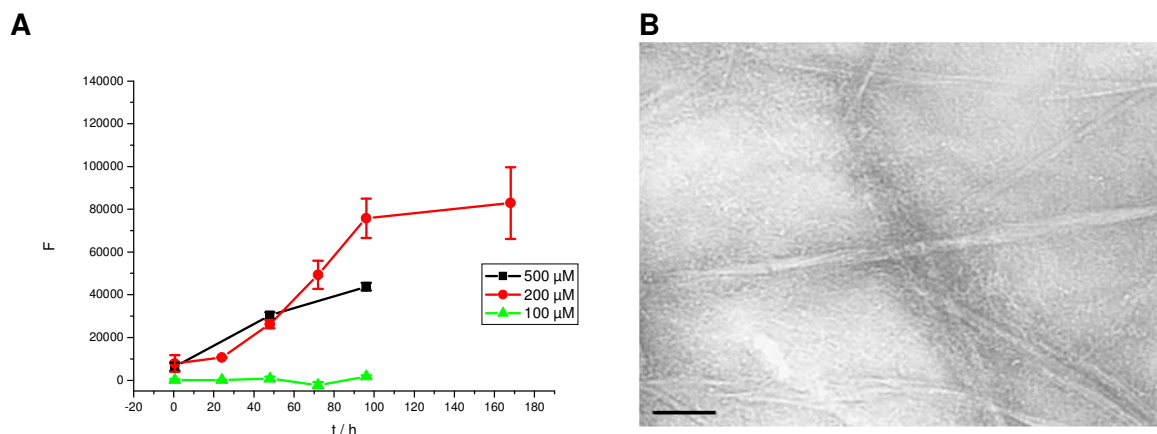


Fig. 220: (A) ThT binding assays of H-NKGAIL-GGG-NFGAILS-OH at different concentrations in 1xb 1% HFIP, pH 7.4. Data are means of 3 assays after subtraction of buffer values +/- standard error of the mean (SEM) with each experiment performed in multiple replicates (n = 3).

(B) TEM picture of an aged incubation of H-NKGAIL-GGG-NFGAILS-OH. The peptide was incubated at 200 μM for 7 d in 1xb 1% HFIP, pH 7.4. Scale bar: 100 nm.

The fibril forming potential of H-NKGAIL-GGG-NFGAILS-OH (Fig. 220A) was lower than for H-NKGAIL-Aoc-NFGAILS-OH (Fig. 208A). At a concentration of 100 μM there was no ThT binding up to incubation time points of 5 days. Strong and intense fibril formation was only seen up to a peptide concentration of 200 μM . Also only at a concentration of 200 μM , fibrils were visible on the TEM picture (Fig. 220B).

Congo Red staining of an aged solution of H-NKGAIL-GGG-NFGAILS-OH (Fig. 221A and B) showed weak red color under normal light and green birefringence under cross-polarized light indicating the formation of amyloid structures.

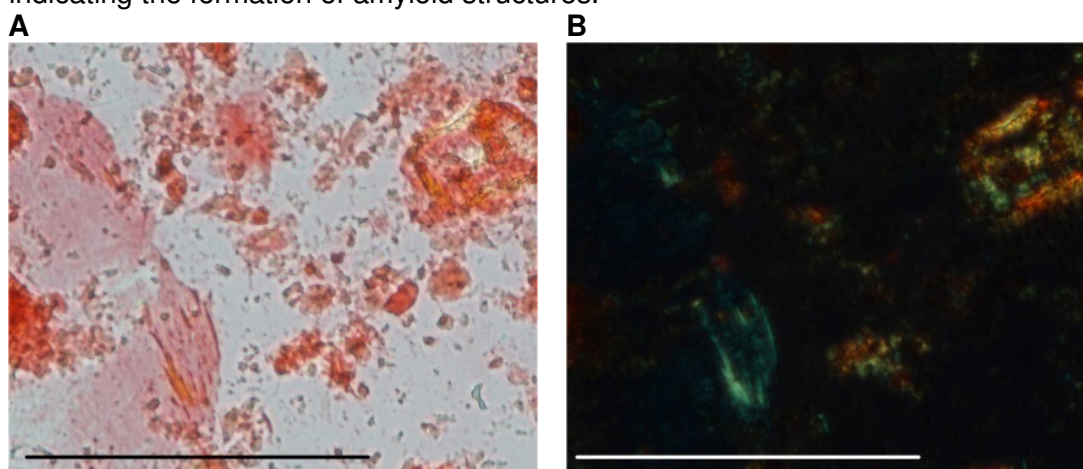


Fig. 221: Microscopic examination of an aged incubation of H-NKGAIL-GGG-NFGAILS-OH stained with Congo Red. The peptide was incubated at a concentration of 1 mM in 1xb 1% HFIP, pH 7.4 for 3 days. Pictures were taken under A normal and B cross-polarized light. Scale bar: 100 μm .

3.2.2.9 H-NKGAIL-AAA-NFGAILS-OH (H18)

H-NKGAIL-AAA-NFGAILS-OH exhibited both random coil and β -sheet structure as indicated by CD spectroscopy (Fig. 222A). Compared to H-NKGAIL-GGG-NFGAILS-OH (Fig. 219A) the intensity of the negative bulge from 210-230 nm was similar, whereas the intensity of the random coil signal at 195 nm was much weaker in the case of H-NKGAIL-AAA-NFGAILS-OH.

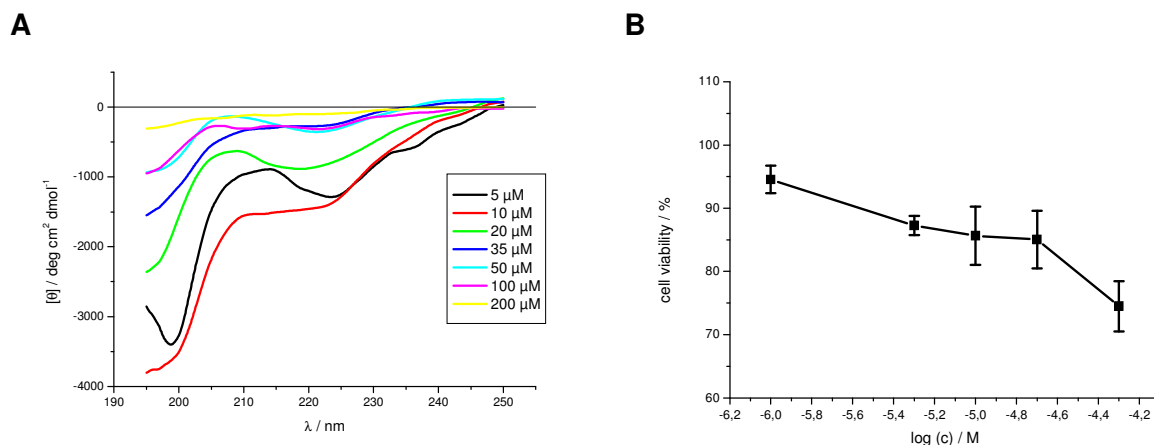


Fig. 222: (A) Far-UV CD spectra of H-NKGAI-AAA-NFGAILS-OH at different concentrations in 1x 1% HFIP, pH 7.4.

(B) Cell viability assay of an aged solution of H-NKGAI-AAA-NFGAILS-OH (5 mM in 1x 1% HFIP, pH 7.4 for 4 days) using PC-12 cells. Data are percentages of control and are the mean (+/-SEM) of three independent experiments with each experiment performed in multiple replicates (n = 3).

H-NKGAI-AAA-NFGAILS-OH was found to be clearly toxic to PC-12 (Fig. 222B) more than H-NKGAI-GGG-NFGAILS-OH (Fig. 219B).

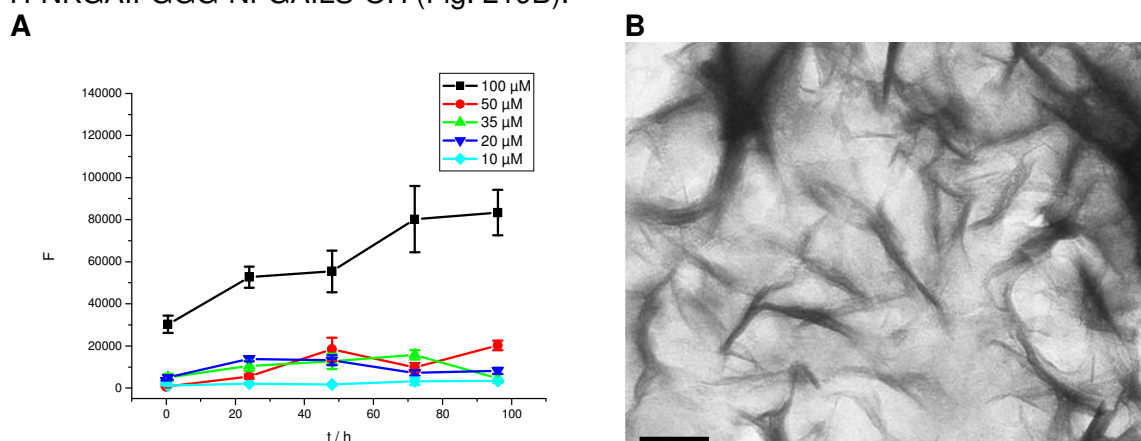


Fig. 223: (A) ThT binding assays of H-NKGAI-AAA-NFGAILS-OH at different concentrations in 1x 1% HFIP, pH 7.4. Data are means of 3 assays after subtraction of buffer values +/- standard error of the mean (SEM) with each experiment performed in multiple replicates (n = 3).

(B) TEM picture of an aged incubation of H-NKGAI-AAA-NFGAILS-OH. The peptide was incubated at 50 μM for 7 d in 1x 1% HFIP, pH 7.4. Scale bar: 100 nm.

In addition, compared to H-NKGAI-GGG-NFGAILS-OH (Fig. 220A), H-NKGAI-AAA-NFGAILS-OH formed fibrils easier (Fig. 223A). Already at a concentration of 20 μM, H-NKGAI-AAA-NFGAILS-OH exhibited a weak increase in the fluorescence signal of ThT. A clear and strong fibril formation was detected at a concentration of 100 μM.

Staining of fibrillar aggregates of H-NKGAI-AAA-NFGAILS-OH with Congo Red was consistent with the presence of amyloid fibrils. Stained aggregates showed intense red color under normal light (Fig. 224A). However, no green/yellow birefringence under cross-polarized light was observed.

TEM imaging of an aged incubation of H-NKGAI-AAA-NFGAILS-OH at a peptide concentration of 50 μM displayed many fibrils that were partially clumped together (Fig. 223B).

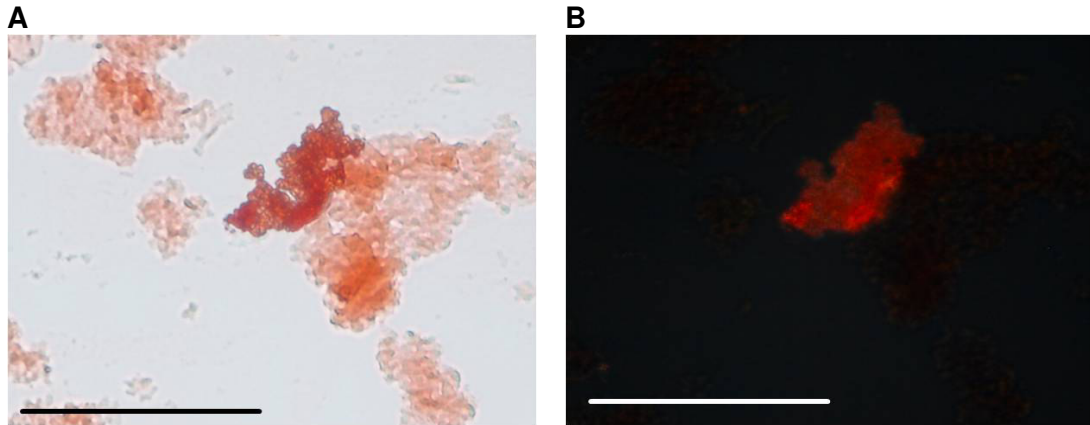


Fig. 224: Microscopic examination of an aged incubation of H-NKGAI-AAA-NFGAILS-OH stained with Congo Red. The peptide was incubated at a concentration of 1 mM in 1xb 1% HFiP, pH 7.4 for 3 days. Pictures were taken under A normal and B cross-polarized light. Scale bar: 100 µm.

3.2.2.10 H-NKGAI-LLL-NFGAILS-OH (H12)

Similar to the other peptides with hydrophobic connecting elements, H-NKGAI-LLL-NFGAILS-OH exhibited β -sheet structure in far-UV CD experiments (Fig. 225A). Compared to the CD spectrum of H-NKGAI-Aoc-NFGAILS-OH (Fig. 207A), the magnitude of the β -sheet signal of the CD spectrum of H-NKGAI-LLL-NFGAILS-OH was weaker and slightly shifted towards higher wavelengths. This shift in the spectra of H-NKGAI-LLL-NFGAILS-OH increased with higher peptide concentrations indicating together with the observed loss of CD signal a stabilization of β -turn elements upon aggregation.

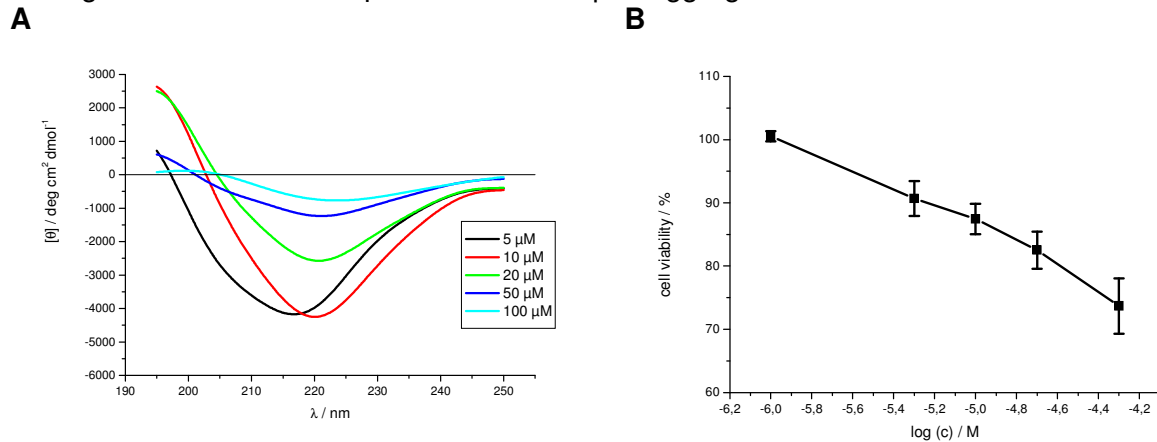


Fig. 225: (A) Far-UV CD spectra of H-NKGAI-LLL-NFGAILS-OH at different concentrations in 1xb 1% HFiP, pH 7.4 (from [159]).

(B) Cell viability assay of an aged solution of H-NKGAI-LLL-NFGAILS-OH (5 mM in 1xb 1% HFiP, pH 7.4 for 4 days) using PC-12 cells. Data are percentages of control and are the mean (+/-SEM) of three independent experiments with each experiment performed in multiple replicates (n = 3).

As shown in Fig. 225B, H-NKGAI-LLL-NFGAILS-OH was toxic to PC-12 cells.

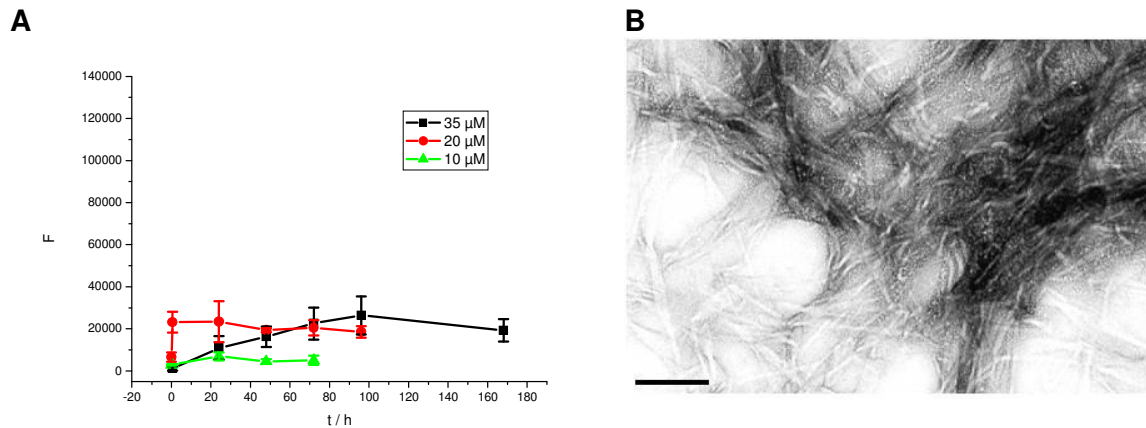


Fig 226: (A) ThT binding assays of H-NKGAI-LLL-NFGA-ILS-OH at different concentrations in 1xb 1% HFIP, pH 7.4 (partially from [159]). Data are means of 3 assays after subtraction of buffer values \pm standard error of the mean (SEM) with each experiment performed in multiple replicates ($n = 3$). (B) TEM picture of an aged incubation of H-NKGAI-LLL-NFGA-ILS-OH. The peptide was incubated at 50 μ M for 7 d in 1xb 1% HFIP, pH 7.4. Scale bar: 100 nm.

ThT assays of H-NKGAI-LLL-NFGA-ILS-OH at different peptide concentrations showed that it started forming fibrils already at 20 μ M (Fig. 226A). Congo Red staining of aged H-NKGAI-LLL-NFGA-ILS-OH (Fig. 227A and B) showed weak green/yellow birefringence under polarized light related to amyloid structures. Fig. 33B shows the TEM image of an aged incubation of H-NKGAI-LLL-NFGA-ILS-OH at a concentration of 50 μ M bundles of fibrils are clearly visible.

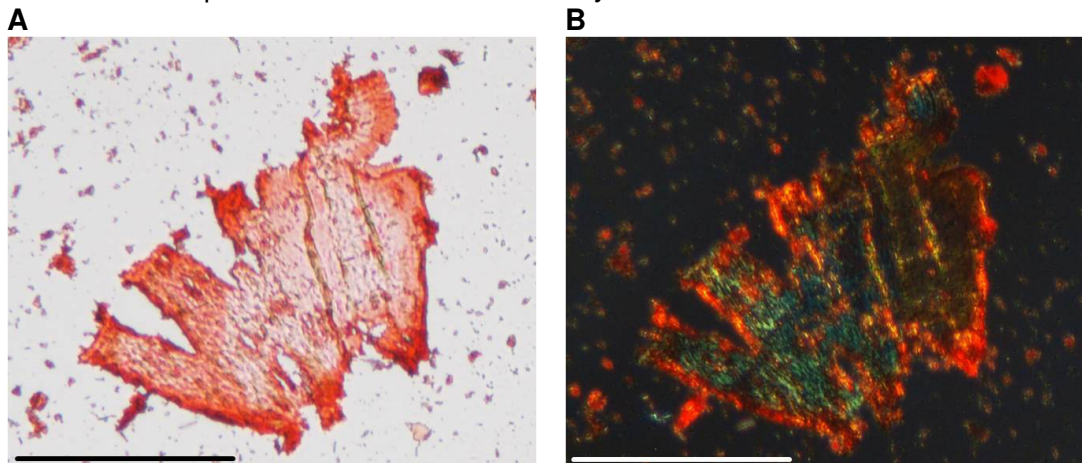


Fig. 227: Microscopic examination of an aged incubation of H-NKGAI-LLL-NFGA-ILS-OH stained with Congo Red. The peptide was incubated at a concentration of 1 mM in 1xb 1% HFIP, pH 7.4 for 3 days. Pictures were taken under A normal and B cross-polarized light (from [159]). Scale bar: 100 μ m.

3.2.2.11 H-KKK- β A-NKGAI-LLL-NFGA-ILS- β A-KKK-OH (H12K6)

Similar to H-NKGAI-Aoc-NFGA-ILS-OH it was intended to improve the solubility of H-NKGAI-LLL-NFGA-ILS-OH by adding C- and N-terminal lysine residues.

Concentration dependent CD spectra of H-KKK- β A-NKGAI-LLL-NFGA-ILS- β A-KKK-OH revealed an intense β -sheet structure.

Contrary to the observations on inducing KKK-stretches in H-NKGAI-Aoc-NFGA-ILS-OH (chapter 3.2.2.5 and 3.2.2.6) the addition lysines did not lead to a loss of the β -sheet structure in the case for H-NKGAI-LLL-NFGA-ILS-OH (Fig. 228A). The hydrophobic connecting element LLL seems thus to be a much more efficient inducer of β -sheet structure than Aoc. At concentrations of 5 and 10 μ M the CD spectra of H-KKK- β A-NKGAI-LLL-

NFGAILS- β A-KKK-OH displayed almost identical shapes and magnitudes. This indicates that the peptide starts aggregating at concentrations higher than 10 μ M.

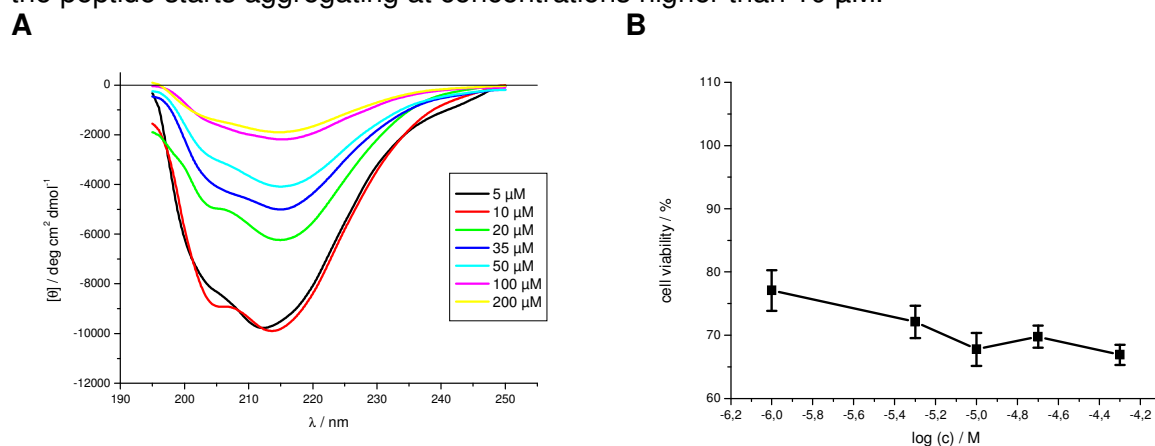


Fig. 228: A) Far-UV CD spectra of H-KKK- β A-NKGAI-LLL-NFGAILS- β A-KKK-OH at different concentrations in 1x1% HFiP, pH 7.4.

B) Cell viability assay of an aged solution of H-KKK- β A-NKGAI-LLL-NFGAILS- β A-KKK-OH (5 mM in 1x1% HFiP, pH 7.4 for 4 days) using PC-12 cells. Data are percentages of control and are the mean (+/-SEM) of three independent experiments with each experiment performed in multiple replicates (n = 3).

Aggregates of H-KKK- β A-NKGAI-LLL-NFGAILS- β A-KKK-OH were also found to be very toxic to PC-12 cells (Fig. 228B).

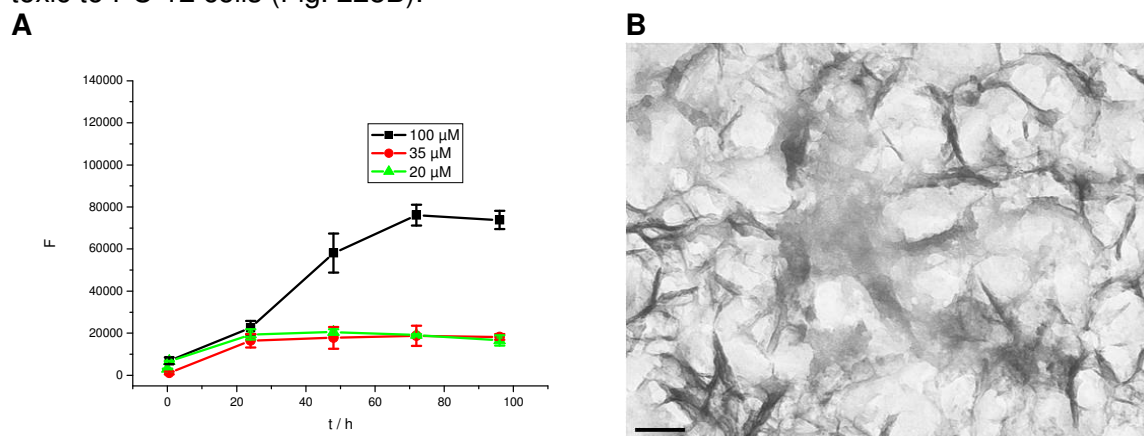


Fig. 229: (A) ThT binding assays of H-KKK- β A-NKGAI-LLL-NFGAILS- β A-KKK-OH at different concentrations in 1x1% HFiP, pH 7.4. Data are means of 3 assays after subtraction of buffer values +/- standard error of the mean (SEM) with each experiment performed in multiple replicates (n = 3).

(B) TEM picture of an aged incubation of H-KKK- β A-NKGAI-LLL-NFGAILS- β A-KKK-OH. The peptide was incubated at 35 μ M for 7 d in 1x1% HFiP, pH 7.4. Scale bar: 100 nm.

The fibril forming potential of H-KKK- β A-NKGAI-LLL-NFGAILS- β A-KKK-OH (Fig. 229A), was similar to that of H-NKGAI-LLL-NFGAILS-OH (Fig. 226A). In fact, ThT assays of H-KKK- β A-NKGAI-LLL-NFGAILS- β A-KKK-OH showed an increase in the fluorescence signal of ThT already at a peptide concentration of 20 μ M.

Aggregates of H-KKK- β A-NKGAI-LLL-NFGAILS- β A-KKK-OH stained with Congo Red revealed intense red color under normal light (Fig. 230A) and displayed red and green birefringence under cross-polarized light (Fig. 230B).

TEM imaging of an aged incubation of H-KKK- β A-NKGAI-LLL-NFGAILS- β A-KKK-OH at a peptide concentration of 35 μ M displayed many short fibrils (Fig. 229B).

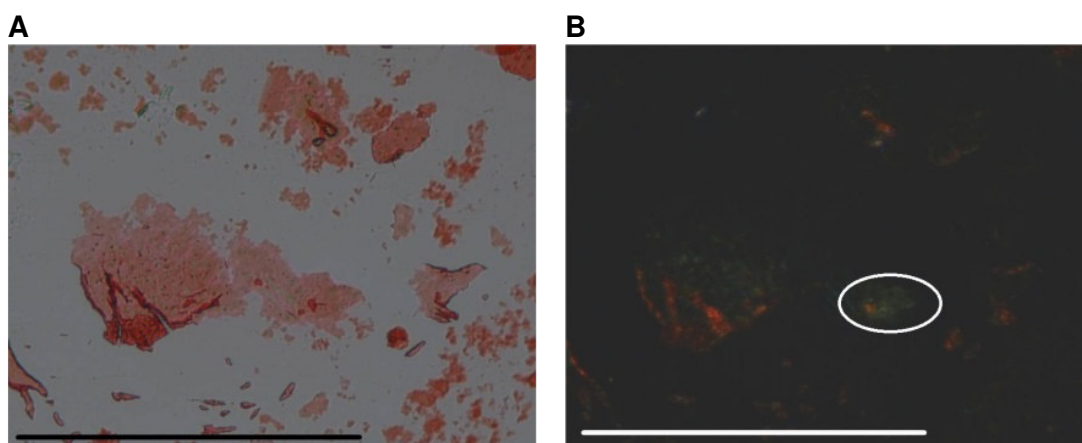


Fig. 230: Microscopic examination of an aged incubation of H-KKK- β A-NKGAI-LLL-NFGAILS- β A-KKK-OH stained with Congo Red. The peptide was incubated at a concentration of 1 mM in 1x 1% HFIP, pH 7.4 for 3 days. Pictures were taken under A normal and B cross-polarized light. Scale bar: 100 μ m.

3.2.2.12 H-NKGAI-KKK-NFGAILS-OH (H13)

The CD spectra of H-NKGAI-KKK-NFGAILS-OH (Fig. 231A) displayed mainly a negative signal at 195 nm indicating random coil structure. A small negative bulge at 210-230 nm indicated the presence of additional structural elements, likely β -sheets and β -turns. The peptide started to aggregate at concentrations higher than 10 μ M.

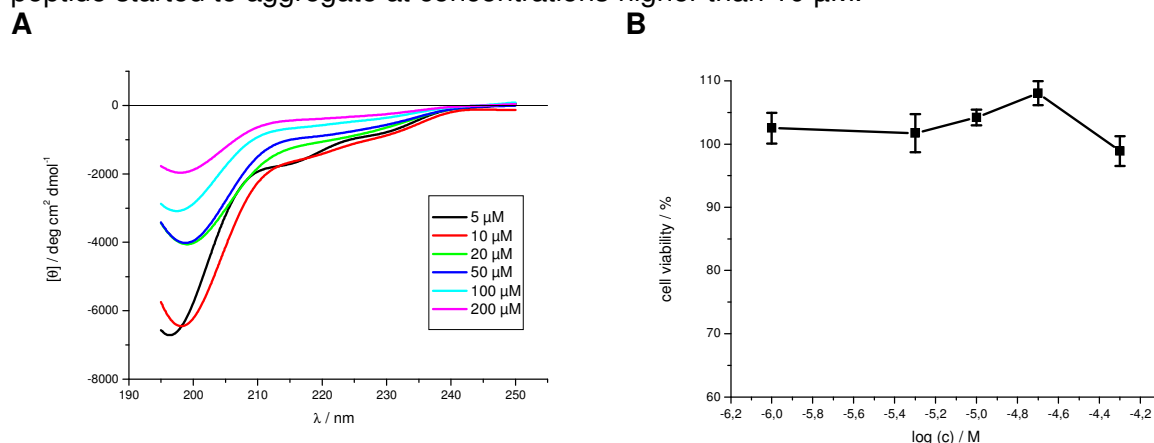


Fig. 231: (A) Far-UV CD spectra of H-NKGAI-KKK-NFGAILS-OH at different concentrations in 1x 1% HFIP, pH 7.4 (from [159]).

(B) Cell viability assay of an aged solution of H-NKGAI-KKK-NFGAILS-OH (5 mM in 1x 1% HFIP, pH 7.4 for 4 days) using PC-12 cells. Data are percentages of control and are the mean (+/-SEM) of three independent experiments with each experiment performed in multiple replicates (n = 3).

Aged solutions of H-NKGAI-KKK-NFGAILS-OH displayed no toxicity towards PC-12 cells under the conditions tested (Fig. 231B) while no fibril formation was observed up to a peptide concentration of 1 mM (Fig. 232A).

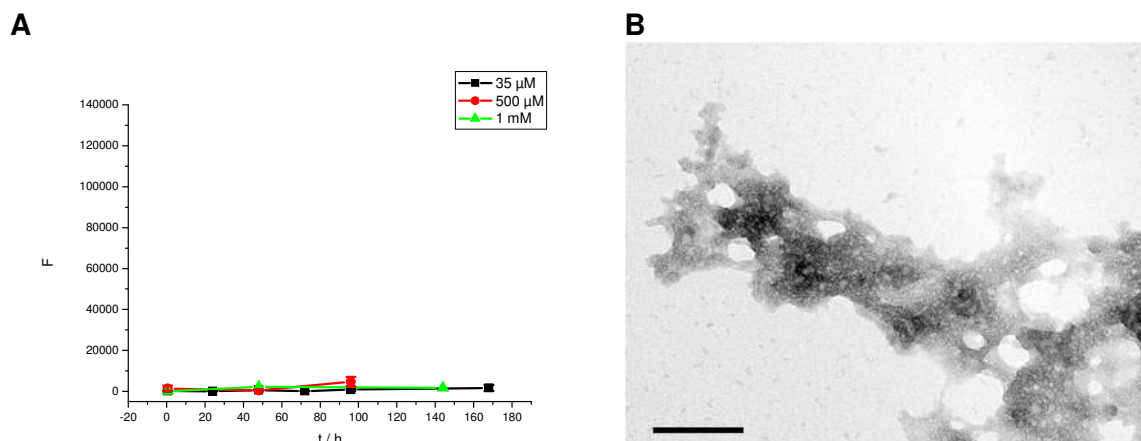


Fig. 232: (A) ThT binding assays of H-NKGAI-KKK-NFGAILS-OH at different concentrations in 1xb 1% HFIP, pH 7.4 (partially from [159]). Data are means of 3 assays after subtraction of buffer values +/- standard error of the mean (SEM) with each experiment performed in multiple replicates (n = 3). (B) TEM picture of an aged incubation of H-NKGAI-KKK-NFGAILS-OH. The peptide was incubated at 5 mM for 7 d in 1xb 1% HFIP, pH 7.4. Scale bar: 100 nm.

The following staining of aggregates of H-NKGAI-KKK-NFGAILS-OH with Congo Red showed red color under normal light but no birefringence under cross-polarized light (Fig. 233A and B).

TEM imaging of an aged incubation of H-NKGAI-KKK-NFGAILS-OH at a concentration of 5 mM, which reflected the conditions used for cell viability assays, also did not reveal fibril formation (Fig. 232B).

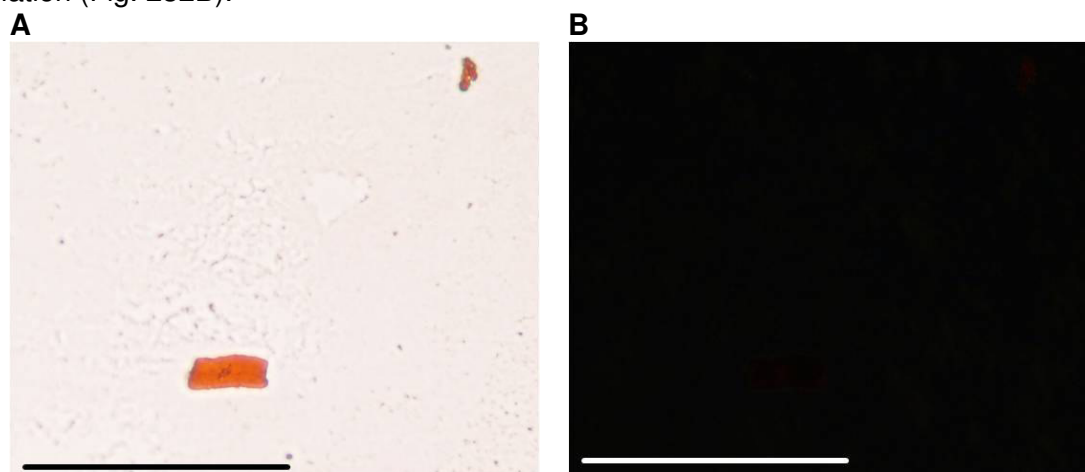


Fig. 233: Microscopic examination of an aged incubation of H-NKGAI-KKK-NFGAILS-OH stained with Congo Red. The peptide was incubated at a concentration of 1 mM in 1xb 1% HFIP, pH 7.4 for 3 days. Pictures were taken under A normal and B cross-polarized light (from [159]). Scale bar: 100 μm.

3.2.2.13 H-NKGAI-K(Ac)K(Ac)K(Ac)-NFGAILS-OH (H20)

Similar to the spectra of H-NKGAI-KKK-NFGAILS-OH (Fig. 231A) the CD spectra of H-NKGAI-K(Ac)K(Ac)K(Ac)-NFGAILS-OH (Fig. 234A) displayed a strong negative signal at 195 nm indicating random coil structure. However, the negative bulge at 210-230 nm, indicating the presence of β -sheet and β -turn elements, was much more intense for H-NKGAI-K(Ac)K(Ac)K(Ac)-NFGAILS-OH. The aggregation of H-NKGAI-K(Ac)K(Ac)K(Ac)-NFGAILS-OH went along with a loss of CD signal. This signal loss was more intense within the random coil region. At a peptide concentration of 100 and 200 μM, the CD spectra

displayed additionally to the random coil signal at 195 nm a clear minimum at 220 nm (Fig. 235). This might be an indication for the formation of β -turns during aggregation.

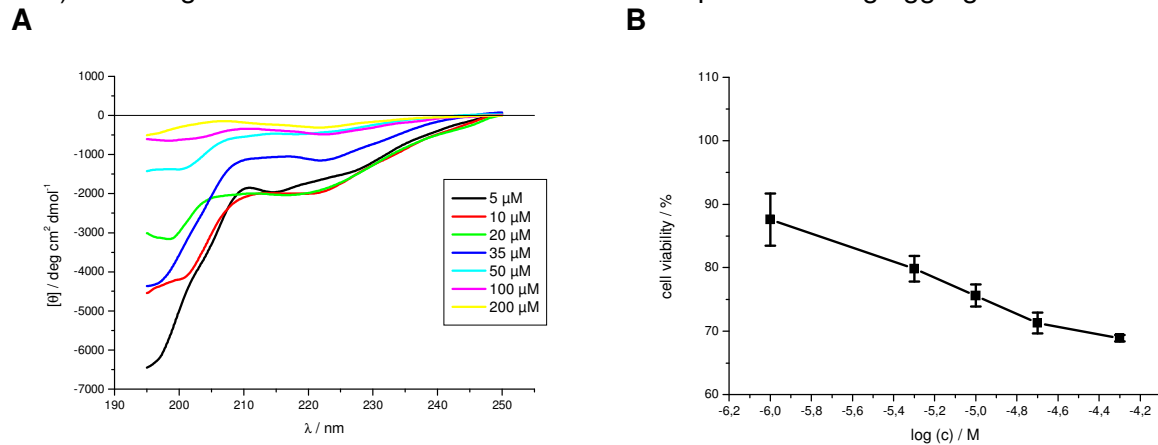


Fig. 234: A) Far-UV CD spectra of H-NKGAI-K(Ac)K(Ac)K(Ac)-NFGAILS-OH at different concentrations in 1x 1% HFIP, pH 7.4.

B) Cell viability assay of an aged solution of H-NKGAI-K(Ac)K(Ac)K(Ac)-NFGAILS-OH (5 mM in 1x 1% HFIP, pH 7.4 for 4 days) using PC-12 cells. Data are percentages of control and are the mean (+/-SEM) of three independent experiments with each experiment performed in multiple replicates (n = 3).

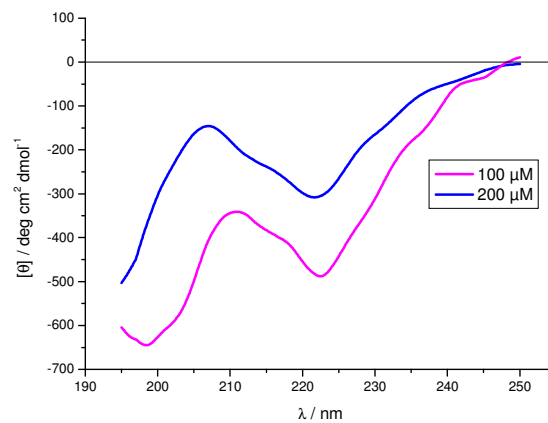


Fig. 235: Far-UV CD spectra of H-NKGAI-K(Ac)K(Ac)K(Ac)-NFGAILS-OH at a peptide concentration of 100 μ M and 200 μ M.

Among the peptides with the sequence H-NKGAI-XXX-NFGAILS-OH, H-NKGAI-K(Ac)K(Ac)K(Ac)-NFGAILS-OH was the most toxic one (Fig. 234B).

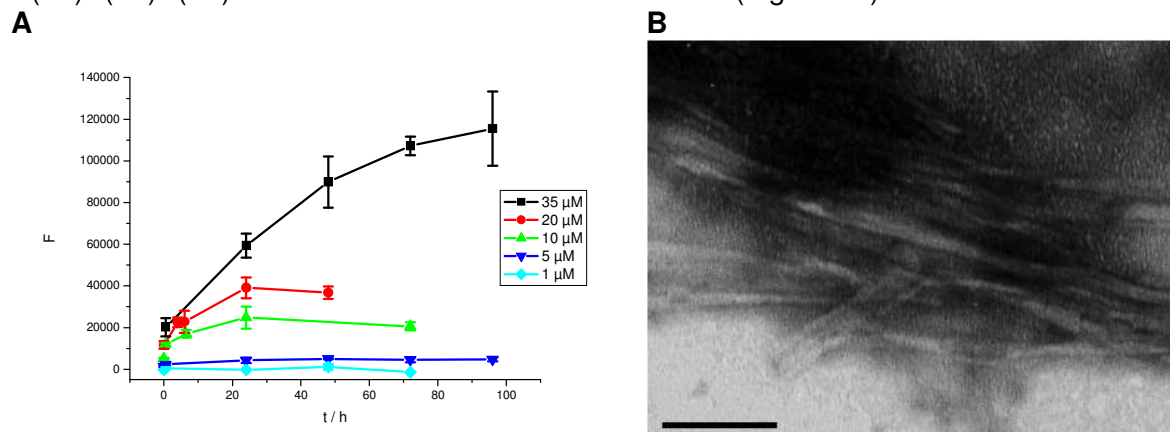


Fig. 236: (A) ThT binding assays of H-NKGAI-K(Ac)K(Ac)K(Ac)-NFGAILS-OH at different concentrations in 1xb 1% HFiP, pH 7.4. Data are means of 3 assays after subtraction of buffer values +/- standard error of the mean (SEM) with each experiment performed in multiple replicates (n = 3). (B) TEM picture of an aged incubation of H-NKGAI-K(Ac)K(Ac)K(Ac)-NFGAILS-OH. The peptide was incubated at 35 μ M for 7 d in 1xb 1% HFiP, pH 7.4. Scale bar: 100 nm.

In addition, it formed fibrils extremely fast (Fig. 236A). Indeed, fibril formation was observed already at a peptide concentration of 5 μ M. Congo Red stained aggregates of H-NKGAI-K(Ac)K(Ac)K(Ac)-NFGAILS-OH (Fig. 237A and B) showed weak green/yellow birefringence under cross-polarized light related to amyloid structures.

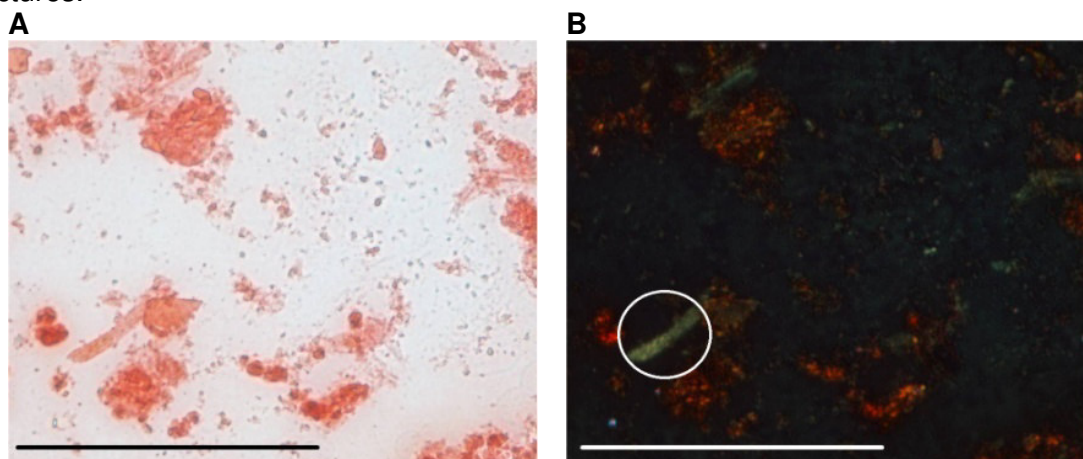


Fig. 237: Microscopic examination of an aged incubation of H-NKGAI-K(Ac)K(Ac)K(Ac)-NFGAILS-OH stained with Congo Red. The peptide was incubated at a concentration of 1 mM in 1xb 1% HFiP, pH 7.4 for 3 days. Pictures were taken under A normal and B cross-polarized light. Scale bar: 100 μ m.

3.2.2.14 H-NKGAI-EEE-NFGAILS-OH (H22)

Concentration dependent CD spectra of H-NKGAI-EEE-NFGAILS-OH (Fig. 238A) showed a strong minimum at 195 nm related to random coil structure. From all the peptides of this group, H-NKGAI-EEE-NFGAILS-OH displayed the most intense random coil signal. There was also a clear negative signal between 210 and 230 nm.

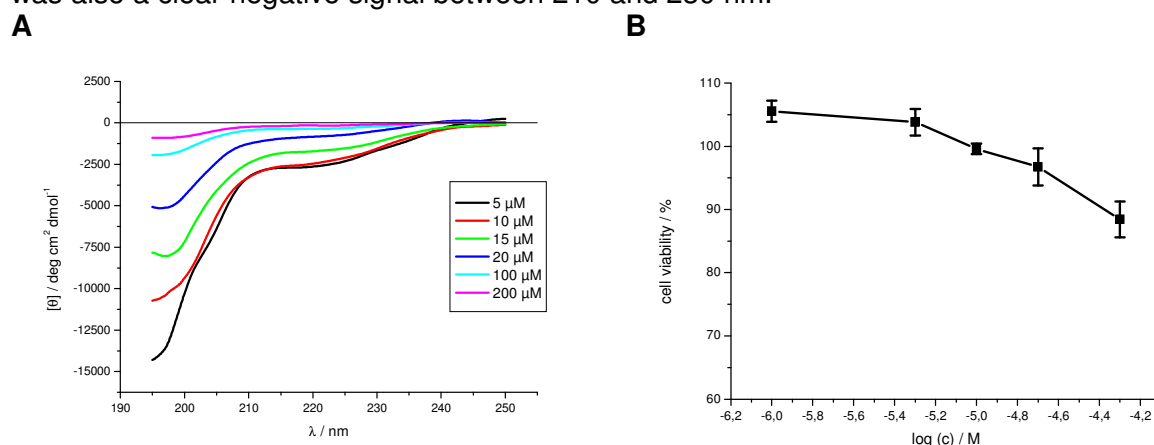


Fig. 238: (A) Far-UV CD spectra of H-NKGAI-EEE-NFGAILS-OH at different concentrations in 1xb 1% HFiP, pH 7.4.

(B) Cell viability assay of an aged solution of H-NKGAI-EEE-NFGAILS-OH (5 mM in 1xb 1% HFiP, pH 7.4 for 4 days) using PC-12 cells. Data are percentages of control and are the mean (+/-SEM) of three independent experiments with each experiment performed in multiple replicates (n = 3).

Notably, aggregates of H-NKGAI-EEE-NFGAILS-OH were only weakly toxic to PC-12 cells (Fig. 238B).

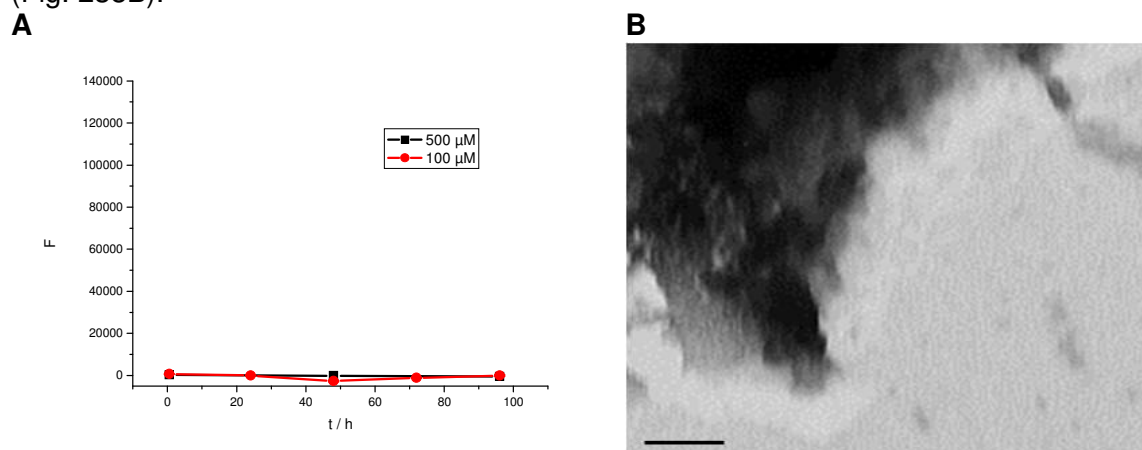


Fig. 239: (A) ThT binding assays of H-NKGAI-EEE-NFGAILS-OH at different concentrations in 1xb 1% HFIP, pH 7.4. Data are means of 3 assays after subtraction of buffer values \pm standard error of the mean (SEM) with each experiment performed in multiple replicates ($n = 3$).

(B) TEM picture of an aged incubation of H-NKGAI-EEE-NFGAILS-OH. The peptide was incubated at 500 μ M for 7 d in 1xb 1% HFIP, pH 7.4. Scale bar: 100 nm.

ThT binding studies of H-NKGAI-EEE-NFGAILS-OH showed no fibril formation at peptide concentrations up to 500 μ M within 96 h (Fig. 239A) which was verified by TEM. The TEM picture of an incubation of H-NKGAI-EEE-NFGAILS-OH at a concentration of 500 μ M also just showed amorphous aggregates but no fibrils (Fig. 239B).

Staining of an aged solution of H-NKGAI-EEE-NFGAILS-OH with Congo Red displayed small aggregates that were very weakly stained with Congo Red as indicated by a red color visible under normal light (Fig. 240A) and exhibited no birefringence under cross-polarized light (Fig. 240B).

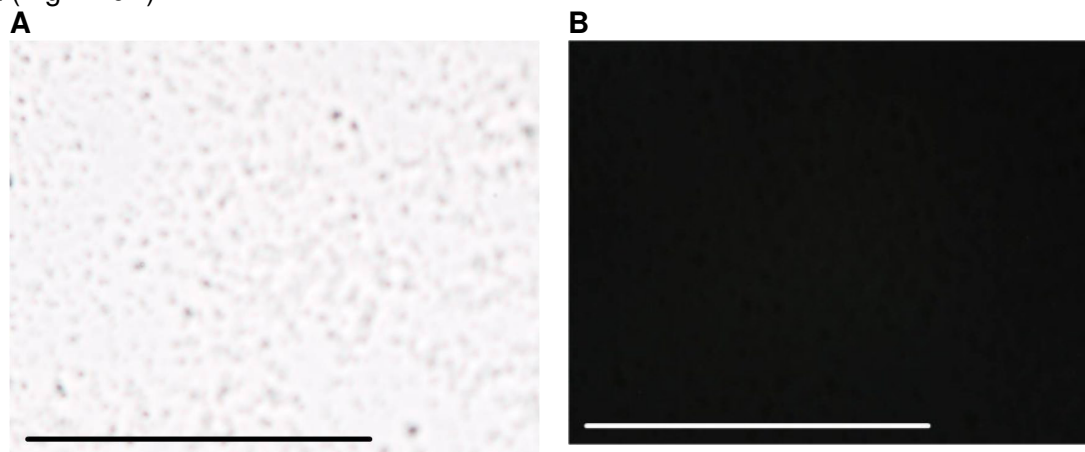


Fig. 240: Microscopic examination of an aged incubation of H-NKGAI-EEE-NFGAILS-OH stained with Congo Red. The peptide was incubated at a concentration of 1 mM in 1xb 1% HFIP, pH 7.4 for 3 days. Pictures were taken under A normal and B cross-polarized light. Scale bar: 100 μ m.

Table 19: Overview of ThT binding assays and cell viability assays performed with peptides containing the sequence H-NKGAI-XXX-NFGAILS-OH at different concentrations.

Results of “+” indicate fibril formation, whereas “-“ indicate no fibril formation within the 5 days of incubation of the solution at the given peptide concentration.

For the cell viability assays, results of “+++” mean high toxicity towards PC-12 cell, “++” means medium toxicity and “+/-” means low to no toxicity. Low toxicity refers to peptides with >90% cell viability, medium toxicity refers to a cell viability between 80% and 90%, and high toxicity refers to a cell viability of <80% for aged incubations at a peptide concentration of 50 μ M.

Abbrev.	Sequence	ThT											Tox.	
		1 μ M	5 μ M	10 μ M	20 μ M	35 μ M	50 μ M	100 μ M	200 μ M	350 μ M	500 μ M	1 mM		
H5	H-NKGAI-Peg-NFGAILS-OH					-	-					+		++
H5a	H-NKGAI-Aoc-NFGAILS-OH		-	+	+	+	+							++
H5aK3	H-NKGAI-Aoc-NFGAILS- β A-KKK-OH					-	+	+						
H5aK6	H-KKK- β A-NKGAI-Aoc-NFGAILS- β A-KKK-OH							-	+	+	+			++
H5b	H-NKGAI-Aoc-NFGAILS-OH			+		+		+						++
H16	H-NKGAI-GGG-NFGAILS-OH							-	+			+		+/-
H18	H-NKGAI-AAA-NFGAILS-OH			-	+	+	+	+						+++
H12	H-NKGAI-LLL-NFGAILS-OH			-	+	+								+++
H12K6	H-KKK- β A-NKGAI-LLL-NFGAILS- β A-KKK-OH				+	+		+						+++
H13	H-NKGAI-KKK-NFGAILS-OH					-						-	-	+/-
H20	H-NKGAI-K(Ac)K(Ac)K(Ac)-NFGAILS-OH	-	+	+	+	+								+++
H22	H-NKGAI-EEE-NFGAILS-OH							-				-		+/-

3.2.3 Peptides containing the segments A β (32-27) and IAPP(22-28)

NKGAI is forming steric zippers with both *face-to-face* and *back-to-back* orientation. In order to test these findings, peptides containing this sequence in an inverted order were also synthesized and studied.

3.2.3.1 A β (32-27) or H-IIAGKN-OH

The CD spectra of H-IIAGKN-OH (Fig. 241A) showed both a minimum at 200 nm related to random coil structure but also a negative signal at 215-220 nm that could be related to β -sheet structure, similar to those of H-NKGAI-OH (Fig. 201A). The signal intensity was however much lower for H-IIAGKN-OH compared to H-NKGAI-OH illustrating less structural integrity for H-IIAGKN-OH.

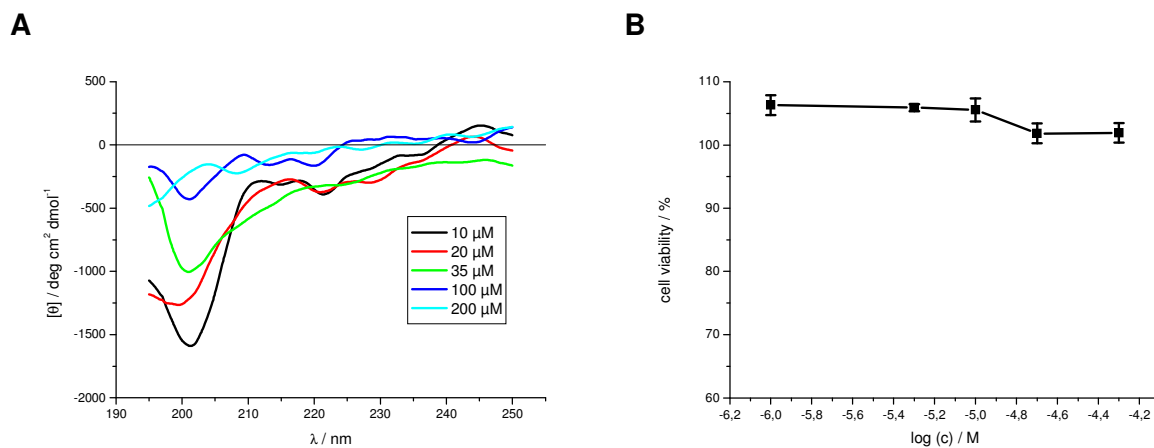


Fig. 241: (A) Far-UV CD spectra of H-IIAGKN-OH at different concentrations in 1x 1% HFIP, pH 7.4. (B) Cell viability assay of an aged solution of H-IIAGKN-OH (5 mM in 1x 1% HFIP, pH 7.4 for 4 days) using PC-12 cells. Data are percentages of control and are the mean (+/-SEM) of three independent experiments with each experiment performed in multiple replicates (n = 3).

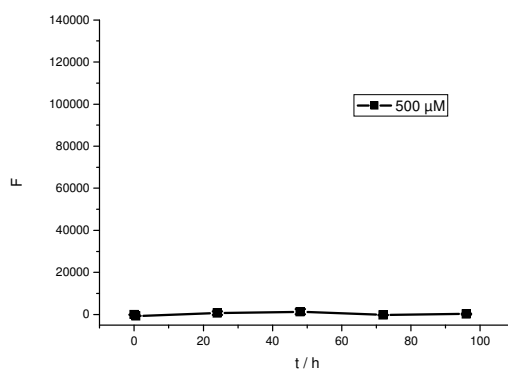


Fig. 242: ThT binding assay of H-IIAGKN-OH at a peptide concentration of 500 μM in 1x 1% HFIP, pH 7.4. Data are means of 3 assays after subtraction of buffer values +/- standard error of the mean (SEM) with each experiment performed in multiple replicates (n = 3).

H-IIAGKN-OH did not display toxicity to PC-12 cells under the conditions tested (Fig. 241B) and did not form fibrils up to a concentration of 500 μM as assessed by the ThT assay (Fig. 242) and Congo Red staining (Fig. 243A and B).

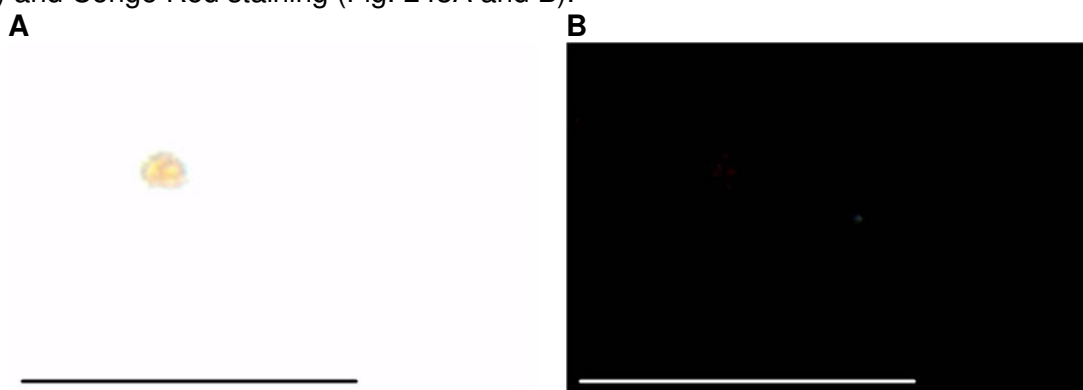


Fig. 243: Microscopic examination of an aged incubation of H-IIAGKN-OH stained with Congo Red. The peptide was incubated at a concentration of 1 mM in 1x 1% HFIP, pH 7.4 for 3 days. Pictures were taken under A normal and B cross-polarized light. Scale bar: 100 μm.

3.2.3.2 H-IIAGKN-Peg-NFGAILS-OH (H6)

The concentration dependent CD spectra of H-IIAGKN-Peg-NFGAILS-OH (Fig. 244A) showed a minimum at 195 - 200 nm that is related to random coil structure. The weaker negative signal between 210 nm and 230 nm intended the presence of additional structural elements like β -sheets and β -turns. H-NKGAI-Peg-NFGAILS-OH expressed a weak aggregation potential as indicative by a weak reduction of the CD signal at 195 nm upon increasing concentrations.

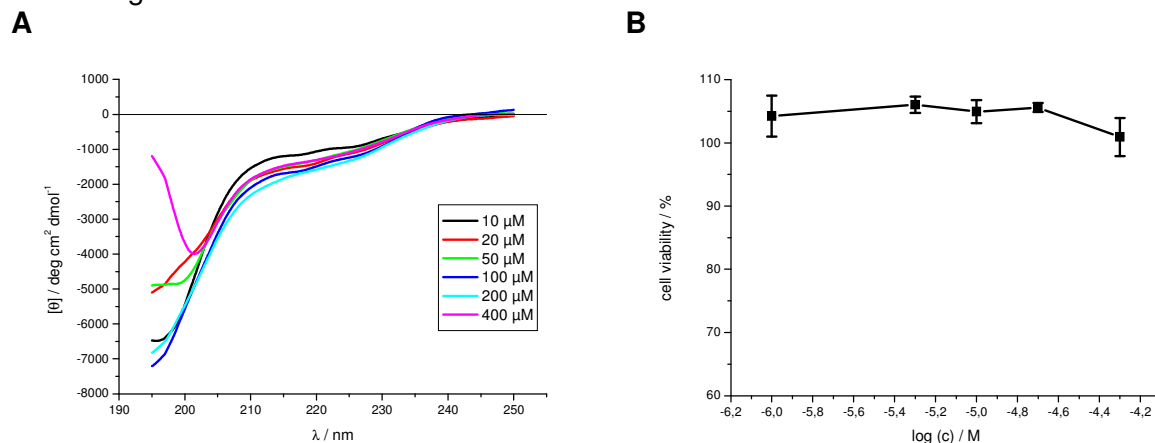


Fig. 244: A) Far-UV CD spectra of H-IIAGKN-Peg-NFGAILS-OH at different concentrations in 1x 1% HFIP, pH 7.4.

B) Cell viability assay of an aged solution of H-IIAGKN-Peg-NFGAILS-OH (5 mM in 1x 1% HFIP, pH 7.4 for 4 days) using PC-12 cells. Data are percentages of control and are the mean (+/-SEM) of three independent experiments with each experiment performed in multiple replicates (n = 3).

The MTT reduction assay showed that H-IIAGKN-Peg-NFGAILS-OH was non-toxic to PC-12 cells (Fig. 244B).

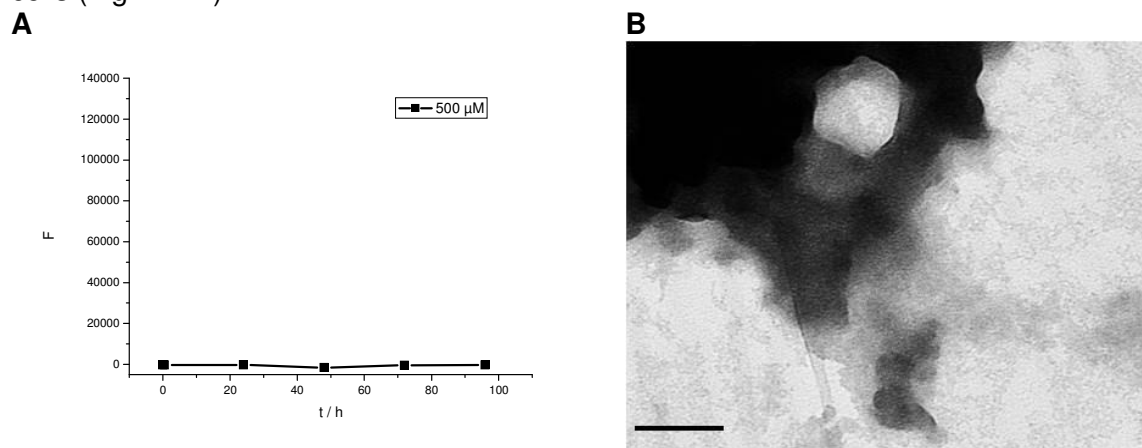


Fig. 245: (A) ThT binding assays of H-IIAGKN-Peg-NFGAILS-OH at a peptide concentration of 500 μM in 1x 1% HFIP, pH 7.4. Data are means of 3 assays after subtraction of buffer values +/- standard error of the mean (SEM) with each experiment performed in multiple replicates (n = 3).

(B) TEM picture of an aged incubation of H-IIAGKN-Peg-NFGAILS-OH. The peptide was incubated at 500 μM for 7 d in 1x 1% HFIP, pH 7.4. Scale bar: 100 nm.

Also, the ThT binding assay of H-IIAGKN-Peg-NFGAILS-OH at 500 μM peptide concentration did not reveal fibril formation (Fig. 245A). This was verified by TEM analysis of this aged solution (Fig. 245B).

Congo Red stained aggregates of H-IIAGKN-Peg-NFGAILS-OH showed red color under normal light but no birefringence at all under cross-polarized light (Fig. 246A and B). Aggregates of H-IIAGKN-Peg-NFGAILS-OH were obviously able to bind to Congo Red but

they did not possess the typical amyloid structure that is responsible for the appearance of birefringence under cross-polarized light.

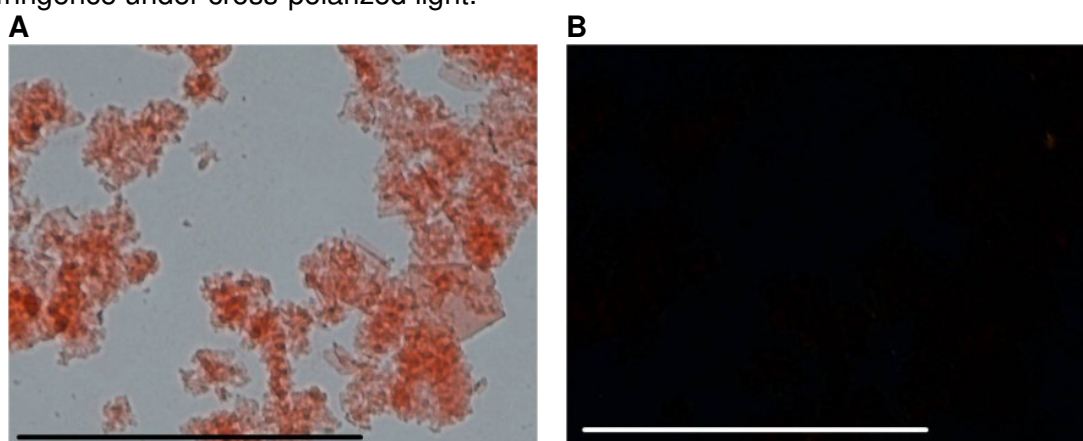


Fig. 246: Microscopic examination of an aged incubation of H-IIAGKN-Peg-NFGAILS-OH stained with Congo Red. The peptide was incubated at a concentration of 1 mM in 1xb 1% HFIP, pH 7.4 for 3 days. Pictures were taken under A normal and B cross-polarized light. Scale bar: 100 μ m.

3.2.3.3 H-IIAGKN-Aoc-NFGAILS-OH (H6a)

Similar to H-NKGAI-Aoc-NFGAILS-OH (Fig. 207A), the far-UV CD spectra of H-IIAGKN-Aoc-NFGAILS-OH (Fig. 247A) displayed a broad and intense minimum from 195 nm to 225 nm. Compared to H-NKGAI-Aoc-NFGAILS-OH, this signal was broader but less intense. The signal intensity decreased already at a peptide concentration of 5 μ M. This indicates a higher aggregation potential compared to H-NKGAI-Aoc-NFGAILS-OH (Fig. 207A).

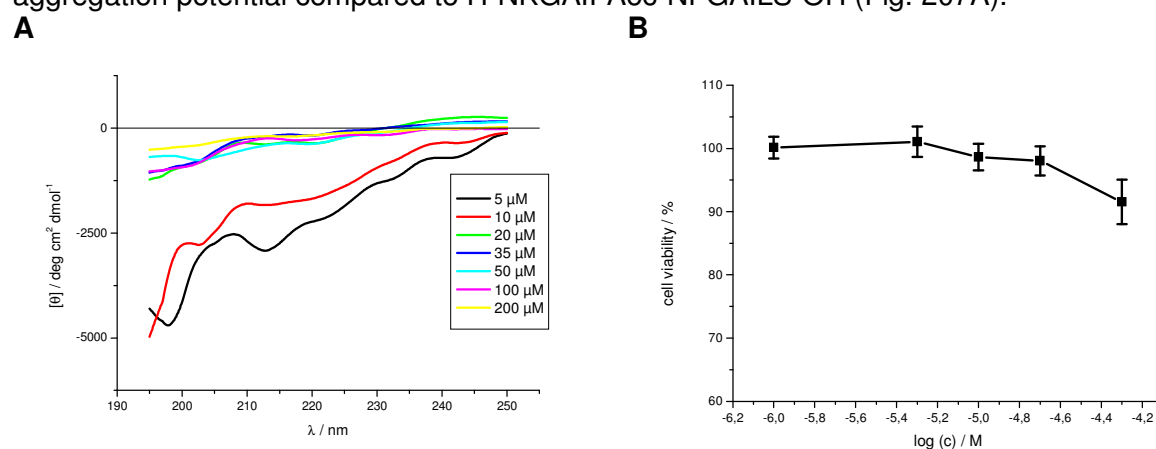


Fig. 247: (A) Far-UV CD spectra of H-IIAGKN-Aoc-NFGAILS-OH at different concentrations in 1xb 1% HFIP, pH 7.4.

(B) Cell viability assay of an aged solution of H-IIAGKN-Aoc-NFGAILS-OH (5 mM in 1xb 1% HFIP, pH 7.4 for 4 days) using PC-12 cells. Data are percentages of control and are the mean (+/-SEM) of three independent experiments with each experiment performed in multiple replicates (n = 3).

Contrary to H-NKGAI-Aoc-NFGAILS-OH (Fig. 207B), H-IIAGKN-Aoc-NFGAILS-OH was only slightly toxic to PC-12 cells (Fig. 247B).

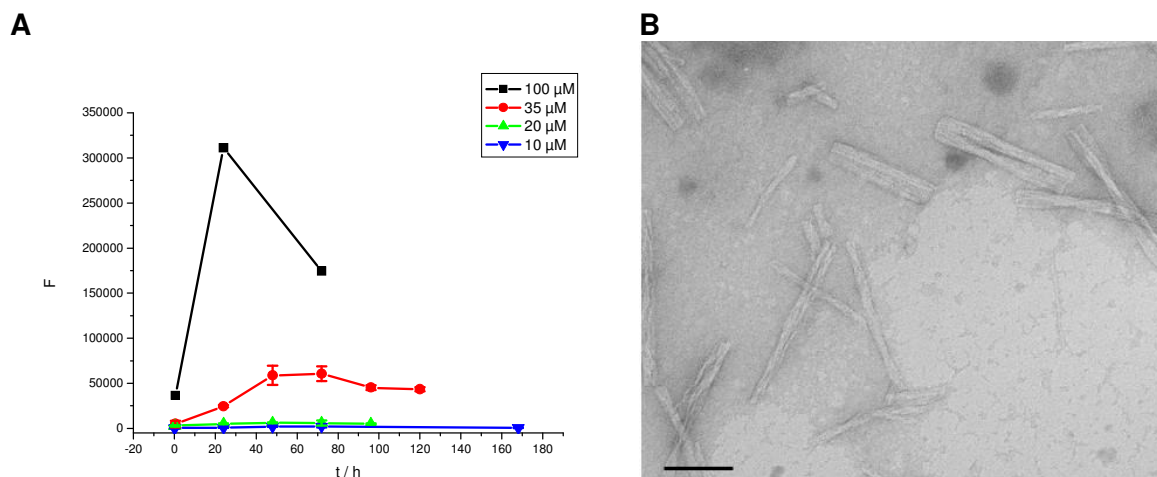


Fig. 248: (A) ThT binding assays of H-IIAGKN-Aoc-NFGAILS-OH at different concentrations in 1xb 1% HFiP, pH 7.4. Data are means of 3 assays after subtraction of buffer values +/- standard error of the mean (SEM) with each experiment performed in multiple replicates (n = 3).

(B) TEM picture of an aged incubation of H-IIAGKN-Aoc-NFGAILS-OH. The peptide was incubated at 35 μM for 7 d in 1xb 1% HFiP, pH 7.4. Scale bar: 100 nm.

As shown in Fig. 248A, H-IIAGKN-Aoc-NFGAILS-OH started forming fibrils at a peptide concentration of 35 μM . At 20 μM only a weak but distinct increase of ThT fluorescence was detected.

Fig. 248B displays the TEM picture of an aged solution of H-IIAGKN-Aoc-NFGAILS-OH. It showed mainly isolated fibrils and in between few amorphous aggregates.

Congo Red staining of fibrillar aggregates of H-IIAGKN-Aoc-NFGAILS-OH indicated some green/ yellow birefringence under cross-polarized light (Fig. 249B). This is a strong indication for fibril formation.

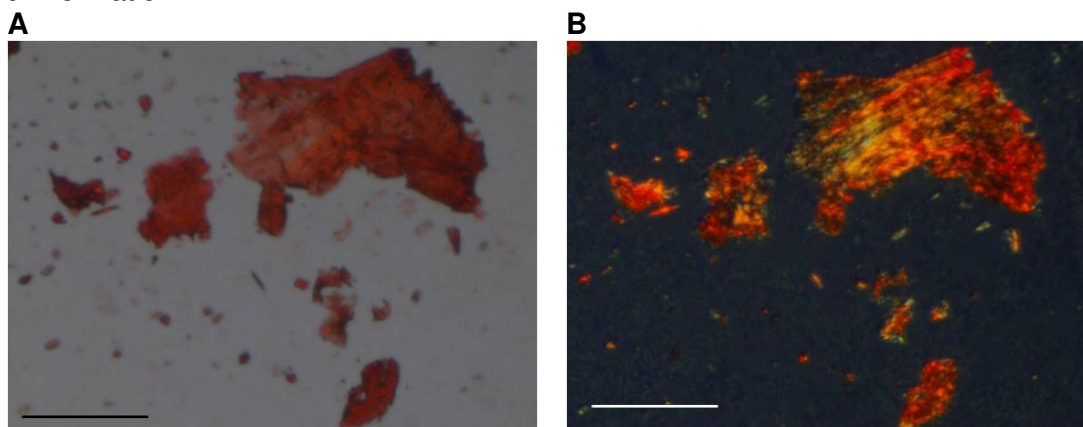


Fig. 249: Microscopic examination of an aged incubation of H-IIAGKN-Aoc-NFGAILS-OH stained with Congo Red. The peptide was incubated at a concentration of 1 mM in 1xb 1% HFiP, pH 7.4 for 3 days. Pictures were taken under A normal and B cross-polarized light. Scale bar: 100 μm .

3.2.3.4 H-IIAGKN-Adc-NFGAILS-OH (H6b)

The CD spectra of H-IIAGKN-Adc-NFGAILS-OH (Fig. 250A) had a similar shape as the CD spectra of H-NKGAIL-Aoc-NFGAILS-OH (Fig. 207A) and H-IIAGKN-Aoc-NFGAILS-OH (Fig. 54A). Compared to H-NKGAIL-Adc-NFGAILS-OH (Fig. 216A), the magnitude of the CD signal was weaker.

Similar to H-NKGAIL-Aoc-NFGAILS-OH, the CD spectrum of H-IIAGKN-Aoc-NFGAILS-OH at a peptide concentration of 2 μM expressed a minimum at around 200 nm indicating the

presence of random coil structure, whereas for higher peptide concentrations the spectra indicated mainly β -sheet structure.

The signal intensity decreased already at a peptide concentration of 5 μ M. This indicates a higher aggregation potential compared to H-NKGAI-Adc-NFGAILS-OH (Fig. 216A).

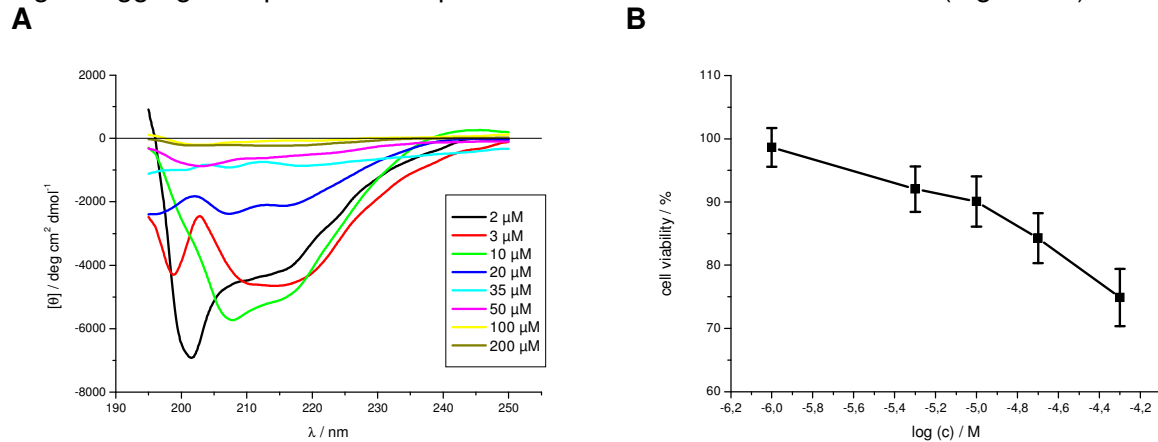


Fig. 250: (A) Far-UV CD spectra of H-IIAGKN-Adc-NFGAILS-OH at different concentrations in 1xb 1% HFIP, pH 7.4.

(B) Cell viability assay of an aged solution of H-IIAGKN-Adc-NFGAILS-OH (5 mM in 1xb 1% HFIP, pH 7.4 for 4 days) using PC-12 cells. Data are percentages of control and are the mean (+/-SEM) of three independent experiments with each experiment performed in multiple replicates (n = 3).

H-IIAGKN-Adc-NFGAILS-OH was toxic to PC-12 cells (Fig. 250B). H-IIAGKN-Adc-NFGAILS-OH was already forming fibrils at a concentration of 10 μ M (Fig. 251A).

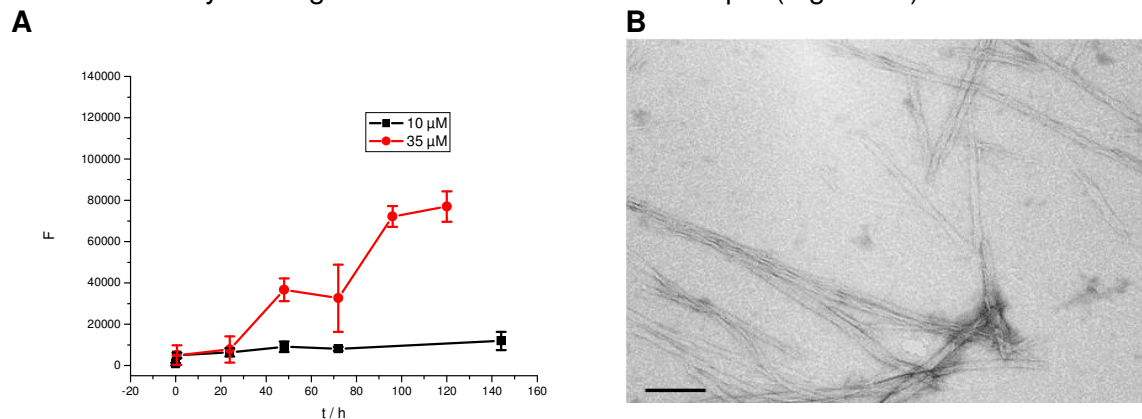


Fig. 251: (A) ThT binding assays of H-IIAGKN-Adc-NFGAILS-OH at different concentrations in 1xb 1% HFIP, pH 7.4. Data are means of 3 assays after subtraction of buffer values +/- standard error of the mean (SEM) with each experiment performed in multiple replicates (n = 3).

(B) TEM picture of an aged incubation of H-IIAGKN-Adc-NFGAILS-OH. The peptide was incubated at 100 μ M for 7 d in 1xb 1% HFIP, pH 7.4. Scale bar: 100 nm.

Congo Red staining of an aged solution of H-IIAGKN-Adc-NFGAILS-OH showed clear green-golden birefringence under cross-polarized light (Fig. 252B).

In addition, long fibrils were found by TEM studies of an aged incubation of H-IIAGKN-Adc-NFGAILS-OH (Fig. 251B).

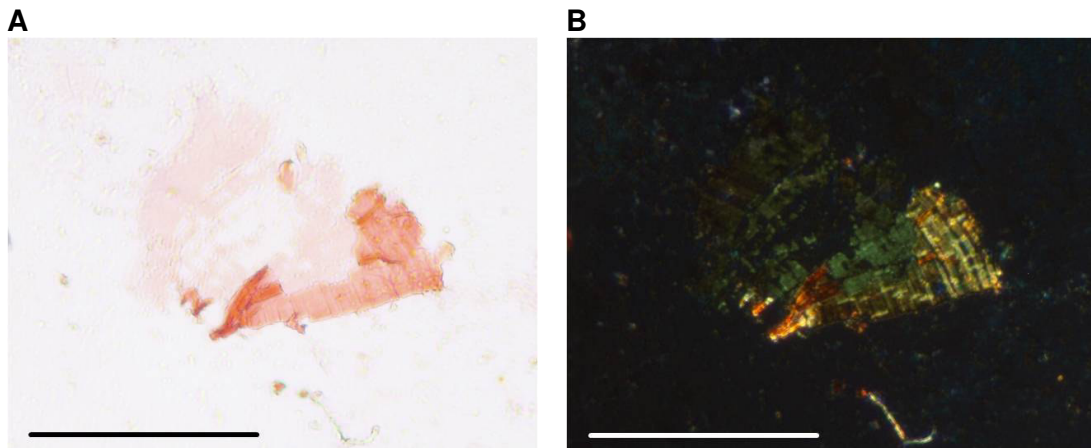


Fig. 252: Microscopic examination of an aged incubation of H-IIAGKN-Adc-NFGAILS-OH stained with Congo Red. The peptide was incubated at a concentration of 1 mM in 1xb 1% HFIP, pH 7.4 for 3 days. Pictures were taken under A normal and B cross-polarized light. Scale bar: 100 μm .

3.2.3.5 H-IIAGKN-GGG-NFGAILS-OH (H24)

The concentration dependent CD spectra of H-IIAGKN-GGG-NFGAILS-OH (Fig. 253A) showed a strong minimum at 195 - 200 nm that can be related to random coil structure. The weaker negative signal between 210 nm and 220 nm indicated the presence of some additional structural elements like β -sheets and β -turns. H-NKGAILI-GGG-NFGAILS-OH started forming aggregates at concentrations higher than 10 μM .

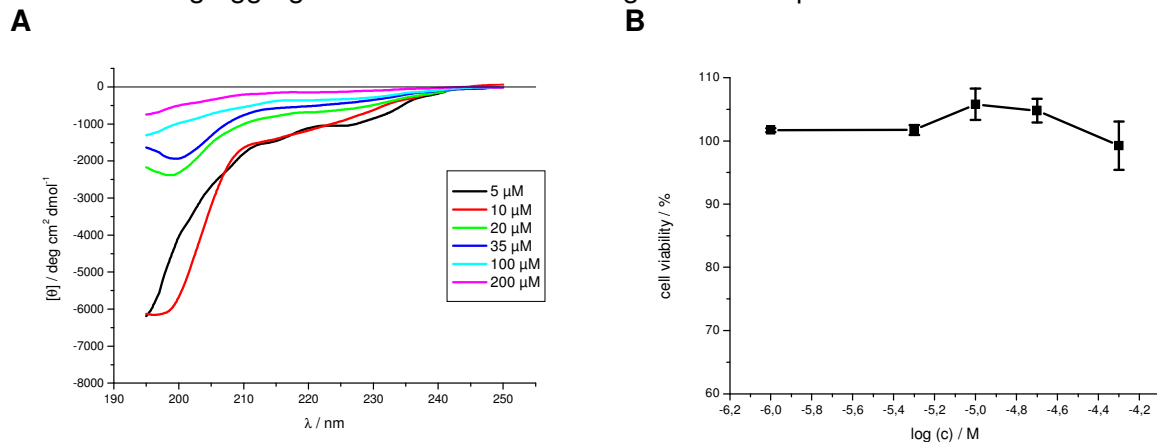


Fig. 253: (A) Far-UV CD spectra of H-IIAGKN-GGG-NFGAILS-OH at different concentrations in 1xb 1% HFIP, pH 7.4.

(B) Cell viability assay of an aged solution of H-IIAGKN-GGG-NFGAILS-OH (5 mM in 1xb 1% HFIP, pH 7.4 for 4 days) using PC-12 cells. Data are percentages of control and are the mean (+/-SEM) of three independent experiments with each experiment performed in multiple replicates ($n = 3$).

Under the conditions tested H-IIAGKN-GGG-NFGAILS-OH did not display toxicity towards PC-12 cells (Fig. 253B) and did not form fibrils up to a concentration of 500 μM (Fig. 254A).

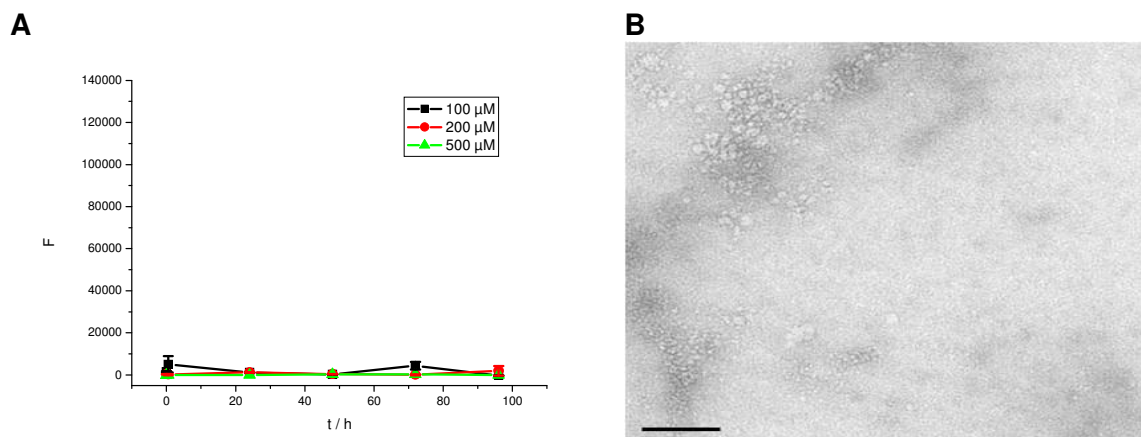


Fig. 254: (A) ThT binding assays of H-IIAGKN-GGG-NFGAILS-OH at different concentrations in 1xb 1% HFIP, pH 7.4. Data are means of 3 assays after subtraction of buffer values \pm standard error of the mean (SEM) with each experiment performed in multiple replicates ($n = 3$). (B) TEM picture of an aged incubation of H-IIAGKN-GGG-NFGAILS-OH. The peptide was incubated at 500 μ M for 7 d in 1xb 1% HFIP, pH 7.4. Scale bar: 100 nm.

The TEM picture of H-IIAGKN-GGG-NFGAILS-OH also only showed amorphous aggregates (Fig. 254B).

Congo Red staining revealed no birefringence under cross-polarized light (Fig. 255B). Congo Red stained aggregates of H-IIAGKN-GGG-NFGAILS-OH showed red staining under normal light (Fig. 255A) but no birefringence under cross-polarized light. Aggregates of H-IIAGKN-GGG-NFGAILS-OH were obviously able to bind to Congo Red but they did not express the typical amyloid structure that is responsible for the appearance of birefringence under cross-polarized light.

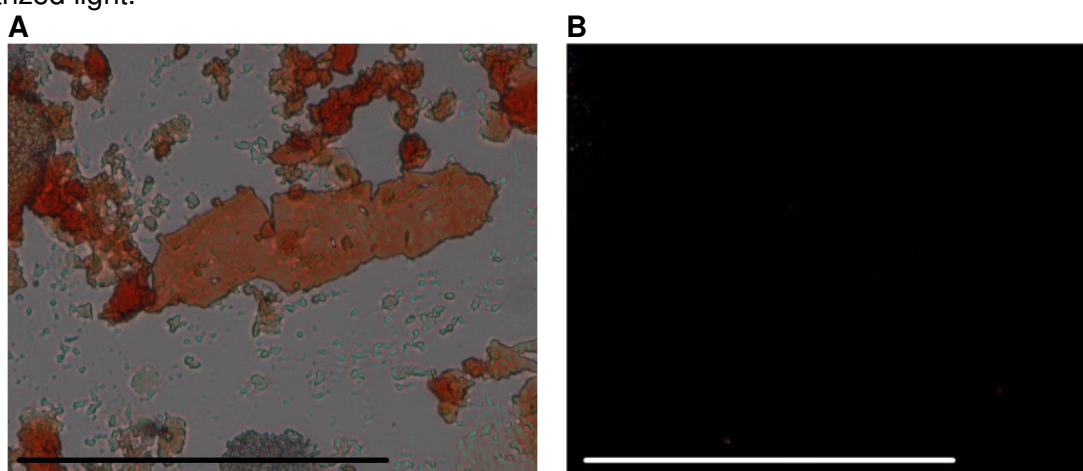


Fig. 255: Microscopic examination of an aged incubation of H-IIAGKN-GGG-NFGAILS-OH stained with Congo Red. The peptide was incubated at a concentration of 1 mM in 1xb 1% HFIP, pH 7.4 for 3 days. Pictures were taken under A normal and B cross-polarized light. Scale bar: 100 μ m.

3.2.3.6 H-IIAGKN-AAA-NFGAILS-OH (H23)

Concentration dependent CD spectra of H-IIAGKN-AAA-NFGAILS-OH (Fig. 256A) also displayed both a strong minimum at 195 - 200 nm that can be related to random coil structure and a weaker negative signal between 210 nm and 225 nm intending the presence of additional structural elements like β -sheet or β -turn. H-IIAGKN-AAA-NFGAILS-OH started forming aggregates at concentrations higher than 10 μ M.

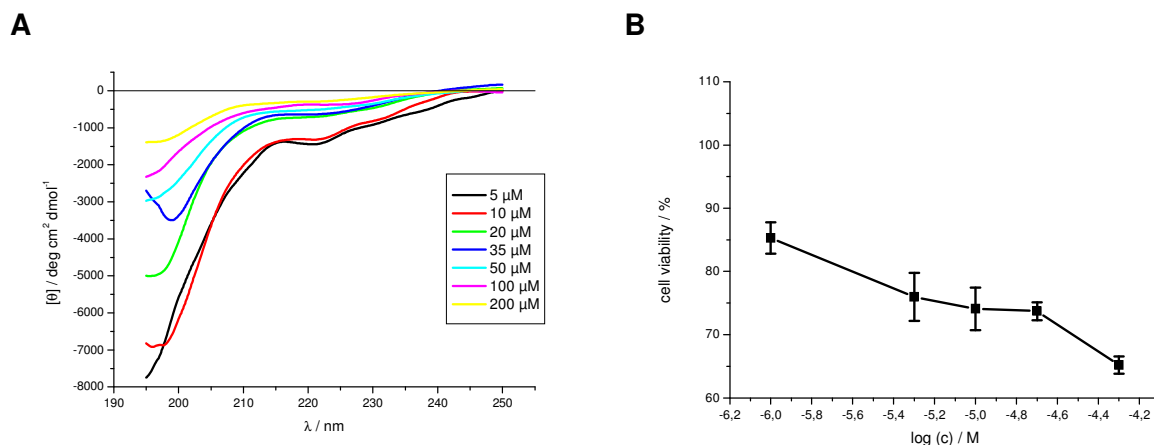


Fig. 256: (A) Far-UV CD spectra of H-IIAGKN-AAA-NFGAILS-OH at different concentrations in 1x 1% HFIP, pH 7.4.

(B) Cell viability assay of an aged solution of H-IIAGKN-AAA-NFGAILS-OH (5 mM in 1x 1% HFIP, pH 7.4 for 4 days) using PC-12 cells. Data are percentages of control and are the mean (+/-SEM) of three independent experiments with each experiment performed in multiple replicates (n = 3).

Among the peptides with the sequence H-IIAGKN-XXX-NFGAILS-OH, H-IIAGKN-AAA-NFGAILS-OH was the most toxic one to PC-12 cells (Fig. 256B).

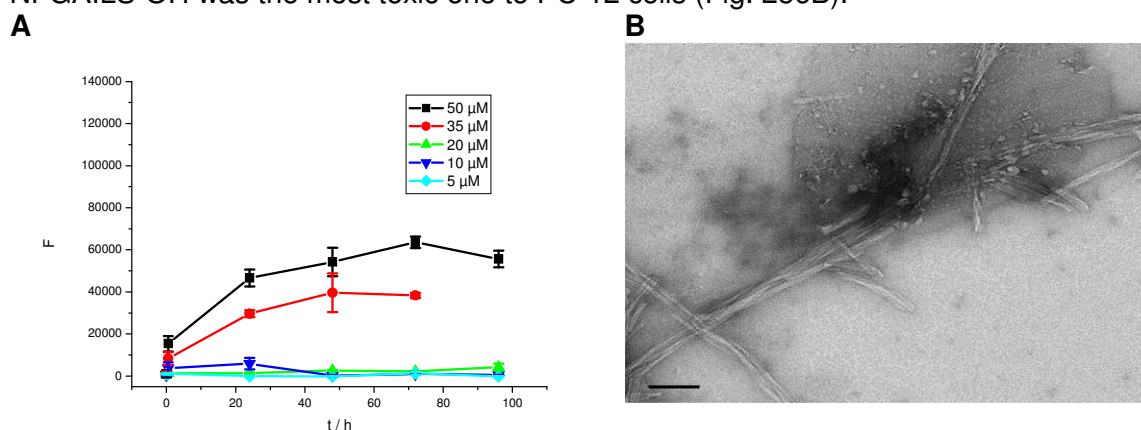


Fig. 257: (A) ThT binding assays of H-IIAGKN-AAA-NFGAILS-OH at different concentrations in 1x 1% HFIP, pH 7.4. Data are means of 3 assays after subtraction of buffer values +/- standard error of the mean (SEM) with each experiment performed in multiple replicates (n = 3).

(B) TEM picture of an aged incubation of H-IIAGKN-AAA-NFGAILS-OH. The peptide was incubated at 100 μM for 7 d in 1x 1% HFIP, pH 7.4. Scale bar: 100 nm.

H-IIAGKN-AAA-NFGAILS-OH started forming amyloid fibrils at a concentration of 35 μM as indicated by ThT assays at different concentrations (Fig. 257A).

Staining of aged aggregates of H-IIAGKN-AAA-NFGAILS-OH with Congo Red revealed the formation of amyloid fibrils. Stained aggregates showed intense red color under normal light (Fig. 258A) and in part green birefringence under cross-polarized light (Fig. 258B).

Fibril formation was additionally verified by TEM (Fig. 257B).

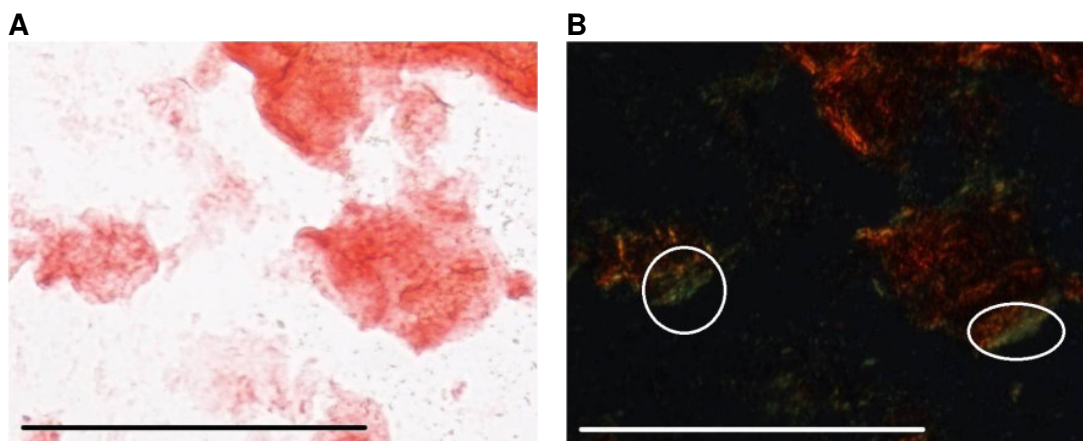


Fig. 258: Microscopic examination of an aged incubation of H-IIAGKN-AAA-NFGAILS-OH stained with Congo Red. The peptide was incubated at a concentration of 1 mM in 1xb 1% HFIP, pH 7.4 for 3 days. Pictures were taken under A normal and B cross-polarized light. Scale bar: 100 μ m.

3.2.3.7 H-IIAGKN-LLL-NFGAILS-OH (H14)

Similar to other peptides with a hydrophobic connecting element, H-IIAGKN-LLL-NFGAILS-OH displayed a clear β -sheet structure in Far-UV CD experiments (Fig. 259A). The intensity of the β -sheet signal of H-IIAGKN-LLL-NFGAILS-OH was higher than for H-NKGAI-Aoc-NFGAILS-OH (Fig. 207A) and H-NKGAI-LLL-NFGAILS-OH (Fig. 225A). Contrary to the spectra of H-NKGAI-LLL-NFGAILS-OH the minimum was not shifted towards higher wavelengths upon peptide aggregation and the related loss of signal.

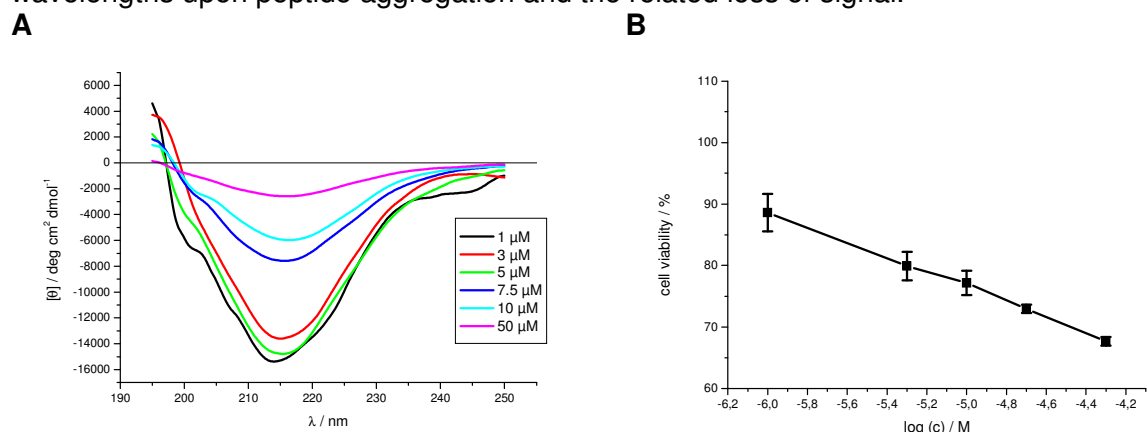


Fig. 259: (A) Far-UV CD spectra of H-IIAGKN-LLL-NFGAILS-OH at different concentrations in 1xb 1% HFIP, pH 7.4.

(B) Cell viability assay of an aged solution of H-IIAGKN-LLL-NFGAILS-OH (5 mM in 1xb 1% HFIP, pH 7.4 for 4 days) using PC-12 cells. Data are percentages of control and are the mean (+/-SEM) of three independent experiments with each experiment performed in multiple replicates (n = 3).

H-IIAGKN-LLL-NFGAILS-OH showed to be highly toxic to PC-12 cells (Fig. 259B) just like H-NKGAI-LLL-NFGAILS-OH (Fig. 225B).

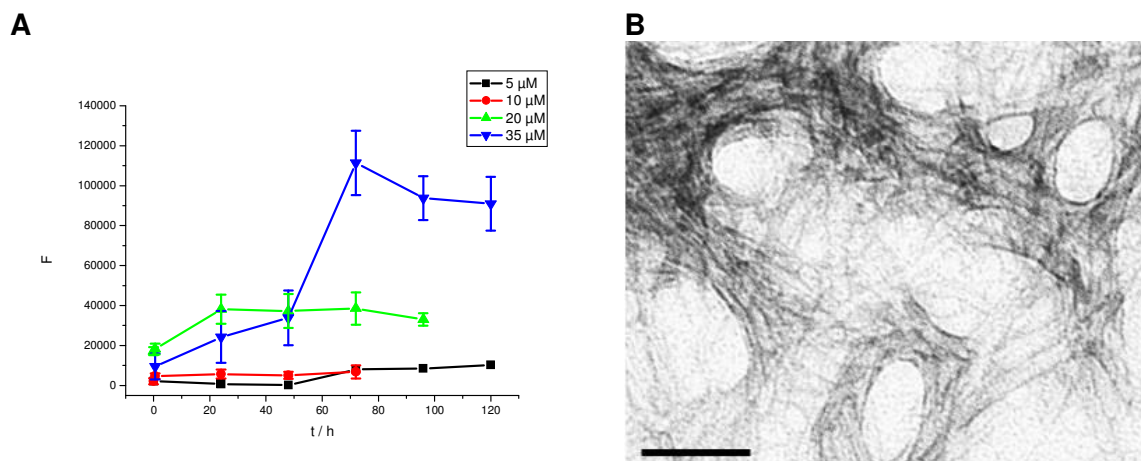


Fig. 260: (A) ThT binding assays of H-IIAGKN-LLL-NFGAILS-OH at different concentrations in 1xb 1% HFIP, pH 7.4. Data are means of 3 assays after subtraction of buffer values +/- standard error of the mean (SEM) with each experiment performed in multiple replicates (n = 3).

(B) TEM picture of an aged incubation of H-IIAGKN-LLL-NFGAILS-OH. The peptide was incubated at 35 μM for 7 d in 1xb 1% HFIP, pH 7.4. Scale bar: 100 nm.

ThT studies at different concentrations revealed, that H-IIAGKN-LLL-NFGAILS-OH was already forming fibrils at a concentration of 5 μM (Fig. 260A). The concentration dependent CD spectrum at 7.5 μM and also at 10 μM already showed a signal loss related to oligomerisation (Fig. 259A). This correlates with a fast fibril formation observed by ThT assay at a concentration of 10 μM .

Congo Red staining of a aged solution of H-IIAGKN-LLL-NFGAILS-OH displayed red staining under normal light (Fig. 261A) and green birefringence under cross-polarized light (Fig. 261B).

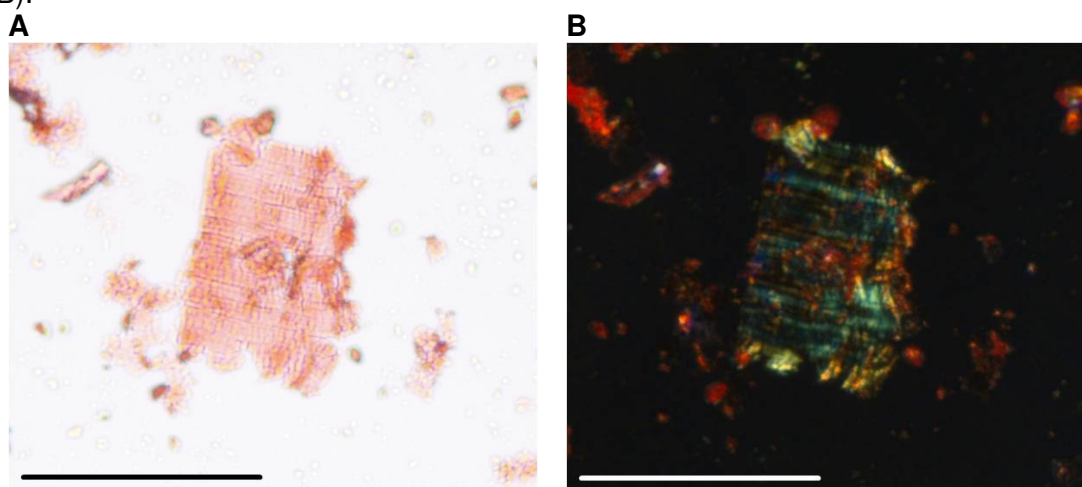


Fig. 261: Microscopic examination of an aged incubation of H-IIAGKN-LLL-NFGAILS-OH stained with Congo Red. The peptide was incubated at a concentration of 1 mM in 1xb 1% HFIP, pH 7.4 for 3 days. Pictures were taken under A normal and B cross-polarized light. Scale bar: 100 μm .

3.2.3.8 H-IIAGKN-KKK-NFGAILS-OH (H15)

The CD spectra of H-IIAGKN-KKK-NFGAILS-OH (Fig. 262A) displayed mainly a negative signal at 195 nm indicating random coil structure. A tiny negative bulge was observed at 210-230 nm indicating the presence of additional β -sheet and β -turn elements. The peptide started to aggregate already between a concentration of 5 μM and 10 μM .

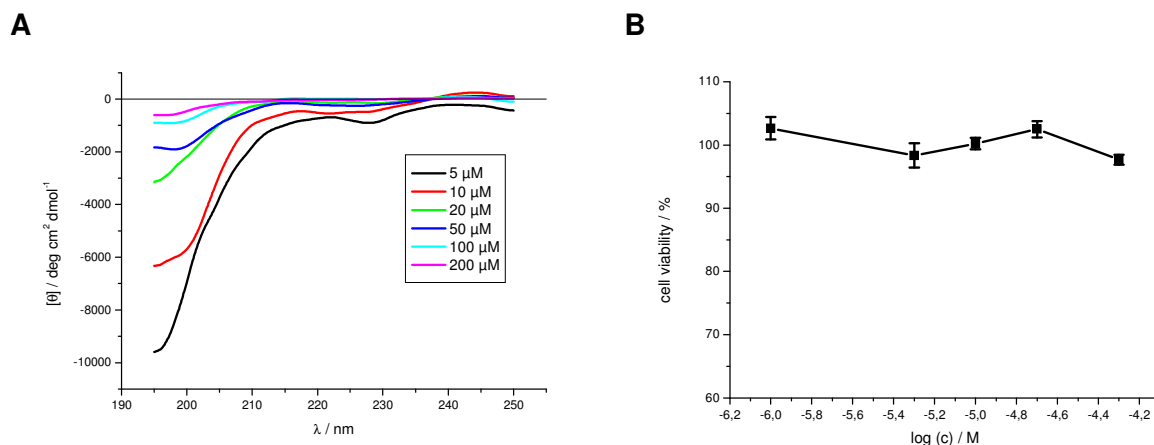


Fig. 262: (A) Far-UV CD spectra of H-IIAGKN-KKK-NFGAILS-OH at different concentrations in 1x 1% HFIP, pH 7.4.

(B) Cell viability assay of an aged solution of H-IIAGKN-KKK-NFGAILS-OH (5 mM in 1x 1% HFIP, pH 7.4 for 4 days) using PC-12 cells. Data are percentages of control and are the mean (+/-SEM) of three independent experiments with each experiment performed in multiple replicates (n = 3).

Similar to H-NKGAI-KKK-NFGAILS-OH (Fig. 232B) H-IIAGKN-KKK-NFGAILS-OH did not display toxicity to PC-12 cells (Fig. 262B).

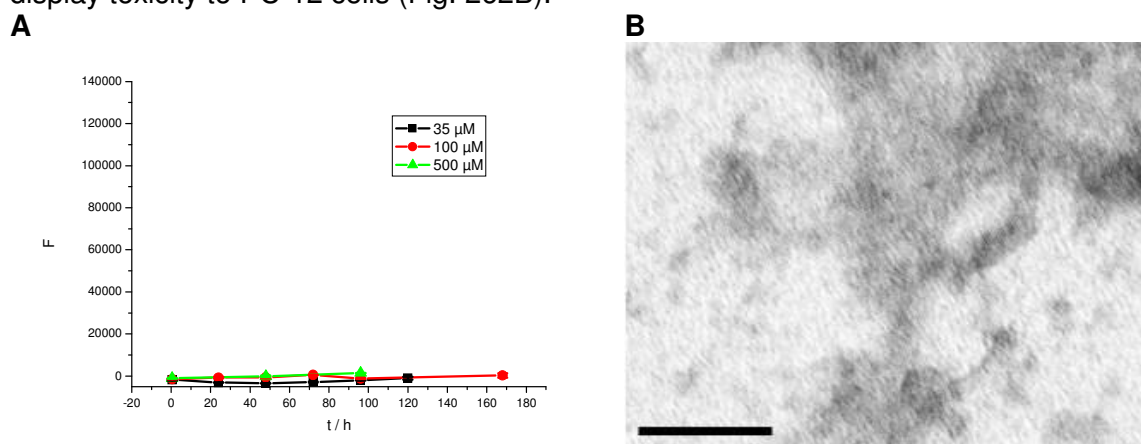


Fig. 263: (A) ThT binding assays of H-IIAGKN-KKK-NFGAILS-OH at different concentrations in 1x 1% HFIP, pH 7.4. Data are means of 3 assays after subtraction of buffer values +/- standard error of the mean (SEM) with each experiment performed in multiple replicates (n = 3).

(B) TEM picture of an aged incubation of H-IIAGKN-KKK-NFGAILS-OH. The peptide was incubated at 35 μM for 7 d in 1x 1% HFIP, pH 7.4. Scale bar: 100 nm.

ThT studies of H-IIAGKN-KKK-NFGAILS-OH did not reveal fibril formation at concentrations up to 500 μM within 96 h (Fig. 263A).

Similar to Congo red stained aggregates of H-NKGAI-KKK-NFGAILS-OH (Fig. 233A and B), staining of an aged incubation of H-IIAGKN-KKK-NFGAILS-OH with Congo Red displayed only small aggregates that weakly stained with Congo Red whereas no birefringence was detected under cross-polarized light (Fig. 264B).

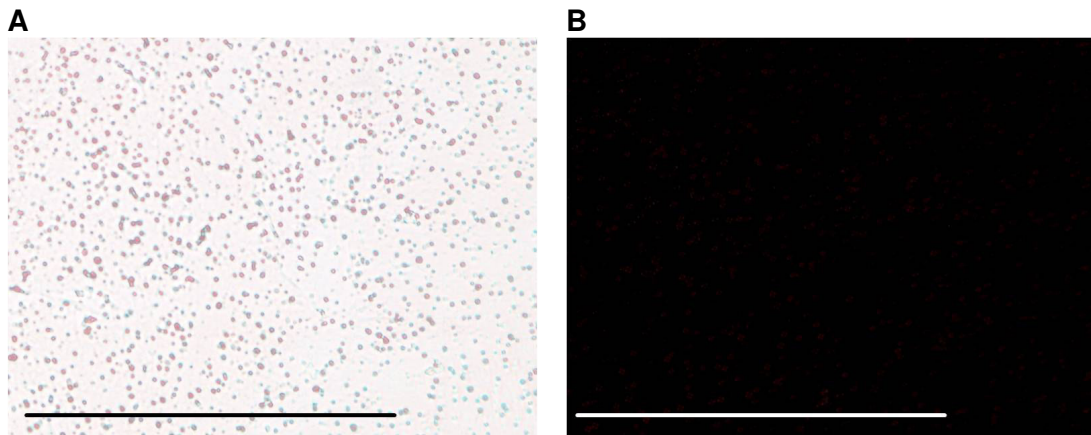


Fig. 264: Microscopic examination of an aged incubation of H-IIAGKN-KKK-NFGAILS-OH stained with Congo Red. The peptide was incubated at a concentration of 1 mM in 1xb 1% HFIP, pH 7.4 for 3 days. Pictures were taken under A normal and B cross-polarized light. Scale bar: 100 µm.

3.2.3.9 H-IIAGKN-K(Ac)K(Ac)K(Ac)-NFGAILS-OH (H19)

The CD spectra of H-IIAGKN-K(Ac)K(Ac)K(Ac)-NFGAILS-OH (Fig. 265A) showed an intense minimum at 195 - 200 nm related to random coil structures and a less intense negative signal between 220 nm and 230 nm related to β -sheets and β -turns. The signal intensity decreased at peptide concentrations higher than 10 µM.

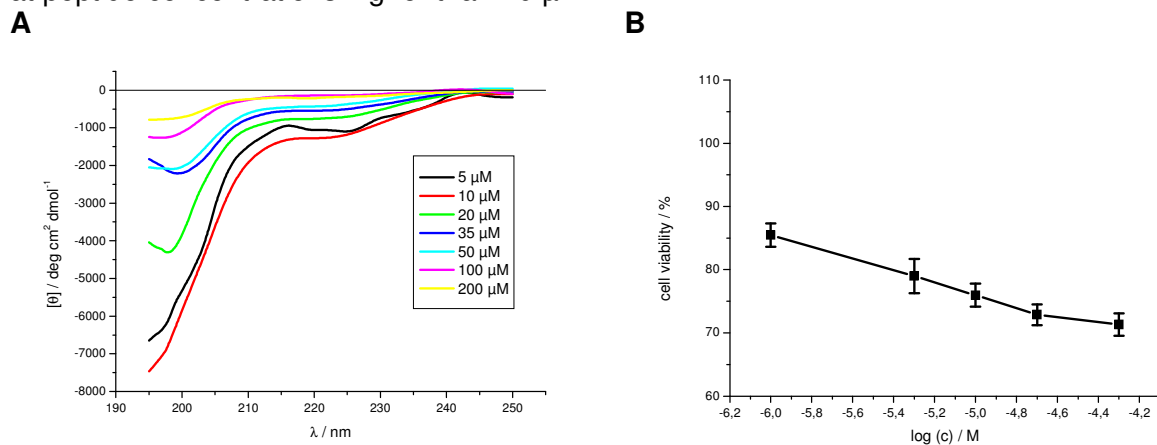


Fig. 265: (A) Far-UV CD spectra of H-IIAGKN-K(Ac)K(Ac)K(Ac)-NFGAILS-OH at different concentrations in 1xb 1% HFIP, pH 7.4.

(B) Cell viability assay of an aged solution of H-IIAGKN-K(Ac)K(Ac)K(Ac)-NFGAILS-OH (5 mM in 1xb 1% HFIP, pH 7.4 for 4 days) using PC-12 cells. Data are percentages of control and are the mean (+/-SEM) of three independent experiments with each experiment performed in multiple replicates (n = 3).

As shown in Fig. 265B H-IIAGKN-K(Ac)K(Ac)K(Ac)-NFGAILS-OH was highly toxic to PC-12 cells.

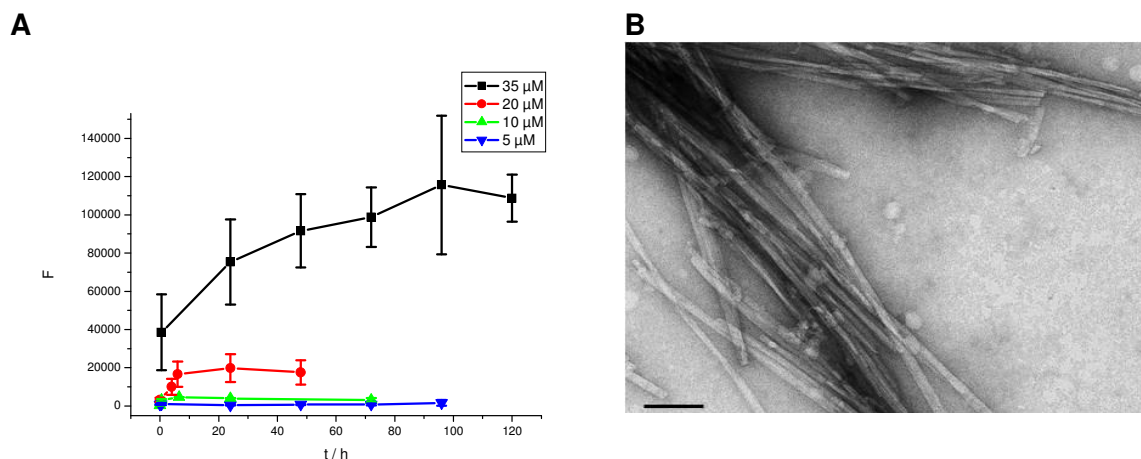


Fig. 266: (A) ThT binding assays of H-IIAGKN-K(Ac)K(Ac)K(Ac)-NFGAILS-OH at different concentrations in 1xb 1% HFIP, pH 7.4. Data are means of 3 assays after subtraction of buffer values +/- standard error of the mean (SEM) with each experiment performed in multiple replicates (n = 3). (B) TEM picture of an aged incubation of H-IIAGKN-K(Ac)K(Ac)K(Ac)-NFGAILS-OH. The peptide was incubated at 35 μ M for 7 d in 1xb 1% HFIP, pH 7.4. Scale bar: 100 nm.

H-IIAGKN-K(Ac)K(Ac)K(Ac)-NFGAILS-OH started forming fibrils at 10 μ M (Fig. 266A). The TEM picture of H-IIAGKN-K(Ac)K(Ac)K(Ac)-NFGAILS-OH displayed thick bundles of fibrils (Fig. 266B). Congo Red staining and microscopic examination of fibrillar aggregates formed by H-IIAGKN-K(Ac)K(Ac)K(Ac)-NFGAILS-OH displayed green/orange birefringence under cross-polarized light (Fig. 267B).

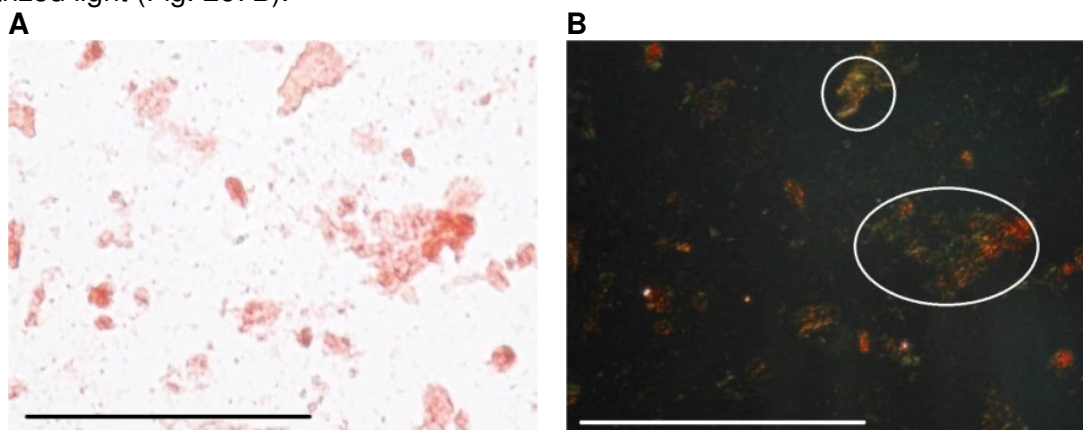


Fig. 267: Microscopic examination of an aged incubation of H-IIAGKN-K(Ac)K(Ac)K(Ac)-NFGAILS-OH stained with Congo Red. The peptide was incubated at a concentration of 1 mM in 1xb 1% HFIP, pH 7.4 for 3 days. Pictures were taken under A normal and B cross-polarized light. Scale bar: 100 μ m.

3.2.3.10 H-IIAGKN-EEE-NFGAILS-OH (H17)

Concentration dependent CD spectra of H-IIAGKN-EEE-NFGAILS-OH (Fig. 268A) displayed both a strong minimum at 195 - 200 nm that can be related to random coil structure and a weaker negative signal between 220 nm and 225 nm intending the presence of additional structural elements like β -sheet and β -turn, similar to the spectra of H-NKGAI-EEE-NFGAILS-OH (Fig. 238A). Compared to H-NKGAI-EEE-NFGAILS-OH the overall signal intensity was however much lower for H-IIAGKN-EEE-NFGAILS-OH. H-IIAGKN-EEE-NFGAILS-OH started forming aggregates at concentrations higher than 10 μ M.

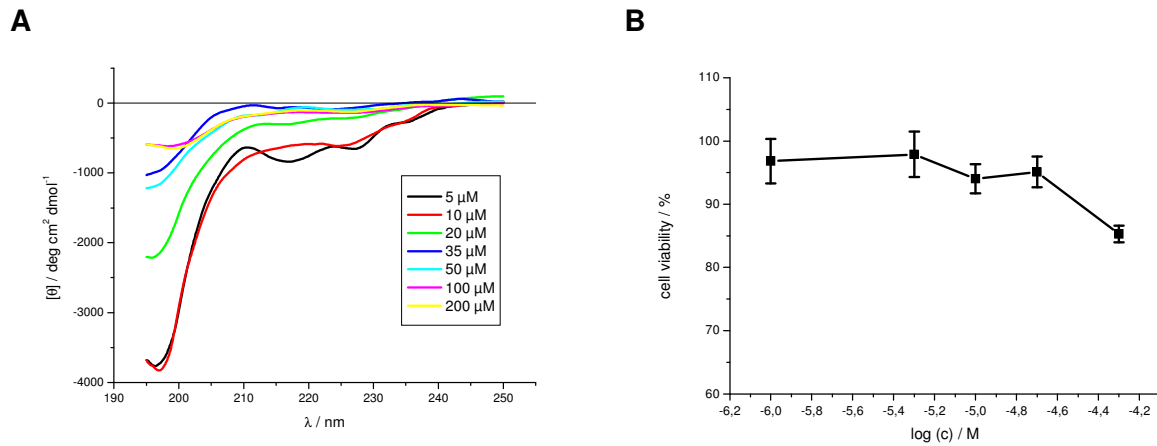


Fig. 268: A) Far-UV CD spectra of H-IIAGKN-EEE-NFGAILS-OH at different concentrations in 1x 1% HFIP, pH 7.4.

B) Cell viability assay of an aged solution of H-IIAGKN-EEE-NFGAILS-OH (5 mM in 1x 1% HFIP, pH 7.4 for 4 days) using PC-12 cells. Data are percentages of control and are the mean (+/-SEM) of three independent experiments with each experiment performed in multiple replicates (n = 3).

H-IIAGKN-EEE-NFGAILS-OH proved to be only weakly toxic to PC-12 cells under the conditions tested (Fig. 268B) and was unable to form fibrils up to a concentration of 500 μM (Fig. 269A). There were no Congo Red stained aggregates of H-IIAGKN-EEE-NFGAILS-OH and thus no birefringence visible under cross-polarized light (Fig. 270B).

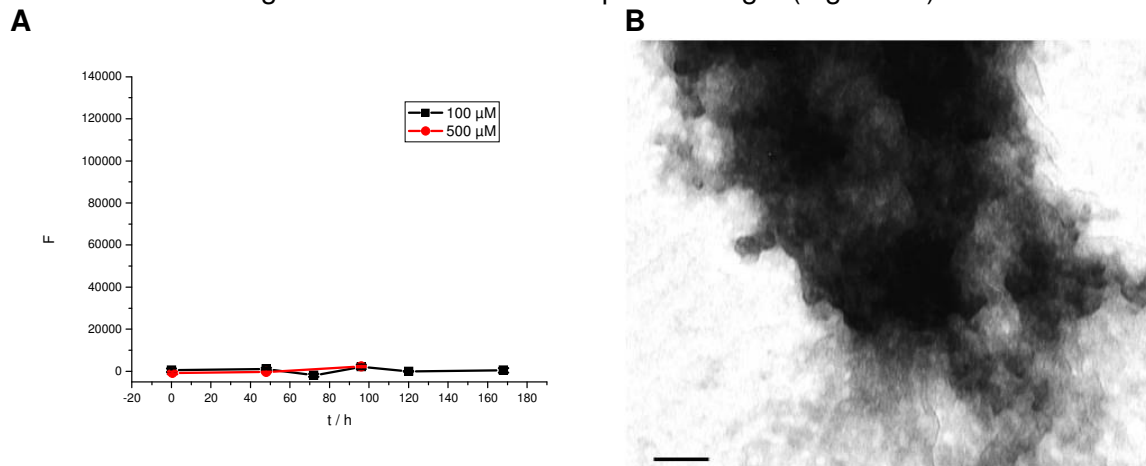


Fig. 269: (A) ThT binding assays of H-IIAGKN-EEE-NFGAILS-OH at different concentrations in 1x 1% HFIP, pH 7.4. Data are means of 3 assays after subtraction of buffer values +/- standard error of the mean (SEM) with each experiment performed in multiple replicates (n = 3).

(B) TEM picture of an aged incubation of H-IIAGKN-EEE-NFGAILS-OH. The peptide was incubated at 500 μM for 7 d in 1x 1% HFIP, pH 7.4. Scale bar: 100 nm.

TEM imaging of H-IIAGKN-EEE-NFGAILS-OH also only displayed amorphous aggregates (Fig. 269B) confirming the suggestion that H-IIAGKN-EEE-NFGAILS-OH was unable to form fibrils.

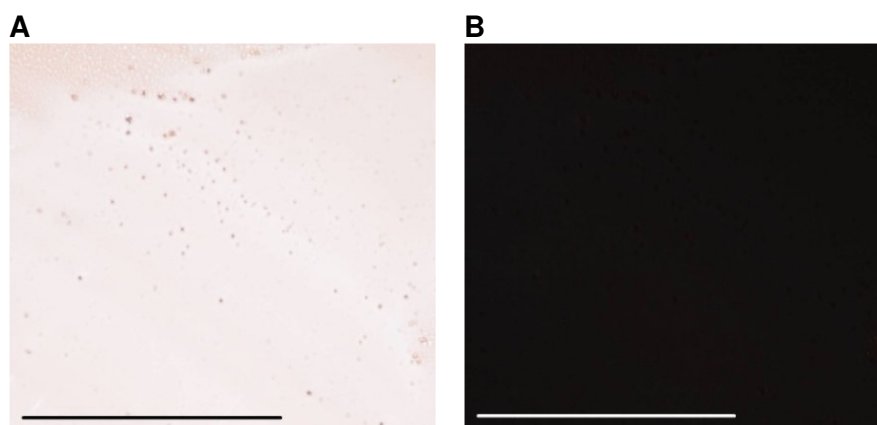


Fig. 270: Microscopic examination of an aged incubation of H-IIAGKN-EEE-NFGAILS-OH stained with Congo Red. The peptide was incubated at a concentration of 1 mM in 1x 1% HFIP, pH 7.4 for 3 days. Pictures were taken under A normal and B cross-polarized light. Scale bar: 100 μ m.

Table 20: Overview of ThT binding assays and cell viability assays performed with peptides containing the sequence H-IIAGKN-XXX-NFGAILS-OH at different concentrations.

Results of “+” indicate fibril formation, whereas “-” indicate no fibril formation within the 5 days of incubation of the solution at the given peptide concentration.

For the cell viability assays, results of “+++” mean high toxicity towards PC-12 cell, “++” means medium toxicity and “+/-” means low to no toxicity. Low toxicity refers to peptides with >90% cell viability, medium toxicity refers to a cell viability between 80% and 90%, and high toxicity refers to a cell viability of <80% for aged incubations at a peptide concentration of 50 μ M.

Abbrev.	Sequence	ThT									Tox.	
		5 μ M	10 μ M	20 μ M	35 μ M	50 μ M	100 μ M	200 μ M	350 μ M	500 μ M		
H6	H-IIAGKN-Peg-NFGAILS-OH										-	+/-
H6a	H-IIAGKN-Aoc-NFGAILS-OH		-	+	+		+					++
H6b	H-IIAGKN-Adc-NFGAILS-OH		+		+							+++
H24	H-IIAGKN-GGG-NFGAILS-OH						-	-			-	+/-
H23	H-IIAGKN-AAA-NFGAILS-OH	-	-	-	+	+						+++
H14	H-IIAGKN-LLL-NFGAILS-OH		+	+	+							+++
H15	H-IIAGKN-KKK-NFGAILS-OH				-		-				-	+/-
H19	H-IIAGKN-K(Ac)K(Ac)K(Ac)-NFGAILS-OH	-	+	+	+		+					+++
H17	H-IIAGKN-EEE-NFGAILS-OH						-				-	++

3.2.4 Other combinations of the segments A β (27-32) and IAPP(22-28)

To additionally verify the amyloidogenic potential of the two sequences NFGAILS and NKGAI compared to each other as well as the influence of the linker region, peptides consisting of either twice NFGAILS or twice NKGAI that are connected with LLL, Aoc or KKK were synthesized and studied.

3.2.4.1 H-NFGAILS-LLL-NFGAILS-OH (CB1)

The first peptide tested consisted of twice the sequence NFGAILS with a hydrophobic connecting element consisting of three leucines.

Similar to the other peptides with hydrophobic connecting elements, H-NFGAILS-LLL-NFGAILS-OH displayed a β -sheet structure in far-UV CD experiments (Fig. 271A) similar to H-NKGAI-LLL-NFGAILS-OH (Fig. 225A). A clear signal loss indicating the formation of oligomers appeared at a peptide concentration of 20 μ M.

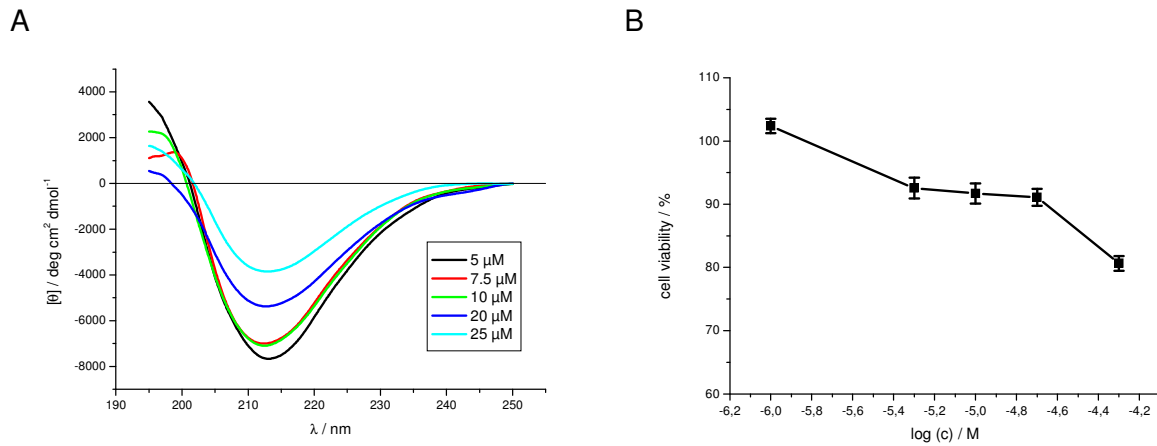


Fig. 271: (A) Far-UV CD spectra of H-NFGAILS-LLL-NFGAILS-OH at different concentrations in 1x 1% HFIP, pH 7.4. (B) Cell viability assay of an aged solution of H-NFGAILS-LLL-NFGAILS-OH (5 mM in 1x 1% HFIP, pH 7.4 for 4 days) using PC-12 cells. Data are percentages of control and are the mean (+/-SEM) of three independent experiments with each experiment performed in multiple replicates (n = 3).

H-NFGAILS-LLL-NFGAILS-OH proved to be medium toxic to PC-12 cells (Fig. 271B) and started forming fibrils at a concentration of 10 μM as indicated by ThT binding assays at different peptide concentrations (Fig. 272A).

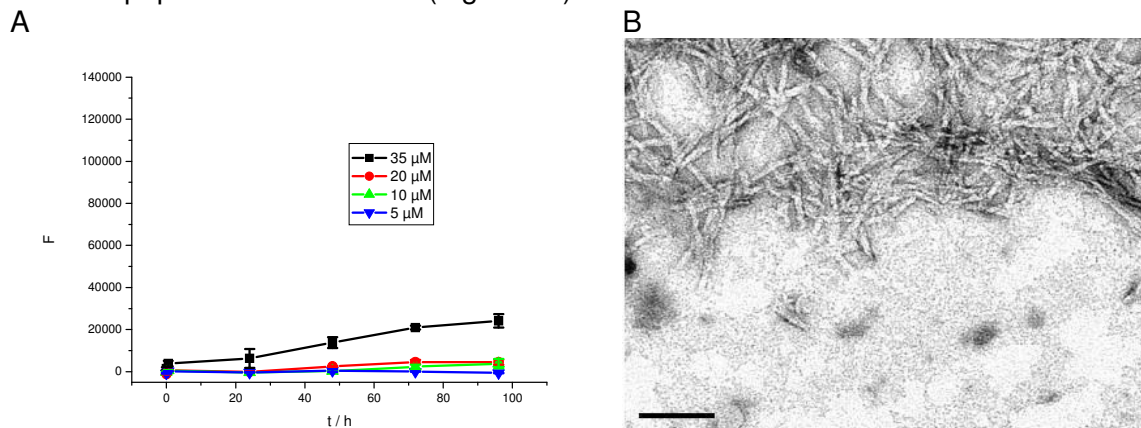


Fig. 272: (A) ThT binding assays of H-NFGAILS-LLL-NFGAILS-OH at different concentrations in 1x 1% HFIP, pH 7.4. Data are means of 3 assays after subtraction of buffer values +/- standard error of the mean (SEM) with each experiment performed in multiple replicates (n = 3). (B) TEM picture of an aged incubation of H-NFGAILS-LLL-NFGAILS-OH. The peptide was incubated at 500 μM for 7 d in 1x 1% HFIP, pH 7.4. Scale bar: 100 nm.

This fibril forming potential was verified by both Congo Red staining (Fig. 273A and B) and TEM imaging (Fig. 272B). The TEM picture of an aged incubation of H-NFGAILS-LLL-NFGAILS-OH showed the presence of many fibrils that were tightly packed together.

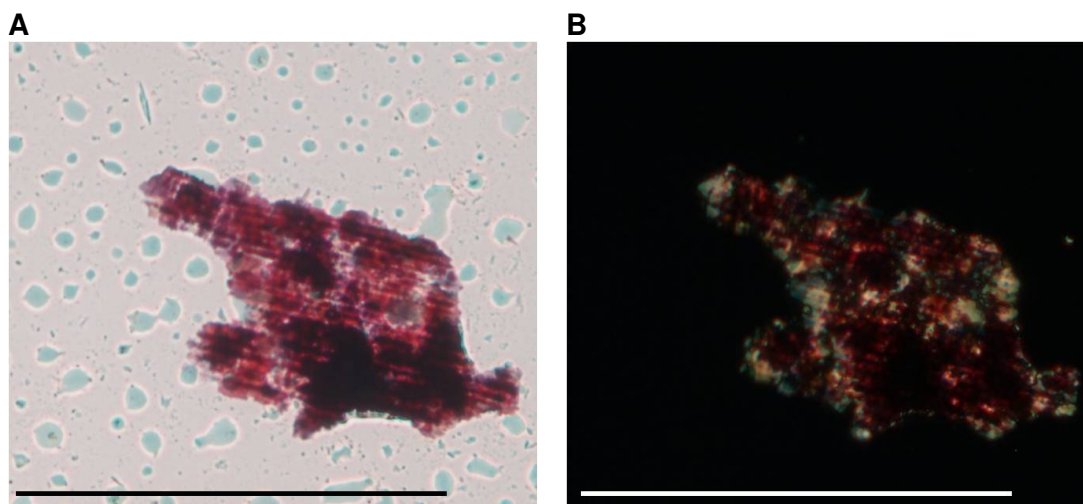


Fig. 273: Microscopic examination of an aged incubation of H-NFGAILS-LLL-NFGAILS-OH stained with Congo Red. The peptide was incubated at a concentration of 1 mM in 1x 1% HFIP, pH 7.4 for 3 days. Pictures were taken under A normal and B cross-polarized light. Scale bar: 100 μm .

3.2.4.2 H-NKGAI-LLL-NKGAI-OH (CB3)

The main conformation expressed by H-NKGAI-LLL-NKGAI-OH in CD spectra is random coil (Fig. 274A) as they displayed a strong negative signal at 195 nm but also a rather broad negative bulge at 215-225 nm indicating the presence of β -sheet and β -turn elements. The signal intensity decreased intensely between a peptide concentration of 10 μM and 20 μM . This was a strong indication for peptide aggregation and the formation of oligomers. For comparison, H-NKGAI-LLL-NFGAILS-OH (Fig. 225A) and H-NFGAILS-LLL-NFGAILS-OH (Fig. 271A) displayed mainly β -sheet structure in CD. As mentioned before, the connecting element LLL seems to be a strong β -sheet inducer. But obviously the peptide segment NKGAI ($\text{A}\beta(27-32)$) does not adapt a β -sheet structure as NFGAILS (IAPP(22-28)) in the context of the linked structures studied here.

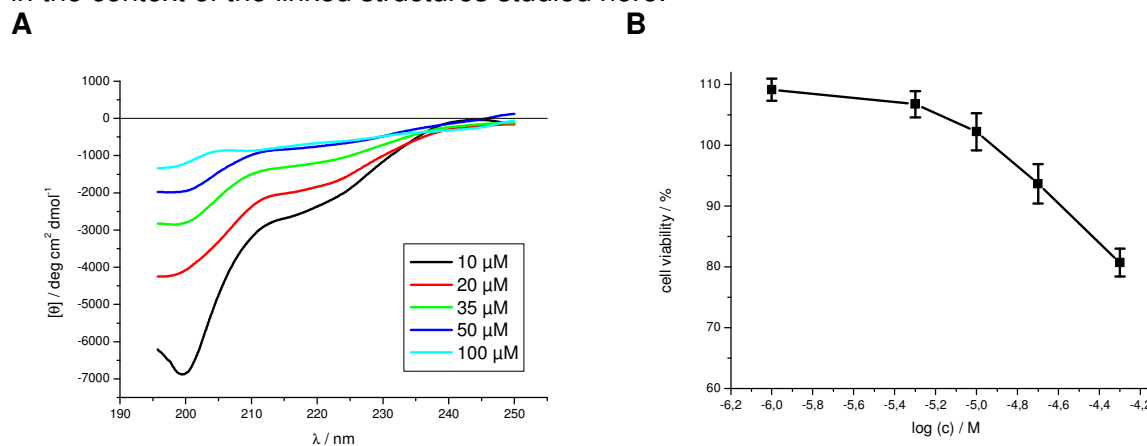


Fig. 274: (A) Far-UV CD spectra of H-NKGAI-LLL-NKGAI-OH at different concentrations in 1x 1% HFIP, pH 7.4.

(B) Cell viability assay of an aged solution of H-NKGAI-LLL-NKGAI-OH (5 mM in 1x 1% HFIP, pH 7.4 for 4 days) using PC-12 cells. Data are percentages of control and are the mean (+/-SEM) of three independent experiments with each experiment performed in multiple replicates ($n = 3$).

Like the other peptides containing LLL as connecting motif, H-NKGAI-LLL-NKGAI-OH proved to be toxic to PC-12 cells (Fig. 274B).

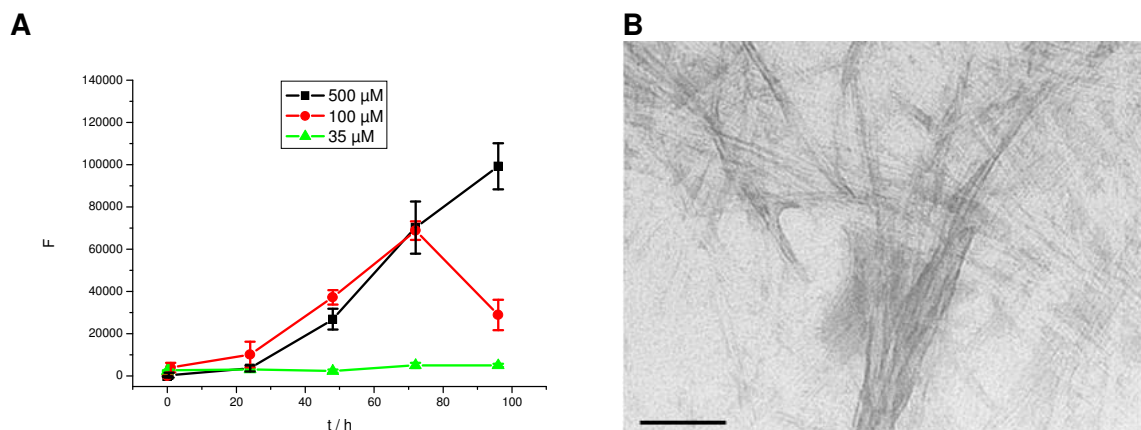


Fig. 275: (A) ThT binding assays of H-NKGAI-LLL-NKGAI-OH at different concentrations in 1xb 1% HFIP, pH 7.4. Data are means of 3 assays after subtraction of buffer values +/- standard error of the mean (SEM) with each experiment performed in multiple replicates (n = 3).

(B) TEM picture of an aged incubation of H-NKGAI-LLL-NKGAI-OH. The peptide was incubated at 500 μM for 7 d in 1xb 1% HFIP, pH 7.4. Scale bar: 100 nm.

However, H-NKGAI-LLL-NKGAI-OH displayed a weaker fibril forming potential compared to H-NKGAI-LLL-NFGAILS-OH (Fig. 226A) and H-NFGAILS-LLL-NFGAILS-OH (Fig. 272A). Only at a peptide concentration of 100 μM, the ThT assays of H-NKGAI-LLL-NKGAI-OH showed an increase in the fluorescence signal of ThT (Fig. 275A).

TEM images of an aged incubation of H-NKGAI-LLL-NFGAILS-OH at a peptide concentration of 50 μM showed the presence of many fibrils that were partially clumped together (Fig. 275B).

Staining of fibrillar aggregates of H-NKGAI-LLL-NKGAI-OH with Congo Red also indicated the presence of amyloid fibrils. Stained aggregates showed intense red color under normal light (Fig. 276A) and displayed in part green birefringence under cross-polarized light (Fig. 276B).

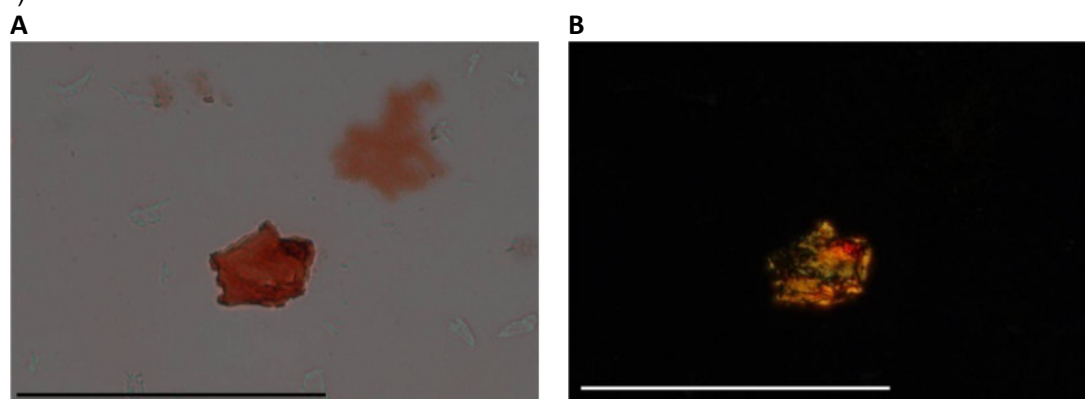


Fig. 276: Microscopic examination of an aged incubation of H-NKGAI-LLL-NKGAI-OH stained with Congo Red. The peptide was incubated at a concentration of 1 mM in 1xb 1% HFIP, pH 7.4 for 3 days. Pictures were taken under A normal and B cross-polarized light. Scale bar: 100 μm.

3.2.4.3 H-NFGAILS-Aoc-NFGAILS-OH (CB5)

Concentration dependent far-UV CD experiments of H-NFGAILS-Aoc-NFGAILS-OH showed β-sheet structure (Fig. 277A). Compared to H-NKGAI-Aoc-NFGAILS-OH (Fig. 207A), the β-sheet signal intensity was lower and slightly shifted towards higher wavelengths for H-NFGAILS-Aoc-NFGAILS-OH.

Similar to H-NKGAI-Aoc-NFGAILS-OH (Fig 207A), the far-UV CD spectra of H-NFGAILS-Aoc-NFGAILS-OH (Fig. 277A) displayed a minimum at around 200 nm indicating the

presence of random coil structure at a peptide concentration of 3 μM . At a concentration of 5 μM the signal indicated no random coil structure anymore but its shape suggested the presence of β -sheet structure. The signal intensity already started to decrease at a peptide concentration of 10 μM which was indicative of a higher aggregation potential as compared to H-NKGAIL-Aoc-NFGAILS-OH (Fig. 207A).

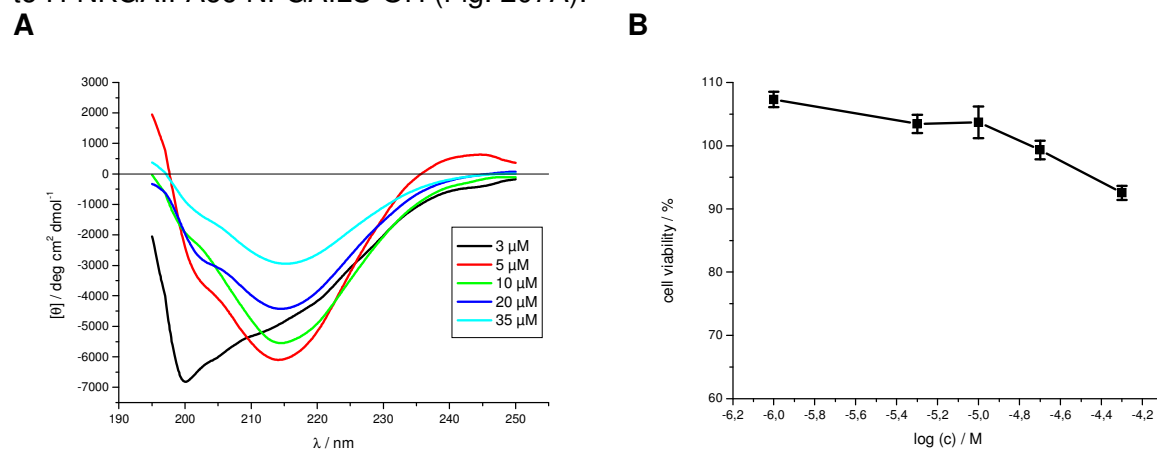


Fig. 277: A) Far-UV CD spectra of H-NFGAILS-Aoc-NFGAILS-OH at different concentrations in 1x 1% HFIP, pH 7.4.

B) Cell viability assay of an aged solution of H-NFGAILS-Aoc-NFGAILS-OH (5 mM in 1x 1% HFIP, pH 7.4 for 4 days) using PC-12 cells. Data are percentages of control and are the mean (+/-SEM) of three independent experiments with each experiment performed in multiple replicates (n = 3).

Aged H-NFGAILS-Aoc-NFGAILS-OH solutions proved to be only weakly toxic to PC-12 cells (Fig. 277B) while the ThT binding assays showed that it started forming fibrils already at a peptide concentration of 20 μM (Fig. 278A).

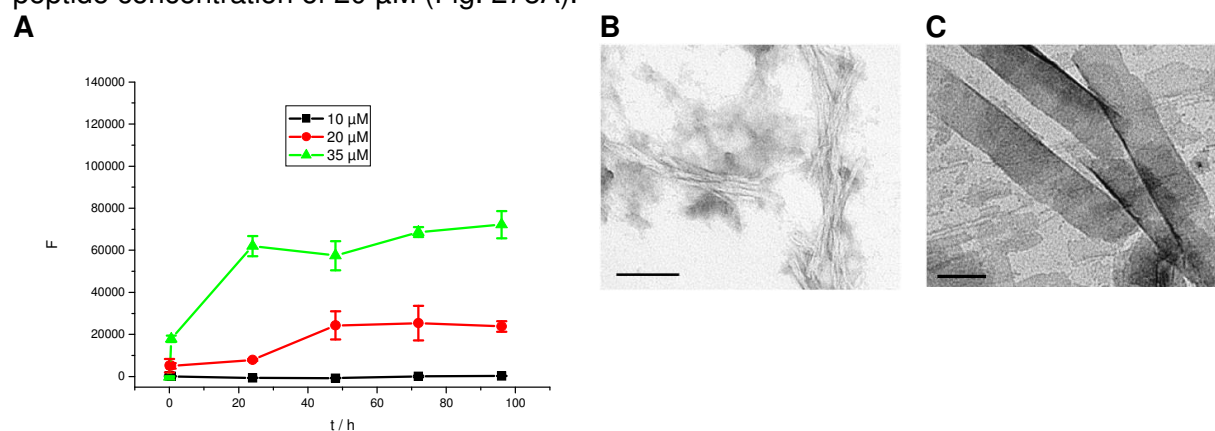


Fig. 278: (A) ThT binding assays of H-NFGAILS-Aoc-NFGAILS-OH at different concentrations in 1x 1% HFIP, pH 7.4. Data are means of 3 assays after subtraction of buffer values +/- standard error of the mean (SEM) with each experiment performed in multiple replicates (n = 3).

(B) TEM picture of an aged incubation of H-NFGAILS-Aoc-NFGAILS-OH. The peptide was incubated at 50 μM for 7 d in 1x 1% HFIP, pH 7.4. Scale bar: 100 nm.

(C) TEM picture of an aged incubation of H-NFGAILS-Aoc-NFGAILS-OH. The peptide was incubated at 500 μM for 7 d in 1x 1% HFIP, pH 7.4. Scale bar: 100 nm.

Fibril formation ability was verified by Congo Red staining studies (Fig. 279A and B) and TEM imaging of an aged incubations. At a peptide concentration of 50 μM , the TEM grid showed the presence of many fibrils (Fig. 278B) and at a peptide concentration of 500 μM , the TEM image even displayed large nanotubes (Fig. 278C).

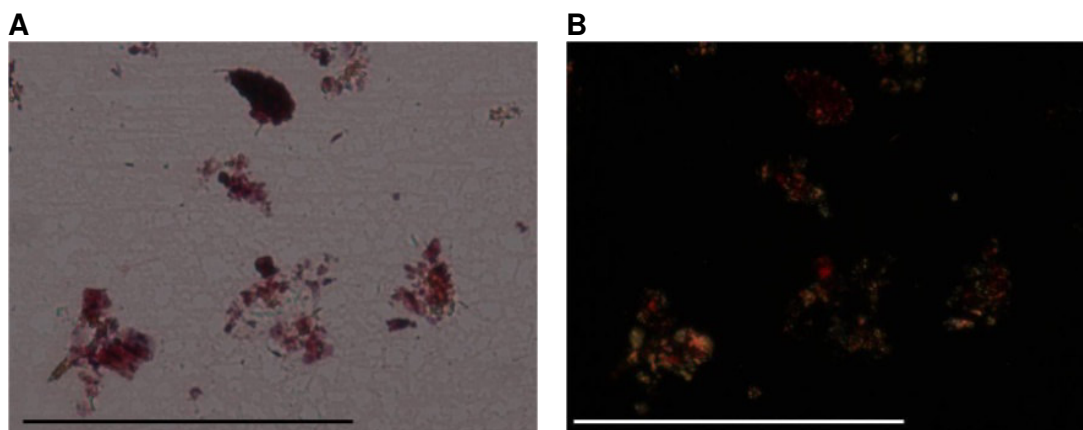


Fig. 279: Microscopic examination of an aged incubation of H-NFGAILS-Aoc-NFGAILS-OH stained with Congo Red. The peptide was incubated at a concentration of 1 mM in 1xb 1% HFIP, pH 7.4 for 3 days. Pictures were taken under A normal and B cross-polarized light. Scale bar: 100 μm .

3.2.4.4 H-NKGAI-Aoc-NKGAI-OH (CB6)

CD spectra of H-NKGAI-Aoc-NKGAI-OH (Fig. 280A) displayed a strong negative signal at 195 nm indicating random coil structure and a broad negative bulge at 210-230 nm indicating the presence of β -sheet and β -turn elements. These spectra are reminiscent to the spectra of H-NKGAI-Aoc-NFGAILS- β A-KKK-OH (Fig. 210) that displayed a similar shape and intensity of the signal.

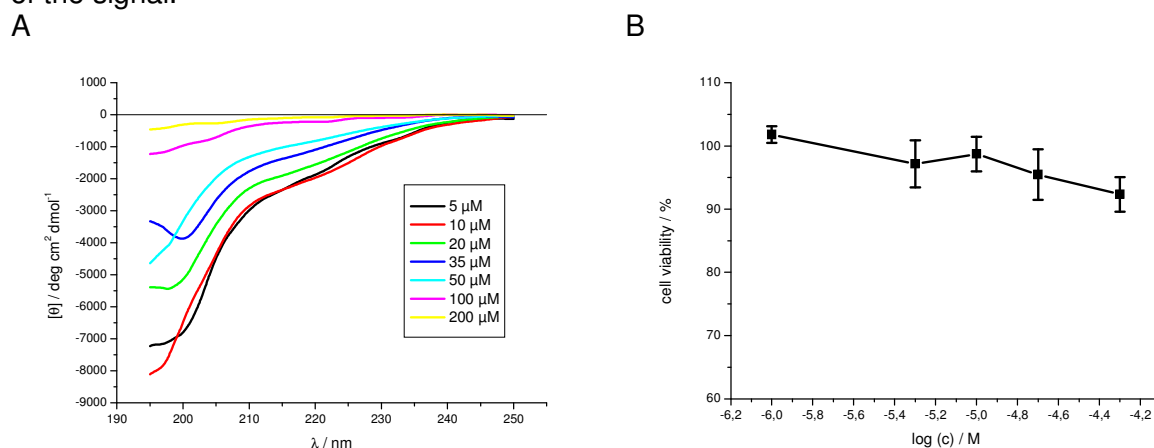


Fig. 280: (A) Far-UV CD spectra of H-NKGAI-Aoc-NKGAI-OH at different concentrations in 1xb 1% HFIP, pH 7.4.

(B) Cell viability assay of an aged solution of H-NKGAI-Aoc-NKGAI-OH (5 mM in 1xb 1% HFIP, pH 7.4 for 4 days) using PC-12 cells. Data are percentages of control and are the mean (\pm SEM) of three independent experiments with each experiment performed in multiple replicates ($n = 3$).

Cell viability assays revealed that H-NKGAI-Aoc-NKGAI-OH was only weakly toxic to PC-12 cells (Fig. 280B) while ThT binding assays revealed that H-NKGAI-Aoc-NKGAI-OH was not able to form fibrils until up to a concentration of 500 μM under (Fig. 281A). TEM imaging of a solution of H-NKGAI-Aoc-NKGAI-OH at a peptide concentration of 500 μM also confirmed the above findings (Fig. 281B).

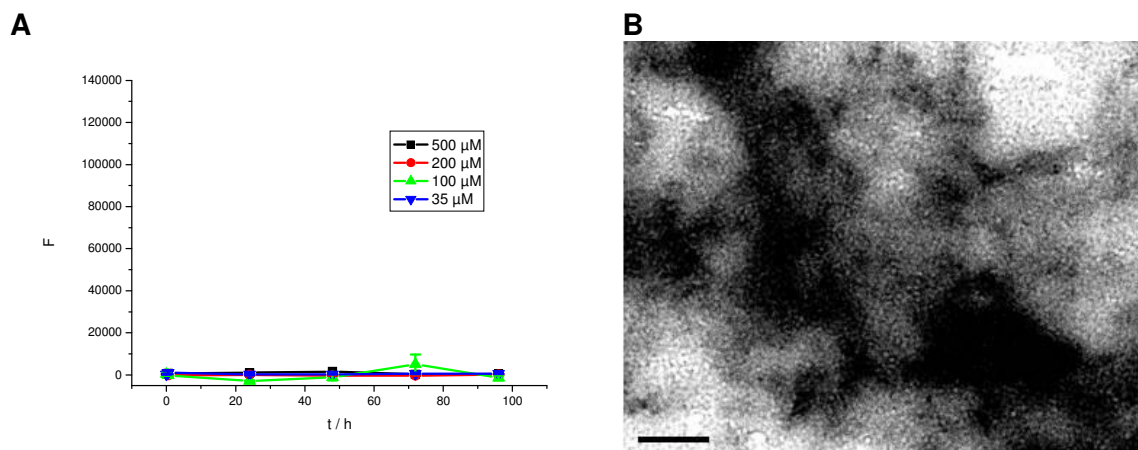


Fig. 281: (A) ThT binding assays of H-NKGAI-Aoc-NKGAI-OH at different concentrations in 1xb 1% HFIP, pH 7.4. Data are means of 3 assays after subtraction of buffer values +/- standard error of the mean (SEM) with each experiment performed in multiple replicates (n = 3). (B) TEM picture of an aged incubation of H-NKGAI-Aoc-NKGAI-OH. The peptide was incubated at 500 μM for 7 d in 1xb 1% HFIP, pH 7.4. Scale bar: 100 nm.

Aged aggregates of H-NKGAI-Aoc-NKGAI-OH did not bind Congo Red and thus did not display birefringence under cross-polarized light (Fig. 282B). This was another indication that H-NKGAI-Aoc-NKGAI-OH was not forming amyloid fibrils under the conditions tested.

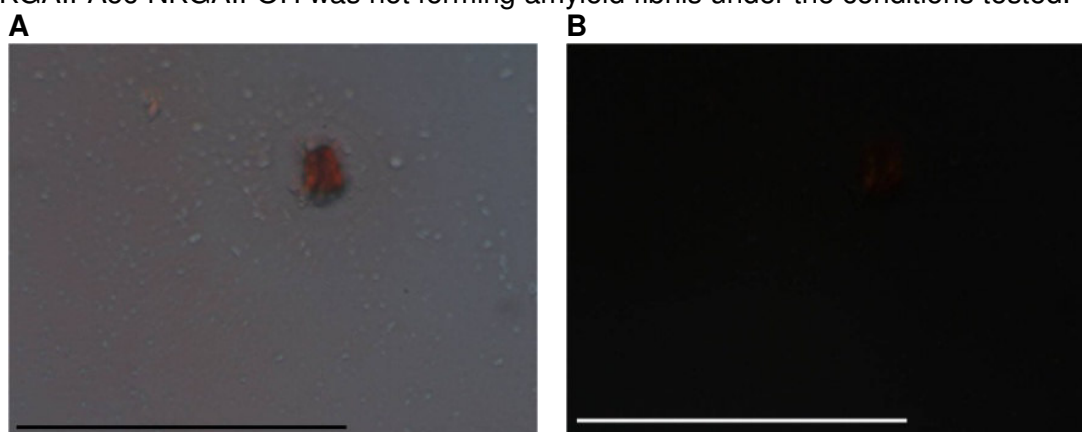


Fig. 282: Microscopic examination of an aged incubation of H-NKGAI-Aoc-NKGAI-OH stained with Congo Red. The peptide was incubated at a concentration of 1 mM in 1xb 1% HFIP, pH 7.4 for 3 days. Pictures were taken under A normal and B cross-polarized light. Scale bar: 100 μm.

3.2.4.5 H-NFGAILS-Aoc-NKGAI-OH (CB7)

As shown in Fig. 283A, CD spectra of H-NFGAILS-Aoc-NKGAI-OH also displayed both random coil and β-sheet structure. The spectra are similar to those of H-NKGAI-Aoc-NKGAI-OH (Fig. 280A).

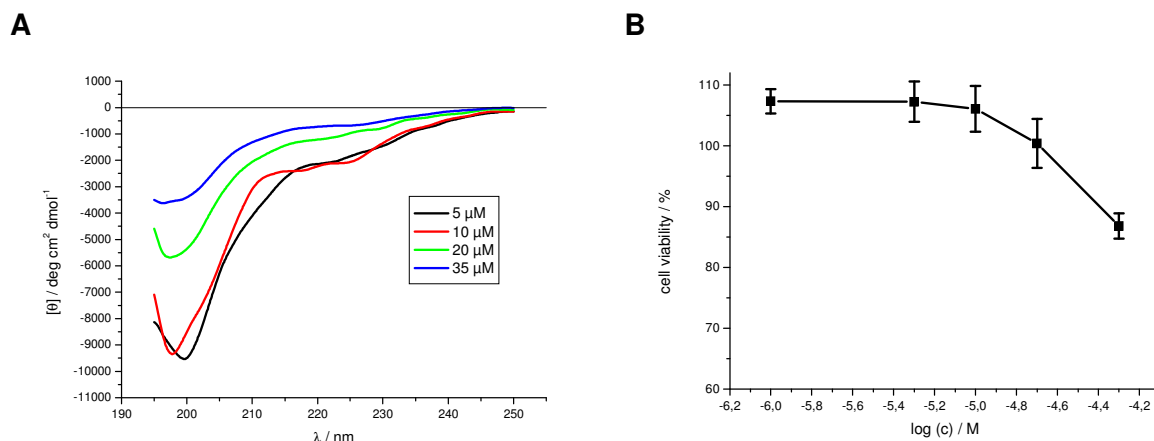


Fig. 283: (A) Far-UV CD spectra of H-NFGAILS-Aoc-NKGAI-OH at different concentrations in 1xb 1% HFIP, pH 7.4.

(B) Cell viability assay of an aged solution of H-NFGAILS-Aoc-NKGAI-OH (5 mM in 1xb 1% HFIP, pH 7.4 for 4 days) using PC-12 cells. Data are percentages of control and are the mean (+/-SEM) of three independent experiments with each experiment performed in multiple replicates (n = 3).

H-NFGAILS-Aoc-NKGAI-OH showed weak toxicity to PC-12 cells (Fig. 283B) similar to H-NKGAI-OH (Fig. 280B) and did not form fibrils as shown by ThT binding assays up to a concentration of 500 μM (Fig. 284A). TEM imaging of an aged solution of H-NFGAILS-Aoc-NKGAI-OH at a peptide concentration of 500 μM showed no fibrils but only amorphous aggregates (Fig. 284B).

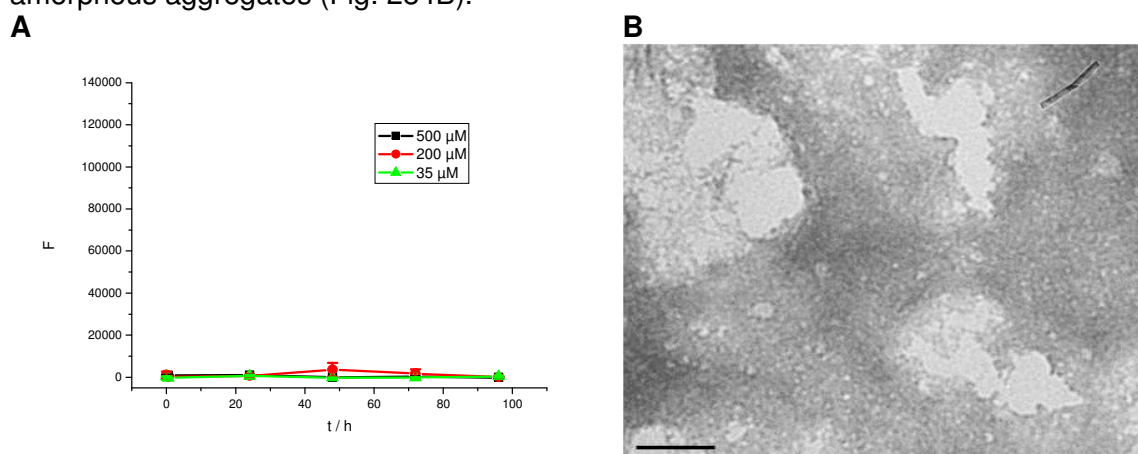


Fig. 284: (A) ThT binding assays of H-NFGAILS-Aoc-NKGAI-OH at different concentrations in 1xb 1% HFIP, pH 7.4. Data are means of 3 assays after subtraction of buffer values +/- standard error of the mean (SEM) with each experiment performed in multiple replicates (n = 3).

(B) TEM picture of an aged incubation of H-NFGAILS-Aoc-NKGAI-OH. The peptide was incubated at 500 μM for 7 d in 1xb 1% HFIP, pH 7.4. Scale bar: 100 nm.

Finally, aged solutions of H-NFGAILS-Aoc-NKGAI-OH also did not bind Congo Red or if bound it showed no birefringence under cross-polarized light (Fig. 285B).

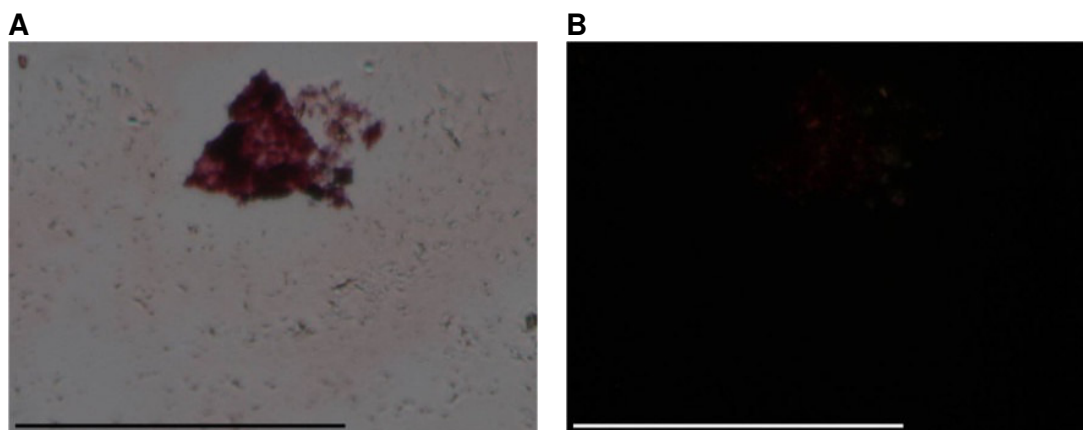


Fig. 285: Microscopic examination of an aged incubation of H-NFGAILS-Aoc-NKGAIL-OH stained with Congo Red. The peptide was incubated at a concentration of 1 mM in 1xb 1% HFIP, pH 7.4 for 3 days. Pictures were taken under A normal and B cross-polarized light. Scale bar: 100 µm.

3.2.4.6 H-NFGAILS-KKK-NFGAILS-OH (CB2)

As a third connecting segment between two NFGAILS sequences, three times Lysine was chosen.

The CD spectra of H-NFGAILS-KKK-NFGAILS-OH (Fig. 286A) displayed mainly a negative signal between 195 and 200 nm indicating random coil structure. A small negative bulge at 210-230 nm indicated the presence of additional structural elements like β -sheets or β -turns. The peptide started to aggregate into soluble oligomers at concentrations higher than 20 µM as indicated by a strong signal loss in the spectra between 20 µM and 35 µM.

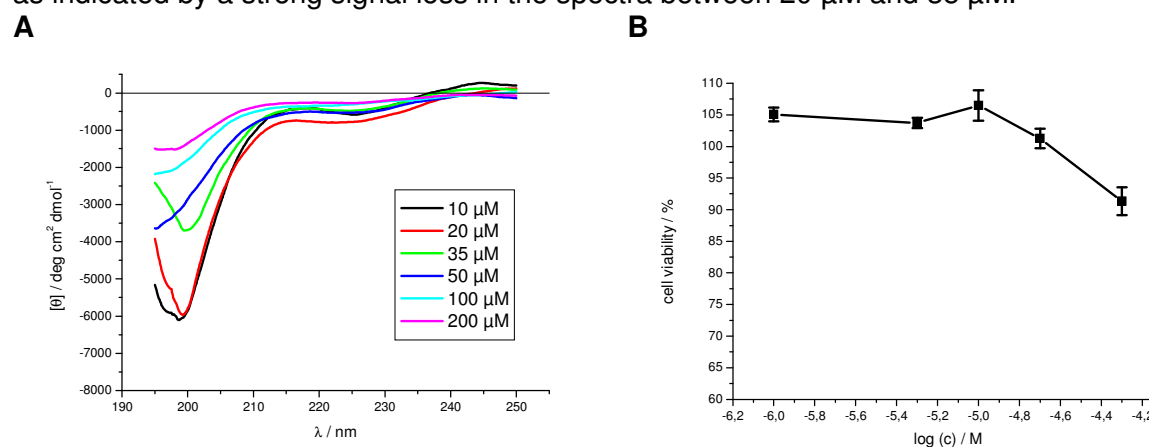


Fig. 286: (A) Far-UV CD spectra of H-NFGAILS-KKK-NFGAILS-OH at different concentrations in 1xb 1% HFIP, pH 7.4.

(B) Cell viability assay of an aged solution of H-NFGAILS-KKK-NFGAILS-OH (5 mM in 1xb 1% HFIP, pH 7.4 for 4 days) using PC-12 cells. Data are percentages of control and are the mean (+/-SEM) of three independent experiments with each experiment performed in multiple replicates (n = 3).

Similar to other peptides with the connecting element KKK, H-NFGAILS-KKK-NFGAILS-OH was only weakly toxic to PC-12 cells (Fig. 286B) and it did not display fibril formation until a peptide concentration of up to 500 µM as seen on Fig. 287A. TEM imaging of an aged incubation of H-NFGAILS-KKK-NFGAILS-OH also did not reveal fibril formation (Fig. 287B). Only amorphous aggregates were observed.

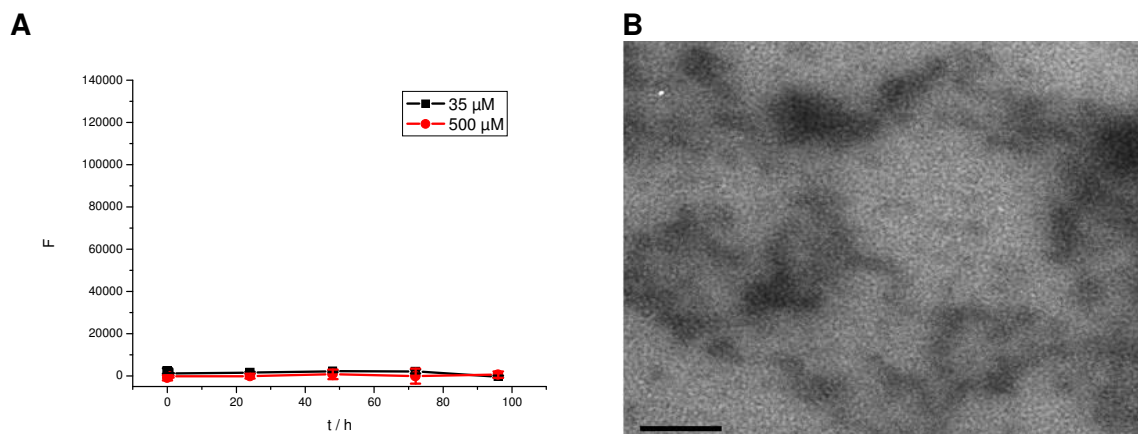


Fig. 287: (A) ThT binding assays of H-NFGAILS-KKK-NFGAILS-OH at different concentrations in 1xb 1% HFIP, pH 7.4. Data are means of 3 assays after subtraction of buffer values \pm standard error of the mean (SEM) with each experiment performed in multiple replicates ($n = 3$).

(B) TEM picture of an aged incubation of H-NFGAILS-KKK-NFGAILS-OH. The peptide was incubated at 500 μ M for 7 d in 1xb 1% HFIP, pH 7.4. Scale bar: 100 nm.

Congo Red stained aggregates of H-NFGAILS-KKK-NFGAILS-OH showed red color under normal light (Fig. 288A) but no birefringence under cross-polarized light at all (Fig. 288B).

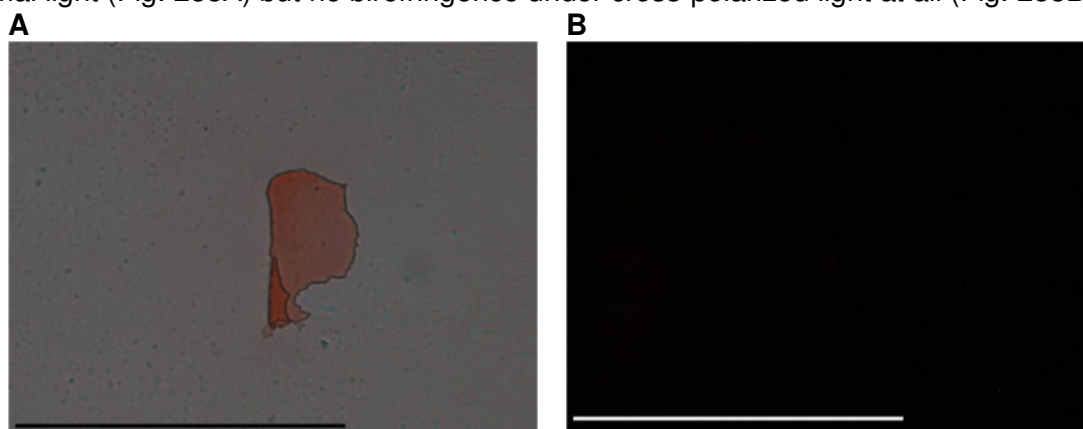


Fig. 288: Microscopic examination of an aged incubation of H-NFGAILS-KKK-NFGAILS-OH stained with Congo Red. The peptide was incubated at a concentration of 1 mM in 1xb 1% HFIP, pH 7.4 for 3 days. Pictures were taken under A normal and B cross-polarized light. Scale bar: 100 μ m.

3.2.4.7 H-NKGAI-KKK-NKGAI-OH (CB4)

The CD spectra of H-NKGAI-KKK-NKGAI-OH displayed mainly a random coil structure as indicative by the negative signal at 195-200 nm. A small negative bulge at 210-230 nm indicated the presence of additional structural elements like β -sheets and β -turns. The peptide started to aggregate at concentrations higher than 10 μ M (Fig. 289A).

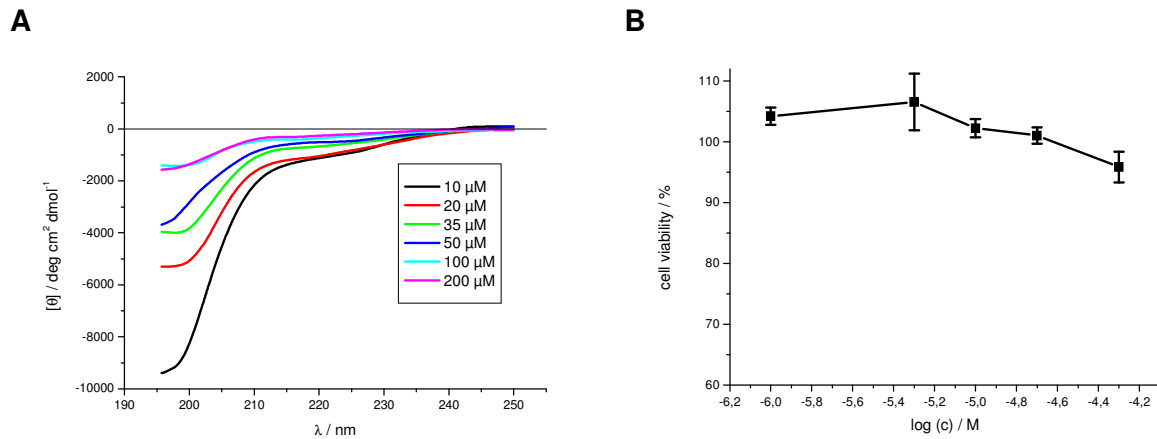


Fig. 289: (A) Far-UV CD spectra of H-NKGAI-KKK-NKGAI-OH at different concentrations in 1x 1% HFIP, pH 7.4. (B) Cell viability assay of an aged solution of H-NKGAI-KKK-NKGAI-OH (5 mM in 1x 1% HFIP, pH 7.4 for 4 days) using PC-12 cells. Data are percentages of control and are the mean (+/-SEM) of three independent experiments with each experiment performed in multiple replicates (n = 3).

H-NKGAI-KKK-NKGAI-OH was found to be non-toxic to PC-12 cells (Fig. 289B) and it did not form fibrils up to a peptide concentration of 500 μM (Fig. 290A). TEM imaging of an incubation of H-NKGAI-KKK-NKGAI-OH at a concentration of 500 μM was also indicative of the presence of amorphous aggregates (Fig. 290B).

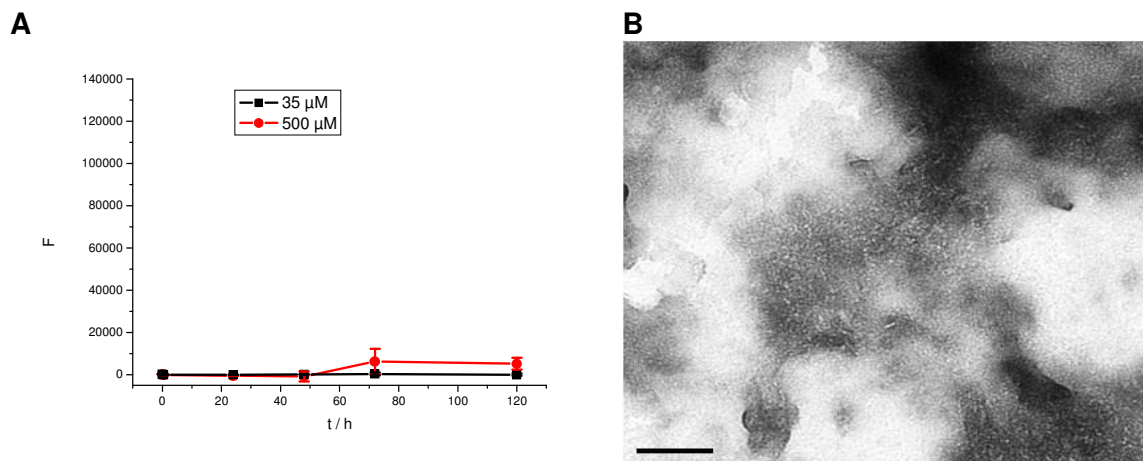


Fig. 290: (A) ThT binding assays of H-NKGAI-KKK-NKGAI-OH at different concentrations in 1x 1% HFIP, pH 7.4. Data are means of 3 assays after subtraction of buffer values +/- standard error of the mean (SEM) with each experiment performed in multiple replicates (n = 3). (B) TEM picture of an aged incubation of H-NKGAI-KKK-NKGAI-OH. The peptide was incubated at 500 μM for 7 d in 1x 1% HFIP, pH 7.4. Scale bar: 100 nm.

Aged incubations of H-NKGAI-KKK-NKGAI-OH only weakly if at all bound Congo Red and showed no sign of birefringence under cross-polarized light (Fig. 291A and B).

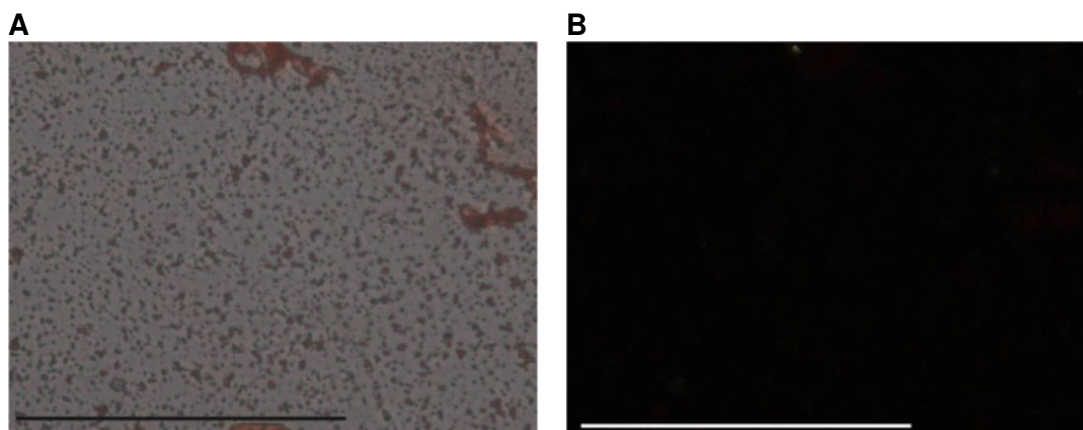


Fig. 291: Microscopic examination of an aged incubation of H-NKGAI-KKK-NKGAI-OH stained with Congo Red. The peptide was incubated at a concentration of 1 mM in 1x 1% HFIP, pH 7.4 for 3 days. Pictures were taken under A normal and B cross-polarized light. Scale bar: 100 μ m.

Table 21: Overview of ThT binding assays and cell viability assays performed with peptides at different concentrations.

Results of “+” indicate fibril formation, whereas “-” indicate no fibril formation within the 5 days of incubation of the solution at the given peptide concentration.

For the cell viability assays, results of “+++” mean high toxicity towards PC-12 cell, “++” means medium toxicity and “+/-” means low to no toxicity. Low toxicity refers to peptides with >90% cell viability, medium toxicity refers to a cell viability between 80% and 90%, and high toxicity refers to a cell viability of <80% for aged incubations at a peptide concentration of 50 μ M.

Abbrev.	Sequence	ThT								Tox.
		5 μ M	10 μ M	20 μ M	35 μ M	100 μ M	200 μ M	350 μ M	500 μ M	
CB1	H-NFGAILS- LLL -NFGAILS-OH	-	+	+	+					+++
CB3	H-NKGAII- LLL -NKGAII-OH				-	+			+	+++
CB5	H-NFGAILS- Aoc -NFGAILS-OH		-	+	+					+/-
CB6	H-NKGAII- Aoc -NKGAII-OH				-	-	-		-	+/-
CB7	H-NFGAILS- Aoc -NKGAII-OH				-		-		-	++
CB2	H-NFGAILS- KKK -NFGAILS-OH				-				-	+/-
CB4	H-NKGAII- KKK -NKGAII-OH				-				-	+/-

3.2.5 Comparisons

3.2.5.1 Influence of the different connecting elements

Similar tendencies were observed in all different groups for segments linked with same connecting elements.

With regard to toxicity, the connecting elements can be classified into three groups: high, medium and low toxicity. Low toxicity refers to peptides with >90% cell viability, medium toxicity refers to a cell viability between 80% and 90%, and high toxicity refers to a cell viability of <80% for aged incubations at a peptide concentration of 50 μ M using PC-12 cells. Peptides with the connecting elements AAA, K(Ac)K(Ac)K(Ac) and LLL displayed high toxicity. Peptides with the connecting elements EEE, GGG, KKK and Peg showed low to almost no toxicity. In the group of peptides that displayed medium toxicity belong the connecting elements Aoc and Adc (Fig 292A and Fig. 293A).

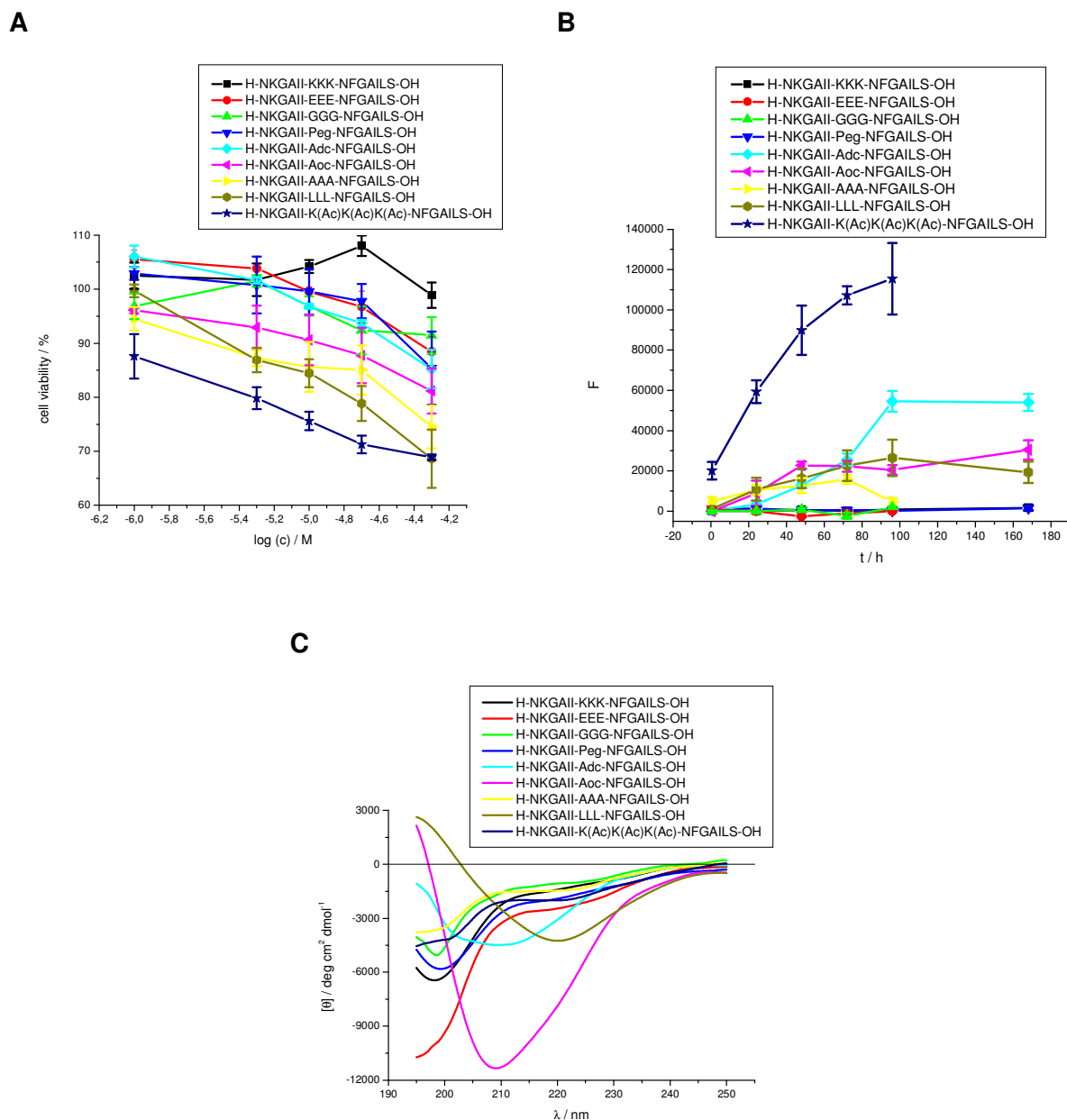


Fig. 292: Comparison of peptides with the sequence H-NKGAI-XXX-NFGAILS-OH.

(A) Cell viability assays of aged solutions of the respective peptide (5 mM in 1x 1% HFiP, pH 7.4 for 4 days) using PC-12 cells. Data are percentages of control and are the mean (+/-SEM) of three independent experiments with each experiment performed in multiple replicates (n = 3).

(B) ThT binding assays at a peptide concentration of 35 μ M in 1x 1% HFiP, pH 7.4, except for H-NKGAI-GGG-NFGAILS-OH and H-NKGAI-EEE-NFGAILS-OH. For these two peptides, ThT binding assays at a peptide concentration of 100 μ M in 1x 1% HFiP, pH 7.4 are shown. Data are means of 3 assays after subtraction of buffer values +/- standard error of the mean (SEM) with each experiment performed in multiple replicates (n = 3).

(C) Far-UV CD spectra at a peptide concentration of 10 μ M in 1x 1% HFiP, pH 7.4.

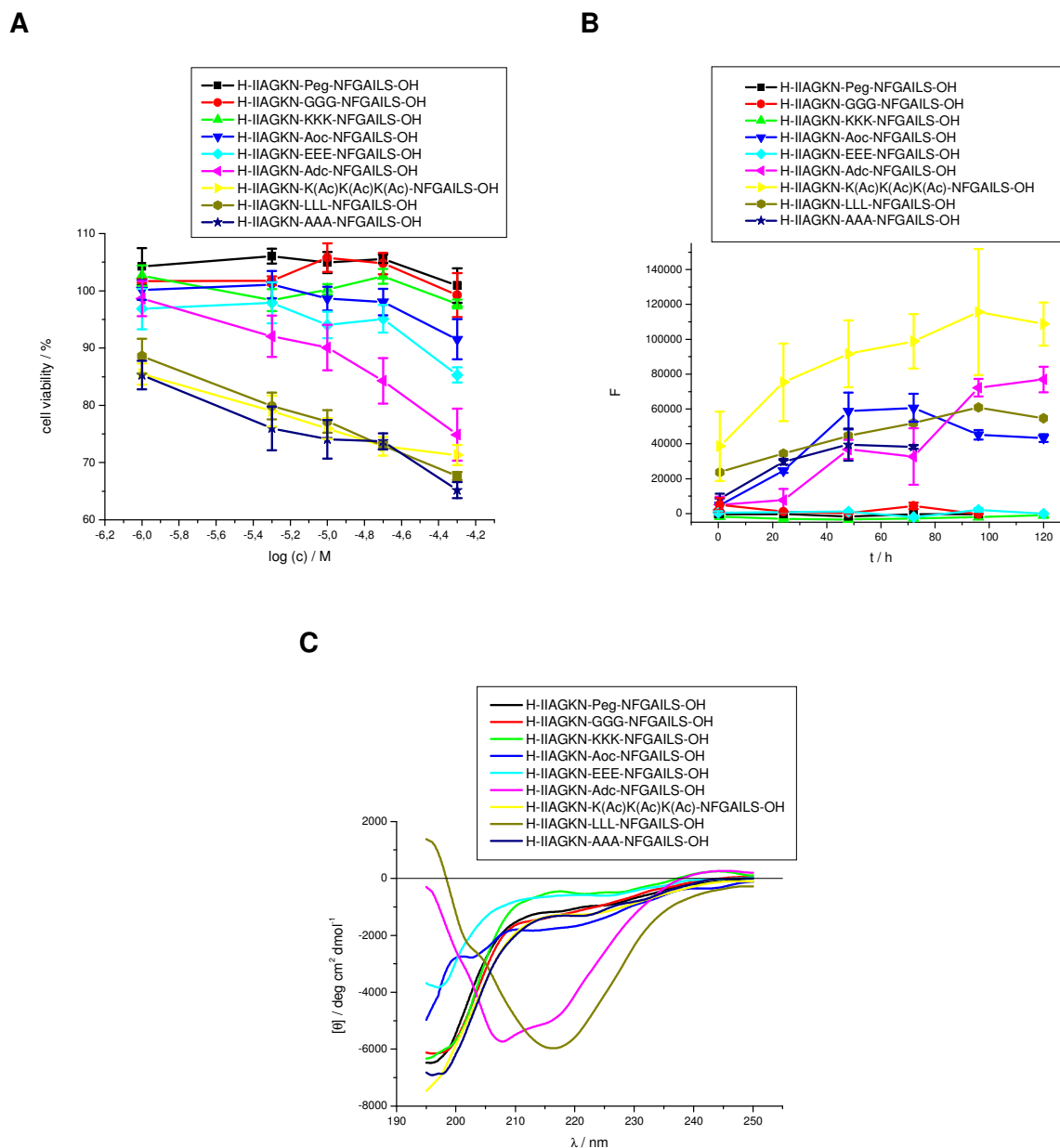


Fig. 293: Comparison of the peptides with the sequence H-IIAGKN-XXX-NFGAILS-OH.

(A) Cell viability assays of aged solutions of the respective peptide (5 mM in 1xb 1% HFIP, pH 7.4 for 4 days) using PC-12 cells. Data are percentages of control and are the mean (+/-SEM) of three independent experiments with each experiment performed in multiple replicates (n = 3).

(B) ThT binding assays at a peptide concentration of 35 μ M in 1xb 1% HFIP, pH 7.4 except for H-IIAGKN-GGG-NFGAILS-OH, H-IIAGKN-EEE-NFGAILS-OH and H-IIAGKN-Peg-NFGAILS-OH. For H-IIAGKN-GGG-NFGAILS-OH and H-IIAGKN-EEE-NFGAILS-OH ThT binding assays at a peptide concentration of 100 μ M in 1xb 1% HFIP, pH 7.4 are shown, for H-IIAGKN-Peg-NFGAILS-OH the ThT binding assay at a peptide concentration of 500 μ M. Data are means of 3 assays after subtraction of buffer values +/- standard error of the mean (SEM) with each experiment performed in multiple replicates (n = 3).

(C) Far-UV CD spectra at a peptide concentration of 10 μ M in 1xb 1% HFIP, pH 7.4.

Peptides with hydrophilic and charged connecting elements were not able to form amyloid fibrils under the conditions tested whereas peptides with hydrophobic connecting elements displayed high fibril forming potentials (Fig. 292B and 293B).

Only peptides with a hydrophobic connecting element like Aoc, Adc and LLL showed β -sheet structures in CD. Peptides with other connecting elements showed mainly random coil structure and only weak β -sheet and β -turn content (Fig. 292C and 293C).

In general, a flexible backbone structure seemed to be rather disadvantageous for fibril formation and toxicity. Peptides with a flexible connecting element like Peg or GGG displayed low fibril forming potential and toxicity. Only peptides with Aoc or Adc as connecting element displayed high fibril forming potentials and were toxic to PC-12 cells. This could be due to the hydrophobicity of these residues rather than due to their flexibility.

The here studied hydrophobic connecting elements Aoc, Adc, and LLL not only promoted toxicity and fibril formation but were also able to induce β -sheet formation. A more detailed discussion about the features and abilities of the hydrophobic motifs LLL and Aoc is presented below.

Charged connecting motifs (KKK and EEE) were also disadvantageous for fibril formation and toxicity. Both positive and negative charges rather disturbed fibril formation due to electrostatic repulsion. CD spectra of peptides with charged connecting motifs displayed mainly random coil structure. This was an additional hint that charges disrupted the formation of ordered structures.

The connecting element AAA also displayed strong fibril forming potential and toxicity, especially when compared to the connecting element GGG.

Alanine residues are less flexible than glycine ones. Additionally, alanine contains a small hydrophobic side chain. This hydrophobicity was albeit not strong enough to induce clear β -sheet conformation as shown by CD studies.

The segment K(Ac)K(Ac)K(Ac) represents a polar connecting motif and some features of the the side chain are reminiscent of glutamine. Aggregation of polyglutamine sequences is involved in neurodegenerative diseases like Huntington's disease[156, 157]. It is interesting that removing the charge in the side chain of lysine and replacing it with a polar group by simply acetylating the side chain leads to such a big difference in toxicity and fibril forming potential. This was also another prove that charges were rather disadvantageous for aggregation and the formation of fibrils.

The backbone structures of the connecting elements that displayed the most toxic and fibrillogenic behaviour, LLL, AAA and K(Ac)K(Ac)K(Ac), were all constrained peptide bonds. A rather rigid structure with less conformational freedom obviously favoured amyloid structures. In addition the ability to form intermolecular backbone hydrogen bonds between peptides also in the area of the connecting element might be important for the formation of amyloid structures by the different peptides.

Table 22: Overview of ThT binding assays and cell viability assays performed with peptides containing different connecting elements.

Results of “+” indicate fibril formation, whereas “-” indicate no fibril formation within the 5 days of incubation of the solution at the given peptide concentration.

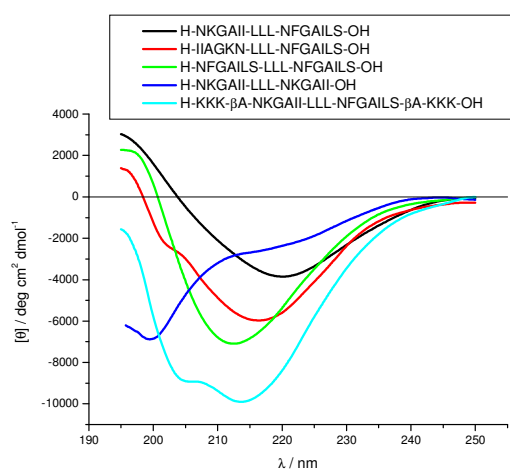
For the cell viability assays, results of “+++” mean high toxicity towards PC-12 cell, “++” means medium toxicity and “+/-” means low to no toxicity. Low toxicity refers to peptides with >90% cell viability, medium toxicity refers to a cell viability between 80% and 90%, and high toxicity refers to a cell viability of <80% for aged incubations at a peptide concentration of 50 μ M.

Abbrev.	Sequence	ThT											Tox.	
		1 μ M	5 μ M	10 μ M	20 μ M	35 μ M	50 μ M	100 μ M	200 μ M	350 μ M	500 μ M	1 mM		
H5	H-NKGAII-Peg-NFGAILS-OH					-	-					+		++
H5a	H-NKGAII-Aoc-NFGAILS-OH		-	+	+	+	+							++
H5aK3	H-NKGAII-Aoc-NFGAILS- β A-KKK-OH					-	+	+						
H5aK6	H-KKK- β A-NKGAII-Aoc-NFGAILS- β A-KKK-OH							-	+	+	+			++
H5b	H-NKGAII-Adc-NFGAILS-OH			+		+		+						++
H16	H-NKGAII-GGG-NFGAILS-OH							-	+			+		+/-
H18	H-NKGAII-AAA-NFGAILS-OH			-	+	+	+	+						+++
H12	H-NKGAII-LLL-NFGAILS-OH			-	+	+	+							+++
H12K6	H-KKK- β A-NKGAII-LLL-NFGAILS- β A-KKK-OH				+	+		+						+++
H13	H-NKGAII-KKK-NFGAILS-OH					-						-	-	+/-
H20	H-NKGAII-K(Ac)K(Ac)K(Ac)-NFGAILS-OH	-	+	+	+	+								+++
H22	H-NKGAII-EEE-NFGAILS-OH							-				-		+/-
H6	H-IIAGKN-Peg-NFGAILS-OH											-		+/-
H6a	H-IIAGKN-Aoc-NFGAILS-OH			-	+	+		+						++
H6b	H-IIAGKN-Adc-NFGAILS-OH			+		+								+++
H24	H-IIAGKN-GGG-NFGAILS-OH							-	-			-		+/-
H23	H-IIAGKN-AAA-NFGAILS-OH		-	-	-	+	+							+++
H14	H-IIAGKN-LLL-NFGAILS-OH			+	+	+								+++
H15	H-IIAGKN-KKK-NFGAILS-OH					-		-				-		+/-
H19	H-IIAGKN-K(Ac)K(Ac)K(Ac)-NFGAILS-OH		-	+	+	+		+						+++

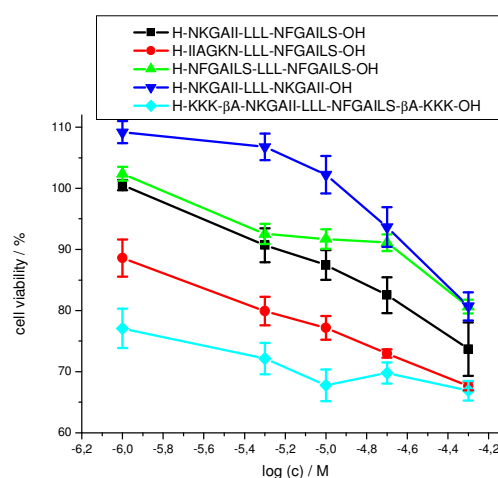
3.2.5.2 Peptides with the connecting element LLL

The hydrophobic connecting element LLL was found to be highly effective in inducing β -sheet structure, amyloidogenicity and toxicity.

A



B



C

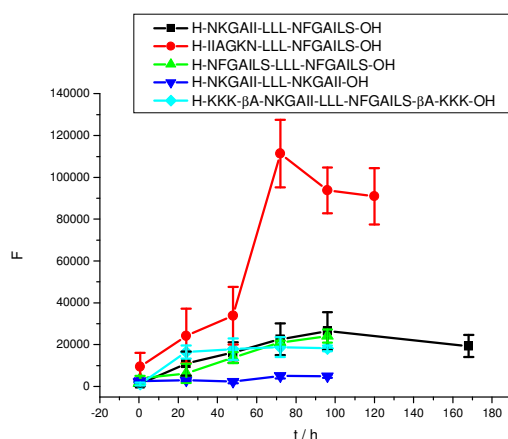


Fig. 294: (A) Far-UV CD spectra of peptides with LLL as a connecting element at a peptide concentration of 10 μM in 1xb 1% HFIP, pH 7.4.

(B) Cell viability assays of aged solutions of peptides with LLL as a connecting element (5 mM in 1xb 1% HFIP, pH 7.4 for 4 days) using PC-12 cells. Data are percentages of control and are the mean (+/-SEM) of three independent experiments with each experiment performed in multiple replicates (n = 3).

(C) ThT binding assays of peptides with LLL as a connecting element at a peptide concentration of 35 μM in 1xb 1% HFIP, pH 7.4. Data are means of 3 assays after subtraction of buffer values +/- standard error of the mean (SEM) with each experiment performed in multiple replicates (n = 3).

Peptides containing the motif LLL displayed these features independent from the adjacent sequences at the C- or N-terminus. The effect of LLL was however less dominant in the case of H-NKGAI-LLL-NKGAI-OH which indicated the influence of the sequence and not only of the connecting motif. Except for H-NKGAI-LLL-NKGAI-OH all peptides with the connecting element LLL displayed clear β -sheet structure in CD (Fig. 294A) and were highly toxic (Fig. 294B) and amyloidogenic (Fig. 294C and table 23). Even the addition of C- and N-terminal lysine residues to improve solubility did not disrupt these features.

Table 23: Results of ThT binding assays of all peptides with LLL as a connecting element at different peptide concentrations.

Results of "+" indicate fibril formation, whereas "-" indicate no fibril formation within the 5 days of incubation of the solution at the given peptide concentration.

For the cell viability assays, results of "+++" mean high toxicity towards PC-12 cell, "++" means medium toxicity and "+/-" means low to no toxicity. Low toxicity refers to peptides with >90% cell viability, medium toxicity refers to a cell viability between 80% and 90%, and high toxicity refers to a cell viability of <80% for aged incubations at a peptide concentration of 50 μM .

Abbrev.	Sequence	ThT									Tox.
		5 μM	10 μM	20 μM	35 μM	50 μM	100 μM	200 μM	350 μM	500 μM	
H12	H-NKGAI-LLL-NFGAILS-OH		-	+	+						+++
H12K6	H-KKK- β A-NKGAI-LLL-NFGAILS- β A-KKK-OH			+	+		+				+++
H14	H-IIAGKN-LLL-NFGAILS-OH		+	+	+						+++
CB1	H-NFGAILS-LLL-NFGAILS-OH	-	+	+	+						+++
CB3	H-NKGAI-LLL-NKGAI-OH				-	+				+	+++

An interesting candidate for future studies would be the peptide with the sequence H-NFGAILS-LLL-NKGAI-OH to further investigate the ability of the connecting element LLL to induce the formation of β -sheet structure and amyloid fibrils.

3.2.5.3 Peptides with the connecting element Aoc

One of the applied connecting elements was Aoc (8-aminooctanoic acid). Aoc is a hydrophobic, flexible motif with an overall length similar to that of a tripeptide sequence. It was therefore used as a non-peptidic linker instead of a tripeptide sequence.

Similar to LLL, the connecting element Aoc was also found to be able to induce the formation of β -sheet structure and fibrils. Compared to the effect of the connecting sequence LLL this effect of Aoc was weaker. Peptides with this connecting element mainly displayed β -sheet formation and a high fibril forming potential if there was the sequence NFGAILS C-terminally adjacent to Aoc (Fig. 295).

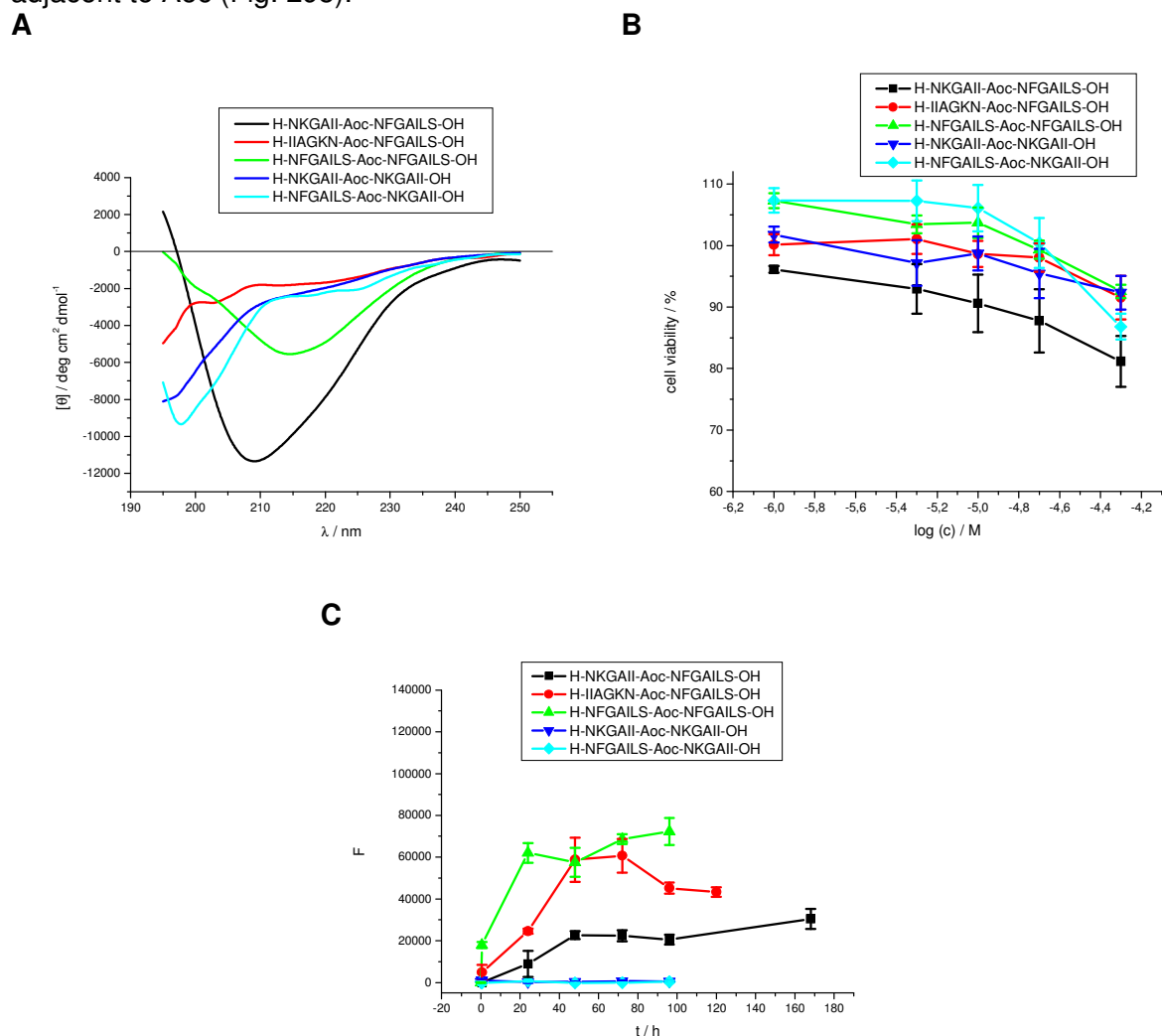


Fig. 295: (A) Far-UV CD spectra of peptides with Aoc as a connecting element at a peptide concentration of 10 μ M in 1xb 1% HFIP, pH 7.4.

(B) Cell viability assays of aged solutions of peptides with Aoc as a connecting element (5 mM in 1xb 1% HFIP, pH 7.4 for 4 days) using PC-12 cells. Data are percentages of control and are the mean (+/-SEM) of three independent experiments with each experiment performed in multiple replicates (n = 3).

(C) ThT binding assays of peptides with Aoc as a connecting element at a peptide concentration of 35 μ M in 1xb 1% HFIP, pH 7.4. Data are means of 3 assays after subtraction of buffer values +/- standard error of the mean (SEM) with each experiment performed in multiple replicates (n = 3).

The addition of lysines at the C- and N-terminus of H-NKGAIL-Aoc-NFGAILS-OH also seemed to interfere with the β -sheet structure of the monomer as indicated by the CD spectra of these peptides. The spectra of H-KKK- β A-NKGAIL-Aoc-NFGAILS- β A-KKK-OH were characterized by a loss of intensity of the negative signal at around 210 nm of H-NKGAIL-

Aoc-NFGAILS-OH which correlated with an appearance of a negative signal at around 195 nm indicating random coil structure. This indicated a structural change from mainly β -sheet for H-NKGAI-Aoc-NFGAILS-OH towards a more unordered structure in H-KKK- β A-NKGAI-Aoc-NFGAILS- β A-KKK-OH. The core region however remained unchanged indicating that this region was responsible for the foundation of β -sheet structure.

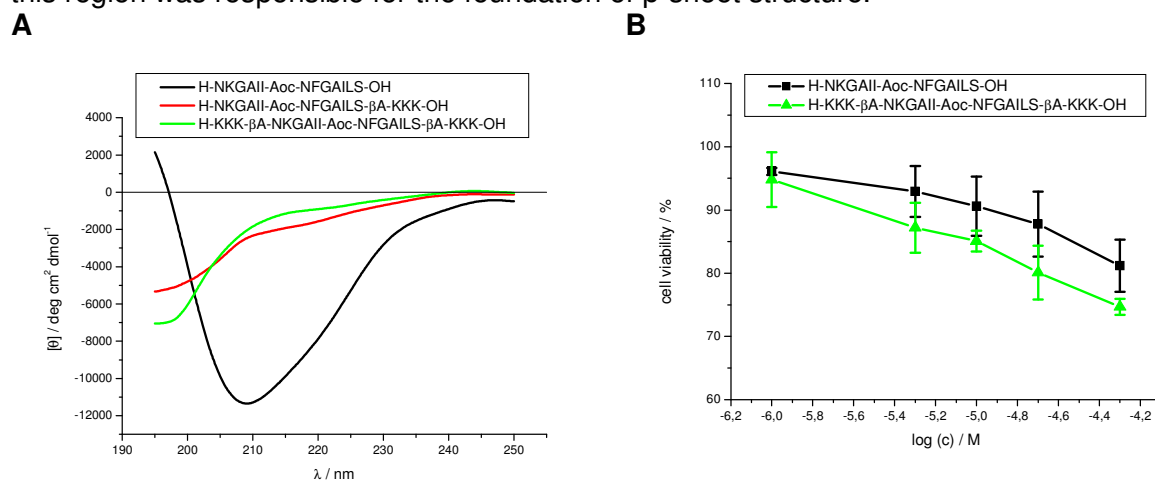


Fig. 296: (A) Far-UV CD spectra of peptides with Aoc as a connecting element with and without terminal lysine residues at a peptide concentration of 10 μM in 1xb 1% HFIP, pH 7.4.

(B) Cell viability assays of aged solutions of peptides with Aoc as a connecting element with and without terminal lysine residues (5 mM in 1xb 1% HFIP, pH 7.4 for 4 days) using PC-12 cells. Data are percentages of control and are the mean (+/-SEM) of three independent experiments with each experiment performed in multiple replicates (n = 3).

The fibril forming potential of H-KKK- β A-NKGAI-Aoc-NFGAILS- β A-KKK-OH was lower than for H-NKGAI-Aoc-NFGAILS-OH (Fig. 297B and table 24). However, H-KKK- β A-NKGAI-Aoc-NFGAILS- β A-KKK-OH was found to be slightly more toxic to PC-12 cells than H-NKGAI-Aoc-NFGAILS-OH. Maybe the equilibrium between mature fibrils and toxic oligomers is shifted towards the formation of oligomers for H-KKK- β A-NKGAI-Aoc-NFGAILS- β A-KKK-OH as formation of amyloid fibrils appeared to be disrupted by the presence of the charged lysine residues at the ends of H-KKK- β A-NKGAI-Aoc-NFGAILS- β A-KKK-OH.

Table 24: ThT binding assays and cell viability assays of all peptides with Aoc as a connecting element at different peptide concentrations.

Results of “+” indicate fibril formation, whereas “-” indicate no fibril formation within the 5 days of incubation of the solution at the given peptide concentration.

For the cell viability assays, results of “+++” mean high toxicity towards PC-12 cell, “++” means medium toxicity and “+/-” means low to no toxicity. Low toxicity refers to peptides with >90% cell viability, medium toxicity refers to a cell viability between 80% and 90%, and high toxicity refers to a cell viability of <80% for aged incubations at a peptide concentration of 50 μM .

Abbrev.	Sequence	ThT									Tox.
		5 μM	10 μM	20 μM	35 μM	50 μM	100 μM	200 μM	350 μM	500 μM	
H5a	H-NKGAI-Aoc-NFGAILS-OH	-	+	+	+	+					++
H5aK3	H-NKGAI-Aoc-NFGAILS- β A-KKK-OH				-	+	+				
H5aK6	H-KKK- β A-NKGAI-Aoc-NFGAILS- β A-KKK-OH						-	+	+	+	++
H6a	H-IIAGKN-Aoc-NFGAILS-OH		-	+	+		+				++
CB5	NFGAILS-Aoc-NFGAILS		-	+	+						+/-
CB6	NKGAI-Aoc-NKGAI				-		-	-		-	+/-
CB7	NFGAILS-Aoc-NKGAI				-			-		-	++

3.2.5.4 Peptides with the connecting element KKK

All four peptides sharing the charged, hydrophilic connecting element KKK (H-NKGAI-KKK-NFGAILS-OH, H-NFGAILS-KKK-NFGAILS-OH, and H-NKGAI-KKK-NKGAI-OH) displayed similar biochemical and biophysical features.

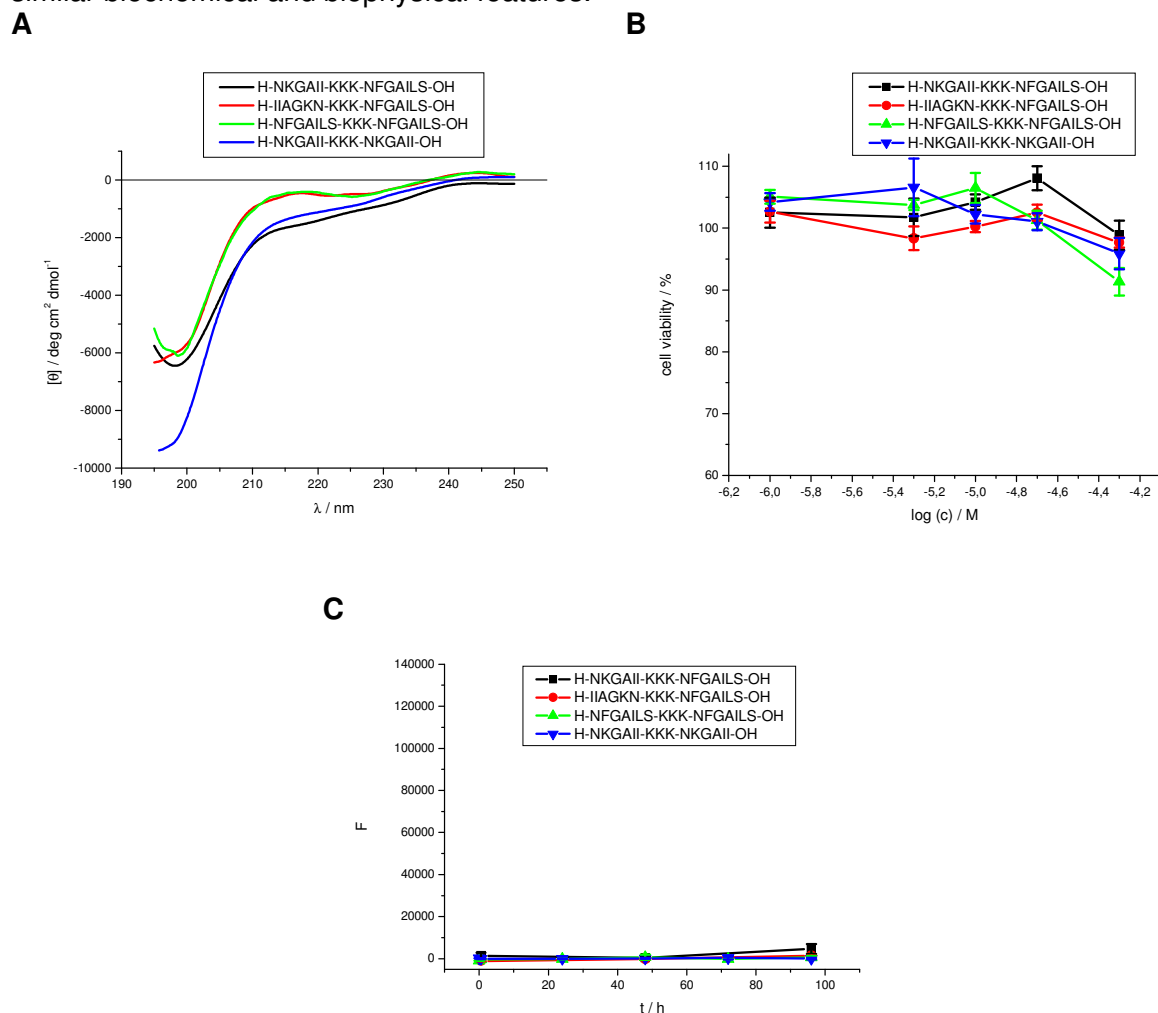


Fig. 297: (A) Far-UV CD spectra of all peptides with KKK as a connecting element at a peptide concentration of 10 μ M in 1xb 1% HFIP, pH 7.4.

(B) Cell viability assays of aged solutions of peptides with KKK as a connecting element (5 mM in 1xb 1% HFIP, pH 7.4 for 4 days) using PC-12 cells. Data are percentages of control and are the mean (\pm SEM) of three independent experiments with each experiment performed in multiple replicates ($n = 3$).

(C) ThT binding assays of peptides with KKK as a connecting element at a peptide concentration of 500 μ M in 1xb 1% HFIP, pH 7.4. Data are means of 3 assays after subtraction of buffer values \pm standard error of the mean (SEM) with each experiment performed in multiple replicates ($n = 3$).

The CD spectra of the four peptides displayed mainly random coil structure (Fig. 297A) and all of them were not toxic to PC-12 cells (Fig. 297B). Another common feature of all peptides with the connecting element KKK was that they were not able to form amyloid fibrils up to a concentration of 500 μ M as evident by ThT binding assays, TEM, and Congo Red staining.

In fact, TEM analysis of an aged incubation of H-NKGAI-KKK-NFGAILS-OH at a concentration of 5 mM (Fig. 232B) consisted also of amorphous aggregates.

The connecting element KKK in general proved to be disadvantageous for fibril formation and toxicity. This might be due to electrostatic repulsion of the positively charged lysine side chains or due to a specific structure of these peptides that was induced by the KKK motif.

Table 25: ThT binding assays of all peptides with KKK as a connecting element at different peptide concentrations.

Results of “+” indicate fibril formation, whereas “-” indicate no fibril formation within the 5 days of incubation of the solution at the given peptide concentration.

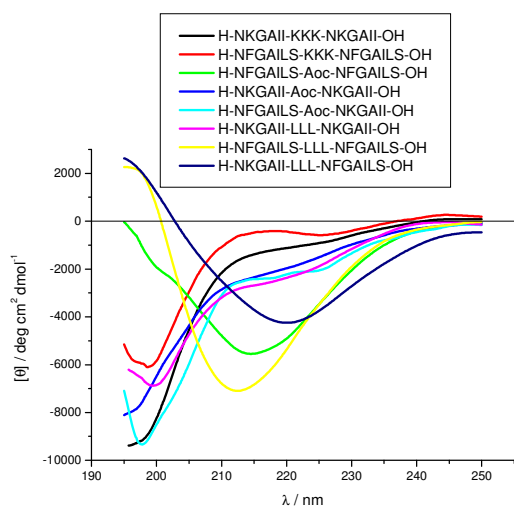
For the cell viability assays, results of “+++” mean high toxicity towards PC-12 cell, “++” means medium toxicity and “+/-” means low to no toxicity. Low toxicity refers to peptides with >90% cell viability, medium toxicity refers to a cell viability between 80% and 90%, and high toxicity refers to a cell viability of <80% for aged incubations at a peptide concentration of 50 μ M.

Abbrev.	Sequence	ThT									Tox.
		5 μ M	10 μ M	20 μ M	35 μ M	50 μ M	100 μ M	200 μ M	350 μ M	500 μ M	
H13	H-NKGAI-KKK-NFGAILS-OH				-					-	+/-
H15	H-IIAGKN-KKK-NFGAILS-OH				-		-			-	+/-
CB2	H-NFGAILS-KKK-NFGAILS-OH				-					-	+/-
CB4	H-NKGAI-KKK-NKGAI-OH				-					-	+/-

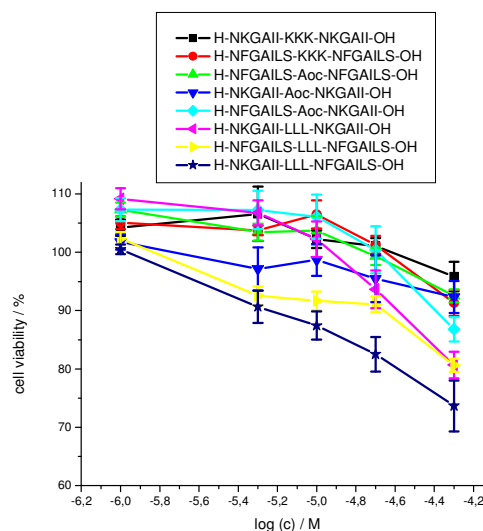
3.2.5.5 Influence of the sequence

Not only the connecting element alone but also the sequences were important for the biochemical and biophysical properties of the designed peptides.

A



B



C

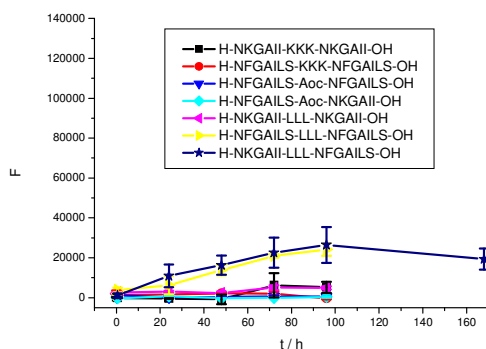


Fig. 298: Comparison of several peptides with different connecting elements and sequence arrangement.

(A) Far-UV CD spectra of a peptide concentration of 10 μM in 1x 1% HFIP, pH 7.4.

(B) Cell viability assays of aged solutions of (5 mM in 1x 1% HFIP, pH 7.4 for 4 days) using PC-12 cells. Data are percentages of control and are the mean (+/-SEM) of three independent experiments with each experiment performed in multiple replicates (n = 3).

(C) ThT binding assays of peptides with KKK as a connecting element at a peptide concentration of 35 μM in 1x 1% HFIP, pH 7.4. Data are means of 3 assays after subtraction of buffer values +/- standard error of the mean (SEM) with each experiment performed in multiple replicates (n = 3).

A clear difference can be made between peptides with the sequence NFGAILS (IAPP(22-28)) at the N-terminal position and those containing the sequence NKGAIL ($\text{A}\beta(27-32)$) as N-terminal part.

From the peptides consisting of twice the same hot region connected with different linking elements (that is H-NFGAILS-XXX-NFGAILS-OH and H-NKGAIL-XXX-NKGAIL-OH), those with the sequence H-NFGAILS-XXX-NFGAILS-OH displayed similar biophysical properties as peptides with the sequence H-NKGAIL-XXX-NFGAILS-OH and the same connecting element. Peptides with the sequence H-NKGAIL-XXX-NKGAIL-OH showed in general lower to no fibril forming potential and toxicity and displayed mainly random coil structure in CD studies independent from the connecting element used when compared to peptides with the sequence H-NKGAIL-XXX-NFGAILS-OH or H-IIAGKN-XXX-NFGAILS-OH (Fig. 298 and 299). In general, peptides with the C-terminal sequence NFGAILS showed a higher tendency to form amyloid fibrils and exhibited higher β -sheet content in CD, when compared to peptides with the same connecting element but the C-terminal sequence NKGAIL.

Also, only weak differences in biophysical properties between peptides with the sequence H-NKGAIL-XXX-NFGAILS-OH and peptides with the sequence H-IIAGKN-XXX-NFGAILS-OH were observed if they possessed the same connecting element (Fig. 292 and Fig. 293). The exchange of the N-terminal NKGAIL ($\text{A}\beta(27-32)$) with its inverted sequence IIAGKN ($\text{A}\beta(32-27)$) did not result in considerable changes. By contrast, the exchange of the C-terminal NFGAILS by NKGAIL led to enormous differences in the properties of the peptides.

A

B

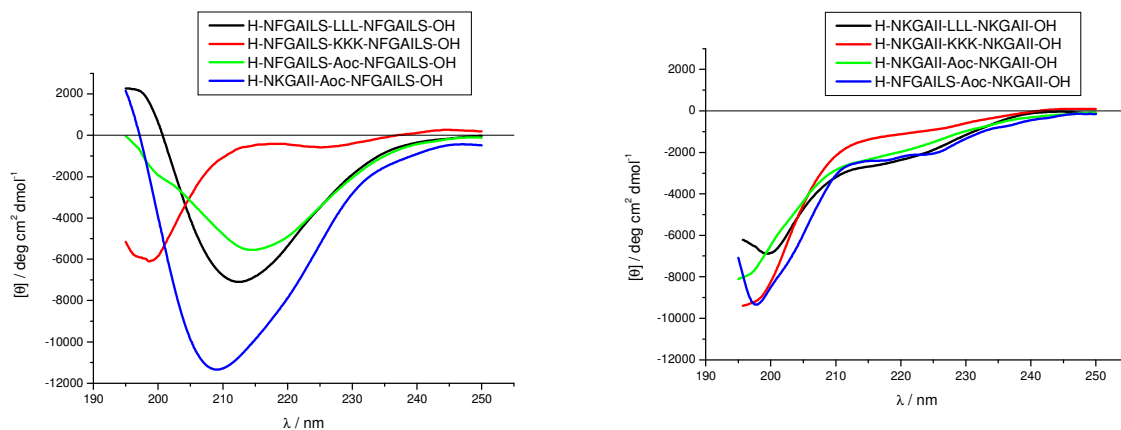


Fig. 299: (A) Far-UV CD spectra of some peptides containing the C-terminal sequence NFGAILS at a peptide concentration of 10 μM in 1x 1% HFIP, pH 7.4.

(B) Far-UV CD spectra of peptides containing the C-terminal sequence NKGAIL at a peptide concentration of 10 μM in 1x 1% HFIP, pH 7.4.

From the peptides with a C-terminal NKGAIL, only H-NKGAIL-LLL-NKGAIL-OH was able to form fibrils. This is again a hint towards the importance of the connecting element and the ability of these different connecting elements to induce amyloidogenicity.

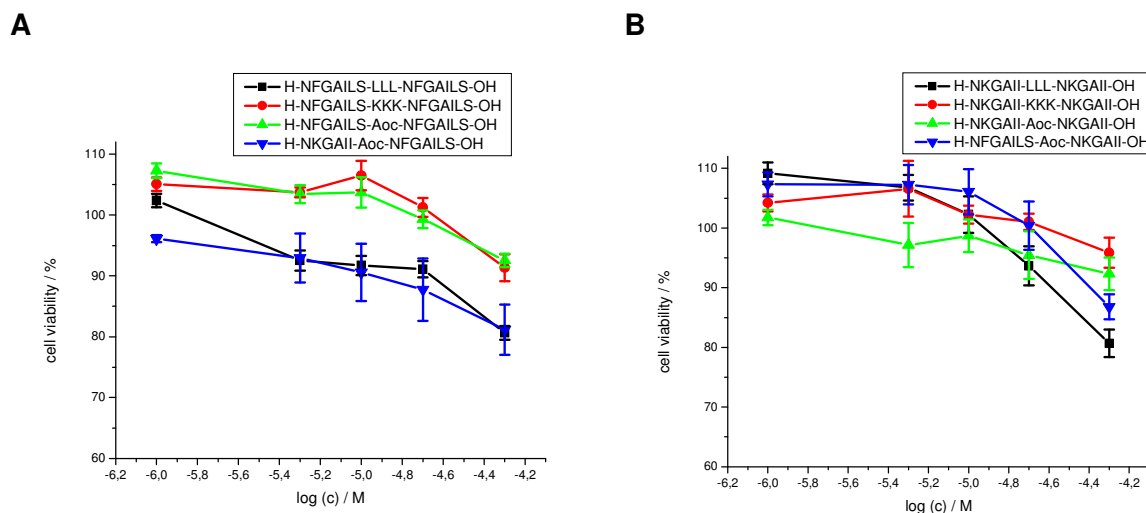


Fig. 300: (A) Cell viability assays of aged solutions of some peptides containing the C-terminal sequence NFGAILS (5 mM in 1x 1% HFiP, pH 7.4 for 4 days) using PC-12 cells. Data are percentages of control and are the mean (+/-SEM) of three independent experiments with each experiment performed in multiple replicates (n = 3).

(B) Cell viability assays of aged solutions of peptides containing the C-terminal sequence NKGAIL (5 mM in 1x 1% HFiP for 4 days) using PC-12 cells. Data are percentages of control and are the mean (+/-SEM) of three independent experiments with each experiment performed in multiple replicates (n = 3).

3.2.5.6 Conclusions

Taken together, the results presented in this chapter suggest that the connecting element as well as the different sequences and also the order in which they were aligned played an important role in conformation and amyloidogenicity of the different peptides. In general the results indicated that the nature of the connecting element had a bigger influence compared to the nature of the segments used.

The connecting element LLL for example was found to be a strong inducer of β -sheet structure and amyloidogenicity whereas KKK completely blocked β -sheet and fibril formation. The sequence at the C-terminus of the peptides was found to be almost as important as the connecting motif. The sequence NFGAILS proved to be more likely induce β -sheet structure or fibril formation in the hybrid peptide than the sequence NKGAIL.

The least important seemed to be the N-terminal sequence of the designed peptides since peptides with the same C-terminal sequence and connecting element displayed similar biophysical features independent from the N-terminal sequence used.

The segments NFGAILS and NKGAIL did not reveal fibril formation under the conditions tested here. It is however known that both segments are able to form amyloid fibrils at higher concentrations.

In contrary, if these two sequences were connected with hydrophobic connecting motifs like Aoc or LLL, the resulting peptides were able to form amyloid fibrils even at low concentrations. The peptide H-NKGAIL-K(Ac)K(Ac)K(Ac)-NFGAILS-OH was already forming fibrils at a concentration of 5 μ M. this is an acceleration by the factor 1000 compared to the segments alone.

On the other hand, peptides with charged connecting motifs like KKK and EEE did also not reveal fibril formation under the conditions used here, also not at high peptide concentrations. The effect of accelerated fibril formation must be related to hydrophobic connecting elements.

Peptides with the flexible and rather hydrophilic connecting motifs Peg and GGG only revealed a weak acceleration of the fibril forming potential and only in the case of peptides with the sequence H-NKGAIL-XXX-NFGAILS-OH.

Table 26: Overview on the results of studies shown in this chapter.

Displayed is the lowest peptide concentration at which an increase in ThT fluorescence emission was observed. Under CD the magnitude of the CD spectrum at a concentration of 10 μ M peptide is displayed. In the column r.c. the local minimum of the signal at around 195-200 nm is displayed, if the peptide showed a mainly random coil structure in CD studies. In the column β -sheet the local minimum of the signal at around 209-225 nm is displayed, if the peptide showed mainly a β -sheet structure in CD studies. For the cell viability assays, results of “+++” mean high toxicity towards PC-12 cell, “++” means medium toxicity and “+/-” means low to no toxicity. Low toxicity refers to peptides with >90% cell viability, medium toxicity refers to a cell viability between 80% and 90%, and high toxicity refers to a cell viability of <80% for aged incubations at a peptide concentration of 50 μ M.

Abbrev.	Sequence	Conc. of earliest ThT binding	CD		Tox
			r.c.	β -sheet	
H5	H-NKGAII-Peg-NFGAILS-OH	500 μ M	-5818 (199.3 nm)		++
H5a	H-NKGAII-Aoc-NFGAILS-OH	10 μ M		-11341 (209.1 nm)	++
H5aK3	H-NKGAII-Aoc-NFGAILS- β A-KKK-OH	50 μ M	-5339 (195.0 nm)		
H5aK6	H-KKK- β A-NKGAII-Aoc-NFGAILS- β A-KKK-OH	200 μ M	-7039 (195.4 nm)		++
H5b	H-NKGAII-Adc-NFGAILS-OH	10 μ M		-4490 (209.4 nm)	++
H16	H-NKGAII-GGG-NFGAILS-OH	200 μ M	-5057 (198.6 nm)		+/-
H18	H-NKGAII-AAA-NFGAILS-OH	20 μ M	-3804 (195.0 nm)		+++
H12	H-NKGAII-LLL-NFGAILS-OH	20 μ M		-4250 (220.1 nm)	+++
H12K6	H-KKK- β A-NKGAII-LLL-NFGAILS- β A-KKK-OH	20 μ M		-9900 (213.6 nm)	+++
H13	H-NKGAII-KKK-NFGAILS-OH	>1 mM	-6448 (198.2 nm)		+/-
H20	H-NKGAII-K(Ac)K(Ac)K(Ac)-NFGAILS-OH	5 μ M	-4544 (195.0 nm)		+++
H22	H-NKGAII-EEE-NFGAILS-OH	>500 μ M	-10731 (195.0 nm)		+/-
H6	H-IIAGKN-Peg-NFGAILS-OH	>500 μ M	-6486 (195.7 nm)		+/-
H6a	H-IIAGKN-Aoc-NFGAILS-OH	20 μ M		-1832 (212.9 nm)	++
H6b	H-IIAGKN-Adc-NFGAILS-OH	10 μ M		-5731 (207.8 nm)	+++
H24	H-IIAGKN-GGG-NFGAILS-OH	>500 μ M	-6158 (196.2 nm)		+/-
H23	H-IIAGKN-AAA-NFGAILS-OH	35 μ M	-6917 (196.0 nm)		+++
H14	H-IIAGKN-LLL-NFGAILS-OH	10 μ M		-5970 (216.4 nm)	+++
H15	H-IIAGKN-KKK-NFGAILS-OH	>500 μ M	-6334 (195.0 nm)		+/-
H19	H-IIAGKN-K(Ac)K(Ac)K(Ac)-NFGAILS-OH	10 μ M	-7465 (195.0 nm)		+++
H17	H-IIAGKN-EEE-NFGAILS-OH	>500 μ M	-3828 (196.9 nm)		++
CB1	H-NFGAILS-LLL-NFGAILS-OH	10 μ M		-7096 (212.5 nm)	+++
CB3	H-NKGAII-LLL-NKGAII-OH	100 μ M	-6878 (199.5 nm)		+++
CB5	H-NFGAILS-Aoc-NFGAILS-OH	20 μ M		-5548 (214.5 nm)	+/-
CB6	H-NKGAII-Aoc-NKGAII-OH	>500 μ M	-8105 (195.0 nm)		+/-
CB7	H-NFGAILS-Aoc-NKGAII-OH	>500 μ M	-9341 (197.8 nm)		++
CB2	H-NFGAILS-KKK-NFGAILS-OH	>500 μ M	-6105 (198.7 nm)		+/-
CB4	H-NKGAII-KKK-NKGAII-OH	>500 μ M	-9390 (195.7 nm)		+/-

3.3 Cyclic peptides containing the segments A β (27-32) and IAPP(22-28)

3.3.1 Design of the peptides

Cyclization of peptides is a commonly used feature to stabilize specific structural features or to make peptides more resistant to proteolytic degradation [181, 182]. Compared to their corresponding linear equivalents cyclic peptides are also less flexible making it more difficult to undergo structural changes [183-185].

Cyclic variants of several peptides containing the amyloidogenic segments A β (27-32) and IAPP(22-28) as described in chapter 3.2.2 were designed in order to force these sequences into close distance and therefore promoting intramolecular interaction with each other.

The peptides were designed in such a way that intramolecular cyclization would lead to hetero-association of the sequences from IAPP and A β within the peptide chain. This was supposed to lead to a constrained conformation that should induce a U-shaped structure containing a β -hairpin motif (Fig. 301).

Goal was to study the effect of conformational restriction by cyclization on the amyloidogenicity of the peptides. In order to achieve this, several of the peptides described in chapter 1.2 were chosen for cyclization according to their ability to form β -sheet structure, to form amyloid fibrils, and to display toxicity in cell viability assays.

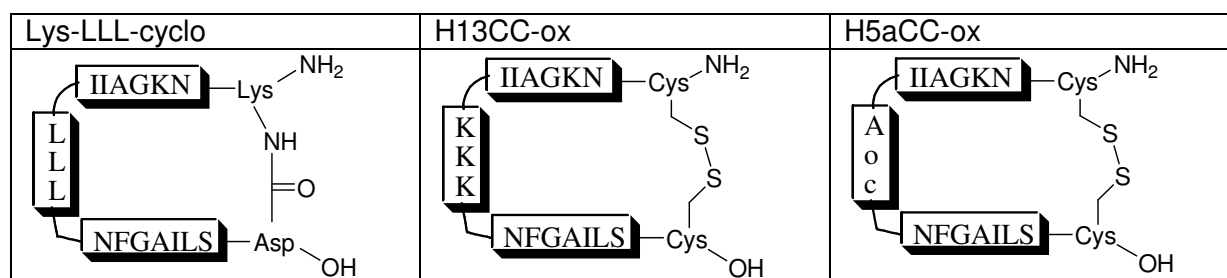


Fig. 301: Possible U-shaped structure of some of the cyclic peptides designed and synthesized in this work.

It was planned to achieve cyclization by two different ways. First, a cysteine residue was added at each the C- and the N-terminus of a chosen core sequence and then cyclization was to be accomplished by an intramolecular disulfide bridge between these two cysteines (Fig. 301). As a control, the same peptides were also synthesized with C- and N-terminal serine residues instead of the cysteines since serine is the closest replacement for cysteine. This was done to evaluate the effects of additional polar residues on the amyloidogenic properties of the peptides.

The second cyclization way involved the method of side-chain-to-side-chain-cyclization [133, 134] by forming a peptide bond between a carboxylic side chain group (C-terminal, from aspartic acid) and a primary amine side chain (N-terminal, from lysine or 2,3-diaminopropionic acid).

Three different connecting elements were chosen according to their individual features and their properties in previous studies (chapter 3.2): The tripeptides LLL and KKK and the amino acid Aoc. Hydrophobic elements were known to favor fibril formation according to the hydrophobic collapse model of fibril formation. In addition, the connecting sequence -LLL- already demonstrated its ability to induce toxicity, fibril formation, and β -sheet structure in our studies on the hot region of the IAPP self-association interface (chapter 3.2). Aoc was used as linker, since it is a hydrophobic and flexible residue with a length of about 3 amino acids. Similar to LLL, Aoc was already proven to induce fibril formation and β -sheet structure (see chapter 3.2). Compared to LLL, Aoc displays, however, much more conformational flexibility. The hydrophilic charged sequence KKK was thought to reduce fibril formation due to electrostatic repulsion and by preventing the formation of a hydrophobic core that is thought

3.3.2 Synthesis and studies of cyclic peptides and their linear equivalents

3.3.2.1 H-C-NKGAI-LLL-NFGAILS-C-OH (H12CC)

The synthesis of H12CC worked without any difficulties. The purification of the crude product was, however, very difficult. It was not possible to purify the peptide in its monomeric form. Even the addition of reducing agents could reduce but not prevent the formation of oligomers as shown by oligomerization assays (Fig. 304) and MALDI-TOF (Fig. 303). There was obviously a strong tendency of H12CC to oxidize and oligomerize on its own. The broad peak observed in HPLC was also an indication for the formation of oligomers (Fig. 302). It could however not be verified, whether these were covalent or non covalent oligomers.

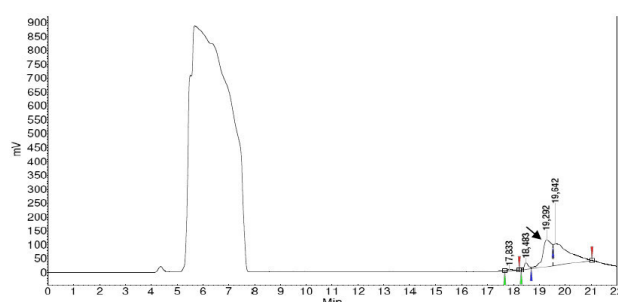


Fig. 302: HPLC of H12CC. The peptide eluted after 19.292 minutes as marked by the black arrow. 0.5 mg crude peptide was dissolved in 150 μ l TFA and 350 μ l 80% buffer B in A.

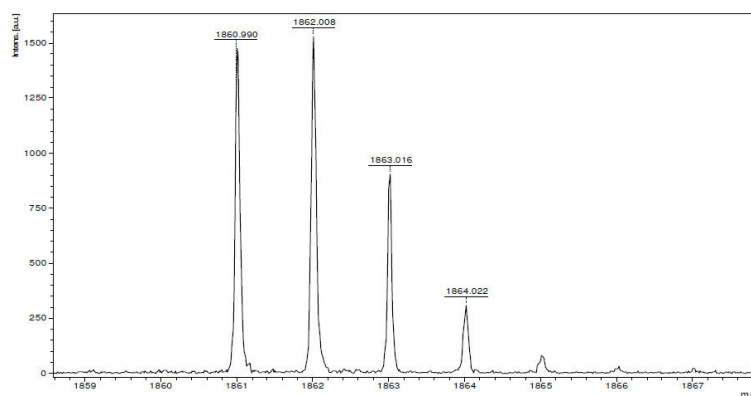


Fig. 303: Mass analysis of the HPLC purified peak at 19.292 minutes of H12CC. The expected monoisotopic molecular weight ($[M+H]^+$) for the reduced form was 1863 g/mol and 1861 g/mol for the oxidized form. Both masses as well as isotopes of both forms were found with MALDI-TOF.

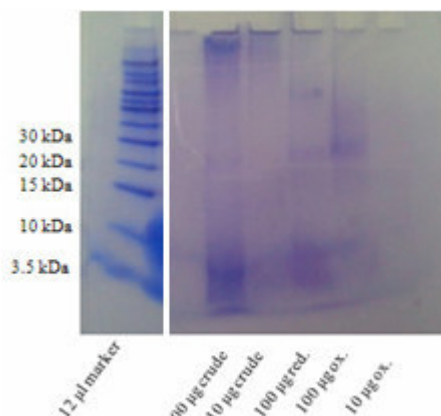


Fig. 304: Oligomerization assay of H12CC. Shown are the marker, 100 μ g crude H12CC, 10 μ g crude H12CC, 100 μ g H12CC reduced using DTT, 100 μ g H12CC oxidised under anaerobic conditions, and 10 μ g H12CC

oxidised under anaerobic conditions. The gel was stained with Coomassie Brilliant Blue. For H12CC, bands referring to both monomers and oligomers were visible in every sample.

Data presented below and their discussions always refer to a mixture of reduced and oxidized monomeric and oligomeric forms of this peptide.

As shown in Fig. 305A H12CC displayed β -sheet structure in far-UV CD experiments (similar to H-NKGAI-LLL-NFGAILS-OH (Fig. 225A)). A clear signal loss indicating the formation of oligomers appeared at a peptide concentration of 20 μ M.

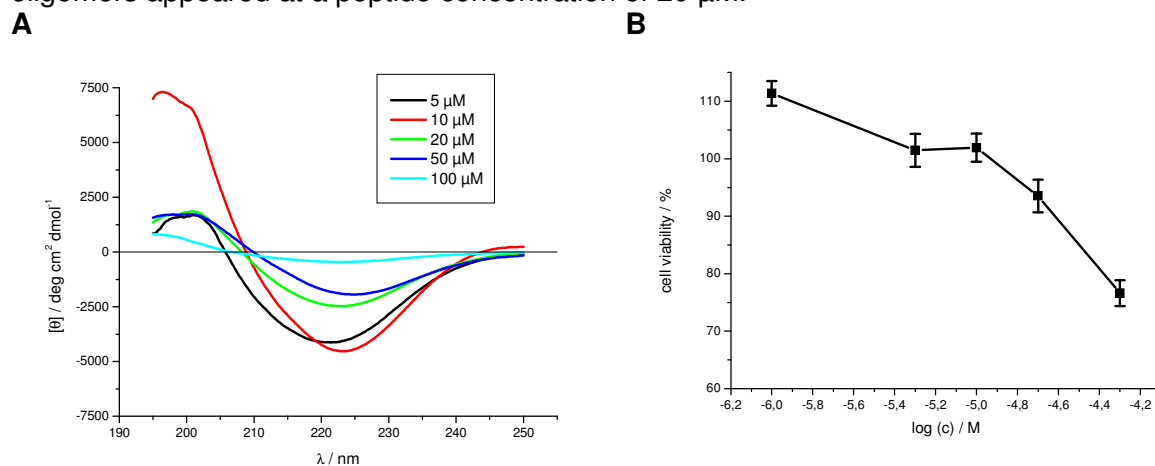


Fig. 305: (A) Far-UV CD spectra of H12CC at different concentrations in 1x 1% HFIP, pH 7.4. (B) Cell viability assay of an aged solution of H12CC (5 mM in 1x 1% HFIP, pH 7.4 for 4 days) using PC-12 cells. Data are percentages of control and are the mean (+/-SEM) of three independent experiments with each experiment performed in multiple replicates ($n = 3$).

Cell viability assays revealed that H12CC was very toxic to PC-12 cells (Fig. 305B).

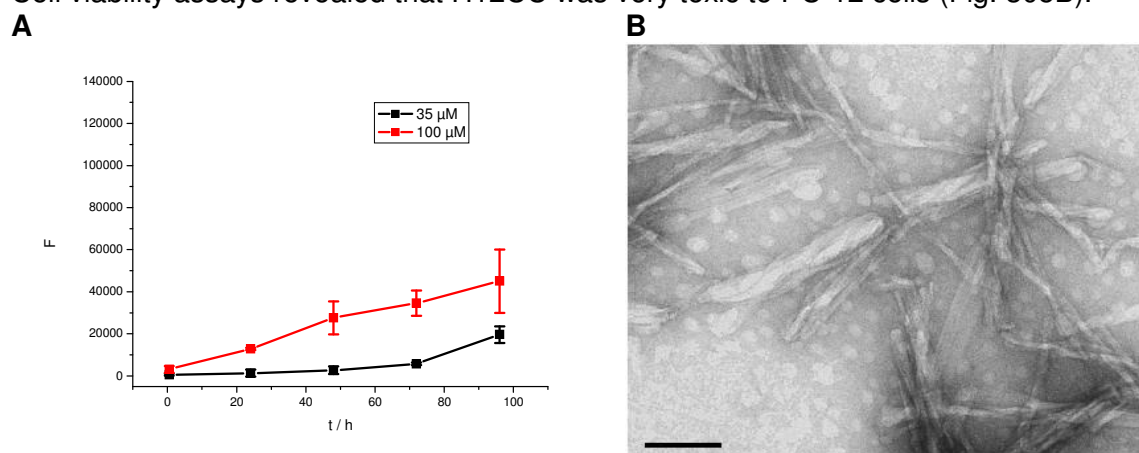


Fig. 306: (A) ThT assays of H12CC at different concentrations in 1x 1% HFIP, pH 7.4. Data are means of 3 assays after subtraction of buffer values +/- standard error of the mean (SEM) with each experiment performed in multiple replicates ($n = 3$). (B) TEM picture of an aged incubation of H12CC. The peptide was incubated at 100 μ M for 7 d in 1x 1% HFIP, pH 7.4. Scale bar: 100 nm.

Compared to H-NKGAI-LLL-NFGAILS-OH (Fig. 226A), H12CC was forming fibrils less easily (Fig. 306A). At a concentration of 35 μ M, the ThT assays of H12CC displayed only a weak increase in the fluorescence signal of ThT after 72 h. A clear and strong fibril formation was, however, detected at 100 μ M.

TEM imaging of an aged incubation of showed the presence of large amounts of fibrils (Fig. 306B).

Staining of fibrillar aggregates of H12CC with Congo Red also revealed the presence of amyloid. Stained aggregates displayed intense red color under normal light (Fig. 307A) and showed yellow birefringence under cross-polarized light (Fig. 307B).

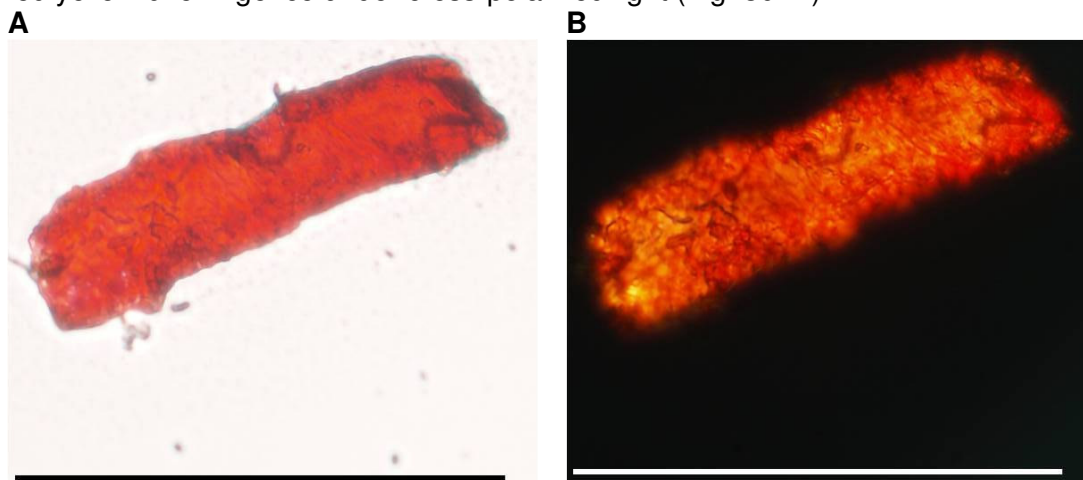


Fig. 307: Microscopic examination of an aged incubation of H12CC stained with Congo Red. The peptide was incubated at a concentration of 1 mM in 1xb 1% HFiP, pH 7.4 for 3 days. Pictures were taken under A normal and B cross-polarized light. Scale bar: 100 μm .

3.3.2.2 H-S-NKGAIL-LLL-NFGAILS-S-OH (H12Ser)

Far-UV CD spectra of H12Ser showed an intense negative signal at 216-218 nm, a clear indication for the presence of β -sheet structure (Fig. 308A). Compared to H12CC (Fig. 305A) but also H-NKGAIL-LLL-NFGAILS-OH (Fig. 225A), this β -sheet signal was much more intense. Signal loss appeared at peptide concentrations larger than 10 μM .

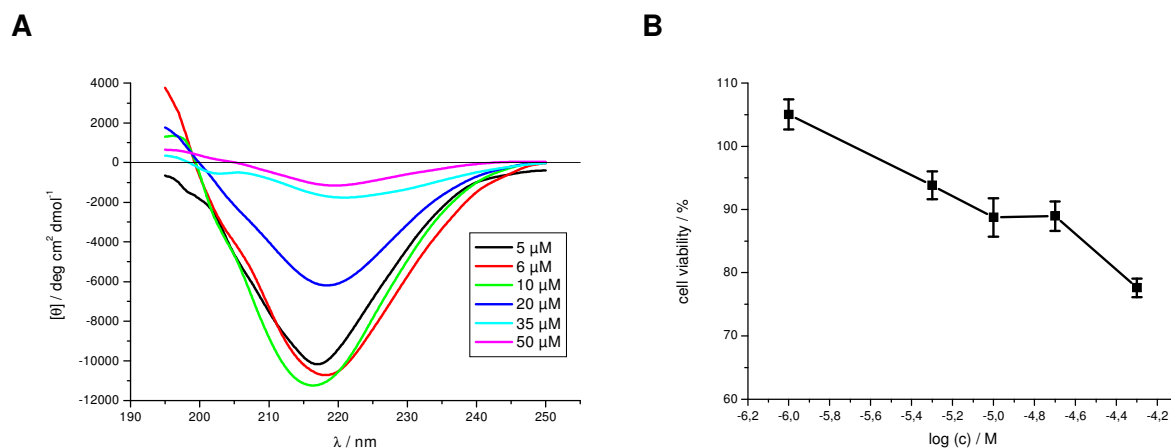


Fig. 308: (A) Far-UV CD spectra of H12Ser at different concentrations in 1xb 1% HFiP, pH 7.4. (B) Cell viability assay of an aged solution of H12Ser (5 mM in 1xb 1% HFiP, pH 7.4 for 4 days) using PC-12 cells. Data are percentages of control and are the mean (+/-SEM) of three independent experiments with each experiment performed in multiple replicates ($n = 3$).

Cytotoxicity assays of H12Ser displayed toxicity towards PC-12 cells (Fig. 308B). In addition, H12Ser was found to form fibrils already at a concentration of 35 μM H12Ser as indicated by ThT fluorescence assays (Fig. 309A).

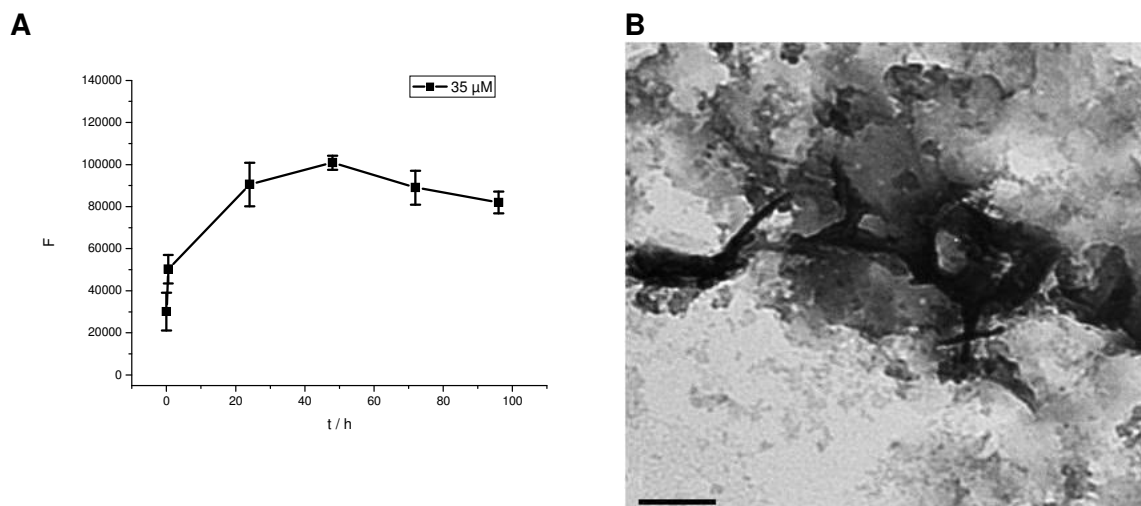


Fig. 309: (A) ThT assay of H12Ser at a peptide concentration of 35 μM in 1xb 1% HFIP, pH 7.4. Data are means of 3 assays after subtraction of buffer values +/- standard error of the mean (SEM) with each experiment performed in multiple replicates (n = 3).

(B) TEM picture of an aged incubation of H12Ser. The peptide was incubated at 35 μM for 7 d in 1xb 1% HFIP, pH 7.4. Scale bar: 100 nm.

Fibril formation was verified by both Congo Red staining (Fig. 310A and B) and TEM (Fig. 309B). The TEM picture of an aged incubation of H12Ser showed short dark fibrils.

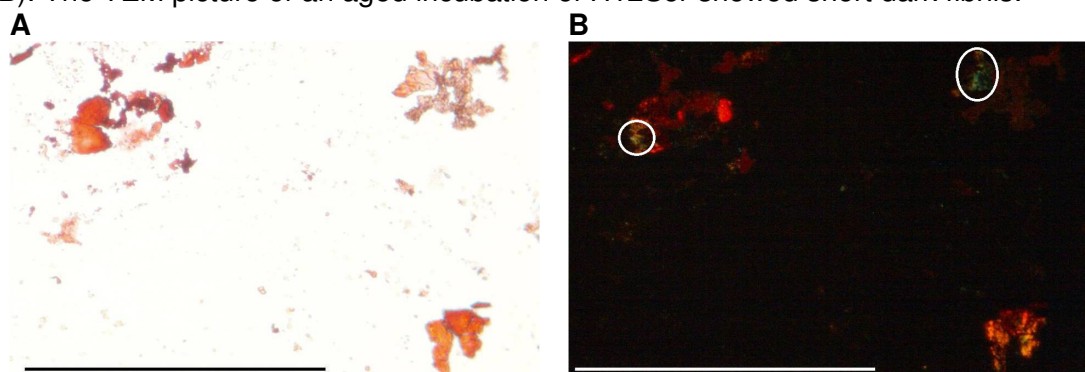


Fig. 310: Microscopic examination of an aged incubation of H12Ser stained with Congo Red. The peptide was incubated at a concentration of 1 mM in 1xb 1% HFIP, pH 7.4 for 3 days. Pictures were taken under A normal and B cross-polarized light. Scale bar: 100 μm.

3.3.2.3 Linear H-Lys-NKGAI-LLL-NFGAILS-Asp-OH (Lys-LLL-lin)

As seen on Fig. 311A Lys-LLL-lin also displayed β-sheet structure in far-UV CD experiments as indicated by the minimum at 218 nm. Compared to the CD spectra from H-NKGAI-LLL-NFGAILS-OH (Fig. 225A), the signal intensity but also the overall shape and the aggregation potential indicated by signal loss upon increased concentration were similar for the two peptides. Aggregation of Lys-LLL-lin started at concentrations higher than 10 μM.

The β-sheet signal was slightly shifted towards higher wavelengths upon increased peptide concentrations indicating a conformational shift towards β-turn elements upon aggregation.

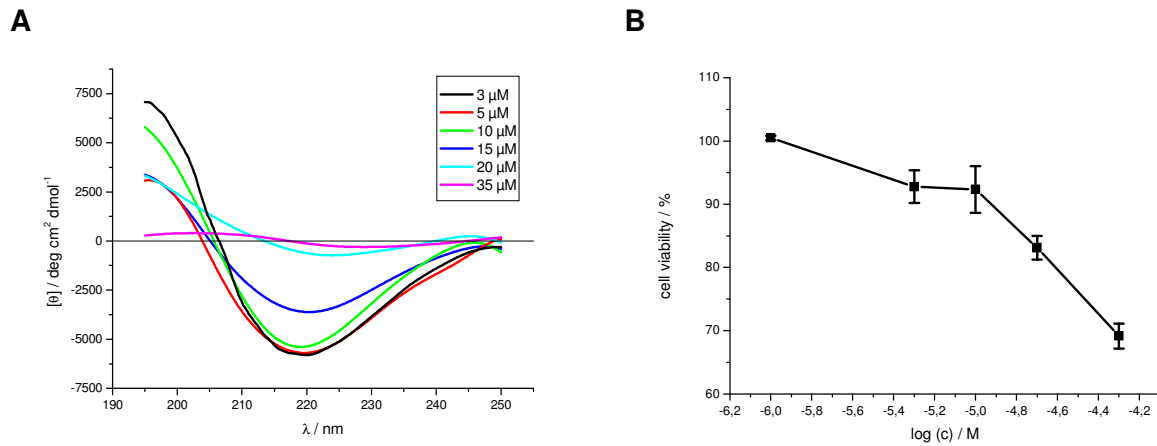


Fig. 311: (A) Far-UV CD spectra of Lys-LLL-lin at different concentrations in 1x 1% HFIP, pH 7.4 (from [186]). (B) Cell viability assay of an aged solution of Lys-LLL-lin (5 mM in 1x 1% HFIP, pH 7.4 for 4 days) using PC-12 cells. Data are percentages of control and are the mean (+/-SEM) of three independent experiments with each experiment performed in multiple replicates ($n = 3$).

In cell viability assays, Lys-LLL-lin proved to be very toxic to PC-12 cells under the conditions tested (Fig. 311B). ThT assays indicated fibril formation already at a concentration of 10 μ M (Fig. 312A).

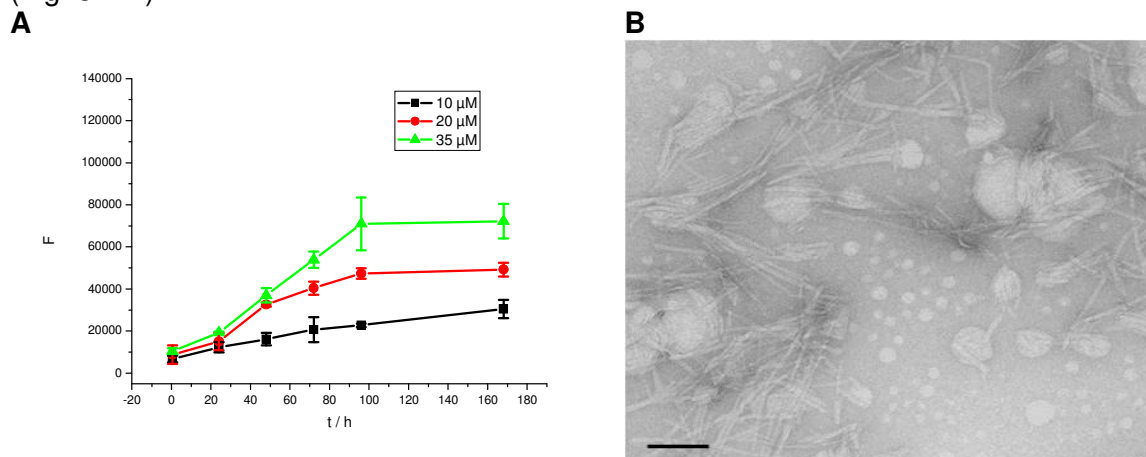


Fig. 312: (A) ThT assays of Lys-LLL-lin at different concentrations in 1x 1% HFIP, pH 7.4 (from [186]). Data are means of 3 assays after subtraction of buffer values +/- standard error of the mean (SEM) with each experiment performed in multiple replicates ($n = 3$). (B) TEM picture of an aged incubation of Lys-LLL-lin. The peptide was incubated at 100 μ M for 7 d in 1x 1% HFIP, pH 7.4. Scale bar: 100 nm.

Fibril formation was verified by both TEM imaging (Fig. 312B) and Congo Red staining (Fig. 313A and B). The TEM picture of an aged incubation of Lys-LLL-lin displayed many unbranched straight fibrils. Congo Red stained aggregates of Lys-LLL-lin expressed yellow birefringence under cross-polarized light.

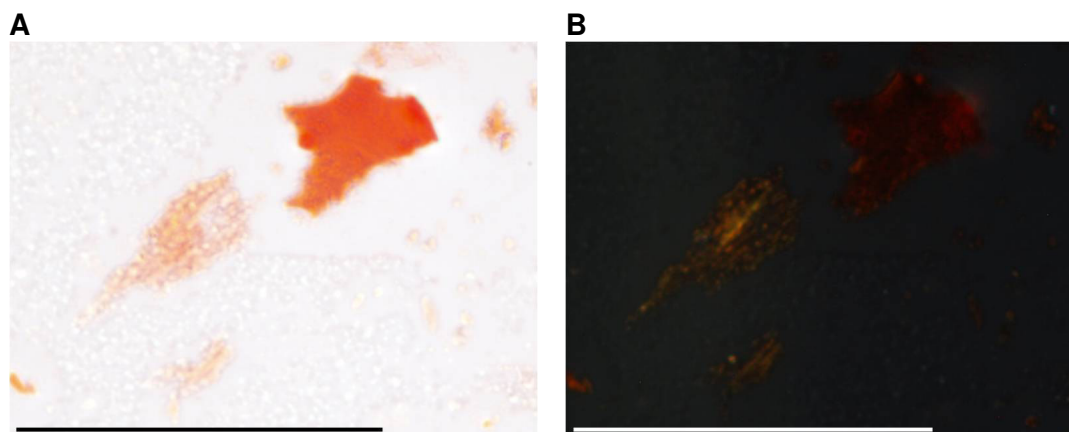


Fig. 313: Microscopic examination of an aged incubation of Lys-LLL-lin stained with Congo Red. The peptide was incubated at a concentration of 1 mM in 1xb 1% HFIP, pH 7.4 for 3 days. Pictures were taken under A normal and B cross-polarized light. Scale bar: 100 μm (from [186]).

3.3.2.4 Cyclic H-Lys-NKGAI-LLL-NFGAILS-Asp-OH (Lys-LLL-cyclo)

In Far-UV CD experiments Lys-LLL-cyclo displayed a β -sheet structure (Fig. 314A). Compared to Lys-LLL-lin (Fig. 311A), the β -sheet signal was much less intense and slightly shifted towards higher wavelengths. This shift in the spectra of Lys-LLL-cyclo increased with higher peptide concentrations indicating a conformational shift towards β -turn elements upon aggregation. These changes of the signal upon aggregation were often observed for peptides with the connecting element LLL.

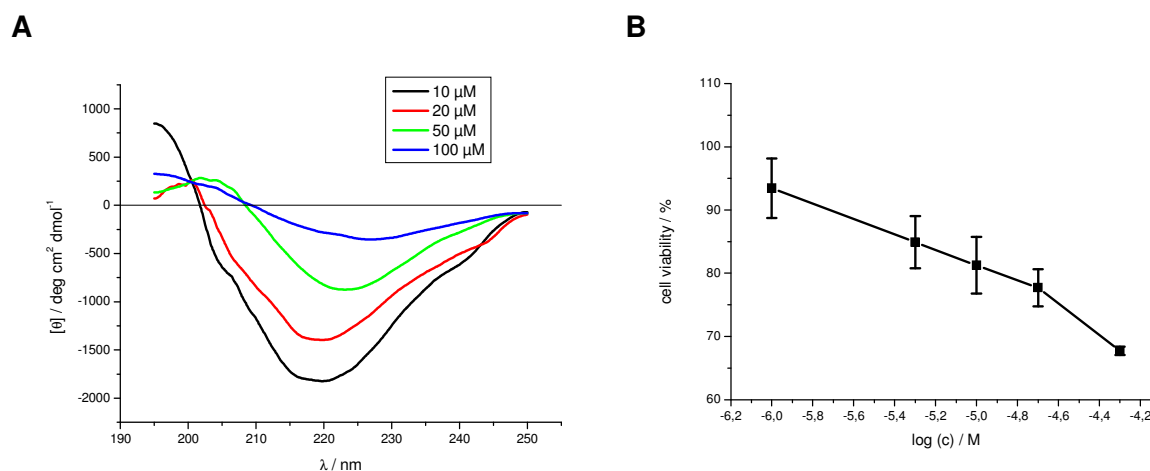


Fig. 314: (A) Far-UV CD spectra of Lys-LLL-cyclo at different concentrations in 1xb 1% HFIP, pH 7.4 (from [186]). (B) Cell viability assay of an aged solution of Lys-LLL-cyclo (5 mM in 1xb 1% HFIP, pH 7.4 for 4 days) using PC-12 cells. Data are percentages of control and are the mean (+/-SEM) of three independent experiments with each experiment performed in multiple replicates ($n = 3$).

Under the conditions tested Lys-LLL-cyclo was also highly toxic to PC-12 cells (Fig. 314B), even slightly more than Lys-LLL-lin (Fig. 311B).

The fibril forming potential of Lys-LLL-cyclo (Fig. 315A), was however lower than that of Lys-LLL-lin (Fig. 312A). Only at a peptide concentration of 100 μM , ThT assays of Lys-LLL-cyclo showed a clear increase in the fluorescence signal of ThT.

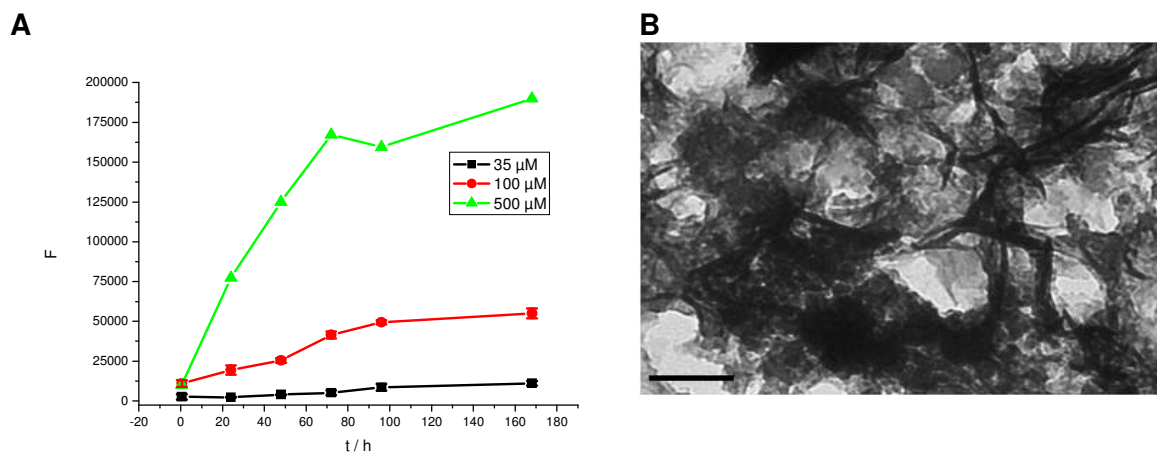


Fig. 315: (A) ThT assays of Lys-LLL-cyclo at different concentrations in 1xb 1% HFIP, pH 7.4 (from [186]). Data are means of 3 assays after subtraction of buffer values \pm standard error of the mean (SEM) with each experiment performed in multiple replicates ($n = 3$).

(B) TEM picture of an aged incubation of Lys-LLL-cyclo. The peptide was incubated at 500 μ M for 7 d in 1xb 1% HFIP, pH 7.4. Scale bar: 100 nm.

TEM imaging of an aged incubation of Lys-LLL-cyclo at a peptide concentration of 500 μ M showed the presence of mixtures of both short needle-like fibrils and amorphous aggregates (Fig. 315B).

Fibrillar aggregates of Lys-LLL-cyclo stained with Congo Red revealed intense red color under normal light (Fig. 316A) and displayed red and green birefringence under cross-polarized light (Fig. 316B).

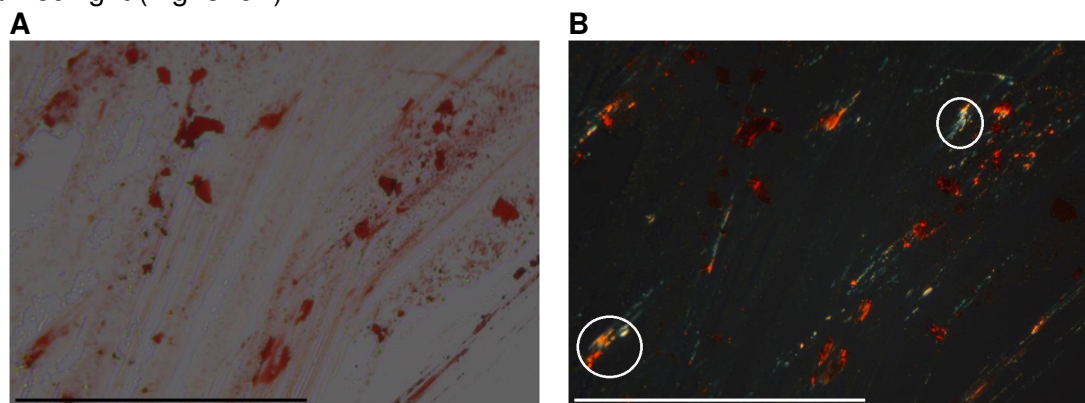


Fig. 316: Microscopic examination of an aged incubation of Lys-LLL-cyclo stained with Congo Red. The peptide was incubated at a concentration of 1 mM in 1xb 1% HFIP, pH 7.4 for 3 days. Pictures were taken under A normal and B cross-polarized light. Scale bar: 100 μ m (from [186]).

3.3.2.5 Linear H-Dap-NKGAI-LLL-NFGAILS-Asp-OH (Dap-LLL-lin)

CD experiments of Dap-LLL-lin also revealed the presence of significant amounts of β -sheet structure (Fig. 317A). Compared to Lys-LLL-lin (Fig. 311A), the β -sheet signal was slightly less intense. A clear loss of signal intensity was again visible for peptide concentrations higher than 10 μ M.

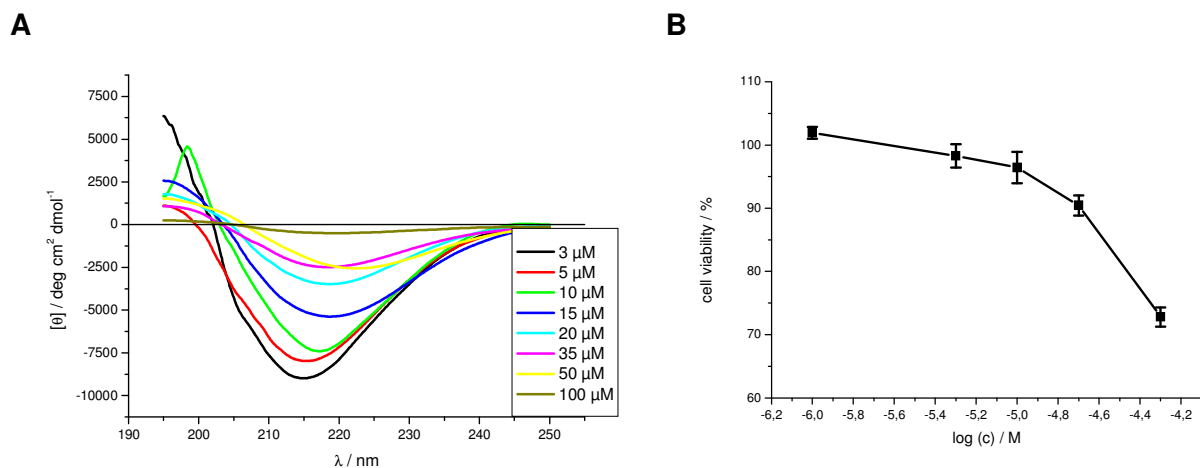


Fig. 317: (A) Far-UV CD spectra of Dap-LLL-lin at different concentrations in 1x 1% HFIP, pH 7.4 (from [186]). (B) Cell viability assay of an aged solution of Dap-LLL-lin (5 mM in 1x 1% HFIP, pH 7.4 for 4 days) using PC-12 cells. Data are percentages of control and are the mean (+/-SEM) of three independent experiments with each experiment performed in multiple replicates (n = 3).

As seen on Fig. 317B, Dap-LLL-lin was found to be highly toxic to PC-12 cells. Similar to Lys-LLL-lin, Dap-LLL-lin displayed a high fibril forming potential and was already forming fibrils at a peptide concentration of 10 μM (Fig. 318A). The TEM picture of an aged solution of Dap-LLL-lin indicated the presence of many short dark fibrils (Fig. 318B).

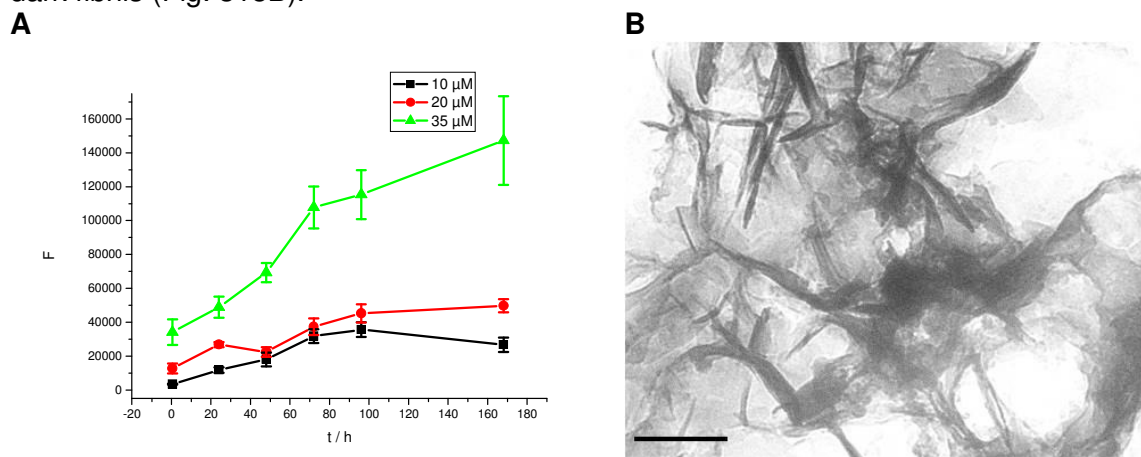


Fig. 318: (A) ThT assays of Dap-LLL-lin at different concentrations in 1x 1% HFIP, pH 7.4 (from [186]). Data are means of 3 assays after subtraction of buffer values +/- standard error of the mean (SEM) with each experiment performed in multiple replicates (n = 3). (B) TEM picture of an aged incubation of Dap-LLL-lin. The peptide was incubated at 100 μM for 7 d in 1x 1% HFIP, pH 7.4. Scale bar: 100 nm.

Some of the fibrillar aggregates of Dap-LLL-lin bound Congo Red (Fig. 319A) and exhibited green birefringence under cross-polarized light (Fig. 319B).

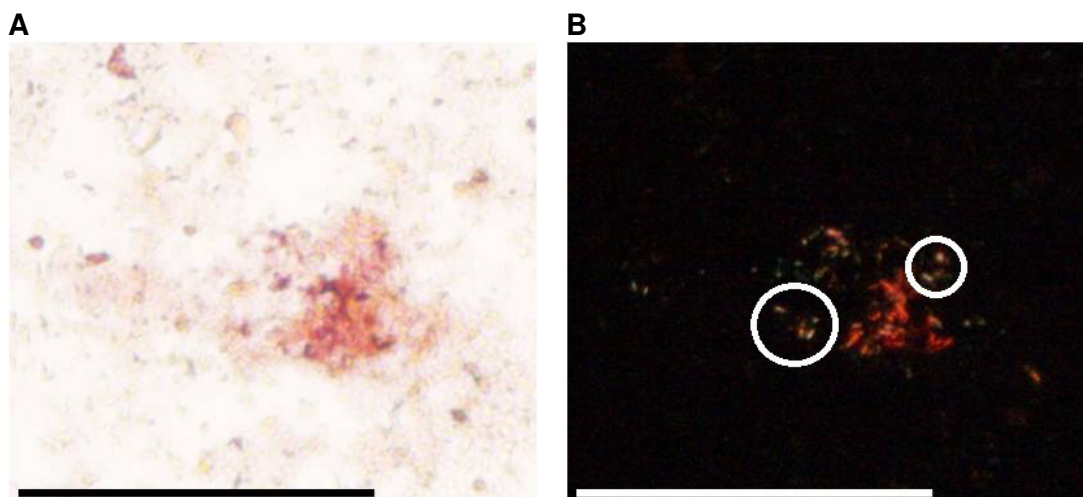


Fig. 319: Microscopic examination of an aged incubation of Dap-LLL-lin stained with Congo Red. The peptide was incubated at a concentration of 1 mM in 1xb 1% HFIP, pH 7.4 for 3 days. Pictures were taken under A normal and B cross-polarized light. Scale bar: 100 μm .

3.3.2.6 Linear H-C-NKGAI-KKK-NFGAILS-C-OH (H13CC-red)

The CD spectra of H13CC-red (Fig. 320A) displayed mainly a negative signal at 195 nm indicating random coil structure. A small negative bulge at 210-230 nm indicated the presence of additional structural elements like β -sheets or β -turns. The peptide started to aggregate at concentrations higher than 20 μM .

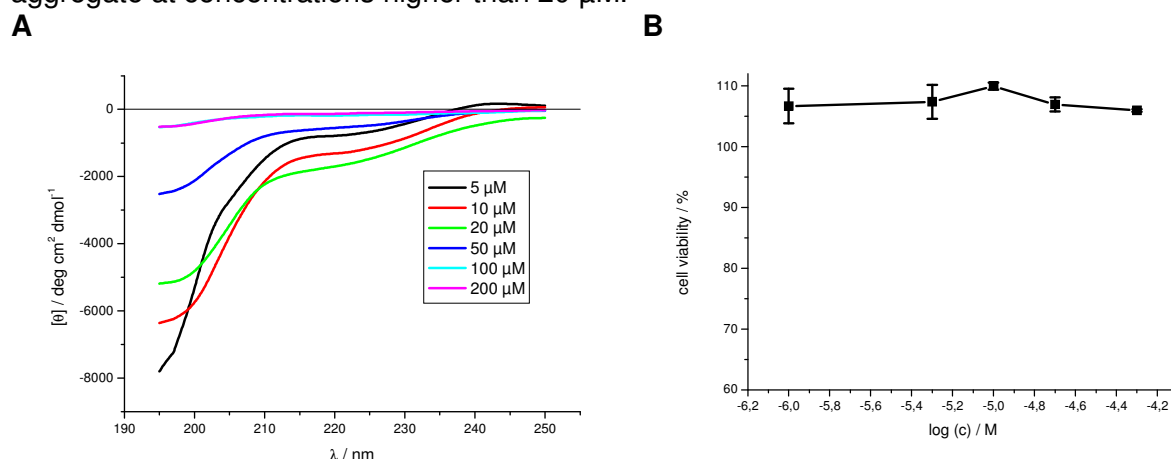


Fig. 320: (A) Far-UV CD spectra of H13CC-red at different concentrations in 1xb 1% HFIP, pH 7.4. (B) Cell viability assay of an aged solution of H13CC-red (5 mM in 1xb 1% HFIP, pH 7.4 for 4 days) using PC-12 cells. Data are percentages of control and are the mean (+/-SEM) of three independent experiments with each experiment performed in multiple replicates ($n = 3$).

Cell viability assays revealed that H13CC-red did not display toxicity to PC-12 cells (Fig. 320B).

ThT studies of H13CC-red, however, showed fibril formation already at a peptide concentration of 50 μM (Fig. 321A). To avoid oxidation of the cysteine residues these studies were performed with the addition of 10 μM DTT.

TEM imaging of an aged solution of H13CC-red showed the presence of a large amount of amyloid fibrils (Fig. 321B).

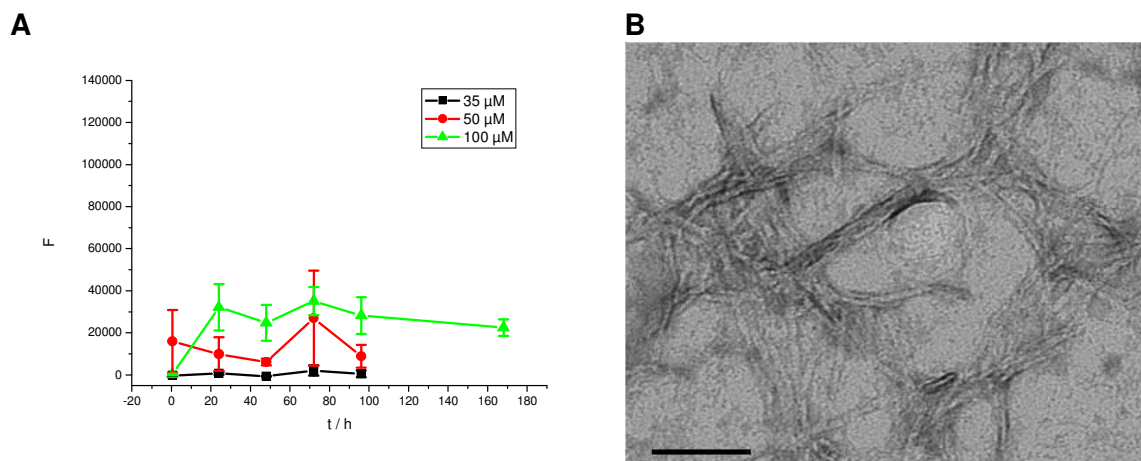


Fig. 321: (A) ThT assays of H13CC-red at different peptide concentrations in 1xb 1% HFIP, pH 7.4, 10 mM DTT. Data are means of 3 assays after subtraction of buffer values +/- standard error of the mean (SEM) with each experiment performed in multiple replicates (n = 3).

(B) TEM picture of an aged incubation of H13CC-red. The peptide was incubated at 100 μ M for 7 d in 1xb 1% HFIP, pH 7.4, 10 mM DTT. Scale bar: 100 nm.

Congo red stained aggregates of H13CC-red (Fig. 322A and B) bound Congo Red (Fig. 322A) but exhibited no green/yellow birefringence under cross-polarized light (Fig. 322B).

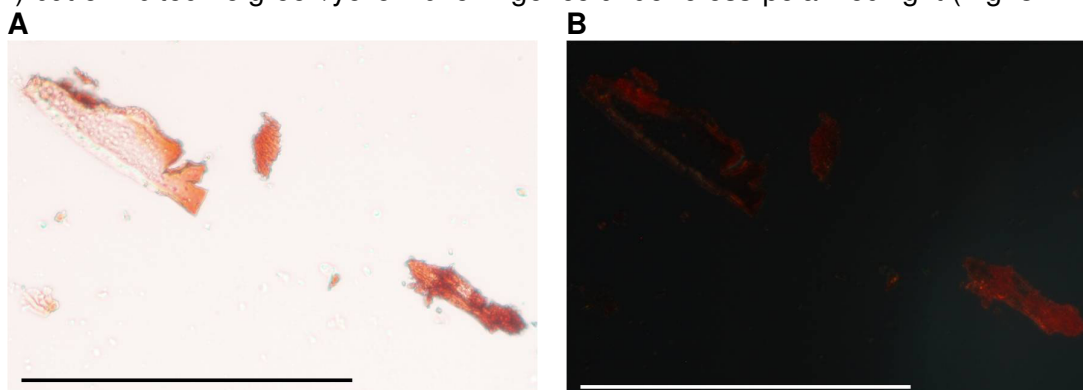


Fig. 322: Microscopic examination of an aged incubation of H13CC-red stained with Congo Red. The peptide was incubated at a concentration of 1 mM in 1xb 1% HFIP, pH 7.4 for 3 days. Pictures were taken under A normal and B cross-polarized light. Scale bar: 100 μ m.

3.3.2.7 Cyclic H-C-NKGAI-KKK-NFGAILS-C-OH (H13CC-ox)

Far-UV CD spectra of H13CC-ox (Fig. 323A) showed a strong negative signal at 195 nm indicating significant amounts of random coil structure and a broad negative bulge at 210-230 nm indicating the presence of some β -sheet and β -turn elements. For comparison, H13CC-red (Fig. 320A) displayed almost identical CD spectra.

The aggregation of H13CC-ox went along with a loss of intensity of the CD signal. This signal loss was more intense for the random coil signal. At a peptide concentration of 200 μ M, there was a slightly positive bulge in the CD spectrum ranging from 200 nm up to 230 nm (Fig. 323A).

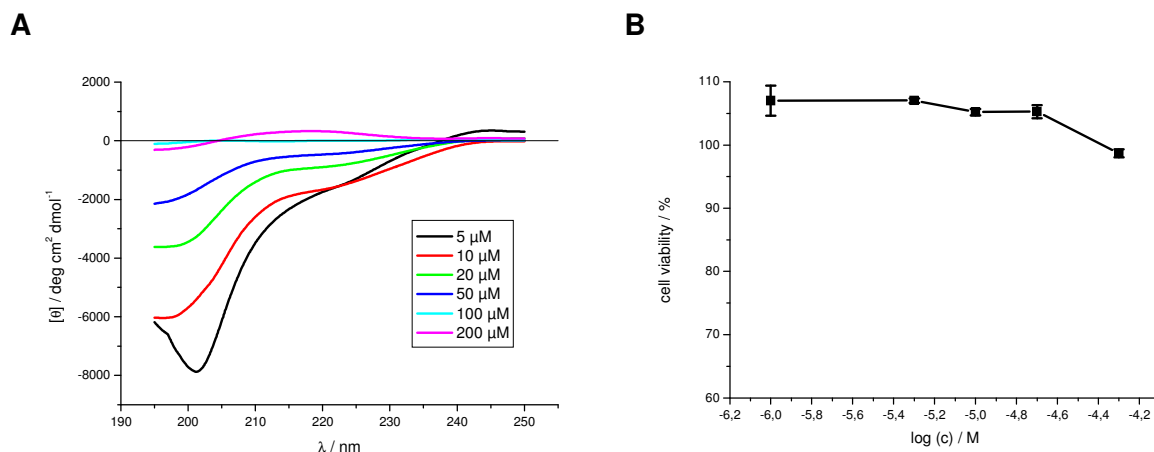


Fig. 323: (A) Far-UV CD spectra of H13CC-ox at different concentrations in 1x 1% HFIP, pH 7.4. (B) Cell viability assay of an aged solution of H13CC-ox (5 mM in 1x 1% HFIP, pH 7.4 for 4 days) using PC-12 cells. Data are percentages of control and are the mean (+/-SEM) of three independent experiments with each experiment performed in multiple replicates (n = 3).

As shown on Fig. 323B H13CC-ox was not toxic to PC-12 cells.

ThT studies of H13CC-ox showed that fibril formation started at a concentration of 500 μM (Fig. 324A). At a concentration of 200 μM , the solutions of the ThT assays exhibited only a slight increase of ThT fluorescence. Importantly, fibril formation at a concentration of 500 μM was confirmed by TEM imaging (Fig. 324B).

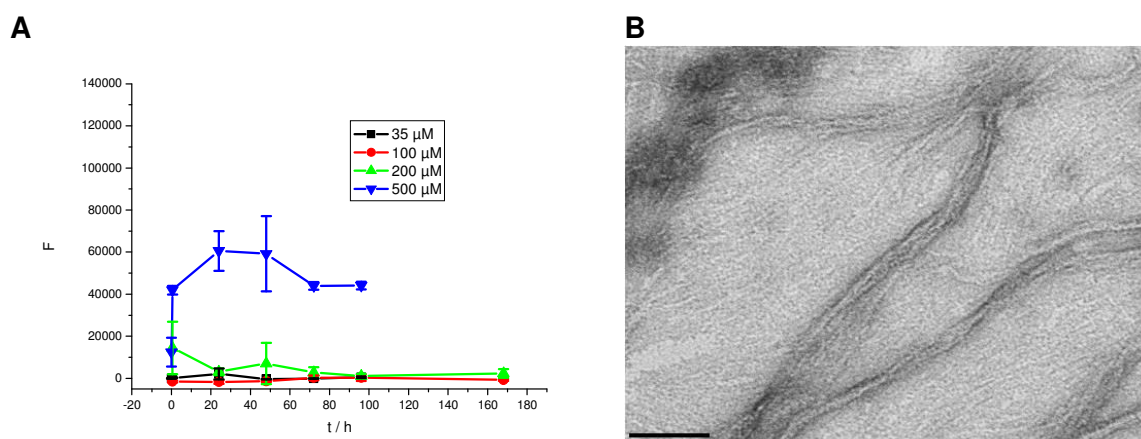


Fig. 324: (A) ThT assays of H13CC-ox at different concentrations in 1x 1% HFIP, pH 7.4. Data are means of 3 assays after subtraction of buffer values +/- standard error of the mean (SEM) with each experiment performed in multiple replicates (n = 3).

(B) TEM picture of an aged incubation of H13CC-ox. The peptide was incubated at 500 μM for 7 d in 1x 1% HFIP, pH 7.4. Scale bar: 100 nm.

Staining of an aged incubation of H13CC-ox with Congo Red indicated aggregates that bound Congo Red as indicated by a red color under normal light (Fig. 325A) and some of them were found to exhibit green birefringence under cross-polarized light (Fig. 325B).

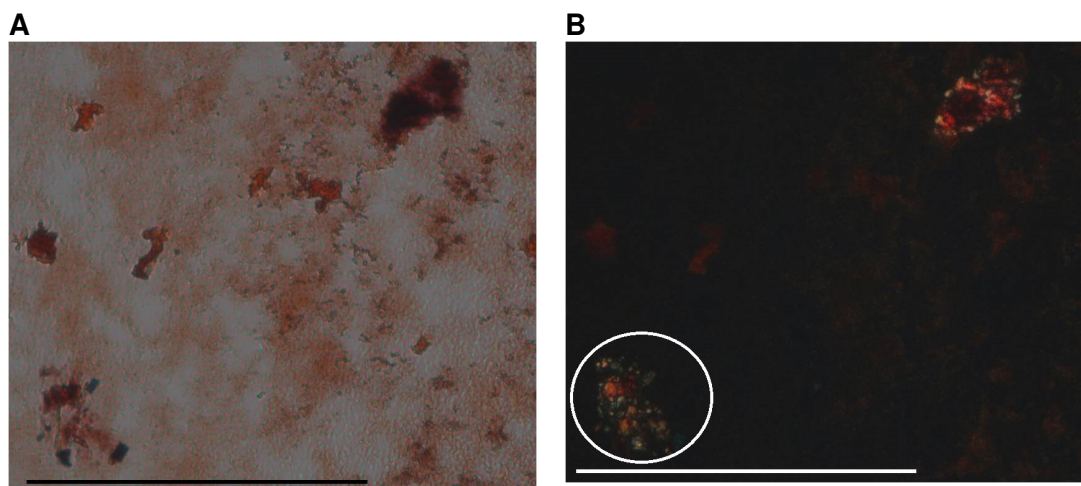


Fig. 325: Microscopic examination of an aged incubation of H13CC-ox stained with Congo Red. The peptide was incubated at a concentration of 1 mM in 1xb 1% HFIP, pH 7.4 for 3 days. Pictures were taken under A normal and B cross-polarized light. Scale bar: 100 μm .

3.3.2.8 H-S-NKGAI-KKK-NFGAILS-S-OH (H13Ser)

Far-UV CD spectra of H13Ser (Fig. 326A) showed a strong negative signal at 195 nm indicating random coil structure and a broad negative bulge at 210-230 nm indicating the presence of β -sheet or β -turn elements. For comparison, CD spectra of H13CC-red (Fig. 320A) showed a similar shape but significantly less intensity.

The aggregation of H13Ser indicated by a loss of signal intensity started at a peptide concentration higher than 10 μM (Fig. 326A).

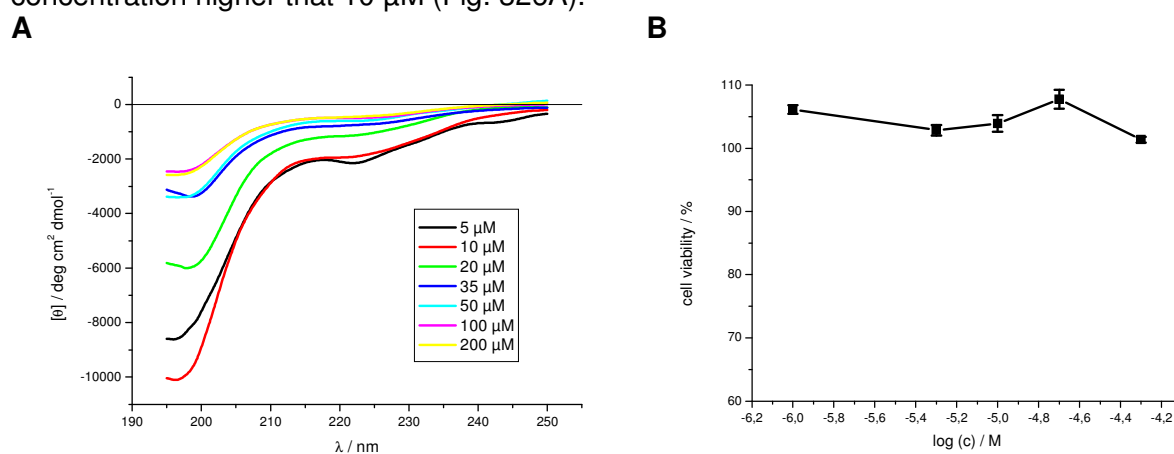


Fig. 326: (A) Far-UV CD spectra of H13Ser at different concentrations in 1xb 1% HFIP, pH 7.4.

(B) Cell viability assay of an aged solution of H13Ser (5 mM in 1xb 1% HFIP, pH 7.4 for 4 days) using PC-12 cells. Data are percentages of control and are the mean (\pm -SEM) of three independent experiments with each experiment performed in multiple replicates ($n = 3$).

Similar to H13CC-red (Fig. 310B) H13Ser did not display toxicity to PC-12 cells (Fig. 326B). ThT studies of H13Ser revealed fibril formation at concentration of 200 μM within 48h (Fig. 327A). TEM imaging of an aged solution of H13Ser showed the presence of a large amount of amyloid fibrils (Fig. 327B).

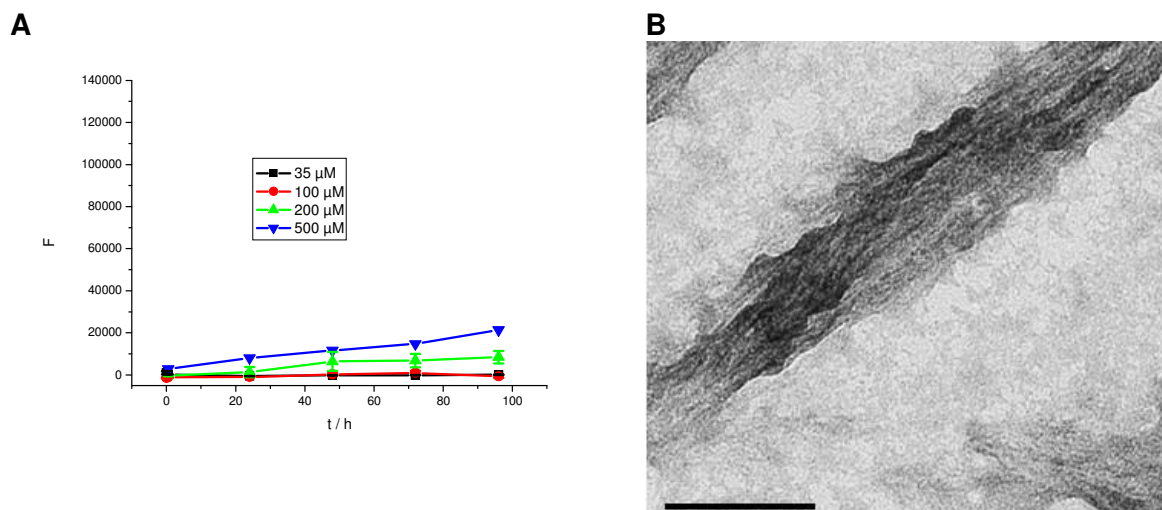


Fig. 327: (A) ThT assays of H13Ser at different concentrations in 1xb 1% HFIP, pH 7.4. Data are means of 3 assays after subtraction of buffer values \pm standard error of the mean (SEM) with each experiment performed in multiple replicates ($n = 3$).

(B) TEM picture of an aged incubation of H13Ser. The peptide was incubated at 500 μ M for 7 d in 1xb 1% HFIP, pH 7.4. Scale bar: 100 nm.

Congo red stained aggregates of H13Ser (Fig. 328A and B), showed aggregates that could be stained with Congo Red as indicated by a red color under normal light (Fig. 328A) and displayed green birefringence under cross-polarized light indicating amyloid structures (Fig. 328B).

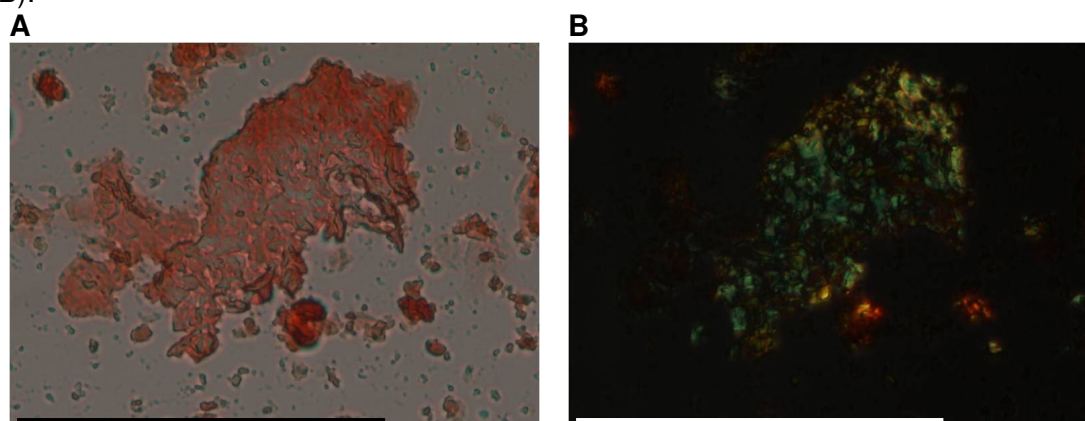


Fig. 328: Microscopic examination of an aged incubation of H13Ser stained with Congo Red. The peptide was incubated at a concentration of 1 mM in 1xb 1% HFIP, pH 7.4 for 3 days. Pictures were taken under A normal and B cross-polarized light. Scale bar: 100 μ m.

3.3.2.9 Linear H-Lys-NKGAI-KKK-NFGAILS-Asp-OH (Lys-KKK-lin)

The CD spectra of Lys-KKK-lin (Fig. 329A) displayed mainly a negative signal at 195 nm indicating random coil structure. There was also a small negative bulge at 210-230 nm visible indicating the presence of additional β -sheet or β -turn elements. These kinds of spectra were typical for peptides with the connecting element KKK.

The peptide started to aggregate already between a concentration of 5 μ M and 10 μ M.

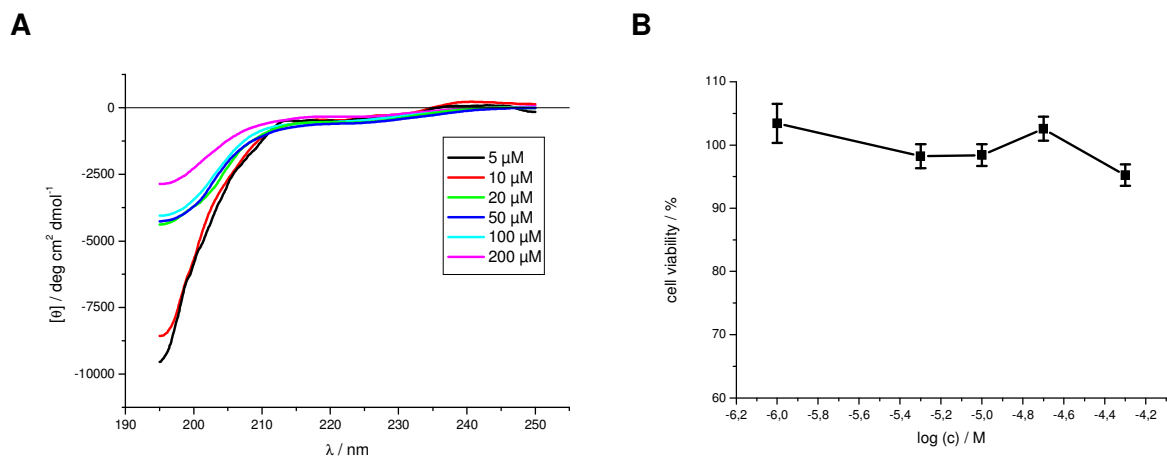


Fig. 329: (A) Far-UV CD spectra of Lys-KKK-lin at different concentrations in 1x 1% HFIP, pH 7.4 (from [186]). (B) Cell viability assay of an aged solution of Lys-KKK-lin (5 mM in 1x 1% HFIP, pH 7.4 for 4 days) using PC-12 cells. Data are percentages of control and are the mean (+/-SEM) of three independent experiments with each experiment performed in multiple replicates (n = 3).

Cell viability assays using Lys-KKK-lin and PC-12 cells did not reveal toxicity (Fig. 329B). Under the conditions used for ThT assays Lys-KKK-lin was also not forming fibrils (Fig. 330A).

The TEM picture of an aged incubation of Lys-KKK-lin also only displayed amorphous aggregates but no fibrils (Fig. 330B).

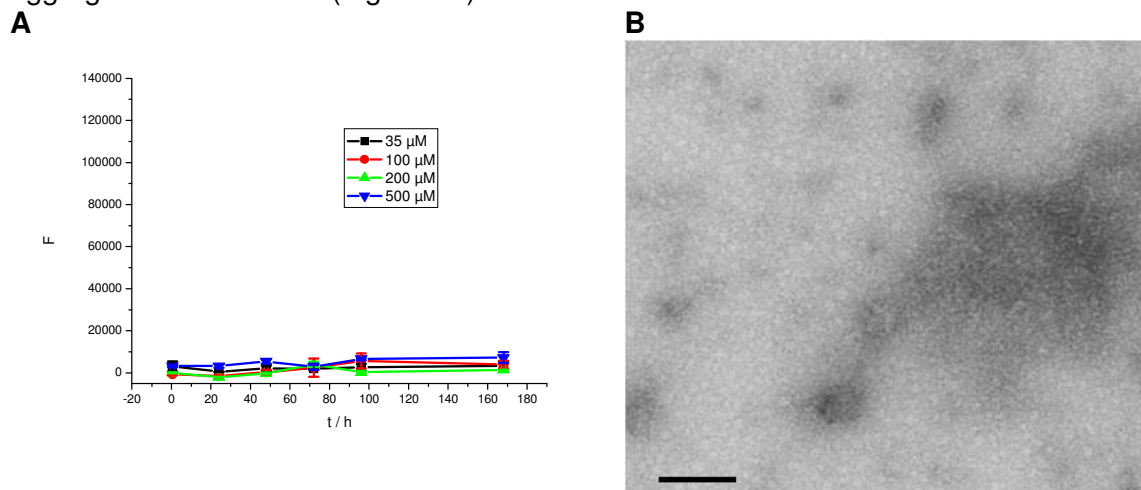


Fig. 330: (A) ThT assays of Lys-KKK-lin at different concentrations in 1x 1% HFIP, pH 7.4 (from [186]). Data are means of 3 assays after subtraction of buffer values +/- standard error of the mean (SEM) with each experiment performed in multiple replicates (n = 3). (B) TEM picture of an aged incubation of Lys-KKK-lin. The peptide was incubated at 500 μM for 7 d in 1x 1% HFIP, pH 7.4. Scale bar: 100 nm.

Similar to Congo red stained aggregates of H-NKGAI-KKK-NFGAILS-OH (Fig. 233A and B), staining of an Aged incubations of Lys-KKK-lin displayed aggregates that could be stained with Congo Red as indicated by a red color under normal light (Fig. 331A). However no birefringence could be detected under cross-polarized light (Fig. 331B).

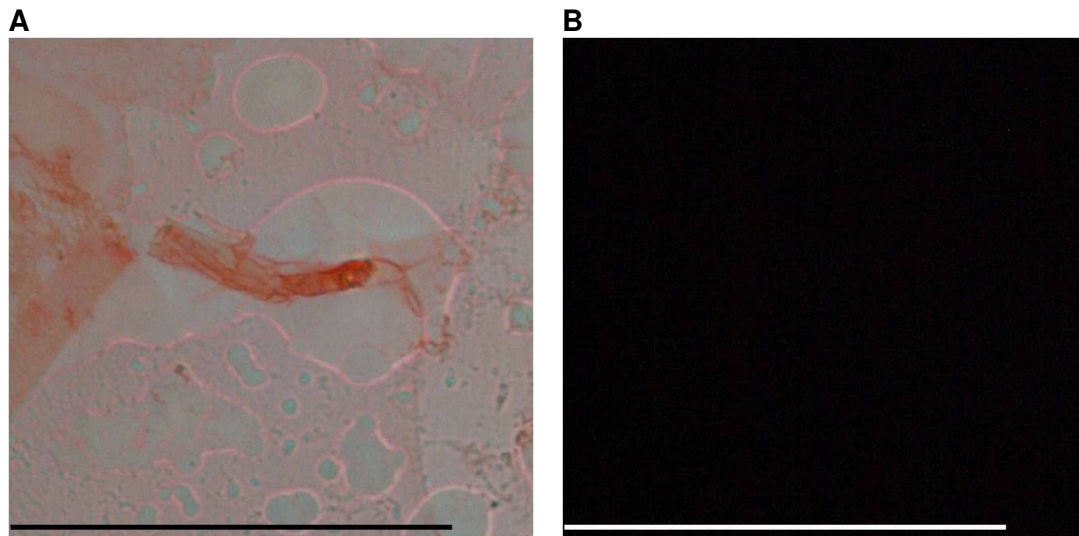


Fig. 331: Microscopic examination of an aged incubation of Lys-KKK-lin stained with Congo Red. The peptide was incubated at a concentration of 1 mM in 1xb 1% HFiP, pH 7.4 for 3 days. Pictures were taken under A normal and B cross-polarized light. Scale bar: 100 μ m. (from [186]).

3.3.2.10 Linear H-Dap-NKGAI-KKK-NFGAILS-Asp-OH (Dap-KKK-lin)

The CD spectra of Dap-KKK-lin (Fig. 332A) displayed a negative signal at 195 nm indicating random coil structure and additionally a negative signal at 210-230 nm indicating the presence of additional β -sheet or β -turn elements. The peptide started to form soluble oligomers already between a concentration of 5 μ M and 10 μ M.

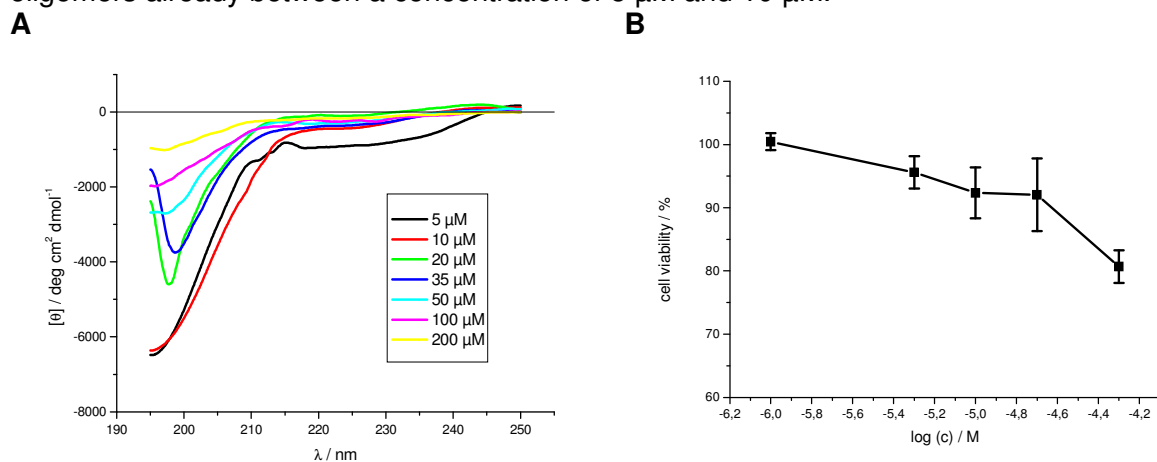


Fig. 332: (A) Far-UV CD spectra of Dap-KKK-lin at different concentrations in 1xb 1% HFiP, pH 7.4 (from [186]). (B) Cell viability assay of an aged solution of Dap-KKK-lin (5 mM in 1xb 1% HFiP, pH 7.4 for 4 days) using PC-12 cells. Data are percentages of control and are the mean (+/-SEM) of three independent experiments with each experiment performed in multiple replicates (n = 3).

Under the conditions tested Dap-KKK-lin was toxic to PC-12 cells (Fig. 332B).

The fibril forming potential of Dap-KKK-lin (Fig. 333A), was similar to that of H13Ser (Fig. 327A). ThT assays of Dap-KKK-lin at a peptide concentration of 200 μ M showed an increase in the fluorescence signal of ThT indicating fibril formation.

TEM examination of an aged incubation of Dap-KKK-lin at a peptide concentration of 35 μ M displayed many short fibrils (Fig. 333B).

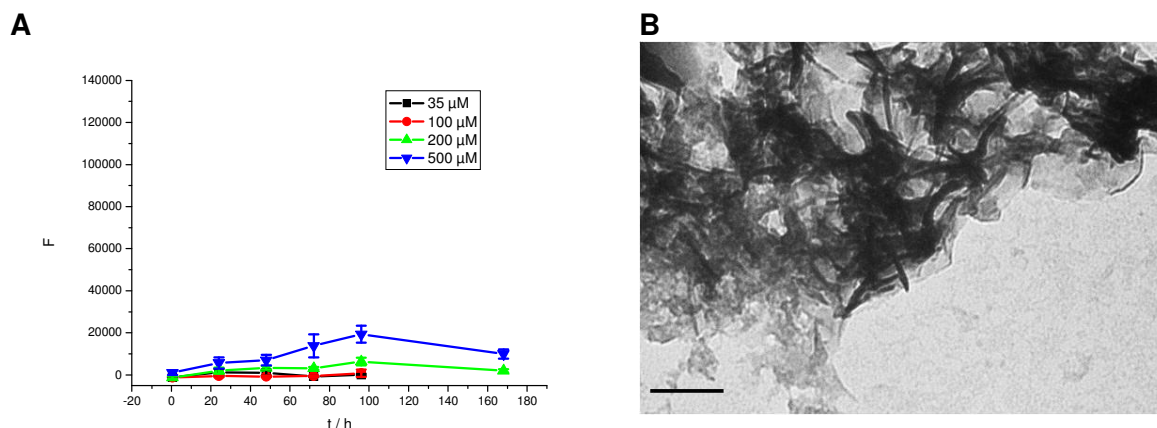


Fig. 333: (A) ThT assays of Dap-KKK-lin at different concentrations in 1xb 1% HFIP, pH 7.4 (from [186]). Data are means of 3 assays after subtraction of buffer values +/- standard error of the mean (SEM) with each experiment performed in multiple replicates (n = 3).

(B) TEM picture of an aged incubation of Dap-KKK-lin. The peptide was incubated at 500 μM for 7 d in 1xb 1% HFIP, pH 7.4. Scale bar: 100 nm.

Fibrillar aggregates of Dap-KKK-lin stained with Congo Red revealed weak red color under normal light (Fig. 334A) and displayed yellow and orange birefringence under cross-polarized light (Fig. 334B).

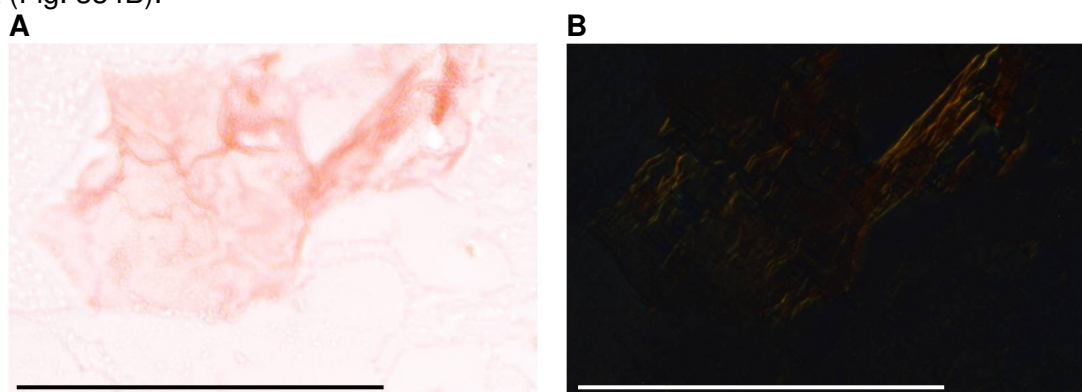


Fig. 334: Microscopic examination of an aged incubation of Dap-KKK-lin stained with Congo Red. The peptide was incubated at a concentration of 1 mM in 1xb 1% HFIP, pH 7.4 for 3 days. Pictures were taken under A normal and B cross-polarized light. Scale bar: 100 μm (from [186]).

3.3.2.11 Cyclic H-Dap-NKGAI-KKK-NFGAILS-Asp-OH (Dap-KKK-cyclo)

Similar to H12CC, Dap-KKK-cyclo could not be obtained in its monomeric form. This could be confirmed by an oligomerization assay. The assay showed no monomeric Dap-KKK-cyclo at all, only covalently bound dimers and higher ordered oligomers (Fig. 336). The oligomerization possibly occurred instead of intramolecular cyclisation during the synthesis. Data presented below and their discussions always refer to a mixture of different oligomeric forms of this peptide.

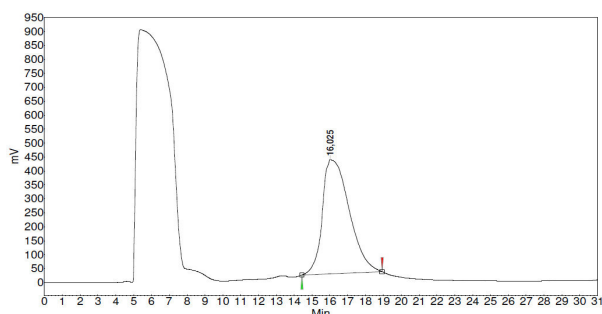


Fig. 335: HPLC of Dap-KKK-cyclo. The peptide eluted after 16.025 minutes. 1.5 mg crude peptide was dissolved in 200 μ l TFA and 800 μ l 80% buffer B in A ([186]).

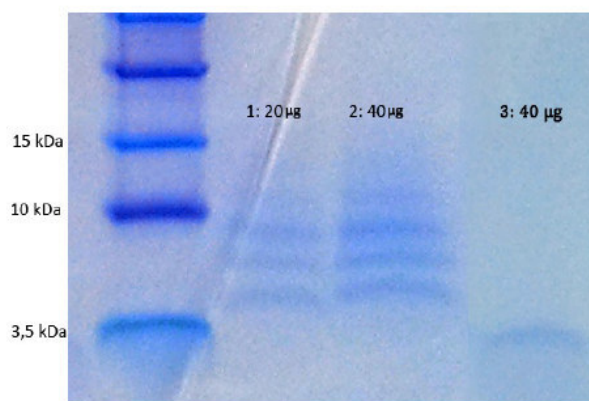
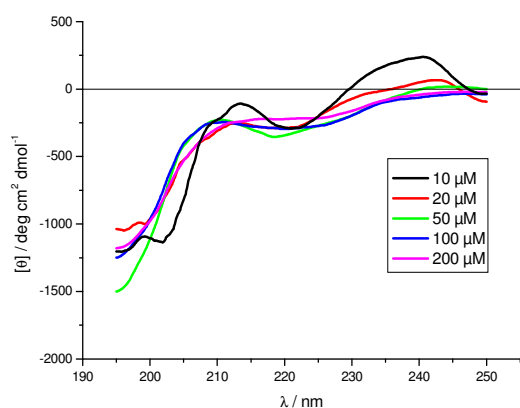


Fig. 336: Oligomerization assay of Dap-KKK-cyclo. Shown are the marker, 20 μ g Dap-KKK-cyclo, 40 μ g Dap-KKK-cyclo and 40 μ g Dap-KKK-lin in 1xb, pH 7.4 (from [186]). The samples were denatured at 95°C for 5 min prior to plotting onto the gel. The gel was stained with Coomassie Brilliant Blue. For Dap-KKK-cyclo, bands referring to dimers, trimers, and tetramers are clearly visible, whereas no band referring to monomers is visible.

Concentration dependent CD spectra of Dap-KKK-cyclo (Fig. 337A) also displayed both a strong minimum at 195 - 200 nm that can be related to random coil structure and a weaker negative signal between 210 nm and 225 nm indicating the presence of additional structural elements like β -sheet or β -turn.

The signal intensity of the CD spectra of Dap-KKK-cyclo is very low. Dap-KKK-cyclo also did not display concentration dependent changes of the CD spectra. Both might be due to the fact that only multimeric but not monomeric Dap-KKK-cyclo was present.

A



B

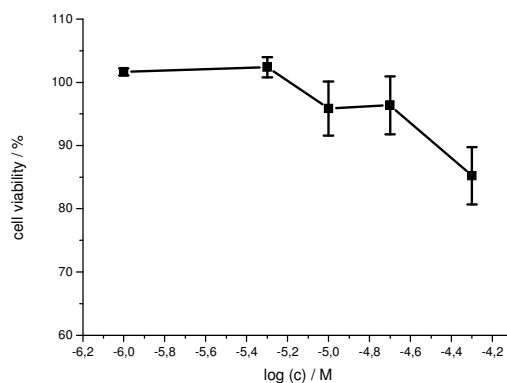


Fig. 337: (A) Far-UV CD spectra of Dap-KKK-cyclo at different concentrations in 1xb 1% HFIP, pH 7.4 (from [186]).

(B) Cell viability assay of an aged solution of Dap-KKK-cyclo (5 mM in 1xb 1% HFIP, pH 7.4 for 4 days) using PC-12 cells. Data are percentages of control and are the mean (+/-SEM) of three independent experiments with each experiment performed in multiple replicates (n = 3).

Under the conditions tested Dap-KKK-cyclo showed some toxicity to PC-12 cells (Fig. 337B). ThT studies of Dap-KKK-cyclo did reveal weak fibril formation at a concentration of 100 μM (Fig. 338A).

The TEM image of aged aggregates of Dap-KKK-cyclo showed lots of fibrils but also some amorphous structures (Fig. 338B).

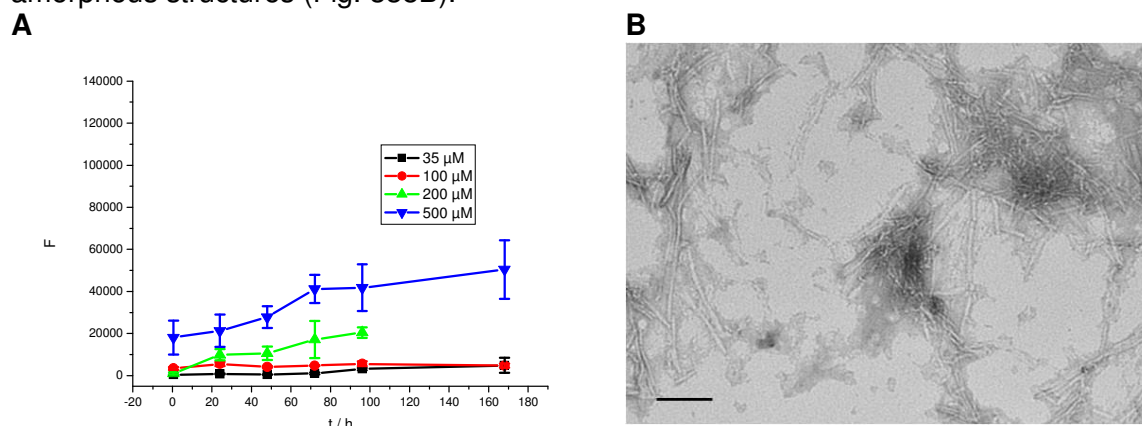


Fig. 338: (A) ThT assays of Dap-KKK-cyclo at different concentrations in 1xb 1% HFiP, pH 7.4 (from [186]). Data are means of 3 assays after subtraction of buffer values \pm standard error of the mean (SEM) with each experiment performed in multiple replicates ($n = 3$).

(B) TEM picture of an aged incubation of Dap-KKK-cyclo. The peptide was incubated at 500 μM for 7 d in 1xb 1% HFiP, pH 7.4. Scale bar: 100 nm.

Congo red stained aggregates of Dap-KKK-cyclo (Fig. 339A and B) displayed red color under normal light (Fig. 339A) and reddish birefringence under cross-polarized light (Fig. 339B).

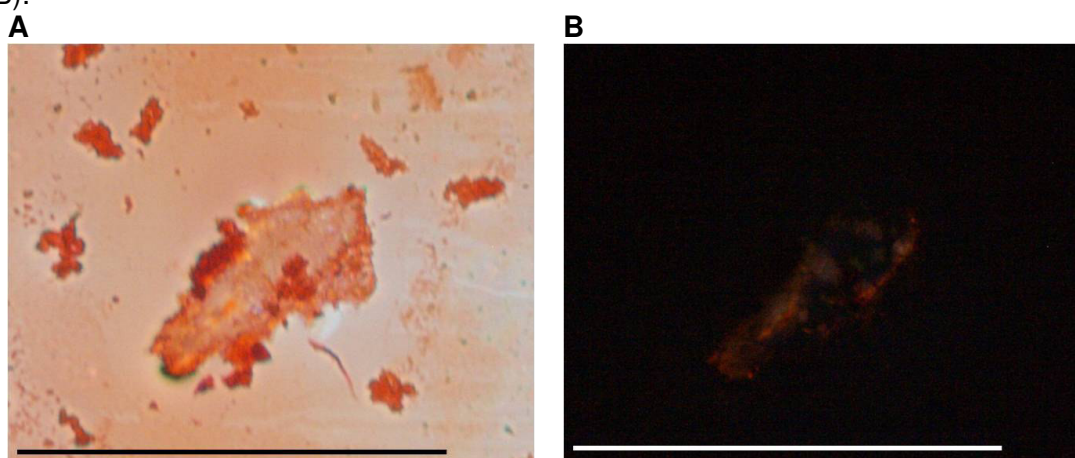


Fig. 339: Microscopic examination of an aged incubation of Dap-KKK-cyclo stained with Congo Red. The peptide was incubated at a concentration of 1 mM in 1xb 1% HFiP, pH 7.4 for 3 days. Pictures were taken under A normal and B cross-polarized light. Scale bar: 100 μm . (From [186]).

3.3.2.12 Linear H-C-NKGAI-Aoc-NFGAILS-C-OH (H5aCC-red)

Far-UV CD spectra of H5aCC-red (Fig. 340A) showed a broad and intense minimum around 205-215 nm indicating the presence of β -sheet structure. The signal intensity decreased at peptide concentrations higher than 5 μM . This signal decrease might be related to the formation of soluble oligomers.

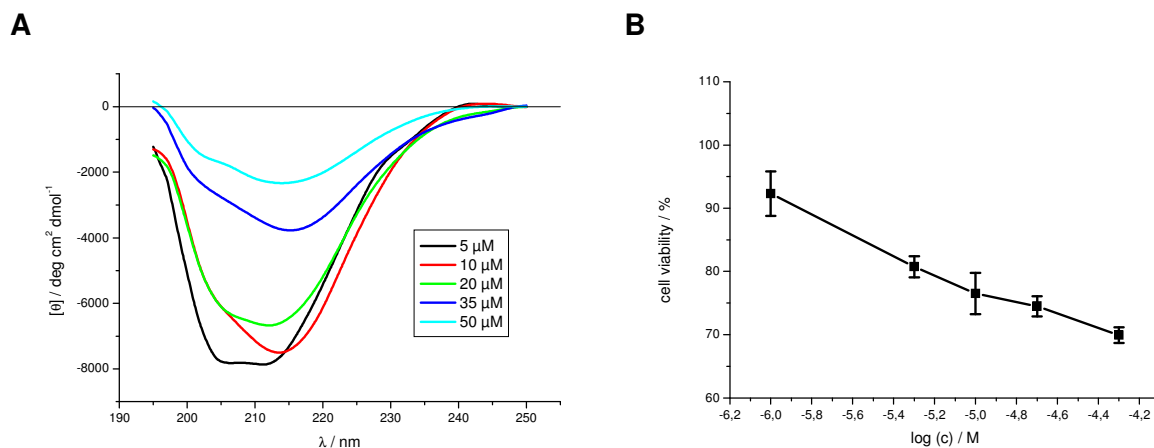


Fig. 340: (A) Far-UV CD spectra of H5aCC-red at different concentrations in 1xb 1% HFIP, pH 7.4 (from [187]). (B) Cell viability assay of an aged solution of H5aCC-red (5 mM in 1xb 1% HFIP, pH 7.4 for 4 days) using PC-12 cells. Data are percentages of control and are the mean (+/-SEM) of three independent experiments with each experiment performed in multiple replicates (n = 3).

As seen on Fig. 340B H5aCC-red proved to be toxic to PC-12 cells under the conditions tested.

The fibril forming potential of H5aCC-red was determined by ThT assays. These assays showed that H5aCC-red started forming fibrils already at a peptide concentration of 10 μM (Fig. 341A). This correlated well with the high aggregation potential of H5aCC-red as determined by CD spectroscopy.

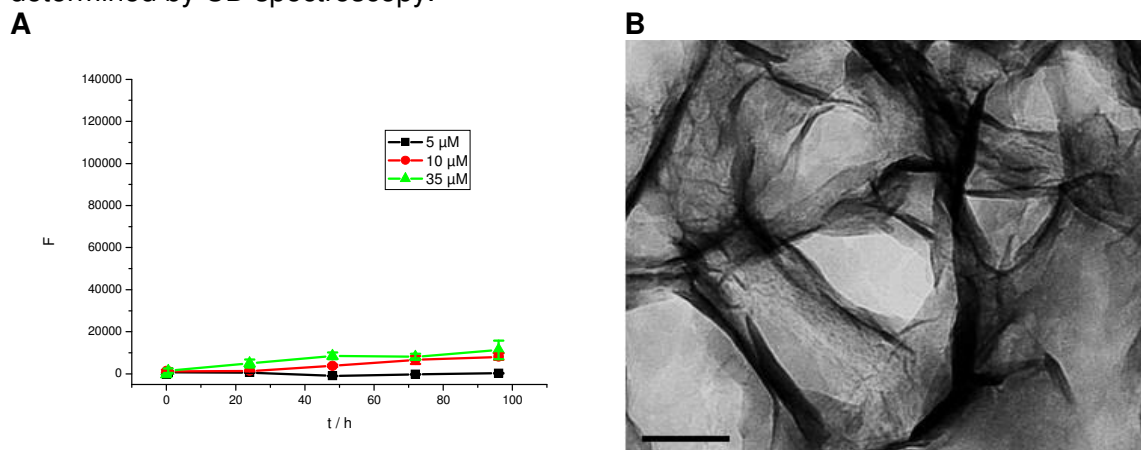


Fig. 341: (A) ThT assays of H5aCC-red at different concentrations in 1xb 1% HFIP, pH 7.4. Data are means of 3 assays after subtraction of buffer values +/- standard error of the mean (SEM) with each experiment performed in multiple replicates (n = 3).

(B) TEM picture of an aged incubation of H5aCC-red .The peptide was incubated at 50 μM for 7 d in 1xb 1% HFIP, pH 7.4. Scale bar: 100 nm.

The fibril formation of H5aCC-red was verified by both Congo Red staining (Fig. 342A and B) and TEM imaging (Fig. 341B) of aged incubations. At a peptide concentration of 50 μM, the TEM image of H5aCC-red displayed many short black fibrils.

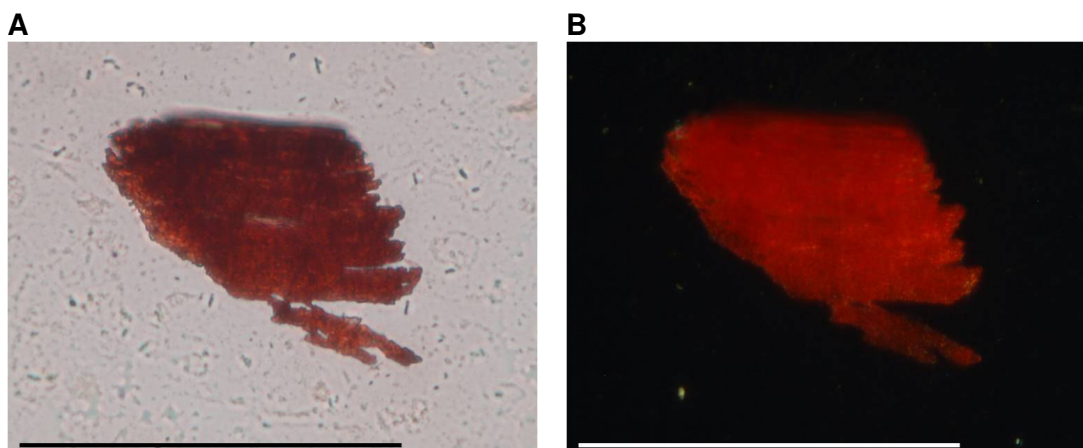


Fig. 342: Microscopic examination of an aged incubation H5aCC-red stained with Congo Red. The peptide was incubated at a concentration of 1 mM in 1xb 1% HFIP, pH 7.4 for 3 days. Pictures were taken under A normal and B cross-polarized light. Scale bar: 100 µm.

3.3.2.13 Cyclic H-C-NKGAI-Aoc-NFGAILS-C-OH (H5aCC-ox)

CD spectra of H5aCC-ox (Fig. 343A) revealed a broad and intense minimum at around 215 nm indicating the formation of β -sheet structures.

Compared to H5aCC-red the minimum of this signal was shifted towards a higher wavelength. Another difference between H5aCC-red and H5aCC-ox concerns their aggregation potential. H5aCC-red aggregated at a slightly faster, whereas the signal loss upon aggregation was much higher for H5aCC-ox. At a concentration of 10 µM the CD signal of H5aCC-ox was similar to that at 5 µM. The signal at a peptide concentration of 20 µM was however already much weaker.

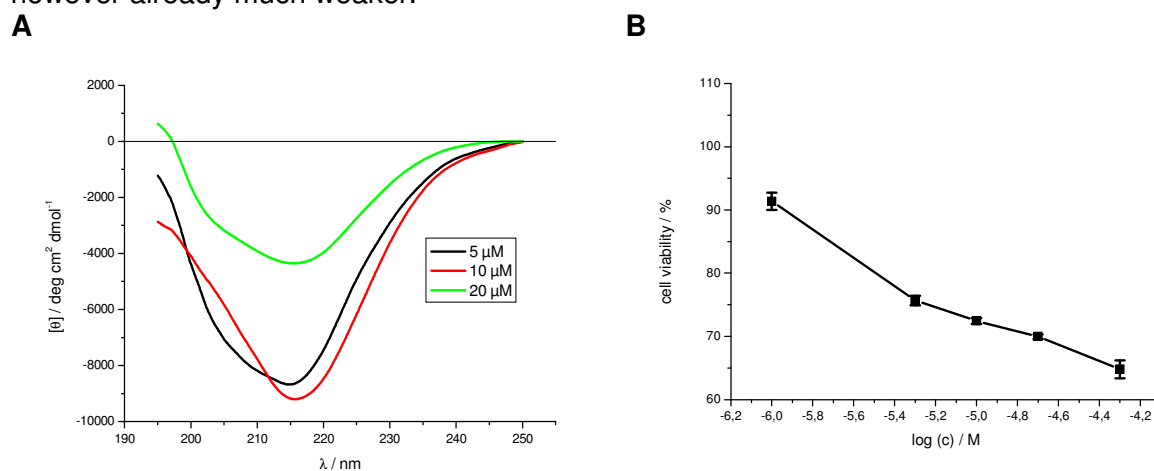


Fig. 343: (A) Far-UV CD spectra of H5aCC-ox at different concentrations in 1xb 1% HFIP, pH 7.4.

(B) Cell viability assay of an aged solution of H5aCC-ox (5 mM in 1xb 1% HFIP, pH 7.4 for 4 days) using PC-12 cells. Data are percentages of control and are the mean (+/-SEM) of three independent experiments with each experiment performed in multiple replicates (n = 3).

Cell viability assays displayed that H5aCC-ox was highly toxic towards PC-12 cells (Fig. 343B), more toxic than H5aCC-red.

ThT studies at different concentrations revealed, that H5aCC-ox started forming fibrils at a peptide concentration of 10 µM (Fig. 344A) similar to H5aCC-red. Fibril formation occurred however after a shorter lag phase indicating a higher fibril forming potential for H5aCC-ox.

Fibril formation could also be verified by TEM. The TEM image of an aged incubation of H5aCC-ox at a concentration of 50 µM clearly displayed amyloid fibrils (Fig. 344B).

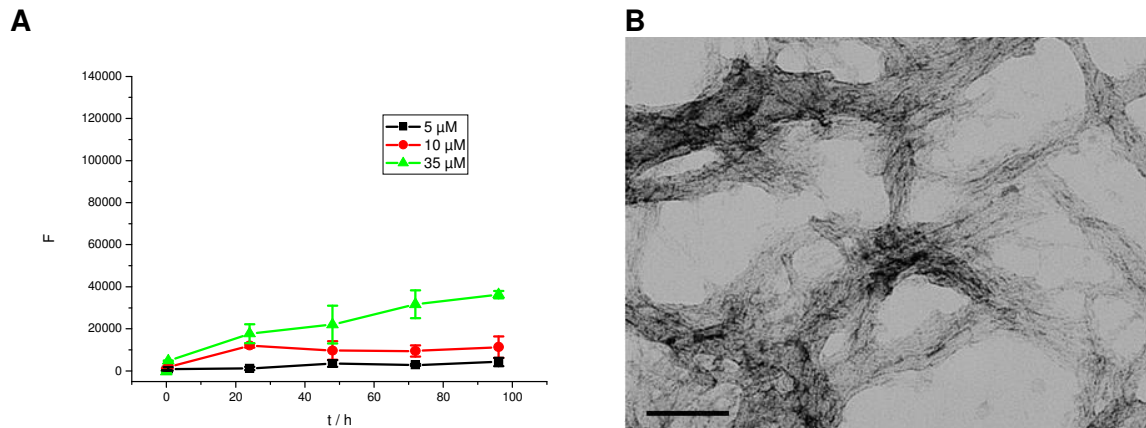


Fig. 344: (A) ThT assays of H5aCC-ox at different concentrations in 1xb 1% HFIP, pH 7.4. Data are means of 3 assays after subtraction of buffer values \pm standard error of the mean (SEM) with each experiment performed in multiple replicates ($n = 3$).

(B) TEM picture of an aged incubation of H5aCC-ox. The peptide was incubated at 50 μ M for 7 d in 1xb 1% HFIP, pH 7.4. Scale bar: 100 nm.

Staining of an aged incubation of H5aCC-ox with Congo Red also confirmed the presence of amyloid fibrils. Stained aggregates showed intense red color under normal light (Fig. 345A) and some of them displayed bright red yellow and green birefringence under cross-polarized light (Fig. 345B).

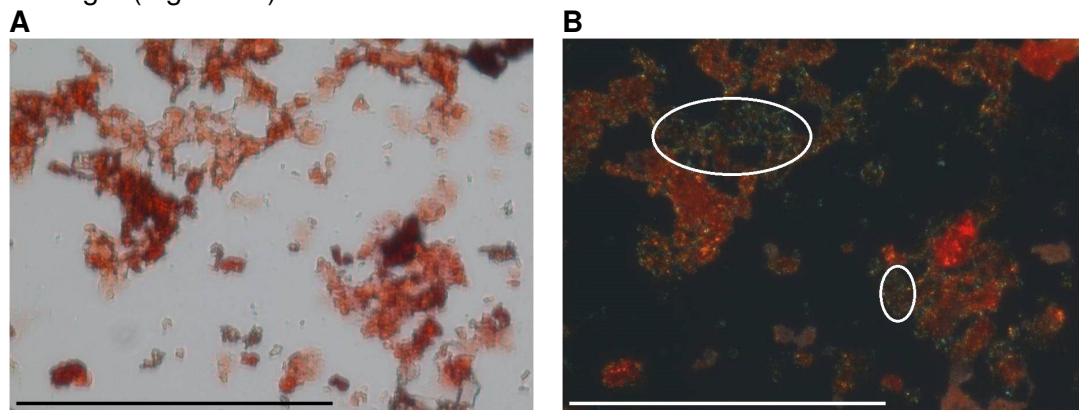


Fig. 345: Microscopic examination of an aged incubation of H5aCC-ox stained with Congo Red. The peptide was incubated at a concentration of 1 mM in 1xb 1% HFIP, pH 7.4 for 3 days. Pictures were taken under A normal and B cross-polarized light. Scale bar: 100 μ m.

3.3.2.14 Dimer 3 red

CD spectra of Dimer 3 red (Fig. 346A) revealed a broad and intense minimum at around 215-220 nm indicating the presence of β -sheet structure. The minimum of this signal was shifted towards higher wavelengths for higher peptide concentrations.

Aggregation of Dimer 3 red started between a concentration of 10 μ M and 20 μ M.

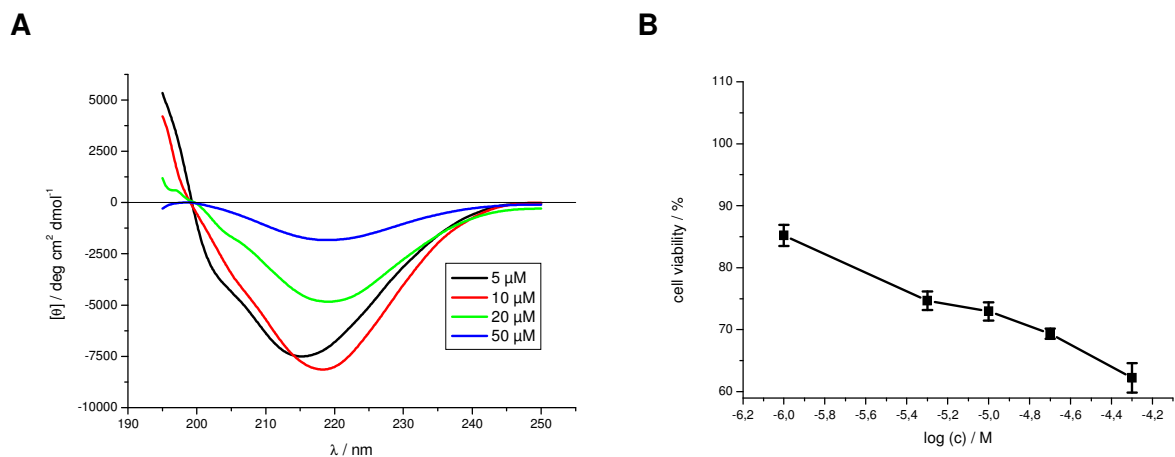


Fig. 346: (A) Far-UV CD spectra of Dimer 3 red at different concentrations in 1x 1% HFIP, pH 7.4 (from [187]). (B) Cell viability assay of an aged solution of Dimer 3 red (5 mM in 1x 1% HFIP, pH 7.4 for 4 days) using PC-12 cells. Data are percentages of control and are the mean (+/-SEM) of three independent experiments with each experiment performed in multiple replicates (n = 3).

Under the conditions tested Dimer 3 red proved to be toxic to PC-12 cells (Fig. 346B). The fibril forming potential of Dimer 3 red was determined by ThT assays. These assays showed that Dimer 3 red started forming fibrils at a peptide concentration of 10 μM (Fig. 347A). The TEM image of an aged incubation of Dimer 3 red at a peptide concentration of 100 μM showed many amyloid fibrils but also some amorphous aggregates (Fig. 347B).

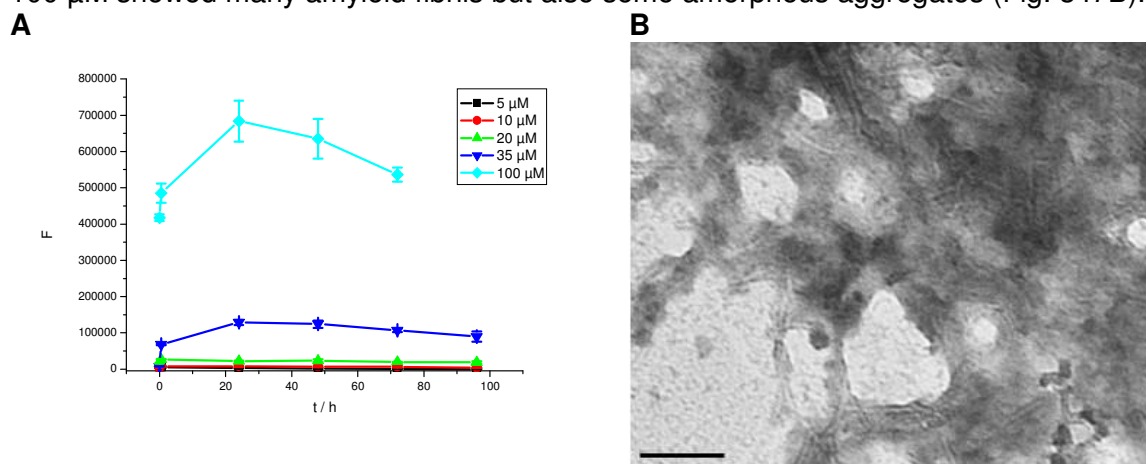


Fig. 347: (A) ThT assays of Dimer 3 red at different concentrations in 1x 1% HFIP, pH 7.4 (partially from [187]). Data are means of 3 assays after subtraction of buffer values +/- standard error of the mean (SEM) with each experiment performed in multiple replicates (n = 3). (B) TEM picture of an aged incubation of Dimer 3 red. The peptide was incubated at 100 μM for 7 d in 1x 1% HFIP, pH 7.4. Scale bar: 100 nm.

Staining of an aged incubation of Dimer 3 red with Congo Red also confirmed the formation of amyloid fibrils. Stained aggregates showed intense red color under normal light (Fig. 348A) and displayed bright red color under cross-polarized light (Fig. 348B).

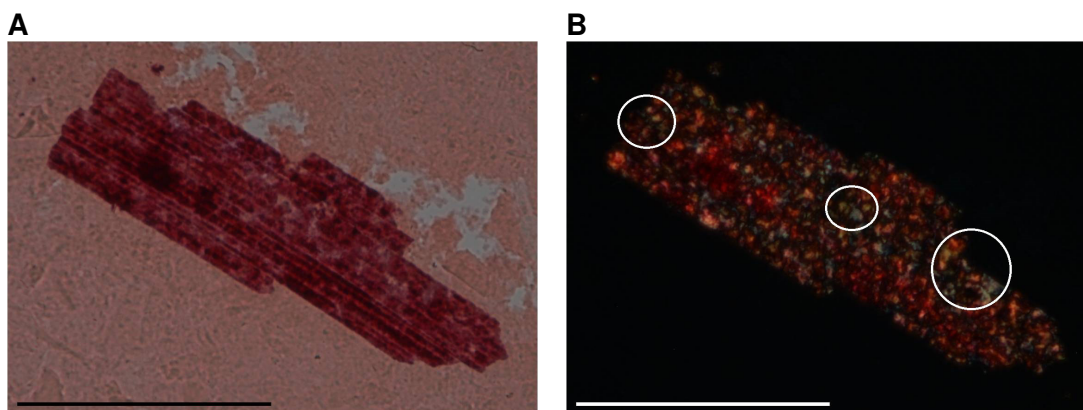


Fig. 348: Microscopic examination of an aged incubation of Dimer 3 red stained with Congo Red. The peptide was incubated at a concentration of 1 mM in 1xb 1% HFIP, pH 7.4 for 3 days. Pictures were taken under A normal and B cross-polarized light. Scale bar: 100 µm.

3.3.2.15 Dimer 3 ox

Fig. 349A shows the CD spectra of Dimer 3 ox. They displayed a broad and intense minimum around 218 nm. The spectra at a concentration of 5 and 10 µM were almost identical, indicating that peptide aggregation started at concentrations higher than 10 µM. Compared to Dimer 3 red (Fig. 346A), the signal intensity was in general much lower than for Dimer 3 ox.

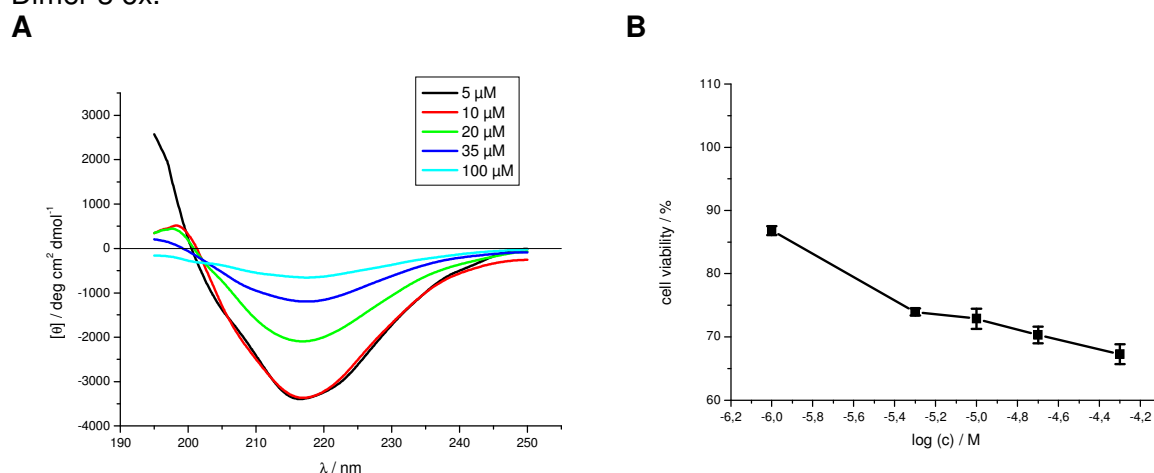


Fig. 349: (A) Far-UV CD spectra of Dimer 3 ox at different concentrations in 1xb 1% HFIP, pH 7.4. (B) Cell viability assay of an aged solution of Dimer 3 ox (5 mM in 1xb 1% HFIP, pH 7.4 for 4 days) using PC-12 cells. Data are percentages of control and are the mean (+/-SEM) of three independent experiments with each experiment performed in multiple replicates (n = 3).

As seen on Fig. 349B, Dimer 3 ox displayed high toxicity towards PC-12 cells. When compared to Dimer 3 red (Fig. 346B), Dimer 3 ox proved to be even more toxic. ThT studies of Dimer 3 ox at different peptide concentrations revealed, that Dimer 3 ox started forming fibrils at a concentration of 20 µM (Fig. 350A). Fibril formation occurred quite fast, already after 30 minutes of incubation. The concentration dependent CD spectrum at 20 µM already showed a signal loss related to oligomerization (Fig. 349A). This correlates with a fast fibril formation observed by ThT assays.

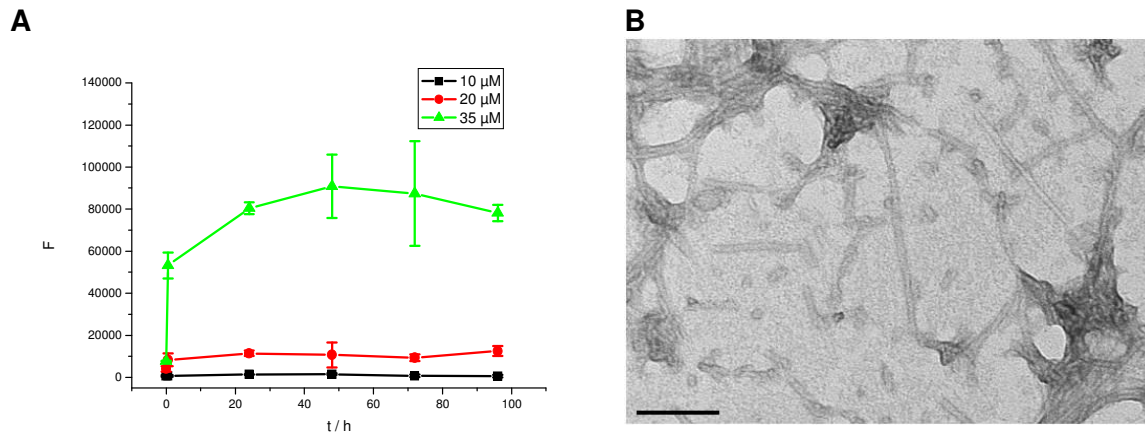


Fig. 350: (A) ThT assays of Dimer 3 ox at different concentrations in 1xb 1% HFIP, pH 7.4. Data are means of 3 assays after subtraction of buffer values \pm standard error of the mean (SEM) with each experiment performed in multiple replicates ($n = 3$). (B) TEM picture of an aged incubation of Dimer 3 ox. The peptide was incubated at 35 μ M for 7 d in 1xb 1% HFIP, pH 7.4. Scale bar: 100 nm.

Fibril formation of Dimer 3 ox could be verified by both Congo Red staining (Fig. 351A and B) and TEM imaging (Fig. 350B) of aged incubations. The TEM image of an aged incubation of Dimer 3 ox at a peptide concentration of 35 μ M showed many straight fibrils (Fig. 350B). Staining of aged aggregates of Dimer 3 ox with Congo Red revealed deep red color under normal light (Fig. 351A) and partially green and yellow color under cross-polarized light (Fig. 351B).

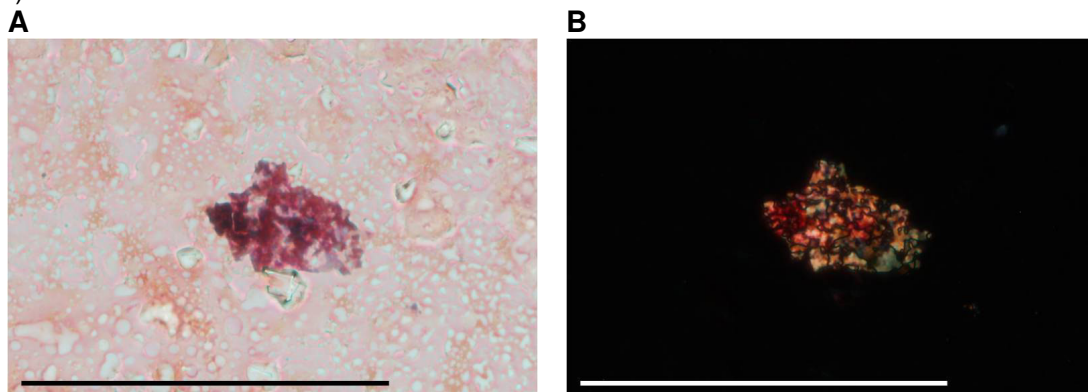


Fig. 351: Microscopic examination of an aged incubation of Dimer 3 ox stained with Congo Red. The peptide was incubated at a concentration of 1 mM in 1xb 1% HFIP, pH 7.4 for 3 days. Pictures were taken under A normal and B cross-polarized light. Scale bar: 100 μ m.

Table 28: Overview of ThT binding assays and cell viability assays performed with cyclic peptides and their linear equivalents at different concentrations.

Results of “+” indicate fibril formation, whereas “-” indicate no fibril formation within the 5 days of incubation of the solution at the given peptide concentration.

For the cell viability assays, results of “+++” mean high toxicity towards PC-12 cell, “++” means medium toxicity and “+/-” means low to no toxicity. Low toxicity refers to peptides with >90% cell viability, medium toxicity refers to a cell viability between 80% and 90%, and high toxicity refers to a cell viability of <80% for aged incubations at a peptide concentration of 50 μ M.

Abbrev.	Sequence	ThT								Tox.
		5 μ M	10 μ M	20 μ M	35 μ M	100 μ M	200 μ M	350 μ M	500 μ M	
H12CC	H-C-NKGAI-LLL-NFGAALS-C-OH				+	+				+++
H12Ser	H-S-NKGAI-LLL-NFGAALS-S-OH				+					+++
Lys-LLL-lin	H-Lys-NKGAI-LLL-NFGAALS-OH		+	+	+					+++
Lys-LLL-cyclo	cyclo-Lys- NKGAI-LLL-NFGAALS-OH				-	+			+	+++
Dap-LLL-lin	H-Dap-NKGAI-LLL-NFGAALS-OH		+	+	+					+++
H13CC-red	H-C-NKGAI-KKK-NFGAALS-C-OH				-	+				+/-
H13CC-ox	H-C-NKGAI-KKK-NFGAALS-C-OH				-	-	-		+	+/-
H13Ser	H-S-NKGAI-KKK-NFGAALS-S-OH				-	-	+		+	+/-
Lys-KKK-lin	H-Lys-NKGAI-KKK-NFGAALS-OH				-	-	-		-	+/-
Dap-KKK-lin	H-Dap-NKGAI-KKK-NFGAALS-OH				-	-	+		+	++
Dap-KKK-cyclo	cyclo-Dap-NKGAI-KKK-NFGAALS-OH				-	+/-	+		+	++
H5aCC-red	H-C-NKGAI-Aoc-NFGAALS-C-OH	-	+		+					+++
H5aCC-ox	H-C-NKGAI-Aoc-NFGAALS-C-OH	+	+		+					+++
Dimer 3 red		-	+	+	+	+				+++
Dimer 3 ox			-	+	+					+++

3.3.3 Comparisons

The results of this work show that it was possible to synthesize and characterize at least one monomeric cyclic peptide for each of the chosen connecting elements between the A β (27-32) and IAPP(22-28) segments. The way to achieve this goal differed nevertheless for each specific peptide. One commonly occurring side reaction was oligomerization rather than cyclization when either a disulfide bridge or a peptide bond was formed between different molecules instead of intramolecularly resulting in covalent oligomers. This problem could be solved by working with low peptide concentrations during cyclization (cyclization of peptides under pseudo-high dilution conditions [188]) and by optimizing of the conditions used for the intramolecular oxidization of cysteines.

The method of cyclization by an intramolecular disulfide bridge between two cysteine residues proved to be more efficient than the cyclisation on the resin involving the formation of a side chain to side chain peptide bond.

In the case of H12CC no monomeric cyclic peptide could be obtained.

The hydrophobic connecting elements Aoc and LLL once again demonstrated their ability to induce β -sheet structure and promote fibril formation even in cyclic structures, whereas the hydrophilic connecting element KKK was found to suppress the formation of fibrils.

3.3.3.1 Peptides with the connecting element LLL

The first connecting element chosen consisted of three leucine residues which made the peptide very hydrophobic.

Previous studies of linear peptides with this connecting element showed that it was able to induce the formation of amyloid fibrils and β -sheet structure. Thus, the ability to form fibrils was also expected for cyclic peptides containing the connecting element LLL.

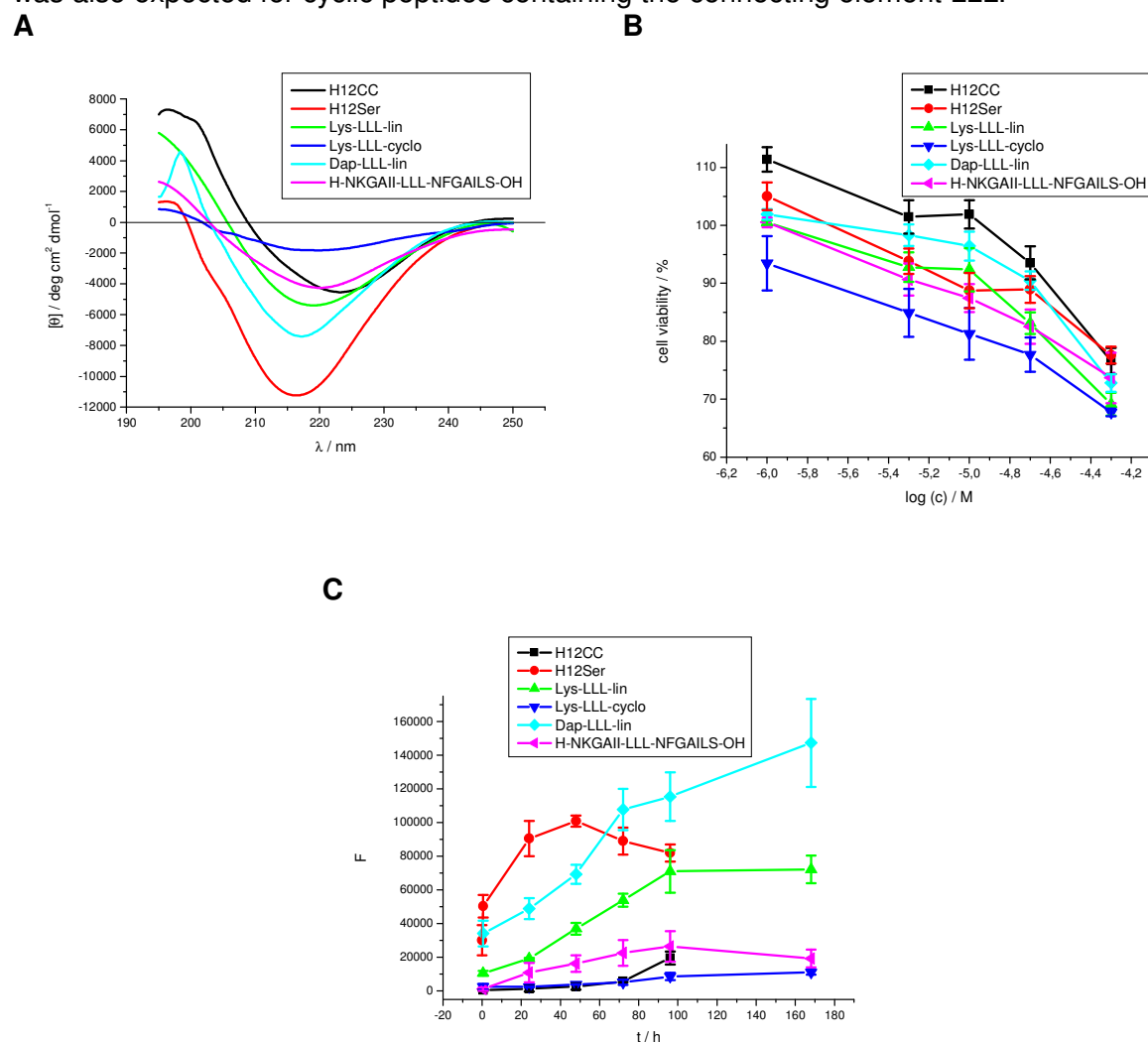


Fig. 352: Comparison of cyclic peptides containing the connecting element LLL and their linear equivalents.

A) Far-UV CD spectra at a peptide concentration of 10 μ M in 1xb 1% HFIP, pH 7.4.

B) Cell viability assays of aged solutions (5 mM in 1xb 1% HFIP for 4 days, pH 7.4) using PC-12 cells. Data are percentages of control and are the mean (+/-SEM) of three independent experiments with each experiment performed in multiple replicates (n = 3).

C) ThT assays at a peptide concentration of 35 μ M in 1xb 1% HFIP, pH 7.4. Data are means of 3 assays after subtraction of buffer values +/- standard error of the mean (SEM) with each experiment performed in multiple replicates (n = 3).

Cyclic peptides containing the connecting element LLL were able to form amyloid fibrils as indicated by ThT assays, Congo Red staining, and TEM imaging. Comparing the fibril

forming potential of cyclic peptides with their linear equivalents, however, revealed that the fibril forming potential was reduced upon cyclisation.

Lys-LLL-lin was already forming fibrils at a peptide concentration of 10 μM whereas its cyclic equivalent Lys-LLL-cyclo did not form fibrils until a peptide concentration of 100 μM as indicated by ThT assays (Fig. 352C and table 29).

All peptides with the connecting element LLL showed β -sheet structure in CD studies and displayed toxicity to PC-12 cells in cell viability assays (Fig. 352A and B).

The red shift of the minimum in the CD spectra of H12CC might have been due to oligomerization. Experiments with the peptide H12cc were difficult to interpret, because the peptide always displayed a mixture of reduced and oxidized, monomeric and oligomeric forms.

Table 29: ThT binding assays of cyclic and linear peptides containing LLL as a connecting element at different peptide concentrations.

Results of “+” indicate fibril formation, whereas “-” indicate no fibril formation within the 5 days of incubation of the solution at the given peptide concentration.

Abbrev.	Sequence	ThT				
		10 μM	20 μM	35 μM	100 μM	500 μM
H12CC	H-C-NKGAI-LLL-NFGAILS-C-OH			+	+	
H12Ser	H-S-NKGAI-LLL-NFGAILS-S-OH			+		
Lys-LLL-lin	H-Lys-NKGAI-LLL-NFGAILSD-OH	+	+	+		
Lys-LLL-cyclo	cyclo-Lys- NKGAI-LLL-NFGAILSD-OH			-	+	+
Dap-LLL-lin	H-Dap-NKGAI-LLL-NFGAILSD-OH	+	+	+		
H12	H-NKGAI-LLL-NFGAILS-OH	-	+	+		

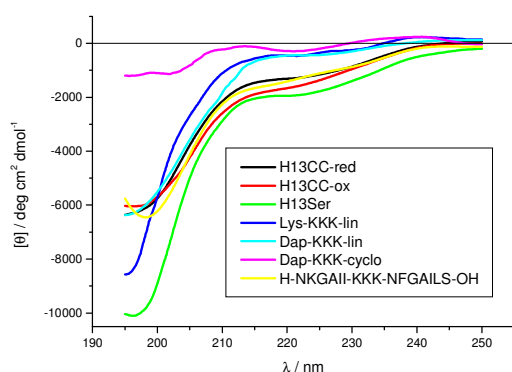
3.3.3.2 Peptides with the connecting element KKK

The influence of positive charges on fibril forming potentials and structure was studied with peptides containing three lysine residues as connecting element.

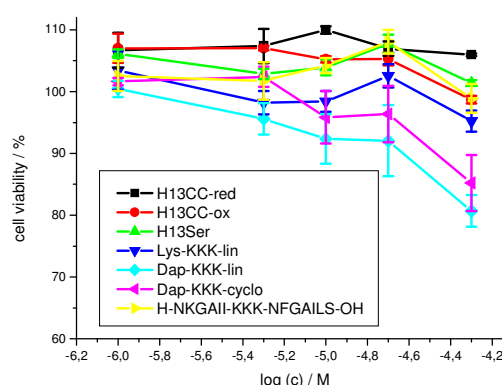
In general, a negative effect of positive charges on fibril formation was expected.

In previous studies H-NKGAI-KKK-NFGAILS-OH without additional residues at the C- and N-terminus was not able to form fibril like structures ([159], chapter 3.2.2) even though two hot spots regions of A β and IAPP that are able to interact with each other were connected.

A



B



C

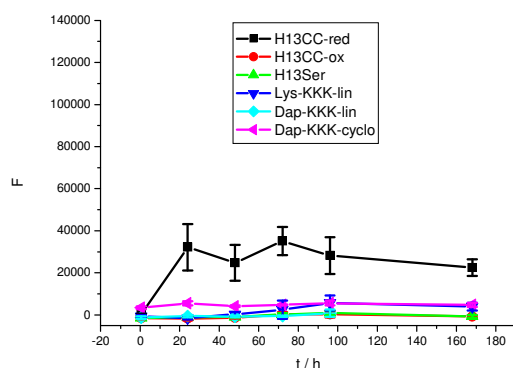


Fig. 353: Comparison of cyclic peptides containing the connecting element KKK and their linear equivalents. A) Far-UV CD spectra at a peptide concentration of 10 μ M in 1xb 1% HFIP, pH 7.4. B) Cell viability assays of aged solutions (5 mM in 1xb 1% HFIP for 4 days, pH 7.4) using PC-12 cells. Data are percentages of control and are the mean (+/-SEM) of three independent experiments with each experiment performed in multiple replicates (n = 3). C) ThT assays at a peptide concentration of 200 μ M in 1xb 1% HFIP, pH 7.4. Data are means of 3 assays after subtraction of buffer values +/- standard error of the mean (SEM) with each experiment performed in multiple replicates (n = 3).

The results shown here displayed that peptides with the charged connecting element KKK were able to form fibrils (Fig. 353C). Only Lys-KKK-lin was not able to form fibrils under the conditions tested. It was also not possible to cyclize Lys-KKK-lin by using the side-chain-to-side-chain cyclisation on the resin method.

The core region of these peptides was the same and possessed the sequence NKGAIL-KKK-NFGAILS. The differences between these analogues were only the additional residues at the C- and N-terminus of the peptides.

In the case for H13CC-red and H13Ser, polar interactions involving the side chains of cysteine or serine residues respectively might have been responsible for their ability to form fibrils by providing additional energy needed for structural rearrangement and fibril formation. The fibril forming ability of these peptides was however still much lower than for example for peptides with hydrophobic connecting motifs.

For Dap-KKK-lin and Lys-KKK-lin, electrostatic attraction between the negatively charged Asp side chain at the C-terminus and the positively charged side chain of Dap or Lys at the N-terminus can be the reason why these peptides form fibrils. The distance between two hot spot regions interacting due to this attraction might have been shorter for Dap-KKK-lin than for Lys-KKK-lin. This shorter distance between two potentially aligning hot spot regions might have enabled them to form a steric zipper like motif that could have functioned as a seed for subsequent fibril formation. One indication for this hypothesis might be that oligomerized Dap-KKK-cyclo was also found to be able to form fibrils, maybe because of the presence of dimers that were able to form such a steric zipper motif.

Dap-KKK-cyclo could not be obtained in monomeric form and was studied in form of a mixture of oligomers. This was probably the reason why Dap-KKK-cyclo expressed such low signal intensity in CD experiments and no concentration dependent change of its CD signal. Dap-KKK-cyclo was slightly less toxic but slightly more fibrillogenic than Dap-KKK-lin.

When comparing cyclic peptides containing the hydrophilic connecting element KKK with their linear equivalents, the cyclic peptides showed slightly more intense β -sheet structure elements in CD studies, especially when comparing the relative signal intensity of random coil and β -sheet structure with each other (Fig. 353A). On the other hand cyclic peptides with the connecting element KKK exhibited lower fibril forming potential than their linear counterparts. Conformational changes or rearrangements occurring upon fibril formation seemed to be more hindered in the case for cyclic peptides.

Table 30: ThT binding assays of cyclic and linear peptides containing Aoc as a connecting element at different peptide concentrations.

Results of “+” indicate fibril formation, whereas “-” indicate no fibril formation within the 5 days of incubation of the solution at the given peptide concentration.

Abbrev.	Sequence	ThT			
		35 μ M	100 μ M	200 μ M	500 μ M
H13CC-red	H-C-NKGAII- KKK -NFGAILS-C-OH	-	+		
H13CC-ox	H-C-NKGAII- KKK -NFGAILS-C-OH	-	-	-	+
H13Ser	H-S-NKGAII- KKK -NFGAILS-S-OH	-	-	+	+
Lys-KKK-lin	H-Lys-NKGAII- KKK -NFGAILSD-OH	-	-	-	-
Dap-KKK-lin	H-Dap-NKGAII- KKK -NFGAILSD-OH	-	-	+	+
Dap-KKK-cyclo	cyclo-Dap-NKGAII- KKK -NFGAILSD-OH	-	+/-	+	+
H13	H-NKGAII- KKK -NFGAILS-OH	-			-

3.3.3.3 Peptides with the connecting element Aoc

For the cyclized version of the peptides, a more flexible connecting element like Aoc seemed to be more advantageous for fibril formation and toxicity than connecting elements with a peptidic backbone like KKK and LLL.

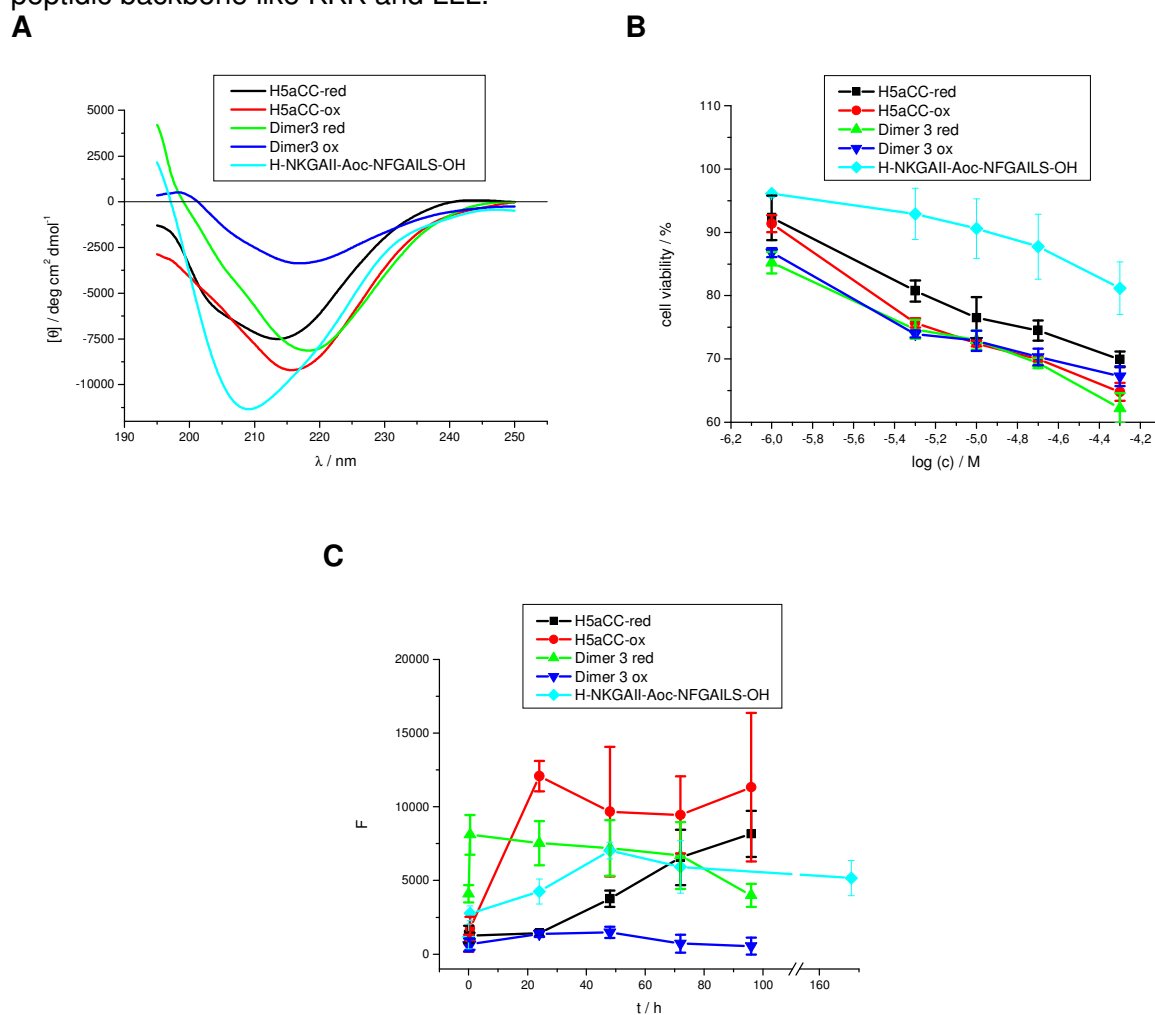


Fig. 354: Comparison of cyclic peptides containing the connecting element Aoc and their linear equivalents.

A) Far-UV CD spectra at a peptide concentration of 10 μ M in 1xb 1% HFiP, pH 7.4.

B) Cell viability assays of aged solutions (5 mM in 1xb 1% HFiP for 4 days, pH 7.4) using PC-12 cells. Data are percentages of control and are the mean (+/-SEM) of three independent experiments with each experiment performed in multiple replicates (n = 3).

C) ThT assays at a peptide concentration of 10 μ M in 1xb 1% HFiP, pH 7.4. Data are means of 3 assays after subtraction of buffer values +/- standard error of the mean (SEM) with each experiment performed in multiple replicates (n = 3).

All peptides containing the hydrophobic connecting element Aoc displayed β -sheet structure in CD studies. Other common features were their high fibril forming potentials and their high toxicity (Fig. 354).

Dimer 3 ox displayed the lowest signal intensity in CD and the lowest fibril forming potential among peptides of this group with Aoc as connecting element.

Cyclic peptides with Aoc as connecting motif between two hot spot regions were in general more toxic than their linear equivalents while their fibril forming potentials were similar.

Table 31: ThT binding assays of cyclic and linear peptides containing Aoc as a connecting element at different peptide concentrations.

Results of “+” indicate fibril formation, whereas “-” indicate no fibril formation within the 5 days of incubation of the solution at the given peptide concentration.

Abbrev.	Sequence	ThT				
		5 μ M	10 μ M	20 μ M	35 μ M	100 μ M
H5aCC-red	H-C-NKGAII-Aoc-NFGAILS-C-OH	-	+		+	
H5aCC-ox	H-C-NKGAII-Aoc-NFGAILS-C-OH	+	+		+	
Dimer 3 red		-	+	+	+	+
Dimer 3 ox			-	+	+	
H5a	H-C-NKGAII-Aoc-NFGAILS-C-OH	-	+	+	+	

3.3.3.4 Conclusions

In general, cyclization did not lead to big changes in the biophysical properties of the peptides when compared with their linear equivalents.

This might be because the open and the cyclized equivalents possessed similar structural features indicating a U-shaped structure for the linear peptides.

CD spectra of Lys-LLL-lin and Dimer 3 red showed a much more intense signal than those of their cyclic equivalents (Fig. 355). The overall shape and the position of the minimum of these signals, however, did not change upon cyclization and suggested β -sheet and β -turn structure for these peptides. The CD spectra of H13CC-ox showed slightly more intensity of the β -sheet signal and slightly less intensity of the random coil signal when compared to H13CC-red (Fig 353A and Fig. 355). This effect might be due to the more rigid conformation of the cyclic peptide H13CC-ox.

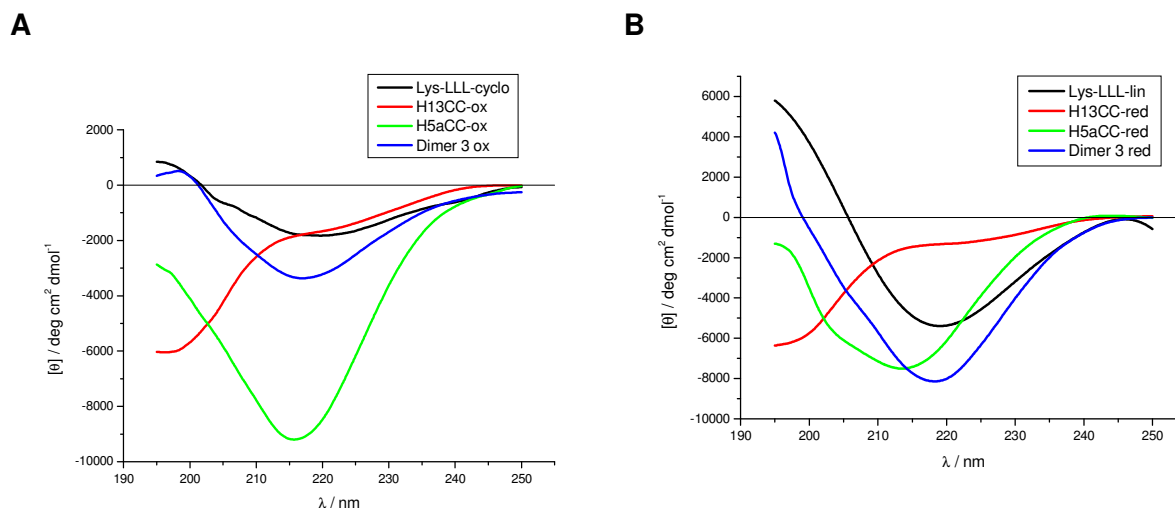


Fig. 355: Far-UV CD spectra of A cyclic peptides and B their linear equivalents at a peptide concentration of 10 μM in 1x 1% HFIP, pH 7.4.

The connecting elements applied here (LLL, KKK, and Aoc) appeared to have a stronger effect on conformation than the cyclisation.

The more rigid conformation expected for the cyclic peptides rather led to a lower fibril forming potential than promoting it. Only the cyclic peptides containing Aoc as a connecting element showed similar fibril forming potentials as their linear equivalents (Fig. 356 and table 31) which might be due to the more flexible connecting motif Aoc as compared to LLL and KKK.

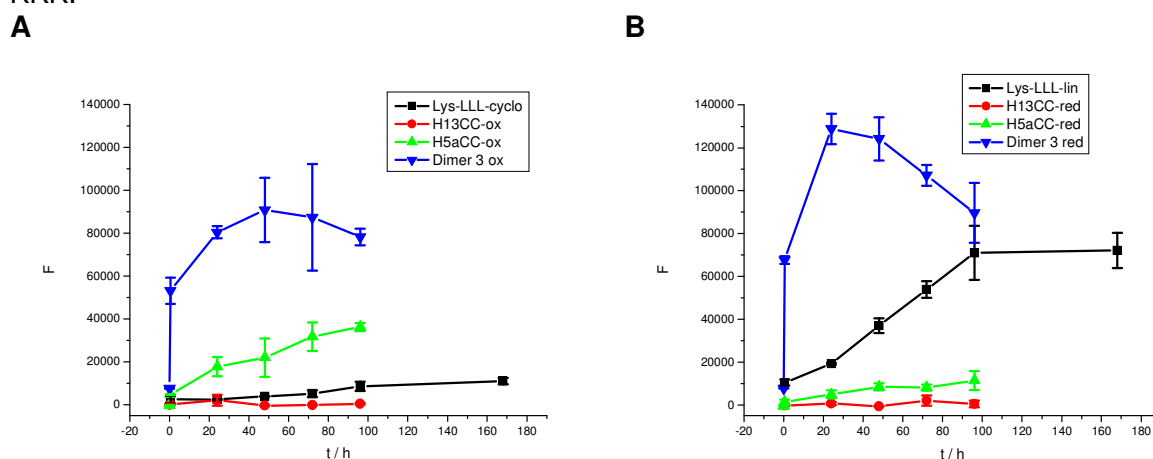


Fig. 356: ThT assays of A cyclic peptides and B their linear equivalents at a peptide concentration of 35 μM in 1x 1% HFIP, pH 7.4. Data are means of 3 assays after subtraction of buffer values \pm standard error of the mean (SEM) with each experiment performed in multiple replicates (n = 3).

Cyclic peptides containing Aoc as connecting element between the two hot spot regions displayed the highest toxicity (Fig. 357). This could be due to an effect of both the hydrophobic connecting element Aoc and of additional cysteine residues at the C- and N-terminus of the peptide. The effect of the cysteines was also present for H13CC-red enabling this peptide to form fibrils but still at much higher concentrations when compared to H5aCC-red.

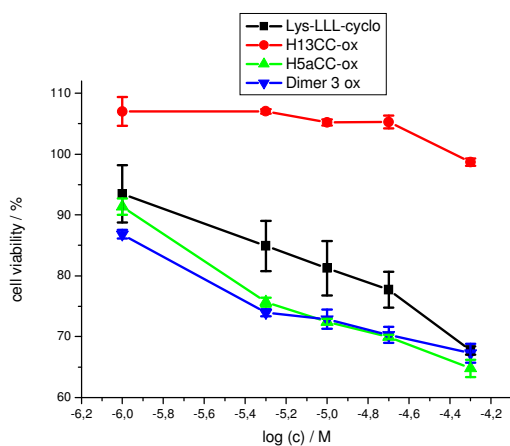
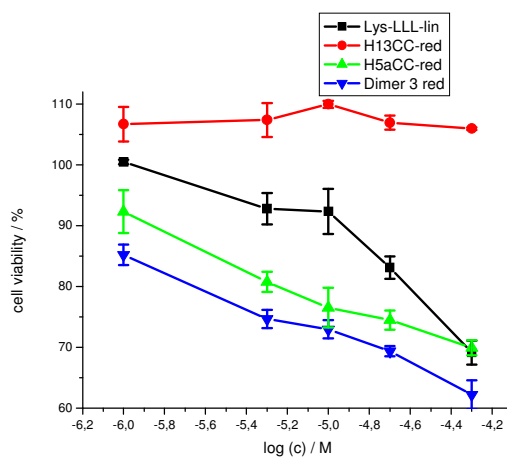
A**B**

Fig. 357: Cell viability assays of aged solutions (5 mM in 1x 1% HFIP for 4 days, pH 7.4) of A cyclic peptides and B their linear equivalents using PC-12 cells. Data are percentages of control and are the mean (+/-SEM) of three independent experiments with each experiment performed in multiple replicates (n = 3).

Crystallization and subsequent X-ray analysis or alternatively NMR analysis would be a necessary tool to reveal the structure of these peptides. This could also reveal whether and what kind of steric zipper motif is formed by the different peptides.

4 References

1. Glenner, G.G. and C.W. Wong, *Alzheimer's disease and Down's syndrome: Sharing of a unique cerebrovascular amyloid fibril protein*. Biochemical and Biophysical Research Communications, 1984. 122(3): p. 1131-1135.
2. Westermark, P., et al., *Islet amyloid in type 2 human diabetes mellitus and adult diabetic cats contains a novel putative polypeptide hormone*. Am J Pathol., 1987. 127(3): p. 414-417.
3. Prusiner, S., *Novel proteinaceous infectious particles cause scrapie*. Science, 1982. 216(4542): p. 136-144.
4. Liepnieks, J.J., B. Kluve-Beckerman, and M.D. Benson, *Characterization of amyloid A protein in human secondary amyloidosis: the predominant deposition of serum amyloid A1*. Biochim Biophys Acta, 1995. 1270(1): p. 81-86.
5. Popescu, A., et al., *Lewy bodies in the amygdala: Increase of α -synuclein aggregates in neurodegenerative diseases with tau-based inclusions*. Archives of Neurology, 2004. 61(12): p. 1915-1919.
6. Häggqvist, B., et al., *Medin: An integral fragment of aortic smooth muscle cell-produced lactadherin forms the most common human amyloid*. Proceedings of the National Academy of Sciences, 1999. 96(15): p. 8669-8674.
7. Furukawa, Y., et al., *Disulfide cross-linked protein represents a significant fraction of ALS-associated Cu, Zn-superoxide dismutase aggregates in spinal cords of model mice*. Proceedings of the National Academy of Sciences, 2006. 103(18): p. 7148-7153.
8. Grundke-Iqbal, I., et al., *Microtubule-associated protein tau. A component of Alzheimer paired helical filaments*. J Biol Chem, 1986. 261: p. 6084-6089.
9. Goedert, M., et al., *Multiple isoforms of human microtubule-associated protein tau: sequences and localization in neurofibrillary tangles of Alzheimer's disease*. Neuron, 1989. 3(4): p. 519-526.
10. Mackay, J.P., et al., *The Hydrophobic EAS Is Largely Unstructured in Solution and Functions by Forming Amyloid-Like Structures*. Structure. 9(2): p. 83-91.
11. Hardy, J. and G. Higgins, *Alzheimer's disease: the amyloid cascade hypothesis*. Science, 1992. 256(5054): p. 184-185.
12. Hardy, J. and D.J. Selkoe, *The Amyloid Hypothesis of Alzheimer's Disease: Progress and Problems on the Road to Therapeutics*. Science, 2002. 297(5580): p. 353-356.
13. McGeer, P.L. and E.G. McGeer, *Inflammation of the brain in Alzheimer's disease: implications for therapy*. Journal of Leukocyte Biology, 1999. 65(4): p. 409-15.
14. Terry, R.D., E. Masliah, and L.A. Hansen, *Structural basis of the cognitive alterations in Alzheimer disease*. Alzheimer disease, 1994: p. 179-196.
15. Lorenzo, A. and B.A. Yankner, *Beta-amyloid neurotoxicity requires fibril formation and is inhibited by Congo red*. Proceedings of the National Academy of Sciences, 1994. 91(25): p. 12243-12247.
16. Lorenzo, A. and B.A. Yankner, *Amyloid Fibril Toxicity in Alzheimer's Disease and Diabetes*. Annals of the New York Academy of Sciences, 1996. 777(1): p. 89-95.
17. Terry, R.D., et al., *Physical basis of cognitive alterations in Alzheimer's disease: Synapse loss is the major correlate of cognitive impairment*. Annals of Neurology, 1991. 30(4): p. 572-580.
18. Thal, D.R., et al., *Phases of A β deposition in the human brain and its relevance for the development of AD*. Neurology, 2002. 58(12): p. 1791-1800.
19. Lemere, C.A., et al., *Sequence of Deposition of Heterogeneous Amyloid β -Peptides and APO E in Down Syndrome: Implications for Initial Events in Amyloid Plaque Formation*. Neurobiology of Disease, 1996. 3(1): p. 16-32.
20. Walsh, D.M. and D.J. Selkoe, *A β Oligomers – a decade of discovery*. Journal of Neurochemistry, 2007. 101(5): p. 1172-1184.
21. Selkoe, D.J., *Soluble oligomers of the amyloid β -protein impair synaptic plasticity and behavior*. Behavioural Brain Research, 2008. 192(1): p. 106-113.
22. Cleary, J., et al., *Beta-amyloid(1-40) effects on behavior and memory*. Brain Research, 1995. 682(1-2): p. 69-74.
23. Cleary, J.P., et al., *Natural oligomers of the amyloid- β protein specifically disrupt cognitive function*. Nat Neurosci, 2005. 8(1): p. 79-84.
24. O'Hare, E., et al., *Delayed behavioral effects following intrahippocampal injection of aggregated Ab(1-42)*. Brain Research, 1999. 815(1): p. 1-10.
25. Glabe, C.G., *Common mechanisms of amyloid oligomer pathogenesis in degenerative disease*. Neurobiology of Aging, 2006. 27(4): p. 570-575.
26. Glabe, C.G., *Structural Classification of Toxic Amyloid Oligomers*. Journal of Biological Chemistry, 2008. 283(44): p. 29639-29643.
27. Glabe, C.G. and R. Kaye, *Common structure and toxic function of amyloid oligomers implies a common mechanism of pathogenesis*. Neurology, 2006. 66(1 suppl 1): p. S74-S78.
28. Bitan, G., et al., *Neurotoxic protein oligomers: what you see is not always what you get*. Amyloid, 2005. 12(2): p. 88-95.

29. Hayden, E. and D. Teplow, *Amyloid beta-protein oligomers and Alzheimer's disease*. *Alzheimer's Research & Therapy*. 5(6): p. 60.
30. Lesné, S.E., *Breaking the Code of Amyloid- Oligomers*. *International Journal of Cell Biology*, 2013. 2013: p. 6.
31. Kaye, R., et al., *Common Structure of Soluble Amyloid Oligomers Implies Common Mechanism of Pathogenesis*. *Science*, 2003. 300(5618): p. 486-489.
32. Kaye, R., et al., *Annular Protofibrils Are a Structurally and Functionally Distinct Type of Amyloid Oligomer*. *Journal of Biological Chemistry*, 2009. 284(7): p. 4230-4237.
33. Kaye, R., et al., *Permeabilization of Lipid Bilayers Is a Common Conformation-dependent Activity of Soluble Amyloid Oligomers in Protein Misfolding Diseases*. *Journal of Biological Chemistry*, 2004. 279(45): p. 46363-46366.
34. Lin, H., R. Bhatia, and R. Lal, *Amyloid b protein forms ion channels: implications for Alzheimer's disease pathophysiology*. *The FASEB Journal*, 2001. 15(13): p. 2433-2444.
35. Lin, M.-C., T. Mirzabekov, and B.L. Kagan, *Channel Formation by a Neurotoxic Prion Protein Fragment*. *Journal of Biological Chemistry*, 1997. 272(1): p. 44-47.
36. McLaurin, J. and A. Chakrabarty, *Membrane Disruption by Alzheimer b-Amyloid Peptides Mediated through Specific Binding to Either Phospholipids or Gangliosides: IMPLICATIONS FOR NEUROTOXICITY*. *Journal of Biological Chemistry*, 1996. 271(43): p. 26482-26489.
37. McLaurin, J. and A. Chakrabarty, *Characterization of the Interactions of Alzheimer β -Amyloid Peptides with Phospholipid Membranes*. *European Journal of Biochemistry*, 1997. 245(2): p. 355-363.
38. Yip, C.M., A.A. Darabie, and J. McLaurin, *Ab42-Peptide Assembly on Lipid Bilayers*. *Journal of Molecular Biology*, 2002. 318(1): p. 97-107.
39. Soto, C., *Unfolding the role of protein misfolding in neurodegenerative diseases*. *Nat Rev Neurosci*, 2003. 4(1): p. 49-60.
40. Levinthal, C., *Are there pathways for protein folding?* *Journal de Chimie Physique et de Physico-Chimie Biologique*, 1968. 65: p. 44-45.
41. Anfinsen, C.B., et al., *THE KINETICS OF FORMATION OF NATIVE RIBONUCLEASE DURING OXIDATION OF THE REDUCED POLYPEPTIDE CHAIN*. *Proceedings of the National Academy of Sciences*, 1961. 47(9): p. 1309-1314.
42. Wilson, M.R., J.J. Yerbury, and S. Poon, *Potential roles of abundant extracellular chaperones in the control of amyloid formation and toxicity*. *Molecular BioSystems*, 2008. 4(1): p. 42-52.
43. DeToma, A.S., et al., *Misfolded proteins in Alzheimer's disease and type II diabetes*. *Chemical Society Reviews*, 2012. 41(2): p. 608-621.
44. Perutz, M.F., *Glutamine repeats and neurodegenerative diseases: molecular aspects*. *Trends in Biochemical Sciences*, 1999. 24(2): p. 58-63.
45. Perutz, M.F., et al., *Glutamine repeats as polar zippers: their possible role in inherited neurodegenerative diseases*. *Proceedings of the National Academy of Sciences*, 1994. 91(12): p. 5355-5358.
46. DePace, A.H., et al., *A Critical Role for Amino-Terminal Glutamine/Asparagine Repeats in the Formation and Propagation of a Yeast Prion*. *Cell*, 1998. 93(7): p. 1241-1252.
47. Maddelein, M.-L. and R.B. Wickner, *Two Prion-Inducing Regions of Ure2p Are Nonoverlapping*. *Molecular and Cellular Biology*, 1999. 19(6): p. 4516-4524.
48. Michelitsch, M.D. and J.S. Weissman, *A census of glutamine/asparagine-rich regions: Implications for their conserved function and the prediction of novel prions*. *Proceedings of the National Academy of Sciences*, 2000. 97(22): p. 11910-11915.
49. Ross, C.A., et al., *Pathogenesis of neurodegenerative diseases associated with expanded glutamine repeats: new answers, new questions*. *Prog Brain Res*, 1998. 117: p. 397-419.
50. Nelson, R., et al., *Structural Models of Amyloid-Like Fibrils*, in *Advances in Protein Chemistry*. 2006, Academic Press. p. 235-282.
51. Sawaya, M.R., et al., *Atomic structures of amyloid cross- β spines reveal varied steric zippers*. *Nature*, 2007. 447(7143): p. 453-457.
52. Wiltzius, J.J.W., et al., *Atomic structures of IAPP (amylin) fusions suggest a mechanism for fibrillation and the role of insulin in the process*. *Protein Science*, 2009. 18(7): p. 1521-1530.
53. Chapman, M.R., et al., *Role of Escherichia coli Curli Operons in Directing Amyloid Fiber Formation*. *Science*, 2002. 295(5556): p. 851-855.
54. Cherny, I., et al., *The Formation of Escherichia coli Curli Amyloid Fibrils is Mediated by Prion-like Peptide Repeats*. *Journal of Molecular Biology*, 2005. 352(2): p. 245-252.
55. Berson, J.F., et al., *Pmel17 Initiates Premelanosome Morphogenesis within Multivesicular Bodies*. *Molecular Biology of the Cell*, 2001. 12(11): p. 3451-3464.
56. Fowler, D.M., et al., *Functional Amyloid Formation within Mammalian Tissue*. *PLoS Biol*, 2006. 4(1). *Bundesministerium für Familie, Senioren, Frauen und Jugend*.
57. Campion, D., et al., *Early-onset autosomal dominant Alzheimer disease: prevalence, genetic heterogeneity, and mutation spectrum*. *Am J Hum Genet*, 1999. 65(3): p. 664-670.
59. Blennow, K., M.J. de Leon, and H. Zetterberg, *Alzheimer's disease*. *The Lancet*, 2006. 368(9533): p. 387-403.

60. Alzheimer, A.A., *Über eine eigenartige Erkrankung der Hirnrinde*. Allg. Z. Psychiat. Psych.-Gerichtl. Med., 1907. 64(146).
61. Glenner, G.G. and C.W. Wong, *Alzheimer's disease: Initial report of the purification and characterization of a novel cerebrovascular amyloid protein*. Biochemical and Biophysical Research Communications, 1984. 120(3): p. 885-890.
62. Masters, C.L., et al., *Amyloid plaque core protein in Alzheimer disease and Down syndrome*. Proceedings of the National Academy of Sciences, 1985. 82(12): p. 4245-4249.
63. Straub, J.E. and D. Thirumalai, *Toward a Molecular Theory of Early and Late Events in Monomer to Amyloid Fibril Formation*. Annual Review of Physical Chemistry, 2011. 62(1): p. 437-463.
64. Benilova, I., E. Karran, and B. De Strooper, *The toxic A[β] oligomer and Alzheimer's disease: an emperor in need of clothes*. Nat Neurosci, 2012. 15(3): p. 349-357.
65. Kang, J., et al., *The precursor of Alzheimer's disease amyloid A4 protein resembles a cell-surface receptor*. Nature, 1987. 325(6106): p. 733-736.
66. Kumar, S., et al., *Extracellular phosphorylation of the amyloid b-peptide promotes formation of toxic aggregates during the pathogenesis of Alzheimer's disease*. Vol. 30. 2011. 2255-2265.
67. Kumar, S., et al., *Early intraneuronal accumulation and increased aggregation of phosphorylated Abeta in a mouse model of Alzheimer's disease*. Acta Neuropathologica, 2013. 125(5): p. 699-709.
68. Milton, N.G.N., *Phosphorylation of amyloid-b at the serine 26 residue by human cdc2 kinase*. NeuroReport, 2001. 12(17): p. 3839-3844.
69. Näslund, J., et al., *Relative abundance of Alzheimer A beta amyloid peptide variants in Alzheimer disease and normal aging*. Proceedings of the National Academy of Sciences, 1994. 91(18): p. 8378-8382.
70. Barnham, K.J., et al., *Neurotoxic, Redox-competent Alzheimer's b-Amyloid Is Released from Lipid Membrane by Methionine Oxidation*. Journal of Biological Chemistry, 2003. 278(44): p. 42959-42965.
71. Mori, H., et al., *Mass spectrometry of purified amyloid beta protein in Alzheimer's disease*. Journal of Biological Chemistry, 1992. 267(24): p. 17082-6.
72. Saido, T.C., et al., *Dominant and differential deposition of distinct b-amyloid peptide species, AbN3(pE), in senile plaques*. Neuron, 1995. 14(2): p. 457-466.
73. Sevalle, J., et al., *Aminopeptidase A contributes to the N-terminal truncation of amyloid β -peptide*. Journal of Neurochemistry, 2009. 109(1): p. 248-256.
74. De Strooper, B. and W. Annaert, *Proteolytic processing and cell biological functions of the amyloid precursor protein*. Journal of Cell Science, 2000. 113(11): p. 1857-1870.
75. Esch, F., et al., *Cleavage of amyloid beta peptide during constitutive processing of its precursor*. Science, 1990. 248(4959): p. 1122-1124.
76. Petkova, A.T., et al., *A structural model for Alzheimer's b-amyloid fibrils based on experimental constraints from solid state NMR*. Proceedings of the National Academy of Sciences, 2002. 99(26): p. 16742-16747.
77. Riek, R., et al., *NMR studies in aqueous solution fail to identify significant conformational differences between the monomeric forms of two Alzheimer peptides with widely different plaque-competence, A β (1-40)ox and A β (1-42)ox*. European Journal of Biochemistry, 2001. 268(22): p. 5930-5936.
78. Hou, L., et al., *Solution NMR Studies of the A beta(1-40) and A beta(1-42) Peptides Establish that the Met35 Oxidation State Affects the Mechanism of Amyloid Formation*. Journal of the American Chemical Society, 2004. 126(7): p. 1992-2005.
79. Bitan, G., et al., *A Molecular Switch in Amyloid Assembly: Met35 and Amyloid b-Protein Oligomerization*. Journal of the American Chemical Society, 2003. 125(50): p. 15359-15365.
80. Whittemore, N.A., et al., *Hydrogen/Deuterium (H/D) Exchange Mapping of Ab1-40 Amyloid Fibril Secondary Structure Using Nuclear Magnetic Resonance Spectroscopy* Biochemistry, 2005. 44(11): p. 4434-4441.
81. Tycko, R., *Solid-State NMR Studies of Amyloid Fibril Structure*. Annual Review of Physical Chemistry, 2011. 62(1): p. 279-299.
82. Lu, J.-X., et al., *Molecular Structure of b-Amyloid Fibrils in Alzheimer's Disease Brain Tissue*. Cell, 2013. 154(6): p. 1257-1268.
83. Opie, E.L., *On the RELATION OF CHRONIC INTERSTITIAL PANCREATITIS TO THE ISLANDS OF LANGERHANS AND TO DIABETES MELUTUS*. The Journal of Experimental Medicine, 1901. 5(4): p. 397-428.
84. Westermark, P., et al., *Amyloid fibrils in human insulinoma and islets of Langerhans of the diabetic cat are derived from a neuropeptide-like protein also present in normal islet cells*. Proceedings of the National Academy of Sciences, 1987. 84(11): p. 3881-3885.
85. Westermark, P., et al., *A novel peptide in the calcitonin gene related peptide family as an amyloid fibril protein in the endocrine pancreas*. Biochemical and Biophysical Research Communications, 1986. 140(3): p. 827-831.
86. Cooper, G.J., et al., *Purification and characterization of a peptide from amyloid-rich pancreases of type 2 diabetic patients*. Proceedings of the National Academy of Sciences, 1987. 84(23): p. 8628-8632.
87. Cooper, G.J.S., et al., *Amylin and the amylin gene: structure, function and relationship to islet amyloid and to diabetes mellitus*. Biochimica et Biophysica Acta (BBA) - Molecular Cell Research, 1989. 1014(3): p. 247-258.

88. Sanke, T., et al., *An islet amyloid peptide is derived from an 89-amino acid precursor by proteolytic processing*. Journal of Biological Chemistry, 1988. 263(33): p. 17243-6.
89. Marzban, L., G. Soukhatcheva, and C.B. Verchere, *Role of Carboxypeptidase E in Processing of Pro-Islet Amyloid Polypeptide in β -Cells*. Endocrinology, 2005. 146(4): p. 1808-1817.
90. Nolan, C., et al., *The Structure of Bovine Proinsulin*. Journal of Biological Chemistry, 1971. 246(9): p. 2780-2795.
91. Ahmad, E., et al., *A mechanistic approach for islet amyloid polypeptide aggregation to develop anti-amyloidogenic agents for type-2 diabetes*. Biochimie, Elsevier Masson SAS, 2011. 93: p. 793-805.
92. O'Brien, T.D., et al., *Islet Amyloid Polypeptide: A Review of Its Biology and Potential Roles in the Pathogenesis of Diabetes Mellitus*. Veterinary Pathology Online, 1993. 30(4): p. 317-332.
93. Betsholtz, C., et al., *Sequence divergence in a specific region of islet amyloid polypeptide (IAPP) explains differences in islet amyloid formation between species*. FEBS letters, 1989. 251(1-2): p. 261-264.
94. Westermark, P., et al., *Islet amyloid polypeptide: pinpointing amino acid residues linked to amyloid fibril formation*. Proceedings of the National Academy of Sciences, 1990. 87(13): p. 5036-5040.
95. Betsholtz, C., et al., *Sequence divergence in a specific region of islet amyloid polypeptide (IAPP) explains differences in islet amyloid formation between species*. FEBS letters, 1989(251): p. 261-264.
96. Rhoades, E., J. Agarwal, and A. Gafni, *Aggregation of an amyloidogenic fragment of human islet amyloid polypeptide*. Biochimica et Biophysica Acta (BBA) - Protein Structure and Molecular Enzymology, 2000. 1476(2): p. 230-238.
97. Ilangovan, U. and A. Ramamoorthy, *Conformational studies of human islet amyloid peptide using molecular dynamics and simulated annealing methods*. Biopolymers, 1998. 45(1): p. 9-20.
98. Ratner, R.E., et al., *Amylin replacement with pramlintide as an adjunct to insulin therapy improves long-term glycaemic and weight control in Type 1 diabetes mellitus: a 1-year, randomized controlled trial*. Diabetic Medicine, 2004. 21(11): p. 1204-1212.
99. Ryan, G.J., L.J. Jobe, and R. Martin, *Pramlintide in the treatment of type 1 and type 2 diabetes mellitus*. Clinical Therapeutics, 2005. 27(10): p. 1500-1512.
100. Tenidis, K., et al., *Identification of a penta- and hexapeptide of islet amyloid polypeptide (IAPP) with amyloidogenic and cytotoxic properties*. Journal of Molecular Biology, 2000. 295(4): p. 1055-1071.
101. Mazor, Y., et al., *Identification and Characterization of a Novel Molecular-recognition and Self-assembly Domain within the Islet Amyloid Polypeptide*. Journal of Molecular Biology, 2002. 322(5): p. 1013-1024.
102. Sakagashira, S., et al., *S20G Mutant Amylin Exhibits Increased in Vitro Amyloidogenicity and Increased Intracellular Cytotoxicity Compared to Wild-Type Amylin*. The American Journal of Pathology, 2000. 157(6): p. 2101-2109.
103. Sakagashira, S., et al., *Missense Mutation of Amylin Gene (S20G) in Japanese NIDDM Patients*. Diabetes, 1996. 45(9): p. 1279-1281.
104. Ma, Z., et al., *Enhanced in vitro production of amyloid-like fibrils from mutant (S20G) islet amyloid polypeptide*. Amyloid, 2001. 8(4): p. 242-249.
105. Tu, L.-H. and D.P. Raleigh, *Role of Aromatic Interactions in Amyloid Formation by Islet Amyloid Polypeptide*. Biochemistry, 2013. 52(2): p. 333-342.
106. Tracz, S.M., et al., *Role of Aromatic Interactions in Amyloid Formation by Peptides Derived from Human Amylin*. Biochemistry, 2004. 43(50): p. 15901-15908.
107. Charge, S.B.P., E.J.P. de Koning, and A. Clark, *Effect of pH and insulin on fibrillogenesis of islet amyloid polypeptide in vitro*. Biochemistry, 1995. 34(44): p. 14588-14593.
108. Abedini, A. and D.P. Raleigh, *The Role of His-18 in Amyloid Formation by Human Islet Amyloid Polypeptide*. Biochemistry, 2005. 44(49): p. 16284-16291.
109. Jha, S., et al., *pH Dependence of Amylin Fibrillization*. Biochemistry, 2014. 53(2): p. 300-310.
110. Jayasinghe, S.A. and R. Langen, *Lipid Membranes Modulate the Structure of Islet Amyloid Polypeptide*. Biochemistry, 2005. 44(36): p. 12113-12119.
111. Soong, R., et al., *Association of Highly Compact Type II Diabetes Related Islet Amyloid Polypeptide Intermediate Species at Physiological Temperature Revealed by Diffusion NMR Spectroscopy*. Journal of the American Chemical Society, 2009. 131(20): p. 7079-7085.
112. Yonemoto, I.T., et al., *Amylin Proprotein Processing Generates Progressively More Amyloidogenic Peptides that Initially Sample the Helical State*. Biochemistry, 2008. 47(37): p. 9900-9910.
113. Vaiana, S.M., et al., *Evidence for a Partially Structured State of the Amylin Monomer*. Biophysical Journal. 97(11): p. 2948-2957.
114. Andrade, M.A., et al., *Evaluation of secondary structure of proteins from UV circular dichroism spectra using an unsupervised learning neural network*. Protein Engineering, 1993. 6(4): p. 383-390.
115. Kaye, R., et al., *Conformational transitions of islet amyloid polypeptide (IAPP) in amyloid formation in Vitro*. Journal of Molecular Biology, 1999. 287(4): p. 781-796.
116. Luca, S., et al., *Peptide Conformation and Supramolecular Organization in Amylin Fibrils: Constraints from Solid-State NMR*. Biochemistry, 2007. 46(47): p. 13505-13522.
117. Kajava, A.V., U. Aebi, and A.C. Steven, *The Parallel Superpleated Beta-structure as a Model for Amyloid Fibrils of Human Amylin*. Journal of Molecular Biology, 2005. 348(2): p. 247-252.

118. Dupuis, N.F., et al., *Human Islet Amyloid Polypeptide Monomers Form Ordered b-hairpins: A Possible Direct Amyloidogenic Precursor*. Journal of the American Chemical Society, 2009. 131(51): p. 18283-18292.
119. Yan, L.-M., et al., *Ein IAPP-Mimetikum blockiert die zytotoxische Aggregation von A β – die Kreuzunterdrückung der Amyloidtoxizität von A β und IAPP deutet auf einen molekularen Zusammenhang zwischen Alzheimer-Krankheit und Typ-II-Diabetes hin*. Angewandte Chemie, 2007. 119(8): p. 1268-1274.
120. Andreetto, E., et al., *Identification of Hot Regions of the A β –IAPP Interaction Interface as High-Affinity Binding Sites in both Cross- and Self-Association*. Angewandte Chemie International Edition, 2010. 49(17): p. 3081-3085.
121. Sims-Robinson, C., et al., *How does diabetes accelerate Alzheimer disease pathology?* Nature reviews. Neurology. 6(10): p. 551-559.
122. Fawver, J.N., et al., *Islet Amyloid Polypeptide (IAPP): A Second Amyloid in Alzheimer's Disease*. Curr Alzheimer Res., 2014. 11(10): p. 928-940.
123. Jackson, K., et al., *Amylin deposition in the brain: A second amyloid in Alzheimer disease?* Annals of Neurology. 74(4): p. 517-526.
124. Merrifield, R.B., *Solid Phase Peptide Synthesis. I. The Synthesis of a Tetrapeptide*. Journal of the American Chemical Society, 1963. 85(14): p. 2149-2154.
125. Carpino, L.A. and G.Y. Han, *9-Fluorenylmethoxycarbonyl amino-protecting group*. The Journal of Organic Chemistry, 1972. 37(22): p. 3404-3409.
126. Wang, S.-S., *p-Alkoxybenzyl Alcohol Resin and p-Alkoxybenzyloxycarbonylhydrazide Resin for Solid Phase Synthesis of Protected Peptide Fragments*. Journal of the American Chemical Society, 1973. 95(4): p. 1328-1333.
127. Lu, G.-s., et al., *Improved synthesis of 4-alkoxybenzyl alcohol resin*. The Journal of Organic Chemistry, 1981. 46(17): p. 3433-3436.
128. Kaiser, E., et al., *Color test for detection of free terminal amino groups in the solid-phase synthesis of peptides*. Analytical Biochemistry, 1970. 34(2): p. 595-598.
129. Aletras, A., et al., *Preparation of the very acid-sensitive Fmoc-Lys(Mtt)-OH Application in the synthesis of side-chain to side-chain cyclic peptides and oligolysine cores suitable for the solid-phase assembly of MAPs and TASP*s. International Journal of Peptide and Protein Research, 1995. 45(5): p. 488-496.
130. Bourel, L., et al., *The deprotection of Lys(Mtt) revisited*. Journal of Peptide Science, 2000. 6(6): p. 264-270.
131. Yue, C., J. Thierry, and P. Potier, *2-phenyl isopropyl esters as carboxyl terminus protecting groups in the fast synthesis of peptide fragments*. Tetrahedron Letters, 1993. 34(2): p. 323-326.
132. Chhabra, S.R., et al., *An appraisal of new variants of Dde amine protecting group for solid phase peptide synthesis*. Tetrahedron Letters, 1998. 39(12): p. 1603-1606.
133. Schiller, P.W., et al., *Side chain to side chain cyclization of an enkephalin analog results in loss of opioid receptor selectivity*. International Journal of Peptide and Protein Research, 1986. 28(5): p. 493-497.
134. Schiller, P.W., T.M.D. Nguyen, and J. Miller, *Synthesis of side-chain to side-chain cyclized peptide analogs on solid supports*. International Journal of Peptide and Protein Research, 1985. 25(2): p. 171-177.
135. King, D.S., C.G. Fields, and G.B. Fields, *A cleavage method which minimizes side reactions following Fmoc solid phase peptide synthesis*. International Journal of Peptide and Protein Research, 1990. 36(3): p. 255-266.
136. Westermark, G.T., et al., *Staining methods for identification of amyloid in tissue*, in *Methods in Enzymology*. 1999, Academic Press. p. 3-25.
137. Stryer, L., *The interaction of a naphthalene dye with apomyoglobin and apohemoglobin: A fluorescent probe of non-polar binding sites*. Journal of Molecular Biology, 1965. 13(2): p. 482-495.
138. Gill, S.C. and P.H. von Hippel, *Calculation of protein extinction coefficients from amino acid sequence data*. Analytical Biochemistry, 1989. 182(2): p. 319-326.
139. Chiti, F., et al., *Studies of the aggregation of mutant proteins in vitro provide insights into the genetics of amyloid diseases*. Proceedings of the National Academy of Sciences, 2002. 99(suppl 4): p. 16419-16426.
140. López de la Paz, M., et al., *De novo designed peptide-based amyloid fibrils*. Proceedings of the National Academy of Sciences, 2002. 99(25): p. 16052-16057.
141. López de la Paz, M. and L. Serrano, *Sequence determinants of amyloid fibril formation*. Proceedings of the National Academy of Sciences, 2004. 101(1): p. 87-92.
142. Takahashi, Y., A. Ueno, and H. Mihara, *Amyloid Architecture: Complementary Assembly of Heterogeneous Combinations of Three or Four Peptides into Amyloid Fibrils*. ChemBioChem, 2002. 3(7): p. 637-642.
143. Inouye, H. and D.A. Kirschner, *Refined Fibril Structures: The Hydrophobic Core in Alzheimer's Amyloid β -Protein and Prion as Revealed by X-ray Diffraction*, in *Ciba Foundation Symposium 199 - The Nature and Origin of Amyloid Fibrils*. 2007, John Wiley & Sons, Ltd. p. 22-46.
144. Kannan, R., M. Raju, and K.K. Sharma, *The critical role of the central hydrophobic core (residues 71-77) of amyloid-forming A β 66-80 peptide in a-crystallin aggregation: a systematic proline replacement study*. Amyloid, 2014. 21(2): p. 103-109.

145. Ahmed, M., et al., *Structural conversion of neurotoxic amyloid-[beta]1-42 oligomers to fibrils*. Nat Struct Mol Biol, 2010. 17(5): p. 561-567.
146. Marshall, K.E., et al., *Hydrophobic, Aromatic, and Electrostatic Interactions Play a Central Role in Amyloid Fibril Formation and Stability*. Biochemistry, 2011. 50(12): p. 2061-2071.
147. Awasthi, S.K., S. Raghothama, and P. Balaran, *A Designed b-Hairpin Peptide*. Biochemical and Biophysical Research Communications, 1995. 216(1): p. 375-381.
148. Blanch, E.W., et al., *Is polyproline II helix the killer conformation? A Raman optical activity study of the amyloidogenic prefibrillar intermediate of human lysozyme*. Journal of Molecular Biology, 2000. 301(2): p. 553-563.
149. Eker, F., K. Griebenow, and R. Schweitzer-Stenner, *Ab1-28 Fragment of the Amyloid Peptide Predominantly Adopts a Polyproline II Conformation in an Acidic Solution*. Biochemistry, 2004. 43(22): p. 6893-6898.
150. Fändrich, M., et al., *Myoglobin forms amyloid fibrils by association of unfolded polypeptide segments*. Proceedings of the National Academy of Sciences, 2003. 100(26): p. 15463-15468.
151. Schweitzer-Stenner, R., et al., *Salmon Calcitonin and Amyloid b:Two Peptides with Amyloidogenic Capacity Adopt Different Conformational Manifolds in Their Unfolded States*. Biochemistry, 2006. 45(9): p. 2810-2819.
152. Williams, A.D., et al., *Mapping Ab Amyloid Fibril Secondary Structure Using Scanning Proline Mutagenesis*. Journal of Molecular Biology, 2004. 335(3): p. 833-842.
153. Wood, S.J., et al., *Prolines and Amyloidogenicity in Fragments of the Alzheimer's Peptide .beta./A4*. Biochemistry, 1995. 34(3): p. 724-730.
154. Rauscher, S., et al., *Proline and Glycine Control Protein Self-Organization into Elastomeric or Amyloid Fibrils*. Structure, 2006. 14(11): p. 1667-1676.
155. Darnell, G., et al., *Flanking Polyproline Sequences Inhibit b-Sheet Structure in Polyglutamine Segments by Inducing PPII-like Helix Structure*. Journal of Molecular Biology, 2007. 374(3): p. 688-704.
156. Jackson, G.R., et al., *Polyglutamine-Expanded Human Huntingtin Transgenes Induce Degeneration of Drosophila Photoreceptor Neurons*. Neuron, 1998. 21(3): p. 633-642.
157. Nance, M.A., et al., *Analysis of a very large trinucleotide repeat in a patient with juvenile Huntington's disease*. Neurology, 1999. 52(2): p. 392-394.
158. Ruprecht, B., *Synthesen, konformationelle Untersuchungen und Wechselwirkungen mit beta-Amyloid Peptid von Teilsequenzderivaten des Insel-Amyloid-Polypeptids*. Bachelor Thesis, Technische Universität München, 2009.
159. Kracklauer, M., *Synthesen und biophysikalische Untersuchungen von Analoga der "Hot-Spot"-Regionen der Aβ-IAPP-Interaktionsdomänen*. Diploma Thesis, Hochschule München, 2011.
160. Claus, A., *Untersuchungen zur Rolle der hot-spot-Regionen der Ab-IAPP wechselwirkungen*. Bachelor Thesis, Technische Universität München, 2013.
161. De la Portilla Guevara, C., *Synthese und Untersuchungen der Konformation und des Amyloidbildungspotentials von Analoga von Teilsequenzen des Insel-Amyloid-Polypeptids*. Bachelor Thesis, Technische Universität München, 2011.
162. Kümmerling, L., *Synthesen und biophysikalische Untersuchungen von Analoga der Selbsterkennungsdomänen von Inselamyloid-Polypeptid*. Bachelor Thesis, Technische Universität München, 2011.
163. Drake, A.F., G. Siligardi, and W.A. Gibbons, *Reassessment of the electronic circular dichroism criteria for random coil conformations of poly(l-lysine) and the implications for protein folding and denaturation studies*. Biophysical Chemistry, 1988. 31(1-2): p. 143-146.
164. Altmann, I., *Synthesen und biophysikalische Charakterisierung von Analoga der IAPP-Sequenz IAPP(8-28)*. Bachelor Thesis, Technische Universität München, 2012.
165. Greenfield, N.J., *Using circular dichroism spectra to estimate protein secondary structure*. Nat. Protocols, 2007. 1(6): p. 2876-2890.
166. Buchanan, L.E., et al., *Mechanism of IAPP amyloid fibril formation involves an intermediate with a transient β-sheet*. Proc Natl Acad Sci U S A, 2013. 110(48): p. 19285-19290.
167. Soriaga, A.B., *Structural Studies of Amyloid Fibril Polymorphism*. 2013.
168. Jeon, J. and M.S. Shell, *Charge Effects on the Fibril-Forming Peptide KTVIIE: A Two-Dimensional Replica Exchange Simulation Study*. Biophysical Journal, 2012. 102(8): p. 1952-1960.
169. Green, M. and P.M. Loewenstein, *Autonomous functional domains of chemically synthesized human immunodeficiency virus tat trans-activator protein*. Cell, 1988. 55(6): p. 1179-1188.
170. Derossi, D., et al., *The third helix of the Antennapedia homeodomain translocates through biological membranes*. Journal of Biological Chemistry, 1994. 269(14): p. 10444-50.
171. Rothbard, J.B., et al., *Conjugation of arginine oligomers to cyclosporin A facilitates topical delivery and inhibition of inflammation*. Nat Med, 2000. 6(11): p. 1253-1257.
172. Fitzpatrick, A.W.P., et al., *Atomic structure and hierarchical assembly of a cross-β amyloid fibril*. Proceedings of the National Academy of Sciences, 2013. 110(14): p. 5468-5473.
173. Kim, W. and M.H. Hecht, *Generic hydrophobic residues are sufficient to promote aggregation of the Alzheimer's Aβ42 peptide*. Proceedings of the National Academy of Sciences, 2006. 103(43): p. 15824-15829.

174. Bolognesi, B., et al., *ANS Binding Reveals Common Features of Cytotoxic Amyloid Species*. ACS Chemical Biology, 2010. 5(8): p. 735-740.
175. Tiffany, M.L. and S. Krimm, *Circular dichroism of poly-L-proline in an unordered conformation*. Biopolymers, 1968. 6(12): p. 1767-1770.
176. Pace, C.N., B.A. Shirley, and J.A. Thomson, *Measuring the conformational stability of a protein*. In *Protein structure: A practical approach*. IRL Press, Oxford, UK, 1990: p. 311-330.
177. Ahmad, F. and C.C. Bigelow, *Estimation of the stability of globular proteins*. Biopolymers, 1986. 25(9): p. 1623-1633.
178. Hopkins, F.G., *Denaturation of Proteins by Urea and Related Substances*. Nature 1930. 126: p. 383-384.
179. Colletier, J.-P., et al., *Molecular basis for amyloid-b polymorphism*. Proceedings of the National Academy of Sciences, 2011. 108(41): p. 16938-16943.
180. Pal, S.K. and A.H. Zewail, *Dynamics of Water in Biological Recognition*. Chemical Reviews, 2004. 104(4): p. 2099-2124.
181. Angell, Y.M., et al., *Solid-Phase Synthesis of Cyclosporin Peptides*. Journal of the American Chemical Society, 1995. 117(27): p. 7279-7280.
182. Hruby, V.J., *Conformational restrictions of biologically active peptides via amino acid side chain groups*. Life Sciences, 1982. 31(3): p. 189-199.
183. Kessler, H., *Conformation and Biological Activity of Cyclic Peptides*. Angewandte Chemie International Edition in English, 1982. 21(7): p. 512-523.
184. Bogdanowich-Knipp, S.J., et al., *Solution stability of linear vs. cyclic RGD peptides*. The Journal of Peptide Research, 1999. 53(5): p. 530-541.
185. Benfield, A.P., et al., *Ligand Preorganization May Be Accompanied by Entropic Penalties in Protein-Ligand Interactions*. Angewandte Chemie International Edition, 2006. 45(41): p. 6830-6835.
186. Zolg, D., *Synthesen und biophysikalische Untersuchungen von Analoga von Teilsequenzen des Inselamyloid-Polypeptids (IAPP) und des β -Amyloid Peptids (A β)*. Bachelor Thesis, Technische Universität München, 2011.
187. Hinkelmann, J., *Synthesen und Untersuchungen zur Konformation und Amyloidbildungspotential von zyklischen Analoga der partiellen Inselamyloid-Polypeptid-Sequenz IAPP(22-28)* Bachelor Thesis, Technische Universität München, 2012.
188. Malesevic, M., et al., *An improved method for the solution cyclization of peptides under pseudo-high dilution conditions*. Journal of Biotechnology, 2004. 112(1-2): p. 73-77.

5 List of Abbreviations

2Aoc	2-Aminooctanoic acid
Ac	Acetyl
ACN	Acetonitrile
Adc	10-Aminodecanoic acid
AD	Alzheimer`s disease
ANS	8-Anilinonaphthalene-1-sulfonic acid
APP	Amyloid Precursor Protein
Aoc	8-Aminooctanoic acid
Boc	<i>tert</i> -butyloxycarbonyl
BSE	Bovine spongiform encephalopathy
CD	Circular dichroism
CGRP	Calcitonin gene related peptide
Cha	Cyclohexylalanine
CR	Congo Red
Dap	2,3-Diaminopropionic acid
d	Day
DCM	Dichloromethane
DIEA	<i>N,N</i> -diisopropylethylamine
DMF	<i>N,N</i> -dimethylformamide
DMSO	Dimethylsulfoxide
DTT	Dithiothreitol
EDT	1,2-ethanedithiol

EOAD	Early-onset Alzheimer's disease
Fmoc	9-fluorenylmethoxycarbonyl
h	Hour
HATU	2-(7-Aza-1H-benzotriazole-1-yl)-1,1,3,3-tetramethyluronium hexafluorophosphate
HFiP	1,1,1,3,3,3-hexafluoro-2-propanol
HOBt	<i>N</i> -hydroxybenzotriazole
IAPP	Islet amyloid polypeptide
ivDde	(4,4-dimethyl-2,6-dioxocyclohex-1-ylidene)-3-methylbutyl
LOAD	Late-onset Alzheimer's disease
m	Milli
M	Molar
MALDI-TOF	Matrix-assisted laser desorption ionisation time-of-flight
μ	Mikro
min	Minute
MS	Mass spectrometry
Mtt	Methytrityl
MTT	3-[4,5-dimethylthiazol-2-yl]-2,5-diphenyltetrazolium bromide
MW	Molecular weight
Nle	Norleucine
NMP	1-methyl-2-pyrrolidinone
PAGE	Polyacrylamide gel electrophoresis
Peg	3(oxy-1,2-ethanediyl)
PiP	Phenylisopropyl
RP-HPLC	Reverse phase high performance liquid chromatography
SDS	Sodium dodecyl sulfate
SPPS	Solid phase peptide synthesis
ssNMR	Solid-state nuclear magnetic resonance
T2D	Type 2 diabetes
TBTU	2-(1H-Benzotriazole-1-yl)-1,1,3,3-tetramethylamminium tetrafluoroborate
t-Bu	Tert-butyl
TEM	Transmission electron microscopy
TFA	Trifluoroacetic acid
TFE	2,2,2-trifluoroethanol
ThT	Thioflavin T
TIS	Triisopropylsilane
t _R	Retention time
Trt	Trityl
UV	Ultraviolet
VIS	Visual

6 Amino Acid Codes

Amino acid residue	One-letter code	Three-letter code
Alanine	A	Ala
Arginine	R	Arg
Asparagine	N	Asn
Aspartic acid	D	Asp
Cysteine	C	Cys
Glutamine	Q	Gln
Glutamic acid	E	Glu
Glycine	G	Gly

Histidine	H	His
Isoleucine	I	Ile
Leucine	L	Leu
Lysine	K	Lys
Methionine	M	Met
Phenylalanine	F	Phe
Proline	P	Pro
Serine	S	Ser
Threonine	T	Thr
Tryptophan	W	Trp
Tyrosine	Y	Tyr
Valine	V	Val

7 Curriculum Vitae

Personal data

Name: Michael Beißwenger
Date of birth: 14. November 1980
Place of birth: Bad Friedrichshall
Citizenship: German

Education

Since 09/2010	PhD in the group of Prof. Dr. Kapurniotu at the TU Munich
10/2007 - 09/2009	Master of Science in Biochemistry at the Ruhr-University Bochum Master thesis: Characterisation and Modulation of the Conformation of Synthetic Protein Fragments from the Family of the Helix- Loop-Helix Transcription Factors.
10/2004 - 09/2007	Bachelor of Science in Biochemistry at the Ruhr-University Bochum Bachelor thesis: Optimization of reagentless biosensors based on Osmiumcomplex modified redox hydrogels and PQQ dependent glucose dehydrogenase.
10/2001 - 09/2004	Studies in physics at the University Leipzig
1991 - 2000	Albert Schweitzer Gymnasium Neckarsulm
1987 - 1991	Elementary school in Erlenbach

Work Experience

01/2010 - 06/2010	Research associate in the group of Prof. Dr. Seitz at the Humboldt-University in Berlin
-------------------	---

8 Acknowledgements

First, I would like to express my special thanks to Prof. Dr. Kapurniotu for her mentorship and guidance during my graduate studies as well as for all her help in experiments and discussions. I will strive to use gained skills and knowledge in the best possible way. I am using this opportunity to express my gratitude to everyone who supported me throughout the course of this Ph.D. thesis.

A special gratitude I give to Michael Kracklauer for examining of the TEM grids. I also want to acknowledge and thank the following students who worked in the context of their Bachelor or Diploma thesis on the synthesis, purification and biophysical studies of some peptides included in my work: Isabella Altmann, Jens Hinkelmann, Linda Kümmerling, Michael Kracklauer, Carolina De la Portilla Guevara, Benjamin Ruprecht, and Daniel Zolg. Their contributions are indicated in the respective figure legends of my thesis. Furthermore, I would like to thank Cornelia Brönner, Constantin Staudtner, and Carina Steinecke for their contributions in peptide synthesis and characterization.

My thanks and appreciations also go to all my colleagues who have helped me in the course of my Ph.D. work. I am thankful for their aspiring guidance, invaluable constructive criticism and friendly advice during the project work.

I would also like to thank Prof. Dr. Bernd Reif for being the reviewer and Prof. Dr. Iris Antes for being the mentor of my doctoral project.

I hope to continue cooperation with all of you in the future.

9 Declaration

I, Michael Beißwenger, declare that I have written this thesis independently, exclusively based on the literature and tools mentioned in the thesis. This document has not previously been submitted for a degree at any other institution than the Technical University of Munich.

Freising,